Probing mechanisms of synergy between PARP inhibitors and inhibitors of ATR, CHK1 and WEE1 in gynaecological cancers

Hannah Louise Smith

Thesis submitted in part requirement for the degree of Doctor of Philosophy (PhD)

October 2021

Newcastle University Centre for Cancer Research

Faculty of Medical Sciences

Newcastle University

Newcastle upon Tyne

Abstract

PARP inhibitors (PARPi) inhibit the repair of DNA single-strand breaks, resulting in collapsed replication forks, which are repaired by homologous recombination repair (HRR). PARPi are synthetically lethal to cancers which are HRR defective (HRD), although resistance often develops. Replication-associated DNA lesions signal to S and G2/M cell cycle checkpoints via ATR, CHK1 and WEE1. Loss of G1 DNA damage checkpoint control is common in cancer cells, so they are predicted to be more dependent on S and G2/M checkpoints. ATR, CHK1 and WEE1 inhibitors are synergistic with PARPi, although the mechanisms underpinning this synergy are not fully understood.

The aim of this thesis is to determine the mechanisms of synergy between inhibitors of PARP (rucaparib), and ATR (VE-821), CHK1 (PF-477736) and WEE1 (MK-1775) in gynaecological cancer cells.

PARPi induced replication stress (RS) (γH2AX foci formation) 3 to 10-fold across the HRR competent (HRC) cells, with modest induction of RS in HRD cells, which had significantly higher basal RS. Rucaparib (10 μM) increased ATR and CHK1 activity as measured by phosphorylation of targets CHK1^{Ser345} (1.8 to 3.1-fold) and CHK1^{Ser296} (1.4 to 4.5-fold), respectively. Rucaparib also increased levels of pCDK1^{Tyr15} (1.3 to 1.7-fold) targeted directly by WEE1 and indirectly by CHK1 and ATR. VE-821 (1 μM) inhibited rucaparib-induced phosphorylation of all 3 targets (40 – 100%). PF-477736 (50 nM) inhibited CHK1^{Ser296} and CDK1^{Tyr15} phosphorylation (50 – 100 %) but caused a 5 to 31-fold feedback activation of ATR. MK-1775 (0.1 μM) inhibited CDK1^{Tyr15} phosphorylation (80- 100%) but activated CHK1 and ATR (up to 20-fold). VE-821, PF-477736 and MK-1775 each significantly potentiated rucaparib in HRC cells (2 to 5-fold). However, no synergy was observed in matched *BRCA* defective cells suggesting the checkpoint inhibitors impaired HRR. Rucaparib increased RAD51 foci (indicative of HRR) 3 to 5-fold across all HRC cells and this increase was completely ablated by VE-821, PF-477736 and MK-1775, suggesting that they induced an HRD phenotype that was synthetically lethal with PARPi. Similar effects were observed in patient-derived malignant ascites cells. Rucaparib-induced S-phase and G2-M arrest was also abrogated by VE-821, PF-477736 and MK-1775.

The data described in this thesis provide compelling evidence that impairment of HRR is a major mechanism underpinning the synergy of PARPi with ATR, CHK1 or WEE1 inhibition.

Acknowledgments

Firstly, I would like to thank my supervisors Professor Nicola Curtin and Dr Elaine Willmore, for all their guidance and support. I value greatly the suggestions and discussions had over the last 4 years. I would also like to thank Dr Lisa Prendergast, who supervised me for part of my studies.

Thank you to DDR group members, past and present, as well as all my colleagues in lab 1.003, I am grateful for each of you.

A special thanks to my Mum and Dad who have been the best support system to me throughout my studies (and life). Thank you for both for always knowing the right things to say when times get particularly tough.

And finally, thank you to my partner Corey, for endlessly supporting me and showing up for me in every way possible, without any hesitation. I appreciate your patience, particularly over the last few months.

Table of contents

Chapter 1. Introduction 1
1.1 Global and UK cancer burden 1
1.2 Ovarian cancer 1
1.3 Cervical cancer 5
1.4 Common features of cancer 6
1.5 DNA damage and the DNA damage response in cancer 7
1.6 DNA repair 9
1.6.1 Base excision repair/ single-strand break repair 10
1.6.2 Nucleotide excision repair 12
1.6.3 Mismatch repair 14
1.6.4 Double-strand break repair: NHEJ, MMEJ/TMEJ and HRR 16
1.6.4.1 NHEJ 16
1.6.4.2 MMEJ/TMEJ 17
1.6.4.3 HRR 17
1.7 Cell cycle checkpoints 20
1.7.1 G1 checkpoint control 20
1.7.2 S and G2/M checkpoint control 23
1.8 Targeting the DNA damage response 25
1.9 PARP and PARP inhibitors 26
1.9.1 PARP structure and function 26
1.9.2 PARP inhibitors 28
1.9.3 Clinical applications of PARP inhibitors 29
1.9.4 PARP inhibitor resistance 31
1.9.5 Biomarkers for PARPi sensitivity 33
1.10 ATR/CHK1/WEE1 in cancer 33
1.10.1 ATR/CHK1/WEE1 dysfunction in cancer 33
1.10.2 ATR, CHK1 and WEE1 inhibitors 34
1.10.3 Preclinical development of ATR/CHK1/WEE1 inhibitors 35
1.10.3.1 Preclinical development of ATR inhibitors 35
1.10.3.2 Preclinical development of CHK1 inhibitors 36
1.10.3.3 Preclinical development of WEE1 inhibitors 36
1.10.4 Clinical development of ATR/CHK1/WEE1 inhibitors 37
1.10.4.1 ATR inhibitors in clinical trials 37
1.10.4.2 CHK1 inhibitors in clinical trials 37
1.10.4.3 WEE1 inhibitors in clinical trials 38
1.10.5 ATR, CHK1 and WEE1 inhibitor synergy with PARPi 39
1.11 Aims and Objectives 40
Chapter 2. Materials and Methods 41
2.1 Chemicals and reagents 41
2.2 Cell culture of cell lines and patient ascites samples 41
2.3 Assessment of mutational status of DDR genes in the cell lines 43
2.4 Targeted RNA sequencing 45
2.5 Gel electrophoresis and Western blotting 45
2.5.1 Preparation of lysates 46
2.5.2 Pierce assay 46

2.5.3 Gel electrophoresis 46
2.5.4 Incubation of antibodies 47
2.5.5 Chemiluminescence and analyses 49
2.6 SRB growth assay 49
2.7 SRB growth inhibition assays 50
2.8 Colony formation assays 51
2.9 Clonogenic survival assays 52
2.10 Immunofluorescence 52
2.10.1 Assessment of basal replication stress 53
2.10.2 Assessing HRR function 54
2.11 PARP activity assay 55
2.12 Cell cycle analysis 57
Chapter 3. Characterisation of cell lines 59
3.1 Introduction 59
3.2 Aims and Objectives 63
3.3 Hypotheses 63
3.4 Materials and Methods 63
3.4.1 Mutational status of DDR genes across cell lines 63
3.4.2 Comparing baseline mRNA expression of key DDR genes across cell lines 64
3.4.3 Baseline DDR protein expression by western blot 64
3.4.4 Determining growth characteristics of cell lines 64
3.4.5 Measure of baseline RS by immunofluorescence 64
3.5 Results 65
3.5.1 Mutational status of DDR genes across cell line panel 65
3.5.2 Expression of previously identified determinants to PARP, ATR, CHK1 and WEE1 inhibition by mRNA expression 67
3.5.3 Expression of previously identified determinants to PARP, ATR, CHK1 and WEE1 inhibition by protein expression 70
3.5.4 Correlation of protein expression and mRNA expression 73
3.5.5 Growth characteristics and cloning efficiency of cell lines 75
3.5.6 Measuring baseline RS of cells by γH2AX and RPA foci formation 77
3.6 Discussion 82
Chapter 4. Determining target inhibition and cytotoxicity of rucaparib on panel of cell lines 85
4.1 Introduction 85
4.2 Aims and Objectives 86
4.3 Hypotheses 86
4.4 Materials and Methods 87
4.4.1 PARP activity assay 87
4.4.2 Single agent cytotoxicity of rucaparib 87
4.4.3 Assessing PARPi-induced RS by γH2AX foci formation 87
4.4.4 Determining activation of ATR-CHK1 pathway by Western blot 87
4.5 Results 88
4.5.1 Endogenous PAR across cell lines and optimum PARP activity in HRC and HRD matched cells 88

4.5.2 Inhibition of PARP activity by rucaparib in HRC and HRD matched cells 90
4.5.3 Single agent cytotoxicity of rucaparib 91
4.5.4 Rucaparib-induced RS across cell line panel 92
4.5.5 Correlation of rucaparib-induced RS and activation of ATR-CHK1 pathway 97
4.5.6 Correlation of RS and rucaparib cytotoxicity 98
4.5.7 Correlation of determinants of sensitivity and rucaparib cytotoxicity 99
4.6 Discussion 101
Chapter 5. Determining cytotoxicity and target inhibition of checkpoint kinase inhibitors on the panel of cell lines 104
5.1 Introduction 104
5.2 Aims and Objectives 107
5.3 Hypothesis 107
5.4 Materials and Methods 107
5.4.1 Determining target inhibition by Western blot 107
5.4.2 Single agent cytotoxicity of kinase inhibitors 108
5.4.3 Statistical analysis 108
5.5 Results 108
5.5.1 Target inhibition by kinase inhibitors 108
5.5.2 Single agent cytotoxicity of kinase inhibitors 114
5.5.2.1 Single agent cytotoxicity of the ATR inhibitor, VE-821 114
5.5.2.2 Single agent cytotoxicity of the CHK1 inhibitor, PF-477736 116
5.5.2.3 Single agent cytotoxicity of the WEE1 inhibitor, MK-1775 117
5.5.3 Correlation between target inhibition by kinase inhibitors and cell survival 120
5.5.4 Correlation between cell growth and inhibition of cell survival by kinase inhibitors 121
5.5.5 Correlation between RS and inhibition of cell survival by kinase inhibitors 123
5.5.6 Correlation between reported determinants of sensitivity and inhibition of cell survival by kinase inhibitors 127
5.5.6.1 Correlation of ATM level and sensitivity to checkpoint kinase inhibitor 127
5.5.6.2 Correlation of ATR level and sensitivity to checkpoint kinase inhibitors 129
5.5.6.3 Correlation of CHK1 level and sensitivity to checkpoint kinase inhibitors 131
5.5.6.4 Correlation of WEE1 level and sensitivity to checkpoint kinase inhibitors 132
5.5.6.5 Correlation of PARP-1 and XRCC1 level and sensitivity to checkpoint kinase inhibitors 133
5.5.6.6 Correlation of BRCA1 and RAD51 level and sensitivity to checkpoint kinase inhibitors 135
5.6 Discussion 137
Chapter 6. Potentiation of rucaparib cytotoxicity by VE-821, PF-477736 and MK-1775 and underlying mechanisms of synergy 141
6.1 Introduction 141
6.2 Aims and Objectives 143
6.3 Hypotheses 143

6.4 Materials and Methods 144
6.4.1 Determining potentiation by combination cytotoxicity experiments 144
6.4.2 Assessment of homologous recombination repair function by immunofluorescence 144
6.4.3 Assessment of cell cycle by flow cytometry 144
6.4.4 Determining the role of PARP trapping by experiments using AA8 and EM9 cells 144
6.4.4.1 Determining the contribution of BER defect vs PARP inhibition in kinase inhibitor cytotoxicity 144
6.4.4.2 Assessing differences in DNA damage and repair between AA8 and EM9 cells 145
6.5 Results 145
6.5.1 Potentiation of rucaparib by kinase inhibitors 145
6.5.2 Correlation of basal RS and degree of potentiation by kinase inhibitors 150
6.5.3 Correlation of rucaparib-induced RS and degree of potentiation by kinase inhibitors 152
6.5.4 Impact of rucaparib and kinase inhibitors on HRR function 154
6.5.5 Effects of rucaparib and kinase inhibitors on cell cycle 165
6.5.6 The impact of PARP trapping on the observed synergy 169
6.6 Discussion 177
Chapter 7. Investigating the effect of rucaparib and kinase inhibitors on patient ascites samples 182
7.1 Introduction 182
7.2 Aims and Objectives 184
7.3 Materials and Methods 184
7.3.1 Establishing primary cultures 184
7.3.2 Homologous recombination repair assay 184
7.3.3 SRB growth inhibition assay 185
7.4 Results 185
7.4.1 Determining basal RS in patient ascites samples 186
7.4.2 Assessing induction of PARPi-induced RS and HRR function of patient ascites samples 188
7.4.3 Determining cytotoxicity of single agent rucaparib and kinase inhibitors in patient ascites samples 190
7.4.4 Investigating synergy between rucaparib and VE-821, PF-477736 and MK-1775 193
7.4.5 Correlation of PARPi-induced RS and potentiation by VE-821, PF-477736 and MK-1775 195
7.4.6 Exploring the impact of VE-821, PF-477736 and MK-1775 on HRR 196
7.5 Discussion 201
Chapter 8. Differences in durability of PARP inhibition by PARP inhibitors in ovarian cancer cells 205
8.1 Introduction 205
8.2 Aims and Objectives 206
8.3 Hypotheses 206
8.4 Materials and Methods 207
8.4.1 PARP activity assay 207

8.4.2 PARP-ATRi scheduling cytotoxicity experiments 207
8.5 Results 207
8.5.1 Durability of PARPi by rucaparib, olaparib, niraparib, pamiparib and talazoparib 207
8.5.2 Investigating schedules of PARPi and ATRi 209
8.6 Discussion 212
Chapter 9. Final discussion 214
9.1 Final Discussion 214
9.2 Future directions 221
Bibliography 222
Appendix A 250
Appendix B 265

List of Figures

Figure 1.1 Histological subtypes of ovarian cancer and frequency of associated mutations 4
Figure 1.2 Emerging hallmarks and enabling characteristics of cancer 6
Figure 1.3 DNA damaging agents causing lesions and the mechanisms of repair associated with them 9
Figure 1.4 Base excision repair mechanism of action from recognition of SS-breaks 11
Figure 1.5 NER responds to DNA helix structural damage and acts by removing oligonucleotides containing damaged DNA bases 13
Figure 1.6 The mechanism of action of mismatch repair 15
Figure 1.7 The mechanism of action of double-strand break repair 19
Figure 1.8 Cyclins and CDKs and their role in cell cycle regulation 21
Figure 1.9 Cell cycle checkpoint signalling by ATM and ATR 22
Figure 1.10 Overview of ATR signalling in response to DNA damage 24
Figure 1.11 The concept of synthetic lethality 25
Figure 1.12 Synthetically lethal relationship between PARP and HRR defective cells 26
Figure 1.13. The role of PARP1 in the orchestration of DNA repair 27
Figure 2.1 Plate layout of 96-well plate for SRB proliferation assay 50
Figure 2.2 Plate layout for SRB growth inhibition experiments in primary cultures 51
Figure 2.3 Principle of measuring PARP activity 56
Figure 3.1 Mutational status of key DDR genes across human cell lines was assessed using data from the CCLE 66
Figure 3.2 Baseline mRNA expression across human cell lines within the panel 69
Figure 3.3 Baseline protein expression of key DDR proteins across cell lines 72
Figure 3.4 Correlation between mRNA expression and protein expression 74
Figure 3.5 Growth characteristics of cell lines 76
Figure 3.6 Baseline replication stress across cell lines 78
Figure 3.7 Correlation of mean γH2AX foci per cell vs mean pRPA 32 $^{Ser4/8}$ per cell across cell lines 79
Figure 3.8 Correlation of protein expression of Cyclin E and pRPA$^{Ser4/8}$ vs. γH2AX and pRPA $^{Ser4/8}$ foci formation 80
Figure 3.9 Correlation of doubling time of cells vs. markers of RS 81
Figure 4.1 Baseline PARP activity and endogenous PAR across cell lines 89
Figure 4.2 Inhibition of PARP activity in HRR defective and competent matched cells 90
Figure 4.3 Single agent cytotoxicity of rucaparib across cell lines 91
Figure 4.4 PARPi-induced RS 93
Figure 4.5 Activation of ATR-CHK1 pathway by rucaparib 96
Figure 4.6 Correlation of rucaparib-induced RS and signalling to ATR-CHK1 pathway 97
Figure 4.7 Correlation of rucaparib cytotoxicity and RS 98
Figure 4.8 Correlation between protein expression of determinants to PARPi sensitivity and rucaparib cytotoxicity. 100
Figure 5.1 Target inhibition of pCHK1^{S345}, pCHK1^{S296} and pCDK1^{Tyr15} by VE-821, PF-477736 and MK-1775 in IGROV-1 cells 109
Figure 5.2: Target inhibition of pCHK1^{S345}, pCHK1^{S296} and pCDK1^{Tyr15} by VE-821, PF-477736 and MK-1775 in C33A, SiHa, UWB1.289+B1, UWB1.289, V-C8.B2 and V-C8 cells 111

Figure 5.3 Single agent cytotoxicity of VE-821 across the panel of cancer cells..... 115
Figure 5.4 Single agent cytotoxicity of PF-477736 across the panel of cancer cells..... 117
Figure 5.5 Single agent cytotoxicity of MK-1775 in cervical and ovarian cancer cells..... 119
Figure 5.6 Correlation of % target inhibition vs. % cell survival inhibition..... 120
Figure 5.7 Correlation of the doubling time of cells vs. LC_{50} and % cell survival at set concentrations..... 122
Figure 5.8 Correlation of basal γH2AX and pRPA foci in cells vs. LC_{50} and % cell survival at set concentrations..... 125
Figure 5.9 Correlation of basal Cyclin E and pRPA level in cells vs. LC_{50} and % cell survival at set concentrations..... 126
Figure 5.10 Correlation of basal ATM level in cells vs. LC_{50} and % cell survival at set concentrations. 128
Figure 5.11 Correlation of basal ATR level in cells vs. LC_{50} and % cell survival at set concentrations..... 130
Figure 5.12 Correlation of basal CHK1 expression in cells vs. LC_{50} and % cell survival at set concentrations. 131
Figure 5.13: Correlation of basal WEE1 expression in cells vs. LC_{50} and % cell survival at set concentrations..... 132
Figure 5.14 Correlation of basal BER protein expression in cells vs. LC_{50} and % cell survival at set concentrations..... 134
Figure 5.15 Correlation of basal HRR protein expression in cells vs. LC_{50} and % cell survival at set concentrations. 136
Figure 6.1 Cytotoxicity of rucaparib in combination with VE-821, PF-477736 or MK-1775 in all cell lines..... 147
Figure 6.2 Comparison of VE-821, PF-477736 and MK-1775 at sensitising cells to rucaparib. 149
Figure 6.3 The impact of basal levels of replication stress on the degree of sensitisation by kinase inhibitors..... 151
Figure 6.4 The impact of rucaparib-induced replication stress on the degree of sensitisation by kinase inhibitors..... 153
Figure 6.5 Impact of rucaparib single agent and in combination with VE-821, PF-477736 or MK-1775 on HRR..... 155
Figure 6.6 Cell cycle analysis of rucaparib and the kinase inhibitors effects in IGROV-1 cells..... 166
Figure 6.7 Single agent cytotoxicity of kinase inhibitors in matched AA8 and EM9 cells..... 171
Figure 6.8 Single agent rucaparib sensitivity and potentiation of kinase inhibitors with rucaparib in matched AA8 and EM9 cells..... 173
Figure 6.9 Impact of PARP inhibition as single agent and in combination with kinase inhibitors on HRR in matched AA8 and EM9 cells..... 176
Figure 7.1 Basal RS in patient cultures of malignant ascites..... 187
Figure 7.2 PARPi- induced RS and HRR function across patient ascites cells..... 189
Figure 7.3 Single agent cytotoxicity of rucaparib in patient ascites cells..... 191
Figure 7.4 Cytotoxicity of VE-821, PF-477736 and MK-1775 at set concentrations in malignant ascites cells..... 192
Figure 7.5 Correlation of basal γH2AX foci in cells vs. growth inhibition (%) at set concentrations..... 193

Figure 7.6 Cytotoxicity of rucaparib in combination with VE-821, PF-477736 or MK-1775 in malignant ascites cells…… 194
Figure 7.7 Correlation of rucaparib-induced γH2AX foci in cells vs. potentiation by kinase inhibitors at 10 μM rucaparib…… 196
Figure 7.8 Impact of rucaparib single agent and in combination with VE-821, PF-477736 or MK-1775 on HRR in patient ascites cells…… 200
Figure 8.1 Durability of PARP activity inhibition by PARP inhibitors in IGROV-1 cells.... 208
Figure 8.2 Scheduling PARPi-ATRi cytotoxicity experiments…… 211

List of Tables

Table 1.1 FIGO staging of ovarian cancer..... 2
Table 1.2 PARPis and current state of development..... 32
Table 2.1 Determinants of sensitivity to PARP, ATR, CHK1 and WEE1 inhibition..... 44
Table 2.2: Primary antibodies used in western blotting experiments..... 48
Table 2.3: HRP-conjugated secondary antibodies used in western blotting experiments... 49
Table 2.4: Volume of Click-iT™ reagents used per sample for cell cycle analysis..... 58
Table 3.1 Cell line characteristics..... 62
Table 5.1: Specific inhibitors of ATR, CHK1 and WEE1 and their relevant properties..... 106
Table 5.2: Effect of VE-821, PF-477736 and MK-1775 on pCHK1^{S345}, pCHK1^{S296} and pCDK1^{Tyr15}..... 113
Table 6.1 Effect of rucaparib and kinase inhibitors on γH2AX and RAD51 foci formation... 164
Table 6.2 Comparison of single agent kinase inhibition and potentiation with addition of rucaparib..... 174
Table 7.1 Patient ascites samples used within the project..... 185

Abbreviations

ATM Ataxia telangiectasia mutated protein

ATR Ataxia telangiectasia and Rad3 related

ATRIP ATR interacting protein

BER base excision repair

BRCA Breast cancer gene

BRIP1 BRCA1 interacting protein 1

BSA Bovine serum albumin

CCLE Cancer cell line encyclopaedia

CCNE1 Cyclin E1

CDK cyclin-dependent kinases

CNA copy number alterations

DDR DNA damage response

DMSO Dimethyl sulfoxide

DSB double-strand break

EC Endometrioid carcinoma

EMA European Medicines Agency

EOC Epithelial ovarian carcinoma

ERCC Excision-repair cross-complementing

FANC genes Fanconi anaemia complementation group

FDA Food and Drug Administration

GI_{50} Growth inhibition 50%

HGSOC High-grade serous ovarian carcinoma

HPV human papilloma virus

HRC Homologous recombination repair competent

HRD Homologous recombination repair defective

HRR homologous recombination repair

IC_{50} half-maximal inhibitory concentration

IF immunofluorescence

LC_{50} Lethal concentration 50%

LGSOC Low-grade serous ovarian carcinoma

MLH1 MutL Homolog 1

MMEJ Microhomology mediated end joining

MOC Mucinous ovarian carcinoma

MRN MRE11-RAD50-NBS1

mRNA messenger ribonucleic acid

MYT1 Myelin transcription factor 1

NAD+ Nicotinamide adenine dinucleotide

NER Nucleotide excision repair

NHEJ Non-homologous end joining

OCC Ovarian clear cell carcinoma

PALB2 Partner and localizer of BRCA2

PARP1 Poly (ADP-ribose) polymerase 1

PBS Phosphate buffer saline

PLK1 polo-like kinase 1

pRB retinoblastoma protein

PTEN Phosphatase and tensin homolog

ROS reactive oxygen species

RPA replication protein A

RS replication stress

SD standard deviation

SEM standard error mean

SETD2 SET domain-containing 2

SRB Sulforhodamine B

SSB single-strand break

SSBR single-strand break repair

TNKS1 Tankyrase 1

TP53 tumour protein p53

WGS/WES whole genome sequencing/whole exome sequencing

WT wildtype

XRCC1 X-ray repair cross-complementing protein 1

Chapter 1. Introduction

1.1 Global and UK cancer burden

Cancer is a leading cause of death worldwide, causing 10 million deaths across the world in 2020 (Ferlay *et al.,* 2020). In 2018 there were 17 million new cases of cancer diagnosed, with the prediction that by 2040 this figure will rise to 27.5 million new cases yearly (Cancer Research UK, 2018). In the United Kingdom (UK) around 375,000 new cancer cases are diagnosed each year (Cancer Research UK, 2016-2018). In 2015 it was estimated that 2.5 million people in the UK were living with cancer, highlighting the necessity for continued research efforts and development of novel therapies.

1.2 Ovarian cancer

Ovarian cancer is the 18th most common cancer worldwide (Sung *et al.,* 2021) and the 6th most common cancer in women in the UK, with approximately 7,500 new cases of ovarian cancer each year (Cancer Research UK, 2016- 2018). Only 43% of women survive 5 years or more from the time of diagnosis (Cancer Research UK, 2013- 2017). Many patients are diagnosed at a later stage and present with metastases, with 30 % and 20 % presenting with stage III and IV disease, respectively, at the time of diagnosis (Cancer Research UK, 2018).

There are ~ 4,200 ovarian cancer deaths in the UK yearly, accounting for ~5% of all cancer deaths in women (Cancer Research UK, 2018), despite the current treatment of platinum- based chemotherapy carboplatin combined with another chemotherapeutic agent such as paclitaxel (American Cancer Society, 2018). Ovarian cancer often presents with less noticeable symptoms so is diagnosed at a later, harder to treat, stage (Gritsina et al., 2015). Ovarian cancers are staged using the International Federation of Gynaecology and Obstetrics (FIGO) system (Table 1.1). Further classification by subtype is based on histological protein expression patterns, epigenetic signatures and mutations (Hirst *et al.,* 2018).

Stage	Description
I	Tumour confined to ovaries of fallopian tube (s)
II	Tumour involves ovary (s) and/or fallopian tube(s) and has progressed to pelvis
III	Tumour involves ovary (s) and/or fallopian tube(s) and has progressed to pelvis, with cytologically or histologically confirmed spread to the peritoneum outside of the pelvis and/or metastasis to the retroperitoneal lymph nodes
IV	Distant metastases

Table 1.1: FIGO staging of ovarian cancer. Ovarian cancers are staged following primary cytoreductive surgery (Hirst *et al.,* 2018).

Ovarian cancer is a heterogeneous disease. Approximately 90 % of ovarian tumours are epithelial and these epithelial ovarian cancers (EOCs) are divided into 5 histological subtypes: high-grade serous, low-grade serous, endometrioid, clear cell and mucinous carcinoma (Figure 1.1)

Serous is the most common epithelial ovarian cancer, with high-grade serous ovarian carcinoma (HGSOC) accounting for the majority of cases (Domcke *et al.,* 2013). This subtype is often aggressive and diagnosed at a late stage of disease. A high percentage of HGSOC cases are *TP53* mutated (96 %) and this likely occurs in precursor lesions of ovarian cancer, as mutated p53 drives early tumourigenesis (Cole *et al.,* 2016). The majority of HGSOC cases are treated with a combination of primary debulking surgery and chemotherapy, with carboplatin and paclitaxel described as the backbone of chemotherapy treatment for advanced HGSOC (Nero *et al.,* 2021). Although the majority of patients show a good initial response to platinum-based chemotherapeutics, the development of primary resistance occurs in ~15% of patients (Nero *et al.,* 2021). PARPi offer a promising therapeutic for exerting anti-tumour activity in recurrent, platinum-resistant HGSOC, with the greatest benefits observed thus far in *BRCA* mutant cancers, in the capacity of use as a monotherapy (Morgan *et al.,* 2018).

The next most common subtype is endometrioid carcinoma (EC). This subtype has a more favourable prognosis and often responds better to chemotherapy treatment (Hirst

et al., 2018). ECs are often MMR defective and *PTEN* is the most frequently observed genetic defect in this subtype (Figure 1.1), which is predictive of poor patient survival (Akiyama-Abe *et al.,* 2013, Martins *et al.,* 2014)

Ovarian clear cell carcinoma (OCCC) has a similar frequency to ECs, with *TP53* mutations and HRR defects occurring much less often compared to HGSOC cases. Clear cell carcinomas respond best to the combination of paclitaxel with platinum (22- 56 %), compared to other platinum-based chemotherapy (11- 27 %) (Iida *et al.,* 2021). Unlike HGSOC, OCCC often presents at an early stage. However, when adjusted for stage, women with OCCC had poorer survival overall compared to HGSOC, owing to the resistance of this subtype to platinum-based therapies (Tang *et al.,* 2018).

Low grade serous ovarian carcinomas (LGSOC) account for a small proportion of ovarian cancer cases and are often diagnosed in younger patients. It is characterised as being less aggressive and more genomically stable (Hirst *et al.,* 2018). Similarly to OCCCs, LGSOCs typically present without *TP53* mutations or HRR defects which are observed with HGSOCs. However, this subsequently means patients with this subtype have a limited response to chemotherapeutics (< 10 %) or PARPis, which typically exploit these defects (Myshko, 2021). So, although LGSOC patients have more favourable survival rates, compared to other subtypes, LGSOCs are relatively chemo-resistant (Ricciardi *et al.,* 2018).

Mucinous ovarian cancer (MOC) is also a rare subtype of ovarian cancers. In ~ 80 % of cases MOC is diagnosed at stage I (Siedman *et al.,* 2004). However, similarly to LGSOC and OCCC, compared to HGSOCs MOCs tend to respond less to platinum-based chemotherapy (12- 35 %), with studies suggesting this subtype is platinum-resistant (Shimada *et al.,* 2009, Babaier and Ghatage, 2020).

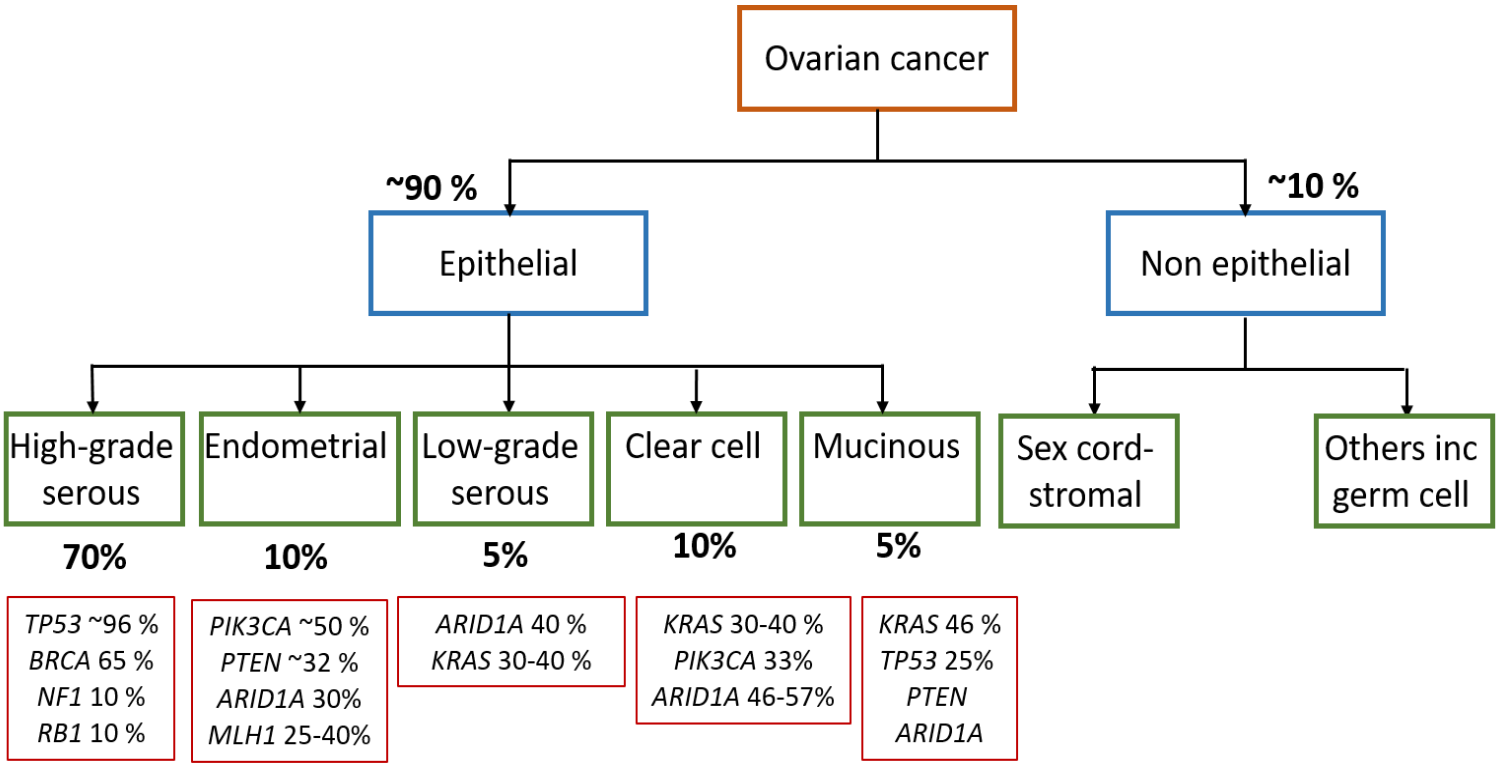


Figure 1.1: Histological subtypes of ovarian cancer and frequency of associated mutations. The most common subtype of epithelial cancer is high-grade serous (HGSOC). *TP53* is mutated in almost all HGSOC cases (Cole *et al.,* 2016). *BRCA* mutations are also common in this subtype in 65% of cases (Mukhopadhyay *et al.,* 2010). Other mutations include *NF1* and *RB1* (Yamulla *et al.,* 2020). *CCNE1* overexpression is also common in this subtype (Chan *et al.,* 2020). Endometrial subtype is associated with mutations in *PIK3CA* (Malentacchi *et al.,* 2019), *PTEN* (Akiyama-Abe *et al.,* 2013), *ARID1A* (Guan *et al.,* 2011) and *MLH1.* Low-grade serous (LGSOC) has mutations in *ARID1A* (Guan *et al.,* 2011) and *KRAS*. Clear cell carcinoma has mutations in *KRAS, PIK3CA* and *ARID1A.* The mucinous subtype has mutations in *PTEN, ARID1A*, *KRAS* and *TP53* (Babaier and Ghatage, 2020, Shimada *et al.,* 2009). Image structure adapted from Banerjee and Kaye, 2013.

1.3 Cervical cancer

On average there are 3,197 new cases of cervical cancer each year in the UK (Cancer research UK, 2016- 2018), with the peak age of incidence 30- 34 years in 2016- 2018. When detected early, the 5-year survival rate for cervical cancer is 92%. However, due to unnoticeable symptoms and lack of screening methods such as the papanicolaou test, which detects abnormal cells and human papillomavirus (HPV) status, in deprived countries many patients are diagnosed at a later stage of the disease. In cases where the cancer has spread to other organs/tissues, this survival decreases to 57% and in patients at the latest stage of the disease the 5-year survival is only 17% (Cancer Research UK, 2015).

HPV infection is a cause of over 90% of cervical cancer cases. HPV16 is the most prominent strain and has seven coding regions: E1-E7. The E6 gene coding proteins target p53 for degradation, thus nearly all cervical cancer cases are p53 defective. E7 works by coding proteins that bind to the tumour suppressor, the retinoblastoma protein (pRb) thus allowing cell progression through the cell cycle (Faridi *et al.,* 2011).

Although the HPV vaccine against HPV 16 and 18 (which account for ~70% cervical cancer) has been introduced in over 80 countries in the last 12 years, these are upper-middle or high-income countries, resulting in cervical cancer still being a great burden in low-income countries (Gallagher *et al.,* 2018). A recent study reported the vaccine reduced the incidence of cervical cancer by 90 % in those vaccinated at 12-13 years old. The vaccine still reduced incidence in those who received it aged 14 to 16 and 16 to 18, although this was to a lesser extent (62 % and 34 % reductions, respectively) (CRUK, 2021). This study also highlighted the importance of giving the vaccine to those who were unlikely to have yet been exposed to HPV, for increased effectiveness.

One of the leading standard treatment options for cervical cancer is surgery, such as radical hysterectomy or trachelectomy. For locally advanced cases external radiotherapy is used alongside chemotherapy, followed up with internal radiotherapy. Cisplatin is a platinum-based, chemotherapeutic agent used in the treatment cervical cancer. However, platinum resistance often occurs as sensitivity to cisplatin decreases with each

successive relapse of the disease (Fong *et al.,* 2010), urging the necessity for new treatment options in both ovarian and cervical cancer.

1.4 Common features of cancer

In 2000, Hanahan and Weinburg proposed that although neoplastic diseases appear extremely diverse in nature, the fundamental underlying molecular mechanisms can be categorised into six characteristics or "hallmarks". The six biological processes determined initially were: the ability to sustain proliferative signalling, resistance to cell death, evasion of growth suppressors, replicative immortality, ability to induce angiogenesis and the ability to activate invasion and metastasis (Hanahan and Weinburg, 2000). Four enabling characteristics of cancer were also established: genome instability, tumour-promoting inflammation, deregulation of cellular energetics and the ability to evade immune destruction (Figure 1.2) (Hanahan and Weinburg, 2011).

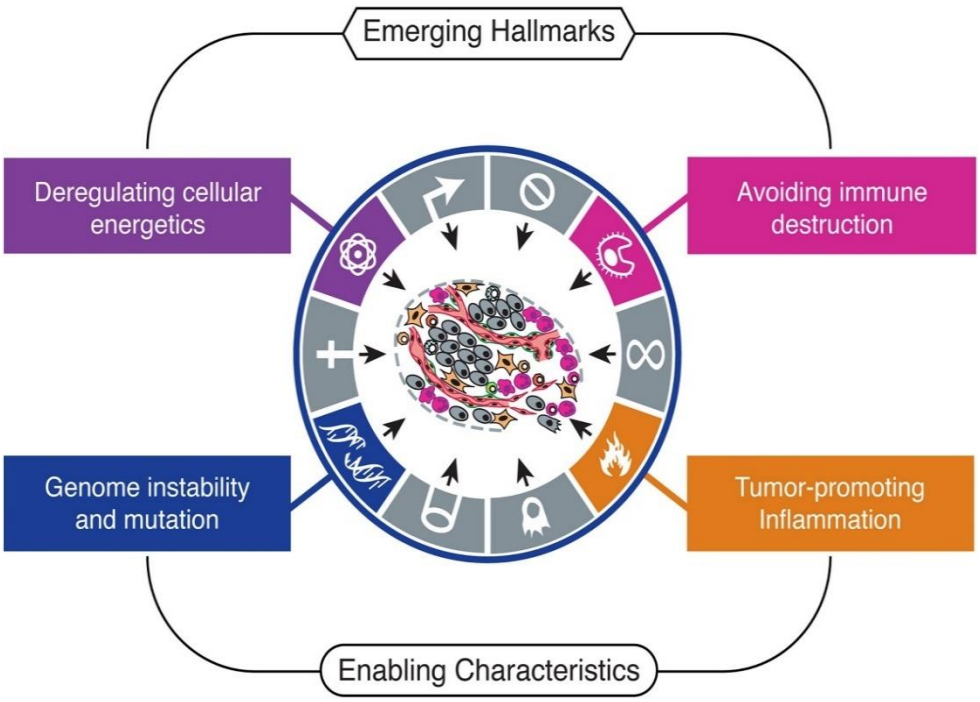


Figure 1.2 Emerging hallmarks and enabling characteristics of cancer. Genetic instability is one of two enabling characteristics that assists in the acquisition of previously mentioned hallmarks, to drive tumour progression. Tumour promoting inflammation is an enabling characteristic as it produces reactive oxygen species (ROS) which damages DNA and leads to DNA damage response (DDR) defects and thus genomic instability (Figure taken from: Hanahan and Weinburg, 2011).

Genomic instability is an enabling molecular characteristic shared amongst almost all human cancers. Cells acquire tens of thousands of DNA lesions on a daily basis, which if left unrepaired can block transcription and replication, leading to loss of genome integrity and cell death (Jackson and Bartek, 2009). Typically, genome maintenance is a tightly regulated surveillance system, referred to as the DDR, which is comprised of caretaker genes that detect genetically damaged cells and either repair the damage, halt the cell cycle, or force them into apoptosis (Campisi, 2005). Mutations in DNA repair genes are a leading cause of genomic instability which drives cancer progression (Broustas and Lieberman, 2014). The mutator phenotype hypothesis states that genomic instability in pre-cancerous lesions facilitates tumour progression. An increase in rate of mutations is a key early event in tumourigenesis and results in a mutation cascade diffusing throughout the genome, effecting genes associated with maintaining genomic integrity (Yao and Dai, 2014).

Replication stress (RS) is a major cause of genomic instability and is common feature in cancer cells due to two factors; 1) oncogenic drivers such as Ras, Myc and Cyclin E that promote entry into S-phase and 2) impairment of the G1/S cell cycle checkpoint e.g., due to loss of p53 or pRb function (Gaillard *et al.,* 2015, Ngoi *et al.,* 2021). Myc is an oncogene that is often deregulated in cancer, and it regulates proliferation, expression of deoxynucleoside triphosphate (dNTP) biosynthesis factors and cyclin dependent kinases (CDKs) (Sarni and Karem, 2017). When the cell cycle is dysregulated, origin firing can occur earlier than it would normally, leading to hyper-origin activation which induces DNA damage. Licensing factors are proteins allowing an origin of replication to begin DNA replication. *In vivo* studies have shown overexpression of licencing factors Cdt1 and Cdc6 lead to an increase in origin activation and the induction of DDR (Blow and Hodgson, 2013).

1.5 DNA damage and the DNA damage response in cancer

As genomic instability is an enabling characteristic of cancer, DNA damage has a fundamental role in carcinogenesis and mutagenesis and can be caused by both endogenous and exogenous factors (Bont and Larebeke, 2004). Tomas Lindahl was the

first to discover the high rate of endogenous damage and the necessity for an equivalent rate of repair (Lindahl and Nyberg, 1972). Endogenous DNA damage is caused by four key processes: methylation, oxidation, depurination and deamination (Ames, 1989). The endogenous production of DNA damaging agents such as reactive oxygen species (ROS), reactive nitrogen species, reactive carbonyl species and alkylating agents lead to single-strand breaks (SSB), which, if left unrepaired, result in RS and collapsed replication forks.

Exogenous DNA damaging agents include environmental factors such as UV, ionizing radiation and genotoxic chemicals, which cause a variety of lesions, including double-strand breaks (DSBs). Orchestration of repair pathways and signalling to cell cycle checkpoints are essential to stop damage being replicated (G1 and S checkpoints), or having the damage passed on to the next generation (G2/M checkpoints) (Figure 1.3). Loss of the DNA damage response (DDR) results in an accumulation of damage, acquisition of mutations and loss of genomic stability.

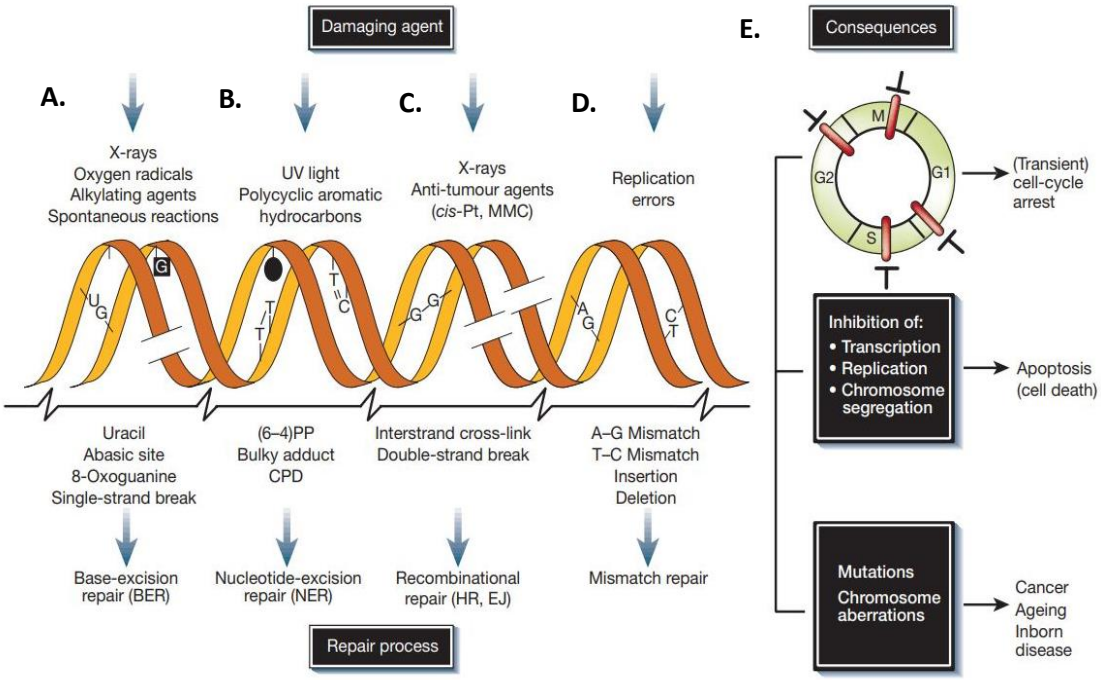


Figure 1.3 DNA damaging agents causing lesions and the mechanisms of repair associated with them. **A**. damaging agents such as X-rays, oxygen radicals, alkylating agents and spontaneous reactions can result in base damage which relies on repair by the base excision repair pathway, which removes specific non-helix distorting base lesions. **B**. UV light and hydrocarbons can result in bulky adducts which must be repaired by nucleotide excision repair. These bulky adducts can interfere with the helix thus the undamaged other strand of DNA is used as a template to replace and correct the site of the lesion. **C**. X-rays and anti-tumour agents such as cisplatin have the ability to induce significant DNA damage, leading to an increase in cross-links and double strand breaks. These double-strand breaks can either be repaired via non-homologous end joining or homologous recombination repair. HRR is the more evolutionary conserved mechanism of repair out of the two and more orchestrated than NHEJ. **D**. Replication errors lead to mismatched base pairs either via an incorrect insertion or deletion, these are dealt with via mismatch repair which rectifies the incorrect "proofreading" of the DNA. **E**. This damage signals to the cell cycle checkpoints. If the damage is too severe then cells are forced into apoptosis. If damage is left unrepaired then mutations can arise such as chromosomal rearrangements. Image from Hoeijmakers, 2001.

1.6 DNA repair

DNA damage is repaired via a number of pathways including base excision repair/ single-strand break repair (BER/SSBR), nucleotide excision repair (NER), mismatch repair (MMR), non-homologous end joining (NHEJ), microhomology-mediated end joining/ POLQ-mediated end joining (MMEJ/TMEJ) and homologous recombination repair (HRR).

1.6.1 Base excision repair/single-strand break repair

BER/SSBR are the front-line of defence against the most common endogenous lesions. Base damage caused by oxidation or alkylation is repaired by BER (Drablos *et al.,* 2004). This involves recognition and removal of the damaged base, creating an AP-site. This AP-site is cleaved by AP-endonuclease 1 (APE1), which creates a single-strand break (SSB). These SSBs, as well as those caused by oxidative damage to the ribose- phosphate backbone are repaired by single-strand break repair (SSBR). SSBs activate PARP1 to recruit XRCC1, DNA polymerase β and DNA ligase III in order to execute SSBR (Figure 1.4). There are two types of BER: short-patch and long-patch repair. Short-patch repair, also termed single-nucleotide BER, is the more dominant pathway and requires DNA polymerase β and DNA ligase III. Long-patch repair also requires PCNA, Fen1, DNA polymerase δ/ε and DNA ligase I. Short-patch BER is equally as proficient in both proliferating and non-proliferating cells, whereas long-patch BER is confined to proliferating cells due to the use of replication proteins (Krokan and Bjoras, 2013) (Figure 1.4).

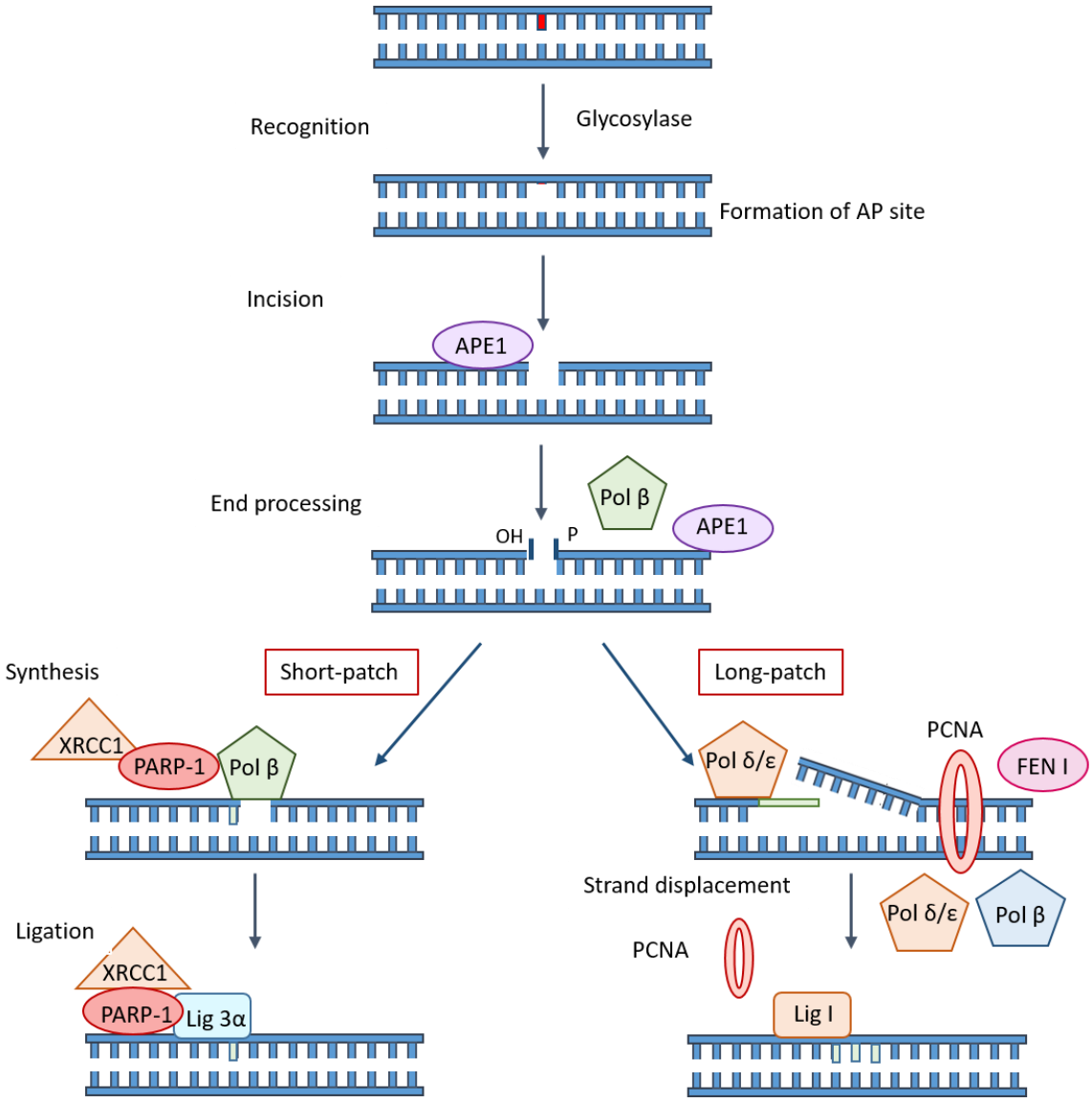


Figure 1.4: Base excision repair mechanism of action from recognition of SS-breaks. BER is required when bases have minor alterations. Specific DNA glycosylases recognize and remove the incorrect base, leaving an abasic site that is later cleaved by abasic endonuclease (APE1) to create an SSB. PARP is drawn to this SSB (see figure 1.14) and recruits XRCC1, which acts as a scaffolding protein for the rest of BER. In short-patch repair DNA polymerase β fills in a single nucleotide and ligase III reseals the break. Long-patch repair is in place for more complex lesions, for example as DNA polymerase can only act on a 3'-OH strand end so when strands are lacking this LP repair is required. PNPK will give 3'-OH and 5-P ends that are able to be ligated. Polymerase δ and ε synthesise the new strand which subsequently creates a flap of the old strand. This old strand is removed by FEN1 in a PCNA-dependent manner. Ligase I acts by joining the two ends together. Image adapted from Akbari *et al.* 2015.

1.6.2 Nucleotide excision repair

Nucleotide excision repair (NER) repairs bulky lesions on one strand of DNA. NER repairs helix-distorting damage often caused by shortwave UV, which leads to 6-4 photoproducts (6-4PPs) and cyclobutene pyrimidine dimers (CPDs) (Kusakabe *et al.,* 2019) (Figure 1.5).

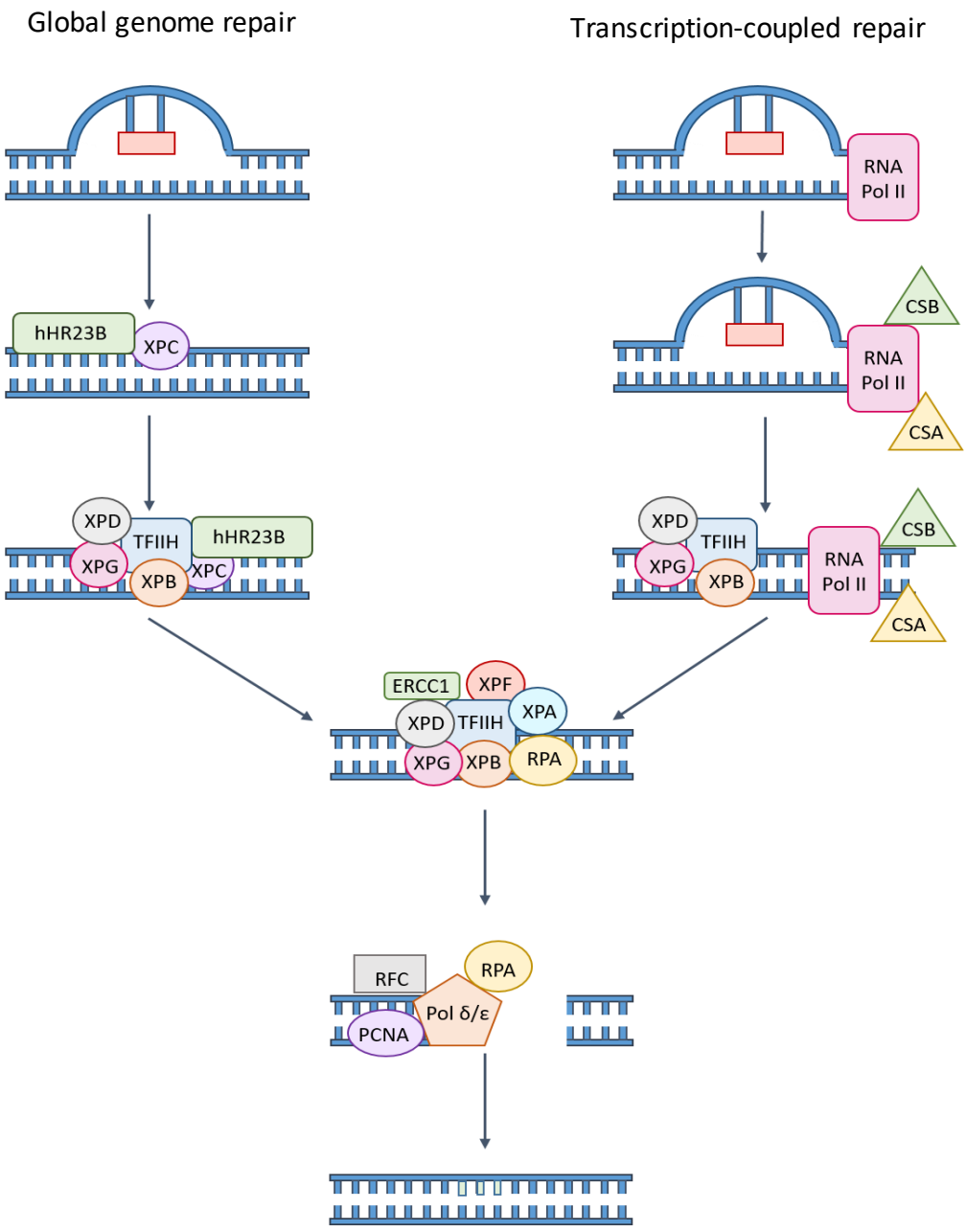


Figure 1.5: NER responds to DNA helix structural damage and acts by removing oligonucleotides containing damaged DNA bases. There are 2 types of NER. Global genome repair (GGR) takes place in the majority of the genome, in DNA not undergoing transcription. Transcription-coupled repair (TCR) takes place in the transcribed strand of activated genes. In GGR XPC/hHR23B binds and in TCR RNA polymerase causes stalling. XPA, RPA, XPG and TFIIH bind before TFIIH unwinds DNA and XPG, XPF/ERCC1 excise the lesion. DNA polymerase fills the gap and ligase seals to ensure the nucleotide sequence is restored (Fuss and Cooper, 2006). XP proteins are derived from xeroderma pigmentosum, a genetic disease characterized by a decrease in repair of DNA damage caused specifically by UV light. CS proteins are linked to Cockayne syndrome, a disease of premature aging and extreme photosensitivity. Image adapted from Olsen *et al.,* 2005.

1.6.3 Mismatch repair

Mismatch repair (MMR) corrects base mismatches, insertions and deletions. MMR acts by recognising and repairing errors made by incorrect DNA "proof reading". The strand-specific rectification is a highly conserved process (Figure 1.6) (Guillotin and Martin, 2014). MMR is less understood in mammalian cells, compared to a less complex MMR mechanism observed in prokaryotes. Mismatches are recognised by either MutSα (heterodimer complex of MSH2/MSH6) or MutSβ (heterodimer complex of MSH2/MSH3). The selection of which MutS homolog is bound to mismatches is based on the size, with MutSα binding to mismatches of up to 3 nucleotides and MutSβ up to 13 nucleotides. MMR is heavily associated with S-phase and PCNA activates MutSα, MutLα and EXO1 at sites of replication (Liu *et al.,* 2017). For excision to occur either MutS homolog recruits MutLα (heterodimer complex of MLH1/PMS2) in an ATP-dependent manner (Liu *et al.,* 2017, Plotz *et al.,* 2006).

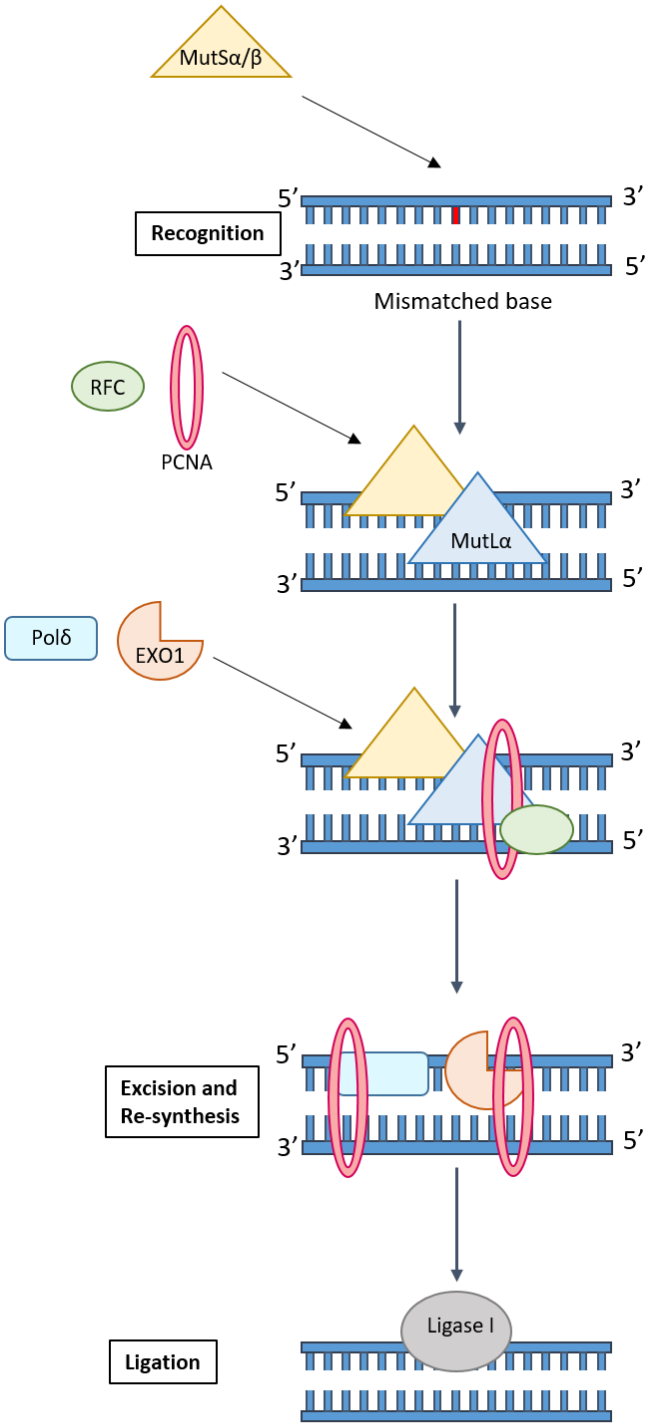


Figure 1.6: The mechanism of action of mismatch repair.
Initially a mismatched base is recognised by either MutSα or MutSβ. One of the MutS homologs is bound to the mismatch and is loaded by proliferating cell nuclear antigen (PCNA)/ RFC. MutLα is recruited and subsequently forms a complex with MutS. EXO1 is recruited to facilitate excision and PCNA fuels Polδ-catalysed re-synthesis. Ligase I seals the resulting nick. Image adapted from Liu *et al.,* 2017.

1.6.4 Double strand break repair: NHEJ, MMEJ/TMEJ and HRR

Double-strand breaks (DSBs) are considered the most cytotoxic DNA lesion and are caused both endogenously and exogenously. Unrepaired SSBs, which in turn collide with the replication fork, trigger fork collapse, which results in single-ended DSBs (Vitor *et al.,* 2020). DSBs can also occur due to environmental exposure to ultraviolet light (UV) (Negritto *et al.,* 2010). Exogenous factors which cause DSBs include irradiation (IR) and topoisomerase II poisons and anti-tumour agents such as cisplatin, which results in persistent DSBs (Hoeijmakers, 2001, Sears and Turchi, 2012). If unrepaired, DSBs can result in genomic rearrangements and ultimately cell death. Therefore, repair of these lesions is crucial.

1.6.4.1 NHEJ

The majority of DSBs are repaired by NHEJ, which is exclusive to G1 and S- phases of cell cycle (Lieber *et al.,* 2010). A major component of this pathway is the Ku70/Ku80 heterodimer complex, which is the DNA binding component of the repair pathway, as it binds to DNA and acts as a scaffold for other NHEJ proteins such as DNA-dependent protein kinase catalytic subunit (DNA-PKcs) (Fell and Schild-Pulter, 2012). Following its recruitment, DNA-Pkcs forms a holoenzyme with the Ku70/Ku80 complex, which promotes the synapsis of the broken DNA ends (Spagnolo *et al.,* 2006). Artemis is a nuclease which is activated by binding to/phosphorylation by DNA-Pkcs. Subsequently, it assists in DNA end resection (Figure 1.7 A) (Davis *et al.*, 2013). Addition of nucleotides occurs via polymerase μ and λ, which interact with Ku via their N-terminal BRCA1 C terminus (BRCT) domains. XRCC4 stimulates Lig IV enzymatic activity to ensure ligation can occur. XRCC4-like-factor (XLF) has a weak structural similarity to XRCC4 and acts by forming a sleeve-like complex with XRCC4 around a DNA duplex (Chang *et al.,* 2017). Paralog of XRCC4 and XLF (PAXX) has also been proposed as a factor involved in NHEJ repair, based on its structural similarity with XRCC4 and XLF (Liu *et al.,* 2017). PAXX has been shown to interact directly with the Ku complex, as well as being recruited to sites of DNA damage in cells. Ochi *et al.,* identified PAXX as a component of NHEJ machinery by showing PAXX promoted Ku-dependent ligation (Ochi *et al.,* 2015).

1.6.4.2 MMEJ/ TMEJ

Microhomology-mediated end joining (MMEJ) or as it is was termed later polymerase theta-mediated end joining (TMEJ), is a DSB repair mechanism which has been shown to be essential in cells deficient in NHEJ or HRR (Wyatt *et al.,* 2016, Feng *et al.,* 2019). It is instigated by PARP1 recruitment to DNA-ends (Schrempf *et al.,* 2021) (Figure 1.7 B). 3' ssDNA overhangs are generated by helicases such as the MRE11-RAD50-NBS1 (MRN) complex. POLQ aligns the 3' ssDNA tails and binds to these, then anneals 2-6 base pair patches of complementary sequence (microhomologies) (Carvajal-Garcia *et al.,* 2020). DNA ends are ligated by Lig III-XRCC1 or Lig I (Liang *et al.,* 2008, Schrempf *et al.,* 2020).

1.6.4.3 HRR

HRR is a template-directed DSB repair mechanism, which is restricted to late S/G2 phase of the cell cycle. NHEJ is a considerably more error-prone mechanism of repair compared to HRR, as the process does not use a complimentary DNA template (Hsu *et al.,* 2002). DSBs are recognised in the first instance by the MRN complex. CtIP is a BRCA-associated protein and the formation of BRCA1-MRN-CtIP complex is cell cycle dependent and vital for end resection in HRR (Chen *et al.,* 2008). The complex generates 3' ssDNA, which is coated with replication protein A (RPA), leading to subsequent ATR activation. BRCA1 and PALB2 assist BRCA2 with replacing RPA with repair protein RAD51, which subsequently forms a filament to search for the specific homologous sequence on the sister chromatid. Strand invasion occurs, and DNA is extended using the template sequence (Brandsma and Gnet, 2012) (Figure 1.7 C). Factors such as PARI, RECQL5, FANCJ and BLM ensure the process is negatively regulated and act to prevent hyper recombination (Brown *et al.,* 2017).

HRR also has a role in resolving stalled replication forks and single-ended DSBs and is therefore crucial in maintaining genomic stability. These collapsed replication forks are caused by RS – the prime activator ATR-CHK1-WEE1 pathway, with each of these cell cycle checkpoint kinases playing a key role in HRR (reviewed in Smith *et al.,* 2020, Appendix A). ATR acts independently of BRCA1 to recruit RAD51 to DSBs, in cells with *BRCA* defects and ATRi was shown to disrupt RAD51 loading in these cells (Yazinski *et al.,*

2017). CHK1 promotes HRR by phosphorylation of BRCA2 and RAD51 (Sorensen *et al.,* 2005). WEE1 is also involved due to its inhibitory phosphorylation of CDK activity when activated. The resection of DNA ends, a necessary step in HRR is antagonised by CDK activity (Buisson *et al.,* 2017), inhibition of CDK activity by WEE1 (or cdc25 inactivation downstream of CHK1) promotes HRR, therefore inhibition of either CHK1 or WEE1 will result in higher CDK activity and compromise HRR (Krajewska *et al.,* 2012).

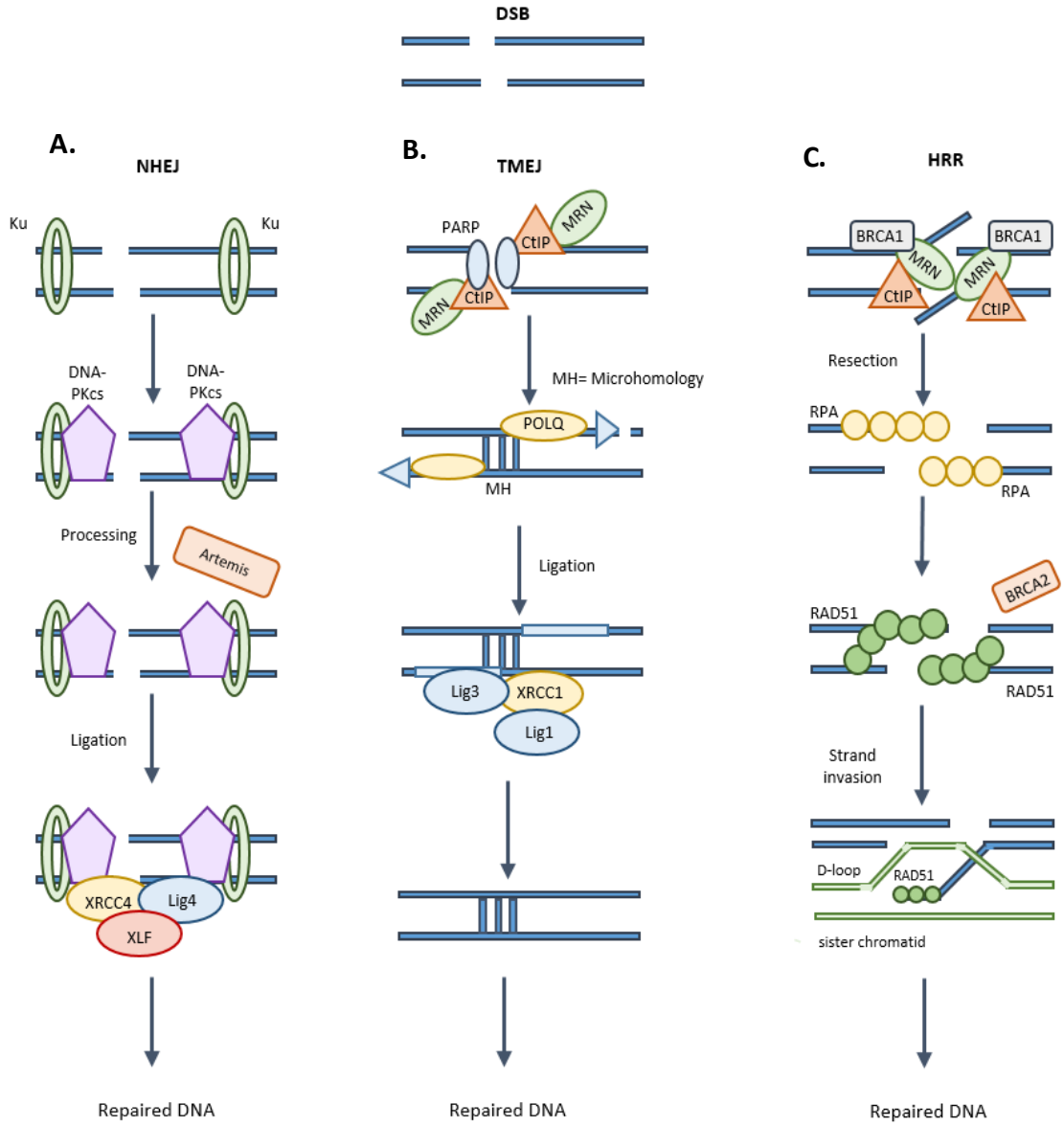


Figure 1.7: The mechanism of action of double-strand break repair. A. NHEJ acts by relegating DNA ends by introducing small insertions and deletions at break sites, without extensive processing. The Ku70/Ku80 complex binds to DNA and recruits DNA-PKcs. Artemis assists in DNA end resection following binding to/phosphorylation by DNA-PKcs. Ligation occurs via XRCC4, LigIV and XLF (Davis and Chen, 2013). **B.** TMEJ is initiated by recruitment of PARP1 to DNA ends. Following activation by CtIp, overhangs are generated by the MRN complex. POLQ binds to ssDNA overhangs and subsequently anneals sequences consisiting of 2-6 base pairs of microhomology (MH). These are used as primers for DNA synthesis. Ligation occurs by Lig 3-XRCC1 or Lig 1 (Schrempf *et al.,* 2020). **C.** HRR uses a complementary sister chromatid to act as a template for DNA repair. The formation of BRCA1-MRN-CtIP complex is vital for end resection in HRR. The complex generates ssDNA, which is coated with replication protein A (RPA). BRCA2 facilitates replacing RPA with repair protein RAD51, which subsequently forms a filament to search for the specific homologous sequence on the sister chromatid (Brandsma and Gnet, 2012). Image adapted from Brandsma and Gent, 2012 and Schrempf *et al.,* 2020.

1.7 Cell cycle checkpoints

Arresting the cell to stop DNA damage passing through the cell cycle and therefore allowing time for DNA repair to occur is just as pivotal as repair mechanisms in preventing oncogenesis or cell death. This ensures cell integrity is maintained from one generation to the next and if DNA damage is deemed irreparable, signalling to apoptosis occurs (Barnum and O' Connell, 2014).

1.7.1 G1 checkpoint control

p53 is a transcription factor and cell cycle regulator at the G1 checkpoint (Figure 1.8). DNA damage activates p53 which subsequently results in transcription of p21. p21 stops DNA replication in two ways: 1) by binding to cyclin-CDK complexes to block cell cycle progression and 2) binding to PCNA to prevent it from acting as a DNA polymerase processivity factor. p53 is a key tumour suppressor mutated in 50% of all cancers, however, a large proportion of patients that do retain wildtype p53 also have significantly altered p53 function (Duffy et al., 2017). CHK1- and CHK2- mediated phosphorylation is vital for the stabilisation and activation of p53. Inhibition of CHK1/2 function leads to a loss of p53 phosphorylation and increased p53 degradation, thus leading to loss of cell cycle regulation and an increase in cell proliferation (Maclaine and Hupp, 2009). Both ATR/ATM and CHK1/CHK2 phosphorylate p53, which further promotes transcription of CDK inhibitor proteins: p16 and p21, leading to cell cycle arrest (Bartek and Lukas, 2003).

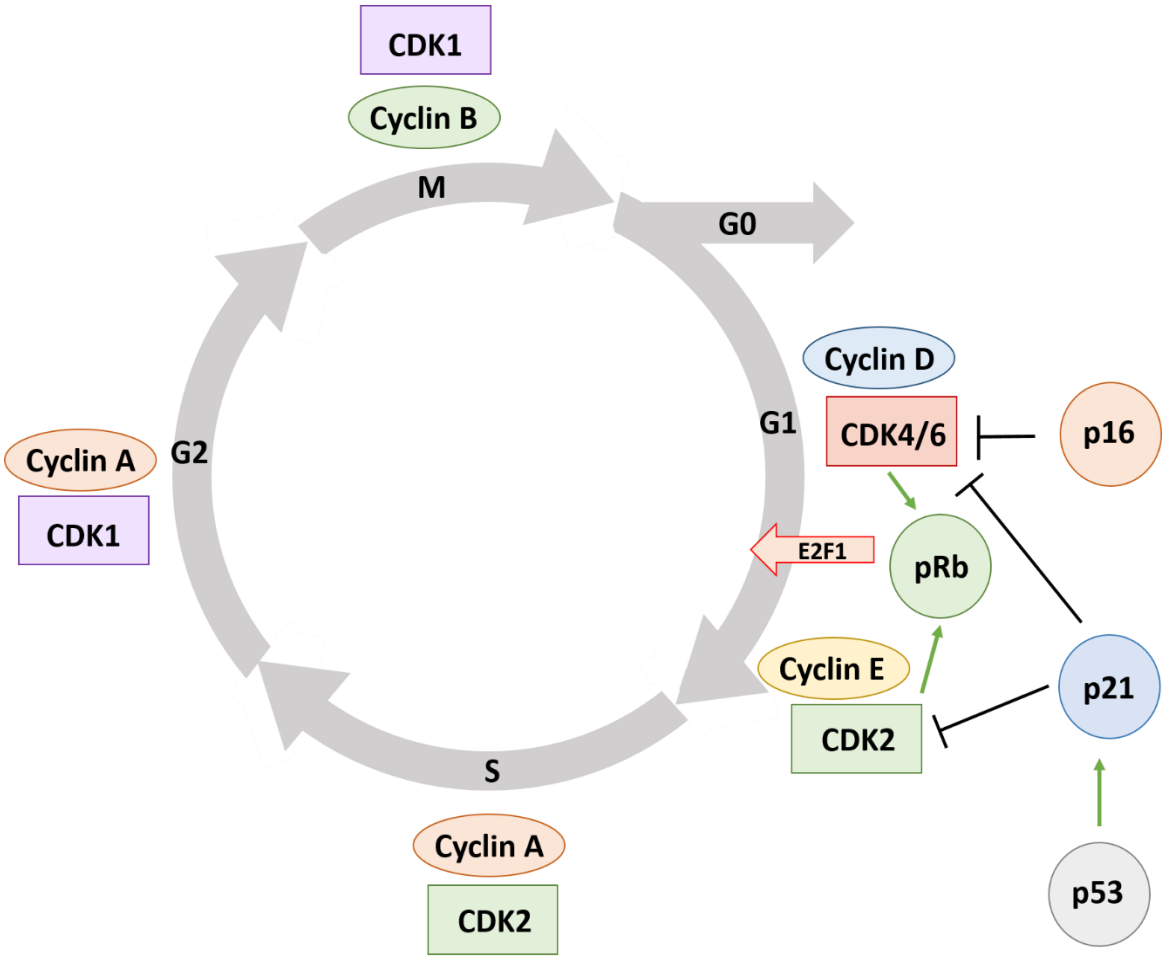


Figure 1.8: Cyclins and CDKs and their role in cell cycle regulation. In G1 phase cyclin D/ CDK4/6 complex triggers phosphorylation of pRb which is completed in late G1/S phase by cyclin E/ CDK2. pRB releases E2F transcription factors and S-phase entry occurs. P16 and p21 inhibit CDK 4/6 and CDK2. When activated p53 results in the transcription of p21 which subsequently blocks cell cycle progression. Image adapted from Hardwick *et al.,* 2018.

Rb protein (pRb) is a tumour suppressor that represses transcription required for G1 to S phase transition. pRb plays a key role in the G1 checkpoint and can bind to E2F transcription factors and viral oncoproteins. When pRb is functionally inactivated E2F is freed, relieving splicing suppression and allowing E2F to activate transcription (Ahlander and Bosco, 2009). As previously described, the most common HPV strain (HPV16) E7 coding region destabilizes pRb, resulting in the majority of cervical cancer cases having defective G1 checkpoint control.

CDKs are key drivers of cell cycle progression (Figure 1.8) and act by phosphorylating their substrates to encourage DNA synthesis and advancement to mitosis. CDC25A is able to remove the inhibitory phosphorylation of CDK2 and cyclin E/CDK2, which

typically prevents cells from entering S phase. Both CHK1 and CHK2 inhibit CDC25A which can therefore no longer act upon cyclin-dependent kinases. When CDKs are inhibited in response to checkpoints being triggered, this subsequently causes cell cycle arrest and allows DNA repair to occur (Hughes et al., 2013).

In most cancers the key regulators involved in the G1 checkpoint control such as p53 and pRb are defective due to alterations/mutations. However, the S and G2 checkpoints remain intact, thus cells can still replicate/excessively proliferate, making pathways such as ATR-CHK1 potential therapeutic targets.

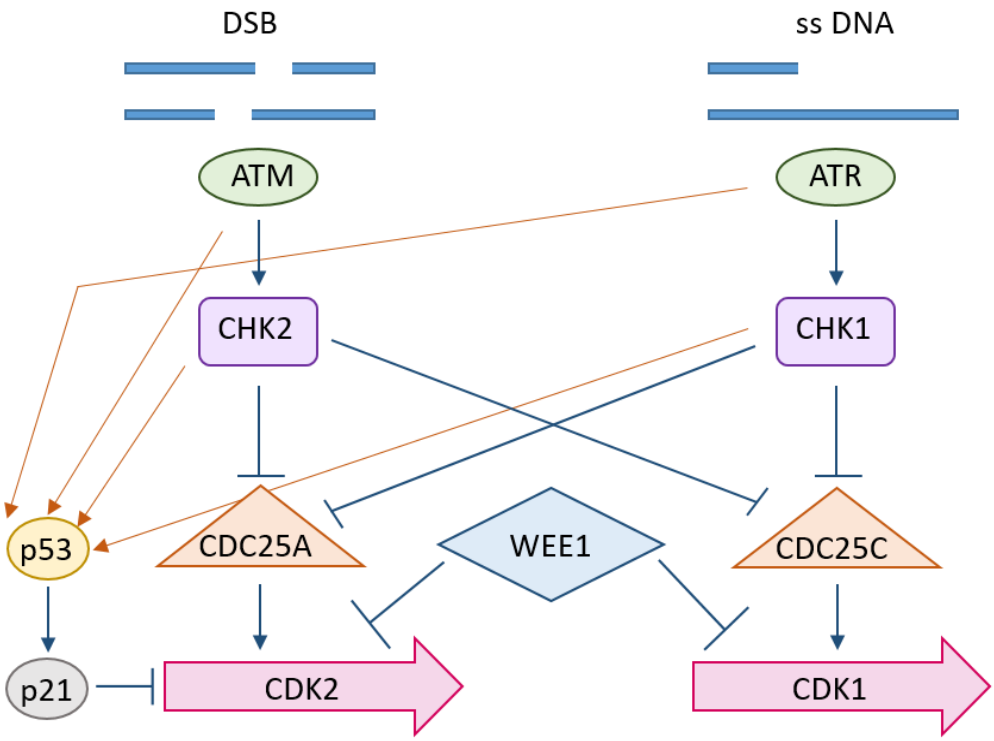


Figure 1.9: Cell cycle checkpoint signalling by ATM and ATR. ATM is activated by DSBs and signals to CHK2 which phosphorylates and inactivated CDC25A, preventing the removal of an inhibitory phosphorylation on CDK2, preventing S-phase entry and cell cycle progression. ATR is activated by ssDNA which phosphorylates CHK1, this phosphorylates and inactivates CDC25C, preventing the removal of an inhibitory phosphorylation on CDK1, preventing G2-M progression. DNA lesions also activate WEE1, which phosphorylates and inactivate CDK1 and 2. Image from Smith *et al.,* 2020.

1.7.2 S and G2/M checkpoint control

In most cancers the G1/S checkpoint is impaired, meaning that cells rely on the S and G2/M checkpoints for survival. The ATR-CHK1-WEE1 pathway has a key role in cell cycle control, specifically in activating both intra-S and G2/M checkpoint control in response to RS. The predominant activator of the pathway is ss-DNA, which primarily arises from stalled replication forks, although NER intermediates and resected DSBs also contribute to this.

Replication protein A (RPA) coats the ss-DNA, protecting it from degradation and enabling recruitment of ATR via ATR-interacting protein (ATRIP). ATR is activated by either TOPBP1, which is recruited by interaction with MRN complex that resects DSB to give long ss-DNA overhangs and the 9-1-1 complex (a proliferating cell nuclear antigen (PCNA)-like clamp that binds ss-ds DNA junctions) or by ETAA1, which is recruited to ss-DNA by inter- action with RPA (Thada and Cortez, 2019). Upon activation, ATR activates CHK1 by phosphorylation at serine 345 causing CHK1 to autophosphorylate at serine 296, to achieve full activation. CHK1 causes the inactivating phosphorylation of CDC25A/C (Rundle *et al.,* 2017, Lewis *et al.,* 2017), thereby preventing them from removing the inhibitory phosphorylation on CDK2 and 1, respectively (as shown in Figure 1.10). In yeast and xenopus, CHK1 phosphorylates and activates Wee1 kinase activity to phosphorylate, and hence inactivate, CDK 1 and 2 (Lin *et al.,* 2017, Lee *et al.,* 2001). This is yet to be shown in mammalian cells. The net result of kinase activation and phosphatase inhibition is inhibition of CDK2, and thus S-phase entry and progression, and inhibition of CDK1 preventing entry into mitosis.

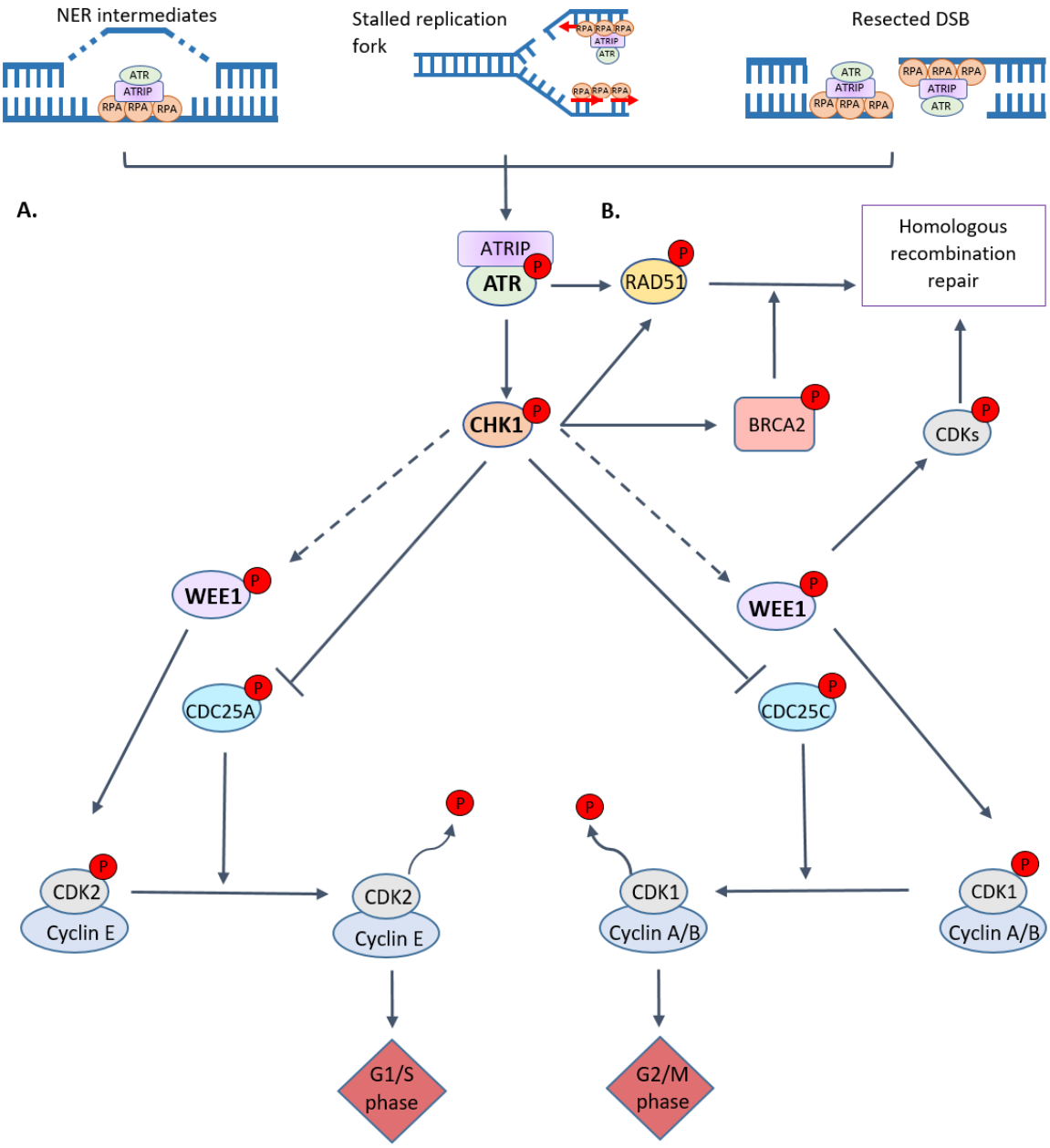


Figure 1.10: Overview of ATR signalling in response to DNA damage. Resected double-strand breaks (DSBs), stalled replication forks and NER intermediates all lead to replication protein A (RPA) recruiting ATR via ATR-interacting protein (ATRIP). **A.** The ATR-CHK1 cascade is heavily involved in cell cycle checkpoint control. ATR activates CHK1 which causes the inactivating phosphorylation of both CDC25C and CDC25A, hence preventing the removal of inhibitory phosphorylation on CDK1 and 2, respectively. These lesions also activate WEE1, directly or via CHK1 (dashed grey arrows) to phosphorylate and inactivate CDK1 and 2. Progression through cell cycle G1/S and G2/M phases is reliant upon activation of CDK2/cyclin E and CDK1/cyclin A/B complexes, respectively. When WEE1, CHK1 or ATR are inhibited, CDK1 and CDK2 are activated so S-phase progression and mitotic entry occur with no delay to allow DNA repair. **B**. ATR, CHK1 and WEE1 also signal to key proteins involved in homologous recombination repair (HRR). ATR promotes repair protein RAD51 recruitment to DSBs and stalled replication forks, independent of BRCA. CHK1 phosphorylates key HRR proteins BRCA2 and RAD51. When activated WEE1 inhibitory phosphorylates CDKs, which play a key role in HRR end resection. Image from Smith *et al.*, 2020, Appendix A.

1.8 Targeting the DNA damage response

Synthetic lethality is a concept that a mutation in one of two genes does not impact cell survival, however mutations in both of these genes results in cell death (Figure 1.11) (Shaheen *et al.,* 2011). In 2005 two studies reported the profound cytotoxicity of PARPis in cells lacking functional *BRCA,* which led to the concept of synthetic lethality, previously described (Bryant *et al.,* 2005, Farmer *et al.,* 2005). Success of PARPi in *BRCA*-mutant ovarian cancers was the first clinical example of using synthetic lethality to target tumour suppressor gene loss (Lord and Ashworth, 2017). As previously described (section 3.1), endogenously generated SSBs rely on PARP-dependent repair mechanisms for resolve. However, when PARP is inhibited these SSBs are unrepaired and when they collide with the replication fork this results in stalled forks and fork collapse, resulting in DSBs which rely on repair by HRR during S and early G2 phase (Figure 1.12). This synthetic lethal relationship is exploitable and can be targeted for therapeutic gain (Setton *et al.,* 2021).

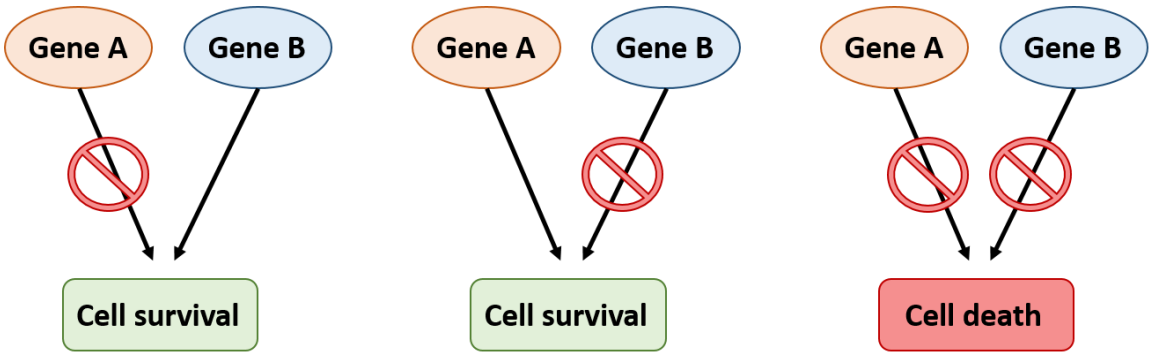


Figure 1.11: The concept of synthetic lethality. Cell survival still occurs when gene 'A' or gene 'B' are mutated or lost. However, mutation/loss of both of these genes simultaneously results in cancer cell death. Image adapted from Jariyal *et al.,* 2020.

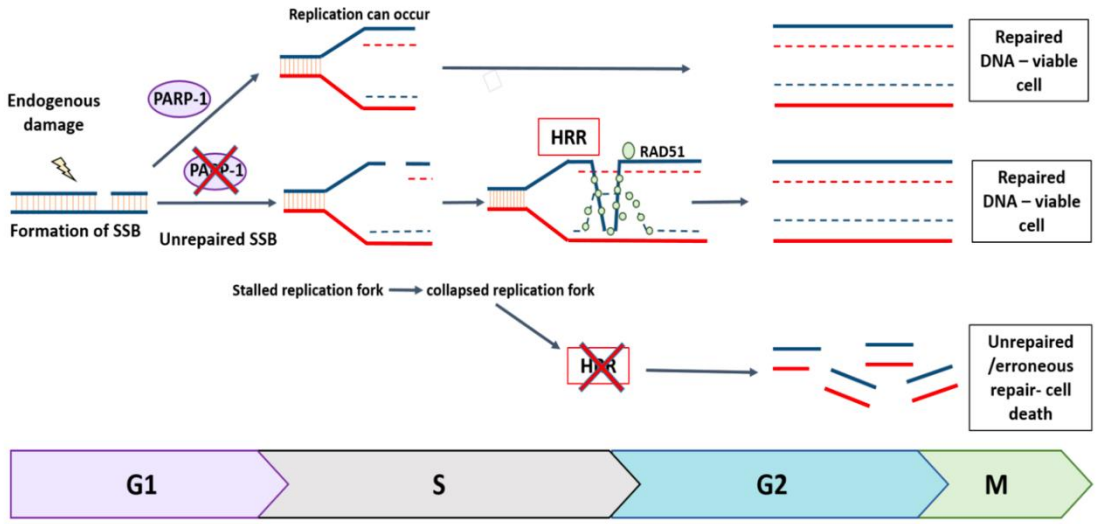


Figure 1.12: Synthetically lethal relationship between PARP and HRR defective cells. Endogenously generated SSB are repaired continuously by PARP dependent repair mechanisms. When PARP is inhibited unrepaired SSB collide with replication forks causing them to stall and collapse resulting in DSBs which can only be repaired by HRR during S and early G2 phase. If HRR is defective, e.g. due to *BRCA* mutation the DNA cannot be repaired accurately, resulting in cell death.

1.9 PARP and PARP inhibitors

1.9.1 PARP structure and function

Poly (ADP-ribose) polymerase 1 (PARP1) is known for its pivotal role in BER/SSBR. PARP recognises SSBs via it's DNA-binding domain and binds to it by its N-terminal zinc fingers, which autoPARylates PARP and causes a conformational change, activating PARP1 to cleave NAD+ into nicotinamide and ADP-ribose moieties (Eustermann *et al.,* 2011) (Bajrami *et al.,* 2012). These moieties covalently attach to PARP, followed by the addition of other ADP-ribose moieties, resulting in the formation of subsequent PAR chains. These polymers have a strong negative charge, which acts as a signal for recruiting essential DNA repair enzymes such as DNA ligase III (Lig III) and DNA polymerase β (Pol β) as well as scaffolding protein, X-ray cross-complementing gene 1 (XRCC1) (Figure 1.13). Following repair, PAR polymers are predominantly degraded by Poly (ADP-ribose) glycohydrolase (PARG) via cleaving of the 2', 1"-*O*-glycosidic ribose-ribose bond within the PAR chains to release ADP-ribose moieties (Wei and Yu, 2016) (Curtin and Szabo *et al.,* 2020).

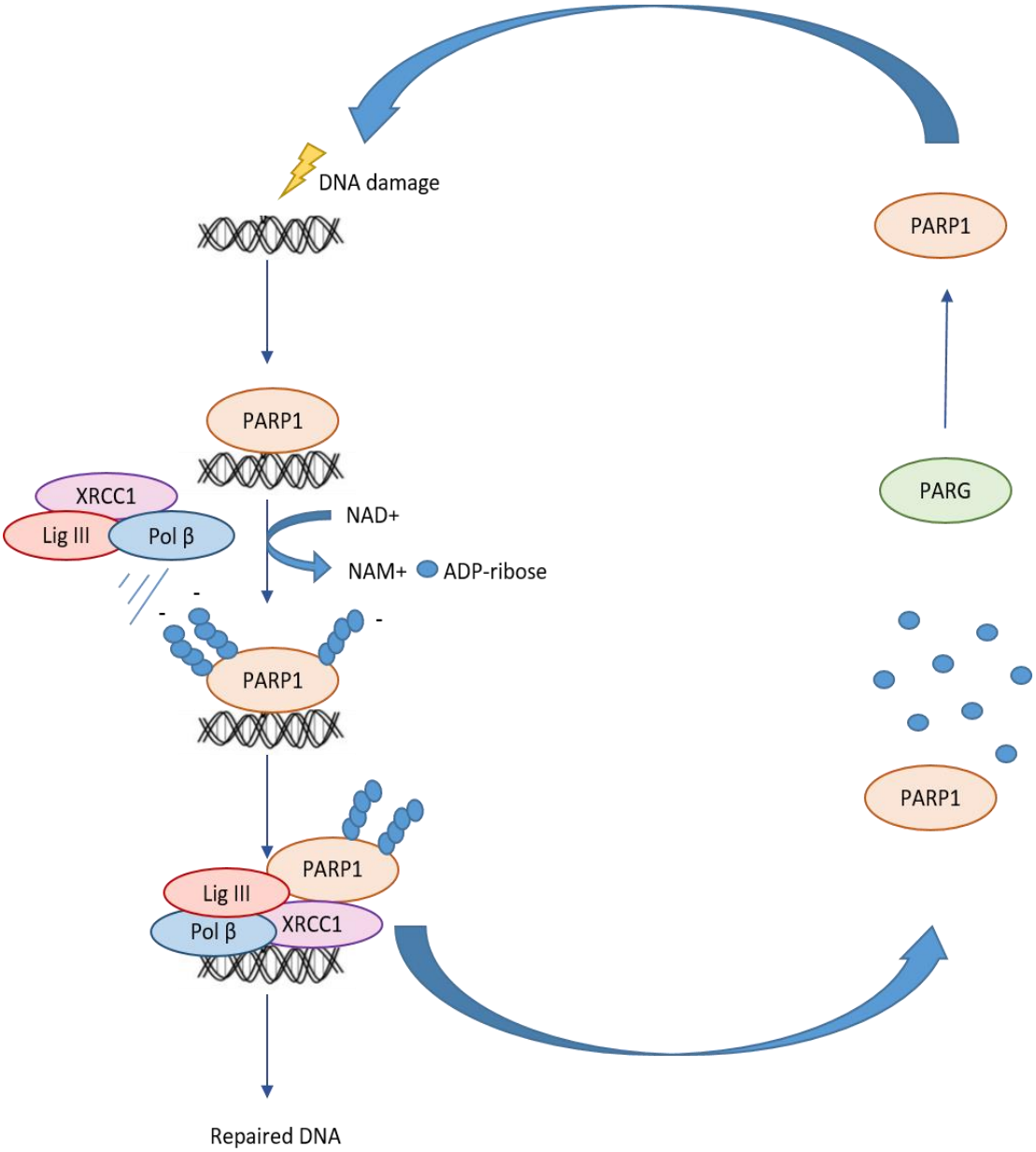


Figure 1.13: The role of PARP1 in the orchestration of DNA repair. DNA is damaged by endogenous/exogenous factors which lead to a SSB. PARP1 detects and binds to the nick in DNA before utilising the ADP-ribose moiety of NAD+ to recruit XRCC1, Lig III and Pol β as well as to form the poly (ADP-ribose) polymer. Polymer formation results in the alteration of acceptor proteins. The auto-modification of PARP leads to dissociation of the enzyme from the DNA. This is temporary as poly (ADP-ribose) is rapidly degraded and proteins are rapidly restored to original states by PARG (Baskar *et al.,* 2012). Image adapted from Singh *et al.,* 2013.

1.9.2 PARP inhibitors

PARP inhibitors (PARPi) usually contain a nicotinamide pharmacophore (Table 1.2) and act by binding to the NAD+ binding site in the catalytic domain of PARP and therefore block enzymatic activity (Alemasova and Lavrik, 2019). This PARP inhibition prevents autoPARylation and PARP1 release from the site of damage, interfering with the catalytic cycle of PARP (Figure 1.13). There are 2 known mechanisms of PARPi action. Inhibition of PARP results in inhibition of SSB repair, eventually resulting in DSBs that rely on HRR for resolve (section 1.6.4). This mechanism of action acts synthetically lethal with cancer cells defective in HRR, as previously described, although is not toxic in cells with competent HRR (reviewed in Murai and Pommier, 2019). The other mechanism of action results in PARP1 becoming "trapped" on the DNA, creating a PARP-DNA complex. This PARP-DNA complex can obstruct replication forks and cause damage to the cell, regardless of HRR function. Clinical PARPis have been shown to "trap" PARP1 to different degrees, with veliparib the least potent trapper and talazoparib the most (Murai *et al.,* 2012).

1.9.3 Clinical applications of PARP inhibitors

The first PARPi phase 1 trial was conducted combining rucaparib and temozolomide to determine the safety and efficacy of this combination with the aim of exploring the use of PARP inhibitor rucaparib (previously AG014699) as a chemo-potentiator (Plummer *et al.,* 2008). A follow-up phase 2 study in 2013 showed evidence of rucaparib acting as a chemo-potentiator in patients with metastatic melanoma (Plummer *et al.,* 2013). However, progression with this combination was halted due to toxicities. Other PARPi have been investigated clinically as chemo- or radio-sensitisers, however toxicity has been a limiting factor and none have progressed past phase 2.

Olaparib was the first PARPi approved by the FDA and EMA in 2014, as a monotherapy in advanced ovarian cancers with germline *BRCA* mutation (Kaufman *et al.,* 2015). This approval of use was extended to maintenance therapy in recurrent cancer with complete or partial response to platinum-based chemotherapy, regardless of *BRCA* mutational status (Friedlander *et al.,* 2018). Further to this, olaparib was also approved for use in breast cancers in 2018 with germline *BRCA1/2* mutations and HER2 negative metastatic cancers treated with chemotherapy or hormone receptor positive cancer treated with endocrine therapy (Moore *et al.,* 2018). More recently, olaparib was approved for use in metastatic pancreatic cancer and HRR defective metastatic castration-resistant prostate cancer (Golan *et al.,* 2019, de Bono *et al.,* 2020).

In 2016 accelerated approval for rucaparib was granted by the FDA for use in advanced ovarian cancers with germline or somatic *BRCA* mutation, following 2 rounds of chemotherapy (Oza *et al.,* 2017). The ARIEL2 study investigated LOH as a marker of HRR deficiency, alongside *BRCA* mutations, to assess whether this was a good predictor of sensitivity to rucaparib. Indeed, patients with *BRCA* mutant or *BRCA* wildtype with LOH had increased platinum sensitivity and sensitivity to rucaparib (NCT01891344) (Swisher *et al.,* 2017). In the follow up ARIEL 3 study, anticancer activity of rucaparib was assessed in a maintenance setting. Patients were grouped into cohorts: patients with deleterious germline or somatic *BRCA* mutations or patients with HRR defective cancers (*BRCA* mutant or *BRCA* wildtype and LOH). Adverse events of grade 3 or higher were reported in 56 % of patients in the rucaparib-treated group vs 15 % in the placebo

group, with anaemia and decreased haemoglobin levels being most common. Overall, rucaparib significantly increased PFS in platinum-sensitive ovarian cancer patients who had received a response to platinum-based chemotherapy (NCT01968213) (Coleman *et al.,* 2017). Following this, in 2018, rucaparib was approved for use in maintenance therapy for recurring ovarian, peritoneal and fallopian cancers, regardless of *BRCA* mutation (Coleman *et al.,* 2017). More recently, following a phase 2 trial (TRITON2, NCT02952534), rucaparib was approved for use in *BRCA* mutated metastatic castration-resistance prostate cancer (Abida *et al.,* 2019).

In 2017 niraparib was approved for use as maintenance therapy in recurrent ovarian, peritoneal and fallopian cancers, regardless of *BRCA* mutation, in cancers that showed a complete or partial response to chemotherapy (Mirza *et al.,* 2016). Further clinical evaluation expanded the eligibility to HRD, platinum-sensitive ovarian cancer, regardless of *BRCA* mutation (Moore *et al.,* 2018). Recently, a phase 3 trial showed niraparib significantly increased PFS in patients with advanced ovarian cancer, independent of HRR status (NCT02655016) (Gonzalez-Martin *et al.,* 2019).

In 2018, talazoparib was approved for breast cancers with germline *BRCA1/2* mutations and HER2 negative metastatic cancer patients, following a phase 3 trial in which talazoparib significantly increased PFS in these patients, compared to chemotherapies (capecitabine, eribulin, gemcitabine or vinorelbine) (NCT01945775) (Ettl *et al.,* 2018)

Veliparib is currently being investigated in clinical trials, although is not yet approved as a treatment. Similarly, pamiparib has shown good anti-tumour activity pre-clinically and is in clinical trials (Table 1.2).

1.9.4 PARP inhibitor resistance

Despite the clear clinical benefit of PARPis, resistance can still occur due to a number of mechanisms. Due to the synthetic lethal relationship between PARPi and tumours with defective HRR, it is unsurprising that restoration of HRR is a primary mechanism of PARPi resistance (reviewed in Li *et al.,* 2020). The most common way HRR is restored is by reverse mutations, resulting in reactivation of *BRCA1/BRCA2*, which was established in 2008 by 2 groups. Edwards *et al.,* derived a PARPi resistant clone by deleting a *BRCA2* mutation from a *BRCA2* deficient cell line and Sakai *et al.,* showed secondary mutations restored wildtype *BRCA2* rendering cells resistant to PARPi and platinum (Edwards *et al.,* 2008, Sakai *et al.,* 2008). Other mechanisms of HRR restoration include restoration of RAD51 paralogs, transcriptional upregulation of genes key to HRR and reacquisition of DNA end resection by loss of 53BP1 or MRE11 (Biegala *et al.,* 2021).

Another key mechanism to PARPi resistance is increased PARPi efflux. P-glycoproteins (P-gp) is an ATP-binding cassette (ABC) transporter, which are often upregulated in cancer cells (Biegala *et al.,* 2021). Previous studies have shown that an overexpression of P-gp is a mechanism of resistance to PARPis (Edwards *et al.,* 2008, Oplustilova *et al.,* 2012). *In vivo* studies have shown PARPi were more effective when P-gp was knocked out in *BRCA1* deficient cells (Jaspers *et al.,* 2013).

The re-stabilisation of replication forks is another mechanism of PARPi resistance. HRR defective cells can evolve to use alternative mechanisms to inhibit fork degradation and to stabilise replication forks. As previously described PARPi induce degradation of replication forks, therefore stabilising these forks, results in PARPi resistance (Kim *et al.,* 2020).

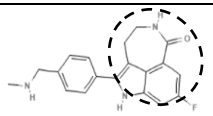
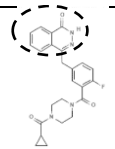
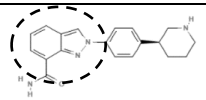
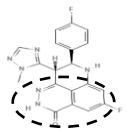
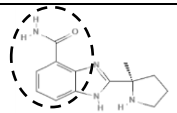
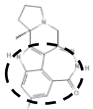
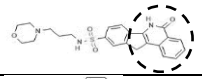
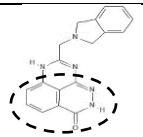
Inhibitor	Chemical structure	Current stage of development
Rucaparib		Approved for treatment in ovarian cancer with germline *BRCA1/2* mutations following 2 rounds of chemotherapy. Approved for maintenance therapy in recurrent ovarian cancer with complete or partial response to platinum-based chemotherapy, regardless of *BRCA* mutation. Approved for use in metastatic castration-resistant prostate cancer, with *BRCA* mutation.
Olaparib		Approved for use as treatment in ovarian cancer with germline *BRCA1/2* mutation, following 3 rounds of chemotherapy. Approved for maintenance therapy in recurrent ovarian cancer with germline/somatic *BRCA* mutations (first line), as well as recurrent cancer without *BRCA* mutation. Approved for treatment in *BRCA* mutated, HER2 negative metastatic breast cancer treated with chemotherapy. Approved as maintenance therapy in germline *BRCA1/2* mutated pancreatic cancer.
Niraparib		Approved for use in HRD ovarian cancers, either by *BRCA* mutation or genomic instability, in patients following 3 rounds of chemotherapy. Approved for maintenance therapy in recurrent ovarian cancer with complete or partial response to platinum-based chemotherapy, regardless of *BRCA* mutation.
Talazoparib		Approved for treatment in *BRCA* mutated, HER2 negative metastatic breast cancer treated with chemotherapy. Phase 2 TALAPRO-1 trial showed good antitumour activity in prostate cancer as a monotherapy. Currently in follow up phase 3 TALAPRO-2 trial in metastatic castrate-resistant prostate cancer (NCT03395197).
Veliparib		Phase I trial with carboplatin and gemcitabine (NCT01063816), as well as phase I trial as monotherapy in solid tumours (NCT01199224). In phase 3 development for use in treatment of HGSOC and *BRCA*-mutated breast cancer in combination with carboplatin and paclitaxel (NCT02163694) (Stodtmann *et al.,* 2021).
Pamiparib		Antitumour activity shown in HGSCO patients in phase I/II trial (NCT03333915). Early phase I trial recruiting to test pamiparib in glioblastoma patients (NCT04614909). Planned trials with tislelizumab or temozolamide, although not yet recruiting (NCT04985721 and NCT04796454). Phase Ib/II trial investigating use with temozolamide and/or IR in glioblastoma (NCT03150862).
INO-1001		Underwent phase I trial with temozolamide in melanoma patients, although study was terminated (NCT00272415).
E7449/2x-121		Phase I trial examining safety and MTD showed supportive data for further clinical trial evaluation (NCT01618136) (Plummer *et al.,* 2018).

Table 1.2: PARPis current state of development. Dashed circle highlights the nicotinamide pharmacophore in each PARPi structure.

1.9.5 Biomarkers for PARPi sensitivity

Over the past decade, several biomarkers for PARPi sensitivity have been identified. Given the well-established synthetic lethal relationship between HRR deficiency and increased anti-tumour activity observed with PARPis, it is not surprising that HRR status of cells has been a focus of biomarkers to select patients for PARPi treatment. An HRR functional assay was developed by Mukhopadhyay *et al.* in 2010, by the assessment of RAD51 foci formation in primary cultures derived from ascitic fluid from patients with EOCs (Mukhopadhyay *et al.,* 2010). However, with the understanding of limitations with obtaining fresh primary samples, RAD51 was further tested as a biomarker in FFPE samples and RAD51 scoring was found to be an effective predictor of sensitivity to PARPi (Castroviejo-bermejo *et al.,* 2018, Hill *et al*., 2018).

Genomic mutational signature 3 has been associated with HRR deficiency, although this required whole genome/exome sequencing and therefore use in clinic was somewhat limited (Alexandrov *et al.,* 2013). The FDA approved FoundationFocusCDx $_{BRCA}$ test is a next-generation sequencing-based diagnostic tool, which was used to identify patients with advanced ovarian cancer suitable for rucaparib treatment by LOH (Balasubramaniam *et al.,* 2017). Similarly, Myriad genetics developed the Myriad myChoice® test, an FDA approved HRD assay, determining HRR status by NGS of tumour tissues to detect deleterious mutations in *BRCA1* and *BRCA2* and HRR status through genomic scarring (Hodgson *et al.,* 2018). Both of these tests were validated in ovarian cancer patients in phase 3 trials, with the FoundationFocusCDx $_{BRCA}$ test detecting sensitivity to rucaparib and Myriad genetics identifying patients sensitive to niraparib (Mirza *et al.,* 2020, Swisher *et al.,* 2017).

1.10 ATR/CHK1/WEE1 in cancer

1.10.1 ATR/CHK1/WEE1 dysfunction in cancer

The importance of the ATR-CHK1-WEE1 cascade is highlighted by the embryonic lethality of all three components (de Klein *et al.,* 2000, Liu *et al.,* 2000, Tominaga *et al.,* 2006). No humans are recorded as being born without these essential kinases but Seckel syndrome

(SS) is a rare, autosomal recessive disorder owing to a hypomorphic mutation in ATR, resulting in delayed development but not cancer predisposition. SS mice are not cancer-prone, even when crossed with p53 defective mice (Murga *et al.,* 2009).

The general consensus seems to be that complete loss of ATR, CHK1 or WEE1 signalling is incompatible with normal development but that compromising the pathway by hypomorphic mutation or heterozygous deletion does not predispose to tumour development. However, upregulation of the pathway in tumours may be indicators of poor prognosis.

As previously described cancer cells have higher levels of RS due to a number of factors, including loss of G1 checkpoint control, often caused by p53 mutation. Targeting the ATR-CHK1 axis in cancer cells that have a loss of G1 control will then also inhibit S/G2 checkpoint control and selectively kill cancer cells, whilst normal cells with intact G1 checkpoint control remain uncompromised. This gives strong rationale for the use of ATR, CHK1 and WEE1 inhibitors, particularly in these cancers.

1.10.2 ATR, CHK1 and WEE1 inhibitors

Since loss of G1 checkpoint control is common in the majority cancers, cancer cells are dependent on S/G2/M checkpoints. Pivotal components of these checkpoints are ATR, CHK1 and WEE1, thus there is a rationale to use inhibitors of this pathway to sensitise cells to chemotherapy and radiotherapy. When loss of p53 is combined with inhibition of ATR it results in loss of both G1 and G2 checkpoints and thus cells become vulnerable and sensitised to DNA damaging agents- such as chemotherapy and radiotherapy treatments (Yeo *et al.,* 2016). The ATR inhibitor VE-821 has shown sensitisation to cisplatin, particularly when p53 was knocked down. ATR inhibitor VE-822, analogue of VE-821, showed cells were sensitised to cisplatin- a standard treatment in ovarian cancer. The ATR inhibitor AZD6738 was shown to increase the activity of carboplatin- a commonly used cervical cancer treatment, *in vivo* (Weber and Ryan, 2015).

As previously described cancer cells have higher levels of RS due to a number of factors, including loss of G1 checkpoint control, often caused by p53 mutation. Targeting the

ATR-CHK1 axis in cancer cells that have a loss of G1 control will then also inhibit S/G2 checkpoint control and selectively kill cancer cells, whilst normal cells with intact G1 checkpoint control remain uncompromised. This gives strong rationale for the use of ATR, CHK1 and WEE1 inhibitors, particularly in these cancers.

1.10.3 Preclinical development of ATR/CHK1/WEE1 inhibitors

1.10.3.1 Preclinical development of ATR inhibitors

Early studies in ATRi development showed that kinase-dead ATR conferred sensitivity to multiple DNA damaging agents (UV, hydroxyurea (HU), irradiation (IR), cisplatin) and that endogenous RS by cyclin E overexpression or p53 inactivation conferred sensitivity to kinase-dead ATR overexpression (Sarkaria *et al.,* 1999, Nghiem *et al.,* 2002). Peasland *et al.,* showed ATRi NU6027 enhanced both cisplatin and HU cytotoxicity and, in the first investigation of its kind, showed that ATRi inhibited HRR and sensitised cells to PARPi (Peasland *et al.,* 2011). As more ATRis were developed a consistent finding across the various inhibitors were that ATRi had chemo and radio-sensitising effects (reviewed in Smith *et al.,* 2020, Appendix A). Another consistent finding across ATRi was that ATM deficiency conferred sensitivity to these inhibitors (Min *et al.,* 2017, Middleton *et al.,* 2015, Shi *et al.,* 2018, Schmitt *et al.,* 2017).

VE-821 was one of the first potent ATRi with greatly improved selectivity for ATR over other PI3K-like kinases discovered in 2011 (ATM, DNAPKcs, mTOR). VE-821, as a single agent, increased apoptosis in cancer cells versus non-cancerous cells (Reaper *et al.,* 2011). VE-821 can sensitise cells to IR (Alsubhi et al., 2016, Fujisawa et al., 2015, Salovska et al., 2018), gemcitabine and camptothecin (Reaper *et al.,* 2011, Josse et al., 2014). However, the strongest synergy observed thus far is with platinum-based therapies cisplatin and carboplatin (Reaper et al., 2011, Huntoon et al., 2013). Interestingly, when used in combination with the PARPi veliparib, VE-821 further sensitised *BRCA* defective cells beyond the sensitivity already observed owing to HRR status (Huntoon et al., 2013). In 2015 Middleton *et al*., showed that defects in ATM, HRR (BRCA2, XRCC3) and BER (XRCC1) resulted in increased sensitivity to VE-821.

Interestingly, defective Ku80 (involved in NHEJ) caused hypersensitivity to VE-821, but the loss of its binding subunit, DNA-PKcs, did not (Middleton *et al.,* 2015).

1.10.3.2 Preclinical development of CHK1 inhibitors

Similarly, to observations with ATRi, many studies have found CHK1 inhibitors to have chemo- and radiosensitising effects (reviewed in Smith *et al.,* 2020, Appendix A). CHK1is have also been found to have synergistic anti-tumour effects with PARPis *in vitro* and *in vivo*.

PF-477736 is a potent ATP-competitive CHK1 inhibitor with >100-fold selectivity over CHK2 developed in 2008 (Blasina *et al.,* 2008). It has potent single-agent activity in triple-negative breast and ovarian cancer cell lines (Bryant *et al.,* 2014), as well as sensitising cells to chemotherapeutic drugs gemcitabine, carboplatin, doxorubicin, mitomycin C and topotecan (Blasina *et al.,* 2008, Kim *et al.,* 2015, Fang *et al.,* 2013). PF-477736 also sensitises HPV positive head and neck cancer cells to radiation (Busch *et al.,* 2013). PF-477736 caused synergistic cytotoxicity in combination with targeted therapies irutinib and bosutinib in mantle cell lymphoma (MCL) and chronic myeloid leukaemia (CML), respectively (Restelli *et al.,* 2015, Nguyen *et al.,* 2015). PF-477736 was more cytotoxic in p53 mutant and Myc-driven cancers (Blasina et al., 2008, Ferrao et al., 2011).

1.10.3.3 Preclinical development of WEE1 inhibitors

Very few small-molecule inhibitors of WEE1 have been developed, in comparison to the plethora of ATRi and CHK1i.

In 2009 AZD1775/MK-1775 was discovered as a specific, potent WEE1 inhibitor that showed excellent selectivity (Hirai et al., 2009). It was effective as a single agent (Kreahling et al., 2012), as well as in synergistically increasing the cytotoxicity of various DNA damaging agents (IR, gemcitabine, carboplatin, cisplatin, 5-FU, pemetrexed, doxorubicin and camptothecin), *in vitro* and *in vivo (*Hirai *et al.,* 2009*,* Hirai *et al.,* 2010, Rajeshkumar *et al.,* 2011, Bridges *et al.,* 2011). Earlier studies reported p53 status as a determinant for sensitivity to AZD1775 (Hirai *et al.,* 2009*,* Rajeshkumar *et al.,* 2011). However, more recent studies have shown MK-1775 cytotoxicity to be independent of

p53 (Kreahling *et al.,* 2012, Heijink *et al.,* 2015). Heijink *et al*. carried out a genome-wide unbiased screen and concluded that the activity of DNA replication proteins, beyond p53, is a key determinant of WEE1 inhibitor sensitivity (Heijink *et al.,* 2015).

1.10.4 Clinical development of ATR/CHK1/WEE1 inhibitors

1.10.4.1 ATR inhibitors in clinical trials

M6620 (VE-822/VX-970) was the first ATR inhibitor to reach clinical trials. Thomas *et al*., first reported ATR inhibition in combination with chemotherapy in patients, with the maximum dose of topotecan being well tolerated when used in combination with M6620 (Thomas *et al.,* 2018). There are currently three active clinical trials using M6620, one of which is the first in a human study looking at the pharmacokinetics of M6620 in combination with gemcitabine, cisplatin, etoposide carboplatin and irinotecan (NCT02157792). A number of phase 1 and 2 studies are currently recruiting patients for the use of M6620 single agent and in combination with a number of DNA damaging agents including irradiation, cisplatin, carboplatin, gemcitabine, irinotecan and topotecan.

Another selective, bioavailable ATR inhibitor currently in phase 1 and 2 trials is AZD6738. Of these trials, nine are investigating the use of AZD6738 with the PARP inhibitor olaparib, which has strong support from pre-clinical data (Kim *et al.,* 2017). The ATR inhibitor BAY1895344 is in a first in human phase I safety trial in patients with advanced solid tumours and lymphomas (NCT03188965).

M4344/VX-803 is an orally bioavailable ATR inhibitor currently recruiting in phase 1 clinical trial where it will be used as a monotherapy and in combination with cisplatin, carboplatin or gemcitabine (NCT02278250). The ATR inhibitor BAY1895344 has recently been shown to have anti-tumour activity and is well tolerated at active doses in cancers with defects in DDR, such as loss of ATM (NCT03188965) (Bono *et al.,* 2019) (reviewed in Smith *et al.,* 2020, Appendix A).

1.10.4.2 CHK1 inhibitors in clinical trials

Although there is significant interest surrounding CHK1 inhibitors, clinical progression has often been hindered because of the lack of bio-availability and off-target effects (Patel *et al.,* 2017). SRA737 is currently in phase 1/2 clinical trials, both as a monotherapy and in combination with gemcitabine +/− cisplatin (NCT02797964) (NCT02797977). MK-8776 is also in phase 1 and 2 trials as a monotherapy and in combination with gemcitabine, cytarabine and hydroxyurea (NCT00779584) (NCT01870596). Phase 1 clinical trials, in patients with advanced solid tumours, of PF-477736 in combination with gemcitabine were terminated early for business reasons, rather than safety concerns (NCT00437203). Prexasertib (LY2606368) is currently in phase 2 trials a monotherapy agent, specifically in patients with cancers that are p53 mutant, have DDR defects such as *BRCA* mutation, increased replication stress or CCNE1 amplification, as these are determinants of CHK1 inhibitor sensitivity (NCT02735980, NCT02203513, NCT03414047, NCT02873975). Prexasertib has also entered phase 1 and 2 clinical trials in combination with pemetrexed (NCT01296568, NCT00415636, NCT01139775, NCT00988858), gemcitabine (NCT01358968, NCT01341457, NCT01296568, NCT00839332) or cisplatin (NCT02555644, NCT01139775) but has currently only been in one clinical trial with a PARP inhibitor (NCT03057145), despite promising synergy being observed pre-clinically (Brill *et al.,* 2017, Yin *et al.,* 2017) (reviewed in Smith *et al.,* 2020, Appendix A).

1.10.4.3 WEE1 inhibitors in clinical trials

AZD17775 is the only WEE1 inhibitor to reach clinical development and is already in a number of phase 1 and 2 trials being used in combination with treatments such as carboplatin, gemcitabine, cisplatin, cytarabine and olaparib (Leijen *et al.,* 2016, Oza *et al.,* 2015). AZD1775 was also shown to inhibit polo-like kinase 1 (PLK1), leading to questioning into its mechanism of action. However, Serpico *et al.,* 2019 showed that at therapeutic concentrations AZD1775 inhibited WEE1 and not PLK1 (Serpico *et al.,* 2019). The majority of clinical trials are still recruiting, suggesting this kinase inhibitor has exciting potential once trials have been completed and data is collected and analysed (reviewed in Smith *et al.,* 2020, Appendix A).

1.10.5 ATR, CHK1 and WEE1 inhibitor synergy with PARPi

Inhibitors of the ATR-CHK1-WEE1 cascade have shown synergy with PARP inhibitors. Peasland *et al.,* were the first to show that the ATR inhibitor, NU6027, was synthetically lethal in combination with the PARP inhibitor, rucaparib in breast and ovarian cancer cells (Peasland *et al.,* 2011). However, this compound was also identified as a CDK2 inhibitor, therefore there may be further activity that would impact cell cycle (Cortese *et al.,* 2016). Subsequently, the ATR inhibitor VE-821 was found to sensitise *BRCA* mutant cells to veliparib (Middleton *et al.,* 2015) and a synthetically lethal screen found VE-821 had profound synergy with PARP inhibition in both HRR competent and defective cells (Mohni *et al.,* 2015). Kim *et al.,* showed that inhibiting PARP resulted in increased reliance on the ATR-CHK1 pathway for genomic stability and that the combination of olaparib with ATRi AZD6738 effectively reduced tumour burden in patient-derived xenografts of serous ovarian cancer (Kim *et al.,* 2017).

A series of PARP inhibitors (rucaparib, olaparib, veliparib and NU1025) synergised with various CHK1 inhibitors (UCN-01, AZD7762 and LY2603618) to increase DNA damage and apoptosis in vitro in breast cancer cells (Booth *et al.,* 2013). The PARPi olaparib in combination with CHK1 inhibitor MK-8776, supressed colony formation in *BRCA* mutant models to a greater degree than either inhibitor as a single agent (Kim *et al.,* 2017). The PARP inhibitor talazoparib was also synergistic with LY2606368, both *in vitro* and *in vivo* in gastric cancer (Yin *et al.,* 2017). Similarly, LY2606368 also showed inhibited HRR function and synergised with olaparib to decrease cell survival in *BRCA* wild-type cells (Brill *et al.,* 2017).

Fewer studies have looked at PARP and WEE1 inhibition combined, perhaps owing to the availability of only one WEE1 inhibitor with the desired selectivity and specificity (AZD1775). AZD1775 has only been tested in combination with olaparib but these results have been promising and when used in combination, the inhibitors act synergistically to radiosensitise pancreatic, and KRAS-mutant NSCLC cells further than when either is used as a single agent (Karnak *et al.,* 2014, Parsels *et al.,* 2018).

1.11 Aims and Objectives

Currently PARPis are only approved for treatment use in *BRCA* mutant, HRR defective tumours, with a proportion of these tumours becoming resistant to PARPis. There is therefore a need to explore mechanisms of resensitising these resistant tumours as well as sensitising *BRCA* competent, HRR competent cells to PARPis, which are intrinsically resistant to PARPi. ATR, CHK1 and WEE1 have key roles in both cell cycle control and signalling to HRR in response to RS and there is *in vitro* and *in vivo* evidence to support the notion of synergy occurring between inhibitors of ATR, CHK1 and WEE1 and PARPi.

The over-arching aim of the investigations presented here was to probe the mechanisms of synergy between PARPi rucaparib and inhibitors of ATR (VE-821), CHK1 (PF-477736) and WEE1 (MK-1775).

Other aims to be addressed include:

- To measure previously reported determinants of sensitivity to PARPi, ATRi, CHK1i and WEE1i (eg. basal RS, DDR genes mutational status, mRNA and protein expression of key DDR genes) and assess correlations with cytotoxicity to the inhibitors
- To assess the induction of RS by rucaparib and the extent to which this RS signals to the ATR-CHK1 axis
- To investigate the impact rucaparib as a single agent and in combination with ATR/CHK1/WEE1 inhibitors has on cell cycle control and HRR function
- To determine the involvement of SSBR inhibition vs PARP trapping on synergy
- To investigate how cell line data translates into a panel of primary cultures consisting of HGSOC, HGSOC/LGSOC and endometrioid G2 subtypes

Chapter 2. Materials and methods

2.1 Chemicals and reagents

The PARP inhibitor, rucaparib, was kindly gifted from Pfizer Global R&D. The other PARPis olaparib, niraparib, talazoparib and pamiparib were purchased from Selleckchem, Houston, TX, USA. ATRi VE-821, CHK1i PF-477736 and WEE1i MK-1775 similarly were each purchased from Selleckchem, Houston, TX, USA, prior to dilution to stock concentrations of 20 mM, 10 mM or 5 mM in dry DMSO, to avoid degradation. Stocks were all stored as aliquots at – 80 °C. Routine chemicals were of the highest purity from Sigma-Aldrich (Burlington, MA, United States) unless otherwise stated.

2.2 Cell culture of cell lines and patient ascites samples

All human cell lines were obtained from American Type Culture Collection (ATCC; Manassas, VA, United States). All cells were used within 30 passages of purchase or subsequent authentication by: STR profiling (PowerPlex Fusion System, Promega), the American type culture collection (ATCC, Manassus, VE, USA) or the European collection of authenticated cell cucltures (ECACC, Salisbury, UK). C33A and SiHa cells were grown in Dulbecco's Modified Eagle Medium (DMEM; Merck, Kenilworth, NJ, United States). IGROV-1 cells were cultured in Roswell Park Memorial Institute (RPMI)-1640 medium (Merck, Kenilworth, NJ, United States). Paired *BRCA1* mutant UWB1.289 and corrected UWB1.289+ *BRCA1* cells by transfection with pcDNA3 plasmid containing wild-type *BRCA1* (DelloRusso *et al.,* 2007) were both grown in 50% RPMI-1640 (Merck, Kenilworth, NJ, United States) and 50% Mammary Epithelial Growth Medium (MEGM; Lonza, Basel, Switzerland), with the addition of bovine pituitary extract (BPE), human epidermal growth factor (hEGF), insulin, hydrocortisone and GA-1000 (Lonza, Basel, Switzerland). Corrected UWB1.289+ B1 cells had the addition of 200 µg/ ml G418 S (Merck, Kenilworth, NJ, United States). Chinese hamster lung fibroblasts with mutant *BRCA2* V-C8 and their *BRCA2* corrected sub-line V-C8.B2 cells were obtained from Thomas Helleday (Kraakman-van der Zwet *et al.,* 2002) cultured in DMEM media, with 200 µg/ml G418 S (Merck, Kenilworth, NJ, United States) being added to the culture media of the *BRCA2* corrected cells to retain the transfected DNA. AA8 are parental Chinese hamster

ovary cells (CHO) and EM9 cells are their XRCC1 mutant derivative (Thompson *et al.,* 1980). Both AA8 and EM9 cells were cultured in RPMI 1640. All cell lines were supplemented with 10% foetal bovine serum (FBS; Gibco, Life Technologies, CA, United States). Cells were kept in exponential phase by passaging cells when they reached 70% confluence. Cells were incubated at 37°C, 5% CO_2 and 95% humidity. Cell lines underwent regular testing for mycoplasma every 2 months (MycoAlert, Lonza, Basel, Switzerland). Prior to being passaged cells were washed once with sterile phosphate buffered saline (PBS) before being incubated with 1.5 ml 1x trypsin-EDTA for 5-15 minutes. Cells were observed under a microscope to ensure detachment from the flask and re-suspended in pre-warmed cell line specific media.

Patient ascites were collected from patients undergoing surgery or palliative drainage of ascites at the Queen Elizabeth Hospital, Gateshead, UK. Ethical approval and written consent was attained from North East Newcastle and North Tyneside 1 Research Ethics Committee for the collection of both clinical material and patient data. All samples were logged in achiever in the Newcastle Biobank collection COL0200. Ascites were collected into a sterile container, which was transported to the lab and processed within 24 h, in compliance with UN3373 regulations for category B biological materials. Patient were anonymised and samples were linked to a unique PA (primary ascites) reference number (referred to in Chapter 7). Samples were handled in accordance with the Human Tissue Act (2004) standards.

Ascites samples were initially processed by mixing ascites fluid 1:1 with RPMI-1640 medium, containing 20 % FBS, 1% penicillin/ streptomycin and transferred to culture flasks. Cultures were incubated at 37°C, 5% CO_2 and 95% humidity, with medium replaced every 3-5 days, until cells had adhered and reached 70- 80 % confluence. Cells were passaged for use in HRR and growth inhibition assays, all of which were conducted within 5 passages.

2.3 Assessment of mutational status of DDR genes in the cell lines

The mutational status of cell lines was noted from the CCLE database, to assess identified determinants of sensitivity to PARP, ATR, CHK1 and WEE1 inhibitors in the literature (Table 2.1), to investigate if these mutations conferred sensitivity to inhibitors (Chapters 4 and 5). Mutational data for each of the human cell lines was collated from the Cancer Cell Line Encyclopedia (CCLE) database. Genes were selected for analysis based on previously identified determinants of sensitivity to PARPi and ATR/CHK1/WEE1 inhibition. Variant allele frequency was calculated using whole genome sequencing and, from these values, mutations were determined homozygous or heterozygous using an allele frequency cut-off value of 0.8.

Inhibitor	Identified determinant of sensitivity
PARP	• HRR genes: *BRCA1*, *BRCA2, RAD51* (Hodgson *et al.,* 2018, Gomez *et al.,* 2020, Pillé *et al.,* 2019) • ATR (Garbarino *et al.,* 2021) • ATM (Bebb *et al.,* 2019) • XRCC1 (Lord *et al.,* 2008) • DNA helicases: *FANCM* and *DDX11* (Stoepker *et al.,* 2015) • CDK12 (Bajrami *et al.,* 2014, Michelena *et al.,* 2018)
ATR	• ATM (Choi *et al.,* 2016, Kwok *et al.,* 2016, Perkhofer *et al.,* 2017, Min *et al.,* 2017, Rafiei *et al.,* 2020, Middelton *et al.,* 2015) • HRR genes: *BRCA2, XRCC3, RAD51* (Krajewska *et al.,* 2015, Middleton *et al.,* 2015) • ATR (Mohni *et al.,* 2014) • CHK1 (Mohni *et al.,* 2014) • BER genes: *XRCC1* and *PARP-1* (Peasland *et al.,* 2011, Sultana *et al.,* 2013, Midleton *et al.,* 2015, Ali *et al.,* 2020) • Basal RS (Murga *et al.,* 2011) • *TP53* mutation (Toledo *et al.,* 2011) • Cyclin E overexpression (Toledo *et al.,* 2011) • Defective Ku80 (Middelton *et al.,* 2015)
CHK1	• Basal RS (Oo *et al.,* 2018) • HRR genes: *RAD51, BRCA1* (Massey *et al.,* 2016, Paculova *et al.,* 2017) • *TP53* mutation (Blasina *et al.,* 2008) • Cyclin E overexpression (Murga *et al.,* 2011)
WEE1	• Basal RS (Kok *et al.,* 2020) • BER genes: *XRCC1* and *PARP-1* (Ali *et al.,* 2020) • *CCNE1* amplification (Gorski *et al.,* 2020) • *PTEN* (Brunner *et al.,* 2020)

Table 2.1: Determinants of sensitivity to PARP, ATR, CHK1 and WEE1 inhibition. These determinants were considered when considering correlations between expression in cells and differential sensitivity of the cell line panel to the inhibitors.

2.4 Targeted RNA-sequencing

Targeted RNA sequencing was performed to assess the baseline mRNA expression of a panel of genes. This was performed by HTG diagnostics, using Illumina Next Generation Sequencing (NGS) in the human cell lines across the panel (C33A, SiHa, IGROV-1, UWB1.289 + B1 and UWB1.289 cells). The HTG EdgeSeq system uses qNPA chemistry and initially cDNA nuclease protection probes to bind to target RNA. Target-specific probes hybridized to target transcripts. Excess probes and unbound RNA are removed with S1 nuclease creating a pool of nuclease protection probes, representative of RNA transcripts from each sample. The remaining probes were amplified with primer and molecular barcodes. The remaining PCR product are purified, quantified and collated into a library. The library is collated and sequenced before quantitation and normalisation. The final step is NGS being performed and data analysed.
Cell lysates comprising of ~40,000 cells were collected in a specialised lysis buffer provided by HTG Molecular Diagnostics prior to shipping. The samples were processed against the HTG Edgeseq Onocology biomarker panel (OBP), encompassing 2, 567 genes, including 4 negative and 4 positive control genes and 15 housekeeper genes. Samples were pooled and sequenced by Illumina NextSeq and the HTG Edgeseq Parser aligned FASTQ files to a probe list. After the process of quality control, raw read outs were normalised using Log_2 (read out of counts per million).

2.5 Gel electrophoresis and Western blotting

Western blotting is a semi-quantitative technique that was used here to assess basal expression of key DDR proteins and the effect of kinase inhibitors on their phosphorylation targets to assess target inhibition. Western blotting uses gel electrophoresis in the first instance to separate proteins based on their molecular weight. The result of the running gel is transferred to a nitrocellulose membrane, which is then incubated with antibodies specific to the protein(s) of interest. As the unbound antibody is washed away the bound antibodies are detected by chemiluminescence, resulting in visible bands. The density of bands directly corresponds to protein present; thus, densitometry can be used to plot the density as a value with a loading control used to normalise samples and investigate target activation or inhibition.

2.5.1 Preparation of lysates

Cells were seeded at 2-5 x 10^5 in 10 cm^2 petri dishes and incubated until reaching 70-80% confluence. Cells were then exposed to media containing drug for 24 hr. The following day cells were lysed using RIPA buffer containing 1 % protease cocktail inhibitor (ThermoFisher, Rockford, USA) for baseline western blots (Chapter 3) or phosphosafe extraction reagent (Merck, Kenilworth, NJ, United States) with protease cocktail inhibitor (Thermo Fisher Scientific, Waltham, MA, United States) used at a 1:100 dilution, when assessing phosphorylation target inhibition (Chapter 4). Lysis buffer was kept on ice until use. Media was aspirated from each dish and gently washed twice with PBS on ice, ensuring adherent cells were not dislodged. Lysis buffer was added 250 µl per dish, before being incubated at 4°C for 5-10 minutes. The lysed cells were rapidly scraped, on ice, before each lysate was collected into a pre-labelled eppendorf. Lysates were centrifuged at 8000 *g* for 10 minutes in a pre-cooled 4°C centrifuge. Lysates were divided into two Eppendorfs. The first was diluted 1:5 and stored in -20°C for protein quantification. The remaining volume of lysate was snap frozen and stored at -80°C.

2.5.2 Pierce assay

To ensure samples ran on western blot had the same protein levels a protein quantification assay was carried out. Protein concentrations of samples were measured using a BCA protein assay kit (Thermo Fisher Scientific, Waltham, MA, United States) as per manufacturer's protocol. Samples were loaded in quadruplicate in a 96-well plate and after an incubation period of 30 minutes at 37°C with a working solution, absorbance was read at 562 nm using the BMG FLUOstar Omega plate reader on a pre-set protocol.

2.5.3 Gel electrophoresis

Samples were diluted in deionised water to achieve a protein concentration of 0.5-1 mg/ml. XT sample buffer (Bio-Rad Laboratories, Hercules, CA, United States) and XT reducing agent (Bio-Rad Laboratories, Hercules, CA, United States) were added at constants of 25% and 0.5%, respectively. Samples were heated at 90°C for 5 minutes to

allow denaturation of protein. 3-8% Criterion XT tris-acetate gels (Bio-Rad Laboratories, Hercules, CA, United States) were used in each instance. After diluting 20x XT tricine with deionised water, HiMark pre-stained protein standard (Thermo Fisher Scientific, Waltham, MA, United States) and samples were loaded, and the gel was run at 150V for approximately 1 hr. Following this, the separated proteins on the gel were transferred onto nitrocellulose membrane (Amersham) at 100V for 1 hr.

In western blot experiments assessing basal DDR protein expression in cells (Chapter 3) Ponceau S staining was performed, as a loading control in these cells, where a housekeeping gene could not be used due to variations across cell lines. The stained membrane was imaged using the G-box (Syngene, Cambridge, UK). Each lane representing a cell line was quantified using Image J software and densitometry of bands was normalised to these obtained values. Prior to membrane blocking Ponceau S was washed off the membrane by PBS-Tween (PBST).

2.5.4 Incubation of antibodies

Prior to the addition of antibodies, the membrane was blocked for 1 hr at room temperature in 5% milk in TBS-tween (TBST) (Merck, Kenilworth, NJ, United States). Using the ladder as guidance the membrane was cut into sections to probe for relevant proteins of interest based on their molecular weight. Primary antibodies were diluted in 5% bovine serum albumin (BSA) (Merck, Kenilworth, NJ, United States) in TBST. Dilutions for each antibody in BSA are specified in Table 2.1. Primary antibodies were left to incubate overnight at 4°C on a rocking platform. The following day the membrane sections were rinsed twice in TBS followed by a 10 minutes wash on a shaking platform, before the addition of relevant secondary antibody (Table 2.2) diluted in 5% milk powder in TBT at room temperature for 1 hr.

Antibody target	Species of antibody	Manufacturer	Product code	Dilution used
ATM	Rabbit	Cell signalling	2873	1:500
ATR	Mouse	Santa-Cruz	Sc515173	1:200
BRCA1	Rabbit	Abcam	Ab191042	1:500
CDK1	Rabbit	Abcam	Ab131450	1:500
CHK1	Mouse	Santa-Cruz	Sc8408	1:500
Cyclin E	Rabbit	Cell signalling	20808	1:1000
pCDK1^{Tyr15}	Rabbit	Cell signalling	9111	1:1000
pCHK1 ^{Ser345}	Rabbit	Cell signalling	2348	1:1000
pCHK1 ^{Ser296}	Rabbit	Cell signalling	90178	1:1000
RAD51	Mouse	Santa-Cruz	Sc398587	1:1000
pRPA $^{Ser 4/8}$	Rabbit	Bethyl laboratories	A300-245A	1:1000
PARP-1	Rabbit	Abcam	Ab227244	1:500
RAD51	Rabbit	Abcam	Ab8875	1:500
TP53	Mouse	Santa-Cruz	Sc126	1:1000
Vinculin	Rabbit	Cell signalling	4650	1:1000
WEE1	Rabbit	Abcam	Ab137377	1:500
XRCC1	Mouse	Santa-Cruz	Sc56254	1:250

Table 2.2: Primary antibodies used in western blotting experiments. The following antibodies were incubated at the stated dilutions, overnight at 4 °C. All antibodies were diluted in 5% BSA (Merck, Kenilworth, NJ, United States) in TBST, with the exception of BRCA1 antibody, which was diluted in 5% milk (Marvel, UK) in TBST.

Target species	Type of antibody	Manufacturer	Product code	Dilution
Anti- mouse	Goat polyclonal	Dako	PO448	1:2000
Anti- rabbit	Goat polyclonal	Dako	PO447	1:2000

Table 2.3: HRP-conjugated secondary antibodies used in western blotting experiments. The following antibodies were added to the relevant primary antibody at the stated dilutions, for 1 h at room temperature. Each of the secondary antibodies were diluted in 5% milk, TBST.

2.5.5 Chemiluminescence and analyses

Following incubation of secondary antibodies membrane sections were washed in TBST for 10 minutes 3 times on a shaking platform. Clarity Max ECL (Bio-rad, Hercules, CA, United States) was prepared at a 1:1 ratio of peroxide reagent and luminol/enhancer reagent was prepared and left on membrane sections for 5 minutes prior to imaging. Membranes were imaged using the G Box (Syngene, Cambridge, UK).

Densitometry was carried out using Genesys software (Syngene, Cambridge, UK). A rectangle was drawn around each band and the same size was consistent for each band assessed. A background value was also obtained and this was subtracted from the value for each band, prior to normalisation to loading control (mean pixel value= ((band densitometry value- background value)/densitometry value for relative sample loading control by Ponceau S or housekeeping gene). Graphs of densitometry were plotted using Graphpad Prism 9.0 software.

2.6 SRB growth proliferation assay

Sulforhodamine B (SRB) assay measures protein content in cells, to determine cell density. Here it was used in proliferation assays, to determine the doubling time of cell lines and assess whether this conferred sensitivity to the kinase inhibitors. Exponentially growing cells were trypsinised and resuspended in pre-warmed media, before being counted and diluted to appropriate cell densities (0.6×10^4, 1.2×10^4, 2.5×10^4, 5.0×10^4 and 1×10^5) (Figure 2.1). 7 plates with this layout were seeded. Plates were each fixed at

24 h time points for evaluation. The outer edges of each plate were filled with cell line specific media, to ensure the edge effect did not affect cells. Once cells had adhered, they were checked under the microscope to ensure viability. Plates were fixed using methanol: acetic acid 3:1. Plates were fixed every 24 hr with the time of fixation recorded. Following fixation plates were stored at 4°C until required for SRB staining.

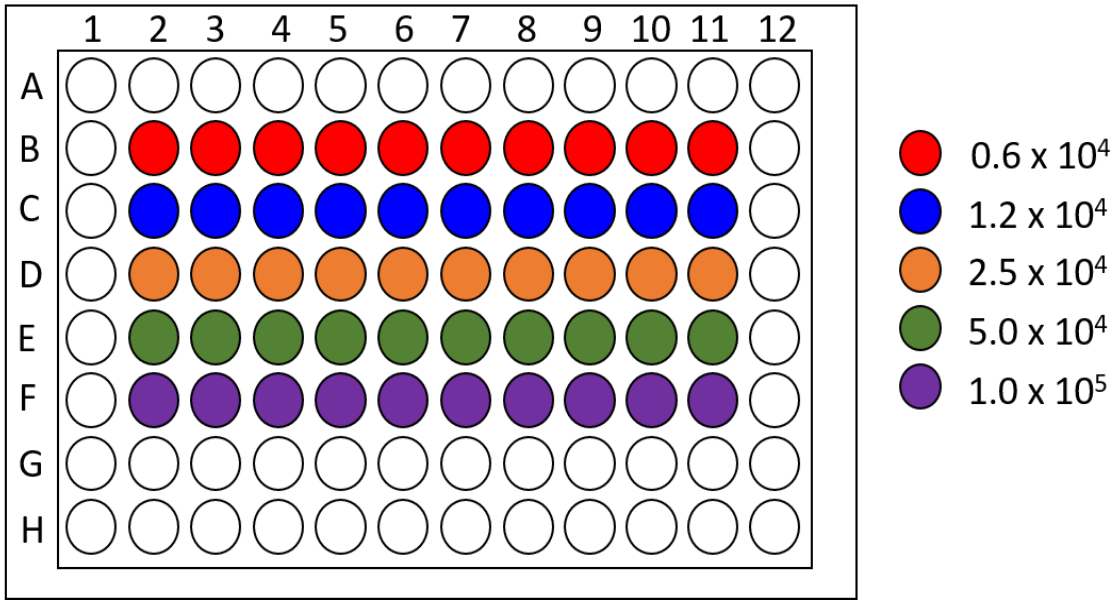


Figure 2.1: Plate layout of 96-well plate for SRB proliferation assay. The cell densities corresponding with each well in the 96-well plate.

Fixed plates were removed from 4°C storage and washed in deionised water, then left to dry prior to the addition of 0.4% SRB solution in 1% acetic acid to all wells for 30 minutes. Dye was then flicked off and plates were washed. After plates were dried, 10 mM Tris was added to each well and left on the plate shaker for 20 minutes, to ensure the stain was solubilised, before being read on the Omega FLUOstar plate reader at an absorbance of 570 nm. Growth curves were constructed using GraphPad Prism 9.0 software and doubling time was calculated using the exponential growth equation on Graphpad Prism 9.0.

2.7 SRB growth inhibition assays

SRB was also used in determining growth inhibition of patient ascites samples, following exposure to the inhibitors (Chapter 7). A known number of cells (500- 1000 cells/well)

were added and left to adhere for 24 h. 2 plates were seeded (Figure 2.2), with the addition of a day 0 plate, to assess how many cell doublings had occurred in the patient cells at the point of fixation.

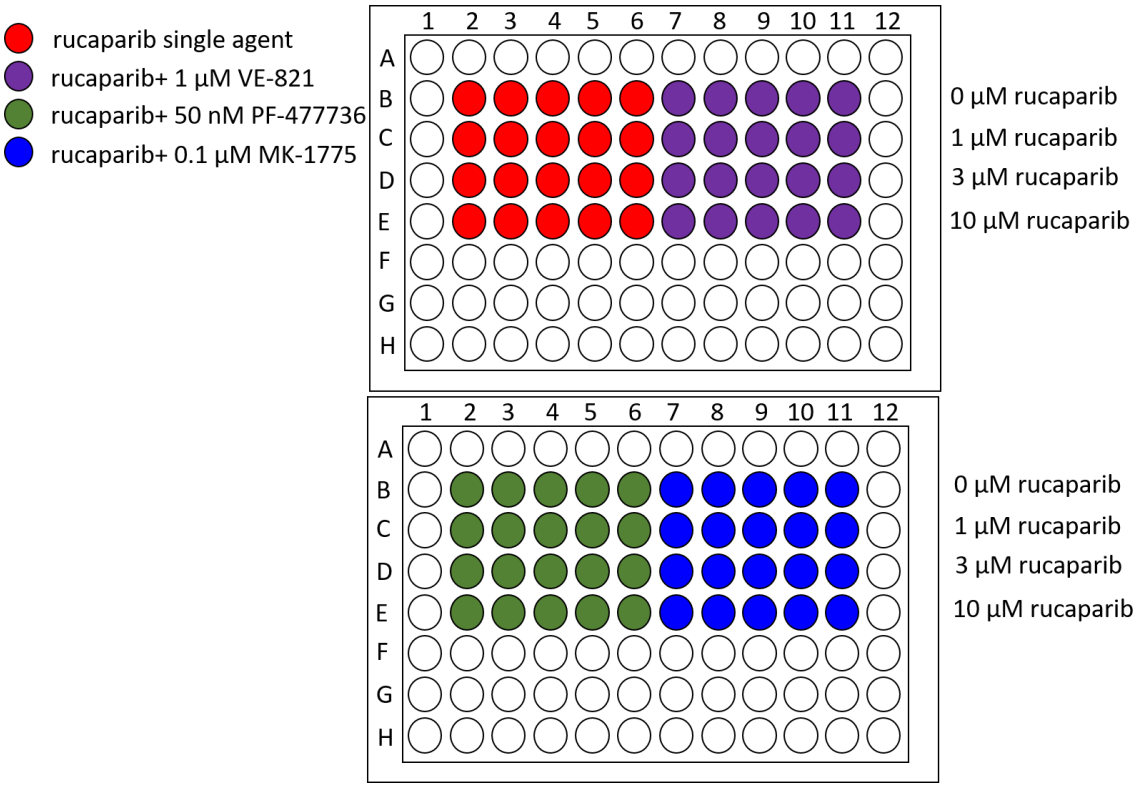


Figure 2.2: Plate layout for SRB growth inhibition experiments in primary cultures

The day 0 plate was fixed following the 24 h period from seeding. At this time the relative drug was added to each well and cells were exposed to drug until control cells reached confluence. Following fixation cells were stained and absorbance was read as described in section 2.6. The absorbance of treated cells was calculated as a percentage of untreated control cells.

2.8 Colony formation assays

Colony formation assays were used in each of the cell lines to determine differences between cell lines cloning efficiencies, which would decide the number of cells seeded in future cytotoxicity experiments. A set number of cells were seeded in 6-well plates that ranged between 50- 1600 cells/well. These cells in growth medium were incubated for 7-14 days before removal of media and fixation with 3:1 methanol acetic acid and

staining with 0.4% crystal violet. Colonies formed were counted and cloning efficiency was calculated as follows:
Cloning efficiency (%) = ((number of colonies counted/ number of cells seeded) x 100)

2.9 Clonogenic survival assays

A clonogenic survival assay is used to determine a single cells capability to form a colony, consisting of approximately 30 cells minimum. Here, clonogenic assays were used to determine the cytotoxicity of inhibitors, as single agents (Chapters 4 and 5) and in combination (Chapter 6), by assessing how drug exposure impacted the number of colonies that subsequently formed, compared to DMSO control cells.

Exponentially growing cells were harvested and counted using a haemocytometer (Merck, Kenilworth, NJ, United States). A selected number of cells were seeded, which varied between cell lines based on growth characteristics and pre-determined cloning efficiency, allowing 3 wells per dose of drug. Cells were left to adhere for 24 hr before media was replaced with media containing drug in DMSO or DMSO alone (0.5 %). After an exposure time of 24 hr to the drug, the medium was changed to 2 mls of fresh medium per well. Cells were left to incubate for 10-14 days, dependent on the time each cell line took to form colonies, before being fixed and stained.

3:1 methanol: acetic acid was added to each well for 5-10 minutes before removing and adding 0.4% crystal violet for 10-20 minutes. Once removed, plates were gently rinsed with diH_2O and left to dry before colonies were counted by eye and data was imported into GraphPad Prism 9.0, where LC_{50} values were calculated and statistical tests performed.

2.10 Immunofluorescence

Immunofluorescence (IF) is a method of identifying a specific target, via a primary antibody and a fluorescent tagged secondary antibody. This was visualised, imaged and analysed via microscopy on Leica DM6 wide-field microscope (Leica Microsystems,

Wetzlar, Germany), which exerts light at the wavelength relative to the fluorophore of the secondary antibody used. Here, IF was used to assess foci formation of key RS markers (γH2AX and pRPA$^{Ser4/8}$) and a marker of HRR function (RAD51 foci).

2.10.1 Assessment of basal replication stress

Basal RS was assessed using the formation of γH2AX and pRPA$^{Ser4/8}$ foci, as detailed in Chapter 3. These data were then correlated with cytotoxicity data, to investigate if basal RS was a determinant of sensitivity of cells to each inhibitor. H2AX is phosphorylated rapidly at serine 139, at the site of DNA damage and blocked replication forks which cause RS (Rogakou *et al.,* 1998, Heylmann and Kaina, 2016) and phosphorylation of RPA at serine 4/8 is pivotal in the response to RS (Ashley *et al.,* 2014), making both of these ideal markers for measuring RS levels in cells. It is important to note that had time permitted other methods of assessing replication stress, such as the DNA fiber assay, would have also been performed as a comparison to the method described here.

Untreated cells were seeded onto sterilised (methanol-dipped) coverslips, which lined each well in a 6-well plate. Cells were left to adhere for 24 h prior to fixation by ice-cold methanol, followed by storage at -20 ^{o}C, for a minimum of 2 hr.

Coverslips were rinsed with 0.2% BSA 0.3% Triton-X-100 in PBS, followed by a further three 10-minute washes. Coverslips were then transferred into a parafilm-lined petri dish and 200 µl of blocking buffer (5% BSA, 1:25 goat serum dissolved in PBS), was added per coverslip and left at room temperature for 1 hr. The blocking buffer was then wicked off the coverslips and replaced with fresh buffer (0.2 % BSA, 0.3 % Triton-X-100 in PBS) containing 1:1000 of γH2AX primary antibody (Merck, Kenilworth, NJ, United States) overnight at 4°C.

The following day coverslips were washed 3 times (0.2% BSA, 0.3% Triton-X-100 in PBS) before incubation with the second primary antibody, pRPA$^{Ser4/8}$ (Bethyl Laboratories, Montgomery, TX, USA) at 1:4000 in the washing buffer for 1 h at room temperature.

Coverslips were washed 3 times in 0.2 % BSA in PBS before incubation with secondary Alexa Fluor 488 and Alexa Fluor 568 secondary antibodies (Invitrogen, Waltham, MA, USA), each diluted 1:1000 in 0.2% BSA in PBS for 1 h at room temperature, protected from the light. Coverslips then underwent 2 quick washes and one 5-minute wash (0.2% BSA in PBS) before being exposed to 0.5 µg/ml DAPI solution for 40 minutes. Coverslips were then mounted onto microscope slides using Prolong Glass Antifade mountant (Thermofisher, Waltham, MA, USA). Slides were stored in dark conditions and left to dry prior to imaging. Cells were imaged at x40 using the Leica DM6 LED fluorescence microscope (Leica Microsystems, Wetzlar, Germany). For analysis the image file was opened in Image J and a line was drawn between 2 foci, one of which was the minimum level deemed to be a focus. This profile was then plotted to give an intensity plot for each pixel intersected by the line. A top hat filter was applied and the value corresponding to the smallest peak was deemed the noise level when running a macro to count foci per cell. A mask was applied to the image to ensure only foci within the perimeter of each nucleus were quantified. Following this, quantification of foci was performed. These raw counts of foci per cell were plotted using Graphpad Prism 9.0 software.

2.10.2 Assessing HRR function

The HRR functional assay uses immunofluorescence to detect γH2AX (a marker of RS previously described) and RAD51 foci (a marker of HRR function) in order to detect levels of DNA damage and repair, respectively, by homologous recombination. HRR function of patient samples and cell lines was established, as well as the impact of rucaparib and the kinase inhibitors on RS and HRR.

Cells were seeded at 0.5 x10^5 cells/ml onto sterile coverslips in 6-well plates, before being incubated for 24 hr. Cells were exposed to DMSO (0.5%), 10 µM rucaparib, 10 µM rucaparib + 1 µM VE-821, 10 µM rucaparib + 50 nM or 10 µM rucaparib + 0.1 µM MK-1775 for 24 h in cell lines and 48 h in patient ascites cells. Media containing drug was then removed and coverslips were washed twice with PBS before being fixed with ice cold methanol for a minimum of 1 hr at -20°C.

Coverslips were rinsed with 0.2% Triton-X-100 in PBS (cell lines) or 0.2% Triton-X-100 in 120 mM potassium chloride, 20 mM sodium chloride, 10 mM Tris and 1 mM EDTA, pH 8.0 (primary cultures), followed by a further three 10-minute washes. Coverslips were then transferred into a parafilm lined petri dish and 200 µl of blocking buffer (2% BSA, 10% skimmed milk powder (Marvel, UK) and 10 % goat serum dissolved in relevant washing buffer), was added per coverslip for 1 hr at room temperature. The blocking buffer was then wicked off the coverslips and replaced with fresh blocking buffer containing 1:500 of RAD51 antibody (Abcam, Cambridge, UK) and incubated at 4°C for 16-18 hr.

The following day coverslips were transferred to 6 well plates containing the relevant washing buffer and placed on the rocker for three 5-minute washes at room temperature. Coverslips were then transferred onto fresh parafilm and 200 µl anti-phospho H2A.X (Merck, Kenilworth, NJ, United States) diluted 1:1000 in buffer (2% BSA) in relevant wash buffer) was added to each coverslip and incubated for 1 hr at room temperature. Coverslips then underwent further washes before being incubated with both secondary antibodies, Alexa Fluor 488 and Alexa Fluor 546 (Invitrogen, Waltham, MA, USA) diluted 1:1000 for 1 hr at room temperature in dark conditions. Coverslips then underwent 2 quick washes and one 5-minute wash with relevant buffer, before being exposed to 0.5 µg/ml DAPI solution for 40 minutes. Coverslips were then mounted onto microscope slides using Prolong Glass Antifade mountant (Thermofisher, Waltham, MA, USA). Slides were stored in dark conditions and left to dry prior to imaging. Cells were imaged and analysed as previously described (section 2.10.1).

2.11 PARP activity assay

A GCLP-validated assay (Plummer *et al.,* 2005) was used here to measure the formation of the product of the PARP reaction (PAR) by immunological detection (Figure 2.3). This was necessary to determine endogenous PAR, optimum PARP activity and extent of PARP inhibition by rucaparib (Chapter 4), as well as to compare durability of PARP inhibition by PARPis (Chapter 8). Cells were incubated with an excess of NAD+ substrate

and a 12 mer palindromic double-stranded oligonucleotide was used (Invitrogen, Waltham, MA, USA), to mimic DNA breaks and activate PARP1.

Cells were harvested and counted, and 800- 1600 cells per reaction tube were required for the assays measuring PARP activity. For experiments measuring baseline PAR (without the addition of NAD+ and oligonucleotide), 100 to 1000-fold more cells were required to detect low levels in unstressed cells. It was essential cells remained on ice following harvesting until use. Following centrifugation (500 x G, 5 minutes, 4 ^{o}C) supernatant was discarded and 1 ml ice-cold PBS was added. Digitonin (0.15 mg/ml) was used to permeabilise cells and 100 µl was added to cells on ice for 5 minutes.

After 5 minutes 900 µl ice-cold isotonic buffer was added (1.9 g HEPES, 1.94 g KCl, 8 g dextran, 152 mg EGTA, 94 mg $MgCl_2$ and 15.4 g sucrose, in 150 ml diH_2O, pH 7.8). Cells were counted and diluted with isotonic buffer to the relative number of cells required. L1210 cells were used as a quality control/ positive control, as these cells had previously shown good PARP activity levels. A standard curve was prepared from PAR standards (Enzo Life Sciences), this was diluted to give a range of 25 -0 pmol PAR monomer, which was ran alongside samples.

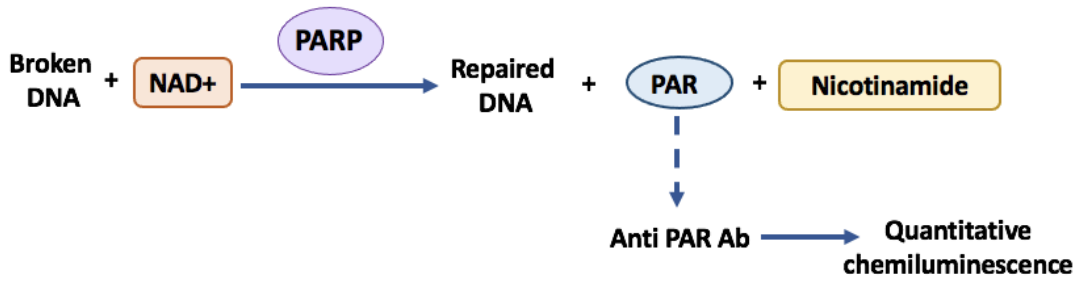


Figure 2.3: Principle of measuring PARP activity. An oligonucleotide was used to mimic broken DNA and an excess of NAD+ was added into the reaction, which resulted in the formation of PAR, which was measurable by 10 H PAR antibody and chemiluminescence.

PARP activity was measured in replicate samples, by the addition of cells to a reaction mixture containing 350 µM NAD+ and 10 µg/ml oligonucleotide in a reaction buffer (100

mM Tris.HCl, 120 mM $MgCl_2$ in diH_2O, pH 7.8). Cells were added in a time-sensitive manner to tubes in an oscillating water bath set to 26°C, ensuring the interval between addition of cells and addition of stop solution (12.5 µM rucaparib in PBS) remained consistent and the reaction ran for precisely 6 minutes. Cells were blotted onto a nitrocellulose membrane (Hybond-N, Amersham) using a 24-well manifold. A T_0 per sample (without oligonucleotide or NAD+ addition) was also loaded onto the blot, as were purified PAR standards (0- 25 pmol monomer equivalent). The membrane was washed 3 x 5 minutes in PBS on a shaking platform. The membrane was then blocked in 5% milk PBS-T for 1 h at room temperature. The membrane was incubated with 10 H PAR antibody diluted 1:1000 (Enzo life sciences) in 5% milk (Marvel, UK) in PBS-T overnight at 4 °C.

Following this the membrane was washed 2 x 5 minutes in PBS-T, prior to incubation with goat anti-mouse HRP conjugated secondary antibody (Dako, Santa Clara, CA, USA) diluted 1:1000 in PBS-MT for 1 h at room temperature. The membrane was then washed every 5 minutes with PBS-T for a minimum of 1 h.

Clarity Max ECL (Bio-rad, Hercules, CA, United States) was prepared at a 1:1 ratio and added to the membrane for 5 minutes prior to imaging. Membranes were imaged using the G Box (Syngene). Densitometry was carried out using Genesys software (Syngene UK, Cambridge, UK). The area surrounding each circle on the dot blot was measured and remained consistent across samples on the membrane. Each circle was assigned a mean pixel value by the software. Regression of the standard curve was calculated using non-linear curve fit (one-site binding) using Graphpad Prism 9.0 software. From this analysis a Bmax and Kd value were reported, which were subsequently used in the calculation of [PAR] per each sample (X= Y*Kd/ (Bmax-Y)).

2.12 Cell cycle analysis

Cell cycle analysis is an innovative application of flow cytometry, used to detect cell populations at various stages of the cell cycle. The role of ATR, CHK1 and WEE1 inhibitors on DNA damage induced cell cycle control has been widely reported and

therefore it was important here to assess both the impact of rucaparib on cell cycle and how the addition of each kinase inhibitor subsequently impacted this.

Initially, all cell lines were due to be used in the following experiment, however due to time restrictions this was not possible and IGROV-1 cells were selected based on these cells often representing the average cytotoxicity to single agents across the HRC cells. Exponentially growing IGROV-1 cells were seeded and left to adhere for 24 h before exposure to drug for 30 h. Cell cycle analysis was performed using a Click-iT™ EdU flow cytometry assay kit (Thermofisher, Waltham, MA, USA). EdU is a nucleoside thymidine analogue, which is transported into dividing cells and incorporated into newly synthesised DNA. This allows a more accurate measurement of S-phase in cells, which can be categorised into EdU positive and EdU negative populations. In the final hr of drug treatment 10 µM EdU was added to the media containing drug. Cells were harvested, prior to fixation by 500 µl 4% PFA per sample (15 minutes, room temperature and dark conditions). The cells were centrifuged (1,600 rpm, 5 minutes) and supernatant discarded before being washed with 1 % BSA/PBS. Cells were centrifuged and the pellet was stored at 4 ^{o}C for 1-2 days, prior to staining. Cells were centrifuged (1,600 rpm, 5 minutes) and Click-iT ™ reaction mixture was prepared as detailed below (Table 2.4). Samples were incubated with reaction mixture for 30 minutes, at room temperature, in dark conditions. Cells were centrifuged (1,600 rpm, 5 minutes) and washed twice with 1% BSA/PBS, with the centrifugation step in between each wash. Cell pellet was resuspended in 1% BSA/PBS and 0.5 mg/ ml DAPI, diluted 1:250 (Thermofisher, Waltham, MA, USA). Analysis was carried out using Attune Nxt Cytometer. De Novo FCS Express 7 software was used to analyse the data.

Reaction component	**Preparation**	**Volume for 1 x sample (µl)**
1 x Click-iT™ reaction buffer	Dilute 10 x stock 1:10 in diH_2O	**438**
$CuSO_4$	Ready to use, 4 ^{o}C	**10**
Fluorescent 488 azide	Ready to use aliquots, - 20 ^{o}C	**2.5**
1 x reaction buffer additive	Dilute 10 x stock 1:10 in diH_2O	**50**
Total volume:		**500**

Table 2.4: Volume of Click-iT™ reagents used per sample for cell cycle analysis.

Chapter 3. Characterisation of cell lines

3.1 Introduction

The overall aim of this thesis was to determine synergy between PARPi and inhibitors of ATR, CHK1 and WEE1. Ovarian cancer cells were used as a model, due to 3 PARPi currently being approved for use in ovarian cancer, although resistance is common and therefore there is an unmet need to re-sensitise these cells. Previous studies have shown ATRi can sensitise ovarian cancer cells to the PARPi rucaparib (Peasland *et al.,* 2011). Cervical cancer cells were also used due to lack of G1 checkpoint control (due to HPV causing p53 and pRb inactivation), which predicts sensitivity to S/G2 checkpoint kinase inhibitors (Nghiem *et al.,* 2001). Cisplatin is often used in the treatment of cervical cancer and platinum sensitivity can be considered a surrogate for PARPi sensitivity (Pennington *et al.,* 2014, Mirza *et al.,* 2016, Coleman *et al.,* 2017, Swisher *et al.,* 2017). Experiments have been performed on more extensive panels of ovarian and cervical cell lines by previous students, to study ATR, CHK1 and WEE1 inhibitor sensitivity (Alice Bradbury, PhD thesis, Stuart Rundle MD thesis, Newcastle University 2020) and, although these were not used in combination with PARPi, data acquired by them was used to select the most suitable cell lines for this study. The aim of this chapter was therefore to determine DDR (genomic, protein and functional) status, growth and levels of replication stress (RS) relevant to the study of PARPi and ATR/CHK1/WEE1i interaction.

The PARPi used in this project, rucaparib (Rubraca®), is currently FDA- and EMA-approved for use in maintenance treatment of recurrent ovarian cancer (Coleman *et al.,* 2017). Since all PARPi are synthetically lethal in cells lacking HRR function, to differing degrees, primarily due to *BRCA* mutations, two sets of isogenic matched cells were used here, with and without a *BRCA1* (UWB1.289+ B1 and UWB1.289 ovarian cancer cells) or *BRCA2* (V-C8 and V-C8.B2 Chinese hamster lung fibroblasts) mutation, to determine the impact of HRR status on synergy between rucaparib and each of the cell cycle checkpoint kinase inhibitors (Chapter 6). A phase 2 trial aimed to evaluate the efficacy of

rucaparib as a maintenance therapy for locally advanced cervical cancer, however the study was withdrawn due to lack of financial support (NCT03795272).

The overwhelming majority of cervical cancers are associated with HPV infection that results in inactivation of two key controllers of the G1 checkpoint, i.e., p53 and pRB. Cervical cancer C33A (HPV negative but p53 and pRb mutated) and SiHa cells (HPV16 +) were selected for their differing HPV statuses. Previous data obtained by Stuart Rundle showed that C33A and SiHa cells had differing sensitivity to the ATR, CHK1 and WEE1 inhibitors used here: VE-821 (LC_{50}: 22.8 µM vs. 5.0 µM, respectively), PF-477736 (LC_{50}: 0.3 µM vs. 0.2 µM, respectively) and MK-1775 (LC_{50}: 0.2 µM vs. 0.3 µM, respectively) (Stuart Rundle MD thesis Newcastle University 2020). The 3 ovarian cancer cell lines used here IGROV-1, UWB1.289+ B1 and UWB1.289 cells were selected on the basis of their differing sensitivity to VE-821, ranking 4th, 11th and 13th, respectively, within a panel of ovarian cancer cells, with LC_{50}s of: 1.9 ± 0.4 µM, 1.0 ± 0.1 µM and 0.6 ± 0.06 µM, respectively (Alice Bradbury, PhD thesis Newcastle University 2020).

UWB1.289 cells are human ovarian cells with a *BRCA1* mutation, together with their BRCA1 corrected isogenic sub-line UWB1.289+*BRCA1* (DelloRusso *et al.,* 2007). They are a good model for studying the effects of *BRCA1* mutation, and thereby HRR function, on the synergy under investigation. Similarly, isogenic matched V-C8 and V-C8.B2 cells were used to explore differences in synergy between *BRCA2* mutated and corrected cells (Kraakman-van der Zwet *et al.,* 2002), as well as investigating any differences between HRD cells with either a *BRCA1* or *BRCA2* mutation. Isogenically-matched cells are able to identify singular determinants of sensitivity as well as key underlying mechanisms of synergy, which was a centre point to this study. The use of isogenic matched cells is favourable in these studies, particularly as these cells only differ by a single gene (*BRCA1* or *BRCA2* in this instance), thereby eliminating any other molecular characteristics as the cause of differing sensitisation by ATR, CHK1 or WEE1 inhibitors to rucaparib.

Matched AA8 and EM9 cells were selected for use in proof-of-concept experiments when determining the importance of single-strand break repair (SSBR) inhibition vs PARP trapping in the synergy between rucaparib and kinase inhibitors (Chapter 6). EM9

cells are defective in XRCC1, an essential component recruited by activated PARP-1 to repair SSBs and are a derivative of AA8 Chinese hamster ovarian cancer cells.

This chapter aims to characterise the panel of cell lines to effectively investigate any differences in cytotoxicity to the inhibitors or combination of rucaparib and the kinase inhibitors throughout the project, in terms of factors hypothesised to affect the response to the drugs used.

Cell line	Origin species	Tissue type	Morphology	HRR status	G1 checkpoint control
C33A	Human	Cervix	Epithelial	Competent	• p53 mutant, pRb null (Crook *et al.,* 1991) • HPV negative (ATCC) • p16 WT (Craig *et al.,* 1998) • High levels of CDK4, CDK6 and cyclin D1 (Xiong *et al.,* 2019)
SiHa	Human	Cervix	Epithelial	Competent	• Inactivation of p53 WT (Srivastava *et al.,* 1992) • HPV 16+ (ATCC) • Express high levels of p16 (Lau *et al.,* 2007)
IGROV-1	Human	Ovary	Epithelial	Competent	• Heterozygous p53 mutation (Domcke *et al.,* 2013) • p16 WT (Kubo *et al.,* 1999) • Express CDK4 and cyclin D1 (Aguirre *et al.,* 2004)
UWB1.289+ B1	Human	Ovary	Epithelial-like	Competent	• p53 mutant (ATCC)
UWB1.289	Human	Ovary	Epithelial-like	Defective	• p53 mutant (ATCC)
V-C8.B2	Chinese hamster	Lung	Fibroblast	Competent	• p53 mutant (Chaung *et al.,* 1997)
V-C8	Chinese hamster	Lung	Fibroblast	Defective	• p53 mutant (Chaung *et al.,* 1997)

Table 3.1: Cell line characteristics. Origin, tissue type, morphology, HRR status and G1 checkpoint control status was collated from information available on the ATCC and Expasy online databases.

3.2 Aims and Objectives

1. To assess the mutational status of key DDR genes across the panel of cell lines as potential determinants of sensitivity to the inhibitors

2. To determine baseline mRNA and protein expression of the same DDR genes *via* RNA-Seq and western blot

3. To establish the growth rate of cell lines, to provide data to explore any relationship between cytotoxicity and proliferation

4. To assess baseline RS in cell line panel, as a potential determinant of cell line sensitivity to kinase inhibitors

3.3 Hypotheses

1. The differences in gene expression data will be reflected in protein levels across cell lines.

2. Basal RS levels will be significantly higher in repair-defective cells, compared to matched repair-competent cells

3.4 Materials and Methods

3.4.1 Mutational status of DDR genes across cell lines

The mutational status of key DDR genes, comprising cell cycle and repair genes, was determined using data retrieved from the CCLE database in the cell lines for which data was available. Variant allele frequency was calculated using whole genome and whole exome sequencing (WGS/ WES). A cut-off value of 0.8 was used to determine heterozygous or homozygous mutations. Genes were selected based on previously

identified determinants to PARP, ATR, CHK1 and WEE1 inhibition from the literature (Chapter 2, Table 2.1).

3.4.2 Comparing baseline mRNA expression of key DDR genes across cell lines

Targeted RNA sequencing was completed by HTG Molecular Diagnostics as previously described (Chapter 2, section 4). Heat maps were created using Morpheus software by Broad institute to compare differences in basal mRNA expression across cell lines tested.

3.4.3 Baseline DDR protein expression by western blot

Lysates were prepared from exponentially growing C33A, SiHa, IGROV-1, UWB1.289+ B1, UWB1.289, V-C8.B2, V-C8, AA8 and EM9 cells and Western blots were performed as described previously (Chapter 2, section 5). Densitometry was analysed as previously described and values were normalised to the staining of Ponceau-S corresponding to each individual cell line, using Image J software.

3.4.4 Determining growth characteristics of cell lines

The doubling time of cell lines was determined by SRB cell proliferation assays described in Chapter 2. Colony formation assays were used to determine cloning efficiency as described in Chapter 2, section 6.

3.4.5 Measure of baseline RS by immunofluorescence

To assess the impact of basal RS on the cytotoxicity to kinase inhibitors (Chapter 5) and synergy with rucaparib (Chapter 6), immunofluorescence assays were performed as described in Chapter 2. Cells were seeded onto coverslips and left to adhere prior to fixation, antibody staining, imaging and analysis as previously described. γH2AX and pRPA 32 $^{Ser4/8}$ foci were used as measures of baseline replication stress across the cell line panel.

3.5 Results

3.5.1 Mutational status of DDR genes across cell line panel

Prior to determining target inhibition and cytotoxicity by PARP and cell cycle checkpoint kinase inhibitors, the mutational status and baseline mRNA expression of key DDR genes involved in cell cycle and DNA repair pathways was assessed by data available on the CCLE database (http://sites.broadinstitute.org/ccle/datasets) and NextSeq sequencing (HTG diagnostics), respectively. It is important to consider that mutational data from the CCLE is based on published data, as opposed to the NextSeq sequencing, which was obtained from the cells used in the work described here, which may include genetic drift during long-term culturing (Fasterius and Szigyarto, 2018). This disparity between cell lines has been previously reported, when an extensive study compared variation between laboratories culturing what were described as the same cell lines (Ben-David *et al.,* 2018).

From data obtained from the CCLE database, none of the cells had mutations in *PARP-1, ATR, CHK1* or *WEE1*. *TP53* was the most commonly mutated, with homozygous mutations in cervical C33A and ovarian UWB1.289 cells, and heterozygous mutation in IGROV-1 cells. Other homozygous mutations identified included *BRCA1* in UWB1.289 cells, HRR gene *FANCM* in SiHa cells, MMR gene *MLH1* in IGROV-1 cells and *TNKS1,* a key regulator of PARylation-dependent ubiquitination, in both SiHa and IGROV-1 cells. Within the selected gene panel, across the cell lines for which data was available, IGROV-1 cells had the most mutations (2 homozygous, 30 heterozygous). C33A cells had 1 homozygous and 27 heterozygous, SiHa cells had 2 homozygous and 2 heterozygous and UWB1.289 cells had 2 homozygous and 1 heterozygous mutation (Figure 3.1).

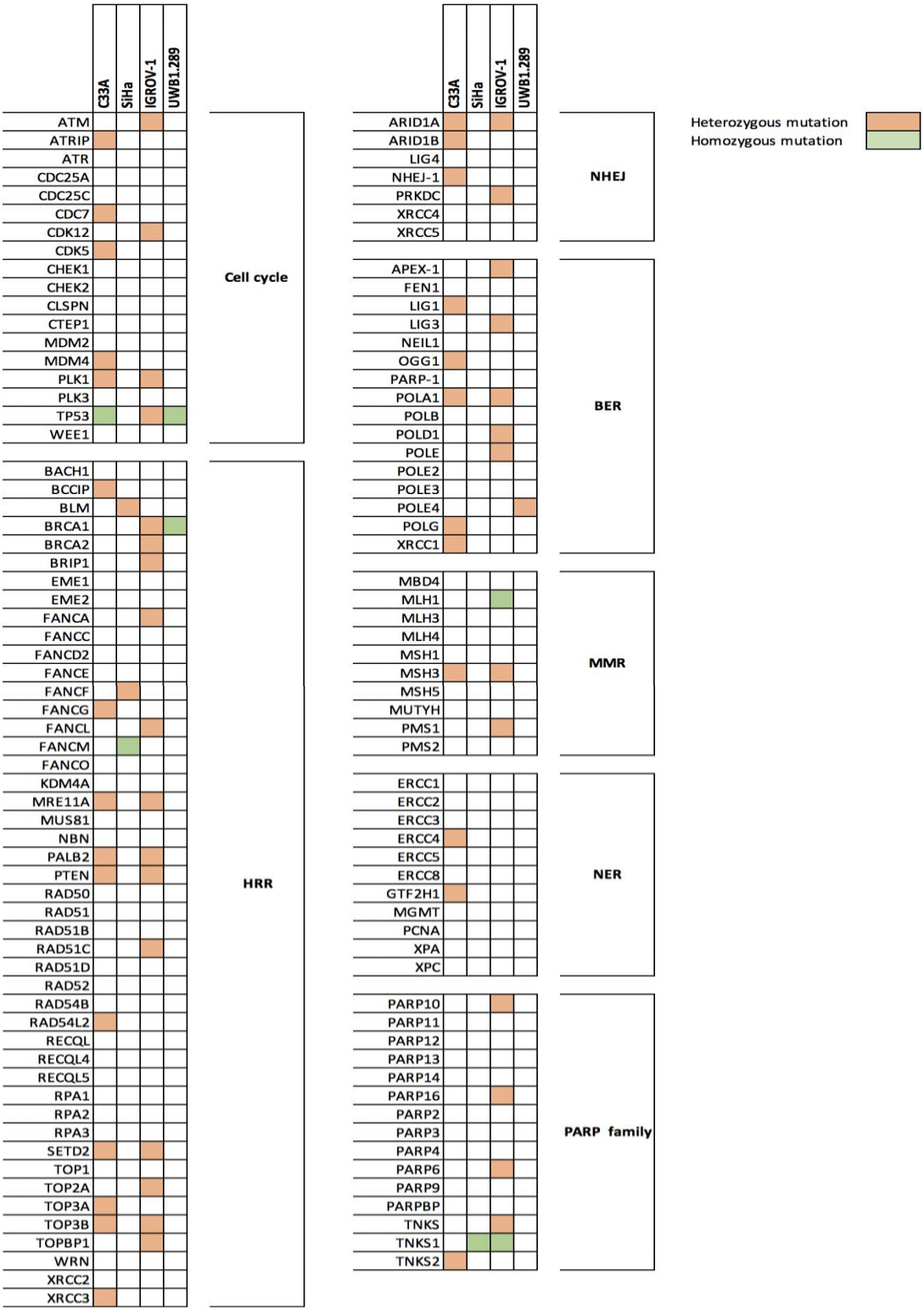


Figure 3.1*:* Mutational status of key DDR genes across human cell lines was assessed using data from the CCLE. Data from the most up to date CCLE database was analysed. Variant allele frequency was calculated, and mutations were identified as heterozygous or homozygous based on a cut-off value of 0.8. A variant allele frequency of above 0.8 was considered a homozygous mutation.

3.5.2 Expression of previously identified determinants to PARP, ATR, CHK1 and WEE1 inhibition by mRNA expression

The baseline mRNA expression of key cell cycle and repair genes was assessed by Illumina NextSeq sequencing by HTG diagnostics (Figure 3.2). The biggest variation between cells was observed with *TP53* mRNA expression, which was lowest in UWB1.289 cells and highest in IGROV-1 cells. This suggests that the heterozygous mutation of *TP53* identified on the CCLE database in IGROV-1 cells is a pathogenic dominant negative one, supressing the wildtype function of p53.

Overall, the mutations identified from the CCLE database (Figure 3.1) related to the mRNA expression data here (Figure 3.2). C33A cells had heterozygous mutations in *ATRIP, PLK1, PALB2, PTEN, SETD2, ARID1A* and *XRCC1* and similarly had the lowest mRNA expression of these across the cell lines. mRNA expression of *MSH3* and *ERCC4* was also lower in C33A cells than the average expression across cell lines, and these were also identified as heterozygous mutations. Similarly, HRR gene *BLM* had the lowest mRNA expression in SiHa cells and this had a heterozygous mutation in these cells. SiHa cells had only 2 homozygous and 2 heterozygous mutations and likewise SiHa cells often had the highest expression of genes tested across the panel. As described, IGROV-1 cells had the most mutations identified by the CCLE database across the genes tested (2 homozygous, 30 heterozygous) and generally had the lowest mRNA expression of the proteins tested. This was especially evident with a lower mRNA expression observed in *ATM, PLK1, BRCA1, BRCA2, BRIP1, FANCA, FANCL, MRE11a, PALB2, PTEN, TOP2A, PRKDC, POLD1, MLH1, MSH3* and *PMS1*, which also had heterozygous mutations.

PARP-1 expression was highest in HRD UWB1.289 cells and lowest in C33A cells. ATR, CHK1 and WEE1 mRNA expression was highest in SiHa cells, with C33A cells having lowest expression of ATR, IGROV-1 cells having lowest expression of CHK1 and UWB1.289 cells lowest expression of WEE1.

Across key HRR genes, in this subset of cell lines, UWB1.289 cells generally had the lowest expression across the panel, with below mean expression in 20/32 of the genes. As expected, UWB1.289 cells had lowest *BRCA1* expression, as well as the lowest

expression for most of the *FANC* genes, compared to the other cells, although C33A cells had the lowest expression of *RAD50* and *RAD51,* which are key to HRR. Similarly, overall UWB1.289 cells had the lowest expression of BER genes, with the exception of PARP-1 and XRCC1, which were lowest in C33A cells.

Across the cell lines tested, UWB1.289 had the lowest mRNA expression of the majority of genes involved in cell cycle control. As expected, these cells had the lowest mRNA expression of *BRCA1,* as well as many other HRR, BER, MMR and NER genes.

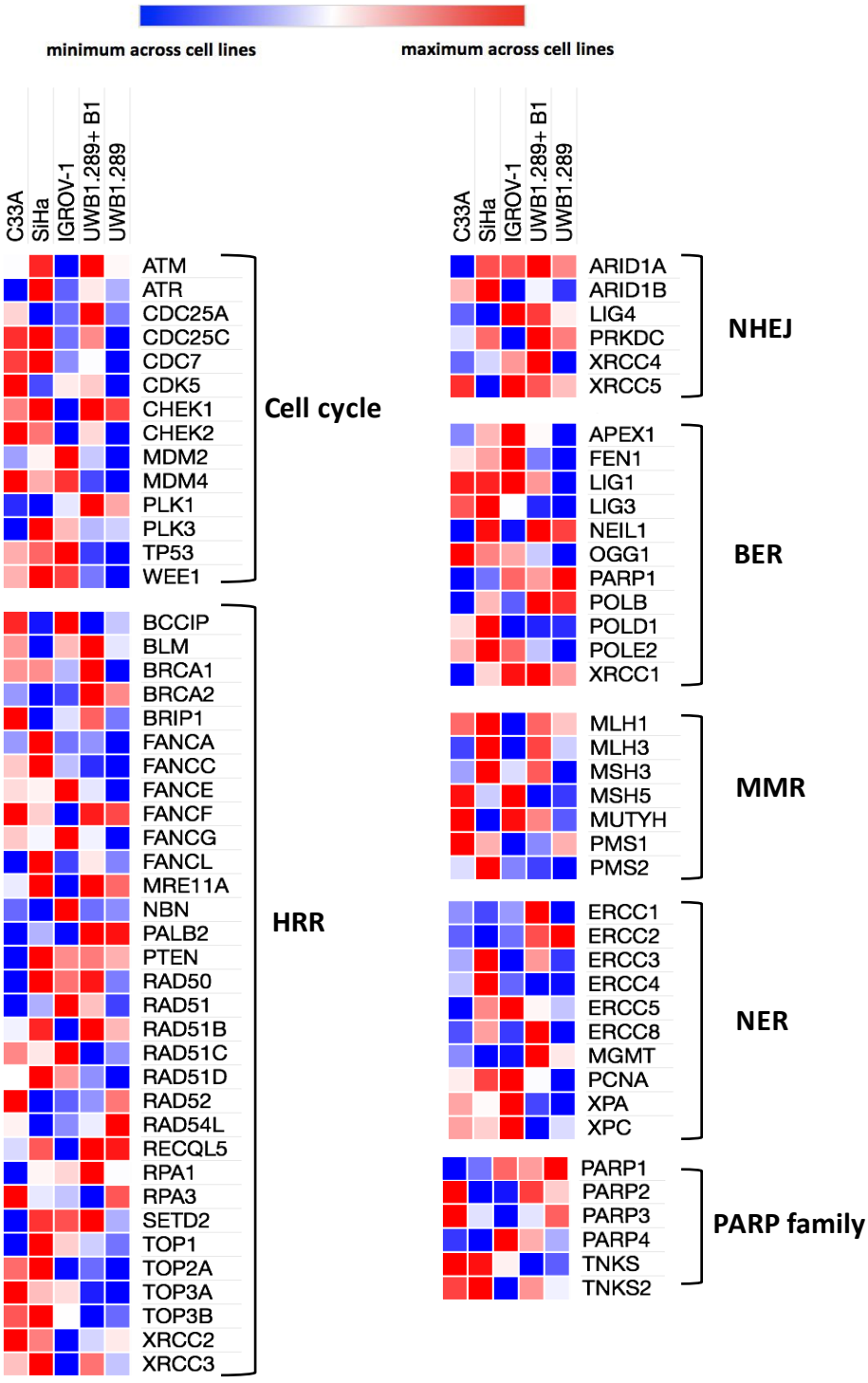


Figure 3.2: Baseline mRNA expression across human cell lines within the panel. Cells were sequenced using HTG NextGen sequencing as part of the Oncology biomarker panel, as described in Chapter 2, Table 1. Data are normalised values from a single experiment, where expression within cells was normalised by: Log_2(CPM). Data was converted into the heat map shown here using Morpheus software (http://software.broadinstitute.org/morpheus), to visualise the range of mRNA expression across cells.

3.5.3 Expression of previously identified determinants to PARP, ATR, CHK1 and WEE1 inhibition by protein expression

Basal expression of 11 key DDR proteins was measured by western blotting. These proteins were selected on the basis of previously being identified as a range of determinants of sensitivity to ATR, CHK1 and WEE1 inhibition, with the inclusion of cyclin E and pRPA Ser4/8, as markers of replication stress in cells (Figure 3.3).

Across human cell lines (C33A, SiHa, IGROV-1, UWB1.289+ B1 and UWB1.289 cells), PARP-1 expression varied 2.0-fold, with the highest expression observed in cervical SiHa cells and lowest in HRD UWB1.289 cells. PARP-1 expression was 8-fold lower in hamster cells (V-C8.B2, V-C8, AA8 and EM9 cells) than human cells (C33A, SiHa, IGROV-1, UWB1.289+ B1 and UWB1.289 cells) (Mann-Whitney, $p < 0.0001$), possibly due to differences in binding affinity of the antibody between species. Within matched hamster AA8 and EM9 cells, XRCC1 defective EM9 cells had 2-fold lower PARP-1 expression than XRCC1 proficient AA8 cells. ATR expression varied 1.9-fold across human cells, with the expression being the highest in cervical SiHa cells and lowest in cervical C33A cells. CHK1 expression varied 3.2-fold across human cells, with the highest expression observed in cervical C33A cells and lowest in IGROV-1 cells. Similarly, the highest expression of WEE1 was observed in C33A cells, with this varying 2.3 -fold across human cells and being lowest in UWB1.289 cells. CDK1 expression varied 1.8-fold, with the highest expression in UWB1.289+ B1 cells and lowest in C33A cells.

Other proteins were selected on the basis of previously being reported as potential determinants of sensitivity to PARP, ATR, CHK1 or WEE1 inhibition. Included in this panel was ATM, which varied 2.6-fold across human cells, with the expression being highest in SiHa cells and lowest in UWB1.289 cells. BRCA1 expression varied 2.3-fold, with this expression highest in SiHa cells and lowest in HRD UWB1.289 cells, and second lowest in UWB1.289+ B1 cells. RAD51 varied 2.8-fold and was highest in IGROV-1 cells and lowest in SiHa cells. XRCC1 varied 1.7-fold with the highest expression in SiHa cells and lowest in UWB1.289+ B1 cells. As expected, XRCC1 defective EM9 cells had 5.7-fold less expression of XRCC1, than matched AA8 XRCC1 competent cells.

Cyclin E and pRPA $^{Ser4/8}$ were assessed as indicators of RS in cells. Across human cells cyclin E varied 2.1-fold with the expression being highest in ovarian IGROV-1 cells and interestingly lowest in HRD UWB1.289 cells. pRPA $^{Ser4/8}$ expression varied 2.0-fold across cells and was highest in HRD UWB1.289 cells and lowest in C33A cells.

Unexpectedly, despite their known *BRCA1* mutation, HRD UWB1.289 cells had similar expression levels of BRCA1 to matched HRC UWB1.289+ B1 cells. The pair of cell lines had the lowest expression of BRCA1, compared to the other cell lines tested. This observation with these same cells was similarly observed in Western blot experiments performed by Alice Bradbury, where it was confirmed that the antibody used here targets a recombinant fragment of BRCA1 relating to C-terminal amino acids 1661-1863, and the mutation in UWB1.289 cells is a frameshift mutation at D825fs, i.e., before the sequence detected by the BRCA1 antibody. These data suggest the antibody is not specific to BRCA1.

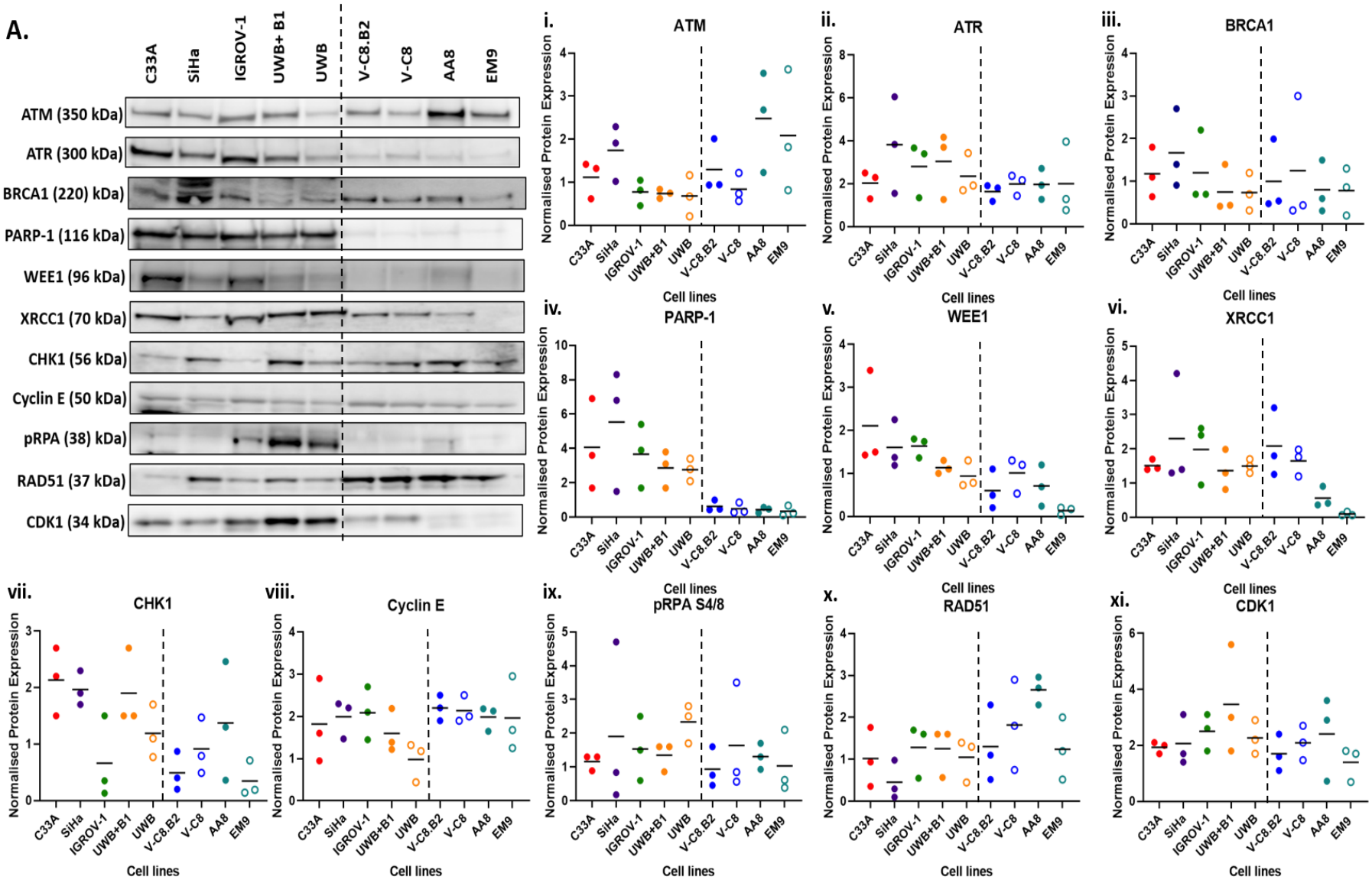

A.
C33A
SiHa
IGROV-1
UWB+ B1
UWB
V-C8.B2
V-C8
AA8
EM9
ATM (350 kDa)
ATR (300 kDa)
BRCA1 (220) kDa)
PARP-1 (116 kDa)
WEE1 (96 kDa)
XRCC1 (70 kDa)
CHK1 (56 kDa)
Cyclin E (50 kDa)
pRPA (38) kDa)
RAD51 (37 kDa)
CDK1 (34 kDa)
i. ATM
ii. ATR
iii. BRCA1
iv. PARP-1
v. WEE1
vi. XRCC1
vii. CHK1
viii. Cyclin E
ix. pRPA S4/8
x. RAD51
xi. CDK1
Normalised Protein Expression
Cell lines

Figure 3.3: Baseline protein expression of key DDR proteins across cell lines. A. Cells were seeded and growing exponentially prior to being lysed. Image is a representative of 3 individual experiments. Protein levels of **i.** ATM, **ii**. ATR, **iii.** BRCA1, **iv.** PARP-1, **v.** WEE1, **vi.** XRCC1, **vii.** CHK1, **viii.** Cyclin E, **ix.** pRPA Ser 4/8, **x.** RAD51 and **xi.** CDK1 were quantified using chemiluminescence and each band was normalised to Ponceau S stain of the corresponding lane to each cell line. This arbitrary unit was plotted. Each data point on the scatter plot represents an individual experiment, with mean bar shown. In each of the graphs hamster cells are separated from human cell lines with a dashed line.

3.5.4 Correlation of protein expression and mRNA expression

Protein and mRNA expression were compared to determine the degree by which mRNA expression of the gene (by HTG diagnostics) and protein expression (by western blotting) correlated and if this varied between genes/proteins (Figure 3.4).

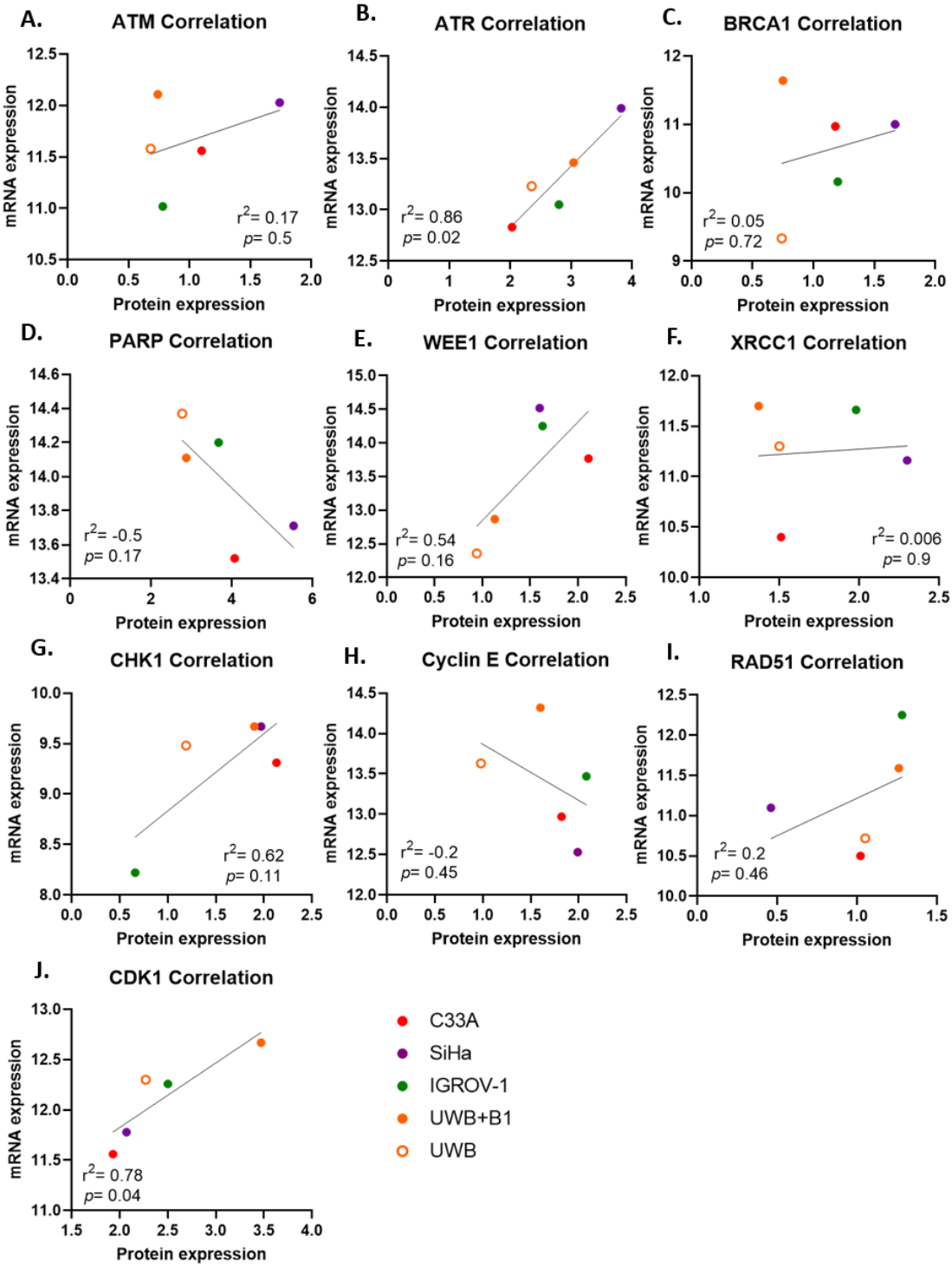


Figure 3.4: Correlation between mRNA expression and protein expression.
Correlations were calculated by Pearson's correlation co-efficient (r) using Graphpad Prism 9.0 for **A.** ATM, **B.** ATR, **C.** BRCA1, **D.** PARP-1, **E.** WEE1, **F.** XRCC1, **G.** CHK1, **H.** Cyclin E, **I.** RAD51 and **J.** CDK1. Each data point represents the normalised mRNA expression from one experiment and the mean protein expression from 3 individual western blots.

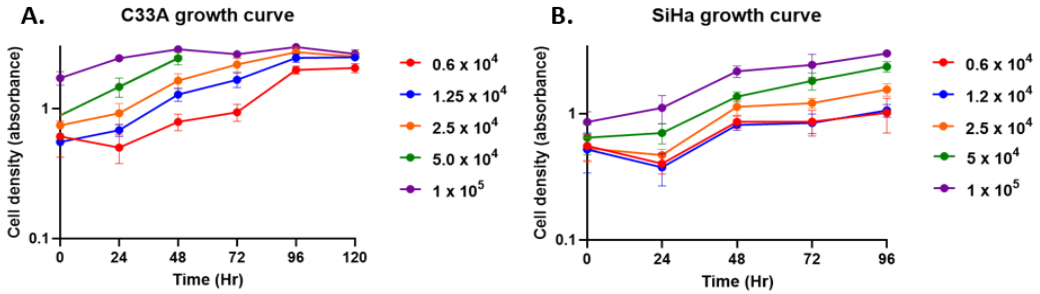
As expected, there were mostly positive correlations between mRNA expression and protein expression. Due to the small number of human cell lines tested it was difficult to class these correlations as statistically significant. The strongest correlations were observed with ATR (r^2= 0.86), CDK1 (r^2= 0.78), CHK1 (r^2= 0.62) and WEE1 (r^2= 0.54). However, of these, only ATR and CDK1 were statistically significant (p= 0.02 and p= 0.04, respectively). Weaker correlations were observed with ATM and RAD51 (both r^2= 0.2) and there was no trend with BRCA1, possibly reflecting the lack of antibody specificity, or XRCC1 (r^2= 0.05 and r^2= 0.006, respectively). Curiously, PARP-1 (r^2= -0.5) and Cyclin E (r^2= -0.2) were negatively correlated.

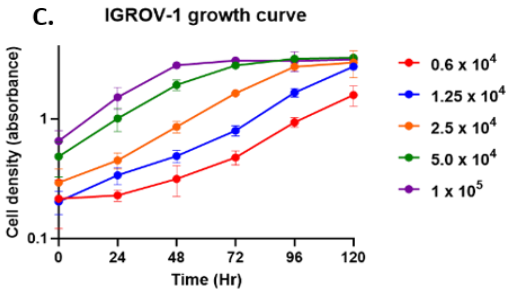
3.5.5 Growth characteristics and cloning efficiency of cell lines

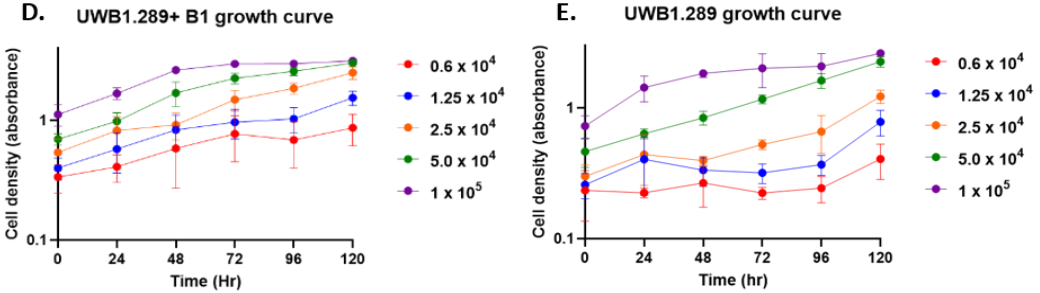
The growth characteristics and cloning efficiency of cells was established prior to cytotoxicity experiments. This was necessary to determine if any observed differential sensitivity of cells to inhibitors is due to cell cycle checkpoint inhibitors being more cytotoxic in rapidly dividing cells. The calculation of cloning efficiencies of cells was required for establishing optimal seeding densities for future cytotoxicity experiments.

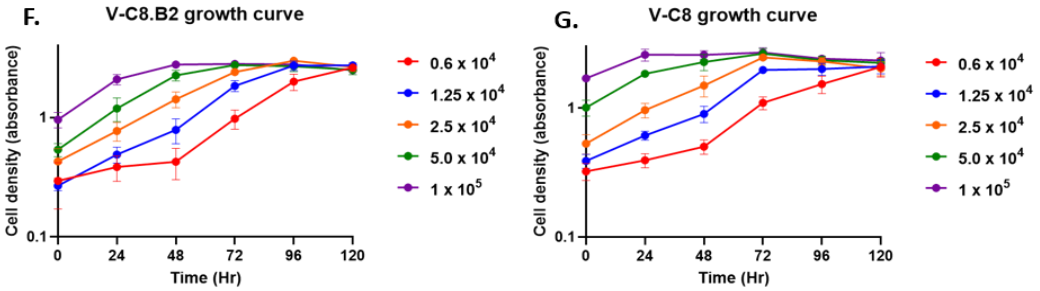
When considering the whole panel of cells, the growth of hamster cells was approximately 2-fold faster than human cells. Correction of DNA repair defect (*BRCA2* and *XRCC1*) in V-C8.B2 and AA8 hamster cells resulted in faster growth (24 vs 21 hours and 24 vs 22 hours, respectively). However, in human UWB1.289 cells corrected with *BRCA1* this effect was less notable.

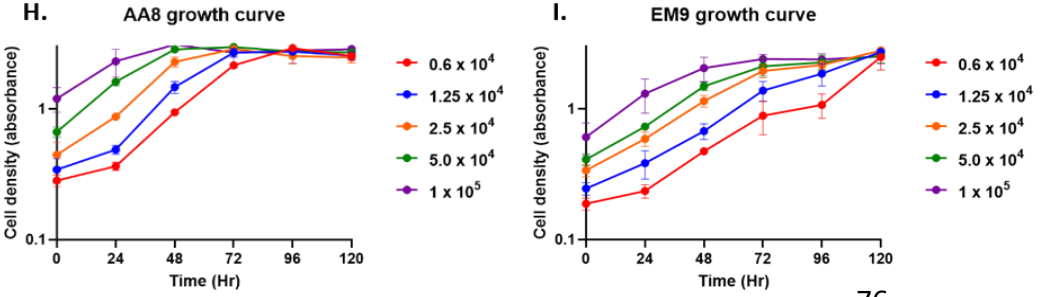
Cloning efficiency varied 5.4-fold across the whole cell line panel. With human repair-competent cells cloning efficiency was 40 to 50% and this was reduced by approximately 50% in *BRCA1* defective UWB1.289 cells. Similarly, DNA repair defective hamster cells had less capacity to form colonies compared to their corrected counterpart, which was similarly reduced by approximately 60 to 70% in repair defective V-C8 and EM9 cells compared to corrected cells.











J.

Cell line	Mean doubling time ± S.D (hours)	Mean cloning efficiency ± S.D (%)
C33A	42.6, 32.7	49.2 ± 5.9
SiHa	47.0 ± 9.2	42.0 ± 6.5
IGROV-1	29.3, 31.7	47.9 ± 4.4
UWB1.289+ B1	56.0, 54.7	38.8 ± 5.5
UWB1.289	52.1, 50.3	22.2 ± 10.6
V-C8.B2	25.6, 19.3	65.0 ± 8.5
V-C8	21.2, 26	26.5 ± 17.0
AA8	21.7 ± 1.9	35.2 ± 20.3
EM9	23.4, 24.8	12.1 ± 7.0

Figure 3.5: Growth characteristics of cell lines. Growth rate of **A.** C33A, **B.** SiHa, **C.** IGROV-1, **D.** UWB1.289+ B1, **E.** UWB1.289, **F.** V-C8.B2, **G.** V-C8, **H.** AA8 and **I.** EM9 cells was assessed by SRB cell proliferation assays described in Chapter 2. Cells were seeded at various densities across 4-5 days. **J.** Doubling time was calculated using the exponentially growing cells with Graphpad Prism software and graphs are representative of a minimum of 2 individual experiments. Cloning efficiency (%) was calculated as: (colonies counted/ number of cells seeded) x 100 and the mean value ± standard deviation reported is from a minimum of 3 individual experiments.

3.5.6 Measuring baseline RS of cells by γH2AX and RPA foci formation

Basal RS was measured by γH2AX and phosphorylated RPA$^{Ser4/8}$ foci formation as previously described (Chapter 2, section 10.1).

Histone H2AX is phosphorylated rapidly at serine 139 at the site of DNA damage and blocked replication forks, making γH2AX foci formation an ideal marker for DNA damage and RS (Rogakou *et al.,* 1998, Heylmann and Kaina, 2016). As previously described (Chapter 1, section 7.2), RPA coats ss-DNA, arising from RS, protecting it from degradation and enabling recruitment of ATR (Thada *et al.,* 2019). Phosphorylation of RPA at serine 4/8 is key in the response to replication stress and is responsible for the regulation of replication fork restart and new origin firing (Ashley *et al.,* 2014).

γH2AX and pRPA 32 $^{Ser4/8}$ foci varied 3.7 and 3.3-fold across repair competent cells (Figure 3.6). C33A had the lowest γH2AX foci levels per cell (1.5 ± 1.6), whilst IGROV-1 cells had the highest (5.5 ± 3.0), excluding HRR and BER defective UWB1.289, V-C8 and EM9 cells. V-C8.B2 cells had the lowest number of pRPA 32 $^{Ser4/8}$ foci per cell (3.9 ± 1.7) and similarly to γH2AX, IGROV-1 cells had the highest number of pRPA 32 $^{Ser4/8}$ foci per cell (12.9 ± 9.8), across repair competent cell lines. HRR defective UWB1.289 and V-C8 cells and XRCC1 defective EM9 cells had significantly higher levels of both γH2AX (4.8, 8.3 and 4.4-fold, respectively) and pRPA 32 $^{Ser4/8}$ foci (6.1, 8.9 and 4.5-fold, respectively), compared to their matched competent cells.

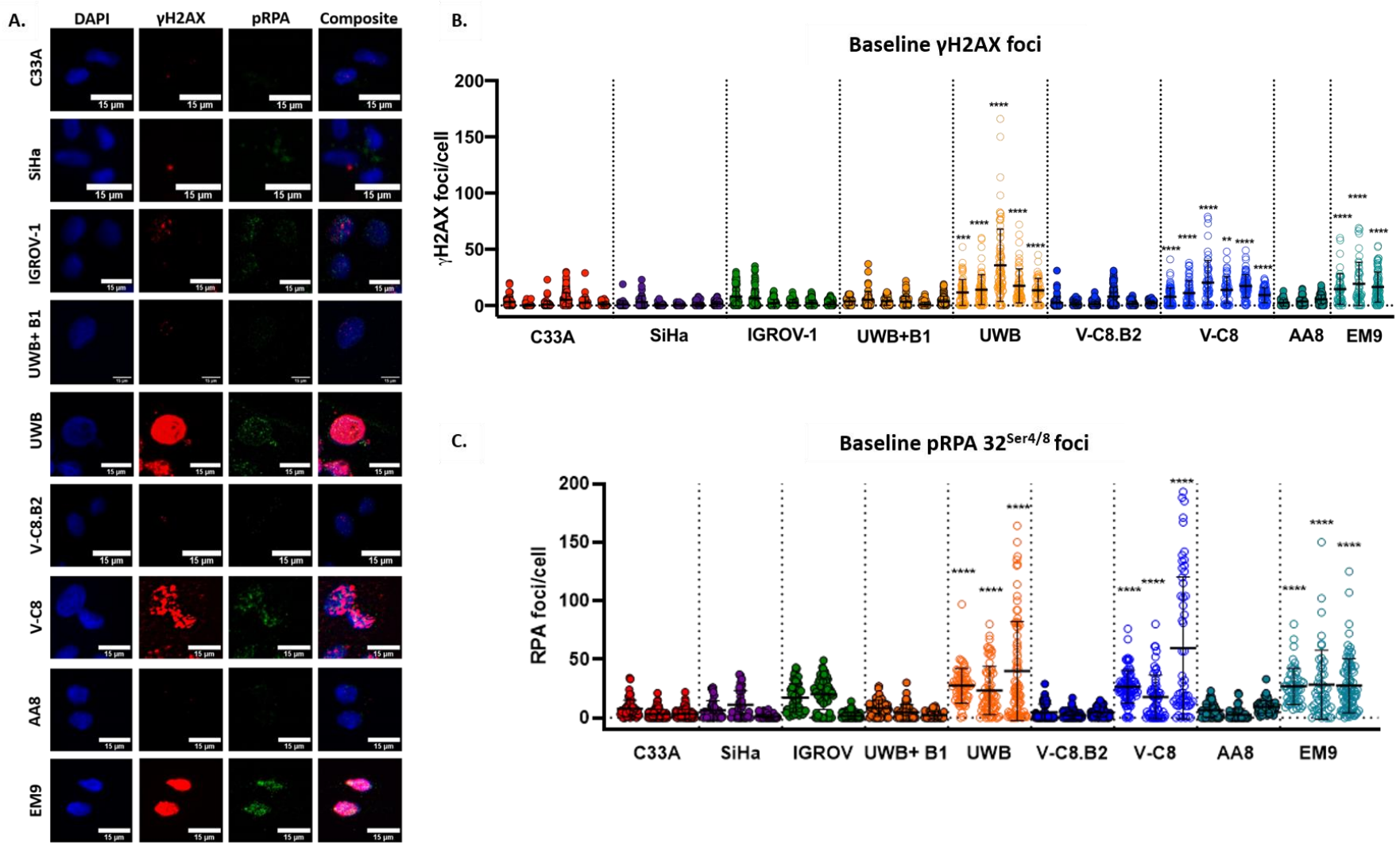

A.
DAPI
γH2AX
pRPA
Composite
C33A
SiHa
IGROV-1
UWB+ B1
UWB
V-C8.B2
V-C8
AA8
EM9
15 μm
B.
Baseline γH2AX foci
γH2AX foci/cell
200
150
100
50
0
C33A
SiHa
IGROV-1
UWB+B1
UWB
V-C8.B2
V-C8
AA8
EM9
C.
Baseline pRPA 32Ser4/8 foci
RPA foci/cell
200
150
100
50
0
C33A
SiHa
IGROV
UWB+ B1
UWB
V-C8.B2
V-C8
AA8
EM9

Figure 3.6: Baseline replication stress across cell lines. γH2AX and pRPA 32 $^{Ser4/8}$ foci were measured by immunofluorescence as previously described. **A.** Images are representative of one experiment. A minimum of three independent experiments were plotted showing **B.** γH2AX foci per cell and **C.** pRPA 32 $^{Ser4/8}$ foci per untreated cell. Unpaired t-tests were performed between matched cells that were imaged as part of the same experiment, to compare differences between matched cells using Graphpad Prism 9.0 software,

The 2 measures of RS correlated well across human repair-competent cells, excluding the correlation being biased by repair defective cells (r^2= 0.5, p=0.3), even considering the limited cell lines tested here (Figure 3.7). As hypothesised the UWB1.289, V-C8 and EM9 repair defective cells had much higher levels of both γH2AX and pRPA$^{Ser4/8}$ foci levels compared to competent matched cells (4.4 to 8.2-fold and 4.5 to 8.9-fold, respectively).

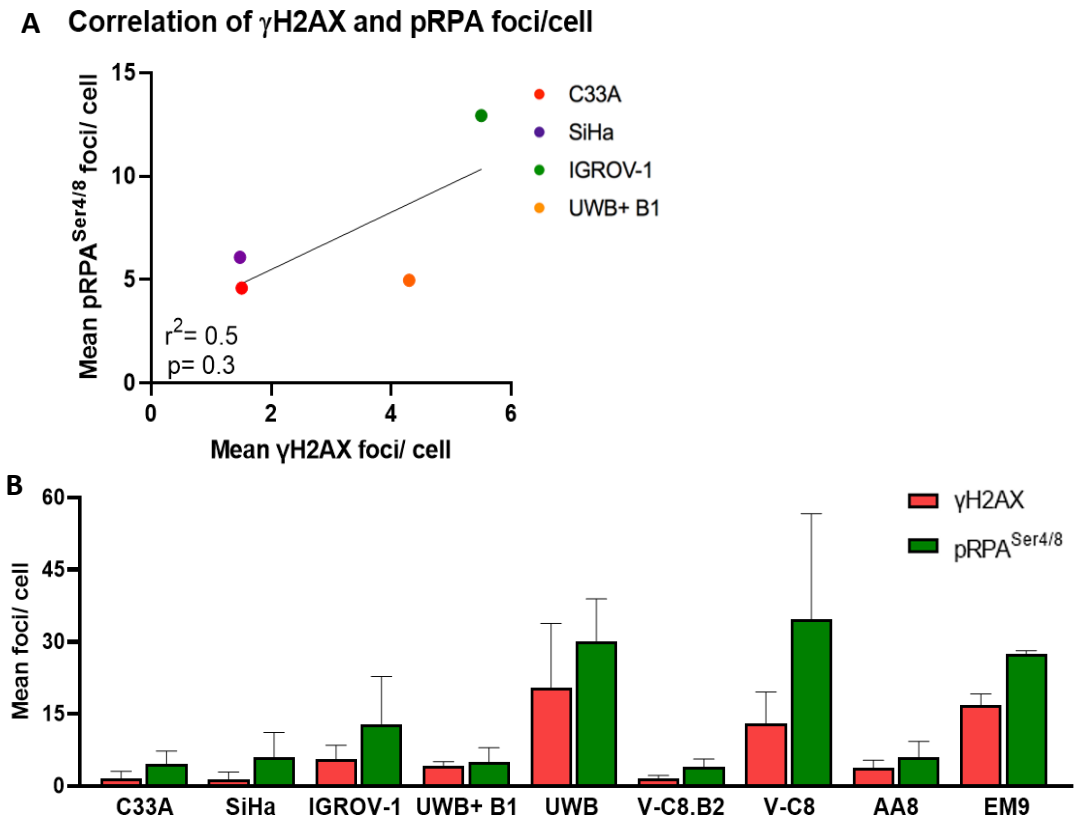


Figure 3.7: Correlation of mean γH2AX foci per cell vs mean pRPA 32 $^{Ser4/8}$ per cell across cell lines. A. Correlation was calculated by Pearson's correlation co-efficient (r) using Graphpad Prism 9.0. The mean γH2AX foci/untreated cell was plotted against the mean pRPA $^{Ser4/8}$ foci/untreated cell over 3 individual experiments in human repair-competent cells. **B.** The mean ± S.D was plotted of mean γH2AX foci (red bar) and pRPA$^{Ser4/8}$ (green bar) across all cell lines.

The two measures of RS by expression (measured by Western blot), cyclin E and pRPA $^{Ser4/8}$, were plotted against immunofluorescence measures of RS, γH2AX and pRPA$^{Ser4/8}$ foci formation, to assess any correlations (Figure 3.8). The number of γH2AX and even pRPA foci/cell was poorly correlated with the pRPA levels by western blot (r^2= 0.01 and 0.1, respectively). Unexpectedly, cyclin E did not correlate with γH2AX foci per cell (r^2=0.004), but did moderately correlate with pRPA$^{Ser4/8}$ foci, although this was not significant, and was only measured across 4 cell lines (r^2= 0.5, p=0.3).

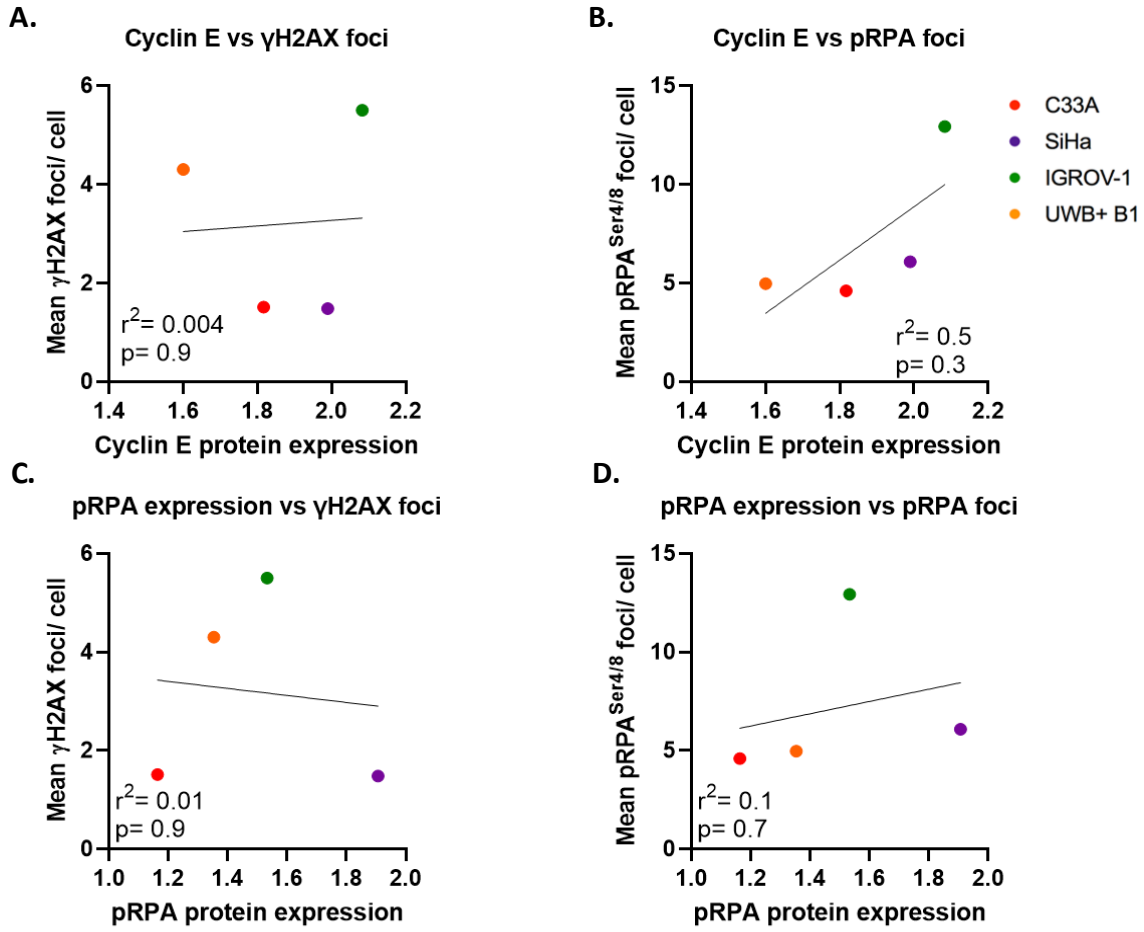


Figure 3.8: Correlation of protein expression of Cyclin E and pRPA$^{Ser4/8}$ vs. γH2AX and pRPA $^{Ser4/8}$ foci formation. The mean normalised protein expression of Cyclin E (arbitrary units) was plotted against **A.** mean γH2AX foci or **B.** mean pRPA$^{Ser4/8}$ foci per untreated cell in repair-competent human cells. Mean normalised protein expression of pRPA (arbitrary units) was plotted against **C.** mean γH2AX foci or **D.** pRPA$^{Ser4/8}$ foci per untreated cell in repair-competent cells human cells. Correlations were calculated using Graphpad Prism 9.0.

It was predicted there would be a negative correlation between the doubling time of cells and markers of RS (Figure 3.9). There was a strong negative correlation observed between cyclin E expression and cell doubling time (r^2= -0.7), although this was non-significant. No correlation was observed between cell doubling time and pRPA expression by western blot or γH2AX foci measured by IF (r^2= 0.0 and -0.1, respectively). There was however a strong negative correlation between cell doubling time and pRPA$^{Ser4/8}$ foci by IF (r^2= -0.7), although again this was not significant (p=0.1). However, the low number of cell lines tested are an important consideration when assessing these trends.

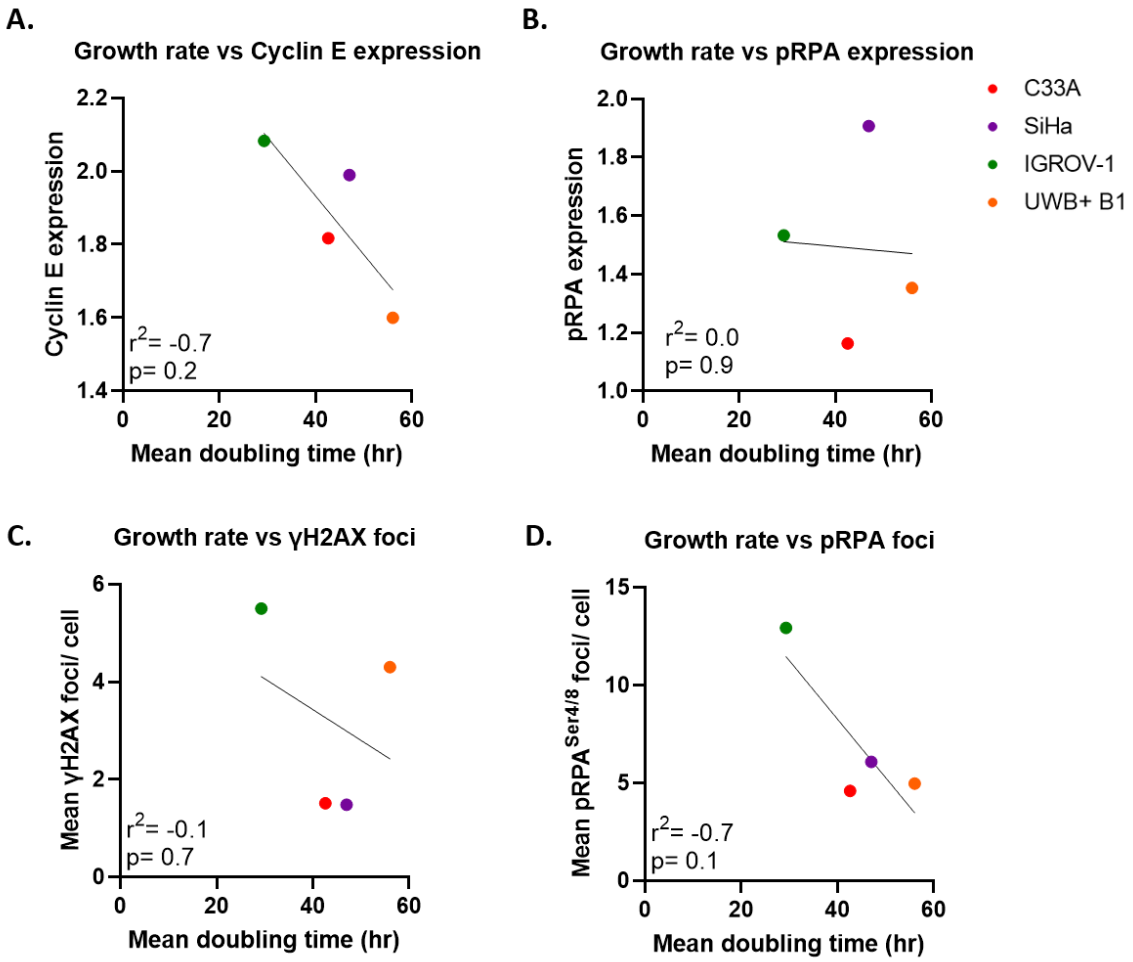


Figure 3.9: Correlation of doubling time of cells vs. markers of RS. The mean doubling time of human repair-competent cells vs. the expression of **(A)** cyclin E and **(B)** pRPA$^{Ser4/8}$, as measured by western blotting. Mean doubling time of cells was also plotted against measures of RS by IF **(C)** mean γH2AX foci or **(D)** pRPA$^{Ser4/8}$ foci per untreated cell in repair-competent human cells. Correlations were calculated using Graphpad Prism 9.0.

3.6 Discussion

The characterisation of these cell lines was essential before further experimentation to assist in determining length of drug exposures, as well as seeding densities for cytotoxicity experiments. Basal expression of key DDR genes and proteins, as well as basal RS was determined so that correlations between these measures and sensitivity to inhibitors as single agents and their synergy could be made.

IGROV-1 cells had the most homozygous and heterozygous mutations (2 homozygous, 30 heterozygous) across the key DDR genes analysed from data available on the CCLE. A study by Domcke *et al.,* compared mutation frequency and degree of copy number alterations (CNA) across a panel of ovarian cancer cell lines and identified IGROV-1 cells as a hypermutated cell line, suggesting that although IGROV-1 cells are regarded as HGSOC, at a genomic level they more closely resemble endometrioid carcinoma cells (Domcke *et al.,* 2013). A key contributor to this hypermutation status could be the homozygous mutation identified here in key MMR gene *MLH1*. Notably, IGROV-1 cells had the highest γH2AX and pRPA 32 $^{Ser4/8}$ foci across repair-competent cells.

mRNA expression and protein expression were compared and correlated across cell lines. Of the 10 proteins examined, only ATR and CDK1 had a significant correlation between basal mRNA expression and basal protein expression (r^2= 0.86, p=0.02 and r^2= 0.78, p=0.04, respectively). mRNA expression alone has been shown to be a poor indicator across most genes in predicting protein expression levels (Koussounadis et al, 2015, Liu *et al.,* 2016). Studies have shown that mRNAs are produced at a much slower rate than proteins are in mammalian cells, suggesting protein turnover rates may be responsible for a lack of correlation between mRNA and protein expression, and inevitably this varies across proteins (Schwanhäusser et al., 2011). Another important consideration is that when correlating only 5 data points, it is possible that a single data point can skew the data and overestimate the strength of correlation. Similarly, the semi-quantitative nature of Western blots may contribute to this discrepancy in correlations across genes/proteins.

The mRNA levels of *BRCA1* were lower in UWB1.289 cells but no correlation was observed between mRNA expression and protein expression which may be due to the suspected lack of specificity of the antibody. DelloRusso *et al.,* characterised UWB1.289 paired cells and found no expression of BRCA1 in UWB1.289 cells and high expression in *BRCA1* corrected UWB1.289+ B1 cells (DelloRusso *et al.,* 2007) using a different BRCA1 antibody (Anti-BRCA1 (AB-1) Mouse mAb (MS110 clone)). Previous studies using the antibody (Ab191042) used in the study presented here, did not detect any BRCA1 in *BRCA1* knock-out cells, compared to control cells (Hamam *et al.,* 2016), although this antibody has only been reported in 9 publications. The observation here and in previous studied by Alice Bradbury, using the same cells and antibodies, may suggest the antibody is not very specific to its target.

Expression of pRPA $^{Ser\,4/8}$ and cyclin E were measured by western blot as high expression of these are considered synonymous with RS. Overexpression of cyclin E expression has been shown to increase sensitivity to ATRi (VE-822) and WEE1i (MK-1775) (Llobet *et al.,* 2020).

Cyclin E expression was similar between human cells, and unexpectedly HRD UWB1.289 cells had 1.6-fold lower expression than UWB1.289+ B1 cells. UWB1.289+ B1 cells have previously been reported to have higher cyclin E protein expression of than UWB1.289 (Wilson *et al.,* 2016), whereas UWB1.289 cells had lower cyclin E expression here. Although *CCNE1* is frequently amplified in cancer cells, the correlation between cyclin E protein expression and *CCNE1* gene amplification has shown to be poor (Aziz *et al.,* 2021).

A positive correlation was observed between cyclin E expression and pRPA$^{Ser4/8}$ foci formation (r^2= 0.5), although this was not observed with γH2AX (r^2= 0.004), despite this being previously reported (Llobet *et al.,* 2020). There was no correlation between pRPA$^{Ser4/8}$ expression by western blot and both γH2AX and pRPA$^{Ser4/8}$ foci levels, when considering repair-competent cells. This suggests focus formation of specific RS markers is a more sensitive measure of RS than expression by western blot. In view of the good correlation between γH2AX and RPA foci and both having been used as measures of RS

in subsequent chapters γH2AX foci alone were used as a measure of RS, although it is important to note γH2AX is also a marker of DNA damage.

Although the panel of cells and the differences between them is limited, the use of matched cells will be advantageous in investigating the main hypotheses of the study. The attributes of cell lines determined in this chapter will further determine the way results of future experiments in the study are interpreted and will give a better insight into the molecular characteristics influencing the cellular response to the PARP and kinase inhibitors used throughout the study.

Chapter 4. Determining target inhibition and cytotoxicity of rucaparib on panel of cell lines

4.1 Introduction

PARP is a fundamental component of the DNA damage response and the first line of defence against the commonest endogenously induced DNA damage, ROS-induced SSBs. It acts by promoting DNA base excision repair (BER)/ single-strand break repair (SSBR), as previously described (Chapter 1, section 9.1) (Dantzer *et al.,* 1999). Rucaparib, like all PARPi, acts by inhibiting the repair of SSBs which, in turn, will collide with the replication fork resulting in lesions that can only be resolved by HRR. These replication lesions caused by PARPi will signal to ATR, CHK1 and WEE1 as previously described in Chapter 1. This increased reliance on HRR following PARP inhibition underpins rucaparib exploitation of HRR defects in cancer cells to selectively kill them through synthetic lethality.

Pre-clinically there is some evidence to suggest that PARPi are more cytotoxic to cells with higher endogenous PAR levels in the absence of external stimuli (Nowsheen *et al.,* 2011, Oplustilova *et al.,* 2012). There is some suggestion that HRD cells upregulate PARP to compensate for their loss of HRR function (Gottipati *et al.,* 2010). However, clinical studies suggest PARP activity and endogenous PAR levels are not a predictor of sensitivity to PARPi (Veskimae *et al.,* 2016, Herriott *et al.,* 2015).

It was important here to establish single agent activity of rucaparib, as well as considering how the extent of PARP activity inhibition and PARPi cytotoxicity relates to the cell line characteristics previously described (Chapter 3). Given the RS caused by PARPi and how this signals to ATR, CHK1 and WEE1, it was important to assess signalling to the cascade in rucaparib-treated cells, to determine whether activation of each kinase is equivalent, which may have implications for combination cytotoxicity studies (Chapter 6).

4.2 Aims and Objectives

The main aims of this chapter are:

- To determine endogenous PAR levels, optimum PARP activity and the extent of PARP inhibition by rucaparib among cell lines and how these correlate with characteristics determined previously (Chapter 3)

- To determine single agent cytotoxicity of rucaparib by colony formation assays

- Determine effect of PARPi on phosphorylation events associated with activation of ATR, CHK1 and WEE1 via Western blot

4.3 Hypotheses

1. Endogenous PAR and baseline PARP activity will be higher in HRR defective cells due to failure to repair endogenous damage by HRR

2. Rucaparib-induced accumulation of SSBs will result in stalled replication forks and RS, which will in turn activate ATR-CHK1 pathway signalling in all cell lines, particularly in HRD cells as these cells have higher basal RS levels (determined in Chapter 3)

4.4 Materials and Methods

4.4.1 PARP activity assay

To measure optimum PARP activity, a biochemical GCLP-validated assay was used in which a 12 mer palindromic double stranded oligonucleotide activates the enzyme in the presence of 350 nM NAD+ as described previously (Chapter 2, section 11). To measure basal levels of PARP activity endogenous PAR levels were measured without exogenous NAD+ and oligonucleotide with 100- 1000-fold more cells needed in the reaction to detect the low levels in unstressed cells.

4.4.2 Single agent cytotoxicity of rucaparib

Cytotoxicity experiments were performed as described in Chapter 2, section 9. The concentration range of 0- 30 µM rucaparib was selected for all HRC cell lines (C33A, SiHa, IGROV-1, UWB1.289+B1, V-C8.B2) and UWB1.289 cells, whilst a lower concentration range of 0- 0.1 µM was used for V-C8 cells. These concentrations were selected based on previous data obtained from members of the DDR group.

4.4.3 Assessing PARPi-induced RS by γH2AX foci formation

Immunofluorescence assays were performed as previously described (Chapter 2, section 10). Exponentially growing C33A, SiHa, IGROV-1, UWB1.289+B1, UWB1.289, V-C8.B2 and V-C8 cells were seeded onto coverslips and incubated for 24 h before being exposed to either DMSO or 10 µM rucaparib for 24 h. Cells were then fixed, prior to antibody staining with γH2AX, imaging and analysis, as previously described.

4.4.4 Determining activation of ATR-CHK1 pathway by Western blot

Activation of ATR, CHK1 and WEE1 was determined by Western blot analysis of pCHK1 ^{S345}, pCHK1^{S296} and CDK1^{Tyr15}, respectively. Cells were treated with either DMSO or 10 µM rucaparib, then lysates were prepared and Western blotting was performed as described previously.

4.5 Results

4.5.1 Endogenous PAR across cell lines and optimum PARP activity in HRC and HRD matched cells

Optimum PARP activity was measured in HRD and HRC matched cells as it has been proposed that HRD cells would have higher PARP activity, to compensate for their lack of HRR function. When PARP was activated by an oligonucleotide mimicking broken DNA in the presence of excess NAD+, there was no significant difference in the activity of UWB1.289 and V-C8 cells (Figure 4.1). *BRCA1* mutant UWB1.289 cells had marginally higher PARP activity than their *BRCA1* corrected counterpart but *BRCA2* defective V-C8 cells had marginally lower PARP activity than their corrected V-C8.B2 counterpart, however neither difference was statistically significant.

Endogenous PAR levels reflect PARP activity in the unperturbed state. To test the hypothesis that HRD cells have higher basal PARP activity, either as a compensatory mechanism, or because of increased DNA damage (Chapter 3), PAR levels were measured in exponentially growing unstressed cells. Endogenous PAR levels were higher in UWB1.289 and V-C8 HRD cells, compared to their matched counterpart, (1.4 ± 0.5-fold, ns and 2.3 ± 0.9-fold, p=0.01, respectively) possibly indicating a higher level of DNA lesions. Interestingly, although endogenous PAR levels were higher in HRD cells compared to their matched HRC cells, HRC C33A, SiHa and IGROV-1 cells had higher endogenous PAR than UWB1.289 and V-C8 cells, suggesting other cellular characteristics also have a strong impact on endogenous PAR.

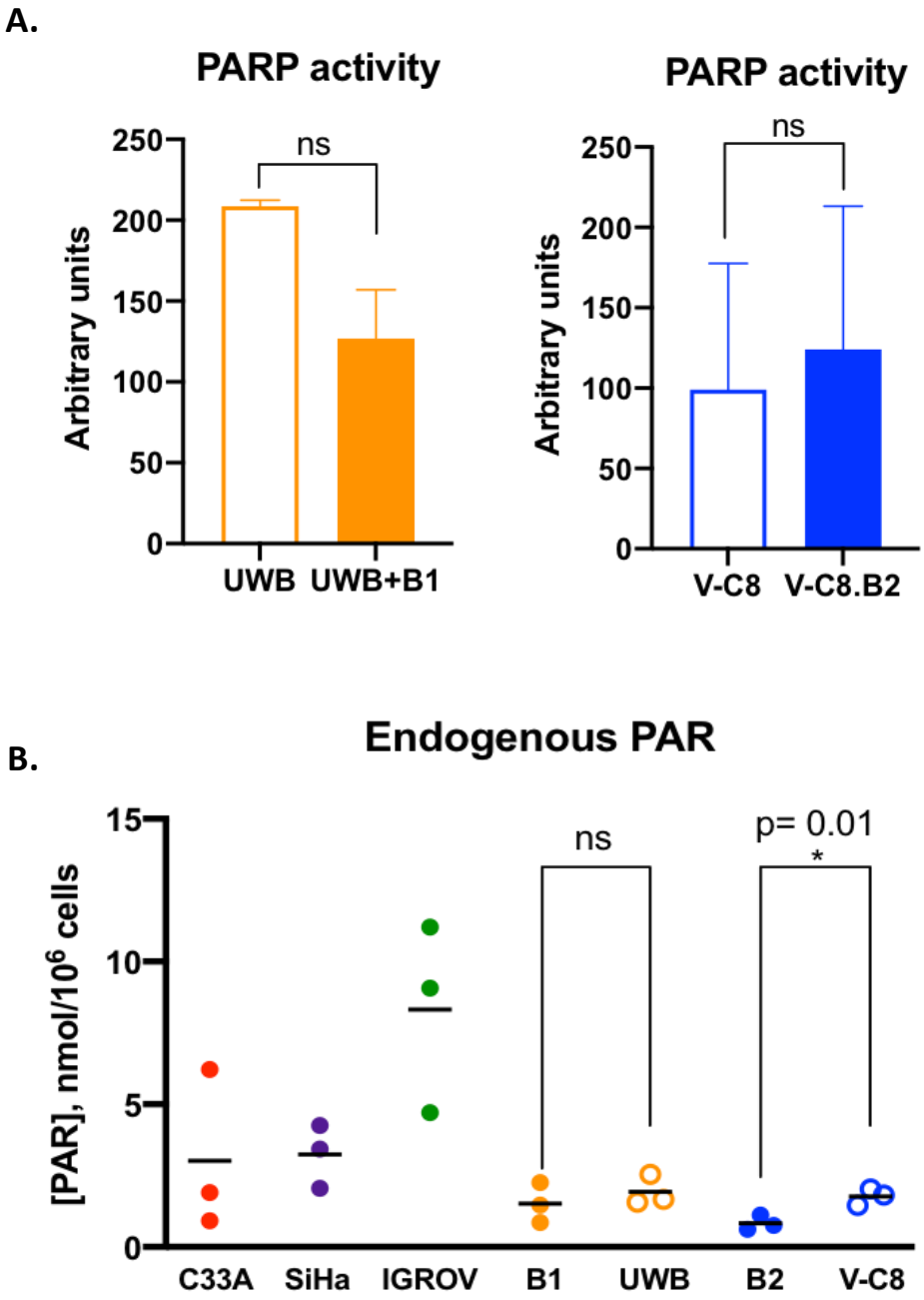
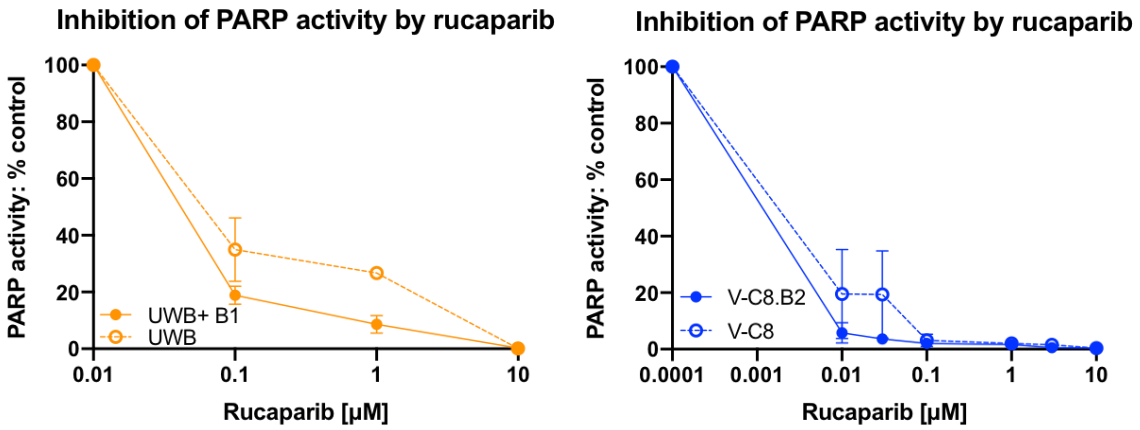


Figure 4.1: Baseline PARP activity and endogenous PAR across cell lines. A. PARP activity/ 10^6 cells was measured in untreated permeabilised cells in the presence of oligonucleotide and NAD+ by mean pixel chemiluminescence. Data are mean and standard deviation of 3 independent experiments. **B.** Endogenous PAR was determined in the absence of oligonucleotide and NAD+ with reference to a standard curve. Data points are individual experiments with mean bar shown. "B1" represents UWB1.289+ B1 cells, "UWB" represents UWB1.289 cells and "B2" represents V-C8.B2 cells.

4.5.2 Inhibition of PARP activity by rucaparib in HRC and HRD matched cells

To determine if rucaparib had a differential effect on PARP activity in the paired HRC and HRD cells, PARP activity was measured following exposure of cells to increasing concentrations of rucaparib.

A.



B.

	IC_{50} [nM]
UWB1.289 +B1	49.8 ± 1.8
UWB1.289	64.0 ± 13.4

	IC_{50} [nM]
V-C8.B2	4.1 ± 0.2
V-C8	5.0 ± 1.0

Figure 4.2: Inhibition of PARP activity in HRR defective and competent matched cells.
A. PARP activity (% control) following exposure to increasing concentrations of rucaparib for 1 h. **B.** IC_{50} values of rucaparib in matched cells. Data are mean and standard error of 3 independent experiments.

IC_{50} values within both pairs of matched cell lines were similar between HRD and HRC cells and inhibition of PARP activity by rucaparib did not significantly differ within each pair of matched cells. However, rucaparib was approximately 100x more potent against the hamster cells compared to the human cells. In UWB1.289 and UWB1.289+ B1 ~1 µM rucaparib was required to achieve >90% inhibition of PARP activity. This was similar to the >90% inhibition achieved with 1 µM rucaparib in IGROV-1 cells (Chapter 8). With V-C8 and V-C8.B2 cells exposure to 10 nM rucaparib inhibited PARP activity >90%.

4.5.3 Single agent cytotoxicity of rucaparib

The cytotoxicity of rucaparib was determined by colony formation assays in all cell lines. For combination studies it was essential to select a concentration that potently inhibited PARP activity but was not excessively cytotoxic (i.e., >50% cell kill).

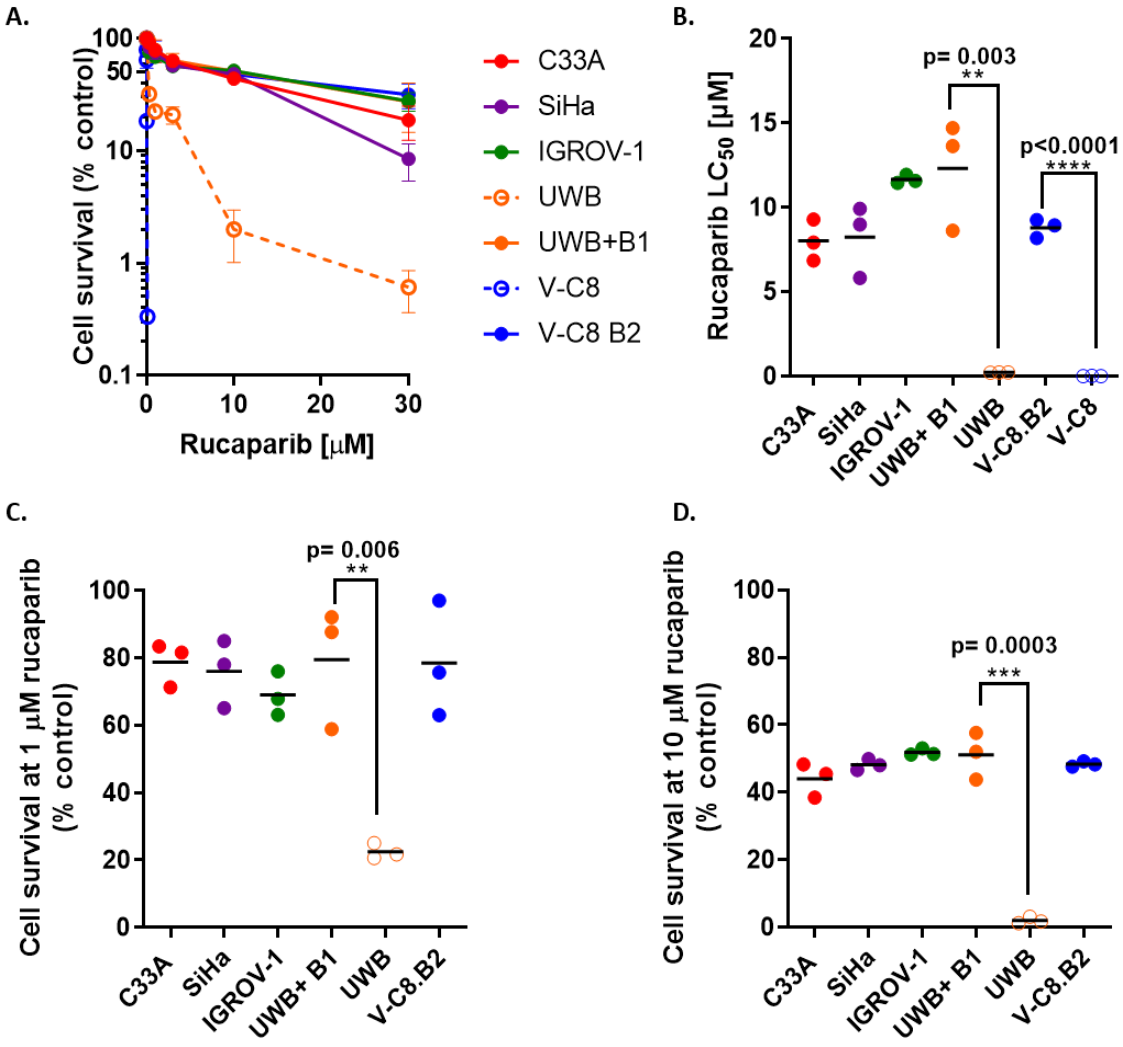


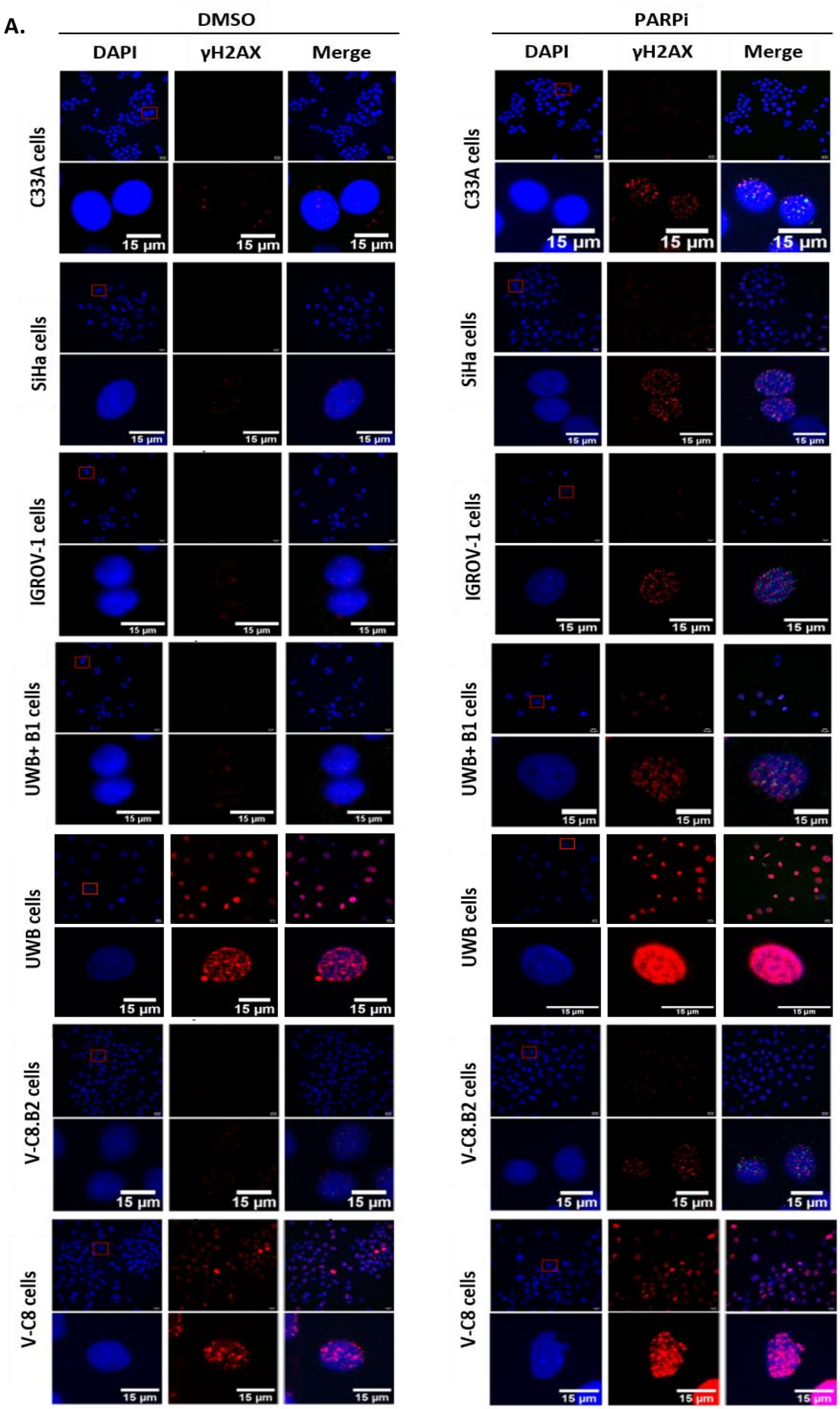
Figure 4.3: Single agent cytotoxicity of rucaparib across cell lines. A. Cells were exposed to rucaparib at indicated concentrations for 24 hr prior to replacement with drug-free medium for 8-10 days to allow colony formation. Data are the mean and SEM of 3 independent experiments. **B.** LC50 values were calculated from data in **A** using GraphPad Prism 8.0 software. To extend analyses of rucaparib sensitivity and separate cell lines further than observed with LC50 values, cell survival (% control) was reported across cell lines at a set concentration of **C.** 1 μM and **D.** 10 μM rucaparib. Data points are individual experiments with mean bar shown (**B, C, D**). Note rucaparib concentrations > 100 nM were not used in V-C8 cells

There was a narrow spectrum of sensitivity to rucaparib across the HRR competent cell lines tested (LC_{50}s: 8.0 µM- 12.3 µM), with cervical cancer cells (C33A and SiHa) being somewhat more sensitive to rucaparib than ovarian cell lines (UWB1.289+ B1 and IGROV-1), although this was not significant. As expected LC_{50} values for rucaparib in HRR defective UWB1.289 and V-C8 cells were 62 and >1000-fold lower than their HRR competent matched cells (p=0.003 and <0.0001), respectively. As previously described 0.1 µM rucaparib inhibited PARP activity >95% in both V-C8 and V-C8.B2 cells. However, a concentration of 0.1 µM rucaparib inhibited cell survival by 99.7% in V-C8 cells but had no significant impact (3.5% cell kill) in V-C8.B2 cells. Similarly, in UWB1.289 and UWB1.289+B1 cells 1 µM rucaparib inhibited PARP activity >75% in both cell lines, but inhibited cell survival 78% in UWB1.289 cells compared to only 21% in UWB1.289+B1 cells. Even at 10 µM rucaparib survival of HRC cells was around 50 %.

4.5.4 Rucaparib-induced RS across cell line panel

Endogenously generated SSBs are repaired continuously by PARP-dependent repair mechanisms. When PARP is inhibited, unrepaired SSBs collide with replication forks, causing them to stall and collapse. This causes RS, which, in turn, signals to the ATR signalling cascade as previously described (Chapter 1, figure 1.10). As there is cross-talk between ATR and ATM signalling cascades (section 1, figure 1.9), it is possible PARPi could also cause activation of ATM and therefore CHK2 also, which could subsequently be signalling to ATR and CHK1 (Aguilar-Quesada *et al.,* 2007). As shown in Chapter 3, γH2AX and $pRPA^{Ser4/8}$ foci correlated within cell lines as measures of RS (r^2= 0.9, p=0.0004), therefore here just γH2AX was used to measure the induction of RS by 10 µM rucaparib (Figure 4.4).

PARPi increased γH2AX significantly (3 to 10.6-fold) in all HRC cells. Although PARPi induced RS in HRD UWB1.289 and V-C8 cells this was mostly non-significant, most likely due to the 5 to 6-fold higher basal γH2AX focus levels in these cells measured in Chapter 3. SiHa cells had the highest increase of RS in response to rucaparib treatment, which was 2.7-fold fold higher than the mean induction across the other HRC cells in the panel.


A.
DMSO
PARPi
DAPI
γH2AX
Merge
C33A cells
SiHa cells
IGROV-1 cells
UWB+ B1 cells
UWB cells
V-C8.B2 cells
V-C8 cells
15 µm

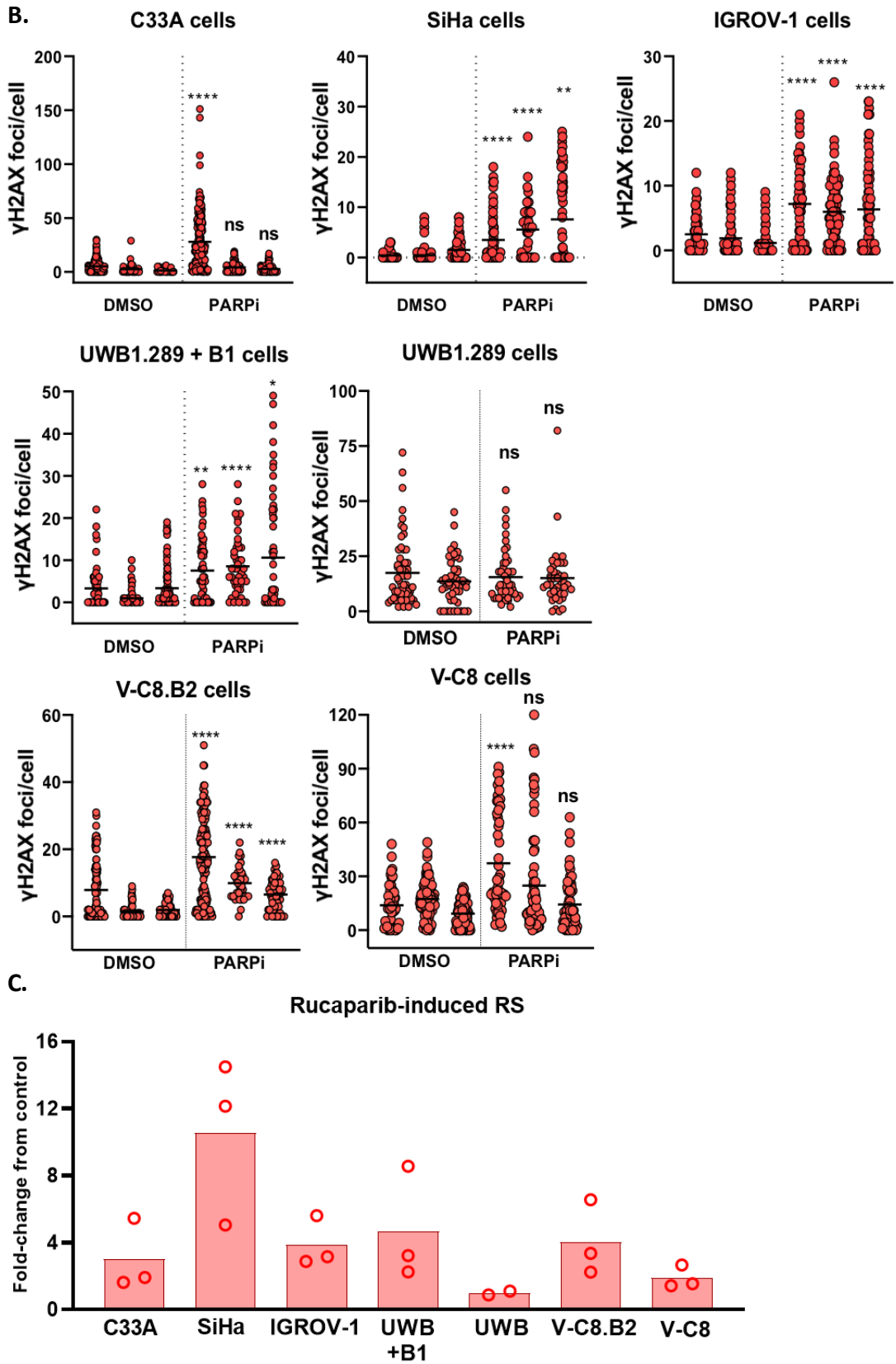

B.
C33A cells
SiHa cells
IGROV-1 cells
UWB1.289 + B1 cells
UWB1.289 cells
V-C8.B2 cells
V-C8 cells
γH2AX foci/cell
DMSO
PARPi
ns
C.
Rucaparib-induced RS
Fold-change from control
C33A
SiHa
IGROV-1
UWB +B1
UWB
V-C8.B2
V-C8

Figure 4.4: PARPi-induced RS. A. Induction of RS across cell lines by PARPi rucaparib, compared to DMSO control cells was measured by γH2AX foci formation with representative images shown. **B.** Data from 3 individual experiments (2 experiments in UWB1.289 cells) was plotted with mean bar from each experiment shown and unpaired t-tests performed using Graphpad prism 9.0 software (* p<0.05, ** p<0.01, ***p<0.001, **** p<0.0001). **C.** Mean fold-increase of γH2AX foci with 10 μM rucaparib across cell lines, with the mean bar shown.

This induction of RS caused by PARPi activates the ATR-CHK1 axis. Here, the signalling of rucaparib-induced RS to ATR, CHK1 and WEE1 was determined by Western blot analysis of phosphorylation targets: pCHK1^{S345}, pCHK1^{S296} and pCDK1^{Tyr15}. It is important to note here that whereas pCHK1^{S345}and pCHK1^{S296} are relatively specific indicators of ATR and CHK1, respectively, increased pCDK1^{Tyr15} results from a combination of direct phosphorylation by WEE1 combined with inhibition of CDC25C dephosphorylation resulting from CHK1 activation (Chapter 1, figure 10). MYT1 also phosphorylates CDK1 at tyrosine 15, which may further complicate the interpretation. The potentially different extent of activation of these kinases was determined as this may impact future combination cytotoxicity experiments.

Rucaparib (10 μM) increased levels of pCHK1^{S345}, pCHK1^{S296} and pCDK1^{Tyr15} in all cell lines. There was a similar induction of ATR and CHK1 upon treatment of rucaparib (1.4 to 4.4-fold), which was highest in the cervical C33A cells and lowest in hamster lung V-C8 cells. However, none of the cells were significantly different from each other due to the inherent inter-assay variability of Western blotting. Activation of ATR-CHK1 signalling was similar between HRC and HRD matched cells, suggesting HRR status did not have an impact. There was a much more modest increase in CDK1 phosphorylation, due to high levels in DMSO control cells.

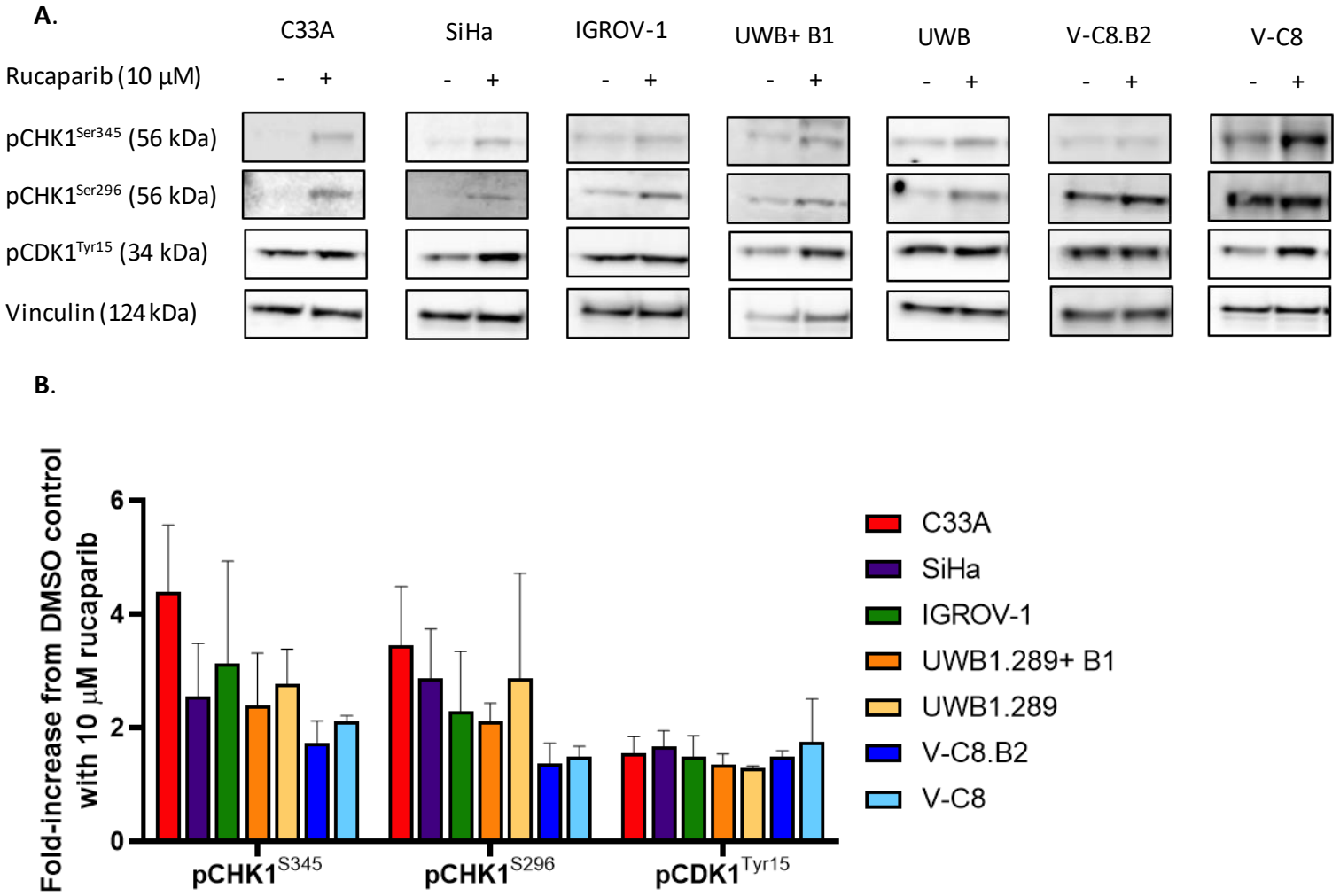


Figure 4.5: Activation of ATR-CHK1 pathway by rucaparib. Cells were treated with 10 µM rucaparib for 24 h before being lysed and Western blotting performed. **A.** Representative Western Blots for C33A, SiHa, IGROV-1, UWB1.289+B1, UWB1.289, V-C8.B2 and V-C8 cells treated with DMSO or 10 µM rucaparib. **B.** Fold-increase induced by rucaparib relative to DMSO control following normalisation to vinculin control. Data are mean and SEM of 3 independent experiments.

4.5.5 Correlation of rucaparib-induced RS and activation of ATR-CHK1 pathway

Due to the activation of the ATR-CHK1 in response to RS, the correlation between rucaparib-induced RS (measured by γH2AX foci formation) and increase of pCHK1^{Ser345}, pCHK1^{Ser296} and pCDK1^{Tyr15} with 10 µM rucaparib was assessed. A positive correlation was observed with pCDK1^{Tyr15} (r^2= 0.4, p=0.4), although with such few data points SiHa cells may be skewing this trend. There was a negative trend between increased pCHK1^{Ser345} (ATR activity) and increased γH2AX by rucaparib. No trend was observed between increased pCHK1^{Ser296} (CHK1 activity) and increased γH2AX by rucaparib (Figure 4.6).

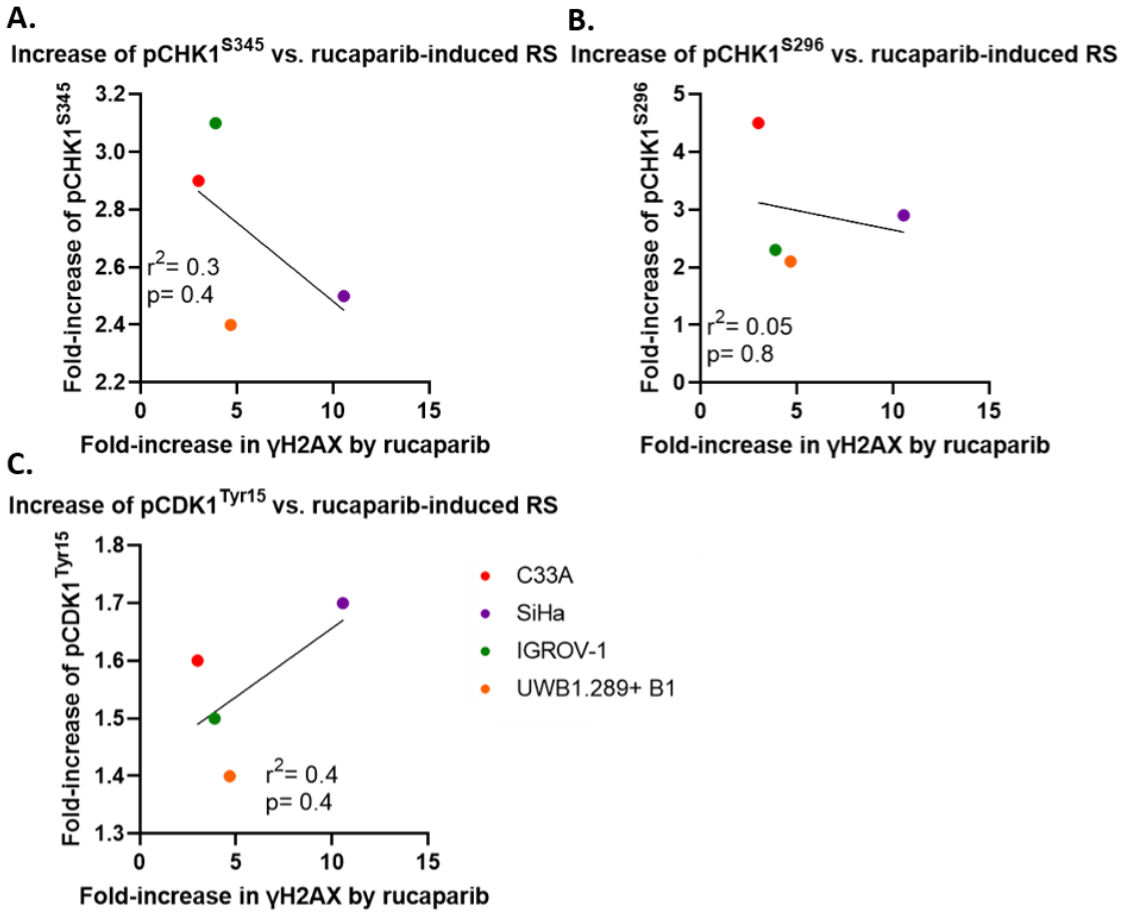


Figure 4.6: Correlation of rucaparib-induced RS and signalling to ATR-CHK1 pathway. Mean fold-increase in γH2AX in cells treated with 10 µM rucaparib compared to DMSO control cells was plotted against fold-increase of **A.** pCHK1^{Ser345}, **B.** pCHK1^{Ser296} and **C.** pCDK1^{Tyr15} by 10 µM rucaparib compared to DMSO control cells. Correlations were calculated by Pearson's correlation coefficient (r) using Graphpad Prism 9.0 in human repair-competent cells. Each data point represents the mean of 3 experiments.

4.5.6 Correlation of RS and rucaparib cytotoxicity

Basal RS and rucaparib-induced RS was plotted against cell survival at 1 µM and 10 µM rucaparib (Figure 4.7). *BRCA* mutant cells were removed from analyses as this would skew the data due to the synthetic lethality of PARPi and HRR defective cells. There was a weak correlation between basal RS and cell survival at 1 µM rucaparib (r^2= 0.3), with the general trend of higher basal RS resulting in higher sensitivity to rucaparib. However this trend was reversed with 10 µM rucaparib (r^2= 0.8). No correlation was observed between fold-induction of RS with 10 µM rucaparib (γH2AX foci) and cell survival at 1 µM or 10 µM rucaparib (r^2= 0.0, for both). Overall, in this limited panel of cell lines rucaparib cytotoxicity was not significantly affected by basal RS or rucaparib-induced RS.

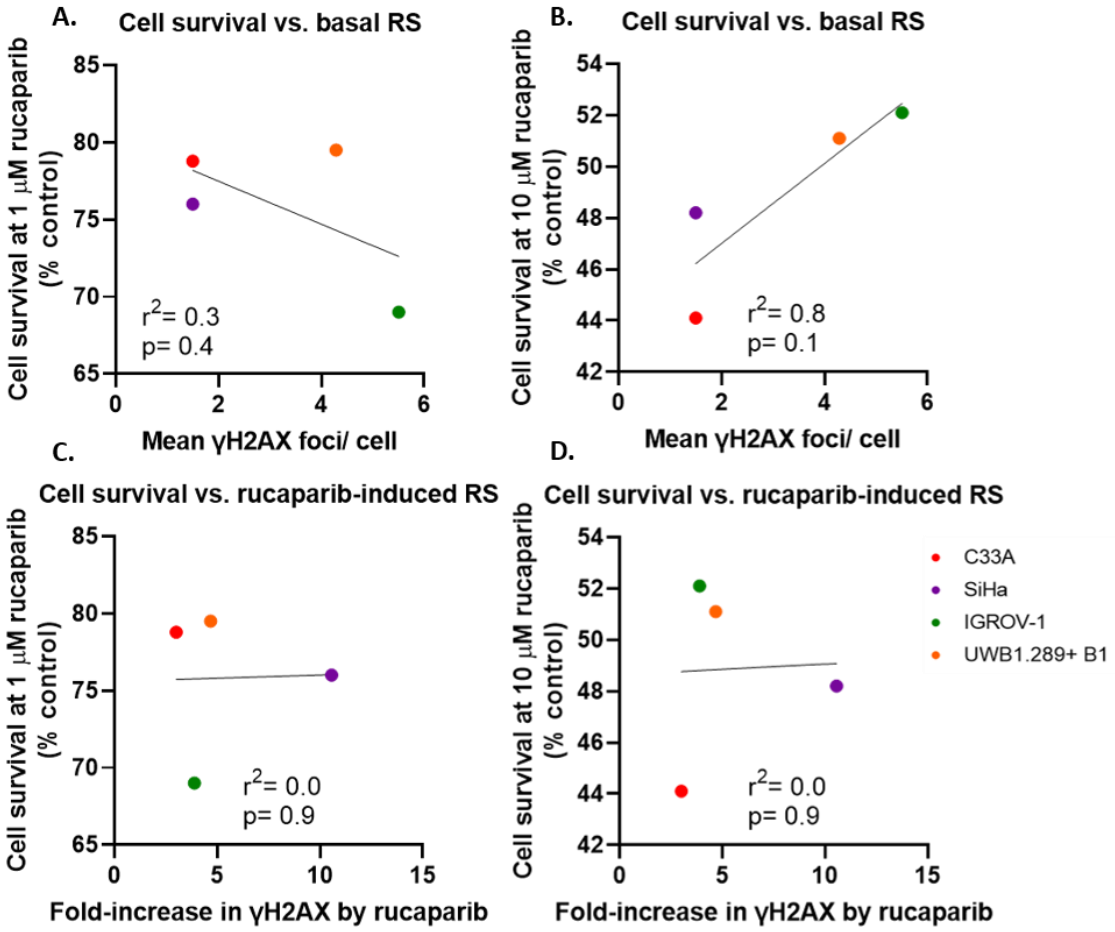


Figure 4.7: Correlation of rucaparib cytotoxicity and RS. Mean γH2AX per untreated cell was plotted against **A.** 1 μM rucaparib and **B.** 10 μM rucaparib. Fold-increase in γH2AX in cells treated with 10 μM rucaparib compared to DMSO control cells was plotted against cell survival with **C.** 1 μM rucaparib and **D.** 10 μM rucaparib. Correlations were calculated by Pearson's correlation coefficient (r) using Graphpad Prism 9.0 and only human repair-competent cells were included in analyses. Each data point represents the mean of 3 experiments.

4.5.7 Correlation of determinants of sensitivity and rucaparib cytotoxicity

As well as *BRCA1* and *BRCA2*, other determinants of PARPi sensitivity have been reported including RAD51, ATR, ATM, CHK1 and XRCC1. Many of the trends observed from correlation analyses were negative trends, where lower protein levels resulted in higher cell survival with rucaparib (Figure 4.8). A weak trend was observed with lower ATR protein levels resulting in lower cell survival at 10 μM rucaparib (r^2= 0.2), however this was non-significant and no trend was observed between ATR protein levels and LC_{50} of rucaparib. Ultimately, in this limited panel of cells, rucaparib cytotoxicity was not significantly affected by any of the previously identified determinants of sensitivity once the *BRCA* mutant cells were taken out of the analysis.

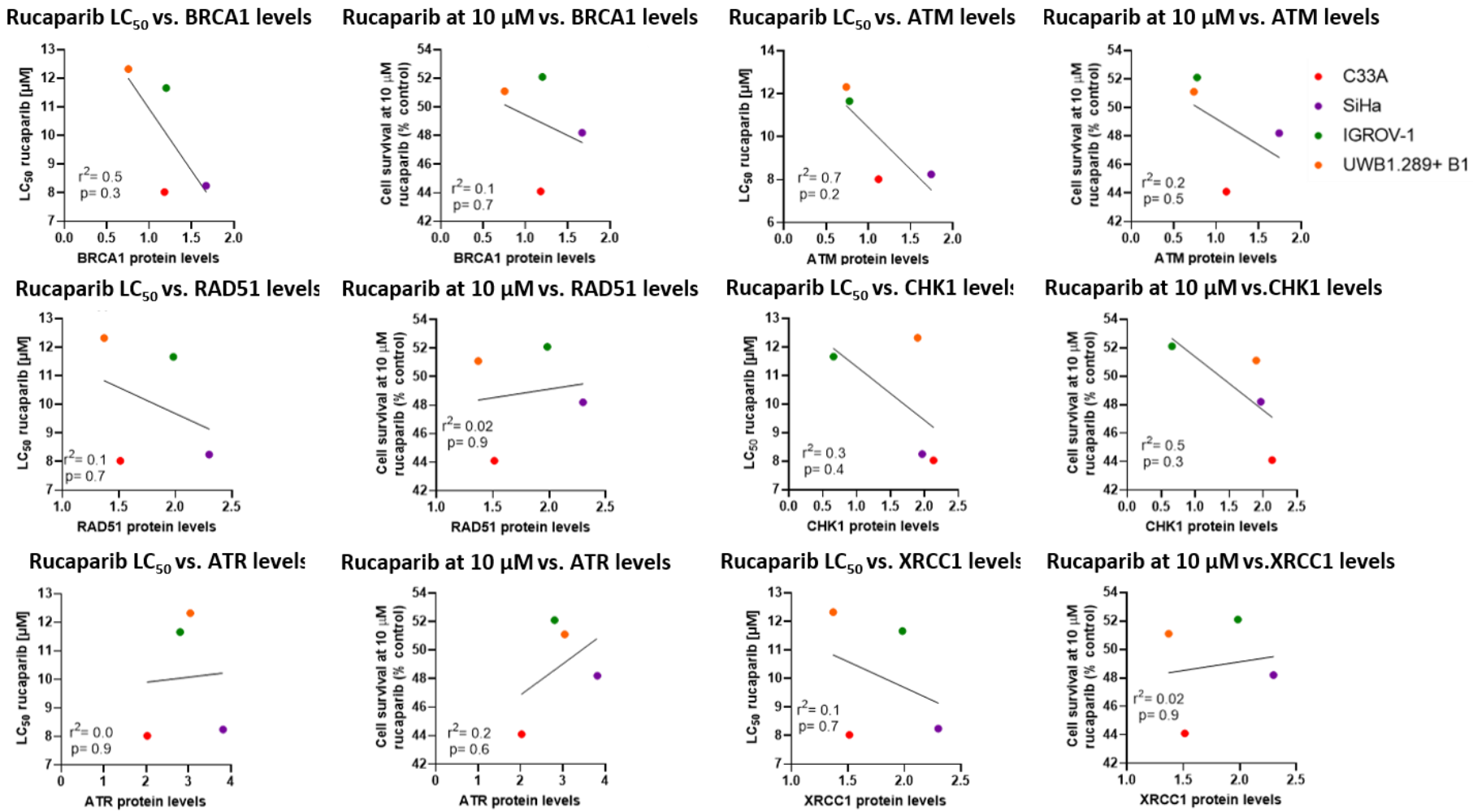


Figure 4.8: Correlation between protein expression of determinants to PARPi sensitivity and rucaparib cytotoxicity. Correlations were calculated by Pearson's correlation co-efficient (r) using Graphpad Prism 9.0. The mean protein expression in untreated cells (assessed by Western blotting in Chapter 3) was correlated with LC_{50} and cell survival at 10 μM rucaparib in human repair-competent cells. Each data point represents the mean of 3 experiments.

4.6 Discussion

The synthetically lethal relationship between PARP and HRR function could suggest that increased PARP activity would be necessary in HRD cells for survival. Gottipati *et al.,* found that in a PARP activity assay, in the absence of activated DNA, HRD V-C8 cells had significantly higher PARP activity than HRC matched V-C8.B2 cells (~8-fold, $p<0.01$) (Gottipati *et al.,* 2010). This concept was confirmed here, with HRD V-C8 cells having significantly higher endogenous PAR levels compared to HRC V-C8.B2 cells (2.3-fold, $p=0.01$). Similarly, the HRD UWB1.289 had 1.3 -fold higher endogenous PAR levels compared to its HRC matched cells. However, following activation with oligonucleotide in the presence of NAD+, there was no difference between the HRC and HRD cells.It was more likely that higher levels of endogenous PAR reflected higher levels of DNA breaks, as indicated by the higher levels of γH2AX foci (Chapter 3) in the HRD cells. Interestingly, endogenous PAR levels were also high in C33A, SiHa and particularly IGROV-1 cells than the UWB1.289 +B1 cells, which suggests there may be other factors besides HRR defects that may cause high endogenous PAR. The extent by which PARP activity was inhibited did not significantly differ within each pair of matched cells, which had similar IC_{50} values, regardless of HRR status. However, there was 10-fold greater potency of PARP inhibition by rucaparib in the V-C8 matched hamster cells compared with the human UWB1.289 paired cells. Similar studies comparing the potency of rucaparib (or other PARPi) across species do not appear to have been made and this observation needs to be investigated further in other cell lines derived from different animal species. Further study into these differences may be necessary as this could have implications in pre-clinical *in vivo* studies in different animal species. The similar inhibition of PARP activity by rucaparib in the HRD and HRC matched cells confirmed that the greater cytotoxicity of PARPi in HRD cells was not due to a greater degree of PARP inhibition.

Rucaparib has previously been documented to be ≥1000× more cytotoxic to *BRCA2* mutant V-C8 cells compared to their matched *BRCA2* corrected V-C8.B2 cells (Patent WO/2005/012305), which was confirmed here. In contrast there was only a 62-fold difference in sensitivity to rucaparib between UWB1.289+B1 and *BRCA1*-defective UWB1.289 cells. Interestingly, recent results from the TRITON2 study (NCT02952534),

showed that the clinical activity of rucaparib was greater in castrate-resistant patients with *BRCA2* mutations than *BRCA1* mutations. This may be due to the fact *BRCA1* has multiple functions as it interacts with tumour suppressors, DNA repair and checkpoint regulation. In contrast, the primary role of *BRCA2* mediating the recruitment of RAD51 to DSBs (Roy, Chun and Powell, 2016). However, Markowski *et al.,* suggested that a larger scale analyses would be required to make any definitive conclusions in further understanding the mechanism underpinning the differences in rucaparib efficacy between *BRCA1* and *BRCA2*- mutated cancer (Markowski *et al.,* 2020, Abida *et al.,* 2020). Although here *BRCA2* status appeared to confer greater sensitivity to rucaparib this is notably only a comparison of two cell line pairs, from human and hamster cells, and a larger panel of cell lines would be necessary to make further distinct comparisons and conclusions.

It has been reported that high levels of baseline RS render cells more sensitive to PARPis, even in the absence of an HRR defect. However, when UWB1.289 and V-C8 cells were excluded from the analysis (because their profound sensitivity to rucaparib-induced synthetic lethality skewed the data) the trend actually suggested that lower basal RS resulted in increased sensitivity to rucaparib (r^2= 0.8, p= 0.1). As these correlations are only between a small number of cell lines, a more molecularly diverse panel would be required to make any conclusions or links between basal RS and sensitivity to PARP inhibition.

The sensitivity to rucaparib observed in SiHa cells compared to the other HRC cells, particularly at higher concentrations, could be due to the SiHa cells being HPV-16 positive. Previous studies have shown HPV positive cells to have downstream defects in both NHEJ and HRR (Weaver *et al.,* 2015, Langsfeld *et al.,* 2015) and from the homozygous mutation in key HRR gene *FANCM* (assessed in Chapter 3, section 5.1), it would be predicted that SiHa cells would be sensitive to PARPi and perhaps be HRD. However, SiHa cells had approximately 11-fold less basal RS than the HRD UWB1.289 and V-C8 cells and formed RAD51 foci when treated with rucaparib (assessed in Chapter 6).

Here, it was confirmed that rucaparib-induced RS led to the increase of pCHK1^{S345}, pCHK1^{S296} and pCDK1^{Tyr15} levels in all cell lines tested. Rucaparib increased ATR activity (as determined by pCHK1^{S345} levels) the most, followed by CHK1 activation (pCHK1^{Ser296}) with only a modest observed increase in pCDK1^{Tyr15}. This could be due to pCDK1^{Tyr15} being further downstream in the response to DNA damage signalling. Untreated cells have a high baseline level of pCDK1^{Tyr15} (Figure 4.5), which may result in lower fold-increase when treated with rucaparib. However, since all cell lines tested had high levels of pCDK1^{Tyr15} but did not have higher levels of pCHK1^{S345} and pCHK1^{S296}, it is unlikely this reflected high levels of RS in the control cells.

Overall, the correlations between the previously identified determinants of PARPi sensitivity (McCabe *et al.,* 2006, Lord *et al.,* 2008) and rucaparib cytotoxicity observed across the cells used here were not supported here. A potential reason for this could be the way these determinants were identified, often by high-throughput siRNA screens, where a single gene is completely knocked-down, and sensitivity is investigated in isolation to other factors at play within cells. Whereas here, protein expression was assessed in a semi-quantitative way and these cells are heterogeneous with an array of molecular complexities that can affect both sensitivity and resistance to an agent.

Data described in this chapter regarding target inhibition and single agent cytotoxicity of rucaparib allowed for the selection of 0- 30 µM rucaparib concentration range to be used in combination cytotoxicity studies in all HRC cells and the selection of 0- 3 µM and 0- 0.3 µM for HRD UWB1.289 and V-C8 cells, respectively, to address the overall aim of the thesis and determine synergy between rucaparib and inhibitors of ATR, CHK1 and WEE1.

Chapter 5. Determining cytotoxicity and target inhibition of checkpoint kinase inhibitors on the panel of cell lines

5.1 Introduction:

HRR status is the major determinant of sensitivity to rucaparib (Chapter 4). The aim of this chapter is to determine whether the cell line characteristics: growth rate, level of DDR proteins and basal replication stress determined in Chapter 3 contribute to the cellular sensitivity to ATR, CHK1 and WEE1 inhibitors.

Defects in G1 checkpoint control e.g. through defects in *TP53* and/or *RB1* are expected to render cells dependent on their S and G2 checkpoints and hence more sensitive to ATR, CHK1 and WEE1 inhibition (see Chapter 1). Most studies suggest p53 is a determinant of chemo- or radio sensitisation by ATR, CHK1 and WEE1 inhibitors (Middleton *et al.,* 2018, Blasina *et al.,* 2008, Hirai *et al.,* 2009). However, at least for VE-821, the inhibitor used here, this may only be apparent in isogenically matched cells and even in matched cells p53 status was not a determinant of single agent cytotoxicity (Middleton et al 2018). These observations may extend to CHK1 and WEE1 inhibition.

Previous studies have shown that defects in key DDR proteins result in increased sensitivity to ATR/CHK1 inhibition. Middleton *et al.,* showed that defects in ATM, HRR (BRCA2, XRCC3) and BER (XRCC1) resulted in increased sensitivity to VE-821. Factors that trigger RS have been shown to increase sensitivity to ATR/CHK1 inhibition (Stover *et al.,* 2016, Glorieux *et al.,* 2017). RS is often caused by oncogenic drivers such as Ras, Myc and cyclin E, which act by forcing cells into S-phase, without allowing repair to occur (Benada and Macurek, 2015, Macheret and Halazonetis, 2015). Cyclin E upregulation was found to confer sensitivity to ATR, CHK1 and WEE1 inhibitors as monotherapies (Toledo *et al.,* 2011, Murga *et al.,* 2011, Chen *et al.,* 2019).

VE-821, PF-477736 and MK-1775 are specific ATR, CHK1 and WEE1 inhibitors, respectively, and are therefore suitable to investigate the downstream consequences of cell cycle checkpoint inhibition and to test hypotheses regarding determinants of sensitivity to them as single agents. Target inhibition data obtained for VE-821, PF-477736 and MK-1775 in the panel of cell lines are shown in Table 5.1, and were used to

guide selection of concentration ranges to be used in the experiments described in this chapter. These data were acquired from theses of previous lab members.

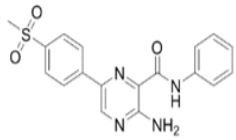
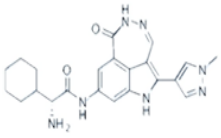
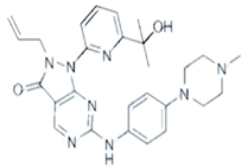
	VE-821	PF-477736	MK-1775
Structure			
Specificity	Selective for ATR. Minimal cross-reactivity with ATM, DNA-PK, mTOR and PI3K	100-fold selective for CHK1 vs CHK2	>100-fold selectivity to WEE1 over Myt1
Published Ki/ IC50	Ki= 13 nM IC50= 26 nM (cell-free)	Ki= 0.49 nM	IC50= 5.2 nM(cell-free)
C33A cells: IC_{50} determined by Western blot	0.6 µM	11.1 nM	0.5 µM
C33A cells: % target inhibition at select concentration	1 µM: 79 %	50 nM: >100 %	0.1 µM: 58 %
C33A cells: LC_{50} (cytotoxicity assay)	22.8 µM	0.3 µM	0.2 µM
SiHa cells: IC_{50} determined by Western blot	0.7 µM	15.7 nM	0.3 µM
SiHa cells: % target inhibition at select concentration	1 µM: 93 %	50 nM: 85%	0.1 µM: 54 %
SiHa cells: LC_{50} (cytotoxicity assay)	5.0 µM	0.2 µM	0.3 µM
IGROV-1 cells: IC_{50} determined by Western blot	0.6 µM		
IGROV-1 cells: % target inhibition at select concentration	1 µM: 59 %		
IGROV-1 cells: LC_{50} (cytotoxicity assay)	1.9 µM		
UWB1.289: IC_{50} determined by Western blot	0.3 µM		
UWB1.289: % target inhibition at select concentration	1 µM: 93%		
UWB1.289: LC_{50} (cytotoxicity assay)	0.6 µM		

Table 5.1: Specific inhibitors of ATR, CHK1 and WEE1 and their relevant properties. Table shows structure of the kinase inhibitors used in the experiments to follow, as well as specificity and published Ki/IC50 values. IC50 and % target inhibition data in cervical cells (C33A and SiHa) was determined by Stuart Rundle using cisplatin as an activator of the ATR/CHK1 pathway (Stuart Rundle MD thesis 2020 Newcastle University). IC50 and % target inhibition data using VE-821 in ovarian cancer cells (IGROV-1 and UWB1.289) was acquired by Alice Bradbury, using 4NQO as an activator of ATR (Alice Bradbury PhD thesis 2020 Newcastle University. In both instances $pCHK1^{345}$ was used as a marker of ATR activity, with $pCHK1^{S296}$ and $pCDK1^{Tyr15}$ phosphorylation targets of CHK1 and WEE1 inhibition in cervical cancer cells. Target inhibition levels were determined in cells treated with 1 µM VE-821, 50 nM PF-477736 and 0.1 µM MK-1775.

5.2 Aims and Objectives:

The main aims of this chapter are:

- To determine target enzyme inhibition and resulting downstream signalling, and how target enzyme inhibition relates to single agent cytotoxicity of the kinase inhibitors

- To investigate whether the observed single agent cytotoxicity links to the molecular phenotype of the cells or characteristics determined in Chapter 3

5.3 Hypothesis

Cytotoxicity of kinase inhibitors will be dependent on the extent of kinase inhibition, DDR dysfunction and endogenous RS

5.4 Materials and Methods

5.4.1 Determining target inhibition by Western blot

Exponentially growing C33A, SiHa, IGROV-1, UWB1.289+B1, UWB1.289, V-C8.B2 and V-C8 cells were treated with either DMSO, 10 µM rucaparib or 10 µM rucaparib with 1 µM VE-821, 50nM PF-477736, 200 nM PF-477736, 0.1 µM MK-1775 or 0.3 µM MK-1775. These concentrations were selected based on data shown in Table 5.1. At the concentrations of 1 µM VE-821, 50 nM PF-477736 and 0.1 µM MK-1775 target inhibition was 59 to 93 %, 85 to >100 % and 54 to 58 %, respectively, across C33A, SiHa, IGROV-1 and UWB1.289 cells (Table 5.1). Lysates were prepared and Western blots were performed as described previously (Chapter 2). Densitometry was analysed as previously described and values were normalised to the corresponding loading control (vinculin) prior to calculation of fold-change from DMSO control.

5.4.2 Single agent cytotoxicity of kinase inhibitors

Exponentially growing cells were seeded at various densities in 6-well plates, allowing 3 different densities per drug concentration estimated to give 20-200 colonies after drug treatment. Following adherence, cells were exposed to various concentrations of VE-821 (0- 10 µM), PF-477736 (0-200 nM) and MK-1775 (0-0.8 µM) for 24 h. Medium was replaced with drug-free medium and cells were left to incubate for 8-10 days to form colonies. Colonies were fixed and counted as previously described. LC_{50} values were calculated using Graphpad Prism 9 software (San Diego, CA, USA).

5.4.3 Statistical analysis

Pearson's correlation was calculated using Graphpad Prism 9 software (San Diego, CA, USA) to determine any relationship between target inhibition and inhibition of cell survival by kinase inhibitors.

5.5 Results

5.5.1 Target inhibition by kinase inhibitors

The effect of each kinase inhibitor on its phosphorylation target was determined by Western blot of pCHK1 ^{S345}, pCHK1^{S296} and pCDK1^{Tyr15}. As indicated in Chapter 4 pCHK1^{S345}and pCHK1^{S296} are indicators of ATR and CHK1, respectively. However, pCDK1^{Tyr15} is the product of direct phosphorylation by WEE1 and MYT1 combined with inhibition of CDC25C dephosphorylation resulting from CHK1 activation (Chapter 1, figure 10). Therefore, pCDK1^{Tyr15} is not exclusively an indicator of WEE1 activation, but a reduction in phosphorylation of this target by MK-1775 is likely to be due to WEE1 inhibition.

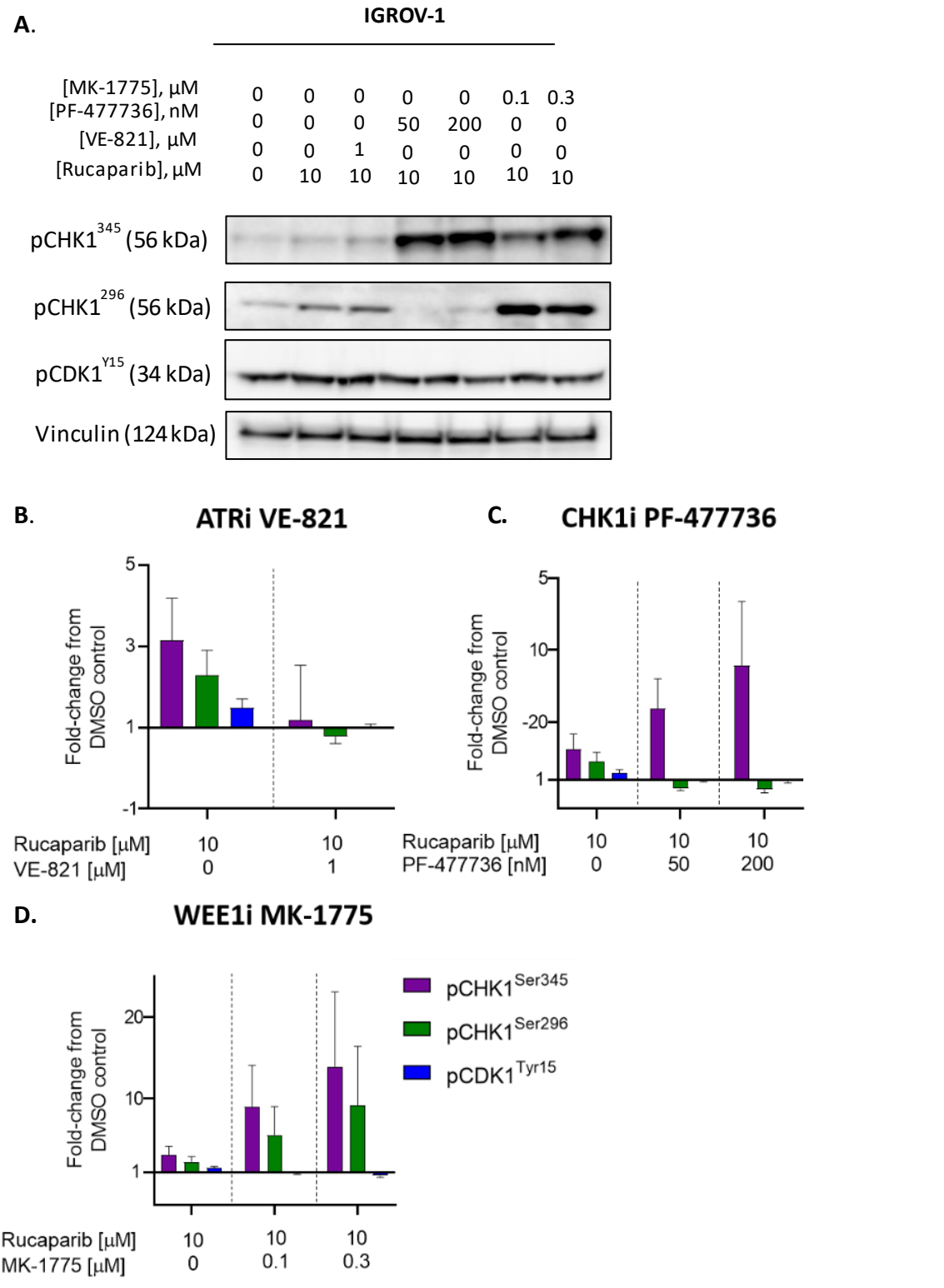
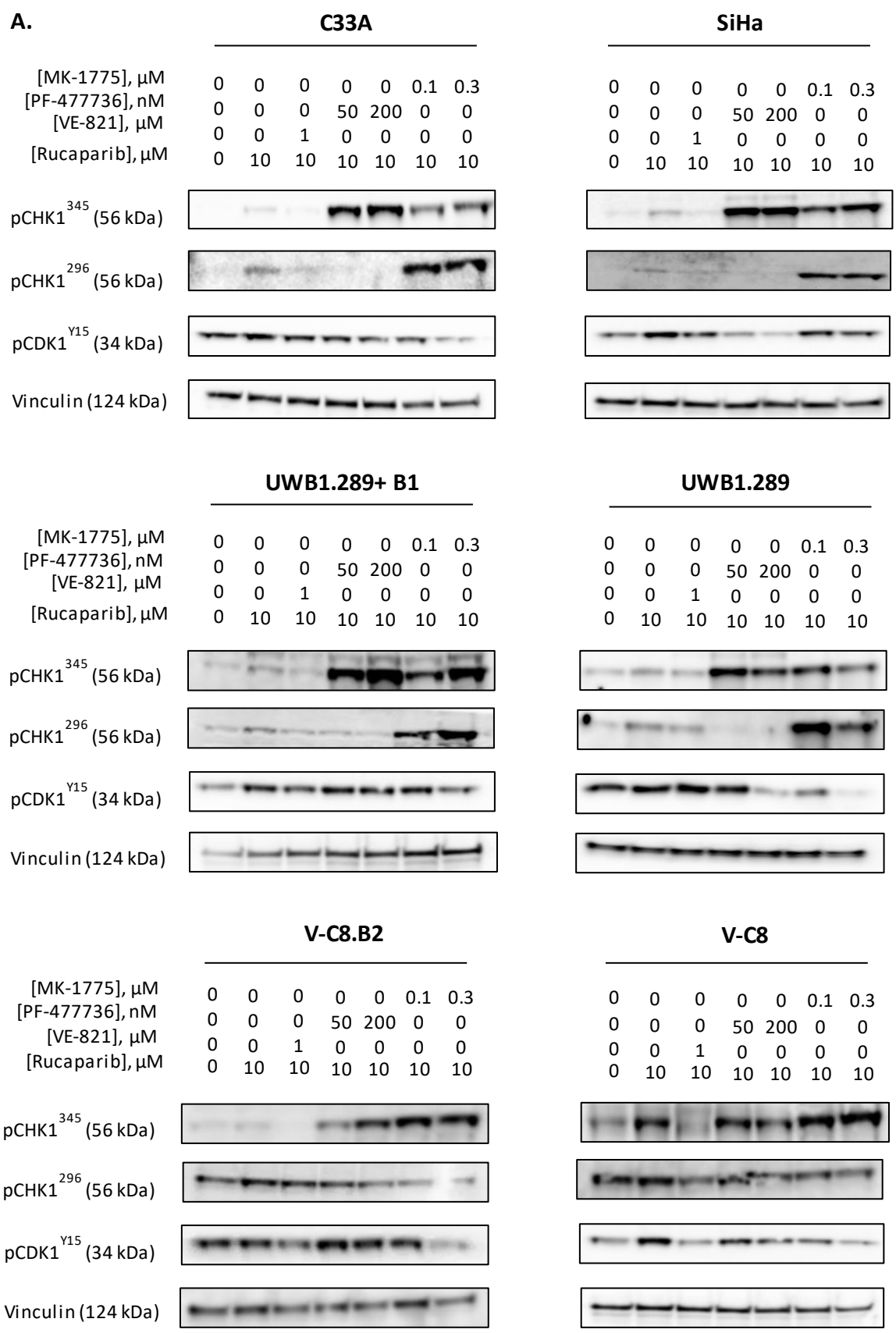


Figure 5.1: Target inhibition of pCHK1^{S345}, pCHK1^{S296} and pCDK1^{Tyr15} by VE-821, PF-477736 and MK-1775 in IGROV-1 cells. A. Representative Western Blot for IGROV-1 cells. Fold-change (determined by densitometry) from DMSO levels of pCHK1^{S345}, pCHK1^{S296} and pCDK1^{Tyr15} in cells treated with rucaparib (10 µM), **B.** rucaparib+ VE-821 (1 µM), **C.** rucaparib+ PF-477736 (50 and 200 nM) and **D.** rucaparib + MK-1775 (0.1 and 0.3 µM). These concentrations were selected based on previous data (Table 5.1). Data are mean and SEM of 3 independent experiments

Rucaparib (10 µM) increased pCHK1^{S345} (indicating ATR activity), pCHK1^{S296} (indicating CHK1 activity) and pCDK1 ^{Tyr15} (3.1-fold, 2.3-fold and 1.5-fold, respectively) in IGROV-1 cells (representative cell line, Figure 5.1). As described previously, in response to RS, ATR is activated and activates CHK1 by phosphorylation at serine 345, causing CHK1 to auto-phosphorylate at serine 296, to achieve full activation. As predicted ATRi VE-821 (1 µM) inhibited pCHK1^{S345} as well as inhibiting pCHK1^{S296} and pCDK1^{Tyr15} downstream. CHK1i PF-477736 inhibited pCHK1^{S296} at both 50 nM and 200 nM in addition to inhibiting pCDK1^{Tyr15}. Inhibition of pCHK1^{Ser296} by PF-477736 resulted in increased pCHK1^{345} upstream, indicating feedback activation of ATR when CHK1 is inhibited. MK-1775 (0.1 µM and 0.3 µM) caused a reduction in CDK1 phosphorylation, as expected. In addition, MK-1775 also caused upstream activation of both CHK1 and ATR, as determined by the increase of CHK1^{S296} and CHK1^{S345}, respectively. These findings were consistent across all cell lines tested (Figure 5.2).


A.
C33A
SiHa
UWB1.289+ B1
UWB1.289
V-C8.B2
V-C8
[MK-1775], µM
[PF-477736], nM
[VE-821], µM
[Rucaparib], µM
0 0 0 0 0 0.1 0.3
0 0 0 50 200 0 0
0 0 1 0 0 0 0
0 10 10 10 10 10 10
pCHK1 345 (56 kDa)
pCHK1 296 (56 kDa)
pCDK1 Y15 (34 kDa)
Vinculin (124 kDa)

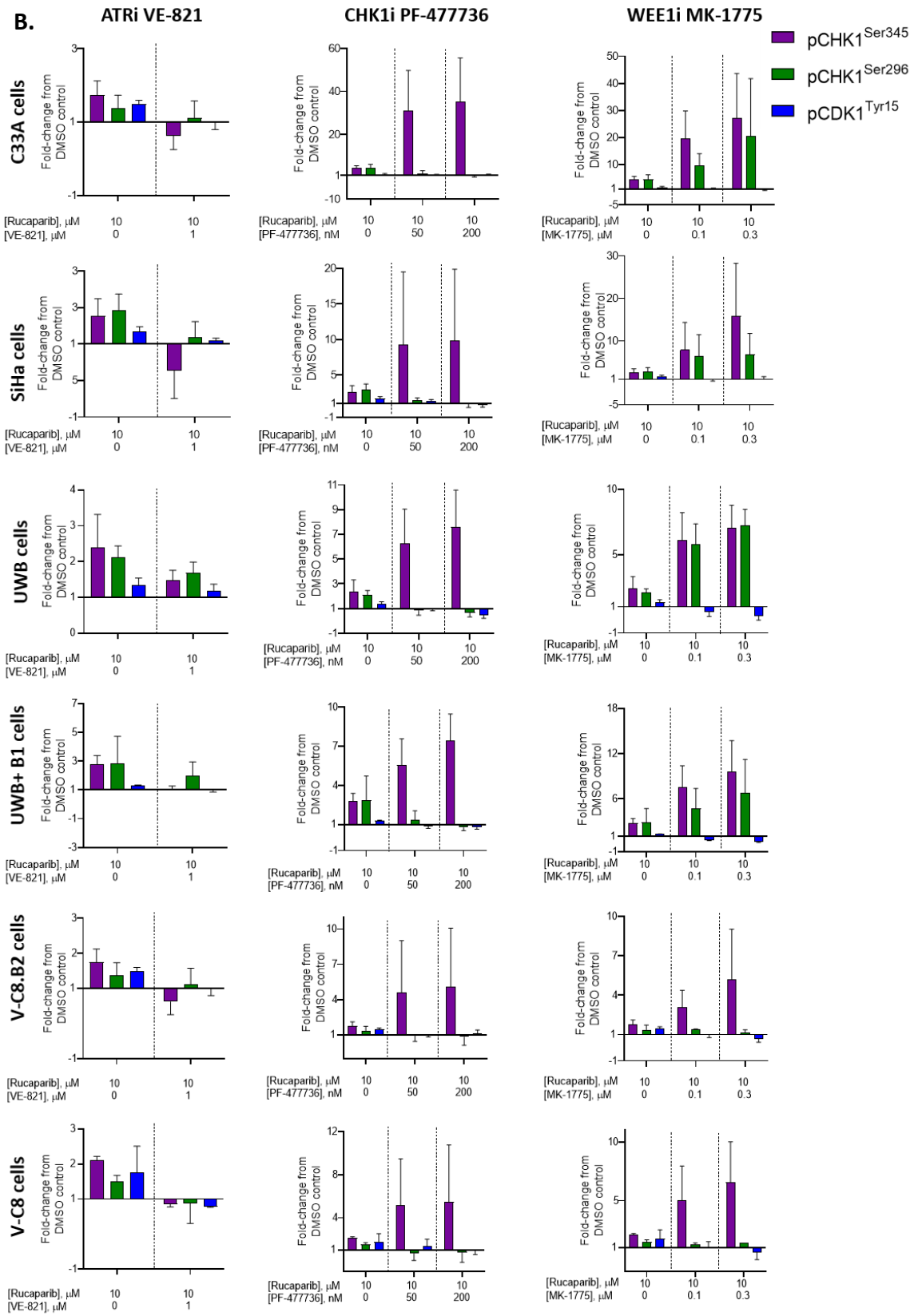

B.
ATRi VE-821
CHK1i PF-477736
WEE1i MK-1775
pCHK1Ser345
pCHK1Ser296
pCDK1Tyr15
C33A cells
SiHa cells
UWB cells
UWB+ B1 cells
V-C8.B2 cells
V-C8 cells
Fold-change from DMSO control
[Rucaparib], µM
[VE-821], µM
[PF-477736], nM
[MK-1775], µM

Figure 5.2: Target inhibition of pCHK1^{S345}, pCHK1^{S296} and pCDK1^{Tyr15} by VE-821, PF-477736 and MK-1775 in C33A, SiHa, UWB1.289+B1, UWB1.289, V-C8.B2 and V-C8 cells. A. Representative Western Blot for C33A, SiHa, UWB1.289+B1, UWB1.289, V-C8.B2 and V-C8 cells. **B.** Fold-change from DMSO levels of pCHK1^{S345}, pCHK1^{S296} and pCDK1^{Tyr15} in cells treated with rucaparib (10 µM), rucaparib+VE-821 (1 µM), rucaparib+ PF-477736 (50 and 200 nM) and rucaparib + MK-1775 (0.1 and 0.3 µM). Densitometry values were normalised to vinculin prior to calculation of fold-change from DMSO control. Data are mean and SEM of 3 independent experiments in C33A, SiHa, UWB1.289 and UWB1.289+B1 cells and 2 independent experiments in V-C8 and V-C8.B2 cells.

A

	pCHK1^{S345}			pCHK1^{S296}			pCDK1^{Tyr15}		
	Rucaparib fold-increase	Rucaparib+ VE fold-change	% target inhibition	Rucaparib fold-increase	Rucaparib+ VE fold-change	% target inhibition	Rucaparib fold-increase	Rucaparib+ VE fold-change	% target inhibition
C33A	2.9 ± 2.3	0.9 ± 1.8	87.7 ± 21.4	4.5 ± 1.8	1.6 ± 0.7	84.4 ± 18.6	1.6 ± 0.3	0.4 ± 1.3	83.7 ± 25.5
SiHa	2.5 ± 0.9	1.0 ± 0.3	95.9 ± 7.1	2.9 ± 0.9	1.4 ± 0.9	75.2 ± 38.3	1.7 ± 0.3	1.2 ± 0.1	73.2 ± 11.6
IGROV-1	3.1 ± 1.8	1.9 ± 1.3	64.4 ± 30.9	2.3 ± 1.1	0.8 ± 0.3	99.3 ± 1.3	1.5 ± 0.4	1.0 ± 0.1	79.5 ± 32.2
UWB1.289+ B1	2.4 ± 0.9	1.5 ± 0.3	65.6 ± 3.1	2.1 ± 0.3	1.7 ± 0.3	38.1 ± 20.9	1.4 ± 0.2	1.2 ± 0.2	49.3 ± 21.8
UWB1.289	2.8 ± 0.6	1.0 ± 0.2	94.8 ± 9.1	2.9 ± 1.9	2.0 ± 1.9	60.9 ± 34.8	1.3 ± 0.04	1.0 ± 0.1	93.3 ± 11.5
V-C8.B2	1.5, 2.0	0.4, 0.9	100.0,100.0	1.1, 1.6	0.8, 1.4	100.0, 29.9	1.4, 1.6	0.9, 1.1	100.0, 77.6
V-C8	2.0, 2.2	0.8, 0.9	100.0,100.0	1.4, 1.6	1.3, 0.5	100.0, 23.7	2.3, 1.2	0.8, 0.8	100.0, 100.0

B.

	pCHK1^{S345}		pCHK1^{S296}			pCDK1^{Tyr15}		
	Rucaparib fold-increase	Rucaparib+ PF fold-change	Rucaparib fold-increase	Rucaparib+ PF fold-change	% target inhibition	Rucaparib fold-increase	Rucaparib+ PF fold-change	% target inhibition
C33A	2.9 ± 2.3	31.3 ± 18.5	4.5 ± 1.8	1.9 ± 1.4	79.9 ± 21.8	1.6 ± 0.3	1.2 ± 0.3	55.3 ± 35.4
SiHa	2.5 ± 0.9	9.3 ± 10.2	2.9 ± 0.9	1.5 ± 0.3	76.5 ± 13.0	1.7 ± 0.3	1.2 ± 0.1	48.5 ± 44.6
IGROV-1	3.1 ± 1.8	6.0 ± 3.6	2.3 ± 1.1	0.4 ± 0.4	100.0 ± 0.0	1.5 ± 0.4	0.9 ± 0.1	100.0 ± 0.0
UWB1.289+ B1	2.4 ± 0.9	6.3 ± 2.7	2.1 ± 0.3	0.8 ± 0.4	100 ± 0.0	1.4 ± 0.2	0.9 ± 0.1	100.0 ± 0.0
UWB1.289	2.8 ± 0.6	5.6 ± 2.0	2.9 ± 1.9	1.4 ± 0.7	85.5 ± 14.4	1.3 ± 0.04	0.9 ± 0.1	100.0 ± 0.0
V-C8.B2	1.5, 2.0	1.5, 7.7	1.1, 1.6	0.6, 1.3	100.0, 100.0	1.4, 1.6	1.0, 0.9	88.9, 24.9
V-C8	2.0, 2.2	2.2, 8.2	1.4, 1.6	1.1, 0.2	100.0, 100.0	2.3, 1.2	1.8, 0.9	100.0,100.0

C.

	pCHK1^{S345}		pCHK1^{S296}		pCDK1^{Tyr15}		
	Rucaparib fold-increase	Rucaparib+ MK fold-change	Rucaparib fold-increase	Rucaparib+ MK fold-change	Rucaparib fold-increase	Rucaparib+ MK fold-change	%target inhibition
C33A	2.9 ± 2.3	19.6 ± 10.3	4.5 ± 1.8	8.5 ± 4.5	1.6 ± 0.3	1.1 ± 0.2	79.8 ± 18.7
SiHa	2.5 ± 0.9	7.9 ± 6.4	2.9 ± 0.9	6.3 ± 5.1	1.7 ± 0.3	1.0 ± 0.4	100.0 ± 0.0
IGROV-1	3.1 ± 1.8	9.0 ± 8.7	2.3 ± 1.1	5.6 ± 6.0	1.5 ± 0.4	0.9 ± 0.3	100.0 ± 0.0
UWB1.289+ B1	2.4 ± 0.9	6.1 ± 2.1	2.1 ± 0.3	5.8 ± 1.6	1.4 ± 0.2	0.6 ± 0.4	100.0 ± 0.0
UWB1.289	2.8 ± 0.6	7.5 ± 2.9	2.9 ± 1.9	4.7 ± 2.7	1.3 ± 0.04	0.5 ± 0.1	100.0 ± 0.0
V-C8.B2	1.5, 2.0	2.2, 4.0	1.1, 1.6	0.7, 1.4	1.4, 1.6	0.8, 1.1	100.0, 100.0
V-C8	2.0, 2.2	2.9, 7.1	1.4, 1.6	1.4, 1.2	2.3, 1.2	1.4, 0.7	100.0, 100.0

Table 5.2: Effect of VE-821, PF-477736 and MK-1775 on pCHK1^{S345}, pCHK1^{S296} and pCDK1^{Tyr15}. Fold-change was calculated relative to DMSO control following exposure to **A.** 1 µM VE-821 **B.** 50 nM PF-477736 or **C.** 0.1 µM MK-1775. Following subtraction of DMSO control to each treatment, target inhibition was calculated as follows: 100-((rucaparib+ kinase inhibitor/ rucaparib single agent)*100). Data are mean and SD across 3 independent experiments (figures 5.1 and 5.2), with the exception of V-C8 and V-C8.B2 cells, which are 2 independent experiments.

Rucaparib (10 µM) increased pCHK1^{345} levels to a similar degree across all cell lines (1.8 to 3.1-fold). Increased levels of pCHK1^{s296} were more varied (1.4 to 4.5-fold) and the observed increase in pCDK1^{Tyr15} was modest across all cells (1.3 to 1.7-fold) (Figure 5.2 and Table 5.2).

VE-821 (1 µM) inhibited induction of target pCHK1^{S345} 64.4 to 100.0 % across cell lines, as well as inhibiting pCHK1^{S296} and pCDK1^{Tyr15} downstream (38.1 to 99.3% and 49.3 to 100.0%, respectively). PF-477736 (50 nM) inhibited pCHK1^{S296} 76.5 to 100.0 % across cell lines, as well as inhibiting pCDK1^{Tyr15} levels (48.5 to 100.0 %). Upstream pCHK1^{345} levels increased 4.6-31.3 -fold upon inhibition of CHK1 by 50 nM PF-477736. MK-1775 (0.1 µM) reduced pCDK1^{Tyr15} levels across all cell lines 79.8 -100.0 %. Reduction of pCDK1^{Tyr15} resulted in an increase of both pCHK1^{S296} and pCHK1^{S345} (1.1 to 8.5-fold and 3.1 to 19.6-fold, respectively) (Figure 5.2 and Table 5.2).

5.5.2 Single agent cytotoxicity of kinase inhibitors

The cytotoxicity of each kinase inhibitor was determined by using colony formation assays. This was necessary to select a concentration for combination studies that inhibited the kinase by >50% but did not result in excessive cytotoxicity.

5.5.2.1 Single agent cytotoxicity of the ATR inhibitor, VE-821

There was a narrow spectrum of sensitivity to VE-821 across the panel of cell lines tested with mean LC_{50} values of 1.6 to 2.1 µM, with the exception of HRR defective UWB1.289 cells, which were more sensitive than HRC paired UWB1.289+ B1 cells (LC_{50}s: 1.6 ± 0.6 µM and 0.6 ± 0.1 µM, respectively, p=0.05, paired t-test). In contrast, there was no difference in VE-821 cytotoxicity between HRC and HRD V-C8 cells (LC_{50}s: 2.1 ± 0.2 µM vs 1.9 ± 0.1 µM, respectively) (Figure 5.3). C33A and UWB1.289 cells were the most sensitive to VE-821, across the cell line panel tested. Survival following exposure to 1 µM VE-821 was >50% in all cells except UWB1.289 cells and this concentration showed >64% target inhibition, therefore 1 µM VE-821 was selected for further combination studies (Figure 5.3, Table 5.2).

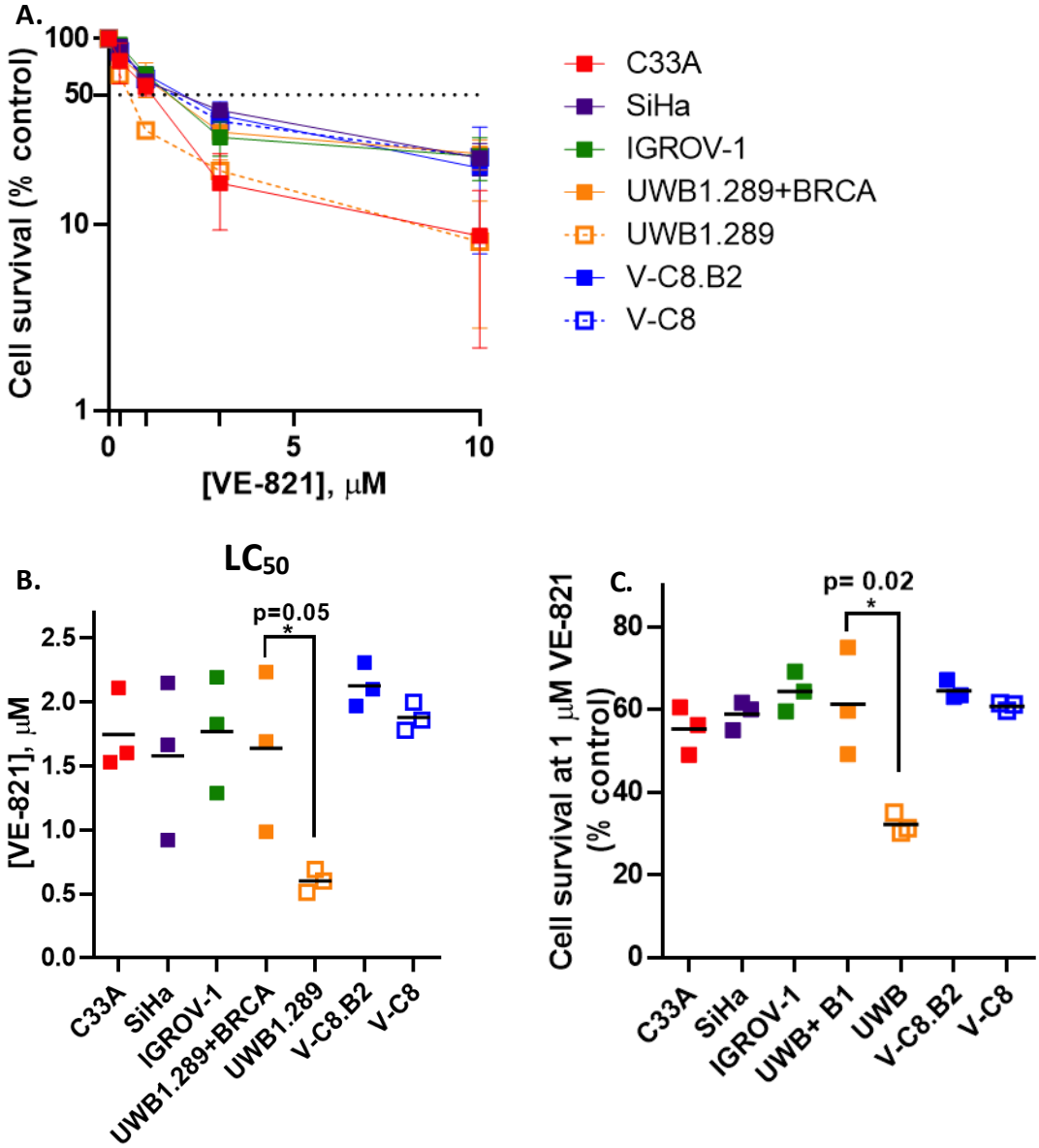


Figure 5.3: Single agent cytotoxicity of VE-821 across the panel of cancer cells. A. Cells were exposed to VE-821 at indicated concentrations for 24 hr prior to replacement with drug-free medium for 8-10 days to allow colony formation. Data are the mean and standard error of 3 independent experiments. **B.** LC_{50} values were calculated using GraphPad Prism 9.0 software. **C.** Using the colony formation assays, % cell survival was reported across cell lines at a set concentration of 1 μM VE-821. **A.** Data are mean and standard deviation of 3 individual experiments. **B, C** Individual experiments shown on scatter plots, with the mean bar shown.

5.5.2.2 Single agent cytotoxicity of the CHK1 inhibitor, PF-477736

There was a greater (approx. 5-fold) spectrum of sensitivity to PF-477736 across cell lines with LC_{50} values of 25.6- 128.4 nM (Figure 5.4). The cytotoxicity of PF-477736 was significantly greater in HRD UWB1.289 cells compared to HRC UWB1.289+B1 cells (LC_{50}s 43.6 ± 11.1 nM and 25.7 ± 9.1 nM, respectively, p= 0.01, paired t-test). Similarly to VE-821 there was no significant difference in sensitivity between HRD V-C8 cells and HRC V-C8.B2 cells to PF-477736 (LC_{50}s: 118.4 ± 37.0 nM and 99.5 ± 40.0 nM, respectively). Ovarian cancer cell lines (IGROV-1 and UWB1.289+B1) were more sensitive to PF-477736 than cervical cancer cells (C33A and SiHa), however due to the small panel of cell lines used no distinct conclusions can be made. A concentration of 50 nM was selected for combination studies as a compromise between potent target inhibition (76-100%) (Table 5.2) and cytotoxicity (20-75%) (Figure 5.4).

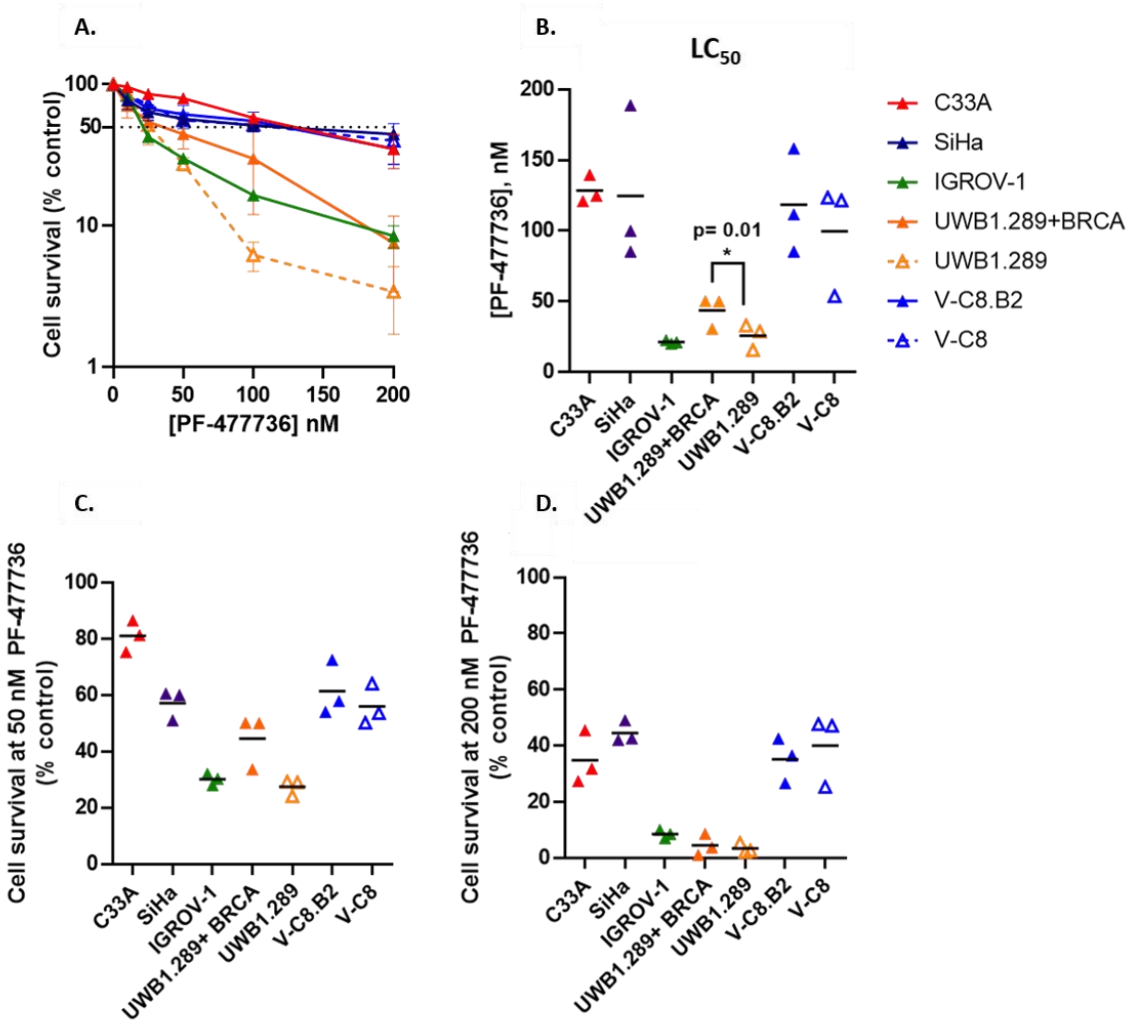


Figure 5.4: Single agent cytotoxicity of PF-477736 across the panel of cancer cells.
A. Cells were exposed to PF-477736 at indicated concentrations (0- 200 nM) for 24 hr prior to replacement with drug-free medium for 8-10 days to allow colony formation. Data are the mean and standard error of 3 independent experiments. Data are mean and standard error of 3 independent experiments. **B.** LC_{50} values were calculated using GraphPad Prism 9.0 software and data are shown as individual experiments, with mean indicated by bar. **C.** Using the colony formation assays, % cell survival was reported across cell line s at set concentrations of 50 and 200 nM PF-477736. **B, C** Individual experiments shown on scatter plots, with the mean bar shown.

5.5.2.3 Single agent cytotoxicity of the WEE1 inhibitor, MK-1775

There was an approximately 4-fold range of sensitivity to MK-1775 with LC_{50} values between 0.1 and 0.5 µM (Figure 5.5). UWB1.289 cells were significantly more sensitive to MK-1775 than UWB1.289 +B1 cells but only at the higher concentrations e.g. at 0.4 µM ($p=0.05$, paired t-test). Interestingly, V-C8 cells appeared no more sensitive to MK-1775 than V-C8.B2 cells. Similarly, to sensitivity to VE-821, C33A and UWB1.289 cells were also most sensitive to MK-1775. The concentration of 0.1 µM was selected for combination studies as at this concentration had <50% cytotoxicity across the panel of cells (Figure 5.5), whilst having >79% target inhibition (Table 5.2).

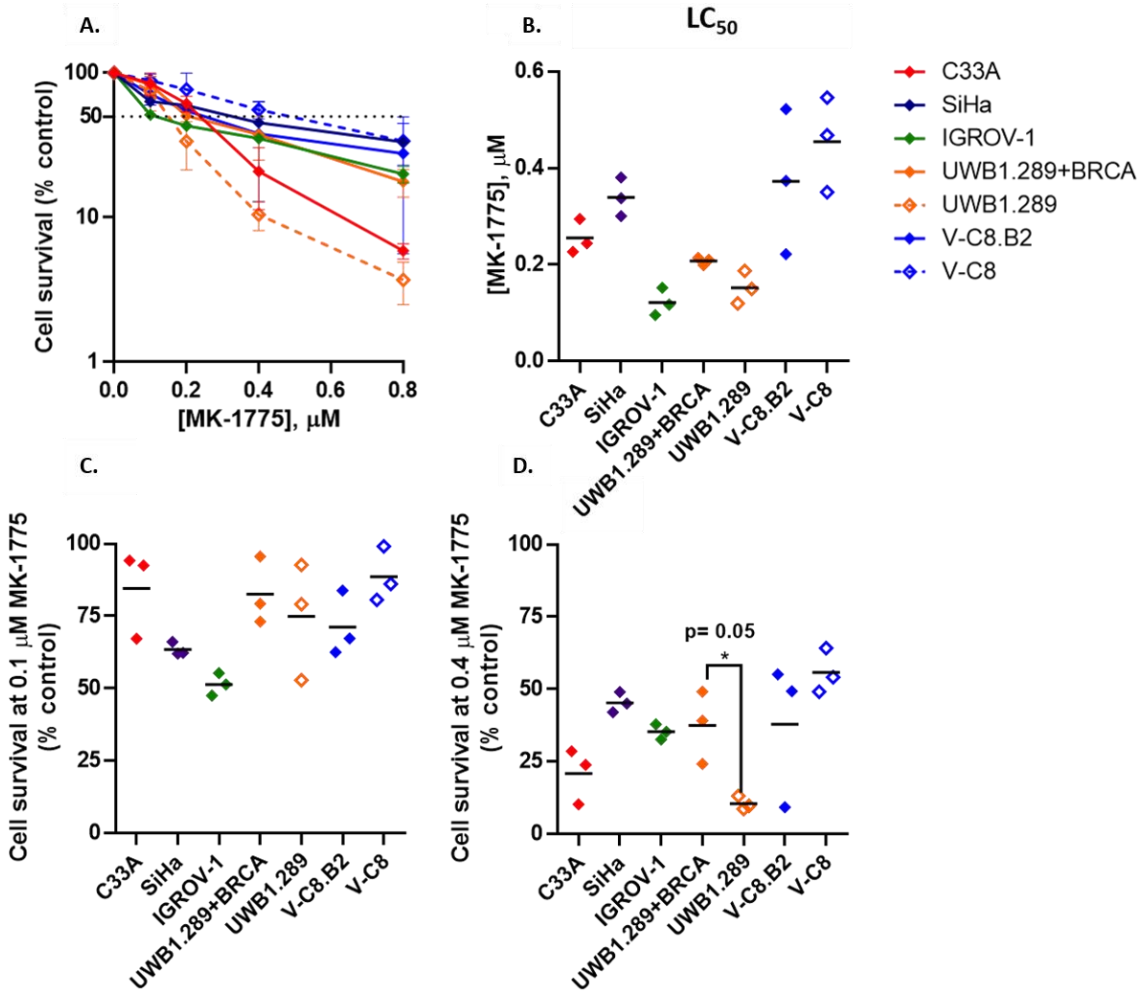


Figure 5.5: Single agent cytotoxicity of MK-1775 in cervical and ovarian cancer cells. A. Cells were exposed to MK-1775 at indicated concentrations (0- 0.8 μM) for 24 hr prior to replacement with drug-free medium for 8-10 days to allow colony formation**.** Data are the mean and standard error of 3 independent experiments. **B.** LC_{50} values calculated using GraphPad Prism 8.0 software. **C.** Using the colony formation assays, % cell survival was reported across cell lines at set concentrations of 0.1 and 0.4 μM MK-1775. **B, C** Individual experiments shown on scatter plots, with the mean bar shown.

5.5.3 Correlation between target inhibition by kinase inhibitors and cell survival

To determine whether the cytotoxicity was merely a reflection of the target inhibition by each of the drugs or if it reflected the complex biology of each cell line, the survival at a given concentration was compared with the inhibition of the target at that concentration (Figure 5.6).

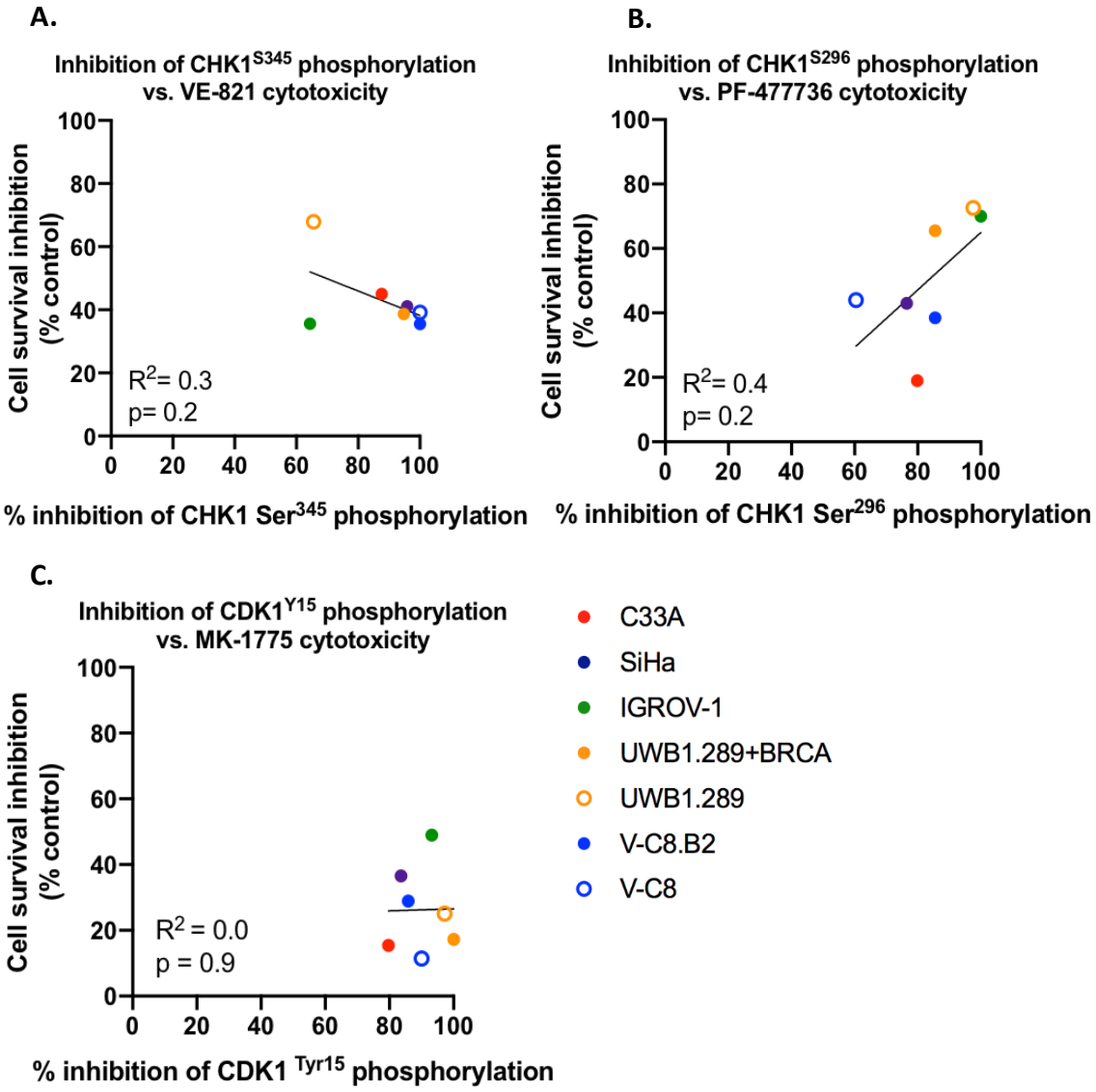


Figure 5.6: Correlation of % target inhibition vs. % cell survival inhibition. A. Both inhibition of CHK1^{S345} phosphorylation and cytotoxicity were measured at a set concentration of 1 µM VE-821. **B.** Inhibition of CHK1^{S296} phosphorylation and cytotoxicity was measured at a set concentration of 50 nM PF-477736. **C.** Inhibition of CDK1^{Tyr15} phosphorylation and cytotoxicity was measured at concentrations of 0.1 µM MK-1775. Data are the mean of 3 independent experiment. Each data point represents a cell line.

No significant correlation was observed between target inhibition and cell survival inhibition across any of the kinase inhibitors, although there appeared to be a weak trend between target inhibition and cell survival inhibition with PF-477736 (r^2=0.4). The lack of significance may reflect the limited number of data points and the semi-quantitative nature of Western blot data for target inhibition, so, although it appears more likely cytotoxicity reflects the cellular biochemistry the extent of target inhibition cannot be excluded as a contributory factor.

5.5.4 Correlation between cell growth and inhibition of cell survival by kinase inhibitors

Doubling times of the cells in the panel ranged from 21 (V-C8.B2) to 55 hours (UWB1.289+ B1), as determined in Chapter 3, section 5.5. ATR, CHK1 and WEE1 have key involvement in cell cycle checkpoint control, as previously described (Chapter 1, section 7.2). It would therefore be predicted that VE-821, PF-477736 and MK-1775 would be more cytotoxic in cells with shorter doubling times.

Doubling time of cells was correlated with LC_{50} values and cell survival at set concentrations of VE-821, PF-477736 and MK-1775, to determine whether cell doubling times is a factor influencing the sensitivity of cells to the checkpoint kinase inhibitors (Figure 5.7). No statistically significant correlations were observed between the doubling time of cells and the sensitivity of cells to the kinase inhibitors.

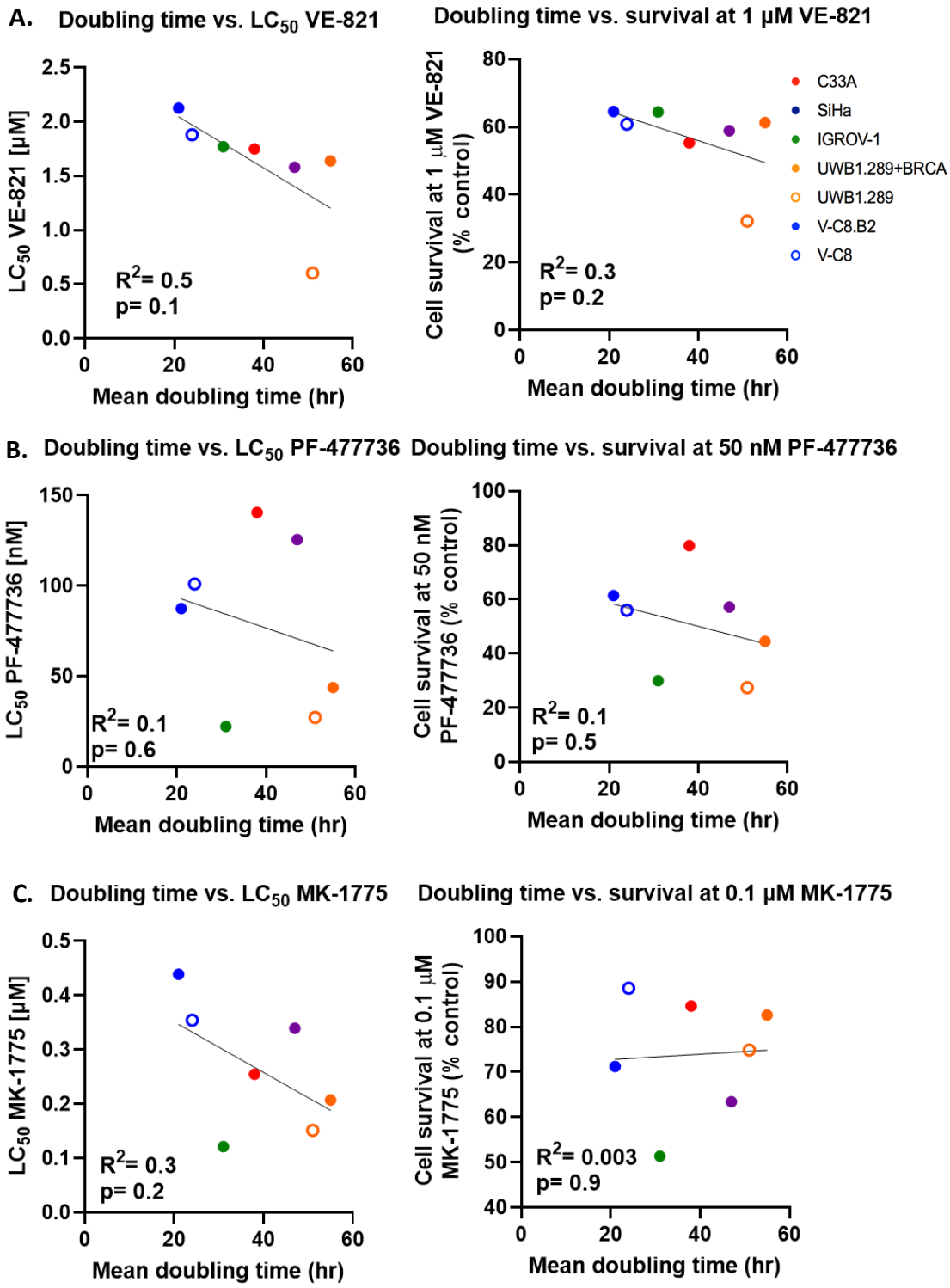


Figure 5.7: Correlation of the doubling time of cells vs. LC_{50} and % cell survival at set concentrations. Mean doubling time of cells was calculated as described in Chapter 3 by SRB cell proliferation assay and plotted against LC_{50} and fixed concentration of **A.** 1 µM VE-821, **B.** 50 nM PF-477736 and **C.** 0.1 µM MK-1775. Correlations were calculated using Graphpad Prism 9.0.

5.5.5 Correlation between RS and inhibition of cell survival by kinase inhibitors

It was predicted a higher level of basal RS would confer cells more sensitive to the ATR, CHK1 and WEE1 inhibitors as this has been previously shown (Murga *et al.,* 2011, Oo *et al.,* 2018, Kok *et al.,* 2020). Basal levels of RS (γH2AX foci and pRPA$^{Ser4/8}$ foci (Chapter 3, section 5.6)) were investigated as determinants of sensitivity to the kinase inhibitors. Cell survival was also correlated with cyclin E and pRPA baseline expression, measured in Chapter 3.

Basal γH2AX foci moderately correlated with both LC_{50} values and cell survival at 1 μM VE-821 (r^2= 0.5 and 0.6, p=0.06 and 0.04, respectively Fig 5.8 A, left panel), with cell lines with lower LC_{50} concentration generally having higher basal γH2AX foci. However, the UWB1.289 cells may have skewed the results and a larger panel of cells would be needed to establish a robust correlation. A weaker trend was observed between basal RS levels and sensitivity to PF-477736 (r^2= 0.2 and 0.4, Fig 5.8 B, left panel), although this was not statistically significant at LC_{50} or 50 nM. No correlation was observed between basal γH2AX foci and sensitivity to MK-1775 (Fig 5.8 C, left panel).

Overall, weaker trends were observed between basal pRPA$^{Ser4/8}$ focus formation and inhibition of cell survival by VE-821 (r^2= 0.2 and 0.3), PF-477736 (r^2= 0.1 and 0.2) and MK-1775 (r^2= 0.03 and 0.1). Similarly, this trend was stronger in VE-821, followed by PF-477736 and a weak trend was observed with MK-1775 (Figure 5.8 right panel).

The relationship between Cyclin E and pRPA level by Western blot and inhibition of cell survival by the checkpoint kinase inhibitors was examined (Figure 5.9). As increased level of these is indicative of increased RS, it would be expected these cells would be more reliant on ATR-CHK1 signalling and would therefore be more sensitive to inhibition of this pathway. Cyclin E had a strong correlation with cell survival inhibition by VE-821 (r^2= 0.8 and 0.9), however this showed that cells with higher basal cyclin E level were less sensitive to VE-821, which was unexpected. It is likely that this is due to the unusual result of HRD UWB1.289 cells, which are most sensitive to VE-821 expressing the lowest levels of cyclin E. This same trend was observed with PF-477736 and MK-1775.

When correlating pRPA protein levels (determined by Western blot) with cell survival a modest trend was observed that higher pRPA levels resulted in increased sensitivity to the kinase inhibitors. This trend was strongest with VE-821 (r^2= 0.5 and 0.7), then PF-477736 (r^2=0.1 and 0.4), with no trend observed with MK-1775 (r^2=0.02 and 0.2). However, the correlations were mostly not significant and appeared to be skewed heavily by UWB1.289 cells, which had the highest level of pRPA and were most sensitive to the kinase inhibitors.

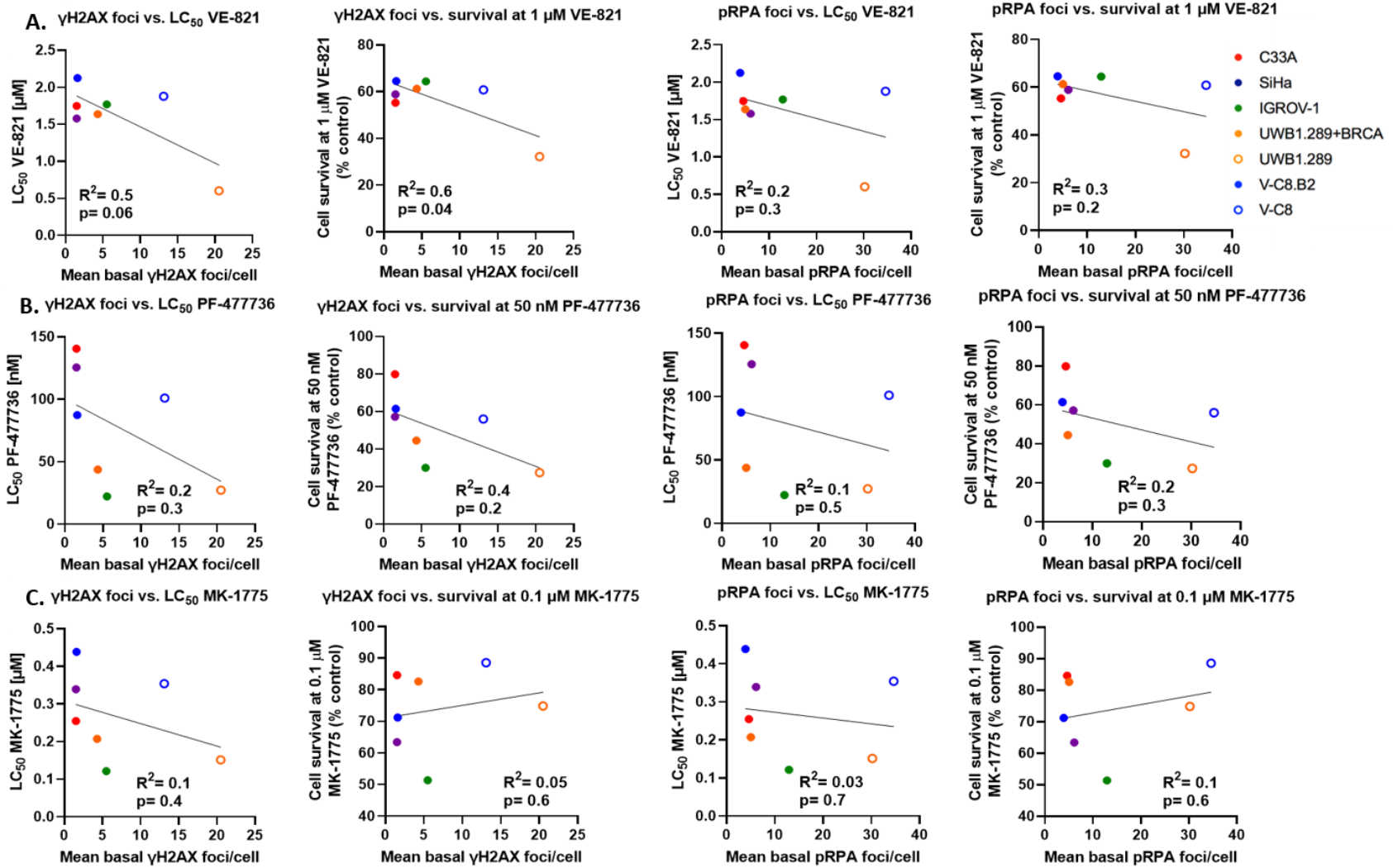


Figure 5.8: Correlation of basal γH2AX and pRPA foci in cells vs. LC_{50} and % cell survival at set concentrations. Mean γH2AX and pRPA foci numbers per untreated cell were calculated as described in Chapter 3 by immunofluorescence and plotted against LC_{50} and fixed concentration of **A.** 1 μM VE-821, **B.** 50 nM PF-477736 and **C.** 0.1 μM MK-1775. Correlations were calculated using Graphpad Prism 9.0.

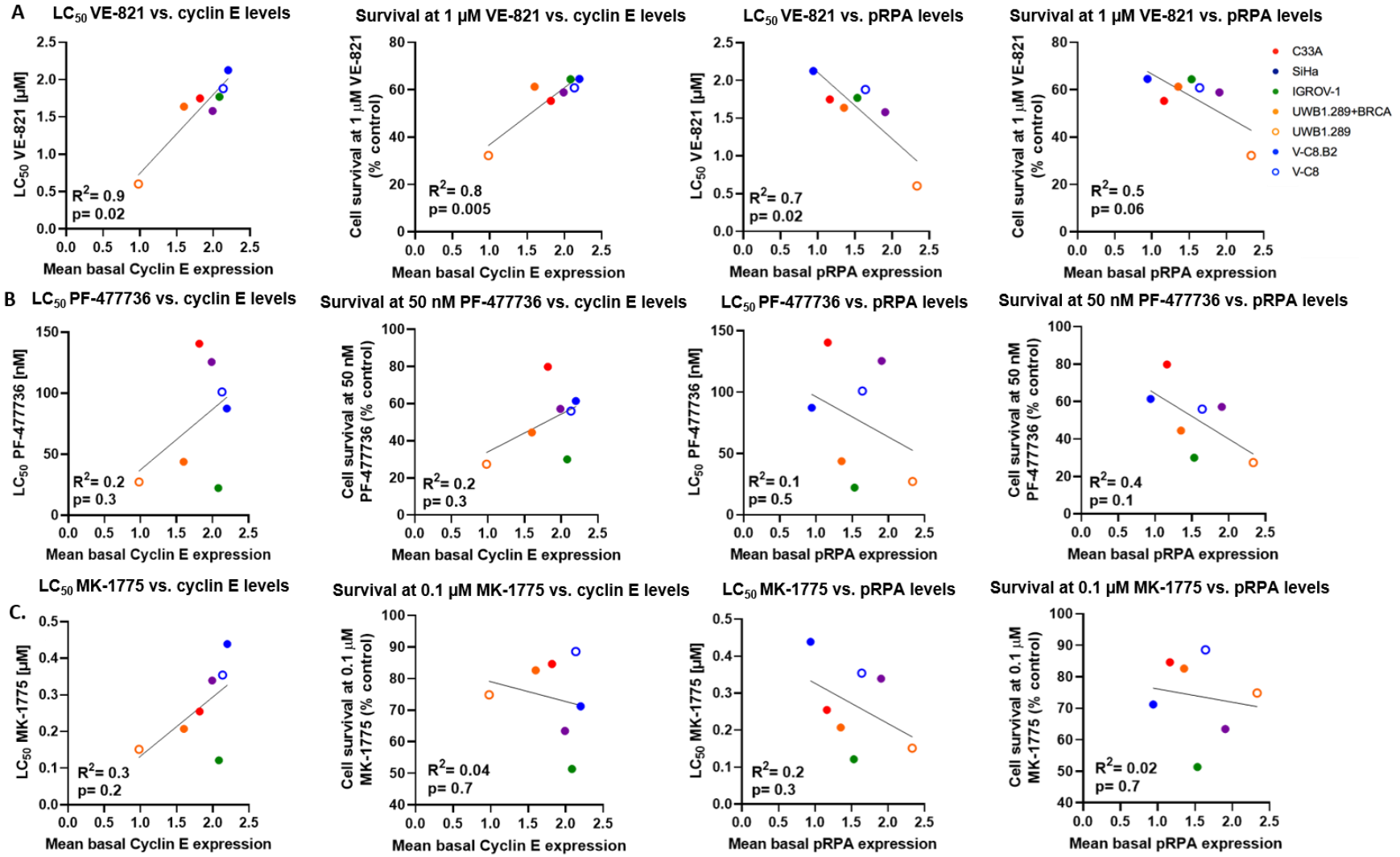


Figure 5.9: Correlation of basal Cyclin E and pRPA level in cells vs. LC_{50} and % cell survival at set concentrations. Mean Cyclin E and pRPA level per untreated cell were calculated as described in Chapter 3 by Western blotting and plotted against LC_{50} and fixed concentration of **A.** 1 µM VE-821, **B.** 50 nM PF-477736 and **C.** 0.1 µM MK-1775. Correlations were calculated using Graphpad Prism 9.0.

5.5.6 Correlation between reported determinants of sensitivity and inhibition of cell survival by kinase inhibitors

Inhibition of cell survival data was correlated against levels of previously identified determinants of sensitivity, as assessed by Western blot in Chapter 3.

5.5.6.1 Correlation of ATM level and sensitivity to checkpoint kinase inhibitors

ATM was analysed, because a range of studies have identified ATM as a key determinant in ATRi sensitivity, with observations that ATRi is synthetically lethal with ATM deficient cancers (Choi *et al.,* 2016, Kwok *et al.,* 2016, Perkhofer *et al.,* 2017, Min *et al.,* 2017).

Across the cell line panel there was a general trend that lower ATM level resulted in increased sensitivity to checkpoint kinase inhibitors (Figure 5.10). This trend was strongest with LC_{50} and cell survival at 50 nM PF-477736 (r^2= 0.5 and 0.3, respectively Figure 5.10 B). The trend was moderate with LC_{50} MK-1775 (r^2= 0.4), and weaker with cell survival at 0.1 µM MK-1775 (r^2 =0.1). The weakest trend was with LC_{50} and 1 µM VE-821 (r^2= 0.1 for both), despite previous reports.

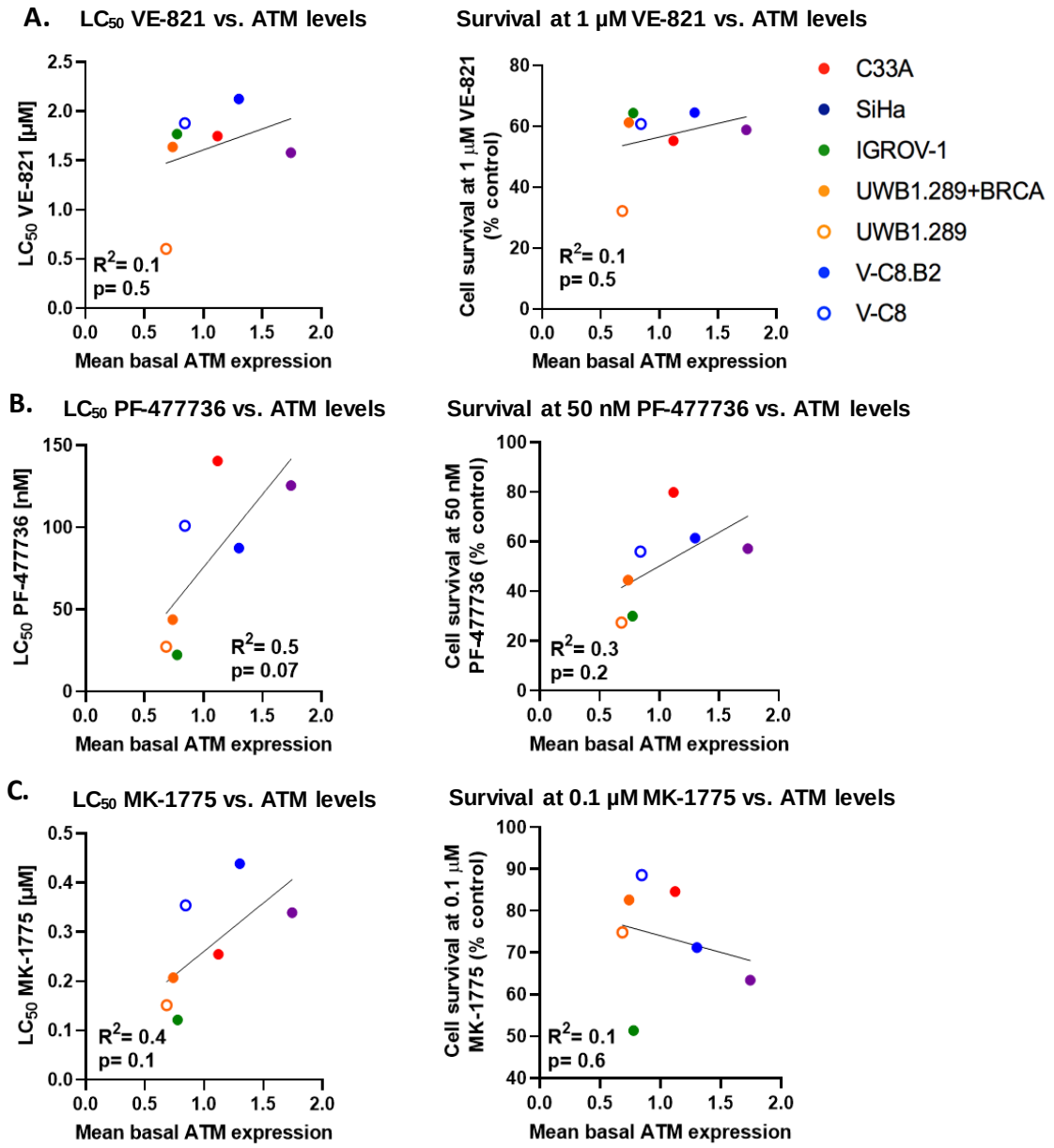


Figure 5.10: Correlation of basal ATM level in cells vs. LC_{50} and % cell survival at set concentrations. Mean ATM level per untreated cell was calculated as described in Chapter 3 by Western blotting and plotted against LC_{50} and fixed concentration of **A.** 1 µM VE-821, **B.** 50 nM PF-477736 and **C.** 0.1 µM MK-1775. Correlations were calculated using Graphpad Prism 9.0.

5.5.6.2 Correlation of ATR level and sensitivity to checkpoint kinase inhibitors

Mohni *et al.,* showed that in a synthetic lethal screen with VE-821, ATR level was identified as a determinant of sensitivity (Mohni *et al.,* 2014). However, here, no correlation was observed between low ATR level and increased cellular sensitivity to the kinase inhibitors. In the majority of instances, the trend indicated that lower ATR level caused less sensitivity to the kinase inhibitors (Fig 5.11).

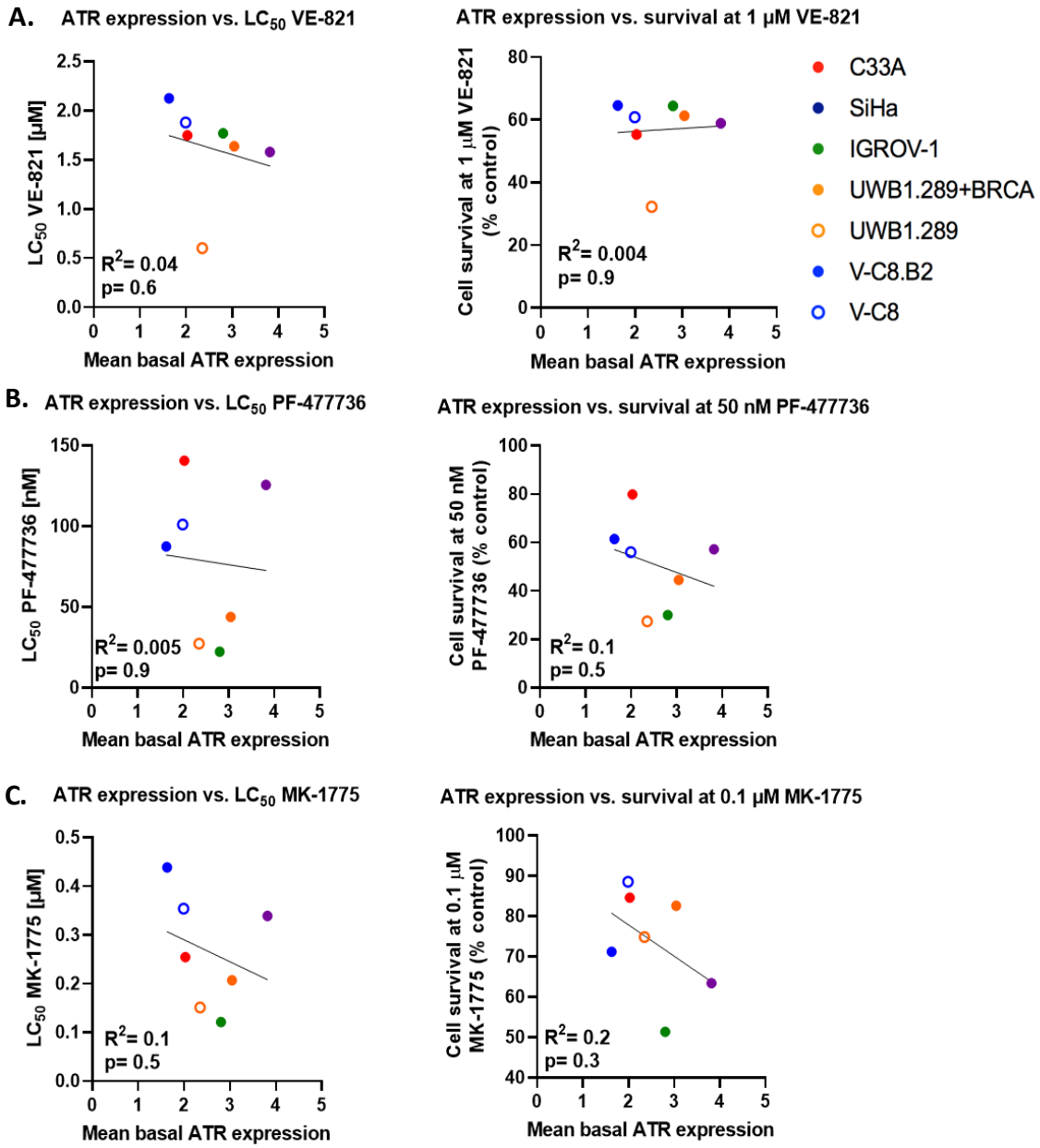


Figure 5.11: Correlation of basal ATR level in cells vs. LC_{50} and % cell survival at set concentrations. Mean ATR level per untreated cell was calculated as described in Chapter 3 by Western blotting and plotted against LC_{50} and fixed concentration of **A.** 1 µM VE-821, **B.** 50 nM PF-477736 and **C.** 0.1 µM MK-1775. Correlations were calculated using Graphpad Prism 9.0.

5.5.6.3 Correlation of CHK1 level and sensitivity to checkpoint kinase inhibitors

The synthetically lethal screen also showed CHK1 silencing was synthetically lethal with ATRi (Mohni *et al.,* 2014).

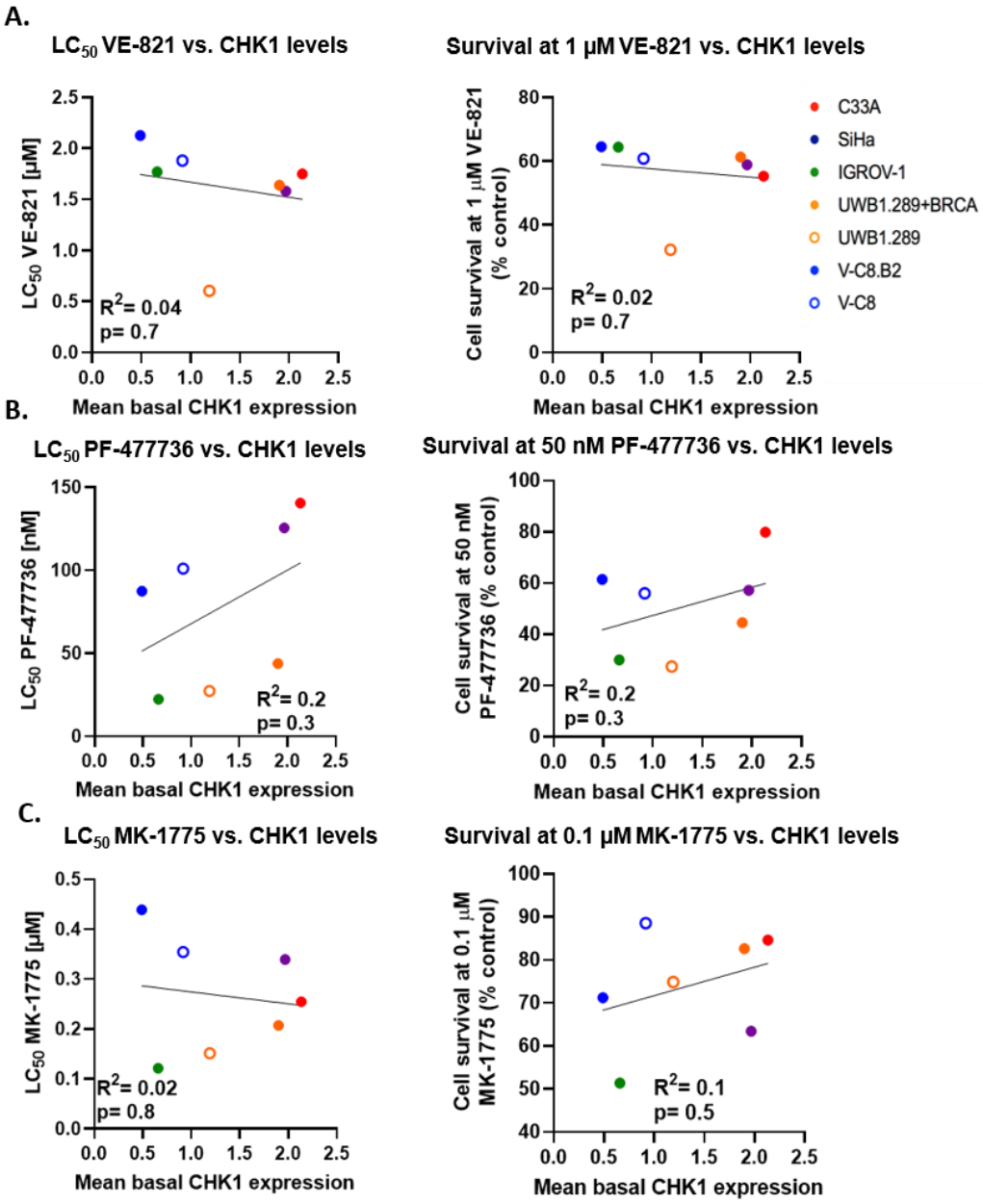


Figure 5.12: Correlation of basal CHK1 expression in cells vs. LC_{50} and % cell survival at set concentrations. Mean CHK1 expression per untreated cell was calculated as described in Chapter 3 by Western blotting and plotted against LC_{50} and fixed concentration of **A.** 1 µM VE-821, **B.** 50 nM PF-477736 and **C.** 0.1 µM MK-1775. Correlations were calculated using Graphpad Prism 9.0.

5.5.6.4 Correlation of WEE1 level and sensitivity to checkpoint kinase inhibitors

Correlation between WEE1 level and sensitivity to the kinase inhibitors was assessed across the panel. However no significant correlations were observed (Fig 5.13)

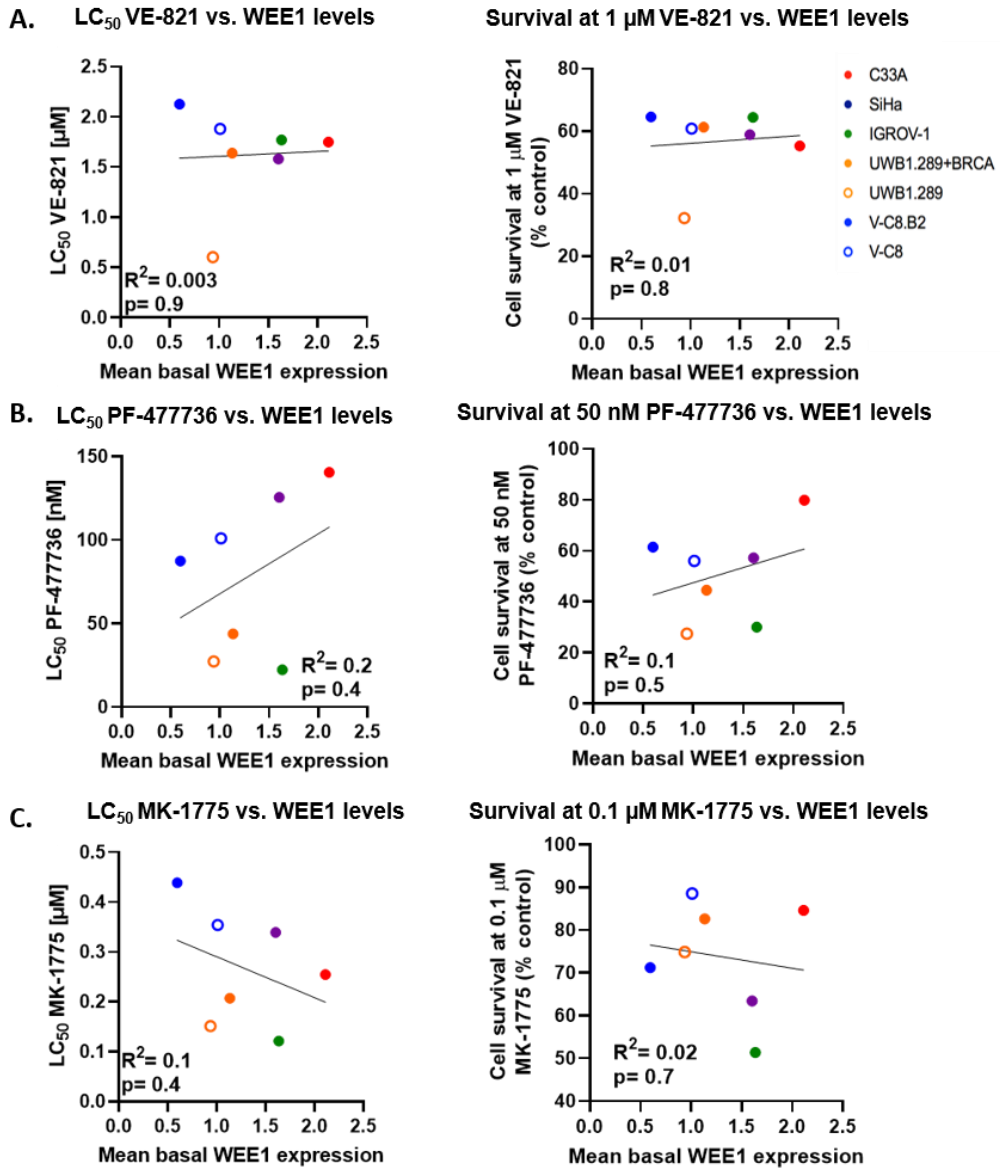


Figure 5.13: Correlation of basal WEE1 expression in cells vs. LC_{50} and % cell survival at set concentrations. Mean WEE1 expression per untreated cell was calculated as described in Chapter 3 by Western blotting and plotted against LC_{50} and fixed concentration of **A.** 1 µM VE-821, **B.** 50 nM PF-477736 and **C.** 0.1 µM MK-1775. Correlations were calculated using Graphpad Prism 9.0.

5.5.6.5 Correlation of PARP-1 and XRCC1 level and sensitivity to checkpoint kinase inhibitors

BER/SSBR proteins (XRCC1 and PARP-1) have been shown to confer sensitivity to ATR, CHK1 and WEE1 inhibition, due to the synthetic lethal relationship between inactivation of SSBR and HRR, and the involvement of the kinases in signalling to HRR (Peasland *et al.,* 2011, Sultana *et al.,* 2013, Middleton *et al.,* 2015, Ali *et al.,* 2020).

However, there was no correlation between PARP-1 or XRCC1 level and sensitivity to ATR, CHK1 or WEE1 inhibition (Fig 5.14).

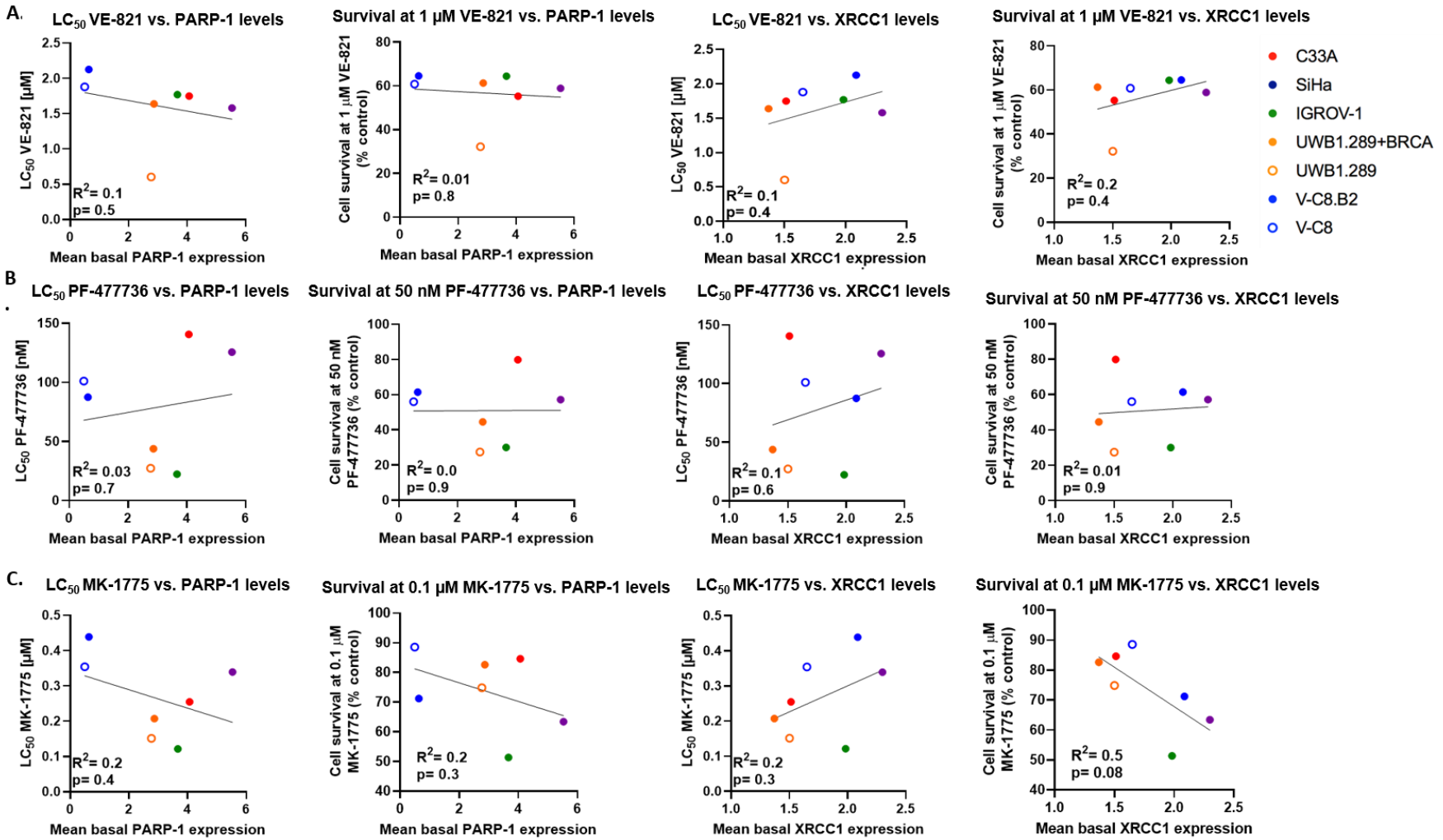


Figure 5.14: Correlation of basal BER protein expression in cells vs. LC_{50} and % cell survival at set concentrations. Mean PARP-1 and XRCC1 expression per untreated cell was calculated as described in Chapter 3 by Western blotting and plotted against LC_{50} and fixed concentration of **A.** 1 µM VE-821, **B.** 50 nM PF-477736 and **C.** 0.1 µM MK-1775. Correlations were calculated using Graphpad Prism 9.0.

5.5.6.6 Correlation of BRCA1 and RAD51 level and sensitivity to checkpoint kinase inhibitors

The downregulation of key HRR proteins have been shown to confer sensitivity to ATR, CHK1 and WEE1 inhibitors (Krajewska *et al.,* 2015, Middleton *et al.,* 2015, Massey *et al.,* 2016). However, analysis of the data on the panel of cells studied here there was no significant correlation between BRCA1 or RAD51 levels and sensitivity to the inhibitors.

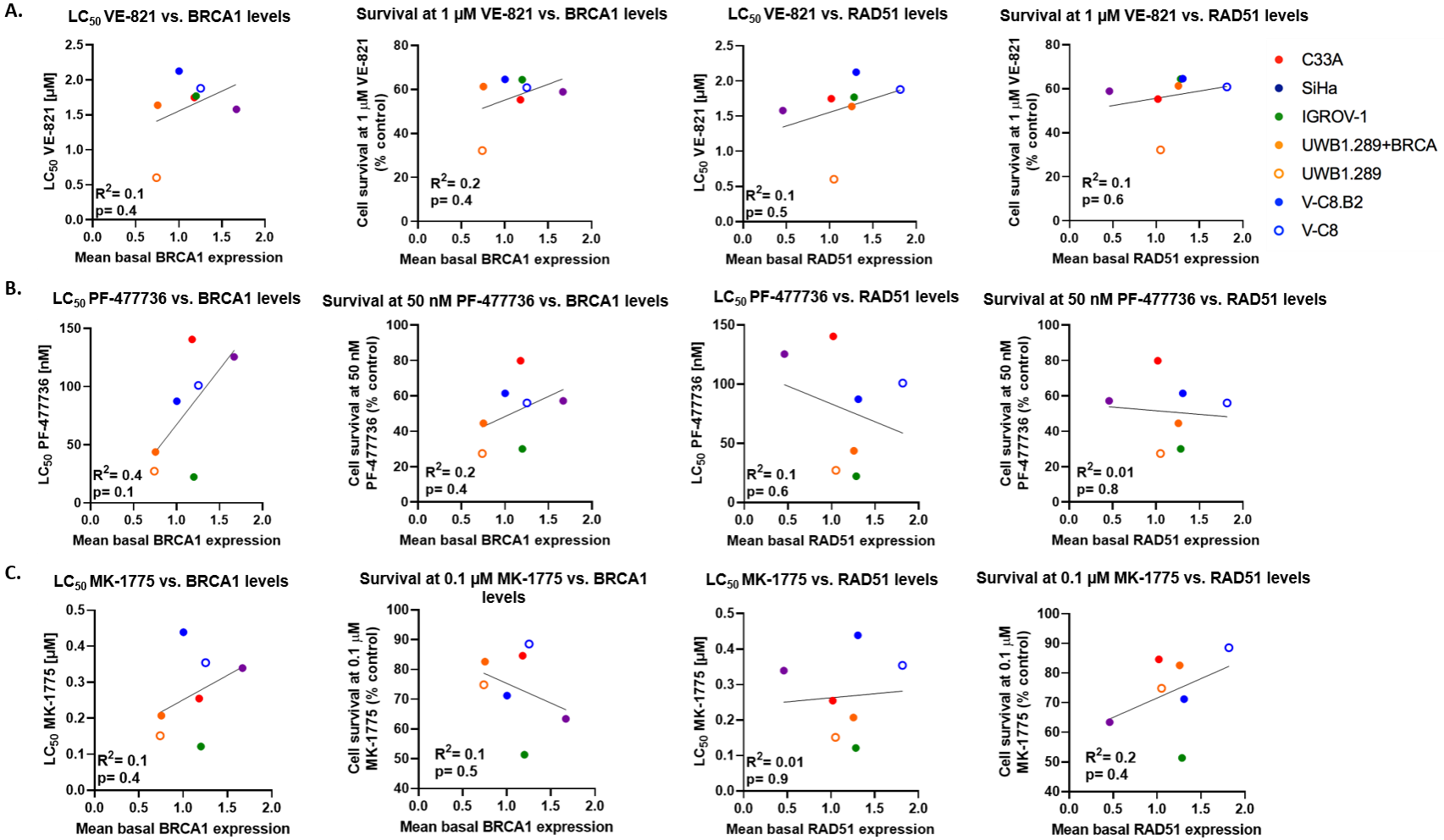


Figure 5.15: Correlation of basal HRR protein expression in cells vs. LC_{50} and % cell survival at set concentrations. Mean BRCA1 and RAD51 expression per untreated cell was calculated as described in Chapter 3 by Western blotting and plotted against LC_{50} and fixed concentration of **A.** 1 µM VE-821, **B.** 50 nM PF-477736 and **C.** 0.1 µM MK-1775. Correlations were calculated using Graphpad Prism 9.0.

5.6 Discussion

PARP inhibition was confirmed as a cause of RS as demonstrated by the 3 to 7-fold increase in γH2AX after exposure to rucaparib, described in Chapter 4, section 5.4, and in the literature (Mukhopadhyay *et al.,* 2010, Michelena *et al.,* 2018). It has previously been shown that ATR, CHK1 and WEE1 are activated by replication stress and DNA damage (Calecott *et al.,* 2014, Kim *et al.,* 2017, Fang *et al.,* 2019). Here we showed that rucaparib-induced RS activated ATR, CHK1 and WEE1 as determined by the increase of pCHK1^{S345}, pCHK1^{S296} and pCDK1^{Tyr15} levels across all cell lines. Rucaparib increased pCHK1^{S345} levels the most, followed by pCHK1^{Ser296} but with only a modest observed increase in pCDK1^{Tyr15} as untreated cells had high levels of pCDK1^{Tyr15}. This could be due to other factors such as Myelin transcription factor 1 (MYT1), which has been shown to act independently of WEE1 and also phosphorylate CDK1 (Chow and Poon, 2013, de Gooijer *et al.,* 2017).

Across all cell lines ATRi VE-821 reduced pCHK1^{S345} levels as well as pCHK1^{S296} and pCDK1^{Tyr15} downstream, as previously shown (Pires *et al.,* 2012). The spectrum of target inhibition ranged from 88-96% in cervical cancer cells and 64-95% in ovarian cancer cell lines, which were similar to target inhibition data obtained in the same cell lines previously within the group (Table 5.1). Cellular IC_{50}s differ from those generated in cell-free biochemical assays, because the ATP (substrate) concentrations differ (1-10 mM intracellular concentrations vs. 1-10 µM used in biochemical assays) (Bonora *et al.,* 2012).

CHK1i PF-477736 decreased pCHK1^{Ser296} levels across all cells at both 50 and 200 nM and also decreased pCDK1^{Tyr15} levels. Increased CHK1^{Ser345} phosphorylation was also observed in response to CHK1 inhibition, suggesting upstream ATR activation as previously described (Massey *et al.,* 2016, Syljuasen *et al.,* 2005).

MK-1775 decreased pCDK1^{Tyr15} levels in cell lines tested but increased both pCHK1^{Ser296} and pCHK1^{Ser345} upstream as previously reported (Bukhari *et al.,* 2019). Inhibition of

CDK1 phosphorylation by MK-1775 may be somewhat counteracted by the activation of CHK1 leading to the inactivation of CDC25C which dephosphorylates CDK1.

Although there was a narrow range of VE-821 LC_{50} values (1.6-2.1 µM, excluding UWB1.289 cells), in this instance LC_{50} is not an accurate representation of the observed sensitivity, particularly at the higher concentrations. HRR defective UWB1.289 cells harbouring a *BRCA1* defect were significantly more sensitive to VE-821 compared to HRR competent matched UWB1.289+ B1 cells (p=0.001). Interestingly at the higher concentrations of VE-821, C33A cells were just as sensitive as HRR defective UWB1.289 cells, perhaps suggesting at the higher concentrations there may be some off-target effects.

There was a wider spectrum of sensitivity to PF-477736 across cell lines, with LC_{50} values varying ~5-fold. The cell line sensitivity could be grouped based on cancer type, with cervical cells (C33A and SiHa) being resistant to PF-477736 and ovarian cells being more sensitive (UWB1.289, UWB1.289+B1, IGROV-1). Previous work comparing single agent sensitivity to PF-477736 across a larger panel of ovarian, lung and breast cancer cell lines, found ovarian cancer cells were not preferentially sensitised (Bryant *et al.,* 2014). The panel of ovarian cells used by Bryant *et al* did not include the 3 tested here, which shows ultimately no distinct conclusions can be made from a small panel of cell lines.

UWB1.289 cells were more sensitive to all 3 kinase inhibitors compared to *BRCA1* competent UWB1.289+ B1 cells indicating a role for BRCA1 in the response to kinase inhibition. HRR status has been shown previously to be a determinant of ATR, CHK1 and WEE1 inhibitor sensitivity (Williamson *et al.,* 2016, Middleton *et al.,* 2015, Kim *et al.,* 2017, Do *et al.,* 2015). However, the *BRCA2* mutant VC8 cells were not significantly more sensitive to any of the inhibitors compared to their *BRCA2* corrected counterpart. This could be due to the differences in *BRCA1* and *BRCA2* involvement in different stages of HRR. Unlike *BRCA2, BRCA1* is heavily involved in the G1/S, S-phase and G2-M checkpoint control, which may be why increased sensitivity to the kinase inhibitors was observed in UWB1.289 cells but not V-C8 cells. The correlation between BRCA1 level and sensitivity to kinase inhibitors was weak and could not be interpreted due to the suspected lack of

specificity of the antibody. RAD51 levels also did not correlate with cytotoxicity either. These data support the notion that the identification of these determinants of sensitivity using paired cell lines may not translate to heterogeneous cell lines, which reflect the real-life situation of a patient with cancer or be suitable for predictive biomarker development.

There was a lack of correlation between target inhibition and cytotoxicity, suggesting sensitivity to the kinase inhibitors was due to the cellular response to kinase inhibition. Across the range of concentrations of kinase inhibitors cells ranked least to most sensitive as: SiHa, UWB1.289+ B1, IGROV-1, C33A and UWB1.289 with VE-821, C33A, SiHa, UWB1.289+B1, IGROV-1 and UWB1.289 with PF-477736 and SiHa, UWB1.289+B1, IGROV-1, C33A then UWB1.289 cells with MK-1775. These orders of sensitivity of the human cell lines were similar across the kinase inhibitors, which may be reflective of their dependence on S/G2/M checkpoint signalling. Various previously identified predictors of sensitivity (ATM, HRR, BER, RS, cyclin E etc.) were therefore investigated.

RS as measured by $pRPA^{Ser4/8}$ level correlated with sensitivity to VE-821 (r^2= 0.5 and 0.7 at LC_{50} and 1 µM). This trend was weaker with PF-477736 (r^2= 0.1 and 0.4 at LC_{50} and 50 nM) and weak with MK-1775 (r^2= 0.2 and 0.2 at LC_{50} and 0.1 µM). Curiously, when RS was measured by pRPA foci there was no significant correlation with any of the inhibitors. There was, however a moderate correlation observed between basal RS when measured by γH2AX and sensitivity to VE-821, a weaker correlation with sensitivity to PF-477736 and no correlation with sensitivity to MK-1775. Moreover, it is clear that the UWB1.289 cells could be skewing the trend between basal RS and VE-821, as when these are removed from analyses the correlation was considerably lower (r^2= 0.04, not significant, for both). Ultimately if RS was a determinant of sensitivity to VE-821 it would be expected that V-C8 cells with high basal RS would have a lower LC_{50} and percentage cell survival, which they do not. Similarly, V-C8 cells were not any more sensitive to PF-477736 cells.

ATM loss is widely reported to confer sensitivity to ATRi (Smith *et al.,* 2020), although there is less in the literature regarding ATM loss and increased sensitivity to CHK1 or

WEE1 inhibition. However, the only significant correlation of ATM levels with the inhibitors observed in the panel of cells used here was with PF-477736. Therefore, it seems unlikely that ATM levels per se can be taken as universally indicative of single agent ATR, CHK1 or WEE1 cytotoxicity when dealing with heterogenous cell types (as here). ATM activity may be a better indicator in more homogeneous cell types as described recently in neuroblastoma (Southgate *et al.,* 2020).

ATR and CHK1 levels were not a determinant of sensitivity, despite previous reports (Mohni *et al.,* 2014). Similarly, levels of XRCC1 or PARP1 did not impact sensitivity to VE-821, PF-477736 or MK-177, despite previous reports of the sensitivity of XRCC1-defective and PARP inhibited cells to ATRi (Peasland *et al.,* 2011, Sultana *et al.,* 2013). As discussed in Chapter 4, these determinants were established via high-throughput siRNA screens, assessing a predictor of sensitivity in isolation. Contrastingly, here, there are many other factors at play within the cells, which could be affecting their response to the kinase inhibitors and therefore masking these correlations.

The data described in this chapter regarding target inhibition and single agent cytotoxicity of the kinase inhibitors allowed for the selection of 1 µM VE-821, 50 nM PF-477736 and 0.1 µM MK-1775 concentrations to be used in combination cytotoxicity and mechanistic experiments with rucaparib, as these concentrations generally inhibit >50% of their relevant targets and cause <50% inhibition of cell survival.

Chapter 6. Potentiation of rucaparib cytotoxicity by VE-821, PF-477736 and MK-1775 and underlying mechanisms of synergy

6.1 Introduction

Increased RS in cancer cells (eg. due to oncogenes or loss of G1 checkpoint control via e.g., p53 mutation) is thought to cause an increased dependence on S/G2 checkpoints (Massague *et al.,* 2004, Magdalou *et al.,* 2014). As shown in Chapter 4, PARP inhibition causes RS, which in turn activates ATR, CHK1 and WEE1 (Chapter 4, section 5.5) as reported by others (Southgate *et al.,* 2020, Gralewska *et al.,* 2020, Wielgos-Bonvallet *et al.,* 2018). There was a trend observed in Chapter 5 between basal RS (measured by γH2AX and pRPA foci formation) and cell survival at 1 μM VE-821 (r^2= 0.6 and 0.3), 50 nM PF-477736 (r^2= 0.4 and 0.2) and 0.1 μM (r^2= 0.05 and 0.1). It was therefore hypothesised that rucaparib would result in increased dependency on ATR, CHK1 and WEE1 signalling for survival and that the correlation of ATR and CHK1 sensitivity with levels of RS meant that co-inhibition of these pathways might be synthetically lethal.

Furthermore, the contribution that ATR, CHK1 and WEE1 are reported to make to HRR, along with the synthetic lethality of PARPi with HRR defects, suggests that a combination of ATR, CHK1 or WEE1 inhibition may be synthetically lethal with PARPi. Peasland *et al.,* were the first to show that the ATR inhibition was synthetically lethal when used in combination with PARP inhibition (Peasland *et al.,* 2011). This was followed by more preclinical studies combining PARPi with ATRi as well as inhibitors of CHK1 and WEE1 also (Mohni *et al.,* 2015, Kim *et al.,* 2017, Booth *et al.,* 2013, Yin *et al.,* 2017, Brill *et al.,* 2017, Karnak *et al.,* 2014, Parsels *et al.,* 2018), although few studies have considered the impact on HRR as the underlying mechanism for the observed synergy.

Many combinations of PARPi and ATR, CHK1 or WEE1 inhibitors have progressed to clinical trials. Several trials with ATRi AZD6738 are being used in combination with PARPi olaparib (NCT03682289, NCT03462342, NCT03428607, NCT03878095, NCT03330847, NCT03787680, NCT02576444, NCT02937818, and NCT02264678). The CHK1i prexasertib (LY2606368) has entered phase 1 and 2 clinical trials in combination with DNA damaging agents, however there is only one clinical trial with a PARPi (NCT03057145) despite promising pre-clinical data. The WEE1i AZD1775 is also being used in ongoing trials with

PARPi olaparib (NCT02511795). However, as yet no study has directly compared the effects of ATR, CHK1 and WEE1 inhibitors on PARPi cytotoxicity and the underlying mechanisms.

Although PARPi have been successful in clinic so far, they are only approved for use in HRD cancers. However, many cancers are not HRD and the development of resistance to PARP inhibition in cells and tumours originally sensitive by virtue of HRD has been observed both pre-clinically and clinically, often due to restoration of HRR function (Li *et al.,* 2020). A way to induce/restore an HRD phenotype therefore offers the possibility of inducing/restoring sensitivity in cancers with inherent or acquired resistance.

Here, to better understand the mechanism underlying the synergy between PARPi and the kinase inhibitors, HRR competent and defective matched cells were used to determine the extent of sensitisation due to impact on HRR function. As shown in Chapter 4, HRD UWB1.289 and V-C8 cells were 62 and <1000-fold more sensitive to rucaparib than their HRC matched counterpart, respectively. It is estimated that >50% of ovarian carcinomas are HRD and therefore sensitive to PARPi treatment (Mukhopadhyay *et al.,* 2010). Cell cycle investigations were also performed, to assess potentiation by kinase inhibitors on PARPi-induced cytotoxicity and the impact on cell cycle checkpoint control.

6.2 Aims and Objectives

The main aims of this chapter are:

- To determine potentiation of rucaparib cytotoxicity by kinase inhibitors across cell lines

- To assess the impact of kinase inhibitors on HRR using a functional immunofluorescence assay

- To measure the impact of rucaparib and kinase inhibitors on cell cycle using flow cytometry

- To assess any correlation between basal RS or rucaparib-induced RS in cells and the degree of sensitisation to rucaparib by the kinase inhibitors

- To determine how much impact the inhibition of SSB repair vs PARP trapping has on any synergy observed between rucaparib and kinase inhibitors

6.3 Hypotheses

1. Inhibition of ATR, CHK1 or WEE1 will potentiate rucaparib-induced cytotoxicity by targeting the G2/M checkpoint and force mitotic entry of damaged cells.

2. Due to their involvement in HRR, ATR/CHK1/WEE1 inhibitors will be synthetically lethal with rucaparib.

3. The synergy between rucaparib and kinase inhibitors is due to inhibition of SSB repair rather than PARP trapping.

6.4 Materials and Methods

6.4.1 Determining potentiation by combination cytotoxicity experiments

Cytotoxicity experiments were performed as described in Chapter 2. Rucaparib was used at 0- 30 μM in HRC C33A, SiHa, IGROV-1, UWB1.289+B1 and V-C8.B2 cells, which was adjusted to 0-3 μM in HRD UWB1.289 cells and 0-0.3 μM in V-C8 cells, to account for increased sensitivity. Cells were treated with single agent rucaparib or a combination of rucaparib with either 1 μM VE-821, 50 nM PF-477736 or 0.1 μM MK-1775 for 24 h. Colonies were fixed and counted as previously described.

6.4.2 Assessment of homologous recombination repair function by immunofluorescence

To assess the impact of the inhibitors on HRR function, immunofluorescence was carried out as described in Chapter 2, section 10.2. Cells were seeded onto coverslips and exposed to DMSO, 10 μM rucaparib or 10 μM rucaparib with either 1 μM VE-821, 50 nM PF-477736 or 0.1 μM MK-1775 for 24 h. Cells were imaged and analysed as previously described.

6.4.3 Assessment of cell cycle by flow cytometry

Exponentially growing IGROV-1 cells were exposed to either DMSO, 1 μM rucaparib, 10 μM rucaparib, 1 μM VE-821, 50 nM PF-477736 or 0.1 μM MK-1775, or co-exposure to 1 μM or 10 μM rucaparib with each of the kinase inhibitors. Following 30 hours (1 cell doubling), in the final hour of treatment cells were exposed to 10 μM EdU. Cells were fixed prior to the addition of Click-iT EdU detection mix (Thermofisher Scientific, Waltham, MA, USA), and analysis was performed using Attune Nxt Cytometer, as previously described. De Novo FCS Express 7 software was used to analyse the data.

6.4.4 Determining the role of PARP trapping by experiments using AA8 and EM9 cells

Matched AA8 (XRCC1/BER competent) and EM9 (XRCC1/BER defective) were used to investigate the role of PARP trapping in the synergy between rucaparib and kinase inhibitors as follows.

6.4.4.1 Determining the contribution of BER defect vs PARP inhibition in kinase inhibitor cytotoxicity

AA8 and EM9 cells were treated for 24 h with either single agent VE-821 (0- 30 µM), PF-477736 (0- 200 nM) or MK-1775 (0- 1.6 µM) or the range of the inhibitors in combination with 1 µM rucaparib. After 7-10 days colonies were fixed and counted as previously described.

6.4.4.2 Assessing differences in DNA damage and repair between AA8 and EM9 cells

As described in Chapter 2, γH2AX and RAD51 were used as markers to determine HRR function in response to DNA damage by the inhibitors. Due to the high percentage of γH2AX pan-stained EM9 cells fluorescence intensity was used to assess induction of DNA damage, as opposed to the foci counts of γH2AX described previously.

6.4.4.2 Statistical analyses

Statistical analyses were performed using GraphPad prism software version 9.0 (San Diego, CA, USA). The type of test used in each analyses is stated and a p-value of <0.05 was considered statistically significant.

6.5 Results

6.5.1 Potentiation of rucaparib by kinase inhibitors

The ability of VE-821, PF-477736 and MK-1775 to sensitise the panel of cells to rucaparib was measured using cytotoxicity assays, in which a set concentration of each inhibitor was added to a range of rucaparib concentrations. The set concentrations of 1 µM VE-821, 50 nM PF-477736 and 0.1 µM MK-1775 were determined from considering target inhibition and single agent cytotoxicity data from Chapter 5 and represent a balance between >50% target inhibition without excessive cytotoxicity (>50% cell survival).

VE-821, PF-477736 and MK-1775 each significantly sensitised HRC C33A (Two-way ANOVA, $p<0.0001$ with each kinase inhibitor), SiHa (Two-way ANOVA, $p= 0.002$, $p=0.0005$, $p=0.0023$, respectively) and IGROV-1 (Two-way ANOVA, $p<0.0001$ with each kinase inhibitor) cells (Figure 6.1, top line). When considering each cell line individually, kinase inhibitors potentiated rucaparib at the LC_{50} to a similar extent across HRC C33A

(13.7 to 23.1-fold), SiHa (26.1 to 34.7-fold), IGROV-1 (6.9 to 22.4-fold), UWB1.289+ B1 (2.0 to 11.9-fold) and V-C8.B2 cells (7.4 to 26.1-fold), with no significant difference between the potentiation of the kinase inhibitors (Figure 6.2). There was some variation in potentiation between cell lines with reduced potentiation in IGROV-1 cells compared to the other cell lines across the panel.

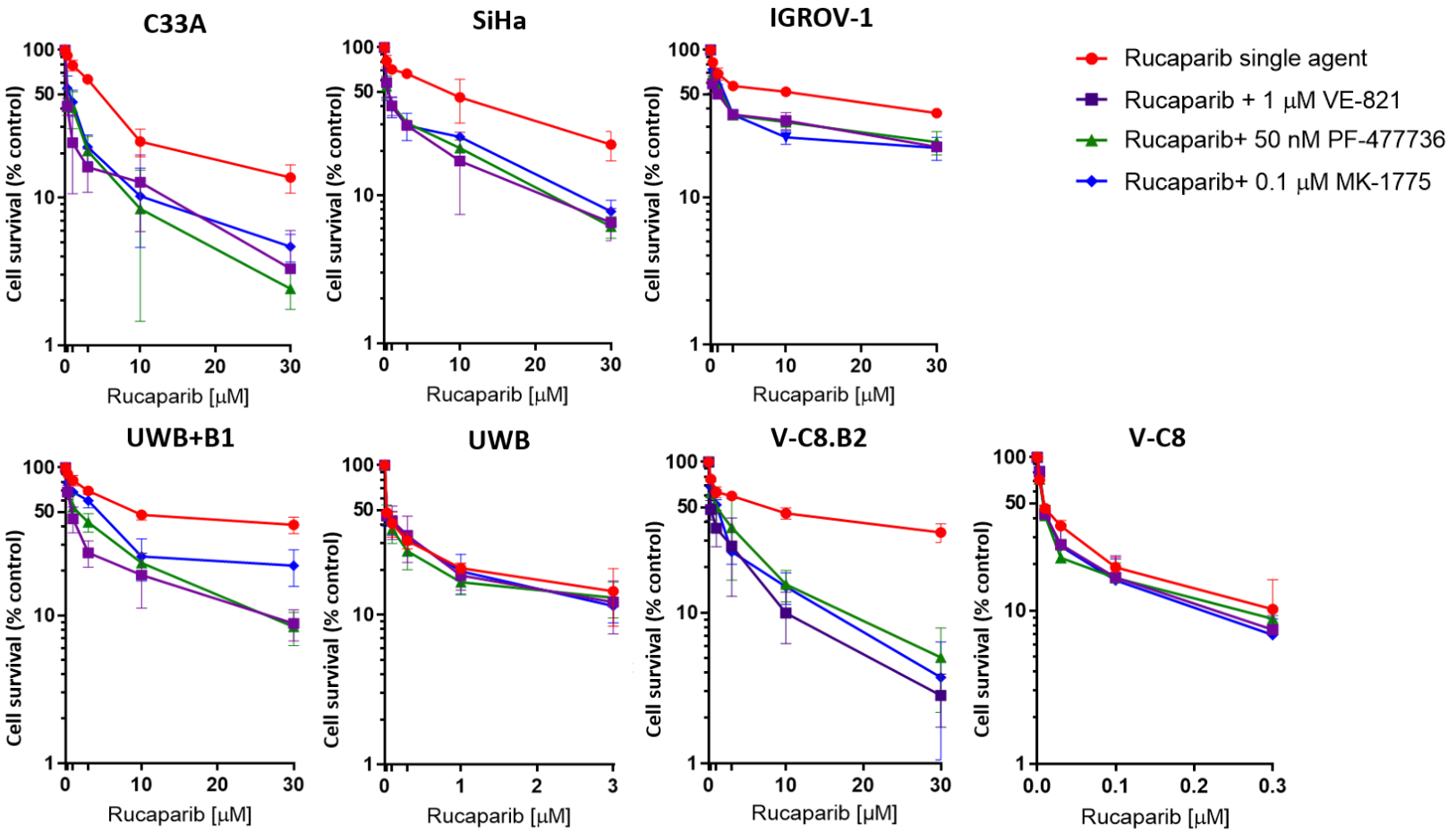


Figure 6.1: Cytotoxicity of rucaparib in combination with VE-821, PF-477736 or MK-1775 in all cell lines. Cells were exposed to rucaparib at indicated concentrations either as single agent or with the addition of 1 μM VE-821, 50 nM PF-477736 or 0.1 μM MK-1775 for 24 hr prior to replacement with drug-free medium for 8-10 days to allow colony formation. Data are representative of the mean and standard error of 3 independent experiments. Cell survivals with exposure to combination treatments were normalised to single agent set concentrations of VE-821 (1 μM), PF-477736 (50 nM) and MK-1775 (0.1 μM).

Matched HRR competent and defective cells were used to investigate whether this synergy was exclusive to HRC cancer cells. VE-821 and PF-477736 significantly sensitised ovarian UWB1.289 *BRCA1* corrected cells to rucaparib (Two-way ANOVA, $p < 0.0001$ and $p = 0.002$, respectively). The sensitisation of UWB1.289+ B1 cells to rucaparib by MK-1775 was not statistically significant (Two-way ANOVA, $p = 0.09$), however, the potentiation at the LC_{50} was 2-fold, indicating potentiation by MK-1775 is does occur. In contrast there was no sensitisation of rucaparib in HRD UWB1.289 cells by VE-821, PF-477736 or MK-1775. A lower concentration range of rucaparib was used for these HRD cells, to account for their increased sensitivity to rucaparib. However, even at a concentration of 1 µM there was no significant sensitisation, in contrast to 1.2 to 1.8-fold sensitisation in UWB1.289+ B1 cells at this concentration of rucaparib.

This difference in sensitisation between HRC and HRD matched cells was similarly observed in Chinese hamster lung cancer V-C8 cells. HRC V-C8 *BRCA2* corrected cells showed significant sensitisation by VE-821, PF-477736 and MK-1775 (Two-way ANOVA, $p<0.0001$ for all kinase inhibitors) (Smith *et al.,* 2020, Appendix B). Again, sensitisation was not observed in HRD *BRCA2* defective V-C8 cells, with any of the kinase inhibitors compared to matched V-C8.B2 cells which have a PF_{50} range of 7.4-26.1-fold (Figure 6.2).

When comparing sensitisation of rucaparib-treated HRC cells by VE-821, PF-477736 and MK-1775 there is a general trend that VE-821 sensitises cells the most, followed by PF-477736 and MK-1775 but this is not statistically significant overall (Figure 6.2)

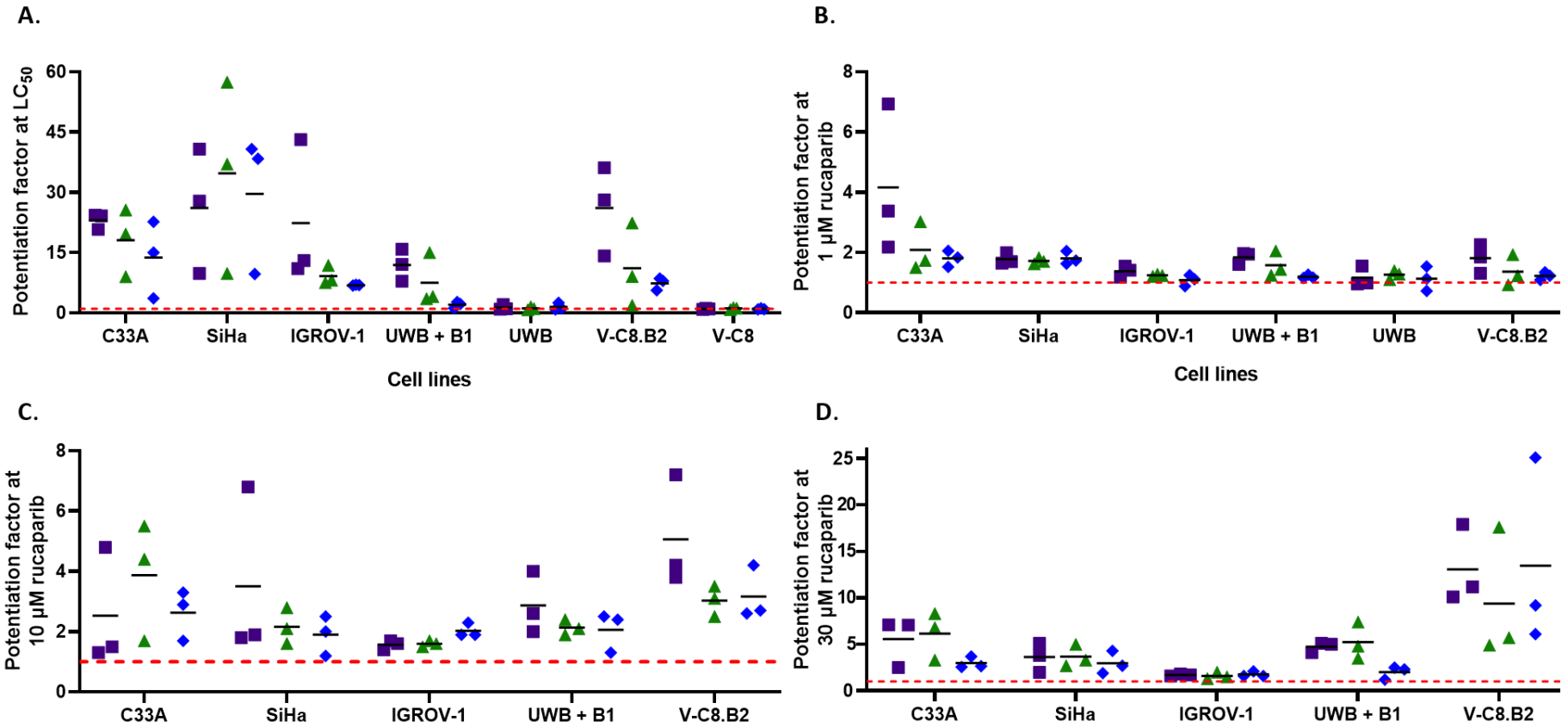


Figure 6.2: Comparison of VE-821, PF-477736 and MK-1775 at sensitising cells to rucaparib. Potentiation was calculated as LC_{50} of rucaparib single agent/ LC_{50} of cells co-exposed to rucaparib and VE-821, PF-477736 or MK-1775 or % cell survival of rucaparib-treated cells/ % cell survival of cells co-exposed to rucaparib and VE-821, PF-477736 or MK-1775 at set concentration of rucaparib. **A.** The potentiation factor at LC_{50} was measured in each individual combination cytotoxicity experiment. **B**. In all cells except HRD V-C8 cells potentiation at 1 µM rucaparib was measured. In all HRC cells potentiation was measured at a set concentration of **C.** 10 µM and **D.** 30 µM rucaparib. Individual experiments are shown on scatter plots, with the mean bar shown. The red dashed line represents y=1, at which no potentiation is occurring.

6.5.2 Correlation of basal RS and degree of potentiation by kinase inhibitors

Cells with increased basal RS are thought to have increased reliance on S/G2 checkpoints controlled by ATR, CHK1 and WEE1. Here, basal RS was correlated with potentiation by the kinase inhibitors, to assess whether this was a contributing factor. Figure 6.3 shows that when cell lines were ranked from lowest to highest basal RS levels (determined in Chapter 3) there was a trend towards cells with the highest baseline replication stress showing the least potentiation of rucaparib by PF-477736 or MK-1775, although this was not apparent with VE-821. Across the cell lines, PF_{50} values were highest in SiHa and C33A cells and these cells also had the lowest basal RS levels (mean γH2AX foci per cell 1.5 ± 1.2 and 1.4 ± 1.3, respectively). The lowest PF_{50} in the HRC cells was observed with UWB1.289+ B1 and IGROV-1 cells and these were the HRC cells with the most basal RS (mean γH2AX foci per cell 4.3 ± 0.6 and 5.5 ± 2.4, respectively).

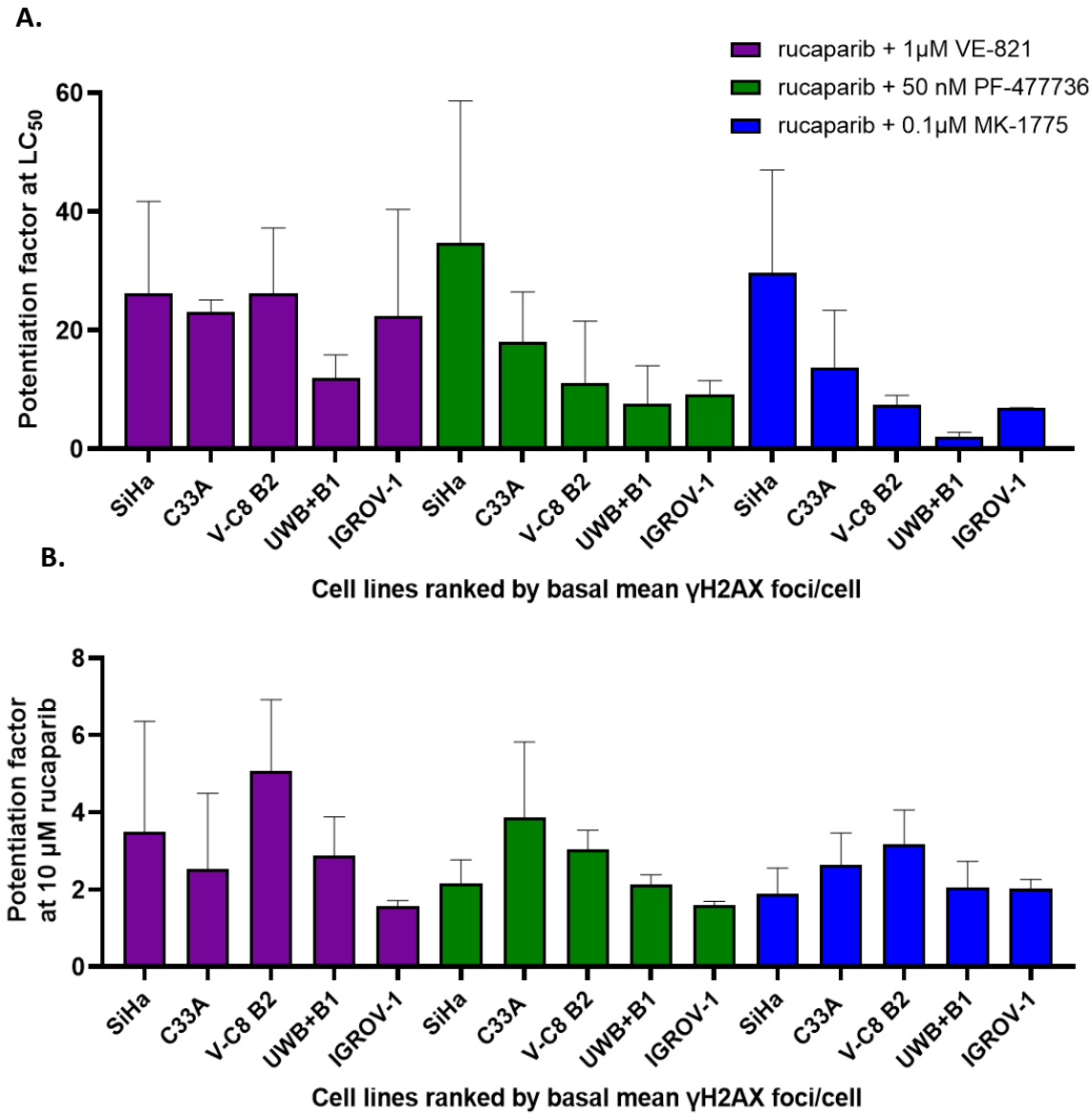


Figure 6.3: The impact of basal levels of replication stress on the degree of sensitisation by kinase inhibitors. Cell lines were ranked from least to most basal replication stress, which was determined in Chapter 3, assessed by the mean γH2AX foci in untreated cells. Each bar represents the mean and standard deviation of 3 independent **A.** PF_{50} and potentiation at **B.** 10 μM values. Potentiation data is from figure 6.2 and basal RS established in Chapter 3.

6.5.3 Correlation of rucaparib-induced RS and degree of potentiation by kinase inhibitors

As previously described, PARPi induce RS which signals to ATR-CHK1-WEE1 axis. It was predicted that there could be a correlation between rucaparib-induced RS (as measured by γH2AX foci in Chapter 4) and sensitisation of cells by ATR, CHK1 and WEE1 inhibitors.

There was a weak trend observed that increased mean γH2AX foci number in rucaparib-treated cells correlated with lower PF_{50} values by VE-821, PF-477736 and MK-1775 (r^2= 0.1, 0.1 and 0.2, respectively) (Figure 6.3). At a fixed concentration of 10 µM rucaparib, where HRD cells were excluded due to a lower concentration range used, the opposite trend was observed and higher mean γH2AX foci number in rucaparib-treated cells resulted in a higher potentiation factor (r^2= 0.2, 0.7 and 0.7, respectively).

It was observed that higher fold-increase in γH2AX foci by 10 µM rucaparib resulted in increased PF_{50} by VE-821, PF-477736 and MK-1775 (r^2= 0.2, 0.7 and 0.7). However the observed trend with PF-477736 and MK-1775 may be overestimated due to SiHa cells having a considerably higher fold-increase of RS, but C33A and V-C8.B2 cells having the highest potentiation factor by the inhibitors, respectively.

These data highlight how trends can differ based on which part of the concentration range of rucaparib is being analysed and how easily skewed data is with a small set of cell lines.

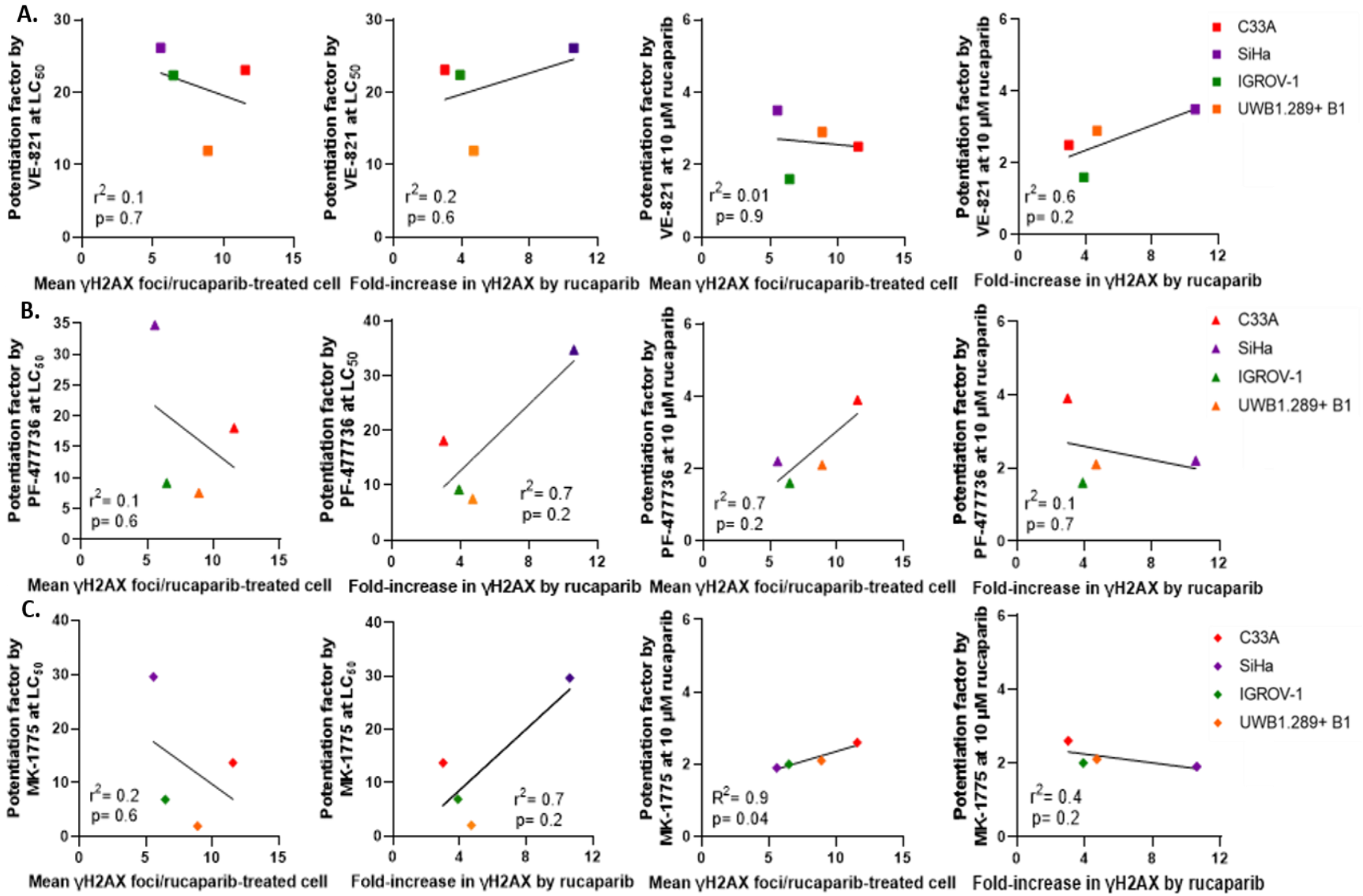
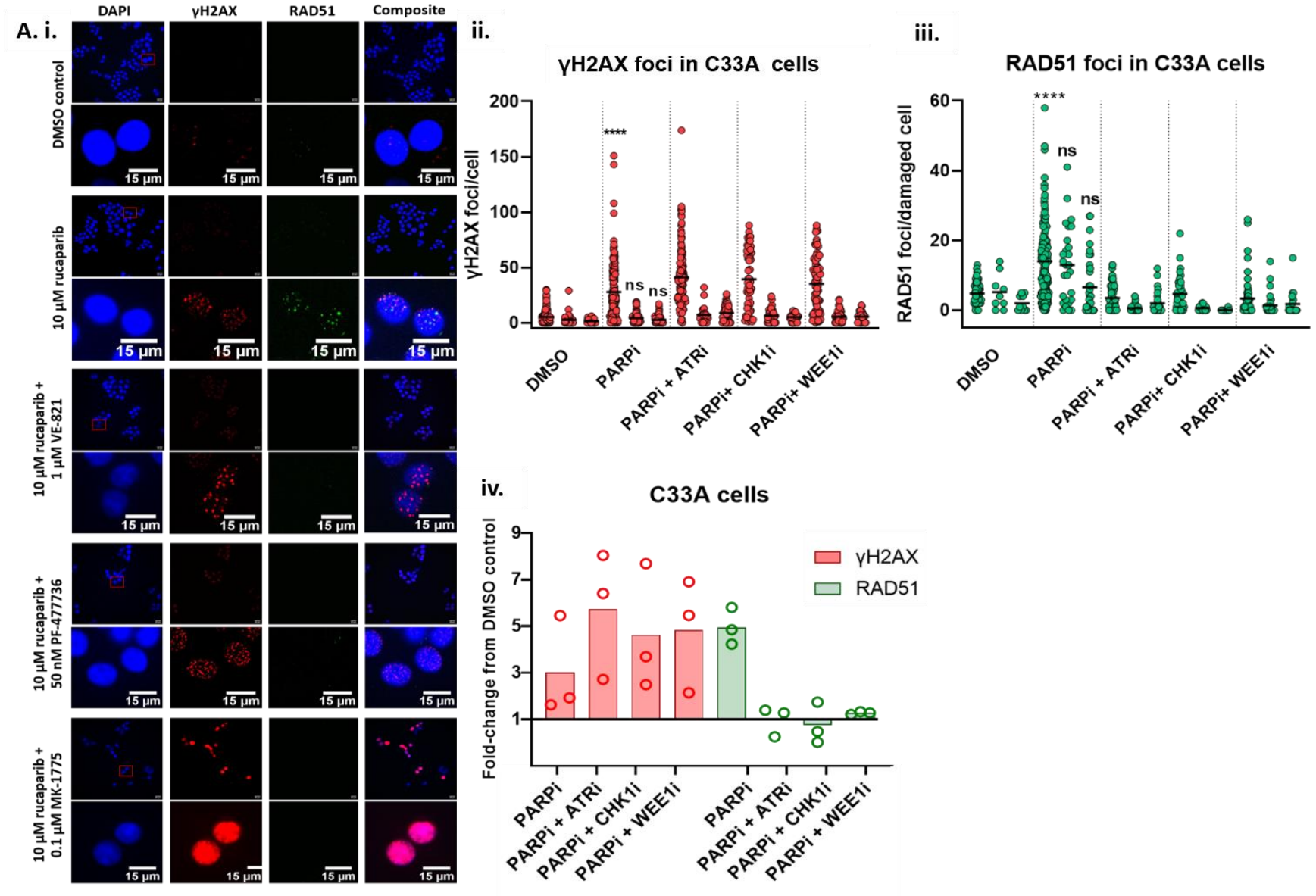
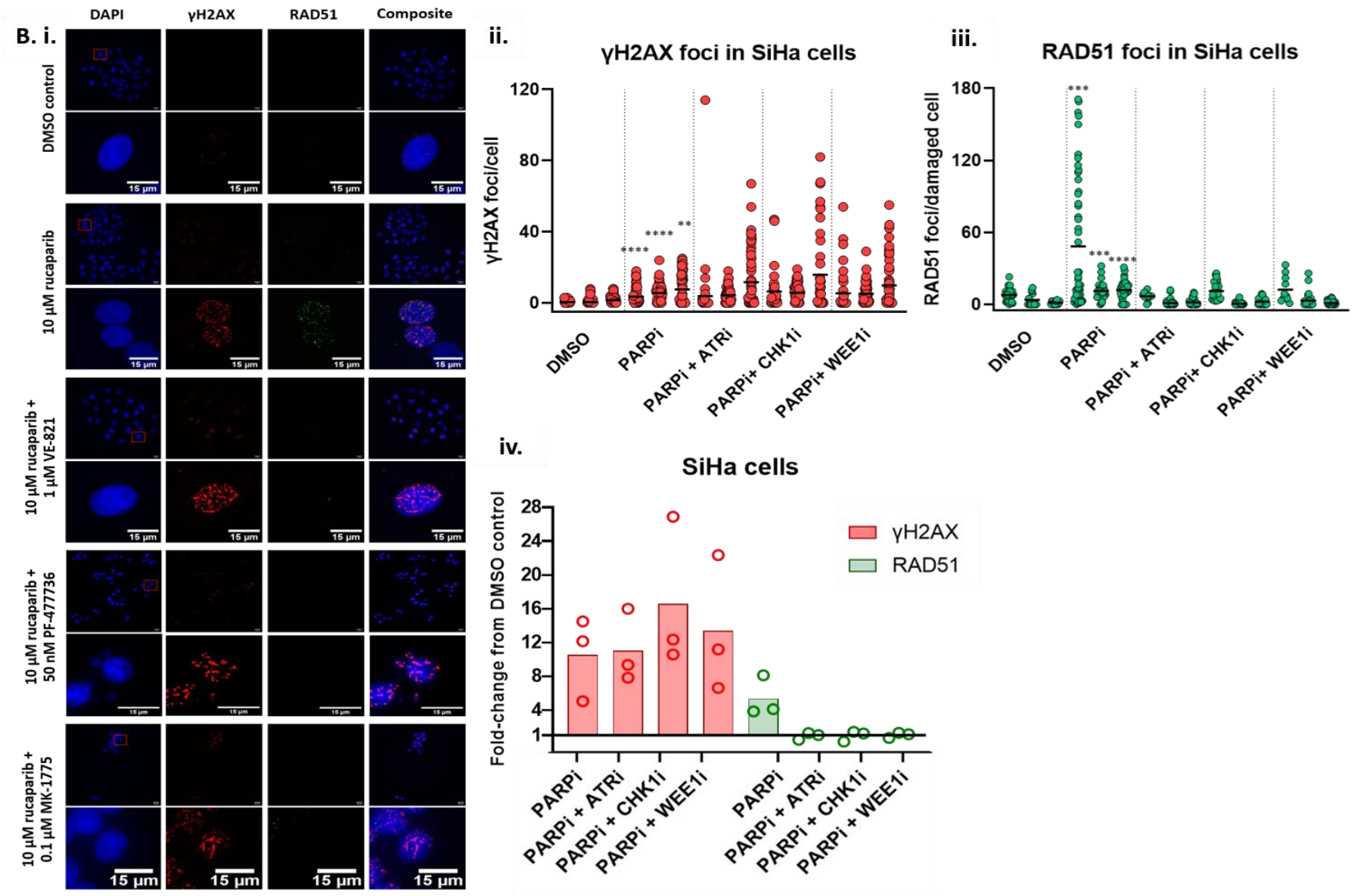

A.
Potentiation factor by VE-821 at LC50
r2= 0.1
p= 0.7
Potentiation factor by VE-821 at LC50
r2= 0.2
p= 0.6
Potentiation factor by VE-821 at 10 μM rucaparib
r2= 0.01
p= 0.9
Potentiation factor by VE-821 at 10 μM rucaparib
r2= 0.6
p= 0.2
C33A
SiHa
IGROV-1
UWB1.289+ B1
Mean γH2AX foci/rucaparib-treated cell
Fold-increase in γH2AX by rucaparib
Mean γH2AX foci/rucaparib-treated cell
Fold-increase in γH2AX by rucaparib
B.
Potentiation factor by PF-477736 at LC50
r2= 0.1
p= 0.6
Potentiation factor by PF-477736 at LC50
r2= 0.7
p= 0.2
Potentiation factor by PF-477736 at 10 μM rucaparib
r2= 0.7
p= 0.2
Potentiation factor by PF-477736 at 10 μM rucaparib
r2= 0.1
p= 0.7
C33A
SiHa
IGROV-1
UWB1.289+ B1
Mean γH2AX foci/rucaparib-treated cell
Fold-increase in γH2AX by rucaparib
Mean γH2AX foci/rucaparib-treated cell
Fold-increase in γH2AX by rucaparib
C.
Potentiation factor by MK-1775 at LC50
r2= 0.2
p= 0.6
Potentiation factor by MK-1775 at LC50
r2= 0.7
p= 0.2
Potentiation factor by MK-1775 at 10 μM rucaparib
R2= 0.9
p= 0.04
Potentiation factor by MK-1775 at 10 μM rucaparib
r2= 0.4
p= 0.2
C33A
SiHa
IGROV-1
UWB1.289+ B1
Mean γH2AX foci/rucaparib-treated cell
Fold-increase in γH2AX by rucaparib
Mean γH2AX foci/rucaparib-treated cell
Fold-increase in γH2AX by rucaparib

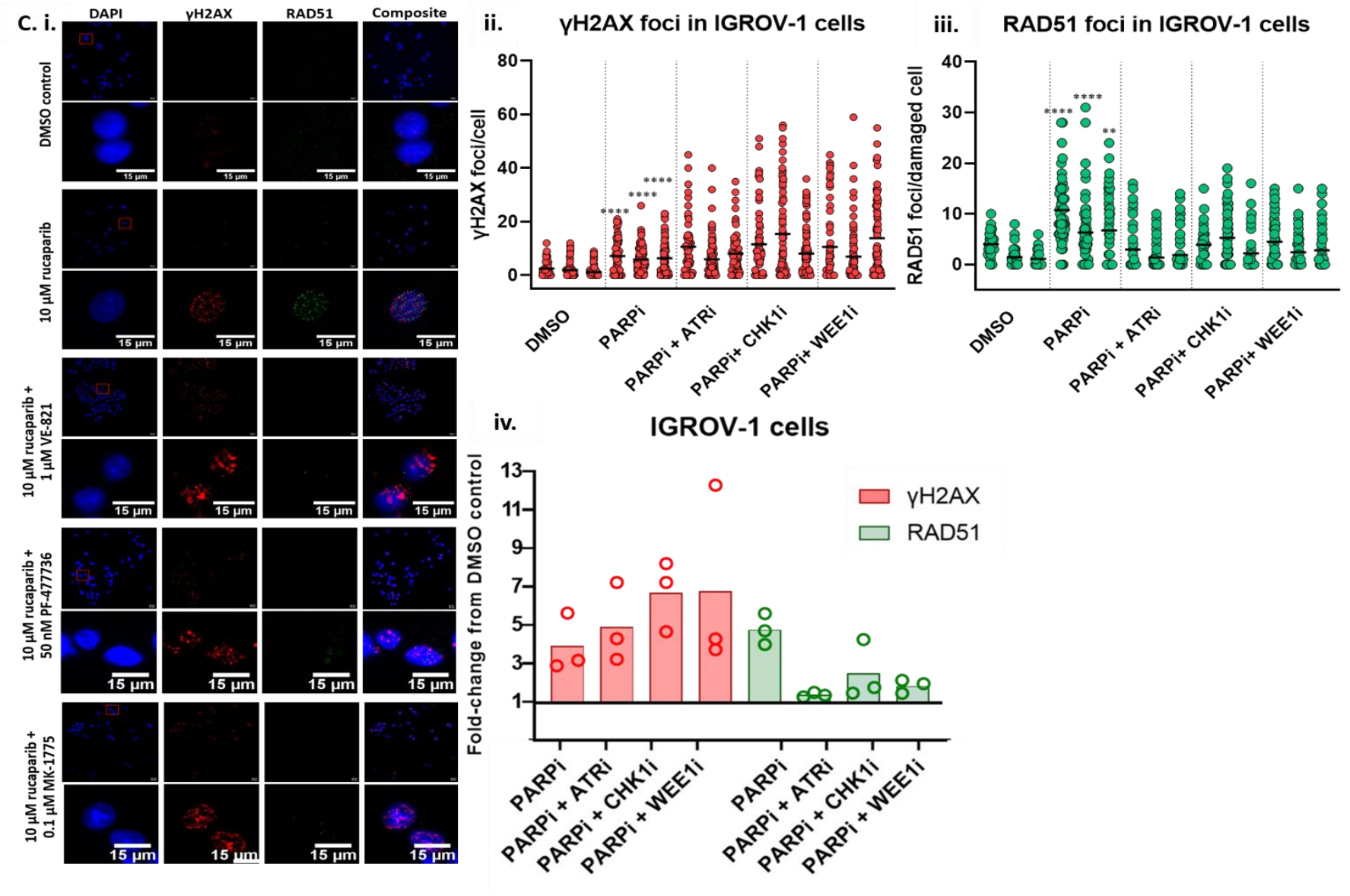
Figure 6.4: The impact of rucaparib-induced replication stress on the degree of sensitisation by kinase inhibitors. Mean absolute γH2AX foci number in cells exposed to 10 μM rucaparib (determined in Chapter 4) was plotted against potentiation at LC_{50} and at a fixed concentration of 10 μM rucaparib with **A**. VE-821, **B.** PF-477736 and **C.** MK-1775. Mean fold-change was calculated between untreated cells and cells treated with 10 μM rucaparib and was plotted against potentiation at LC_{50} and at a fixed concentration of 10 μM rucaparib (as determined in figure 6.2) with **A.** VE-821, **B.** PF-477736 and **C.** MK-1775. Correlation co-efficient and statistical significance was calculated using Graphpad Prism 9.0 software.

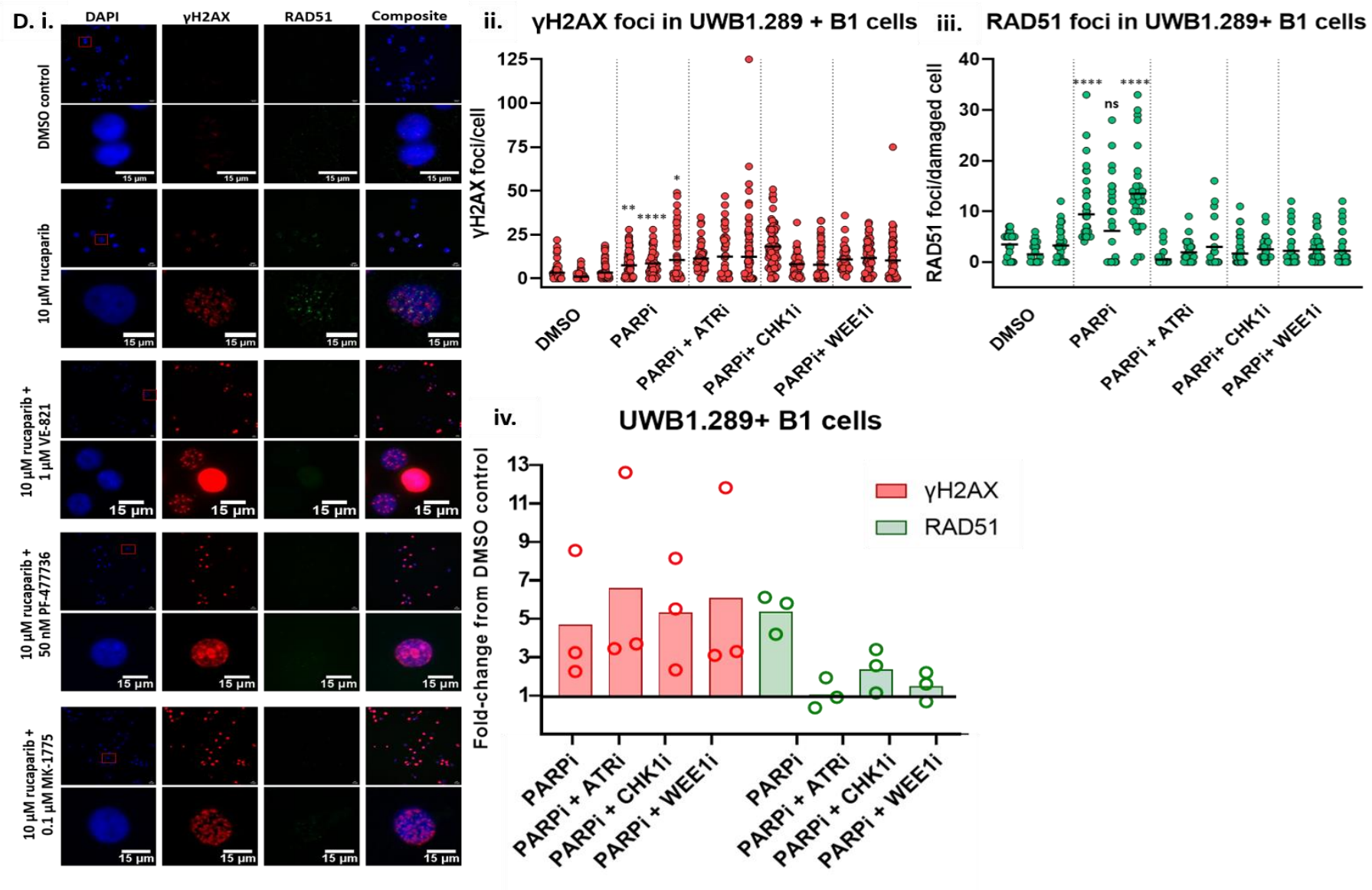
6.5.4 Impact of rucaparib and kinase inhibitors on HRR function

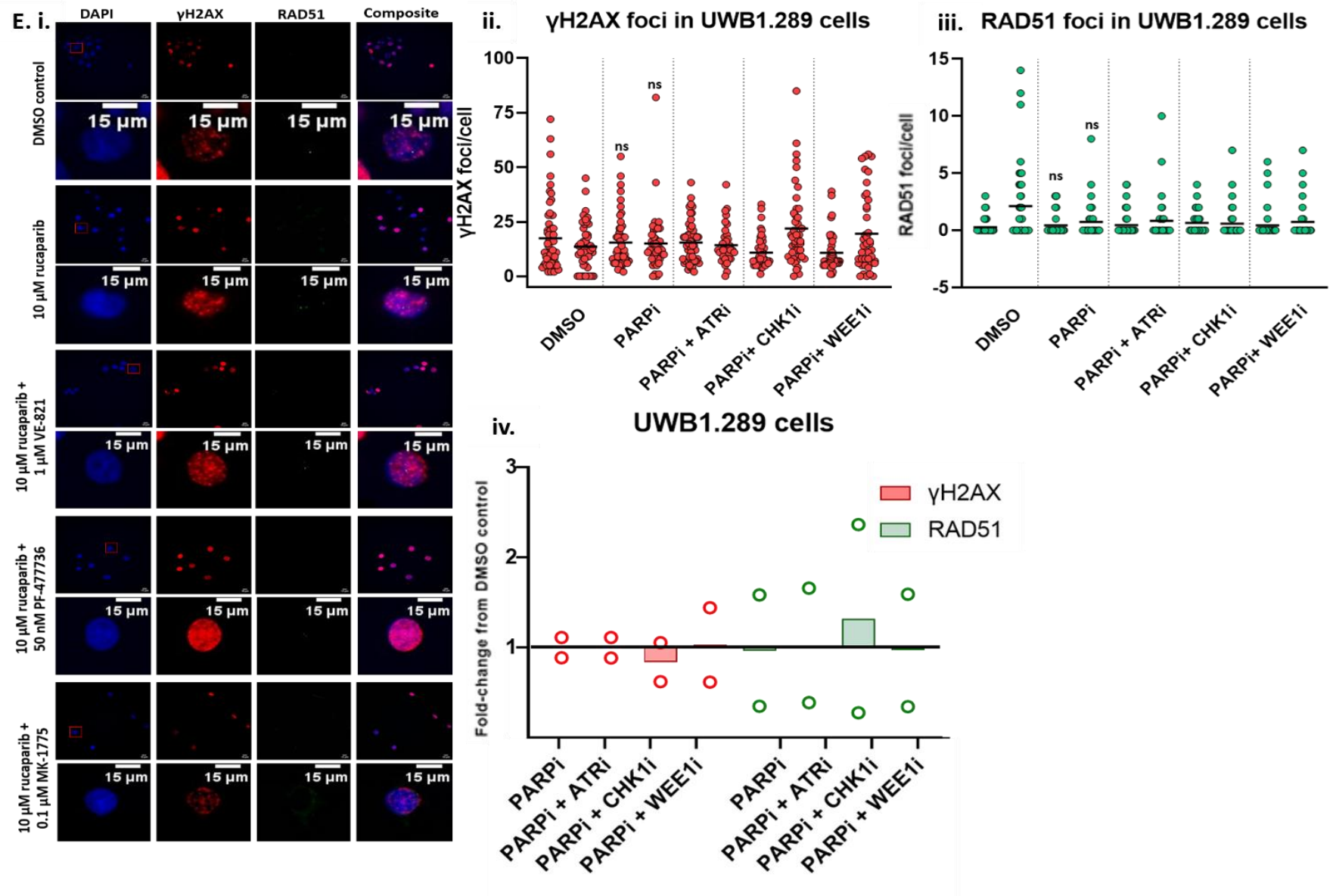
The observation that VE-821, PF-477736 and MK-1775 only sensitised rucaparib in HRC cells combined with the known synthetic lethality of PARPi in cells with HRD cells suggested that the inhibitors were suppressing HRR, as had previously been demonstrated for the prototype ATRi, NU6027 (Peasland *et al.,* 2011). The impact of VE-821, PF-477736 and MK-1775 on HRR was therefore measured by a functional assay where phosphorylation of γH2AX at Ser139 was measured as a marker of DNA damage and RS and RAD51 foci formation as an indicator of HRR occurring in damaged cells (Moeglin *et al.,* 2019, Cruz *et al.,* 2018).

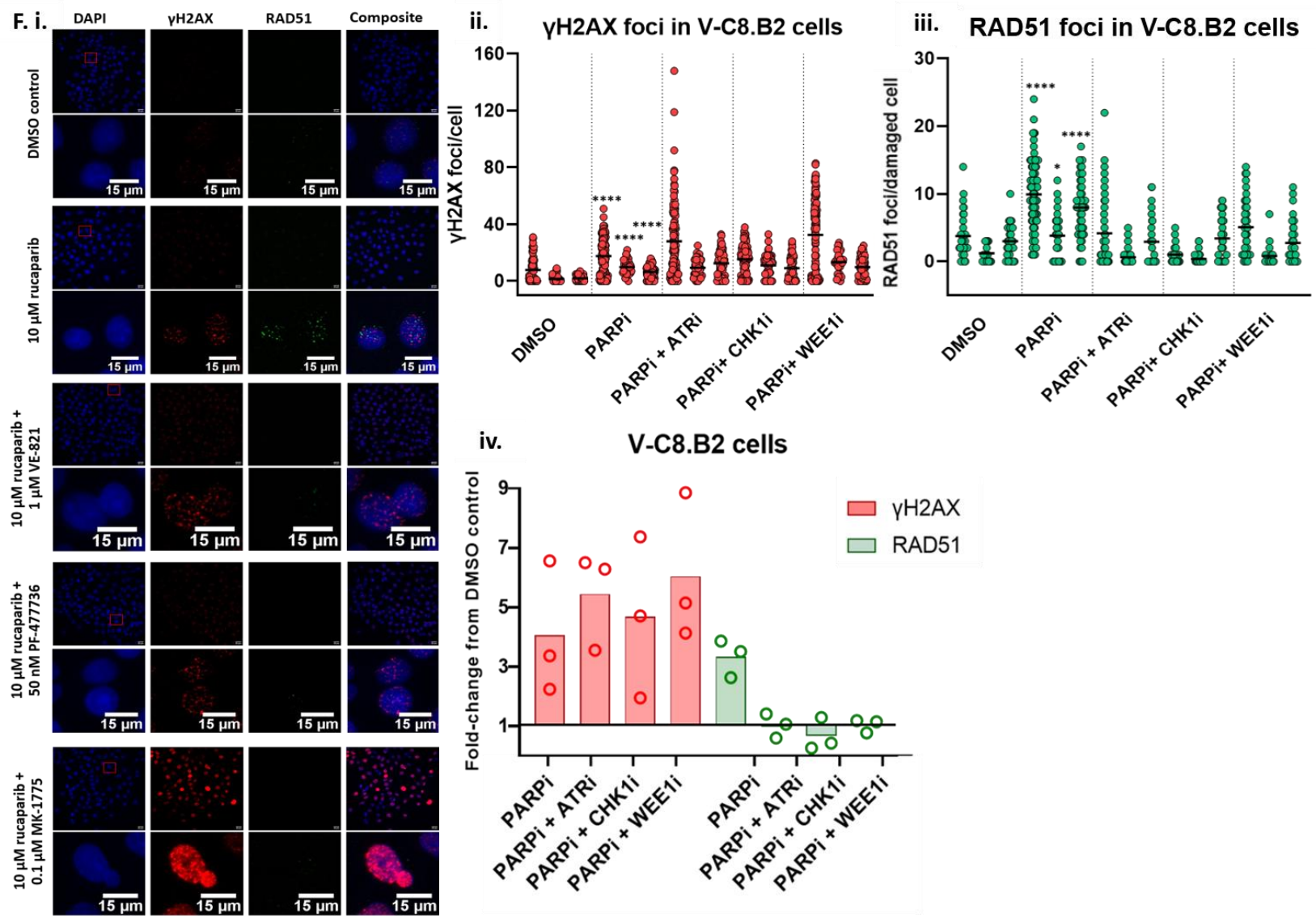

A. i.
DAPI
γH2AX
RAD51
Composite
DMSO control
10 μM rucaparib
10 μM rucaparib + 1 μM VE-821
10 μM rucaparib + 50 nM PF-477736
10 μM rucaparib + 0.1 μM MK-1775
15 μm
ii.
γH2AX foci in C33A cells
γH2AX foci/cell
200
150
100
50
0
****
ns
ns
DMSO
PARPi
PARPi + ATRi
PARPi+ CHK1i
PARPi+ WEE1i
iii.
RAD51 foci in C33A cells
RAD51 foci/damaged cell
60
40
20
0
****
ns
ns
DMSO
PARPi
PARPi + ATRi
PARPi+ CHK1i
PARPi+ WEE1i
iv.
C33A cells
Fold-change from DMSO control
9
7
5
3
1
γH2AX
RAD51
PARPi
PARPi + ATRi
PARPi + CHK1i
PARPi + WEE1i
PARPi
PARPi + ATRi
PARPi + CHK1i
PARPi + WEE1i


B. i.
DAPI
γH2AX
RAD51
Composite
DMSO control
10 μM rucaparib
10 μM rucaparib + 1 μM VE-821
10 μM rucaparib + 50 nM PF-477736
10 μM rucaparib + 0.1 μM MK-1775
15 μm
ii.
γH2AX foci in SiHa cells
γH2AX foci/cell
120
80
40
0
****
****
**
DMSO
PARPi
PARPi + ATRi
PARPi+ CHK1i
PARPi+ WEE1i
iii.
RAD51 foci in SiHa cells
RAD51 foci/damaged cell
180
120
60
0
***
***
****
DMSO
PARPi
PARPi + ATRi
PARPi+ CHK1i
PARPi+ WEE1i
iv.
SiHa cells
Fold-change from DMSO control
28
24
20
16
12
8
4
1
γH2AX
RAD51
PARPi
PARPi + ATRi
PARPi + CHK1i
PARPi + WEE1i
PARPi
PARPi + ATRi
PARPi + CHK1i
PARPi + WEE1i


C. i.
DAPI
γH2AX
RAD51
Composite
DMSO control
10 μM rucaparib
10 μM rucaparib + 1 μM VE-821
10 μM rucaparib + 50 nM PF-477736
10 μM rucaparib + 0.1 μM MK-1775
15 μm
ii.
γH2AX foci in IGROV-1 cells
γH2AX foci/cell
DMSO
PARPi
PARPi + ATRi
PARPi+ CHK1i
PARPi+ WEE1i
iii.
RAD51 foci in IGROV-1 cells
RAD51 foci/damaged cell
iv.
IGROV-1 cells
Fold-change from DMSO control
γH2AX
RAD51


D. i.
DAPI
γH2AX
RAD51
Composite
DMSO control
10 μM rucaparib
10 μM rucaparib + 1 μM VE-821
10 μM rucaparib + 50 nM PF-477736
10 μM rucaparib + 0.1 μM MK-1775
15 μm
ii. γH2AX foci in UWB1.289 + B1 cells
γH2AX foci/cell
DMSO
PARPi
PARPi + ATRi
PARPi+ CHK1i
PARPi+ WEE1i
iii. RAD51 foci in UWB1.289+ B1 cells
RAD51 foci/damaged cell
ns
iv. UWB1.289+ B1 cells
Fold-change from DMSO control
γH2AX
RAD51
PARPi
PARPi + ATRi
PARPi + CHK1i
PARPi + WEE1i


E. i.
DAPI
γH2AX
RAD51
Composite
DMSO control
10 μM rucaparib
10 μM rucaparib + 1 μM VE-821
10 μM rucaparib + 50 nM PF-477736
10 μM rucaparib + 0.1 μM MK-1775
15 μm
ii.
γH2AX foci in UWB1.289 cells
γH2AX foci/cell
ns
DMSO
PARPi
PARPi + ATRi
PARPi+ CHK1i
PARPi+ WEE1i
iii.
RAD51 foci in UWB1.289 cells
RAD51 foci/cell
iv.
UWB1.289 cells
Fold-change from DMSO control
γH2AX
RAD51


F. i.
DAPI
γH2AX
RAD51
Composite
DMSO control
10 μM rucaparib
10 μM rucaparib + 1 μM VE-821
10 μM rucaparib + 50 nM PF-477736
10 μM rucaparib + 0.1 μM MK-1775
15 μm
ii.
γH2AX foci in V-C8.B2 cells
γH2AX foci/cell
160
120
80
40
0
****
****
DMSO
PARPi
PARPi + ATRi
PARPi+ CHK1i
PARPi+ WEE1i
iii.
RAD51 foci in V-C8.B2 cells
RAD51 foci/damaged cell
30
20
10
0
****
*
****
DMSO
PARPi
PARPi + ATRi
PARPi+ CHK1i
PARPi+ WEE1i
iv.
V-C8.B2 cells
Fold-change from DMSO control
9
7
5
3
1
γH2AX
RAD51
PARPi
PARPi + ATRi
PARPi + CHK1i
PARPi + WEE1i
PARPi
PARPi + ATRi
PARPi + CHK1i
PARPi + WEE1i

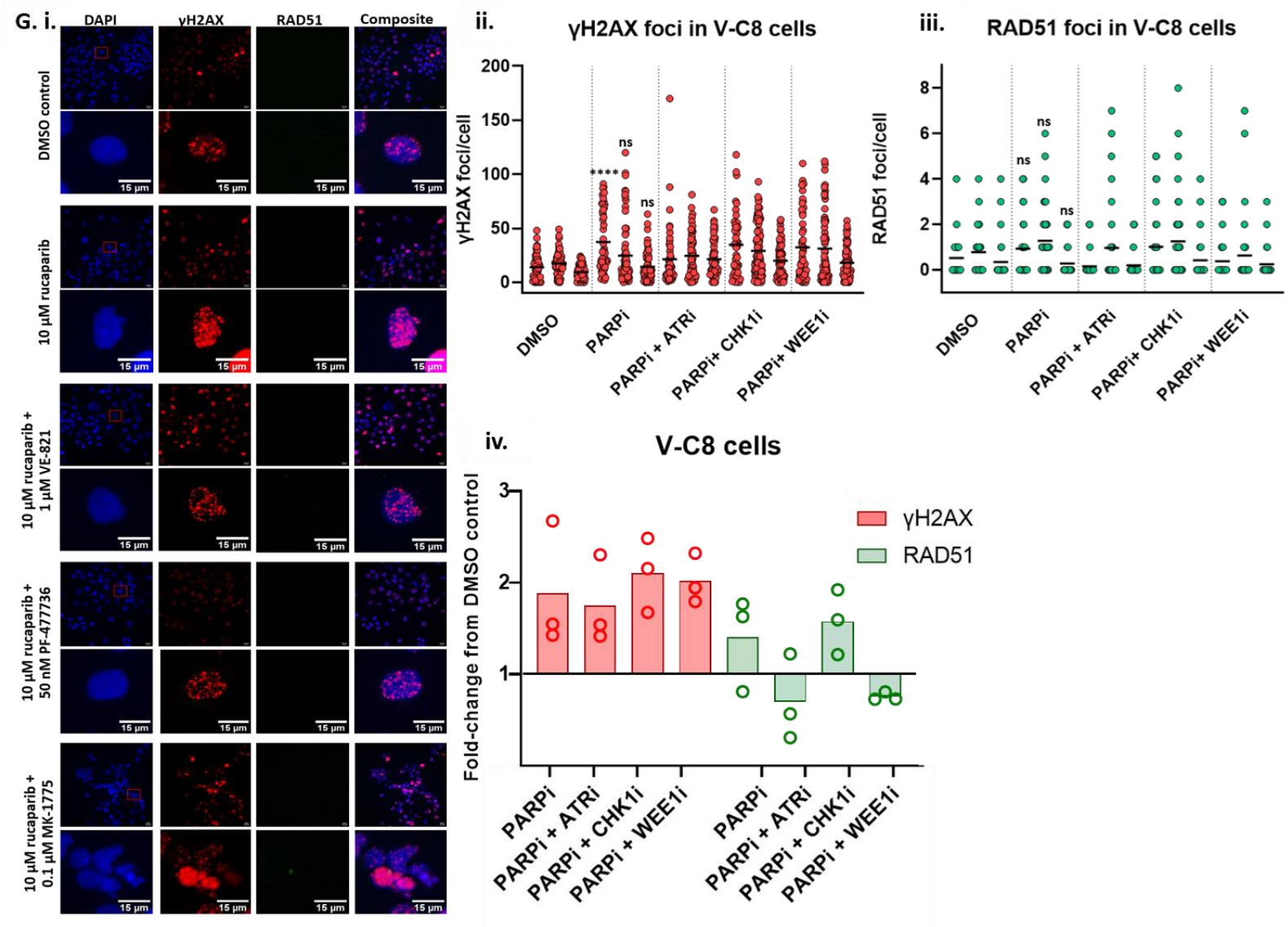

G. i.
DAPI
γH2AX
RAD51
Composite
DMSO control
10 μM rucaparib
10 μM rucaparib + 1 μM VE-821
10 μM rucaparib + 50 nM PF-477736
10 μM rucaparib + 0.1 μM MK-1775
15 μm
ii.
γH2AX foci in V-C8 cells
γH2AX foci/cell
****
ns
DMSO
PARPi
PARPi + ATRi
PARPi+ CHK1i
PARPi+ WEE1i
iii.
RAD51 foci in V-C8 cells
RAD51 foci/cell
iv.
V-C8 cells
Fold-change from DMSO control
γH2AX
RAD51
PARPi
PARPi + ATRi
PARPi + CHK1i
PARPi + WEE1i

Figure 6.5: Impact of rucaparib single agent and in combination with VE-821, PF-477736 or MK-1775 on HRR. Formation of γH2AX foci was measured to indicate the induction of DNA damage and RAD51 foci formation as an indicator of HRR function. Images are representative of one replicate per cell line assessed (i). Three independent experiments (with the exception of UWB1.289 cells) were plotted showing **ii.** γH2AX foci per cell and **iii.** RAD51 foci per γH2AX positive cell (defined as any cell above the mean γH2AX foci in DMSO control cells per individual experiment). **iv.** Fold-change from DMSO was calculated for each independent experiment (Mean γH2AX foci in rucaparib-treated cells/ mean γH2AX foci per untreated cell) and the data pooled to give mean and SD.

In the HRC cell lines 10 μM rucaparib caused a 3.0 (C33A cells) to 10.6-fold (SiHa cells) increase in γH2AX foci compared to DMSO control cells. UWB1.289 and V-C8 HRD cells had increased basal γH2AX foci in these cells compared to their matched HRC cells (Chapter 3), therefore the induction of γH2AX foci by rucaparib was marginal (1.0-fold and 1.9-fold, respectively). VE-821 caused a modest further increase in γH2AX foci in HRC cells ranging between 1.1-fold (SiHa cells) and 2.2-fold (C33A cells). PF-477736 similarly increased γH2AX foci in HRC cells 1.1-fold (UWB1.289+B1 and V-C8.B2 cells) to 1.7-fold (IGROV-1 cells), as did MK-1775 1.3 (SiHa and UWB1.289+B1 cells) to 1.7-fold (IGROV-1 cells), although these were not deemed statistically significant. In HRD cells the addition of VE-821, PF-477736 and MK-1775 did not have a significant impact on γH2AX foci compared to rucaparib as a single agent (1.0 to 1.1-fold, 0.8 to 1.2-fold and 1.0 to 1.1-fold, respectively).

Unrepaired SSBs leading to RS requiring HRR for resolution will manifest as γH2AX foci only in cells that pass-through S-phase during the exposure period. To ensure that HRR was only measured in such cells RAD51 foci were counted in cells that had above mean baseline γH2AX foci (defined as γH2AX positive). In all HRC cells rucaparib increased RAD51 foci in γH2AX positive cells, compared to DMSO control cells. This ranged from 3.3-fold (V-C8.B2 cells) to 5.4-fold (SiHa and UWB1.289 +B1 cells) (Table 6.1). In all HRC cell lines tested here, each of the kinase inhibitors significantly reduced the rucaparib-induced increase in RAD51 foci, such that in no case were RAD51 levels significantly higher in cells treated with the combination than in unperturbed control cells. VE-821 (1 μM) caused the greatest inhibition of rucaparib-induced RAD51 foci formation ranging from 89.0 ± 4.0% (IGROV-1 cells) to in excess of 100 %, i.e., below the levels in DMSO control cells, in SiHa and UWB1.289+B1 cells, indicating complete inhibition of HRR. PF-

477736 (50 nM) caused the next most inhibition of rucaparib-induced RAD51 foci ranging from 64.1 ± 30.7% (IGROV-1 cells) to in excess of 100 % in C33A, SiHa and V-C8.B2 cells. MK-1775 (0.1 μM) reduced rucaparib-induced RAD51 foci the least out of the 3 inhibitors across the cells tested with this ranging from 78.2 ± 7.8% (IGROV-1 cells) to 96.8 ± 10.0% (V-C8.B2 cells). Across the panel of cells the 3 kinase inhibitors reduced RAD51 foci formation the most in V-C8.B2 cells and least in IGROV-1 cells. As expected, there was no significant induction of RAD51 foci in HRD UWB1.289 and V-C8 cells by rucaparib and very few RAD51 foci were observed with any of the treatments.

A

Cell line	Fold-increase of γH2AX foci compared to DMSO control cells				Fold-increase of RAD51 with rucaparib single agent from DMSO control	% inhibition of RAD51 foci formation compared to rucaparib single agent, normalised to DMSO control		
	Rucaparib	Rucaparib + VE-821	Rucaparib + PF-477736	Rucaparib + MK-1775		Rucaparib + VE-821	Rucaparib + PF-477736	Rucaparib + MK-1775
C33A	3.0 ± 2.1	5.7 ± 2.7	4.6 ± 2.7	4.8 ± 2.4	5.0 ± 0.8	98.3 ± 15.1	107.2 ± 25.0	92.8 ± 2.5
SiHa	10.6 ± 4.9	11.1 ± 4.3	16.6 ± 9.0	13.4 ± 8.1	5.4 ± 2.4	102.9 ± 13.7	102.9 ± 20.5	96.3 ± 7.3
IGROV-1	3.9 ± 1.5	4.9 ± 2.1	6.7 ± 1.8	6.8 ± 4.8	4.8 ± 0.8	89.9 ± 4.0	64.1 ± 30.7	78.2 ± 7.8
UWB1.289 + B1	4.7 ± 3.4	6.6 ± 5.2	5.3 ± 2.9	6.1 ± 5.0	5.4 ± 1.0	100.6 ± 19.5	72.3 ± 21.3	87.4 ± 16.6
V-C8.B2	4.1 ± 2.2	5.4 ± 1.6	4.7 ± 2.7	6.0 ± 2.5	3.3 ± 0.6	97.8 ± 15.3	117.8 ± 28.4	96.8 ± 10.0

B.

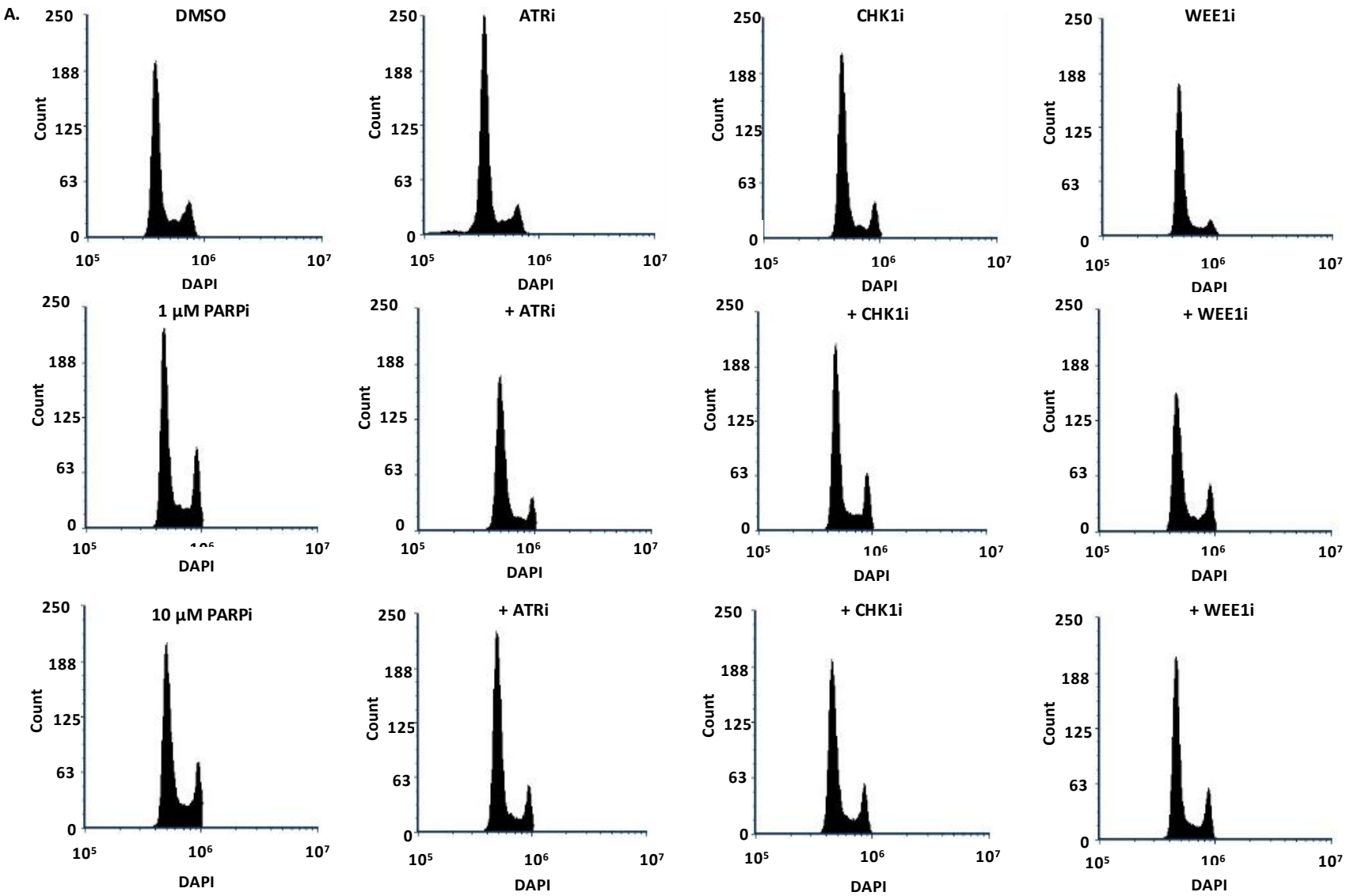
Cell line	Fold-increase of γH2AX foci compared to DMSO control cells				Fold-increase of RAD51 with rucaparib single agent from DMSO control
	Rucaparib	Rucaparib + VE-821	Rucaparib + PF-477736	Rucaparib + MK-1775	
UWB1.289	1.0 ± 0.2	1.0 ± 0.2	0.8 ± 0.3	1.0 ± 0.6	0.9 ± 0.9
V-C8	1.9 ± 0.7	1.8 ± 0.5	2.1 ± 0.4	2.0 ± 0.3	1.4 ± 0.5

Table 6.1: Effect of rucaparib and kinase inhibitors on γH2AX and RAD51 foci formation. Fold-increase of γH2AX by rucaparib single agent and in combination with each kinase inhibitor was calculated in comparison to mean γH2AX foci in DMSO control **A.** HRC and **B.** HRD cells. Fold-increase RAD51 upon treatment with rucaparib was calculated from mean RAD51 foci per γH2AX positive cell. For HRC cells percentage inhibition of RAD51 foci upon addition of kinase inhibitors was calculated (100- ((mean RAD51 foci/cell rucaparib and kinase inhibitor co-exposure – mean RAD51 foci/cell DMSO)/ (mean RAD51 foci rucaparib single agent))*100). Data is representative of 3 independent experiments.

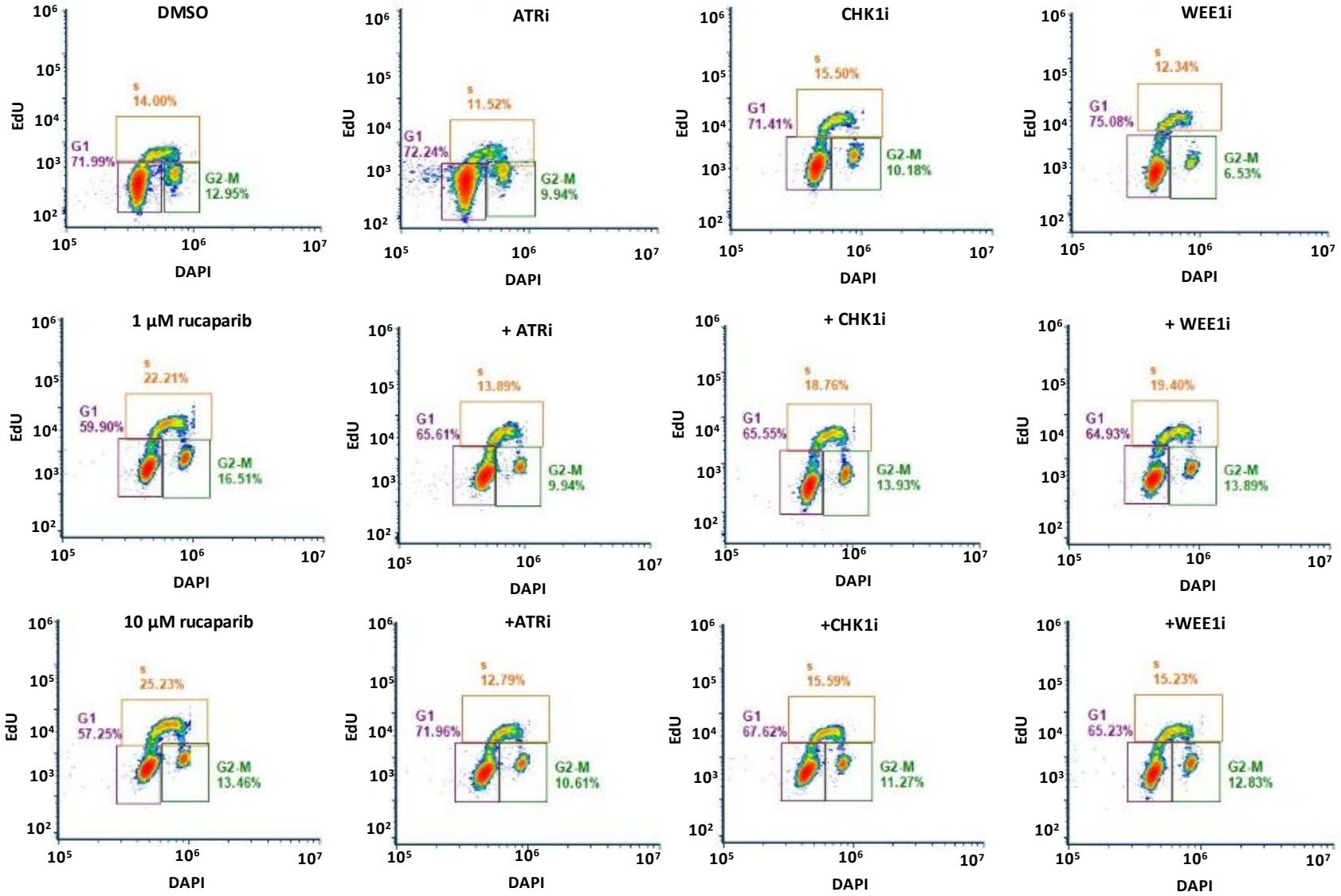
6.5.5 Effects of rucaparib and kinase inhibitors on cell cycle

The role of ATR, CHK1 and WEE1 inhibitors in DNA damage-induced cell cycle control has been widely reported. Here, IGROV-1 cells were used for these experiments, to assess the effect rucaparib had on the cell cycle and how the addition of the kinase inhibitors impacted this. It was predicted that rucaparib would cause S and G2 arrest as SSBs accumulate and convert to stalled forks, which collapse in S-phase as previously described. Given the importance of ATR-CHK1 signalling to cell cycle checkpoints in response to RS, it was predicted these kinase inhibitors would abrogate S and G2 cell cycle arrest.

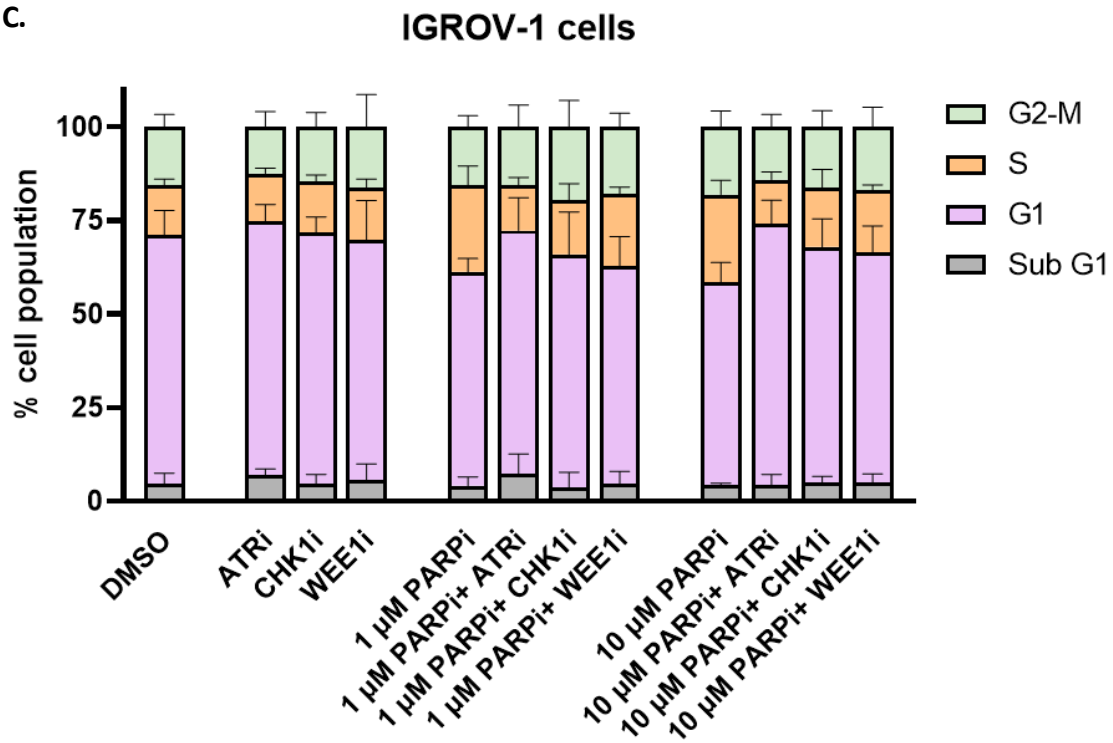
The kinase inhibitors alone did not significantly affect the cell cycle profile compared to control cells. As predicted rucaparib induced S-phase arrest, which was significant with 10 µM ($p=0.01$). The addition of VE-821 (1 µM) to both 1 µM and 10 µM rucaparib completely abrogated this S-phase accumulation to below DMSO control levels (>100%), and this was significant with 10 µM rucaparib ($p=0.007$). PF-477736 (50 nM) reduced S-phase arrest when added to 1 µM and 10 µM rucaparib (88.8 and 78.3 %, respectively), which was again significant at the higher concentration of 10 µM ($p=0.03$). MK-1775 (0.1 µM) also reduced S-phase arrest when added to 1 µM and 10 µM rucaparib (37.8 and 68.0 %, respectively), although this reduction was non-significant at both concentrations. No increase in G2-M cell population was observed when cells were treated with 1 µM rucaparib, although there was an increase in cells treated with 10 µM rucaparib. VE-821 significantly reduced this G2-M accumulation to below DMSO control ($p=0.02$). PF-477736 and MK-1775 also reduced G2-M phase population (78.3 and 47.8 %, respectively), although this was non-significant.


A.
DMSO
ATRi
CHK1i
WEE1i
1 µM PARPi
+ ATRi
+ CHK1i
+ WEE1i
10 µM PARPi
+ ATRi
+ CHK1i
+ WEE1i
Count
DAPI
250
188
125
63
0
10⁵
10⁶
10⁷

B.


DMSO
S 14.00%
G1 71.99%
G2-M 12.95%
ATRi
S 11.52%
G1 72.24%
G2-M 9.94%
CHK1i
S 15.50%
G1 71.41%
G2-M 10.18%
WEE1i
S 12.34%
G1 75.08%
G2-M 6.53%
1 µM rucaparib
S 22.21%
G1 59.90%
G2-M 16.51%
+ ATRi
S 13.89%
G1 65.61%
G2-M 9.94%
+ CHK1i
S 18.76%
G1 65.55%
G2-M 13.93%
+ WEE1i
S 19.40%
G1 64.93%
G2-M 13.89%
10 µM rucaparib
S 25.23%
G1 57.25%
G2-M 13.46%
+ATRi
S 12.79%
G1 71.96%
G2-M 10.61%
+CHK1i
S 15.59%
G1 67.62%
G2-M 11.27%
+WEE1i
S 15.23%
G1 65.23%
G2-M 12.83%
EdU
DAPI

C.



D.

	Mean cell population ± S.D (%)			
	Sub G1	G1	S	G2-M
DMSO	4.5 ± 3.0	66.5 ± 6.7	13.3 ± 1.7	15.7 ± 3.4
1 µM VE-821	6.9 ± 1.8	67.8 ± 4.6	12.9 ± 1.4	12.4 ± 4.0
50 nM PF-477736	4.7 ± 2.5	67.0 ± 4.3	13.8 ± 1.7	14.5 ± 3.8
0.1 µM MK-1775	5.7 ± 4.4	64.0 ± 10.7	14.2 ± 2.3	16.2 ± 8.6
1 µM rucaparib	4.1 ± 2.4	57.1 ± 3.6	23.1 ± 5.3	15.7 ± 3.0
1 µM rucaparib+ VE-821	7.5 ± 5.2	64.8 ± 8.8	12.0 ± 2.2	15.7 ± 5.8
1 µM rucaparib+ PF-477736	3.7 ± 4.0	62.2 ± 11.4	14.4 ± 4.5	19.7 ± 7.0
1 µM rucaparib+ MK-1775	4.5 ± 3.5	58.2 ± 8.0	19.4 ± 1.8	17.9 ± 3.6
10 µM rucaparib	5.0 ± 4.4	54.0 ± 5.3	23.6 ± 3.8	18.0 ± 4.2
10 µM rucaparib+ VE-821	4.3 ± 2.9	69.8 ± 6.4	11.8 ± 2.1	14.1 ± 3.3
10 µM rucaparib+ PF-477736	4.9 ± 1.8	62.9 ± 7.6	15.9 ± 4.9	16.2 ± 4.3
10 µM rucaparib+ MK-1775	5.1 ± 2.3	61.4 ± 7.1	16.6 ± 1.4	16.9 ± 5.2

Figure 6.6: Cell cycle analysis of rucaparib and the kinase inhibitors effects in IGROV-1 cells. Cell cycle analysis of IGROV-1 cells following treatment with rucaparib and kinase inhibitors as single agent and in combination. **A.** Histogram plots are one representative of observations across 3 replicates. **B.** Cells were exposed to 10 µM EdU during the final hour of exposure to drug, prior to harvest. Densitometry plots show how cell populations were gated, which was cross-referenced with a histogram plot. **C.** Data are mean and S.D of 3 independent experiments population (%) of cells in each phase of the cell cycle at the time of fixation. **D.** Mean ± S.D of cell population (%) in each phase of the cell cycle.

6.5.6 The impact of PARP trapping on the observed synergy

PARPi causes an accumulation of SSB through inhibiting BER, which ultimately causes increased RS and an increased reliance on HRR and S/G2 checkpoints for cell survival. PARPi also cause PARP1 to become trapped on the DNA at the SSBs further contributing to replication fork collapse. It was essential to better understand the role of unrepaired SSBs vs PARP trapping on the synergy observed between rucaparib and the kinase inhibitors. Development of a PARP trapping assay would have been the best model to explore this, however due to time limitations this was not possible and a combination of cytotoxicity and immunofluorescence assays were used to attempt to gain a better understanding on the role SSBR inhibition vs PARP trapping, with regards to the observed potentiation.

The purpose of these cytotoxicity assays was to distinguish the effect of unrepaired SSBs vs PARP trapping in the synergy observed between rucaparib and the kinase inhibitors. Although EM9 cells are XRCC1 mutant and AA8 cells XRCC1 wildtype, both cell lines expressed PARP-1. Therefore, if unrepaired SSBs are driving the synergy it would be expected that EM9 cells would have increased sensitivity to ATR, CHK1 and WEE1 inhibition but there would be minimal potentiation observed in these cells with addition of rucaparib, compared to XRCC1 wildtype AA8 cells. If PARP trapping was influencing this synergy it would be expected that EM9 cells would be further sensitised to the kinase inhibitors by rucaparib. It has been previously reported that XRCC1 defective EM9 cells were more sensitive to ATR inhibition than their XRCC1 competent matched AA8 cells (Peasland *et al.,* 2011, Middleton *et al.,* 2015).

Overall EM9 cells were more sensitive to VE-821, PF-477736 and MK-1775 than AA8 cells (ANOVA, p=0.003, 0.006 and 0.003, respectively). The data suggest that deletion of this key SSB repair component confers greater sensitivity to all of the kinase inhibitors (Figure 6.7).

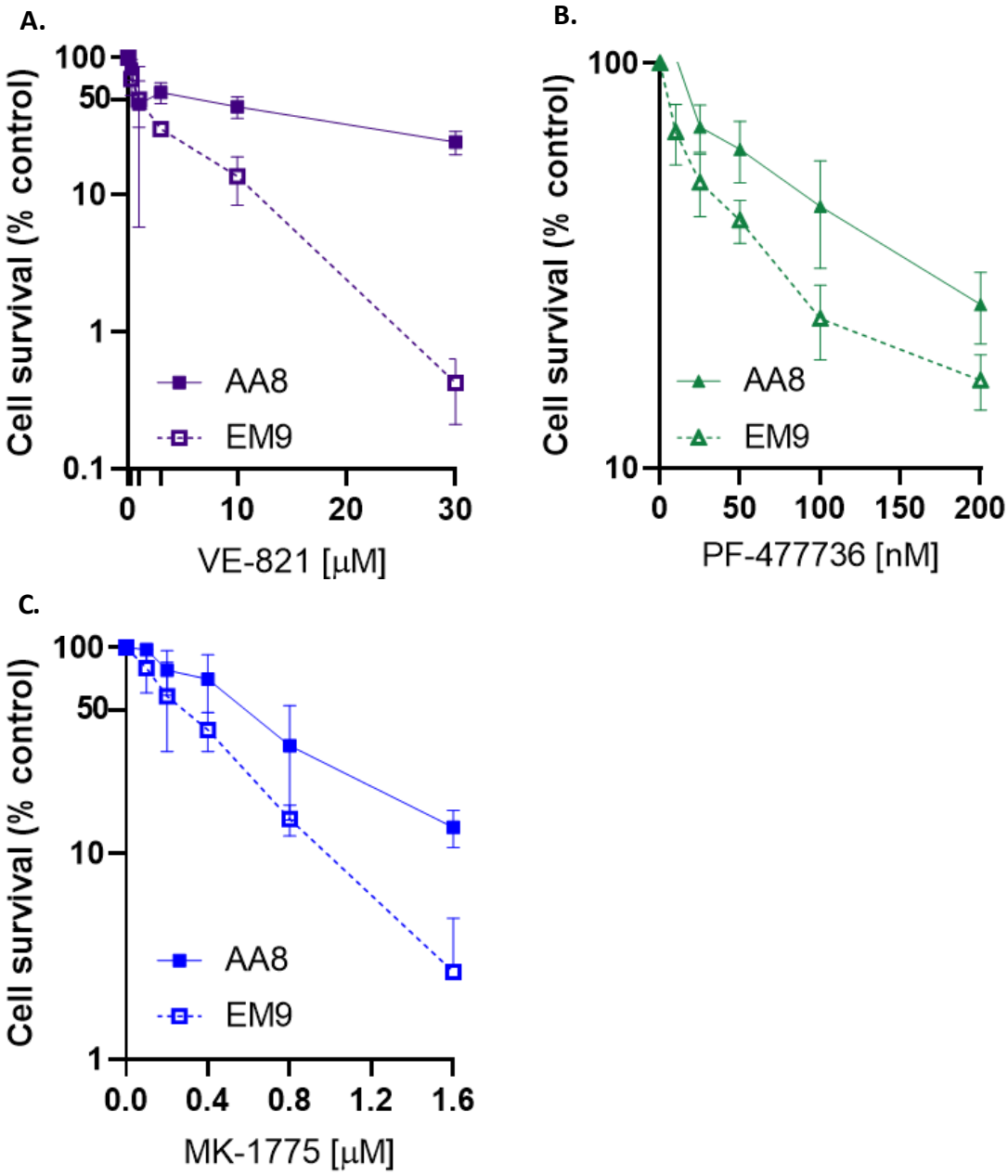


Figure 6.7: Single agent cytotoxicity of kinase inhibitors in matched AA8 and EM9 cells. Cells were exposed to a set concentration range of VE-821 (A), PF-477736 (B) and MK-1775 (C) for 24 h prior to replacement of drug-free media for 7-9 days. Data represents 3 independent experiments ± standard deviation.

To determine whether unrepaired SSB-induced RS or PARP trapping was more important the cytotoxic synergy between rucaparib and the kinase inhibitors was investigated. Overall, rucaparib sensitised both AA8 and EM9 cells to VE-821, PF-477736 and MK-1775 to a similar extent, suggesting PARP trapping was also important in the observed synergy (Figure 6.8). An exception to this was at the highest concentration of 30 µM VE-821 where potentiation by rucaparib in AA8 cells was 12-fold higher than in EM9 cells. Interestingly, XRCC1 defective EM9 cells were found to be more sensitive to rucaparib as a single agent than AA8 cells, possibly reflecting greater PARP trapping at unresolved SSBs.

EM9 cells were more sensitive to VE-821, PF-477736 and MK-1775 as single agent than AA8 cells co-incubated with the kinase inhibitors and rucaparib (Figure 6.8). This indicates that although PARP trapping is having an impact on the observed synergy between rucaparib and kinase inhibitors, but is perhaps less important than the inhibition of SSBR.

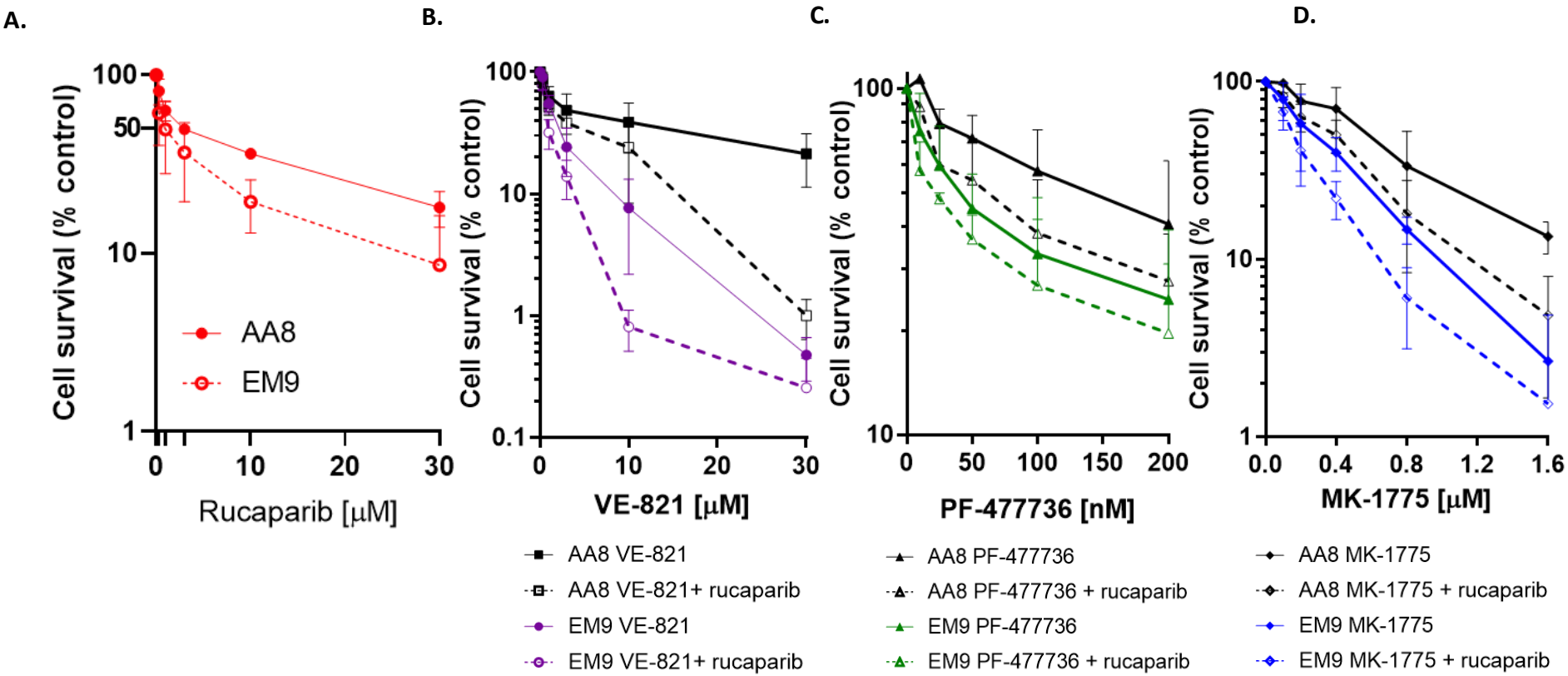


Figure 6.8: Single agent rucaparib sensitivity and potentiation of kinase inhibitors with rucaparib in matched AA8 and EM9 cells. Following single agent rucaparib cytotoxicity experiments **(A.)**, cells were treated with **B.** VE-821, **C.** PF-477736 or **D.** MK-1775, either as single agent or in combination with 1 μM rucaparib. Data are mean and standard deviation of 3 independent experiments.

		AA8	EM9	Magnitude of difference between cell lines
VE-821	LC_{50} single agent	4.8 ± 4.0 µM	1.1 ± 0.7 µM	5.4 ± 3.8-fold, ns, p=0.23
	PF_{50} with rucaparib	1.9 ± 0.6 µM	2.0 ± 0.6 µM	1.2 ± 0.1-fold, ns, p=0.87
	Cell survival (% control) at 3 µM single agent	56.1 ± 9.9 %	30.3 ± 3.1 %	1.9 ± 0.5-fold, ns, p=0.07
	Potentiation at 3 µM with rucaparib	1.3 ± 0.1	1.9 ± 1.2	0.9 ± 0.5-fold, ns, p=0.49
	Cell survival (% control) at 30 µM single agent	24.4 ± 4.7 %	0.4 ± 0.2 %	63.4 ± 20.2-fold, * p=0.01
	Potentiation at 30 µM with rucaparib	20.9 ± 6.82	2.5 ± 1.8	12.0 ± 8.0-fold, ns, p=0.06
PF-477736	LC_{50} single agent	91.3 ± 41.7 nM	25.7 ± 11.4 nM	3.6 ± 0.6-fold, ns, p=0.07
	PF_{50} with rucaparib	3.8 ± 0.4	2.5 ± 1.6	2.3 ± 0.4-fold, ns, p=0.31
	Cell survival (% control) at 50 nM single agent	61.3 ± 10.6 %	40.9 ± 5.0 %	1.5 ± 0.5-fold, ns, p=0.15
	Potentiation at 50 nM with rucaparib	1.4 ± 0.3	1.2 ± 0.1	1.1 ± 0.3-fold, ns, p=0.57
	Cell survival (% control) at 200 nM single agent	25.4 ± 5.1 %	16.5 ± 2.6 %	1.6 ± 0.4-fold, ns, p=0.12
	Potentiation at 200 nM with rucaparib	1.4 ± 0.3	1.3 ± 0.4	1.1 ± 0.2-fold, ns, p=0.65
MK-1775	LC_{50} single agent	0.6 ± 0.3 µM	0.3 ± 0.1 µM	2.3 ± 0.1-fold, ns, p=0.06
	PF_{50} with rucaparib	1.5 ± 0.2	1.5 ± 0.3	1.0 ± 0.1-fold, ns, p=0.06
	Cell survival (% control) at 0.2 µM single agent	77.9 ± 19.1 %	58.1 ± 26.8 %	1.5 ± 0.4, * p= 0.05
	Potentiation at 0.2 µM with rucaparib	1.2 ± 0.1	1.4 ± 0.2	0.9 ± 0.1-fold, ns, p=0.26
	Cell survival (% control) at 1.6 µM single agent	13.4 ± 2.7 %	2.7 ± 2.2 %	7.7 ± 5.9-fold, ** p=0.007
	Potentiation at 1.6 µM with rucaparib	3.3 ± 1.2	1.6 ± 0.5	2.2 ± 1.4-fold, ns, p=0.2

Table 6.2: Comparison of single agent kinase inhibition and potentiation with addition of rucaparib. The magnitude of differences between cell lines was calculated comparing LC_{50} values, PF_{50} values, % cell survival at set concentrations and potentiation factor at set concentrations (e.g LC_{50} of VE-821 in AA8 cells/EM9 cells) to assess the differences. Paired t-test statistical analysis was performed using Graphpad Prism 9.0 to determine if the differences between cell lines were statistically significant.

To understand the effect of unresolved SSB repair vs PARP trapping on cells dependence on HRR RAD51 foci were measured. As expected EM9 cells had higher basal γH2AX (1.5-fold) and RAD51 (2-fold) focus levels, as previously described (Helleday *et al.,* 2005). In AA8 cells the addition of 10 µM rucaparib caused a significant increase in γH2AX foci (Mann-Whitney test, p= 0.04) and an approximately 4-fold increase in RAD51 foci (Mann-Whitney test, p=< 0.0001), however in EM9 cells there was not a significant increase in γH2AX or RAD51 foci, suggesting unrepaired SSBs are the primary trigger of HRR as opposed to PARP trapping in these cells. Similarly to the other HRC cells, the kinase inhibitors each inhibited RAD51 focus formation >100%, to below DMSO control RAD51 levels, however this could be due to increased DMSO RAD51 foci.

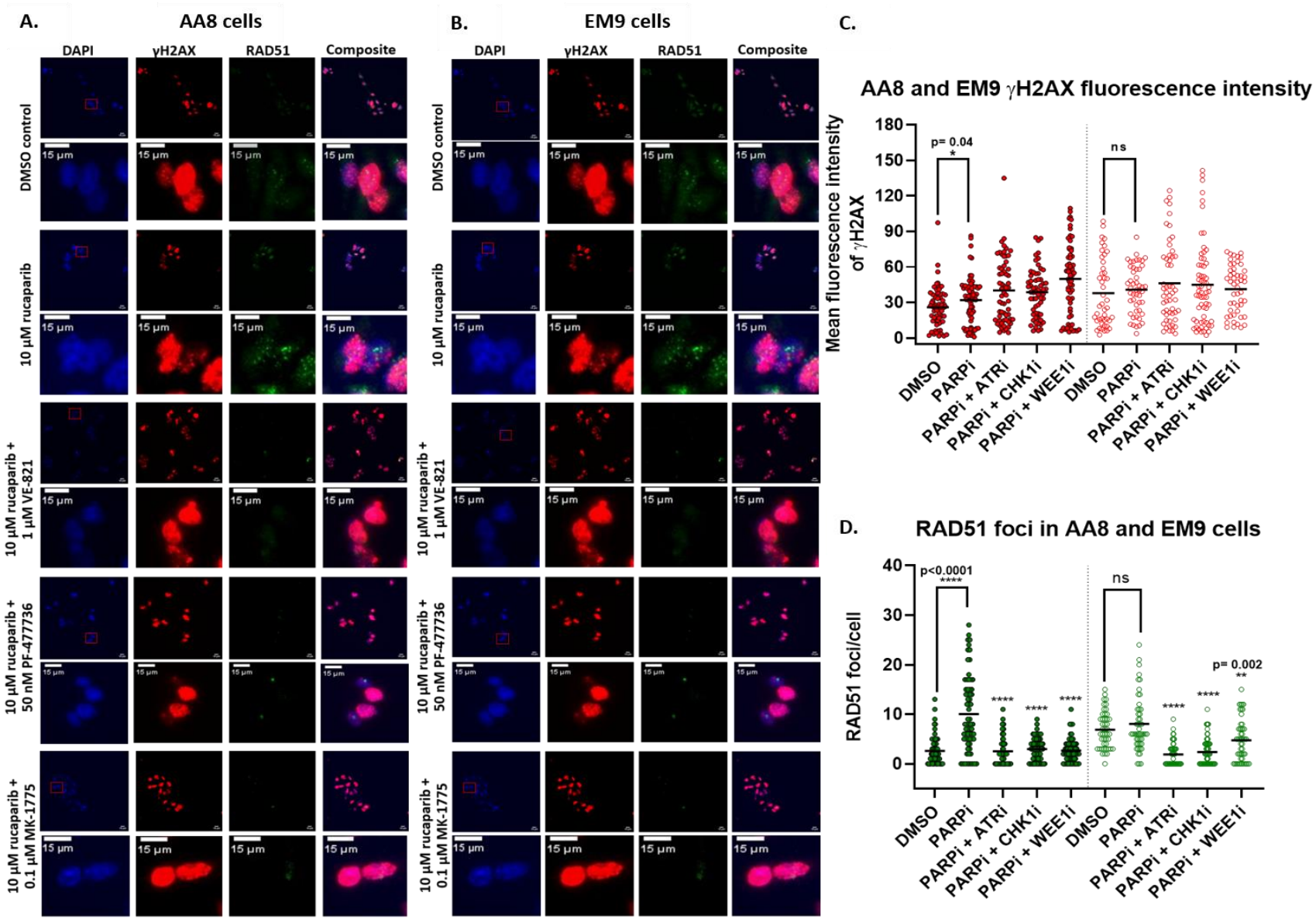

A.
AA8 cells
B.
EM9 cells
DAPI
γH2AX
RAD51
Composite
DMSO control
10 μM rucaparib
10 μM rucaparib + 1 μM VE-821
10 μM rucaparib + 50 nM PF-477736
10 μM rucaparib + 0.1 μM MK-1775
15 μm
C.
AA8 and EM9 γH2AX fluorescence intensity
Mean fluorescence intensity of γH2AX
p= 0.04
*
ns
DMSO
PARPi
PARPi + ATRi
PARPi + CHK1i
PARPi + WEE1i
D.
RAD51 foci in AA8 and EM9 cells
RAD51 foci/cell
p<0.0001
****
ns
p= 0.002
**

Figure 6.9: Impact of PARP inhibition as single agent and in combination with kinase inhibitors on HRR in matched AA8 and EM9 cells. DNA damage and HRR function was measured as mentioned previously in **A.** AA8 and **B.** EM9 cells. **C.** Fluorescence intensity of γH2AX was measured across cells and **D.** corresponding RAD51 foci were counted. Statistical analysis was calculated by Mann-Whitney t-test, **** $p<0.0001$.

6.6 Discussion

Sensitisation of PARPi-treated cells by ATR, CHK1 and WEE1 inhibitors has been demonstrated for the inhibitors individually, but to date there are no studies describing a direct comparison between inhibitors of ATR, CHK1 and WEE1.

In the study reported here sensitisation of cells to rucaparib by VE-821, PF-477736 and MK-1775 was exclusive to HRC cells and no potentiation was observed with HRD UWB1.289 and V-C8 cells. Though there appeared to be a general trend across the cell lines of the most potentiation occurring with VE-821, then PF-477736 followed by MK-1775, this was not statistically significant. Contrastingly, there has been previous data to show that PARPi olaparib in combination with ATR (AZD6738) or CHK1 (MK8776) inhibition resulted in decreased colony formation in both HRC and HRD cells (Gralewska *et al.,* 2020). However, in the study the ATRi was used at highly cytotoxic concentrations, whereas here concentrations were selected that gave good target inhibition but were not overly cytotoxic.

Kim *et al.,* also found both HRC and HRD cells were sensitised to the combination of PARPi olaparib and ATRi (AZD6738). However, the study showed less difference in sensitivity to PARPi between UWB1.289 matched cells, compared to what was observed here with rucaparib, and used the same concentration of olaparib when treating the matched cells in combination with ATRi (Kim *et al.,* 2020). Here, even at the lowest concentration used for UWB1.289+ B1 cells (0.3 μM) the concentration was too cytotoxic for UWB1.289 cells (cell survival: 90.5 vs 31.3%), thus the concentration of rucaparib used in combination experiments using HRD cells was adjusted (0- 30 μM vs. 0-3 μM). Due to the exceptionally increased sensitivity of these HRD cells to rucaparib as a single agent it was not possible to examine potentiation at higher concentrations.

Considering the trend observed in Chapter 5, between basal RS and single agent cytotoxicity by VE-821 and PF-477736, it was of interest to determine if this contributed to the kinase inhibitors ability to potentiate rucaparib. Both PF_{50} and potentiation at a fixed concentration were used as discriminants and, in the first instance, there appeared to be a trend of cells with higher basal RS being potentiated the least at the PF_{50} with PF-477736 and MK-1775, although this was not observed with VE-821. There was however no trend between basal RS and potentiation at 10 µM rucaparib, emphasising the importance of representing the entire concentration curve, when selected values can give opposing results.

As previously shown in Chapter 4, 10 µM rucaparib induced RS 3 to 7-fold in HRC cells and in turn signalled to the ATR-CHK1 axis. Due to the increased signalling to the ATR-CHK1 axis it was predicted that this would cause an increased reliance of cells on the pathway for both cell cycle control and DNA repair, by signalling to HRR. It was therefore predicted that RS induction by 10 µM rucaparib would correlate with the degree of sensitisation to rucaparib by the kinase inhibitors. Absolute mean γH2AX foci numbers in rucaparib-treated cells were used in the correlation analyses, as were mean fold-induction values from DMSO control. At the fixed concentration of 10 µM the hypothesised trend was observed between mean γH2AX foci per rucaparib-treated cell and CHK1 and WEE1 inhibitors (r^2= 0.7 and 0.9, respectively). However there was no trend with γH2AX foci per rucaparib-treated cell and response to ATR inhibition (r^2= 0.01). Fold-increase of γH2AX foci by rucaparib positively correlated with sensitisation by VE-821, PF-477736 and MK-1775 when measuring PF_{50} values (r^2= 0.2, 0.7 and 0.7). It is possible that measuring mean γH2AX foci per cell does not give the most accurate representation of RS caused by rucaparib, especially as this does not account for the vast standard deviation across cells.

The ATR-CHK1 signalling cascade is primarily known for its role in cell cycle checkpoint control at intra-S and G2/M checkpoints (Saldivar *et al.,* 2017, Rundle *et al.,* 2017, Lin *et al.,* 2017, Thada and Cortez, 2019). Here, the effects of rucaparib and the kinase inhibitors on cell cycle was assessed in IGROV1 cells and as predicted, rucaparib caused

S-phase arrest, which was the same at both 1 µM and 10 µM. There was no increase in G2-M population when cells were treated with 1 µM rucaparib, although an increase was observed with 10 µM. Overall there appeared to be a hierarchy in the cell cycle effects, as VE-821 abrogated S-phase arrest by 1 µM and 10 µM rucaparib to below DMSO levels, as well as reducing G2-M levels to below DMSO control. PF-477736 had the next greatest impact at reducing S and G2-M arrest, followed by MK-1775. However, more cell lines would need to be tested to confirm this was not an observation exclusive to IGROV-1 cells. In particular, the effects in the matched *BRCA* mutant and corrected cells is a priority here and would have been done had time allowed.

Due to the exclusive synergy between PARPi and the kinase inhibitors in HRC cells and not in matched HRD cells, it was key to assess how the combination of rucaparib and the kinase inhibitors was impacting HRR function in cells. The synthetic lethal relationship between PARPi and HRD cancer cells is well reported (Chapter 1, section 8), as is the involvement ATR, CHK1 and WEE1 each have with signalling to key components of HRR (Chapter 1, section 4.3.3), therefore it was predicted that as well as cell cycle effects the kinase inhibitors would also be impairing HRR function. RAD51 focus formation was measured exclusively in γH2AX- positive cells. PARPi induced RS and/or DNA damage across HRC cells and induced RAD51 focus formation (3 to 5-fold). This was expected due to the increased reliance PARPi-treated cells have on HRR for the resolution of unrepaired SSBs. VE-821 caused the greatest inhibition of RAD51 (89.0 ± 4.0 % to below DMSO control), then PF-477736 (64.0 ± 30.7 % to below DMSO control) then MK-1775 (78.2 ± 7.8 to 96.8 ± 10.0 %). However, this trend is across cell lines and was not significant within cell lines. The exclusive sensitisation of HRC cells and the impairment of HRR function by the kinase inhibitors, suggests HRR inhibition is a key mechanism underpinning the synergy of rucaparib and the kinase inhibitors. This reveals how key each of the kinases are in the HRR process, which has been demonstrated previously (Yazinski *et al.,* 2017, Sorensen *et al.,* 2005, Krajewska *et al.,* 2012). Yazinski *et al.* found ATRi disrupts BRCA1-independent RAD51 loading to DSBs and stalled forks in PARPi-resistant, *BRCA1*-deficient cells, using UWB1.289 cells to establish a panel of cell lines resistant to PARPi olaparib. This study showed ATRi (VE-821) preferentially sensitised *BRCA*-defective resistant cells over HRR competent UWB1.289+ B1 cells, which differs to

the observations here (Figure 6.1). When expanding the study into mechanistic investigations substantial RAD51 foci were detectable in HRD UWB1.289 cells, showing significant RAD51 were recruited to DSBs, independently of BRCA1. This contrasts the finding here where RAD51 foci formation differed greatly between UWB1.289 and UWB1.289+B1 cells, and UWB1.289 cells failed to increase RAD51 foci upon exposure to rucaparib, compared to the 5-fold increase observed in UWB1.289 + B1 cells (Yazinski *et al.,* 2017). Sorensen *et al.* discovered that abrogation of CHK1 function using siRNA or chemical antagonists inhibited HRR and showed evidence of a functional interplay between CHK1 and RAD51, which is crucial for HRR function. CHK1 inhibitors (UCN-01 and CEP3891) abrogated hydroxyurea (HU)-induced RAD51 foci induction, similar to the complete inhibition of rucaparib-induced RAD51 foci observed here across HRR competent cells. Furthermore, this study showed evidence that CHK1 mediated phosphorylation of RAD51 on Thr309, which was found to be essential for efficient HRR in cells (Sorensen *et al.,* 2005). Krajewska *et al.* investigated the impact of WEE1i by MK-1775, the WEE1i used here, by means of a GFP plasmid assay. The results suggested WEE1i forced activation of CDK1, which impaired HRR and further investigation showed the use of a second WEE1i PD-166285, resulted in more pronounced inactivation of HRR, possibly due to inhibition of Myt1 too with this inhibitor (Krajewska *et al.,* 2012). Here, the addition of MK-1775 to rucaparib-treated cells inhibited HRR to 79 – 97%.

Similar to observations made here, studies have shown that ATRi (AZD6738) alone and in combination with PARP inhibition (olaparib) reduced RAD51 foci to below DMSO control (Kim *et al.,* 2020). Similarly, it has been reported PARPi (olaparib) and CHK1i (Prexasertib) showed synergy in HGSOC cells due to reduced RAD51 foci formation in *BRCA*-wildtype, HRC cells (Brill *et al.,* 2017) and that WEE1i (MK-1775) inhibited the RAD51 foci formation caused by PARP inhibition (Ha *et al.,* 2020).

To further investigate the observed synergy the mechanism of PARP action was probed using XRCC1 defective and competent matched EM9 and AA8 cells. In addition to PARPi preventing BER occurring, persistent PARP inhibition can become “trapped” on DNA. EM9 cells were more sensitive to VE-821, PF-477736 and MK-1775, indicating that persistent SSB contribute to cytotoxicity but these were also sensitised by rucaparib

indicating a role for PARP trapping. However, the greatest difference between cell lines was observed with their sensitivity to VE-821, PF-477736 and MK-1775 alone, where EM9 cells were 5.4, 3.6 and 2.3-fold more sensitive than AA8 cells at the LC_{50}, suggesting the impairment of SSBR is more essential than the role of PARP trapping.

Rucaparib significantly increased RAD51 foci in AA8 but not the EM9 cells, suggesting unrepaired SSBs are the trigger of HRR as opposed to PARP trapping. However, a specific, quantifiable, PARP trapping assay would be necessary to distinguish which mechanism is contributing most to the observed synergy before any distinct conclusions on the role of PARP trapping could be made (Murai *et al.,* 2012).

A significant finding of this chapter is the exclusive sensitisation observed in HRC cells, which was not observed in HRD isogenic matched cells, suggesting HRR inhibition is central to the sensitisation. Indeed, VE-821, PF-477736 and MK-1775 inhibited rucaparib-induced HRR activity, further confirming this mechanism. Undoubtedly, the kinase inhibitors contribution to inhibiting PARPi-induced cell cycle arrest is another mechanism involved in the synergistic effects reported between PARPi and ATR/CHK1/WEE1i. Following these findings in cell lines, the next steps were to determine if the same would be observed in clinically relevant patient samples (Chapter 7).

Chapter 7. Investigating the effect of rucaparib and kinase inhibitors on patient ascites samples

7.1 Introduction

A key finding in the project so far was the exclusive synergy of PARPi and ATR/CHK1/WEE1 inhibitors observed in HRC cells (Chapter 6). The clinical use of PARPi is currently for *BRCA* mutated/ (presumed) HRD cancers. Resistance to PARPi can be acquired by restoration of HRR function (Lee and Matulonis, 2020), additionally, many tumours are intrinsically resistant due to having functional HRR. Therefore, combining PARPi with inhibitors of ATR/CHK1/WEE1 has the potential to overcome both acquired and intrinsic resistance to PARPi and would increase the number of patients who might benefit from PARPi therapy. In order to investigate the translational capacity of these combinations, it was essential to determine if VE-821, PF-477736 and MK-1775 could sensitise HRC patient-derived malignant ascites cells (from relevant tumour types) to rucaparib, and to measure the impact the combination had on HRR in these cells.

The use of patient-derived malignant ascites cells is valuable as these cells are more biologically relevant and a more directly related to the patient than an immortalised cell line. Although primary cultures are a valued tool in research there are disadvantages such as limited growth potential and the need for optimized culture conditions (Theriault *et al.,* 2013, Kodack *et al.,* 2017, Miserocchi *et al.,* 2017). Nevertheless, our lab has had a relatively high rate of success without special medium, provided the cells are initially cultured in a mixture of culture medium and the patient's ascitic fluid (O'Donnell *et al.,* 2014). Using such primary cells, the fraction of ovarian cancers that were HRD and rucaparib-sensitive was established for the first time (Mukhopadhyay *et al.,* 2010), and this was subsequently validated clinically when the survival of the patients was determined (Mukhopadhyay *et al.,* 2012).

Of the ascites samples used here, 4 originated from tumours that were identified as HGSOC and 1 that was mixed HGSOC/LGSOC by histological examination at the pathology department of the Queen Elizabeth Hospital, Gateshead. HGSOC is characterized by chromosomal instability, most likely due to defects in p53 (96% of

cases) and HRR in approximately 50-65% of cases (Mukhopadhyay *et al.,* 2010, Cancer Genome Atlas Research, 2011, Labidi-Galy *et al.,* 2017, Petersen *et al.,* 2020). Other abnormalities include genes encoding HRR proteins (PTEN, RAD51C, ATM and ATR), as well as Fanconi anaemia genes (Antony-Lisio *et al.,* 2019). Defects such as loss of G1 checkpoint control by p53 mutation occurs in >96% of HGSOC cases (Cole *et al.,* 2016), predicting a greater sensitivity to ATR/CHK1/WEE1 inhibitors as previously described in the literature (Nghiem *et al.,* 2002, Graves *et al.,* 2000, Bridges *et al.,* 2016, Wang *et al.,* 2001, Hirai *et al.,* 2009, Rajeshkumar *et al.,* 2011).

The other 2 primary cultures were established from endometrial cancer cultures, both of which were classed as Type 1 endometrioid G2. This subtype is defined as oestrogen-driven (Mang *et al.,* 2017) and most commonly associated with alterations in the PIK3CA pathway (>90%). *KRAS* and *FGFR2* mutations are also common (20% and 12%, respectively) (Morice *et al.,* 2016).

A recent study has shown *CCNE1* as an effective biomarker in predicting response to WEE1i-ATRi combination in aggressive ovarian carcinomas (Xu *et al.,* 2021). Here, cyclin E overexpression did not correlate with sensitivity to single agent ATR, CHK1 or WEE1 inhibitors (Chapter 5). Both ovarian and endometrial cancers have molecular features predicting high levels of RS, such as loss of G1 checkpoint control due to deleterious *TP53* mutations, loss of *RB1*, amplification of *MYC*, *KRAS* amplification and *NF1* loss or mutation, all of which contribute to RS. In chapter 5 basal RS was a predictor of sensitivity to single agent VE-821 and PF-477736, although not for MK-1775.

Here, it was of interest to investigate whether the observations across the cell line panel translated into primary patient-derived ascites samples.

7.2 Aims and Objectives

The main aims of this chapter are:

1. Determine HRR function and basal RS in primary cultures

2. Determine single agent cytotoxicity of VE-821, PF-477736 and MK-1775 in relation to measure of basal RS

3. Determine single agent rucaparib sensitivity in relation to HRR status

4. Determine sensitisation of rucaparib by VE-821/PF-477736/MK-1775 in relation to:

   a) The impact of rucaparib on RS and
   b) The impact of VE-821, PF-477736 and MK-1775 on HRR

7.3 Materials and Methods

7.3.1 Establishing primary cultures

Ascitic fluid samples were collected from patients following informed consent and processed as previously described (Chapter 2, section 1). Prior to the first passage the cells are in 50:50 RPMI-1640 media + 20% FCS: ascitic fluid. Cultures were then grown in RPMI-1640, with the addition of 20% FCS and 1% penicillin/ streptomycin. Of the ascites collected 15/19 were established as growing cultures that were passaged 1-8 times. For 7 of these cultures both SRB growth inhibition and HRR functional assays were successfully performed.

7.3.2 Homologous recombination repair assay

Following a minimum of 1 passage, cells were seeded onto coverslips as previously described (Chapter 2, section 10) and left to adhere. Cells were treated with either DMSO, 10 µM rucaparib single agent, 10 µM rucaparib with 1 µM VE-821, 10 µM

rucaparib with 50 nM PF-477736 or 10 µM rucaparib with 0.1 µM MK-1775 for 48 hr prior to fixation and analyses of γH2AX and RAD51 foci.

7.3.3 SRB growth inhibition assay

Primary cultures were seeded at 500- 1000 cells/well and left to adhere for 24 h. Cells were exposed to increasing concentrations of either single agent rucaparib (0 µM, 1 µM, 3 µM and 10 µM), or rucaparib concentrations with the addition of 1 µM VE-821, 50 nM PF-477736 or 0.1 µM MK-1775 and cells were incubated until control cells reached confluence, before being fixed and stained as previously described (Chapter 2, section 6).

7.4 Results

The following patient ascites samples were used.

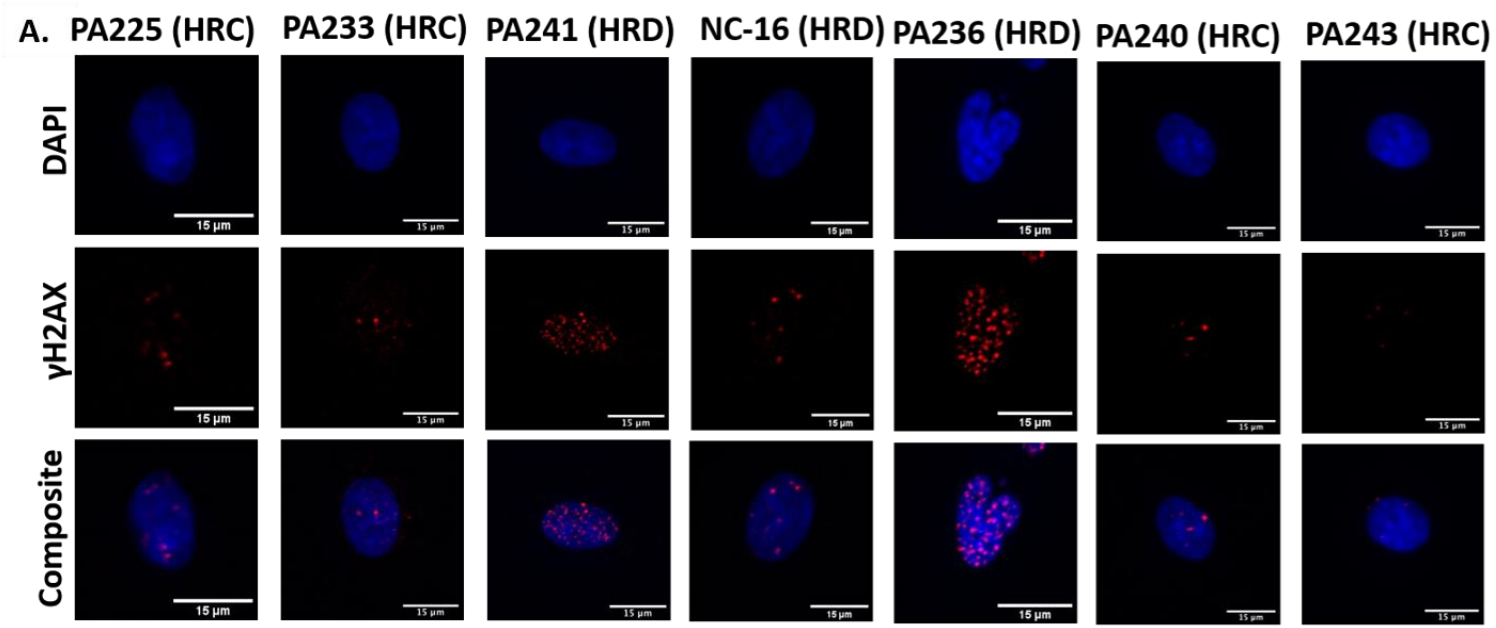
Sample I.D	Tumour site	Histology	Estimated doubling time (hr)
PA225	Ovary	HGSOC	61
PA233	Ovary	HGSOC	38
PA241	Ovary	HGSOC	81
NC-16	Ovary	HGSOC	46
PA236	Ovary	HGSOC and LGSOC	112
PA240	Corpus	Endometrioid G2	52
PA243	Corpus	Endometrioid G2	49

Table 7.1: Patient ascites samples used within the project. Sample ID, tumour site, histology and doubling time of patient ascites samples to be used in ex vivo experiments. Doubling time was calculated by SRB assays as day 0 was measured and compared to DMSO cells following a period of time before fixation, which was recorded to estimate a doubling time (hr). These values are one experiment per culture.

7.4.1 Determining basal RS in patient ascites samples

Basal RS was determined to assess whether correlations observed between kinase inhibitor sensitivity and basal RS observed *in vitro* in cell lines, translated into *ex vivo* experiments. Basal RS was measured in ascites cells by γH2AX foci formation in untreated cells, as previously described (Chapter 2, section 10).

The level of γH2AX foci per cell varied 3.2-fold among the ascites cells used here. The lowest levels were observed in PA243 (mean value 0.6 γH2AX foci/cell) and the highest in PA236 (1.9 γH2AX foci/cell). However, this sample (PA236) has outliers and had the highest standard deviation across the samples (S.D: 4.9), which may indicate a sub-population of cells with much higher γH2AX foci per cell. Interestingly, PA236 cells also had one of the slowest growth rates across the ascites, which may reflect an actively dividing sub-population amongst largely non-dividing cells. The mean basal γH2AX levels across patient ascites (1.3 γH2AX foci/cell) was lower than the mean observed across the cell line panel (7.6 ± 7.3 foci per cell), which was lower when excluding HRD UWB and V-C8 cells and XRCC1 defective EM9 cells (3.0 ± 1.7).


A.
PA225 (HRC)
PA233 (HRC)
PA241 (HRD)
NC-16 (HRD)
PA236 (HRD)
PA240 (HRC)
PA243 (HRC)
DAPI
γH2AX
Composite
15 μm

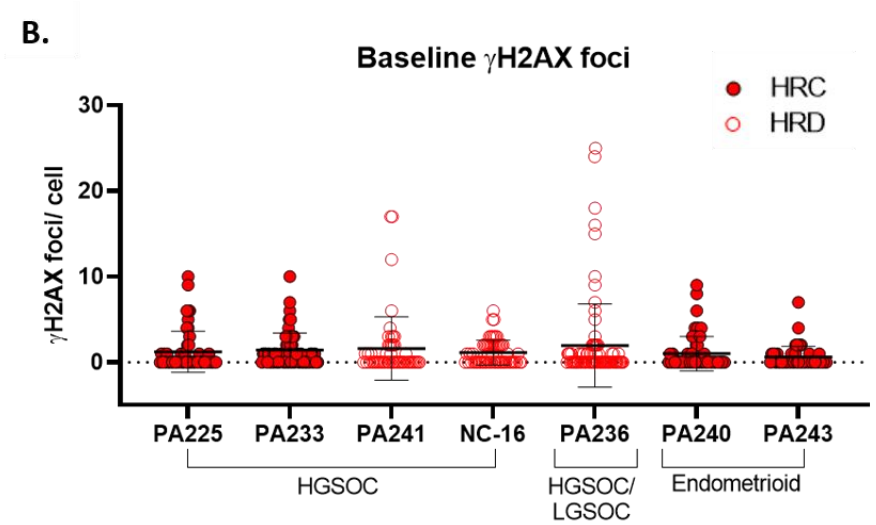

B.
Baseline γH2AX foci
HRC
HRD
γH2AX foci/ cell
30
20
10
0
PA225
PA233
PA241
NC-16
PA236
PA240
PA243
HGSOC
HGSOC/
LGSOC
Endometrioid

Figure 7.1: Basal RS in patient cultures of malignant ascites. γH2AX foci were measured by immunofluorescence as previously described. **A.** Images are representative of one experiment. Data shown are one experiment per patient ascites cells. **B.** γH2AX foci per untreated cell were plotted, with the mean bar and standard deviation shown. Open symbols represent HRD cultures, as determined below in section 7.5.2. Closed circles represent those deemed HRC.

7.4.2 Assessing induction of PARPi-induced RS and HRR function of patient ascites samples

As previously observed (Chapter 4), PARP inhibition by rucaparib induces RS (as measured by γH2AX foci). In the ascites cells tested here rucaparib also induced γH2AX foci formation 1.2- 5.2-fold (Figure 7.2B). Similar to the observation across the cell line panel, HRD cells with higher basal RS tended to have less fold-induction RS by PARPi.

To determine the HRR status of the cells RAD51 focus formation was measured as previously described. Drew *et al*. established the HRR functional assay used here where a rucaparib-induced increase in RAD51 foci of at least 2-fold was determined as indicative of functional HRR (Drew *et al.,* 2011), which was later validated in primary cultures (Mukhopadhyay *et al.,* 2010). Previously, cells which failed to increase in γH2AX foci by 2-fold or higher by rucaparib were excluded from analyses, under the assumption these cells failed to replicate during the exposure period to generate collapsed replication forks caused by PARPi (Gentles *et al.,* 2019). The assay has been further refined to only include γH2AX positive cells (as described in Chapter 6), and this way only replicating cells were assayed. Of the small panel of ascites cells tested here, PA236, PA241 and NC-16 were classified as HRD, as upon exposure to rucaparib there was only a 1.2, 0.9 and 1.6-fold RAD51 foci induction. PA236 cells had the lowest fold-induction of γH2AX foci.

In the HRC cells rucaparib increased RAD51 foci 2.4 to 4.6-fold. This induction of RAD51 was significant in all HRC cells except PA240 and PA243, where RAD51 still increased in excess of 2-fold.

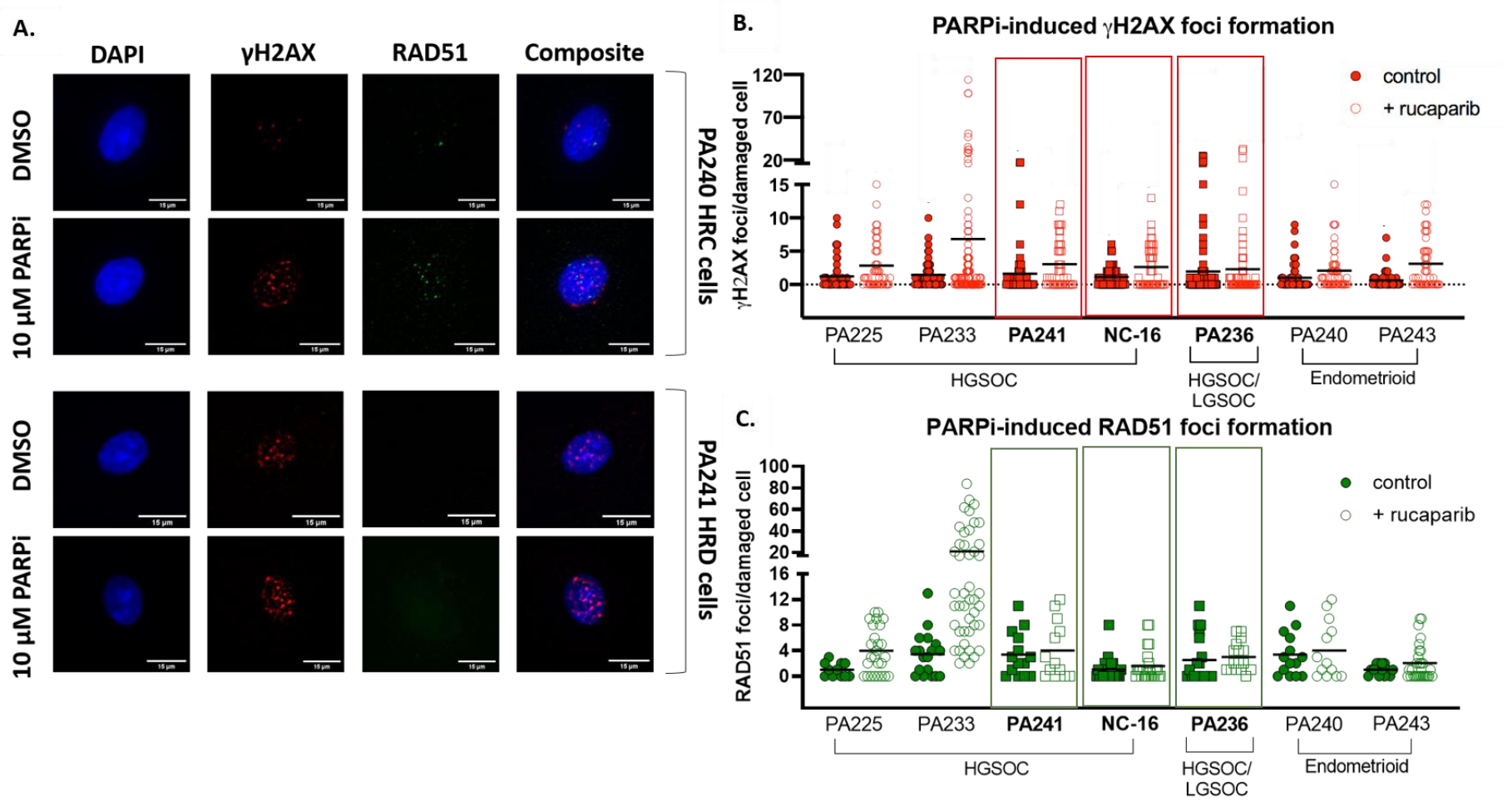

A.
DAPI
γH2AX
RAD51
Composite
DMSO
10 μM PARPi
PA240 HRC cells
DMSO
10 μM PARPi
PA241 HRD cells
B.
PARPi-induced γH2AX foci formation
γH2AX foci/damaged cell
120
70
20
15
10
5
0
control
+ rucaparib
PA225
PA233
PA241
NC-16
PA236
PA240
PA243
HGSOC
HGSOC/
LGSOC
Endometrioid
C.
PARPi-induced RAD51 foci formation
RAD51 foci/damaged cell
100
80
60
40
20
16
12
8
4
0
control
+ rucaparib
PA225
PA233
PA241
NC-16
PA236
PA240
PA243
HGSOC
HGSOC/
LGSOC
Endometrioid

Figure 7.2: PARPi- induced RS and HRR function across patient ascites cells. Cells were treated with 10 μM rucaparib and cells treated with rucaparib with an increase of γH2AX foci and RAD51 foci cells were deemed as HRR competent. When there was no induction of RAD51 foci cells were deemed HRR defective. **A.** Representative images of an HRC culture (PA240) and an HRD culture (PA241) from one experiment. **B.** γH2AX foci per cell and **C.** RAD51 foci/ γH2AX positive cell, as previously described, with each data point representing an individual cell with mean bar shown, from one experiment per culture. Unpaired t-tests were performed between DMSO control and rucaparib-treated cells within each patient ascites sample. *** p<0.001, **p<0.01, * p<0.05, as calculated using Graphpad prism 9.0 software. Cultures with boxes surrounding them are HRD.

7.4.3 Determining cytotoxicity of single agent rucaparib and kinase inhibitors in patient ascites samples

To determine if HRR status determined sensitivity to rucaparib alone as previously reported in similar ascites cultures (Mukhopadhyay *et al.,* 2010). The HRD primary cultures (PA236, PA241 and NC-16) were more sensitive to rucaparib (GI_{50}: 0.6 to 3.6 μM) than the HRC cultures (GI_{50} > 10 μM), as expected (Figure 8.3).

The cytotoxicity of 1 μM VE-821, 50 nM PF-477736 and 0.1 μM MK-1775 was assessed. Figure 8.4 shows that 1 μM VE-821 caused growth inhibition that ranged from no growth inhibition (PA241, HRD) to 30.8% (PA236, HRD). 50 nM PF-477736 ranged from no growth inhibition (PA243, HRC) to inhibiting growth by 54.0% (PA236, HRD). 0.1 μM MK-1775 caused inhibition ranging from 4.1 % (NC-16, HRD) to 38.6% (PA236, HRD). For all 3 inhibitors sample PA236 (HRD) was most susceptible to growth inhibition and interestingly these cells had the highest basal RS, which was previously correlated with sensitivity to VE-821 and PF-477736 (Chapter 5, section 5.5). The other identified HRD samples, PA241 and NC-16, were not more sensitive to any of the kinase inhibitors.

Correlation analyses (Figure 8.5) showed a trend between basal RS and growth inhibition by 1 μM VE-821 (r^2= 0.1), 50 nM PF-477736 (r^2= 0.7) and 0.1 μM MK-1775 (r^2=0.1), although this trend was weak with VE-821 and MK-1775 and only statistically significant with PF-477736 (p=0.02), due to the limited number of observations.

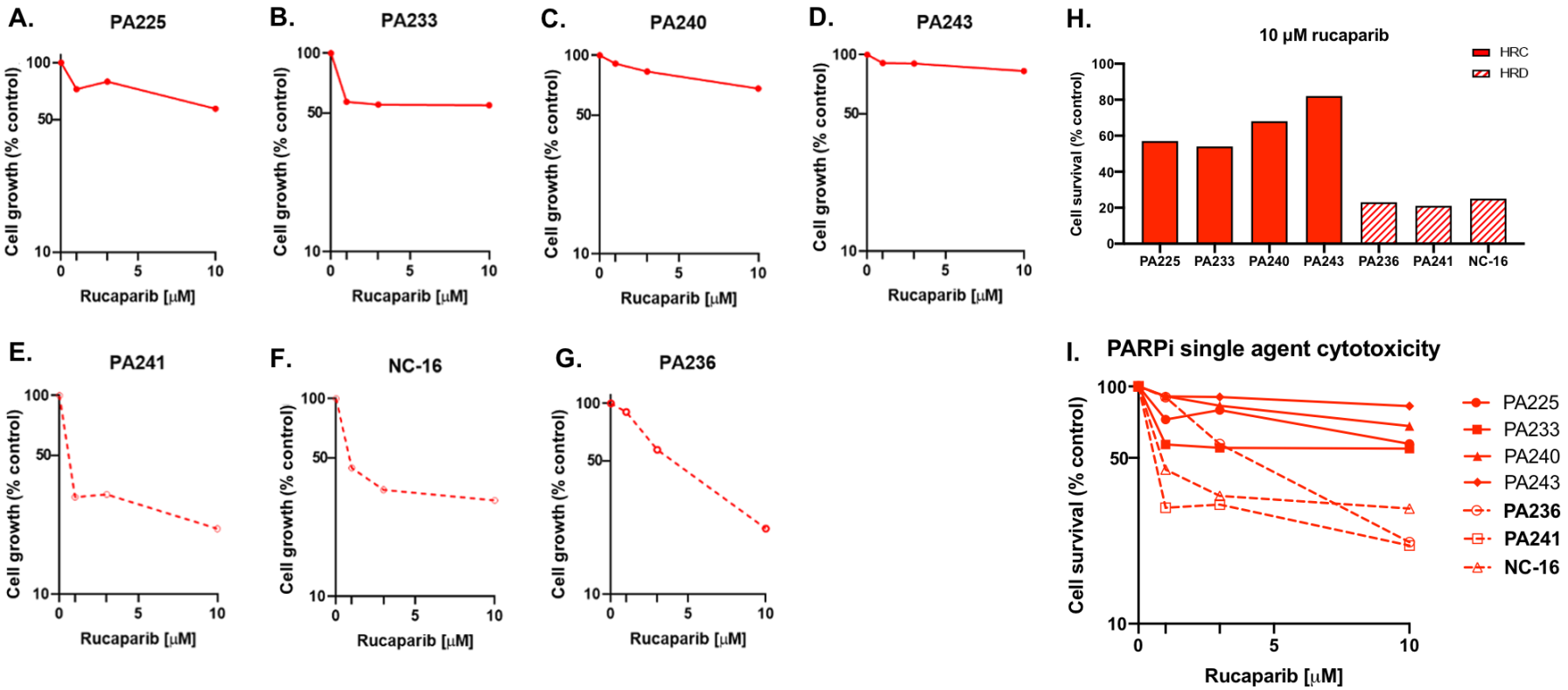


Figure 7.3: Single agent cytotoxicity of rucaparib in patient ascites cells. Cells were exposed to a concentration range of 0- 10 µM rucaparib and cytotoxicity was assessed by SRB growth inhibition assays as previously described in **A.** PA225, **B.** PA233, **C.** PA236, **D.** PA240, **E.** PA241, **F.** PA243, and **G.** NC-16 cells. **H.** Cell survival (% control) was measured at set concentrations of 10 µM rucaparib. **I.** Each of the ascites samples were plotted on one graph to highlight the differences in sensitivity to rucaparib between HRC and HRD cells. The dashed lines represent HRD cells. Data are from one experiment per primary culture.

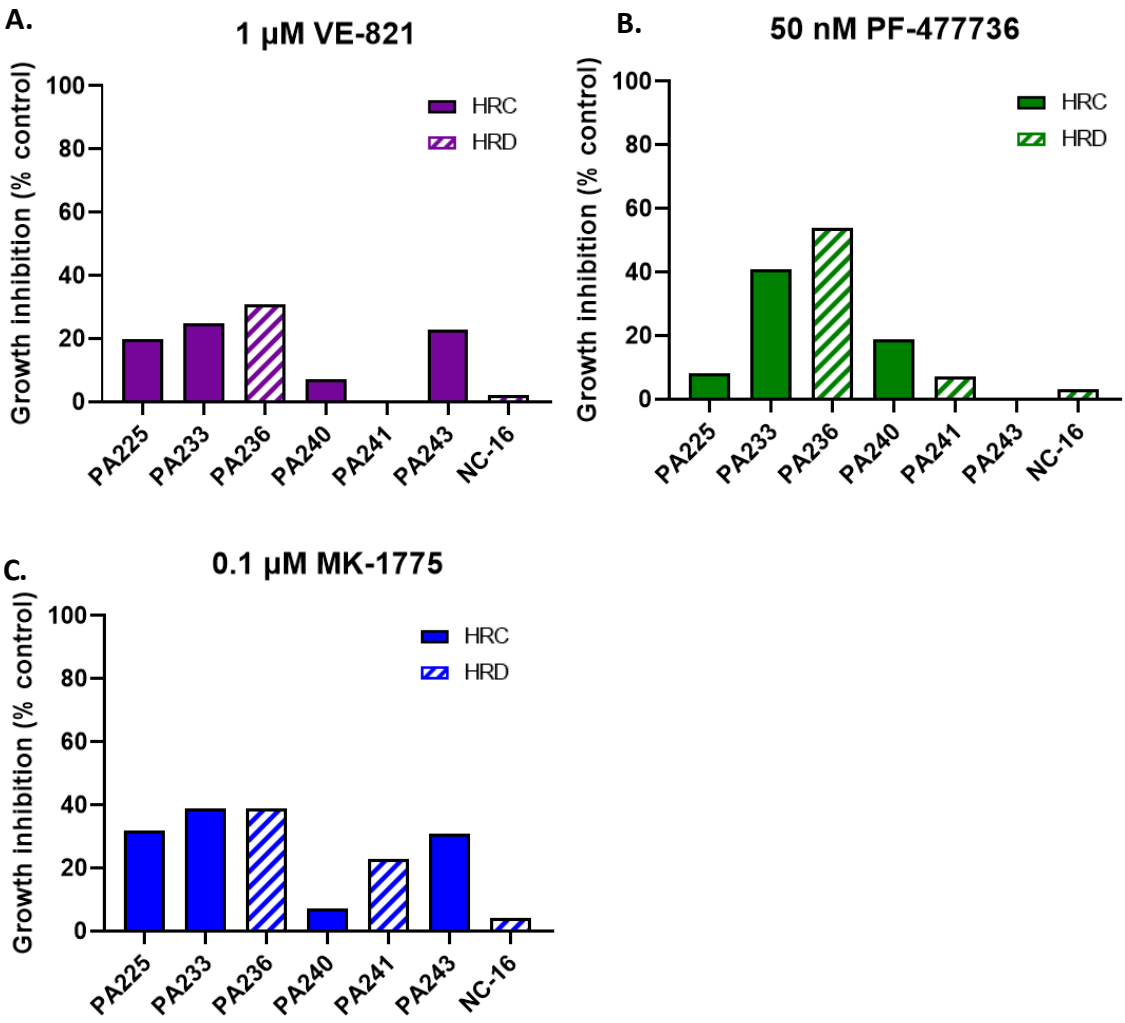


Figure 7.4: Cytotoxicity of VE-821, PF-477736 and MK-1775 at set concentrations in malignant ascites cells. SRB growth inhibition assays were performed to determine growth inhibitory effect of **A.** 1 µM VE-821, **B.** 50 nM PF-477736 and **C.** 0.1 µM MK-1775 on the panel of ascites cells. Data are from one single experiment per primary culture.

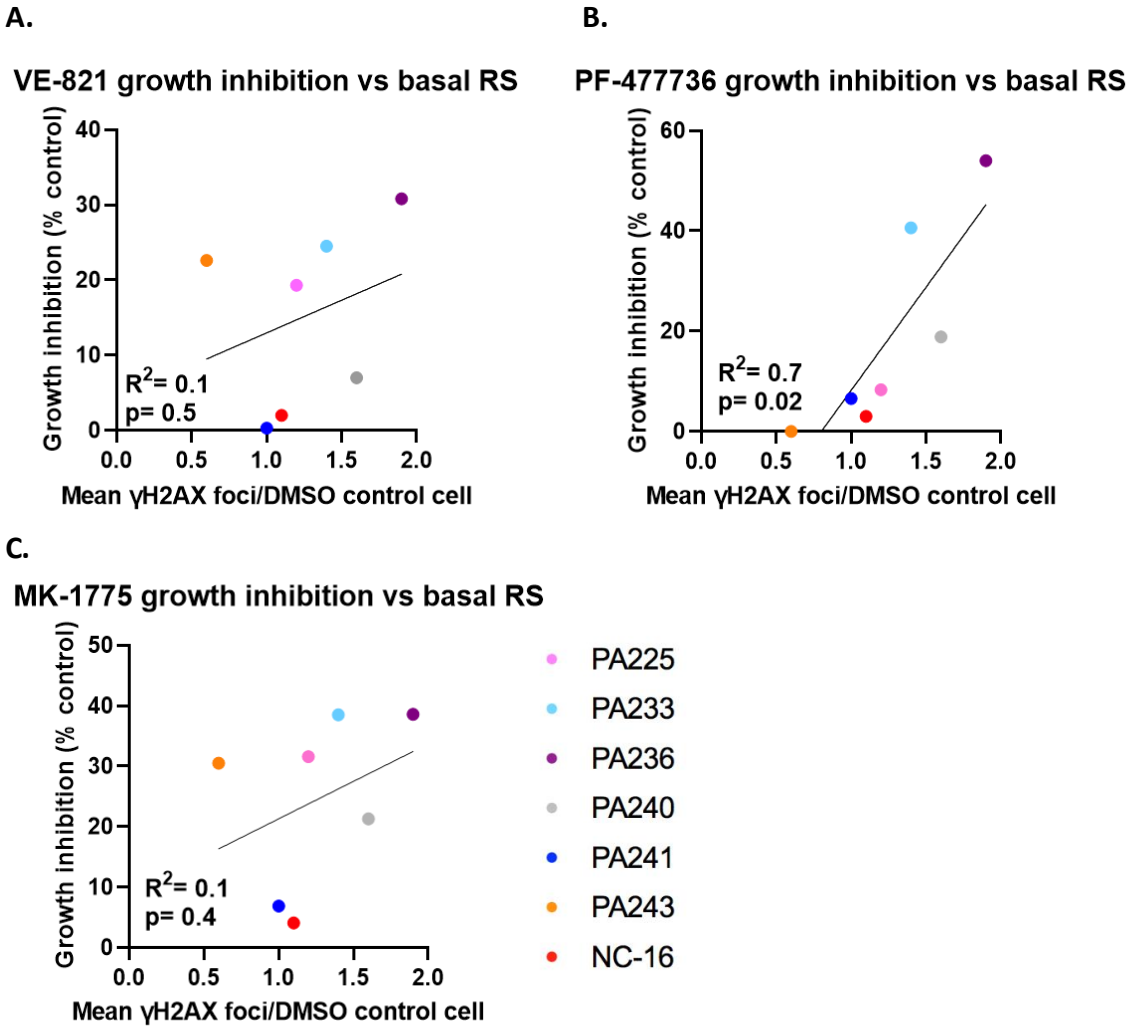


Figure 7.5: Correlation of basal γH2AX foci in cells vs. growth inhibition (%) at set concentrations. Mean γH2AX foci number was calculated as described previously and plotted against growth inhibition at a fixed concentration of **A.** 1 µM VE-821, **B.** 50 nM PF-477736 and **C.** 0.1 µM MK-1775. Correlation was calculated using Graphpad prism 9.0 software.

7.4.4 Investigating synergy between rucaparib and VE-821, PF-477736 and MK-1775

In cultured cell lines 1 µM VE-821, 50 nM PF-477736 and 0.1 µM MK-1775 each potentiated rucaparib cytotoxicity (Chapter 6, section 5.1), exclusively in HRC cells. Here, it was determined if this finding was replicated in primary cultures.

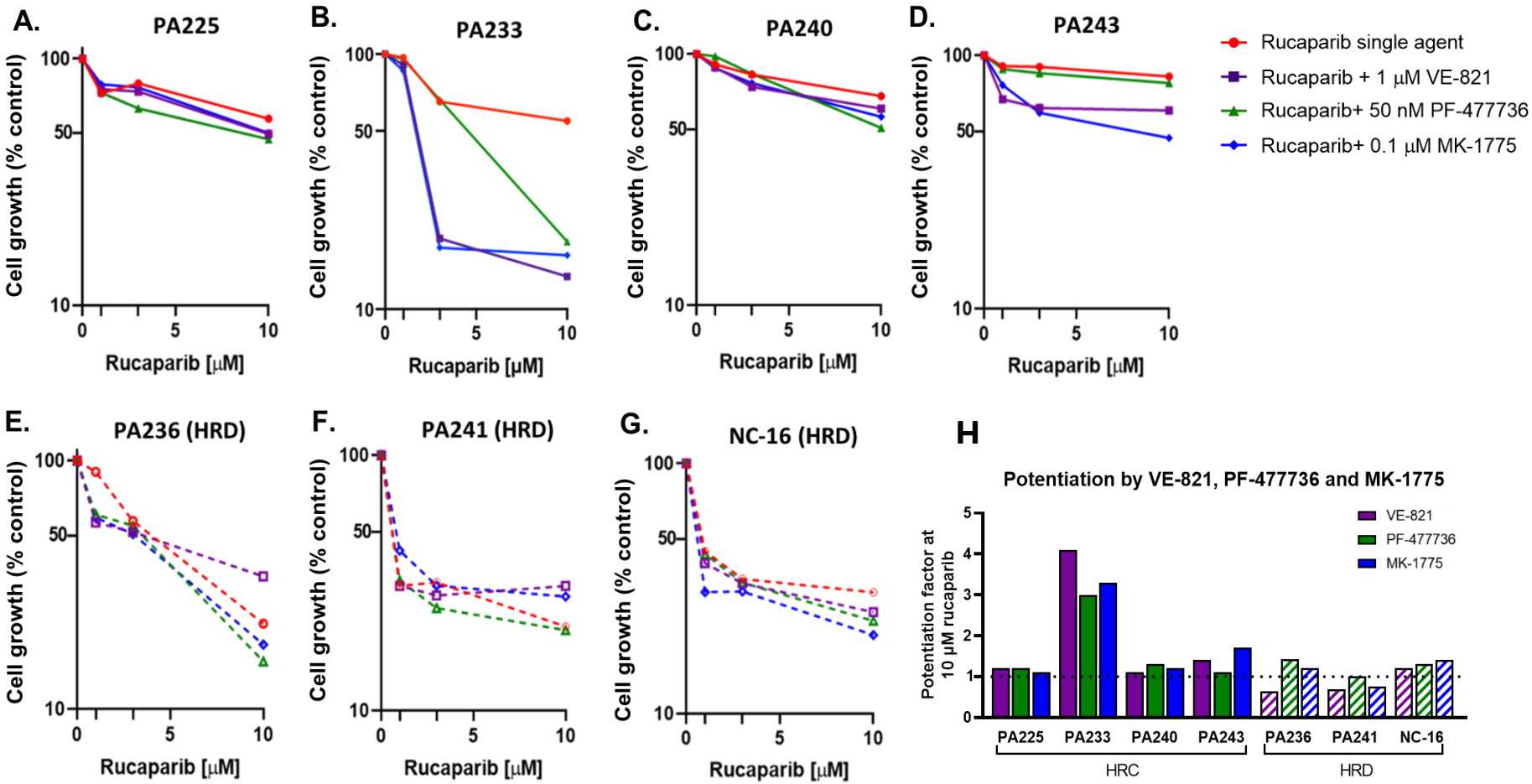


Figure 7.6: Cytotoxicity of rucaparib in combination with VE-821, PF-477736 or MK-1775 in malignant ascites cells.
Cells were exposed to rucaparib at indicated concentrations either as single agent or with the addition of 1 μM VE-821, 50 nM PF-477736 or 0.1 μM MK-1775 as previously described (Chapter 2) in **A.** PA225, **B.** PA233, **C.** PA236, **D.** PA240, **E.** PA241, **F.** PA243 and **G.** NC-16 cells. Each graph represents one individual experiment, with dashed lines representing HRD cells. **H.** A bar chart showing potentiation factor at 10 μM rucaparib in cultures tested.

In the HRC ascites cells some sensitisation by VE-821, PF-477736 and MK-1775 was observed, although this was often only observed at the higher concentration of 10 µM rucaparib (Figure 7.6). Overall, the mean potentiation at 10 µM rucaparib by VE-821, PF-47736 and MK-1775 inhibitors was greater for the HRC cultures than HRD cells (2-fold vs. no potentiation, 1.7-fold vs. 1.2-fold and 1.8 vs. 1.1-fold, respectively). Although there was difficulties in culturing these cells and only one replicate per culture, the data are in line with that obtained with the cell lines described in Chapter 6.

7.4.5 Correlation of PARPi-induced RS and potentiation by VE-821, PF-477736 and MK-1775

In Chapter 6, section 5.3, in human HRC cells, there was a trend that cells with the greatest fold-increase in RS by rucaparib (measured by γH2AX foci) had greater sensitisation by VE-821, PF-477736 and MK-1775 (r^2= 0.2, 0.7 and 0.7, respectively), although this was in a limited panel of cells. Here, it was interesting to investigate this trend further, to assess if this was also the case with patient ascites cultures.

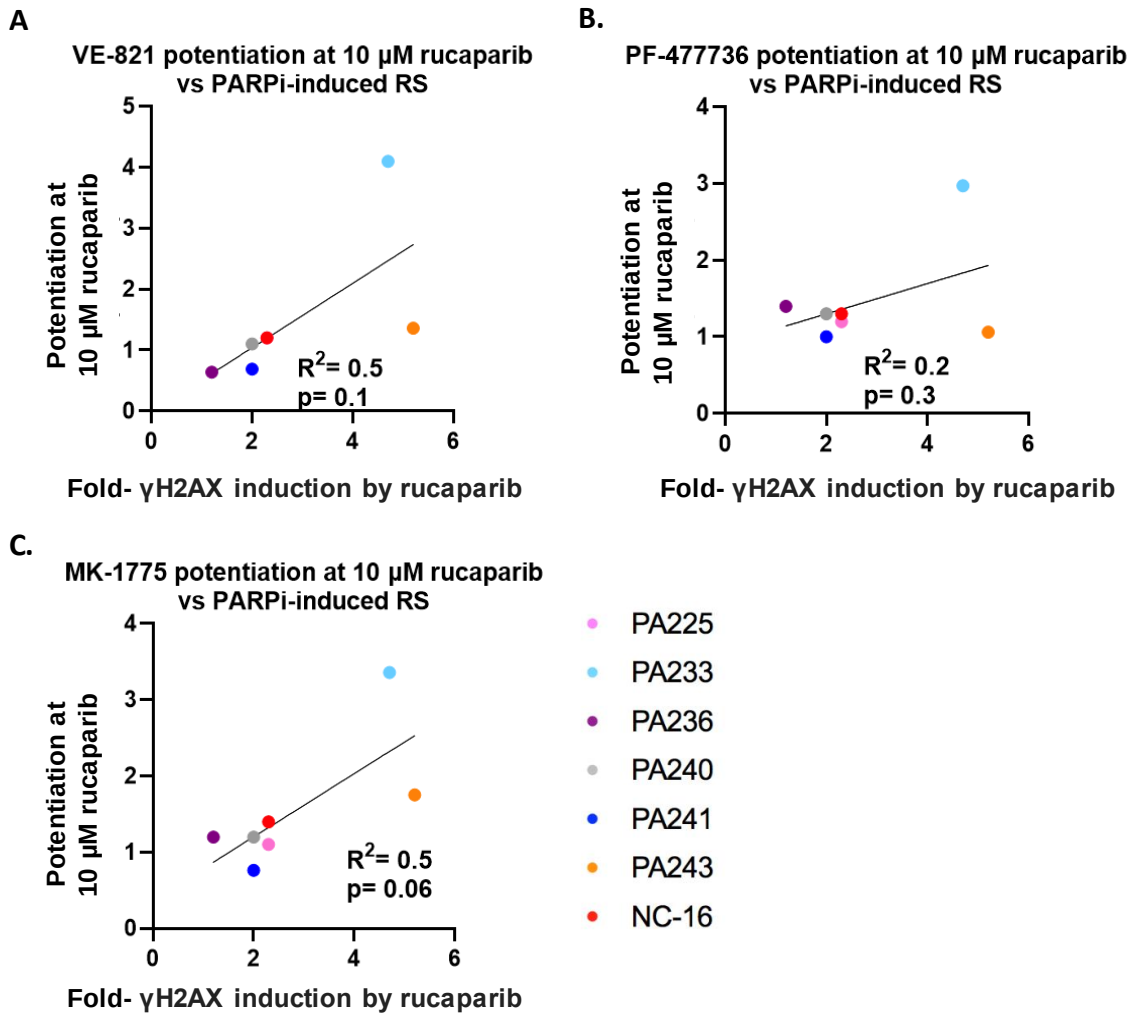


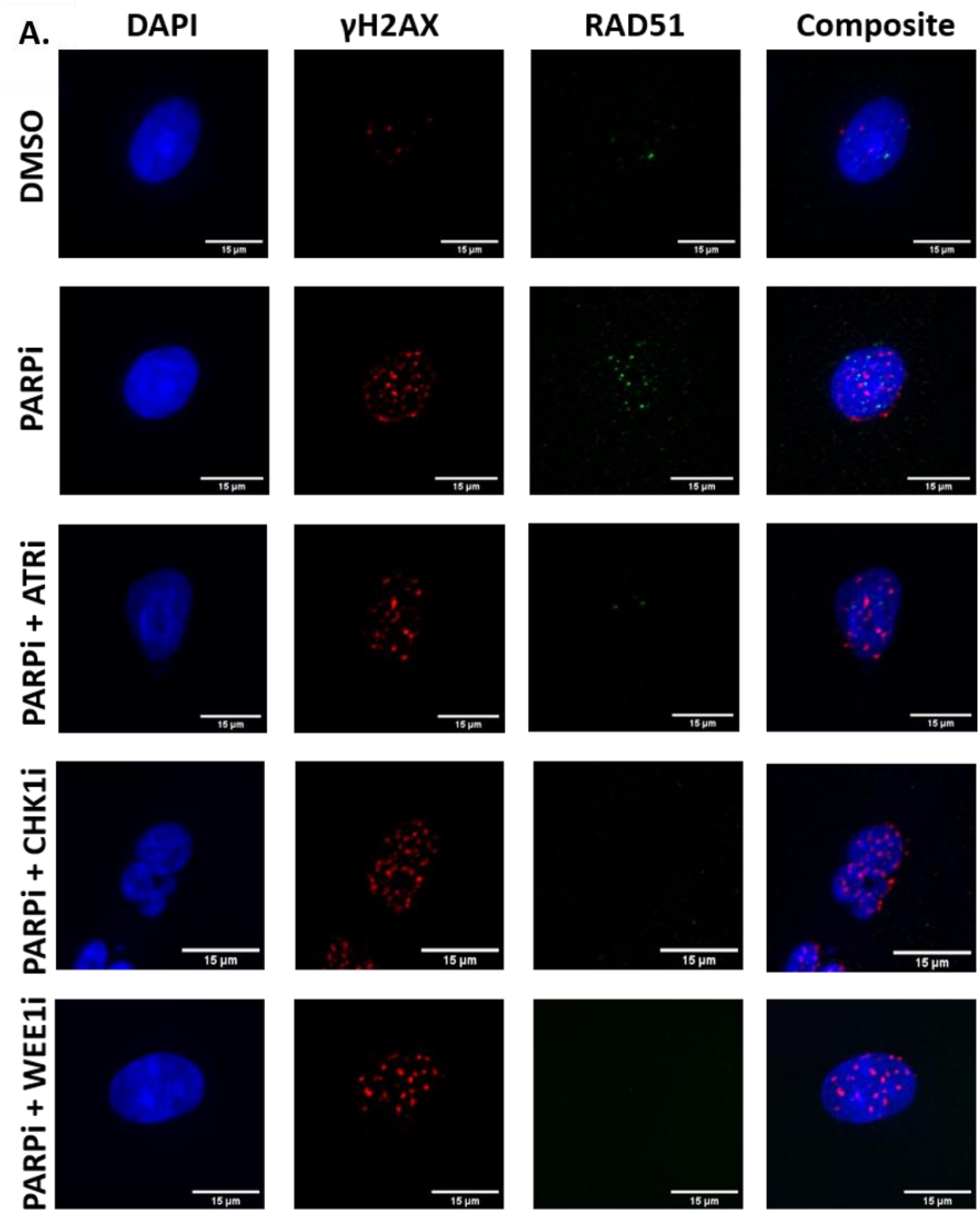
Figure 7.7: Correlation of rucaparib-induced γH2AX foci in cells vs. potentiation by kinase inhibitors at 10 µM rucaparib. Fold-increase of γH2AX foci with exposure to rucaparib was calculated as described previously and plotted against potentiation at 10 µM rucaparib by **A.** 1 µM VE-821, **B.** 50 nM PF-477736 and **C.** 0.1 µM MK-1775. Correlation was calculated using Graphpad prism 9.0 software.

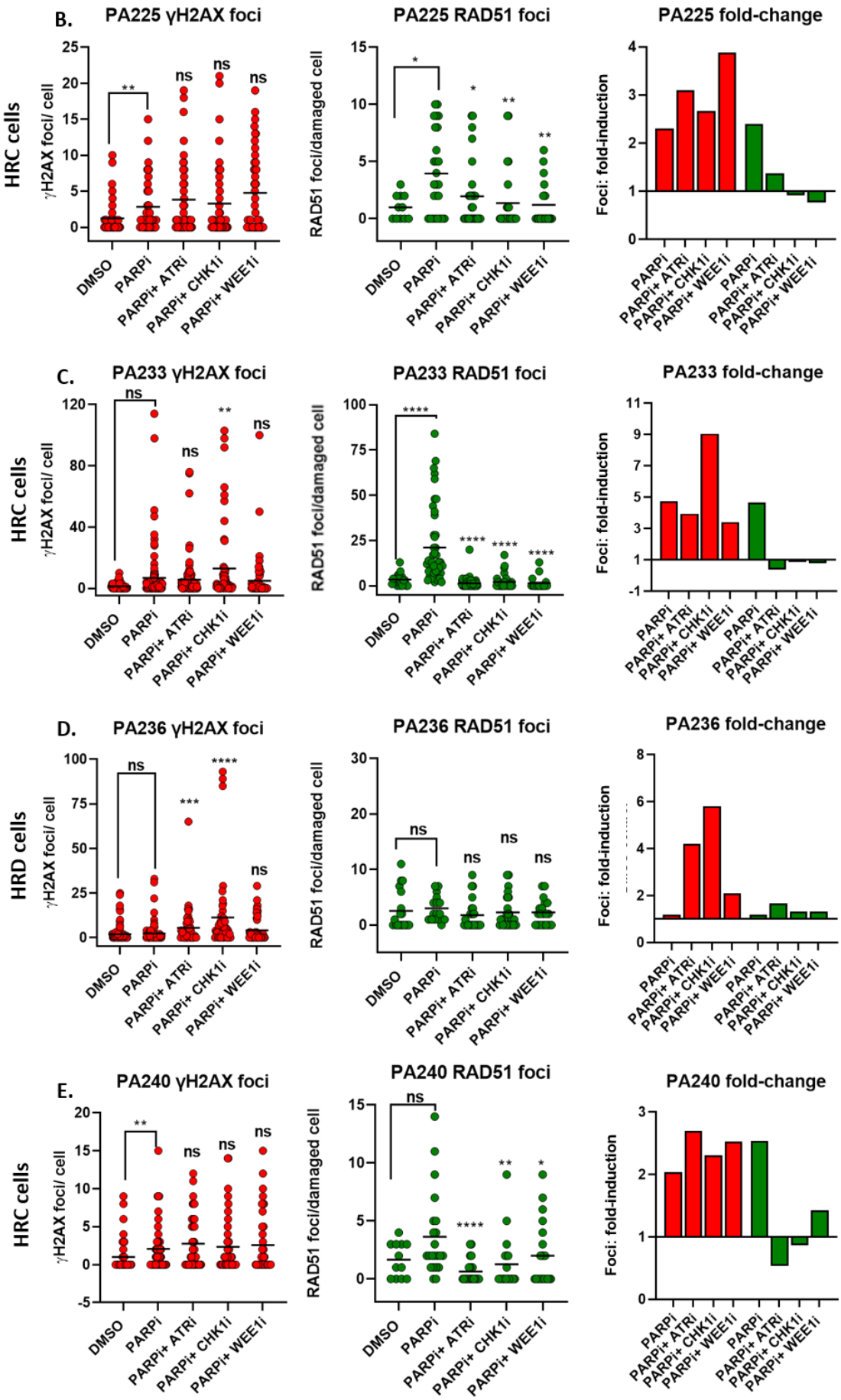
Similarly to observed with cell lines in Chapter 6, there was a modest trend between rucaparib-induced RS and potentiation by VE-821, PF-477736 and MK-1775 (r^2= 0.5, 0.2 and 0.5, respectively), although it was not significant. As with the cell lines, more samples would be required to determine if induction of RS by rucaparib is a true indicator of synergy.

7.4.6 Exploring the impact of VE-821, PF-477736 and MK-1775 on HRR

In the cell lines, inhibition of HRR by VE-821, PF-477736 and MK-1775 was a major factor in their sensitisation of rucaparib (Chapter 6, section 5.4). To determine if they also

inhibited HRR in ascites cultures, HRR function was measured by RAD51 foci formation. PARPi induced RAD51 foci 2.4 to 4.6-fold, which was reduced by the addition of 1 μM VE-821, 50 nM PF-477736 and 0.1 μM MK-1775 in all the HRC ascites cells, and this reduction was significant in all cultures except for, where rucaparib did not significantly induce RAD51 foci formation (Figure 7.8).


A.
DAPI
γH2AX
RAD51
Composite
DMSO
PARPi
PARPi + ATRi
PARPi + CHK1i
PARPi + WEE1i
15 μm


B.
PA225 γH2AX foci
PA225 RAD51 foci
PA225 fold-change
C.
PA233 γH2AX foci
PA233 RAD51 foci
PA233 fold-change
D.
PA236 γH2AX foci
PA236 RAD51 foci
PA236 fold-change
E.
PA240 γH2AX foci
PA240 RAD51 foci
PA240 fold-change
HRC cells
HRD cells
γH2AX foci/ cell
RAD51 foci/damaged cell
Foci: fold-induction
DMSO
PARPi
PARPi+ ATRi
PARPi+ CHK1i
PARPi+ WEE1i
ns

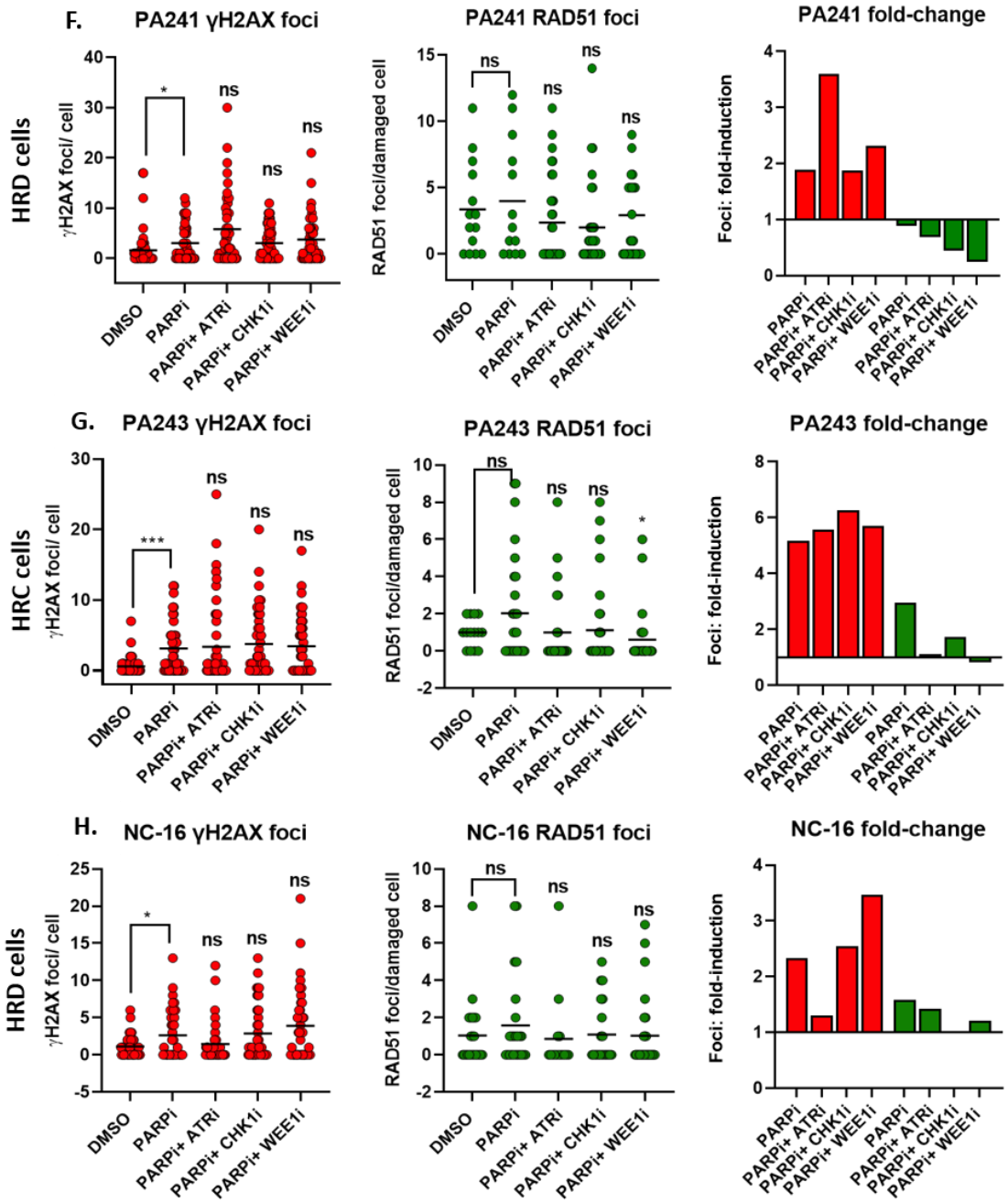


Figure 7.8: Impact of rucaparib single agent and in combination with VE-821, PF-477736 or MK-1775 on HRR in patient ascites cells. A. Representative images of HRC cultures (PA240), where γH2AX foci measured RS and RAD51 foci HRR function. γH2AX foci per cell was plotted for each culture, with mean bar shown. RAD51 foci were counted per damaged cell and mean bar is shown for each culture **B.** PA225, **C.** PA233, **D.** PA236, **E.** PA240, **F.** PA241, **G.** PA243 and **H.** NC-16 cells. Fold-change of γH2AX (red bars) and RAD51 (green bars) from DMSO was calculated and unpaired t-test was performed to calculate significance. * p<0.05, ** p<0.01, ***p<0.001, ****p<0.0001.

7.5 Discussion

The aim of this study was to determine if the findings with the cell lines described in previous chapters were applicable to primary cultures of gynaecological cancers and therefore more likely to be clinically relevant

Due to their limited life span and unpredictable cell growth, it was not possible to characterise these patient ascites samples to the same degree as the cell lines. However, it was possible to measure basal RS, HRR function and the impact of rucaparib, VE-821, PF-477736 and MK-1775 on these parameters and cell proliferation to a limited extent. These limitations meant each experiment could only be performed once per culture, reducing the reliability of results that is associated with replicates. Cell line doublings varied 3-fold, which could have impacted the data as with the cell cycle checkpoint inhibitors it may be expected that cells dividing more rapidly would have increased sensitivity, although this was not the case in cell lines (Chapter 5, section 5.4).

In these primary cultures basal RS varied 3-fold and overall HRD cultures had higher basal RS than HRC ones, as observed in matched cell lines in Chapter 3, section 5.6. Correlation analyses between basal RS and growth inhibition by VE-821, PF-477736 and MK-1775 (Figure 7.5) showed a modest trend but this was only statistically significant with PF-477736 ($p=0.02$), due to the limited number of observations. This was different from correlation analyses in Chapter 5, section 5.5, with cell lines, which showed the strongest trend between sensitivity to 1 µM VE-821 and basal RS, and a weaker trend with 50 nM PF-477736, although these data were skewed by HRD UWB1.289 cells.

The HRR status of patient ascites cultures were determined by the induction of γH2AX foci and RAD51 foci by rucaparib. All cultures deemed HRC by immunofluorescence had rucaparib GI_{50} values of >10 µM, whilst HRD cultures had GI_{50} values of <4 µM. Similarly, Mukhopadhyay *et al.,* showed that primary epithelial ovarian cultures deemed HRD by the same assay had rucaparib GI_{50} value of <2 µM, with HRC > 10 µM (Mukhopadhyay *et al.,* 2010). Myriad myChoice® and Foundation medicine FoundationOne®CDx are FDA approved, commercially available tests to identify HRD ovarian cancers, targetable by

PARPi (Cleary *et al.,* 2020). Other genomic tests can be done to assess LOH, mutations in HRR and COSMIC signature 3 to determine HRR status, but these represent genomic scarring caused when a tumour is HRD at some point in its evolution, although does not necessarily reflect HRR status at the time when treatment decisions have to be made (Chopra *et al.,* 2020). The IF RAD51 focus formation assay represents a cheaper alternative to these tests and gives a rapid read out, at a specific time point although it is somewhat more challenging in the need for viable tumour material.

PA236 (HRD) cells had the highest basal RS levels and were most sensitive to single agent VE-821, PF-477736 and MK-1775 and in general there was a modest trend for a correlation of growth inhibition with basal RS. Although in most studies HRD cells are reported to be more sensitive to VE-821, PF-477736 and MK-1775 (Williamson *et al.,* 2016, Middleton *et al.,* 2015, Kim *et al.,* 2017, Do *et al.,* 2015), this was not the case in this small sample of heterogeneous ascites cells. In Chapter 5, HRD UWB1.289 cells were more sensitive to the kinase inhibitors than HRC UWB1.289+ B1 cells, however, HRD V-C8 cells did not have increased sensitivity compared to corrected V-C8.B2 cells. Another consideration is that there could be many other mutations contributing to the effects observed in patient-derived cells and ideally these cells would have been sequenced, if time would have permitted to further investigate this.

Potentiation by the kinase inhibitors was measured at the set rucaparib concentrations of 10 µM, where it reached up to 4-fold potentiation in the HRC cultures, similar to the observations in HRC cell lines in Chapter 6. In this limited sample there was no clear evidence of one kinase inhibitor being superior to the others. There was no significant sensitisation in any of the HRD cells. As was observed in the cell lines, VE-821, PF-477736 and MK-1775 all inhibited HRR in the HRC ascites cells and so this may be the mechanism underlying rucaparib potentiation. It has been reported that in a *BRCA2* mutant PDX model ATRi (AZD6738) or CHK1i (MK8776) in combination with PARPi (olaparib) significantly reduced tumour volume, when compared to relevant single-agent therapy. (Kim *et al.,* 2017). Although no *BRCA2* competent model was used as a comparison in this instance, to examine any differences or increased response in HRC tumour cells.

In cells co-incubated with rucaparib and VE-821, PF-477736 and MK-1775 it might not entirely be the kinase inhibitors potentiating rucaparib but rucaparib also potentiating VE-821, PF-477736 and MK-1775. Higher levels of rucaparib-induced RS were associated with a greater cytostatic effect of the combination (figure 7.7), suggesting a 2-way synergy rather than potentiation, although a larger sample number would be required to assess this by using Bliss or Loewe analysis.

Although primary cultures are more biologically relevant than cell lines, limitations were experienced in using these cells. A major limitation is the short lifespan of these cultures, and therefore a restricted time for optimizing culture conditions. However, even with the limited number of cultures used here, the same trends were observed as in Chapter 6, in particular the greater sensitivity of HRD cultures to rucaparib, exclusive potentiation of rucaparib by VE-821, PF-477736 and MK-1775 in HRC ascites cells, as well as the same inhibition of HRR function by the addition of the kinase inhibitors to rucaparib-treated cells.

8 clinical trials are currently investigating the use of ATRi AZD6738 with PARPi olaparib (NCT03462342, NCT04090567, NCT03787680, NCT04065269, NCT02576444, NCT03682289, NCT03022409, and NCT03878095), although no results from these trials have yet been published. The PARPi veliparib (ABT-888) is currently being evaluated in combination with cisplatin and ATRi berzosertib (VX-970) in a phase 1 trial in patients with advanced solid tumours, originally hypothesising that the combination would induce a *BRCA*-null phenotype. However, preliminary data shows sensitisation of HRD cells and an increase in RAD51 foci formation with ATRi, which is an unexpected result considering these data and previous studies (Coyne *et al.,* 2021) (NCT02723864).

Currently a PARPi has only been combined with a CHK1i in 1 clinical trial. This phase 1 study showed prexasertib could safely be used in combination with olaparib, resulting in preliminary antitumour activity in HGSOC and other solid tumours. The study highlighted how results support further investigations comparing PARPi-sensitive and resistant models, probing other DDR alterations, such as *ATRX* mutations (Do *et al.,* 2021) (NCT03057145).

A dose-escalating Phase 1b study investigated the safety of adavosertib (MK-1775) combined with olaparib in refractory solid tumours, to determine a MTD and recommended dose for Phase 2 (NCT02511795). Treatment with the combination of olaparib and adavosertib showed antitumour activity, particularly at the MTD (Hamilton *et al.,* 2019). Three trials investigating the combination of olaparib and adavosertib are currently ongoing, with the focus on sensitising PARPi-resistant cancers (NCT04197713, NCT02576444, and NCT03579316).

With further experiments and a greater number of samples used, these preliminary findings may help better the understanding of how to best identify patients more likely to respond to single agent rucaparib/kinase inhibitors or in combination. For example, from these findings combined with the cell line data in Chapter 6, HRD patients would not benefit from the addition of ATR, CHK1 or WEE1 inhibitor, and this would most likely cause more harm, with increased toxicities.

Chapter 8. Differences in durability of PARP inhibition by PARP inhibitors in ovarian cancer cells

8.1 Introduction

As previously described (Chapter 1, section 9.1), endogenously generated SSBs are repaired continuously by PARP-dependent repair mechanisms. When PARP is inhibited these endogenous SSBs persist and collide with replication forks causing them to stall and collapse resulting in DSBs which can only be repaired by HRR during S and early G2 phase. If HRR is defective, e.g. due to *BRCA* mutation, the DNA cannot be repaired accurately, resulting in cell death. Since PARP is in excess of what is needed for the repair of endogenous damage to effectively target these HRD tumours PARP must be completely and continuously inhibited, allowing cells to go through S-phase inhibited (Javle and Curtin, 2011, Michelena *et al.,* 2018). On the other hand, all the preclinical data show that for chemo- and radiosensitisation PARP only needs to be inhibited sufficiently to render the genotoxic damage unrepairable and for a limited period. Therefore the durability of PARP inhibition may have scheduling implications.

As part of the first clinical trial patients received rucaparib for 5 days during which inhibition of PARP activity was measured in patient PBMCs during treatment (Plummer et al 2008). In some cases, it was also measured 3 days later, when it was still found to be suppressed (C Jones MD thesis 2005 Newcastle University). Following this observation, pre-clinical data showed that a single pulse of rucaparib caused persistent PARP inhibition in cell lines for several days and tumour xenografts for at least 7 days after a single dose (Murray *et al.,* 2014). This study also showed a single weekly administration of rucaparib was as effective as 5 daily doses a week in supressing the growth of *BRCA* mutant tumour xenografts. These data clearly show the persistent inhibition of PARP by rucaparib, however, as yet no study has compared rucaparib to other PARP inhibitors to determine if this is a unique characteristic or class effect. Rucaparib, olaparib, niraparib and talazoparib are currently FDA approved for the use in cancer patients as monotherapy, using daily dosing schedules (Jiang *et al.,* 2019). Rucaparib, olaparib and niraparib are approved for use in ovarian cancers with *BRCA1/2* mutations, following at least 2 rounds of chemotherapy with rucaparib and at least 3

rounds with olaparib and niraparib. They are also used as maintenance therapy in ovarian cancer, in patients with recurrent cancer with complete or partial response to platinum-based chemotherapy, regardless of *BRCA* mutation. Rucaparib is also FDA approved for use in prostate cancer, on an accelerated basis. Olaparib and talazoparib are FDA approved for use in germline *BRCA1/2* mutation and HER2 negative breast cancer. Olaparib is also FDA approved for first-line maintenance therapy in pancreatic cancer with germline *BRCA1/2* mutations and HRR defective metastatic castration-resistant prostate cancer. Pamiparib was selected as it is in late-phase clinical trials and is structurally similar to rucaparib (Chapter 1, table 1.2).

Comparing the durability of these PARPis could have important clinical implications when considering the clinical uses of PARPi. For monotherapy in use with HRD cancers, a durable PARPi would be desirable for maximum single agent activity. However, a less durable PARPi may be beneficial and less toxic in combination with cytotoxic agents such as radiotherapy, topotecan and temozolomide.

8.2 Aims and Objectives

- To assess durability of PARP inhibition by the different inhibitors using a GCLP-validated PARP activity assay to determine if persistent inhibition is unique to rucaparib or a class effect

- To assess if differences in durability of PARP inhibition result in differential synergy with ATRi VE-821 when sequential, rather than co-incubations are used

8.3 Hypotheses

1. PARPi by rucaparib in IGROV-1 cells will be durable and persistent, based on data in other cell lines.

2. If PARPi is durable, then sequential PARPi followed by VE-821 exposure will be as synergistic as co-exposure.

8.4 Materials and Methods

8.4.1 PARP activity assay

To measure optimum PARP activity, a 12 mer palindromic oligonucleotide was used to activate the enzyme in permeabilised cells in the presence of 350 nM NAD+ as described previously (Chapter 2, section 11). IGROV-1 cells were used as a representative ovarian cancer cell line, due to the previous approvals of rucaparib, olaparib and niraparib in this cancer type. Cells were exposed to 1 µM rucaparib, olaparib, niraparib, pamiparib or talazoparib for 1 h before drug was washed off and replaced with fresh media prior to cells being harvested immediately or after 1, 24, 48 or 72 h. Cells were permeabilised and PARP activity measured in comparison to untreated cells and cells with 1 uM drug added directly to the reaction mixture.

8.4.2 PARP-ATRi scheduling cytotoxicity experiments

The cytotoxicity of single agent VE-821 was compared with exposure to VE-821 and 1 µM of either rucaparib, olaparib or niraparib. Co-exposed cells were treated with VE-821 (1, 3 or 10 µM) and PARPi for 24 h, before drug was removed and replaced with fresh media. Sequentially exposed cells were treated with PARPi for 24 h before drug was washed off and replaced with media containing VE-821 for another 24 h. Following this time the medium was replaced with drug free medium to allow colony formation. Delayed sequentially exposed cells were similarly treated with PARPi for 24 h but media was replaced with fresh media for a further 24 h. Following this time media containing VE-821 was added for a further 24 h, before being replaced by fresh media. Colonies were fixed and counted as previously described.

8.5 Results

8.5.1 Durability of PARPi by rucaparib, olaparib, niraparib, pamiparib and talazoparib

To assess whether persistent PARP inhibition by rucaparib was unique or is a class effect, PARP inhibition by rucaparib, olaparib, niraparib, pamiparib and talazoparib was measured in IGROV-1 cells.

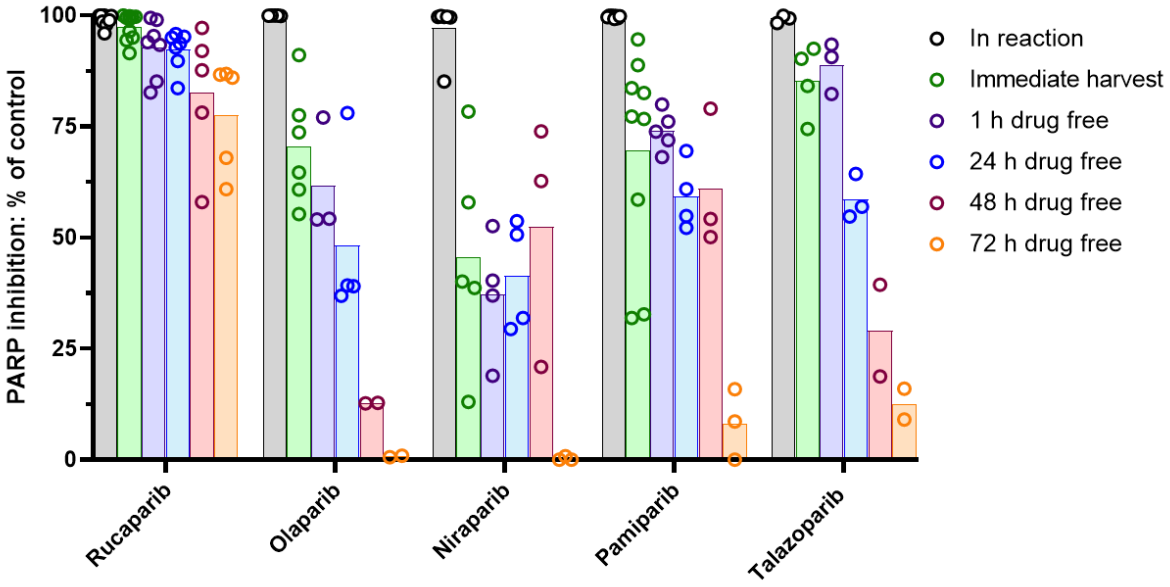


Figure 8.1: Durability of PARP activity inhibition by PARP inhibitors in IGROV-1 cells. PARP activity was measured in cells treated for 1 h with PARPi and harvested immediately and following 1, 24, 48 or 72 h in fresh media. Activity in pre-treated cells were compared to untreated cells and those with PARPi added directly to permeabilised cells in the reaction mix. Each data point on the graph represents an individual experiment and bars represent the mean of these experiments.

Rucaparib, olaparib, niraparib, pamiparib and talazoparib each inhibited PARP activity in excess of 99% in permeabilised cells, where PARPi (1 µM) was added directly into the reaction mix. However, only rucaparib maintained this level of PARP inhibition in the cells harvested immediately after 1 h exposure to PARPi, with the other PARP inhibitors having reduced levels of PARP inhibition in the range of 47% (niraparib) to 85% (talazoparib). This could be due to failure to achieve sufficient intracellular concentration or wash-out during the harvesting process. Similarly, PARP inhibition by rucaparib was maintained after 24 h in drug-free medium (92.3 ± 4.3%), but was much less with talazoparib (58.6 ± 5.0%), pamiparib (56.0 ± 4.5%) olaparib (48.3 ± 19.8%) and niraparib (37.3 ± 11.6%). This effect was also observed at the 48 h time-point with rucaparib maintaining PARP inhibition (82.6 ± 15.4%), which was markedly lower in cells treated with pamiparib (52.2 ± 2.9%), niraparib (41.8 ± 29.6%), talazoparib (29.1 ± 14.6 %) and olaparib (12.8 ± 0.08 %). Notably, after 72 h in drug-free medium, rucaparib-treated cells retained 75% PARP inhibition whereas there was only 12 % inhibition for

pamiparib and talazoparib, and undetectable inhibition after exposure to olaparib and niraparib.

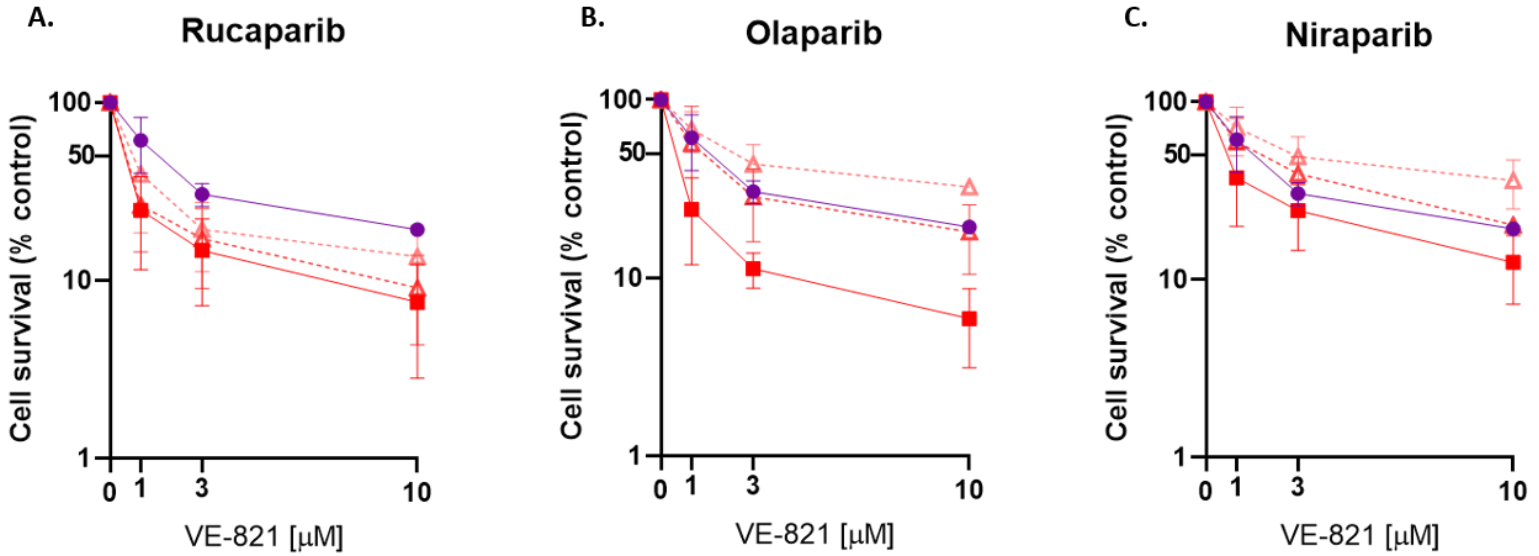
These data show rucaparib is unique in its ability to cause persistent PARP inhibition and that this is not a class effect. This durable inhibition of PARP could be pivotal in the effectiveness of rucaparib in HRD cells, as cells must traverse S-phase while PARP is inhibited for cytotoxic effects. This persistent inhibition is also an important consideration for scheduling when combining rucaparib with ATR, CHK1 and WEE1 inhibitors.

8.5.2 Investigating schedules of PARPi and ATRi

Rucaparib, olaparib and niraparib were selected, to investigate whether the observed differences in durability would affect the cytotoxicity in combination with VE-821 on different schedules. As rucaparib was found to be profoundly more durable it would be expected that when rucaparib was removed from cells, PARP inhibition would persist and therefore synergy with ATRi could still occur, without the need for co-exposure. Rucaparib, olaparib and niraparib each sensitised IGROV-1 cells to VE-821 when cells were co-exposed to 0- 10 µM VE-821 and 1 µM PARPi (Figure 7.2). Rucaparib and olaparib had similar PF_{50} values (2.7 vs. 2.8, respectively) and potentiation at 10 µM VE-821 (4.1 vs. 3.8, respectively), whereas niraparib had less impact sensitising cells (PF_{50}: 1.8 and PF at 10 µM: 1.7).

With sequential exposure, where PARPi was added for 24 h as single agent prior to replacement of media with VE-821 as a single agent, rucaparib caused similar sensitisation to co-exposed cells, indicating PARP inhibition was sustained for the 24 h VE-821 exposure (PF_{50}:. 2.6, PF at 10 µM: 2.7). This was not observed with olaparib (PF_{50}: 1.5, PF at 10 µM: 1.2) and niraparib (no sensitisation). Sequential exposure with olaparib and niraparib had modest potentiation, with the cell survival closely resembling that of cells treated with VE-821 alone, indicating that PARPi had not persisted in these cells. Delayed sequential exposure included a 24 h period between PARPi removal and VE-821 addition. Rucaparib sensitised cells less with this schedule than co-exposure and sequential exposure- although there was still potentiation at the LC_{50} and 10 µM VE-821

(2.2 and 1.8-fold, respectively), indicating some PARPi is sustained after 48 h. No potentiation was observed with olaparib or niraparib, reflective of the durability data (Figure 7.1).



D.

	Rucaparib		Olaparib		Niraparib	
	PF_{50} (mean ± S.D)	PF at 10 μM (mean ± S.D)	PF_{50} (mean ± S.D)	PF at 10 μM (mean ± S.D)	PF_{50} (mean ± S.D)	PF at 10 μM (mean ± S.D)
Co-exposure	2.7 ± 1.0	4.1 ± 3.8 *	2.8 ± 1.5	3.8 ± 1.6 **	1.8 ± 0.4	1.7 ± 0.7
Sequential exposure	2.6 ± 1.2	2.7 ± 1.7 *	1.5 ± 1.0	1.2 ± 0.42	1.0 ± 0.8	0.9 ± 0.03
Delayed sequential exposure	2.2 ± 1.4	1.8 ± 1.1	0.6 ± 0.4	0.6 ± 0.02	0.7 ± 0.6	0.6 ± 0.1

Figure 8.2: Scheduling PARPi-ATRi cytotoxicity experiments. Cells were exposed to VE-821 at indicated concentrations either as single agent or with the addition of **A.** rucaparib, **B.** olaparib or **C.** niraparib, either as co-exposure, sequential exposure or 24 h delayed sequential exposure, as previously described. Prior to replacement with drug-free medium cells were incubated for 10-14 days to allow colony formation. Data are representative of the mean and standard error of 3 independent experiments. **D.** Comparison of PARPi durability based on PF_{50} and potentiation at 10 μM VE-821. Paired t-tests, calculated using Graphpad Prism 9.0, determined any significance difference between LC_{50} and survival at 10 μM of single agent VE-821 compared to the addition of 1 μM PARPi. * $p < 0.05$, ** $p < 0.01$.

8.6 Discussion

Following previous studies highlighting the durability of rucaparib, here rucaparib durability was compared to other FDA approved PARPi and pamiparib, which is currently in clinical trials (NCT03991494, NCT04614909, NCT04985721, NCT04796454, NCT03333915, NCT03427814). It was clear from the PARP activity data that rucaparib was unique in its ability to cause very persistent PARP inhibition and thus the observed durability is not a class effect. There was a progressive loss of PARP inhibition with olaparib, niraparib, pamiparib and talazoparib. Between 24 and 72 h post drug removal durability from most to least was ranked as: rucaparib, talazoparib, pamiparib, olaparib and niraparib. Notably pamiparib did not have similar levels of durability observed in rucaparib, despite structural similarities.

The unique PARP inhibition durability with rucaparib, compared to other approved PARPis, suggests that the current twice daily dosing approved schedule may not be necessary, an intermittent dosing schedule might be equally effective and both more tolerable and affordable.

Scheduling cytotoxicity experiments showed that PARP inhibition was sustained up to 24 h in drug free medium when rucaparib was added sequentially to VE-821, where survival at 10 μM was significantly lower than VE-821 single agent ($p= 0.04$). PARPi by rucaparib persisted between 24 and 48 h with delayed addition of rucaparib to VE-821 (PF_{50}: 2.2, PF at 10 μM: 1.8), although was not significant. PARPi did not persist with olaparib or niraparib for up to 24 h with sequential exposure (PF at 10 μM: 1.2 and 0.9, respectively) or up to 48 h with delayed exposure (PF at 10 μM: 0.6 for both).

These data are preliminary and so further studies would be required before distinct conclusions could be made. Further studies are needed to determine whether sequential dosing would have equivalent anti-cancer activity *in vivo* and to examine the implications for toxicity prior to exploring different schedules clinically.

Chapter 9. Final discussion

9.1 Final Discussion

PARP1 is essential to repair the high volumes of endogenous damage that cells undergo continually and PARPi act by inhibiting SSBs, which collide with replication forks and collapse resulting in DSBs, which can only be repaired by HRR during S and early G2 phase. The relationship between PARPis and HRD tumours has been well established over the last decade and subsequently 4 PARPi, including rucaparib have been approved by the FDA and EMA for use in cancer patients as monotherapy, using daily dosing schedules (Jiang *et al.,* 2019) (Patent WO/2005/012305). Rucaparib is currently used to treat ovarian cancers with *BRCA1/BRCA2* mutations following 2 rounds of chemotherapy and as maintenance therapy in recurrent ovarian cancer, with complete or partial response to platinum-based chemotherapy, regardless of *BRCA* mutation. Despite the success of PARPi in the clinic, resistance is a major difficulty and is often caused by the restoration of HRR, as well as replication fork protection (Li *et al.,* 2020). Moreover, many tumours do not have an HRD phenotype so are intrinsically resistant to PARPi. Recent studies are investigating ways to overcome this resistance and address this unmet clinical need.

PARPi-resistant cells have been shown to have increased ATR-CHK1 activity and greater sensitivity to a combination of PARPi and ATRi (Ray-Coquard *et al.,* 2020, Kim *et al.,* 2020, McMullen *et al.,* 2020). ATR, CHK1 and WEE1 have key roles in both cell cycle control (Sorensen and Syljuasen, 2012, Lewis *et al.,* 2017, Lin *et al.,* 2017, Thada and Cortez, 2019), and signalling to HRR in response to RS (Yazinski *et al.,* 2017, Sorensen *et al.,* 2018, Buisson *et al.,* 2017, Foo *et al.,* 2021). There is plentiful evidence both *in vitro* and *in vivo* to suggest synergy between these kinases and PARPi, which has led to their advances into ongoing clinical trials (Mohni *et al.,* 2015, Kim *et al.,* 2017, Booth *et al.,* 2013, Yin *et al.,* 2017, Brill *et al.,* 2017, Karnak *et al.,* 2014, Parsels *et al.,* 2018, Gorecki *et al.,* 2021). However, most studies of PARPi –ATR/CHK1/WEE1 inhibitors have focussed on cell cycle checkpoint inhibition and not considered this synergy to be driven by HRR inhibition. However, Peasland *et al.* was the first study that considered inhibition of HRR as a mechanism underpinning synergy between rucaparib and a prototype ATRi NU6027.

They showed that XRCC1 defective EM9 cells were significantly more sensitive to NU6027 as a single agent compared to parental XRCC1 competent AA8 cells and found ATRi significantly inhibited rucaparib-induced RAD51 foci, suggesting this was a proposed mechanism of synergy. A major aim of this work was to compare synergy of rucaparib and ATR/CHK1/WEE1 inhibitors in HRC and HRD cells matched, and assess how HRR function was impacted. An additional aim was to determine whether ATR, CHK1 or WEE1 inhibition had the most powerful synergy with rucaparib.

A strength of this study was the use of isogenic matched cells, defective in *BRCA1* or BRCA2, to probe the effect of HRR function on the synergy under investigation. As these cells only differ by a single gene mutation, other molecular complexities within the cells can be eliminated as the cause of any observed differences between matched cells. The other cells used in this study were a small and heterogeneous cell line panel, making correlation analyses challenging with the varied molecular phenotypes. Nevertheless, this is reflective of the clinical reality of heterogeneity within tumours as well as between them. However, despite the differing characteristics of these cells, findings were consistent in all the (HRC) cells e.g. the induction of ATR, CHK1 and WEE1 by rucaparib, feedback inhibition by the kinase inhibitors, potentiation of rucaparib by the kinase inhibitors and impact on HRR. The fact that the panel was heterogeneous, but the effects were consistent, gives confidence that the observed effects are real.

In the study conducted here, the *BRCA* mutated cells were, as predicted, more sensitive to rucaparib. Further determinants of sensitivity, besides HRR status, that had been reported in the literature were also assessed. Basal RS (evaluated by γH2AX and pRPA foci) was only found to strongly correlate with rucaparib single agent cytotoxicity (r^2= 0.7- 0.96), when HRD cells that have high levels of RS or DNA damage and are profoundly sensitivity to rucaparib, were included. When just the HRC cells were analysed they had a weaker correlation between basal RS levels and sensitivity to rucaparib (r^2= 0.3- 0.8). As shown previously, RS signals to ATR, which activates CHK1 and in turn causes the inactivating phosphorylation of CDC25C, which prevents the removal of inhibitory phosphorylation of CDK1. WEE1 is also activated in response to this RS and phosphorylates and inactivates CDK1. Rucaparib (10 μM) increased ATR

(measured by pCHK1^{Ser345}) and CHK1 activity (measured by pCHK1^{Ser296}) across all cells, as well as increasing pCDK1^{Tyr15}. Interestingly, downstream effects were observed when ATR was inhibited by VE-821, as this also inhibited CHK1 activity and pCDK1^{Tyr15}. Upstream feedback was also detected, as inhibition of CHK1 activity by PF-477736 increased ATR activity up to 30-fold, as well as inhibiting CHK1 and pCDK1^{Tyr15} downstream, suggesting signalling occurs between CHK1 and WEE1, although as yet in the literature this has only been proven in xenopus studies (Lee *et al.,* 2001). Similarly, WEE1 inhibited pCDK1^{Tyr15} but activated CHK1 and ATR activity upstream (9 and 20-fold, respectively).

A moderate correlation suggested basal RS was a predictor of sensitivity to single agent ATRi VE-821 (r^2= 0.5). However, a weaker trend was observed with CHK1i PF-477736 (r^2= 0.2) and no correlation with WEE1i MK-1775. This could suggest measuring basal RS by IF would be a good predictor of patients with increased sensitivity to PARPi, ATRi or CHK1i monotherapy.

Previous studies have also shown that increased basal RS conferred sensitivity to the checkpoint kinase inhibitors. High RS gene expression signatures, calculated by a weighted sum of standardized transcript expression for key DDR genes, significantly correlated with ATRi AZD6738 and WEE1i MK1775 cytotoxicity in patient-derived pancreatic cancer cells, where it was suggested a high RS signature was a more reliable predictor of ATRi and WEE1i sensitivity than HRR status (Dreyer *et al.,* 2020). Similarly, here, HRR status was a conflicting determinant of sensitivity between UWB1.289 and V-C8 cells (Chapter 5). A high RS signature also correlated significantly with sensitivity to ATRi M4344 treatment (Jo *et al.,* 2020). Sensitivity to CHK1i correlated with another measurement of basal RS, by pRPA $^{Ser4/8}$, (Oo *et al.,* 2018), which was used here. As additional measures of RS, pRPA and cyclin E expression were measured by Western blot across the cell line panel (Chapter 3). Similarly, the results with IF assessment, pRPA expression correlated with sensitivity to the kinase inhibitors, which was strongest with VE-821 and PF-477736 and weaker with MK-1775. Although with these correlations consisting of such few data points, the true correlations may be masked and this would need to be assessed across a larger panel of cell lines, with more diverse molecular

characteristics, as opposed to the data grouping into 2 subsets here of: i) repair-defective with high pRPA$^{Ser4/8}$ foci levels/expression and increased sensitivity, and ii) repair-competent with low pRPA$^{Ser4/8}$ foci levels/expression and less sensitivity.

Previous studies have shown evidence for HRR status to be a marker of sensitivity to ATRi, CHK1i or WEE1i (Williamson *et al.,* 2016, Middleton *et al.,* 2015, Kim *et al.,* 2017, Do *et al.,* 2015). Here, *BRCA1* defective UWB1.289 cells were significantly more sensitive to VE-821 and PF-477736 (p=0.02 and 0.01, respectively), than their *BRCA1* competent matched cells although this was only significant with MK-1775 at a higher concentration of 0.4 μM (p=0.05). Contrastingly, *BRCA2* mutant V-C8 cells were no more sensitive to any of the kinase inhibitors compared to *BRCA2* competent V-C8.B2 cells. As these isogenic matched cells differed only in a single gene mutation, these data could possibly suggest *BRCA1* may be a more favourable determinant of ATR and CHK1 inhibitor sensitivity than *BRCA2* in this instance, potentially due to *BRCA1* role in cell cycle control. However further investigations in several *BRCA1* and *BRCA2* mutant cells would be required to confirm this. Defects in other key HRR proteins have been shown to confer sensitivity to ATR, CHK1 and WEE1 inhibitors (Krajewska *et al.,* 2015, Middleton *et al.,* 2015, Massey *et al.,* 2016). However, there was no significant trend with HRR protein expression and the inhibitors overall and conflicting trends were observed between them so much more work in many more cell lines is needed to truly define the role of HRR in sensitivity to ATR, CHK1 and WEE1 inhibitors.

In line with previous reported synergy, cells were sensitised to PARPi rucaparib by ATR, CHK1 and WEE1 inhibition. However, here a unique finding was that the sensitisation was exclusive to HRC cells. This led to the hypothesis that ATR, CHK1 and WEE1 involvement in HRR played a greater role as a mechanism underpinning the synergy than has been previously considered. The impact of VE-821, PF-477736 and MK-1775 on HRR function was assessed using RAD51 foci formation and indeed rucaparib-induced HRR activity, was inhibited by VE-821 (89 to >100 %), PF-477736 (64 to >100 %) and MK-1775 (78 to 97 %) in all the HRC cells, as well as further increasing γH2AX foci formation. The exclusivity of HRC cells potentiation combined with the HRR functional data, implied the addition of ATR, CHK1 or WEE1 inhibition was inducing an HRD phenotype in cells,

thereby sensitising HRC cells to rucaparib. Due to the observation that the kinase inhibitors appear to be inducing an HRD phenotype further studies would be required regarding toxicity, to determine whether the inhibitors are effecting non-cancer cells in this way, making PARPi synthetically lethal with these cells too. *In vivo* studies would be required to assess the efficacy vs toxicity of these combinations.

Although inhibition of HRR was considered a mechanism underpinning this synergy, the impact of cell cycle effects on the synergy could not be excluded and analysis was performed. As previously reported PARPi by rucaparib caused S and G2-M arrest and the addition of each of the inhibitors abrogated S and G2-M arrest (Fang *et al.,* 2019, Kim *et al.,* 2020). This abrogation was most evident with VE-821, followed by PF-477736 and then MK-1775, suggesting that both loss of cell cycle checkpoint control and inhibition of HRR are contributors to the synergy between rucaparib and VE-821, PF-477736 and MK-1775. This was only in IGROV-1 cells in this study and so it is unknown if this trend comparing the inhibitors is exclusive to these cells and further studies would be required, particularly in matched HRC and HRD cells. The effect of rucaparib and PF-477736 was measured in V-C8.B2 cells and similarly rucaparib increased S and G2-M arrest, with the addition of PF-477736 (50 nM) reducing S-phase (by 64.5 %) and G2-M (by 33.6 %) (Smith *et al.,* 2020).

A sample of patient cultures (4 HRC and 3 HRD) were used to determine whether, the synergy of rucaparib with VE-821, PF-477736 and MK-1775 observed in cell lines and underlying mechanisms translated to patient cells. Overall, the magnitude of the synergy was lower than in immortalised cells, possibly due to the slower growth rate of the primary cultures and a high proportion of these cells being in senescence. However, there was still greater sensitisation in the HRC than in HRD cells. VE-821, PF-477736 and MK-1775 also blocked rucaparib-induced RAD51 focus formation suggesting that synergy was due to inhibition of HRR, although the sample size needs to be expanded to verify these observations, these data are consistent with those obtained in cell cultures, which suggests that the effect is real. Taking both the cell culture and ascites culture data together it seems likely that PARPi monotherapy would be sufficiently effective in HRD tumours, whereas the addition of ATR/ CHK1/ WEE1 inhibitor would be beneficial

to HRC tumours by inducing an HRD phenotype. Real-time assessment of the HRR function is needed for appropriate patient selection for mono- vs combination therapy and the RAD51 focus assay is a good candidate for a predictive biomarker as it is not merely a measure of a history of HRR as measured by genomic scarring.

PARPi are considered to be synthetically lethal in HRD cells by 2 mechanisms, inhibition of SSBR and PARP trapping but it is not known which of these mechanisms is key to the synergy with ATR, CHK1 and WEE1 inhibitors. Defects in the key SSBR protein, XRCC1, has been shown to confer sensitivity to ATR, CHK1 and WEE1 inhibition, (Peasland *et al.,* 2011, Sultana *et al.,* 2013, Middleton *et al.,* 2015, Ali *et al.,* 2020). Low XRCC1 expression, measured by Western blotting, poorly correlated with increased sensitivity to ATR, CHK1 and WEE1 inhibition (r^2= 0.1, 0.1 and 0.2, respectively). In the limited panel of cells used here there was no significant correlation between XRCC1 levels and VE-821, PF-477736 and MK-1775 cytotoxicity. Therefore, to further probe mechanisms underpinning the sensitisation of cells to rucaparib and to establish the influence of SSBR inhibition vs. PARP trapping matched XRCC1 defective and competent EM9 and AA8 cells were used (Chapter 6). EM9 cells were significantly more sensitive than AA8 cells to each of the kinase inhibitors. Rucaparib sensitised both AA8 and EM9 cells to all three kinase inhibitors, to similar degrees. An interesting observation was that the sensitivity of EM9 to single agent VE-821, PF-477736 and MK-1775 compared to AA8 cells than the sensitisation occurring in AA8 cells when rucaparib was added, indicating SSBR inhibition had a role in the synergy. However, given that EM9 cells were further sensitised by rucaparib it is suggested PARP trapping is also a contributing factor. A specific PARP trapping assay would be necessary before making any assumptions based on these data, to better quantify the effect of trapping on the synergy (Murai *et al.,* 2012). These experiments could be expanded to using PARP null cells, to assess the relative contribution of PARP loss, loss of SSBR function or trapping has on the observed synergy.

For PARP inhibitors to successfully inhibit PARP via synthetic lethality in HRD cells, PARP must be completely and continually inhibited, allowing cells to go through S-phase whilst inhibited (Michelena *et al.,* 2018). For chemo- and radio-sensitisation sufficient

PARP inhibition is required for as long as is needed to block repair of the induced damage, sufficient to exert effects on cell kill (Nguewa *et al.,* 2006, Patel *et al.,* 2012, Murai *et al.,* 2014, Ihnen *et al.,* 2013). Clinical observations and pre-clinical studies showed rucaparib-induced inhibition was durable (Plummer *et al.,* 2008, Murray *et al.,* 2014). Here, the durability of PARPis were compared to investigate whether this durability was unique to rucaparib or a class effect. Rucaparib was found to have a unique ability to persistently inhibit PARP activity and after 72 h PARP inhibition persisted at 75 %, whilst this dropped to 12 % with pamiparib and talazoparib and no PARP inhibition persisted at this time point with olaparib or niraparib. This has potential implications in clinical dosing, particularly regarding the approved twice daily dosing regimens, as this may not be necessary. It is possible that an intermittent schedule of rucaparib would be equally effective, less toxic and more affordable. Rucaparib, olaparib and niraparib were further compared using different dosing schedules of PARPi and VE-821, to explore whether the durability of rucaparib translated into synergy with ATR inhibition. With rucaparib similar synergy was observed with sequential exposure to rucaparib then VE-821 as with co-exposure and even a 24 h drug-free period between rucaparib and VE-821 exposure resulted in some synergy. This was not the case with olaparib and niraparib, which were only synergistic with co-exposure to VE-821.

Many ongoing clinical trials with PARPi and ATRi are administering PARPi twice daily and ATRi daily, which may be unnecessary when using a PARPi as durable as rucaparib (NCT03462342, NCT03462342, NCT04267939, NCT04065269, and NCT03787680). The *in vivo* studies with rucaparib indicated that after a single dose rucaparib was retained in the tumour and inhibited PARP activity longer than in the blood or normal tissue (Murray *et al* 2014). The potential toxicities of the combination of rucaparib and ATR/CHK1/WEE1 inhibitors described above) might be minimised with sequential dosing. Further studies in vivo are needed to investigate if rucaparib followed by ATR/CHK1/WEE1 inhibitor administration, with variable intervals between drug administrations, increases the therapeutic index (greater antitumour efficacy than toxicity). Such experiments could justify investigations of different schedules in clinical trials.

Overall, although synergy between PARPi and ATR, CHK1 or WEE1 inhibitors has been observed in previous studies, to the point of now being tested as clinical candidates in combination, most have not considered HRR inhibition as the underlying mechanism. The data presented in this thesis, particularly in isogenic matched cells, provides compelling evidence that, as well as loss of checkpoint control, impairment of HRR is a major mechanism underpinning the synergy of PARPi with ATR, CHK1 or WEE1 inhibition and this could provide direction on future research into how to expand the use of PARPi to beyond *BRCA* mutated cells.

9.2 Future directions

The following further experiments could be performed to strengthen the work presented in this thesis:

- Use of a wider panel of cell lines with diverse molecular characteristics to further extend correlation analyses between reported determinants of sensitivity and observed sensitivity to the inhibitors.
- An alternative method of investigating RS by DNA fiber assay was not able to be explored due to time limitations of the study, although this would have been a valuable tool for conducting pulse-chase experiments to assess the induction of RS at variable time points, as opposed to the immunofluorescence here, which resembles a snapshot of RS within cells at the time of fixation.
- Cell cycle analysis on matched HRC and HRD cells- to determine any differences in abrogation of cell cycle checkpoint control by the kinase inhibitors in these cells.
- The use of a PARP-trapping assay to better establish the weighting SSBR and PARP trapping have on the mechanism of synergy.
- Expansion of the number of patient samples tested, to strengthen the reliability of the trends observed in the small subset used.
- *In vivo* studies to explore the efficacy vs toxicity of the combinations against HRC and HRD tumours, and if sequential administration of rucaparib followed by ATR/CHK1/WEE1 inhibitors would increase the therapeutic index

Bibliography

Abida, W., Campbell, D., Patnaik, A., Dowson, M., Golsorkhi, T. and Chowdhury, S. (2019) 'Preliminary results from the TRITON2 study of rucaparib in patients (pts) with DNA damage repair (DDR)-deficient metastatic castration-resistant prostate cancer (mCRPC): Updated ', Annals of Oncology., 30(5).

Abida, W., Patnaik, A., Campbell, D., Shapiro, J., Bryce, A.H., McDermott, R., Sautois, B., Vogelzang, N.J., Bambury, R.M., Voog, E., Zhang, J., Piulats, J.M., Ryan, C.J., Merseburger, A.S., Daugaard, G., Heidenreich, A., Fizazi, K., Higano, C.S., Krieger, L.E., Sternberg, C.N., Watkins, S.P., Despain, D., Simmons, A.D., Loehr, A., Dowson, M., Golsorkhi, T., Chowdhury, S. and investigators, T. (2020) 'Rucaparib in Men With Metastatic Castration-Resistant Prostate Cancer Harboring a', J Clin Oncol, 38(32), pp. 3763-3772.

Aguilar-Quesada, R., Munoz-Gamez, J. A., Martin-olivia, D., Peralta, A., Valenzuela, M. T., Matinez-Romero, R., Quiles-Perez, R., Murcia, J. M., Murcia, G., Almodovar, M. R. and Oliver, F. J. (2007), 'Interaction between ATM and PARP-1 in response to DNA damage and sensitization of ATM deficient cells through PARP inhibition', BMC Molecular Biology, 8 (29).

Aguirre, D., Boya, P., Bellet, D., Faivre, S., Troalen, F., Benard, J., Saulnier, P., Hopkins-Donaldson, S., Zangemeister-Wittke, U., Kroemer, G. and Raymond, E. (2004) 'Bcl-2 and CCND1/CDK4 expression levels predict the cellular effects of mTOR inhibitors in human ovarian carcinoma', Apoptosis, 9(6), pp. 797-805

Ahlander, J. and Bosco, G. (2009) 'The RB/E2F pathway and regulation of RNA processing', Biochem Biophys Res Commun, 384(3), pp. 280-3.

Ali, R., Alblihy, A., Toss, M.S., Algethami, M., Al Sunni, R., Green, A.R., Rakha, E.A. and Madhusudan, S. (2020) 'XRCC1 deficient triple negative breast cancers are sensitive to ATR, ATM and Wee1 inhibitor either alone or in combination with olaparib', Ther Adv Med Oncol, 12, p. 1758835920974201.

Akbari, M., Morevati, M., Croteau, D. and Bohr, V.A. (2015) 'The role of DNA base excision repair in brain homeostasis and disease', DNA Repair (Amst), 32, pp. 172-179.

Akiyama-Abe, A., Minaguchi, T., Nakamura, Y., Michikami, H., Shikama, A., Nakao, S., Sakurai, M., Ochi, H., Onuki, M., Matsumoto, K., Satoh, T., Oki, A. and Yoshikawa, H. (2013) 'Loss of PTEN expression is an independent predictor of favourable survival in endometrial carcinomas', Br J Cancer, 109(6), pp. 1703-10.

Alemasova, E.E. and Lavrik, O.I. (2019) 'Poly(ADP-ribosyl)ation by PARP1: reaction mechanism and regulatory proteins', Nucleic Acids Res, 47(8), pp. 3811-3827.

Alexandrov, L.B., Nik-Zainal, S., Wedge, D.C., Aparicio, S.A., Behjati, S., Biankin, A.V., Bignell, G.R., Bolli, N., Borg, A., Børresen-Dale, A.L., Boyault, S., Burkhardt, B., Butler,

A.P., Caldas, C., Davies, H.R., Desmedt, C., Eils, R., Eyfjörd, J.E., Foekens, J.A., Greaves, M., Hosoda, F., Hutter, B., Ilicic, T., Imbeaud, S., Imielinski, M., Imielinsk, M., Jäger, N., Jones, D.T., Jones, D., Knappskog, S., Kool, M., Lakhani, S.R., López-Otín, C., Martin, S., Munshi, N.C., Nakamura, H., Northcott, P.A., Pajic, M., Papaemmanuil, E., Paradiso, A., Pearson, J.V., Puente, X.S., Raine, K., Ramakrishna, M., Richardson, A.L., Richter, J., Rosenstiel, P., Schlesner, M., Schumacher, T.N., Span, P.N., Teague, J.W., Totoki, Y., Tutt, A.N., Valdés-Mas, R., van Buuren, M.M., van 't Veer, L., Vincent-Salomon, A., Waddell, N., Yates, L.R., Zucman-Rossi, J., Futreal, P.A., McDermott, U., Lichter, P., Meyerson, M., Grimmond, S.M., Siebert, R., Campo, E., Shibata, T., Pfister, S.M., Campbell, P.J., Stratton, M.R., Initiative, A.P.C.G., Consortium, I.B.C., Consortium, I.M.-S. and PedBrain, I. (2013) 'Signatures of mutational processes in human cancer', Nature, 500(7463), pp. 415-21.

Alsubhi, N., Middleton, F., Abdel-Fatah, T.M., Stephens, P., Doherty, R., Arora, A., Moseley, P.M., Chan, S.Y., Aleskandarany, M.A., Green, A.R., Rakha, E.A., Ellis, I.O., Martin, S.G., Curtin, N.J. and Madhusudan, S. (2016) 'Chk1 phosphorylated at serine345 is a predictor of early local recurrence and radio-resistance in breast cancer', Mol Oncol, 10(2), pp. 213-23.

Ames, B.N. (1989) 'Endogenous DNA damage as related to cancer and aging', Mutat Res, 214(1), pp. 41-6.

Ashley, A.K., Shrivastav, M., Nie, J., Amerin, C., Troksa, K., Glanzer, J.G., Liu, S., Opiyo, S.O., Dimitrova, D.D., Le, P., Sishc, B., Bailey, S.M., Oakley, G.G. and Nickoloff, J.A. (2014) 'DNA-PK phosphorylation of RPA32 Ser4/Ser8 regulates replication stress checkpoint activation, fork restart, homologous recombination and mitotic catastrophe', DNA Repair (Amst), 21, pp. 131-9.

Aziz, D., Portman, N., Fernandez, K.J., Lee, C., Alexandrou, S., Llop-Guevara, A., Phan, Z., Yong, A., Wilkinson, A., Sergio, C.M., Ferraro, D., Etemadmoghadam, D., Bowtell, D.D., Serra, V., Waring, P., Lim, E., Caldon, C.E. and Investigators, k. (2021) 'Synergistic targeting of BRCA1 mutated breast cancers with PARP and CDK2 inhibition', NPJ Breast Cancer, 7(1), p. 111.

Babaier, A. and Ghatage, P. (2020) 'Mucinous Cancer of the Ovary: Overview and Current Status', Diagnostics (Basel), 10(1).

Bajrami, I., Kigozi, A., Van Weverwijk, A., Brough, R., Frankum, J., Lord, C.J. and Ashworth, A. (2012) 'Synthetic lethality of PARP and NAMPT inhibition in triple-negative breast cancer cells', EMBO Mol Med, 4(10), pp. 1087-96.

Bajrami, I., Frankum, J.R., Konde, A., Miller, R.E., Rehman, F.L., Brough, R., Campbell, J., Sims, D., Rafiq, R., Hooper, S., Chen, L., Kozarewa, I., Assiotis, I., Fenwick, K., Natrajan, R., Lord, C.J. and Ashworth, A. (2014) 'Genome-wide profiling of genetic synthetic lethality identifies CDK12 as a novel determinant of PARP1/2 inhibitor sensitivity', Cancer Res, 74(1), pp. 287-97.

Balasubramaniam, S., Beaver, J.A., Horton, S., Fernandes, L.L., Tang, S., Horne, H.N., Liu, J., Liu, C., Schrieber, S.J., Yu, J., Song, P., Pierce, W., Robertson, K.J., Palmby, T.R., Chiu, H.J., Lee, E.Y., Philip, R., Schuck, R., Charlab, R., Banerjee, A., Chen, X.H., Wang, X., Goldberg, K.B., Sridhara, R., Kim, G. and Pazdur, R. (2017) 'FDA Approval Summary: Rucaparib for the Treatment of Patients with Deleterious', Clin Cancer Res, 23(23), pp. 7165-7170.

Banerjee, S. and Kaye, S.B. (2013) 'New strategies in the treatment of ovarian cancer: current clinical perspectives and future potential', Clin Cancer Res, 19(5), pp. 961-8.

Barnum, K.J. and O'Connell, M.J. (2014) 'Cell cycle regulation by checkpoints', Methods Mol Biol, 1170, pp. 29-40.

Bartek, J. and Lukas, J. (2003) 'Chk1 and Chk2 kinases in checkpoint control and cancer', Cancer Cell, 3(5), pp. 421-9.

Bebb, D.G.P., L. F. and · Moore, J.E., A. Lees-Miller, S. (2019) 'ATM loss in NSCLC increases sensitivity to cisplatin and PARP inhibition.', Annals of Oncology, 30.

Ben-David, U., Siranosian, B., Ha, G., Tang, H., Oren, Y., Hinohara, K., Strathdee, C. A., Dempster, J., Lyons, N. J., Burns, R., Nag, A., Kugener, G., Cimini, B., Tsvetkov, P., Maruvka, Y. E., O'Rourke, R., Garrity, A., Tubelli, A. A., Bandopadhayay, P., Tsherniak, A., … Golub, T. R. (2018) 'Genetic and transcriptional evolution alters cancer cell line drug response', Nature, 560(7718), pp. 325–330.

Benada, J. and Macurek, L. (2015) 'Targeting the Checkpoint to Kill Cancer Cells', Biomolecules, 5(3), pp. 1912-37.

Biegala, L., Gajek, A., Marczak, A. and Rogalska, A. (2021) 'PARP inhibitor resistance in ovarian cancer: Underlying mechanisms and therapeutic approaches targeting the ATR/CHK1 pathway', Biochin Biophys Acta Rev Cancer, 1876 (2), pp. 188633.

Brunner, A., Suryo Rahmanto, A., Johansson, H., Franco, M., Viiliäinen, J., Gazi, M., Frings, O., Fredlund, E., Spruck, C., Lehtiö, J., Rantala, J.K., Larsson, L.G. and Sangfelt, O. (2020) 'PTEN and DNA-PK determine sensitivity and recovery in response to WEE1 inhibition in human breast cancer', Elife, 9.

Blasina, A., Hallin, J., Chen, E., Arango, M.E., Kraynov, E., Register, J., Grant, S., Ninkovic, S., Chen, P., Nichols, T., O'Connor, P. and Anderes, K. (2008) 'Breaching the DNA damage checkpoint via PF-00477736, a novel small-molecule inhibitor of checkpoint kinase 1', Mol Cancer Ther, 7(8), pp. 2394-404.

Bonora, M., Patergnani, S., Rimessi, A., De Marchi, E., Suski, J.M., Bononi, A., Giorgi, C., Marchi, S., Missiroli, S., Poletti, F., Wieckowski, M.R. and Pinton, P. (2012) 'ATP synthesis and storage', Purinergic Signal, 8(3), pp. 343-57.

Booth, L., Cruickshanks, N., Ridder, T., Dai, Y., Grant, S. and Dent, P. (2013) 'PARP and CHK inhibitors interact to cause DNA damage and cell death in mammary carcinoma cells', Cancer Biol Ther, 14(5), pp. 458-65.

Brandsma, I. and Gent, D.C. (2012) 'Pathway choice in DNA double strand break repair: observations of a balancing act', Genome Integr, 3(1), p. 9.

Bridges, K.A., Hirai, H., Buser, C.A., Brooks, C., Liu, H., Buchholz, T.A., Molkentine, J.M., Mason, K.A. and Meyn, R.E. (2011) 'MK-1775, a novel Wee1 kinase inhibitor, radiosensitizes p53-defective human tumor cells', Clin Cancer Res, 17(17), pp. 5638-48.

Bridges, K.A., Chen, X., Liu, H., Rock, C., Buchholz, T.A., Shumway, S.D., Skinner, H.D. and Meyn, R.E. (2016) 'MK-8776, a novel chk1 kinase inhibitor, radiosensitizes p53-defective human tumor cells', Oncotarget, 7(44), pp. 71660-71672.

Brill, E., Yokoyama, T., Nair, J., Yu, M., Ahn, Y.R. and Lee, J.M. (2017) 'Prexasertib, a cell cycle checkpoint kinases 1 and 2 inhibitor, increases', Oncotarget, 8(67), pp. 111026-111040.

Broustas, C.G. and Lieberman, H.B. (2014) 'DNA damage response genes and the development of cancer metastasis', Radiat Res, 181(2), pp. 111-30.

Brown, J.S., O'Carrigan, B., Jackson, S.P. and Yap, T.A. (2017) 'Targeting DNA Repair in Cancer: Beyond PARP Inhibitors', Cancer Discov, 7(1), pp. 20-37.

Bryant, C., Rawlinson, R. and Massey, A.J. (2014) 'Chk1 inhibition as a novel therapeutic strategy for treating triple-negative breast and ovarian cancers', BMC Cancer, 14, p. 570.

Bryant, H.E., Schultz, N., Thomas, H.D., Parker, K.M., Flower, D., Lopez, E., Kyle, S., Meuth, M., Curtin, N.J. and Helleday, T. (2005) 'Specific killing of BRCA2-deficient tumours with inhibitors of poly(ADP-ribose) polymerase', Nature, 434(7035), pp. 913-7.

Buisson, R., Niraj, J., Rodrigue, A., Ho, C.K., Kreuzer, J., Foo, T.K., Hardy, E.J., Dellaire, G., Haas, W., Xia, B., Masson, J.Y. and Zou, L. (2017) 'Coupling of Homologous Recombination and the Checkpoint by ATR', Mol Cell, 65(2), pp. 336-346.

Bukhari, A.B., Lewis, C.W., Pearce, J.J., Luong, D., Chan, G.K. and Gamper, A.M. (2019) 'Inhibiting Wee1 and ATR kinases produces tumor-selective synthetic lethality and suppresses metastasis', J Clin Invest, 129(3), pp. 1329-1344.

Busch, C.J., Kriegs, M., Laban, S., Tribius, S., Knecht, R., Petersen, C., Dikomey, E. and Rieckmann, T. (2013) 'HPV-positive HNSCC cell lines but not primary human fibroblasts are radiosensitized by the inhibition of Chk1', Radiother Oncol, 108(3), pp. 495-9.

Campisi, J. (2005) 'Suppressing cancer: the importance of being senescent', Science, 309(5736), pp. 886-7.

Castroviejo-Bermejo, M., Cruz, C., Llop-Guevara, A., Gutiérrez-Enríquez, S., Ducy, M., Ibrahim, Y.H., Gris-Oliver, A., Pellegrino, B., Bruna, A., Guzmán, M., Rodríguez, O.,

Grueso, J., Bonache, S., Moles-Fernández, A., Villacampa, G., Viaplana, C., Gómez, P., Vidal, M., Peg, V., Serres-Créixams, X., Dellaire, G., Simard, J., Nuciforo, P., Rubio, I.T., Dienstmann, R., Barrett, J.C., Caldas, C., Baselga, J., Saura, C., Cortés, J., Déas, O., Jonkers, J., Masson, J.Y., Cairo, S., Judde, J.G., O'Connor, M.J., Díez, O., Balmaña, J. and Serra, V. (2018) 'A RAD51 assay feasible in routine tumor samples calls PARP inhibitor response beyond BRCA mutation', EMBO Mol Med, 10(12).

Chan, A.M., Enwere, E., McIntyre, J.B., Wilson, H., Nwaroh, C., Wiebe, N., Ou, Y., Liu, S., Wiedemeyer, K., Rambau, P.F., Grevers, X., Morris, D.G., Neri, P., Gilks, C.B., Visser, F., Le, N., Luo, L., Cook, L.S. and Köbel, M. (2020) 'Combined CCNE1 high-level amplification and overexpression is associated with unfavourable outcome in tubo-ovarian high-grade serous carcinoma', J Pathol Clin Res, 6(4), pp. 252-262.

Chang, H.H.Y., Pannunzio, N.R., Adachi, N. and Lieber, M.R. (2017) 'Non-homologous DNA end joining and alternative pathways to double-strand break repair', Nat Rev Mol Cell Biol, 18(8), pp. 495-506.

Chaung, W., Mi, L.J. and Boorstein, R.J. (1997) 'The p53 status of Chinese hamster V79 cells frequently used for studies on DNA damage and DNA repair', Nucleic Acids Res, 25(5), pp. 992-4.

Chen, L., Nievera, C.J., Lee, A.Y. and Wu, X. (2008) 'Cell cycle-dependent complex formation of BRCA1.CtIP.MRN is important for DNA double-strand break repair', J Biol Chem, 283(12), pp. 7713-20.

Choi, M., Kipps, T. and Kurzrock, R. (2016) 'ATM Mutations in Cancer: Therapeutic Implications', Mol Cancer Ther, 15(8), pp. 1781-91.

Chopra, N., Tovey, H., Pearson, A., Cutts, R., Toms, C., Proszek, P., Hubank, M., Dowsett, M., Dodson, A., Daley, F., Kriplani, D., Gevensleben, H., Davies, H.R., Degasperi, A., Roylance, R., Chan, S., Tutt, A., Skene, A., Evans, A., Bliss, J.M., Nik-Zainal, S. and Turner, N.C. (2020) 'Homologous recombination DNA repair deficiency and PARP inhibition activity in primary triple negative breast cancer', Nat Commun, 11(1), p. 2662.

Chow, J.P. and Poon, R.Y. (2013) 'The CDK1 inhibitory kinase MYT1 in DNA damage checkpoint recovery', Oncogene, 32(40), pp. 4778-88.

Cleary, J.M., Aguirre, A.J., Shapiro, G.I. and D'Andrea, A.D. (2020) 'Biomarker-Guided Development of DNA Repair Inhibitors', Mol Cell, 78(6), pp. 1070-1085.

Cole, A.J., Dwight, T., Gill, A.J., Dickson, K.A., Zhu, Y., Clarkson, A., Gard, G.B., Maidens, J., Valmadre, S., Clifton-Bligh, R. and Marsh, D.J. (2016) 'Assessing mutant p53 in primary high-grade serous ovarian cancer using immunohistochemistry and massively parallel sequencing', Sci Rep, 6, p. 26191.

Coleman, R.L., Oza, A.M., Lorusso, D., Aghajanian, C., Oaknin, A., Dean, A., Colombo, N., Weberpals, J.I., Clamp, A., Scambia, G., Leary, A., Holloway, R.W., Gancedo, M.A., Fong,

P.C., Goh, J.C., O'Malley, D.M., Armstrong, D.K., Garcia-Donas, J., Swisher, E.M., Floquet, A., Konecny, G.E., McNeish, I.A., Scott, C.L., Cameron, T., Maloney, L., Isaacson, J., Goble, S., Grace, C., Harding, T.C., Raponi, M., Sun, J., Lin, K.K., Giordano, H., Ledermann, J.A. and investigators, A. (2017) 'Rucaparib maintenance treatment for recurrent ovarian carcinoma after response to platinum therapy (ARIEL3): a randomised, double-blind, placebo-controlled, phase 3 trial', Lancet, 390(10106), pp. 1949-1961.

Cortese, D., Chegaev, K., Guglielmo, S., Wang, L. Z., Golding, B. T., Cano, C. and Fruttero, R. (2016) 'Synthesis and Biological Evaluation of N(2)-Substituted 2,4-Diamino-6-cyclohexylmethoxy-5-nitrosopyrimidines and Related 5-Cyano-NNO-azoxy Derivatives as Cyclin-Dependent Kinase 2 (CDK2) inhibitors', Chem Med Chem, 11 (16), pp. 1705-1708.

Craig, C., Kim, M., Ohri, E., Wersto, R., Katayose, D., Li, Z., Choi, Y.H., Mudahar, B., Srivastava, S., Seth, P. and Cowan, K. (1998) 'Effects of adenovirus-mediated p16INK4A expression on cell cycle arrest are determined by endogenous p16 and Rb status in human cancer cells', Oncogene, 16(2), pp. 265-72.

Crook, T., Wrede, D. and Vousden, K.H. (1991) 'p53 point mutation in HPV negative human cervical carcinoma cell lines', Oncogene, 6(5), pp. 873-5.

Cruz, C., Castroviejo-Bermejo, M., Gutiérrez-Enríquez, S., Llop-Guevara, A., Ibrahim, Y.H., Gris-Oliver, A., Bonache, S., Morancho, B., Bruna, A., Rueda, O.M., Lai, Z., Polanska, U.M., Jones, G.N., Kristel, P., de Bustos, L., Guzman, M., Rodríguez, O., Grueso, J., Montalban, G., Caratú, G., Mancuso, F., Fasani, R., Jiménez, J., Howat, W.J., Dougherty, B., Vivancos, A., Nuciforo, P., Serres-Créixams, X., Rubio, I.T., Oaknin, A., Cadogan, E., Barrett, J.C., Caldas, C., Baselga, J., Saura, C., Cortés, J., Arribas, J., Jonkers, J., Díez, O., O'Connor, M.J., Balmaña, J. and Serra, V. (2018) 'RAD51 foci as a functional biomarker of homologous recombination repair and PARP inhibitor resistance in germline BRCA-mutated breast cancer', Ann Oncol, 29(5), pp. 1203-1210.

Curtin, N.J. and Szabo, C. (2020) 'Poly(ADP-ribose) polymerase inhibition: past, present and future', Nat Rev Drug Discov, 19(10), pp. 711-736.

Dantzer, F., Schreiber, V., Niedergang, C., Trucco, C., Flatter, E., De La Rubia, G., Oliver, J., Rolli, V., MÈnissier-de Murcia, J. and de Murcia, G. (1999) 'Involvement of poly(ADP-ribose) polymerase in base excision repair', Biochimie, 81(1-2), pp. 69-75

Davis, A.J., Lee, K.J. and Chen, D.J. (2013) 'The N-terminal region of the DNA-dependent protein kinase catalytic subunit is required for its DNA double-stranded break-mediated activation', J Biol Chem, 288(10), pp. 7037-46.

de Bono, J., Mateo, J., Fizazi, K., Saad, F., Shore, N., Sandhu, S., Chi, K.N., Sartor, O., Agarwal, N., Olmos, D., Thiery-Vuillemin, A., Twardowski, P., Mehra, N., Goessl, C., Kang, J., Burgents, J., Wu, W., Kohlmann, A., Adelman, C.A. and Hussain, M. (2020) 'Olaparib for Metastatic Castration-Resistant Prostate Cancer', N Engl J Med, 382(22), pp. 2091-2102.

De Bono, J.S., Peng Tan, D.S., Caldwell, R., Terbuch, A., Goh, B.C., Heong, V., Haris, N.M., Bashir, S., Hong, D.S., Meric-Bernstam, F., Bordia, S., Liu, L., Wilkinson, G., Hreiki, J., Wengner, A., Fischer, K., Boix, O., Lagkadinou, E., Plummer, E. and Yap, T.A. (2019) 'First-in-human trial of the oral ataxia telangiectasia and Rad3-related (ATR) inhibitor BAY 1895344 in patients (pts) with advanced solid tumors.', Journal of Clinical Oncology., 37(15).

De Bont, R. and van Larebeke, N. (2004) 'Endogenous DNA damage in humans: a review of quantitative data', Mutagenesis, 19(3), pp. 169-85.

de Gooijer, M.C., van den Top, A., Bockaj, I., Beijnen, J.H., Würdinger, T. and van Tellingen, O. (2017) 'The G2 checkpoint-a node-based molecular switch', FEBS Open Bio, 7(4), pp. 439-455.

de Klein, A., Muijtjens, M., van Os, R., Verhoeven, Y., Smit, B., Carr, A.M., Lehmann, A.R. and Hoeijmakers, J.H. (2000) 'Targeted disruption of the cell-cycle checkpoint gene ATR leads to early embryonic lethality in mice', Curr Biol, 10(8), pp. 479-82.

DelloRusso, C., Welcsh, P.L., Wang, W., Garcia, R.L., King, M.C. and Swisher, E.M. (2007) 'Functional characterization of a novel BRCA1-null ovarian cancer cell line in response to ionizing radiation', Mol Cancer Res, 5(1), pp. 35-45.

Do, K., Wilsker, D., Ji, J., Zlott, J., Freshwater, T., Kinders, R.J., Collins, J., Chen, A.P., Doroshow, J.H. and Kummar, S. (2015) 'Phase I Study of Single-Agent AZD1775 (MK-1775), a Wee1 Kinase Inhibitor, in Patients With Refractory Solid Tumors', J Clin Oncol, 33(30), pp. 3409-15.

Domcke, S., Sinha, R., Levine, D.A., Sander, C. and Schultz, N. (2013) 'Evaluating cell lines as tumour models by comparison of genomic profiles', Nat Commun, 4, p. 2126.
Fasterius, E. and Al-Khalili Szigyarto, C. (2018) 'Analysis of public RNA-sequencing data reveals biological consequences of genetic heterogeneity in cell line populations', Sci Rep, 8(1), p. 11226.

Drabløs, F., Feyzi, E., Aas, P.A., Vaagbø, C.B., Kavli, B., Bratlie, M.S., Peña-Diaz, J., Otterlei, M., Slupphaug, G. and Krokan, H.E. (2004) 'Alkylation damage in DNA and RNA--repair mechanisms and medical significance', DNA Repair (Amst), 3(11), pp. 1389-407.

Drew, Y., Mulligan, E.A., Vong, W.T., Thomas, H.D., Kahn, S., Kyle, S., Mukhopadhyay, A., Los, G., Hostomsky, Z., Plummer, E.R., Edmondson, R.J. and Curtin, N.J. (2011) 'Therapeutic potential of poly(ADP-ribose) polymerase inhibitor AG014699 in human cancers with mutated or methylated BRCA1 or BRCA2', J Natl Cancer Inst, 103(4), pp. 334-46.

Dreyer, S.B., Upstill-Goddard, R., Paulus-Hock, V., Paris, C., Lampraki, E.M., Dray, E., Serrels, B., Caligiuri, G., Rebus, S., Plenker, D., Galluzzo, Z., Brunton, H., Cunningham, R., Tesson, M., Nourse, C., Bailey, U.M., Jones, M., Moran-Jones, K., Wright, D.W., Duthie, F., Oien, K., Evers, L., McKay, C.J., McGregor, G.A., Gulati, A., Brough, R., Bajrami, I.,

Pettitt, S., Dziubinski, M.L., Candido, J., Balkwill, F., Barry, S.T., Gr¸tzmann, R., Rahib, L., Johns, A., Pajic, M., Froeling, F.E.M., Beer, P., Musgrove, E.A., Petersen, G.M., Ashworth, A., Frame, M.C., Crawford, H.C., Simeone, D.M., Lord, C., Mukhopadhyay, D., Pilarsky, C., Tuveson, D.A., Cooke, S.L., Jamieson, N.B., Morton, J.P., Sansom, O.J., Bailey, P.J., Biankin, A.V., Chang, D.K., Glasgow Precision Oncology Laboratory and Initiative, A.P.C.G. (2021) 'Targeting DNA Damage Response and Replication Stress in Pancreatic Cancer', Gastroenterology, 160(1), pp. 362-377.e13.

Duffy, M.J., Synnott, N.C. and Crown, J. (2017) 'Mutant p53 as a target for cancer treatment', Eur J Cancer, 83, pp. 258-265.
Edwards, S. L., Brough, R., Lord, C. J., Natrajan, R., Vatcheva, R., Levine, D. A., Boyd, J., Reis-Filho, J. S. and Ashworth, A. (2008) 'Resistance to therapy caused by intragenic deletion in *BRCA2*' Nature, 451, pp. 1111-1115.

Ettl, J., Quek, R.G.W., Lee, K.H., Rugo, H.S., Hurvitz, S., Gonçalves, A., Fehrenbacher, L., Yerushalmi, R., Mina, L.A., Martin, M., Roché, H., Im, Y.H., Markova, D., Bhattacharyya, H., Hannah, A.L., Eiermann, W., Blum, J.L. and Litton, J.K. (2018) 'Quality of life with talazoparib versus physician's choice of chemotherapy in patients with advanced breast cancer and germline BRCA1/2 mutation: patient-reported outcomes from the EMBRACA phase III trial', Ann Oncol, 29(9), pp. 1939-1947.

Eustermann, S., Videler, H., Yang, J.C., Cole, P.T., Gruszka, D., Veprintsev, D. and Neuhaus, D. (2011) 'The DNA-binding domain of human PARP-1 interacts with DNA single-strand breaks as a monomer through its second zinc finger', J Mol Biol, 407(1), pp. 149-70.

Fang, D.D., Cao, J., Jani, J.P., Tsaparikos, K., Blasina, A., Kornmann, J., Lira, M.E., Wang, J., Jirout, Z., Bingham, J., Zhu, Z., Gu, Y., Los, G., Hostomsky, Z. and Vanarsdale, T. (2013) 'Combined gemcitabine and CHK1 inhibitor treatment induces apoptosis resistance in cancer stem cell-like cells enriched with tumor spheroids from a non-small cell lung cancer cell line', Front Med, 7(4), pp. 462-76.

Fang, Y., McGrail, D.J., Sun, C., Labrie, M., Chen, X., Zhang, D., Ju, Z., Vellano, C.P., Lu, Y., Li, Y., Jeong, K.J., Ding, Z., Liang, J., Wang, S.W., Dai, H., Lee, S., Sahni, N., Mercado-Uribe, I., Kim, T.B., Chen, K., Lin, S.Y., Peng, G., Westin, S.N., Liu, J., O'Connor, M.J., Yap, T.A. and Mills, G.B. (2019) 'Sequential Therapy with PARP and WEE1 Inhibitors Minimizes Toxicity while Maintaining Efficacy', Cancer Cell, 35(6), pp. 851-867.e7.

Faridi, R., Zahra, A., Khan, K. and Idrees, M. (2011) 'Oncogenic potential of Human Papillomavirus (HPV) and its relation with cervical cancer', Virol J, 8, p. 269.

Farmer, H., McCabe, N., Lord, C.J., Tutt, A.N., Johnson, D.A., Richardson, T.B., Santarosa, M.,
Dillon, K.J., Hickson, I., Knights, C., Martin, N.M., Jackson, S.P., Smith, G.C. and Ashworth, A. (2005) 'Targeting the DNA repair defect in BRCA mutant cells as a therapeutic strategy', Nature, 434(7035), pp. 917-21.

Fell, V.L. and Schild-Poulter, C. (2012) 'Ku regulates signaling to DNA damage response pathways through the Ku70 von Willebrand A domain', Mol Cell Biol, 32(1), pp. 76-87.

Feng, W., Simpson, D.A., Carvajal-Garcia, J., Price, B.A., Kumar, R.J., Mose, L.E., Wood, R.D., Rashid, N., Purvis, J.E., Parker, J.S., Ramsden, D.A. and Gupta, G.P. (2019) 'Genetic determinants of cellular addiction to DNA polymerase theta', Nat Commun, 10(1), p. 4286.

Ferlay, J., Colombet, M., Soerjomataram, I., Parkin, D.M., Piñeros, M., Znaor, A. and Bray, F. (2021) 'Cancer statistics for the year 2020: An overview', Int J Cancer.

Ferrao, P.T., Bukczynska, E.P., Johnstone, R.W. and McArthur, G.A. (2012) 'Efficacy of CHK inhibitors as single agents in MYC-driven lymphoma cells', Oncogene, 31(13), pp. 1661-72.

Fong, P.C., Yap, T.A., Boss, D.S., Carden, C.P., Mergui-Roelvink, M., Gourley, C., De Greve, J., Lubinski, J., Shanley, S., Messiou, C., A'Hern, R., Tutt, A., Ashworth, A., Stone, J., Carmichael, J., Schellens, J.H., de Bono, J.S. and Kaye, S.B. (2010) 'Poly(ADP)-ribose polymerase inhibition: frequent durable responses in BRCA carrier ovarian cancer correlating with platinum-free interval', J Clin Oncol, 28(15), pp. 2512-9.

Foo, T.K., Vincelli, G., Huselid, E., Her, J., Zheng, H., Simhadri, S., Wang, M., Huo, Y., Li, T., Yu, X., Li, H., Zhao, W., Bunting, S.F. and Xia, B. (2021) 'ATR/ATM-Mediated Phosphorylation of BRCA1 T1394 Promotes Homologous Recombinational Repair and G', Cancer Res, 81(18), pp. 4676-4684.

Friedlander, M., Matulonis, U., Gourley, C., du Bois, A., Vergote, I., Rustin, G., Scott, C., Meier, W., Shapira-Frommer, R., Safra, T., Matei, D., Shirinkin, V., Selle, F., Fielding, A., Lowe, E.S., McMurtry, E.L., Spencer, S., Rowe, P., Mann, H., Parry, D. and Ledermann, J. (2018) 'Long-term efficacy, tolerability and overall survival in patients with platinum-sensitive, recurrent high-grade serous ovarian cancer treated with maintenance olaparib capsules following response to chemotherapy', Br J Cancer, 119(9), pp. 1075-1085.

Fujisawa, H., Nakajima, N.I., Sunada, S., Lee, Y., Hirakawa, H., Yajima, H., Fujimori, A., Uesaka, M. and Okayasu, R. (2015) 'VE-821, an ATR inhibitor, causes radiosensitization in human tumor cells irradiated with high LET radiation', Radiat Oncol, 10, p. 175.

Gaillard, H., García-Muse, T. and Aguilera, A. (2015) 'Replication stress and cancer', Nat Rev Cancer, 15(5), pp. 276-89.

Gallagher, K.E., Kelly, H., Cocks, N., Dixon, S., Mounier-Jack, S., Howard, N. and Watson-Jones, D. (2018) 'Vaccine programme stakeholder perspectives on a hypothetical single-dose human papillomavirus (HPV) vaccine schedule in low and middle-income countries', Papillomavirus Res, 6, pp. 33-40.

Garbarino, J., Eckroate, J., Sundaram, R.K., Jensen, R.B. and Bindra, R.S. (2021) 'Loss of ATRX confers DNA repair defects and PARP inhibitor sensitivity', Transl Oncol, 14(9), p. 101147.
Gorski, J.W., Ueland, F.R. and Kolesar, J.M. (2020) 'CCNE1 Amplification as a Predictive Biomarker of Chemotherapy Resistance in Epithelial Ovarian Cancer', Diagnostics (Basel), 10(5).

Gentles, L., Goranov, B., Matheson, E., Herriott, A., Kaufmann, A., Hall, S., Mukhopadhyay, A., Drew, Y., Curtin, N.J. and O'Donnell, R.L. (2019) 'Exploring the Frequency of Homologous Recombination DNA Repair Dysfunction in Multiple Cancer Types', Cancers (Basel), 11(3).

Glorieux, M., Dok, R. and Nuyts, S. (2017) 'Novel DNA targeted therapies for head and neck cancers: clinical potential and biomarkers', Oncotarget, 8(46), pp. 81662-81678.

Golan, T., Locker, G.Y. and Kindler, H.L. (2019) 'Maintenance Olaparib for Metastatic Pancreatic Cancer. Reply', N Engl J Med, 381(15), pp. 1492-1493.

González-Martín, A., Pothuri, B., Vergote, I., DePont Christensen, R., Graybill, W., Mirza, M.R., McCormick, C., Lorusso, D., Hoskins, P., Freyer, G., Baumann, K., Jardon, K., Redondo, A., Moore, R.G., Vulsteke, C., O'Cearbhaill, R.E., Lund, B., Backes, F., Barretina-Ginesta, P.,
Haggerty, A.F., Rubio-Pérez, M.J., Shahin, M.S., Mangili, G., Bradley, W.H., Bruchim, I., Sun, K., Malinowska, I.A., Li, Y., Gupta, D., Monk, B.J. and Investigators, P.E.-O.G.-. (2019) 'Niraparib in Patients with Newly Diagnosed Advanced Ovarian Cancer', N Engl J Med, 381(25), pp. 2391-2402.

Gorecki, L., Andrs, M. and Korabecny, J. (2021) 'Clinical Candidates Targeting the ATR-CHK1-WEE1 Axis in Cancer', Cancers (Basel), 13(4).

Gottipati, P., Vischioni, B., Schultz, N., Solomons, J., Bryant, H.E., Djureinovic, T., Issaeva, N., Sleeth, K., Sharma, R.A. and Helleday, T. (2010) 'Poly(ADP-ribose) polymerase is hyperactivated in homologous recombination-defective cells', Cancer Res, 70(13), pp. 5389-98.

Gralewska, P., Gajek, A., Marczak, A., Mikuła, M., Ostrowski, J., Śliwińska, A. and Rogalska, A. (2020a) 'PARP Inhibition Increases the Reliance on ATR/CHK1 Checkpoint Signaling Leading to Synthetic Lethality-An Alternative Treatment Strategy for Epithelial Ovarian Cancer Cells Independent from HR Effectiveness', Int J Mol Sci, 21(24).

Graves, P.R., Yu, L., Schwarz, J.K., Gales, J., Sausville, E.A., O'Connor, P.M. and Piwnica-Worms, H. (2000) 'The Chk1 protein kinase and the Cdc25C regulatory pathways are targets of the anticancer agent UCN-01', J Biol Chem, 275(8), pp. 5600-5.

Gritsina, G., Xiao, F., O'Brien, S.W., Gabbasov, R., Maglaty, M.A., Xu, R.H., Thapa, R.J., Zhou, Y., Nicolas, E., Litwin, S., Balachandran, S., Sigal, L.J., Huszar, D. and Connolly, D.C.

(2015) 'Targeted Blockade of JAK/STAT3 Signaling Inhibits Ovarian Carcinoma Growth', Mol Cancer Ther, 14(4), pp. 1035-47.

Guan, B., Wang, T.L. and Shih, I.M. (2011) 'ARID1A, a factor that promotes formation of SWI/SNF-mediated chromatin remodeling, is a tumor suppressor in gynecologic cancers', Cancer Res, 71(21), pp. 6718-27.

Guerrero Llobet, S., van der Vegt, B., Jongeneel, E., Bense, R.D., Zwager, M.C., Schröder, C.P., Everts, M., Fehrmann, R.S.N., de Bock, G.H. and van Vugt, M.A.T.M. (2020) 'Cyclin E expression is associated with high levels of replication stress in triple-negative breast cancer', NPJ Breast Cancer, 6, p. 40.

Guillotin, D. and Martin, S.A. (2014) 'Exploiting DNA mismatch repair deficiency as a therapeutic strategy', Exp Cell Res, 329(1), pp. 110-5.

Ha, D.H., Min, A., Kim, S., Jang, H., Kim, S.H., Kim, H.J., Ryu, H.S., Ku, J.L., Lee, K.H. and Im, S.A. (2020) 'Antitumor effect of a WEE1 inhibitor and potentiation of olaparib sensitivity by DNA damage response modulation in triple-negative breast cancer', Sci Rep, 10(1), p. 9930.

Hamam, D., Abdouh, M., Gao, Z.H., Arena, V., Arena, M. and Arena, G.O. (2016) 'Transfer of malignant trait to BRCA1 deficient human fibroblasts following exposure to serum of cancer patients', J Exp Clin Cancer Res, 35, p. 80.

Hanahan, D. and Weinberg, R.A. (2000) 'The hallmarks of cancer', Cell, 100(1), pp. 57-70.

Hanahan, D. and Weinberg, R.A. (2011) 'Hallmarks of cancer: the next generation', Cell, 144(5), pp. 646-74.

Hardwick, L.J.A., Azzarelli, R. and Philpott, A. (2018) 'Cell cycle-dependent phosphorylation and regulation of cellular differentiation', Biochem Soc Trans, 46(5), pp. 1083-1091.

Heijink, A.M., Blomen, V.A., Bisteau, X., Degener, F., Matsushita, F.Y., Kaldis, P., Foijer, F. and van Vugt, M.A. (2015) 'A haploid genetic screen identifies the G1/S regulatory machinery as a determinant of Wee1 inhibitor sensitivity', Proc Natl Acad Sci U S A, 112(49), pp. 15160-5.

Helleday, T., Bryant, H.E. and Schultz, N. (2005) 'Poly(ADP-ribose) polymerase (PARP-1) in homologous recombination and as a target for cancer therapy', Cell Cycle, 4(9), pp. 1176-8.

Herriott, A., Tudhope, S.J., Junge, G., Rodrigues, N., Patterson, M.J., Woodhouse, L., Lunec, J., Hunter, J.E., Mulligan, E.A., Cole, M., Allinson, L.M., Wallis, J.P., Marshall, S., Wang, E., Curtin, N.J. and Willmore, E. (2015) 'PARP1 expression, activity and ex vivo sensitivity to the PARP inhibitor, talazoparib (BMN 673), in chronic lymphocytic leukaemia', Oncotarget, 6(41), pp. 43978-91.

Heylmann, D. and Kaina, B. (2016) 'The γH2AX DNA damage assay from a drop of blood', Sci Rep, 6, p. 22682.

Hill, S.J., Decker, B., Roberts, E.A., Horowitz, N.S., Muto, M.G., Worley, M.J., Feltmate, C.M., Nucci, M.R., Swisher, E.M., Nguyen, H., Yang, C., Morizane, R., Kochupurakkal, B.S., Do, K.T.,
Konstantinopoulos, P.A., Liu, J.F., Bonventre, J.V., Matulonis, U.A., Shapiro, G.I., Berkowitz, R.S., Crum, C.P. and D'Andrea, A.D. (2018) 'Prediction of DNA Repair Inhibitor Response in Short-Term Patient-Derived Ovarian Cancer Organoids', Cancer Discov, 8(11), pp. 1404-1421.

Hirai, H., Arai, T., Okada, M., Nishibata, T., Kobayashi, M., Sakai, N., Imagaki, K., Ohtani, J., Sakai, T., Yoshizumi, T., Mizuarai, S., Iwasawa, Y. and Kotani, H. (2010) 'MK-1775, a small molecule Wee1 inhibitor, enhances anti-tumor efficacy of various DNA-damaging agents, including 5-fluorouracil', Cancer Biol Ther, 9(7), pp. 514-22.

Hirai, H., Iwasawa, Y., Okada, M., Arai, T., Nishibata, T., Kobayashi, M., Kimura, T., Kaneko, N., Ohtani, J., Yamanaka, K., Itadani, H., Takahashi-Suzuki, I., Fukasawa, K., Oki, H., Nambu, T., Jiang, J., Sakai, T., Arakawa, H., Sakamoto, T., Sagara, T., Yoshizumi, T., Mizuarai, S. and Kotani, H. (2009) 'Small-molecule inhibition of Wee1 kinase by MK-1775 selectively sensitizes p53-deficient tumor cells to DNA-damaging agents', Mol Cancer Ther, 8(11), pp. 2992-3000.

Hirst, J., Crow, J. and Godwin, A. (2018) Ovarian Cancer Genetics: Subtypes and Risk Factors.
Hodgson, B., Li, A., Tada, S. and Blow, J.J. (2002) 'Geminin becomes activated as an inhibitor of Cdt1/RLF-B following nuclear import', Curr Biol, 12(8), pp. 678-83.

Hodgson, D.R., Dougherty, B.A., Lai, Z., Fielding, A., Grinsted, L., Spencer, S., O'Connor, M.J., Ho, T.W., Robertson, J.D., Lanchbury, J.S., Timms, K.M., Gutin, A., Orr, M., Jones, H., Gilks, B., Womack, C., Gourley, C., Ledermann, J. and Barrett, J.C. (2018) 'Candidate biomarkers of PARP inhibitor sensitivity in ovarian cancer beyond the BRCA genes', Br J Cancer, 119(11), pp. 1401-1409.

Hodgson, D.R., Dougherty, B.A., Lai, Z., Fielding, A., Grinsted, L., Spencer, S., O'Connor, M.J., Ho, T.W., Robertson, J.D., Lanchbury, J.S., Timms, K.M., Gutin, A., Orr, M., Jones, H., Gilks, B., Womack, C., Gourley, C., Ledermann, J. and Barrett, J.C. (2018) 'Candidate biomarkers of PARP inhibitor sensitivity in ovarian cancer beyond the BRCA genes', Br J Cancer, 119(11), pp. 1401-1409.

Hoeijmakers, J.H. (2001) 'DNA repair mechanisms', Maturitas, 38(1), pp. 17-22; discussion 22-3.

Hsu, H.L., Yannone, S.M. and Chen, D.J. (2002) 'Defining interactions between DNA-PK and ligase IV/XRCC4', DNA Repair (Amst), 1(3), pp. 225-35.

Hughes, B.T., Sidorova, J., Swanger, J., Monnat, R.J. and Clurman, B.E. (2013) 'Essential role for Cdk2 inhibitory phosphorylation during replication stress revealed by a human Cdk2 knockin mutation', Proc Natl Acad Sci U S A, 110(22), pp. 8954-9.

Huntoon, C.J., Flatten, K.S., Wahner Hendrickson, A.E., Huehls, A.M., Sutor, S.L., Kaufmann, S.H. and Karnitz, L.M. (2013) 'ATR inhibition broadly sensitizes ovarian cancer cells to chemotherapy independent of BRCA status', Cancer Res, 73(12), pp. 3683-91.

Ihnen, M., zu Eulenburg, C., Kolarova, T., Qi, J.W., Manivong, K., Chalukya, M., Dering, J., Anderson, L., Ginther, C., Meuter, A., Winterhoff, B., Jones, S., Velculescu, V.E., Venkatesan, N., Rong, H.M., Dandekar, S., Udar, N., J‰nicke, F., Los, G., Slamon, D.J. and Konecny, G.E. (2013) 'Therapeutic potential of the poly(ADP-ribose) polymerase inhibitor rucaparib for the treatment of sporadic human ovarian cancer', Mol Cancer Ther, 12(6), pp. 1002-15.

Iida, Y., Okamoto, A., Hollis, R.L., Gourley, C. and Herrington, C.S. (2021) 'Clear cell carcinoma of the ovary: a clinical and molecular perspective', Int J Gynecol Cancer, 31(4), pp. 605-616.

Jackson, S.P. and Bartek, J. (2009) 'The DNA-damage response in human biology and disease', Nature, 461(7267), pp. 1071-8.

Jariyal, H., Weinberg, F., Achreja, A., Nagarath, D. and Srivastava, A. (2020) 'Synthetic lethality: a step forward for personalized medicine in cancer', Drug Discov Today, 25(2), pp. 305-320.

Jaspers, J. E., Kersbergen, A., Boon, U., Sol, W., Van Deemter, L., Zander, S. A., Drost, R., Wientjens, E., Ji, J., Aly, A., Doroshow, J. H., Cranston, A., Martin, N. M. B., Lau, A., O' Connor, M. J., Ganesan, S., Borst, P., Jonkers, J. and Rottenberg, S. (2013) 'Loss of 53BP1 Causes PARP Inhibitor Resistance in *BRCA1*-Mutated Mouse Mammary Tumours,' Cancer Discovery, 3 (1).

Javle, M. and Curtin, N.J. (2011) 'The role of PARP in DNA repair and its therapeutic exploitation', Br J Cancer, 105(8), pp. 1114-22.

Jiang, X., Li, W., Li, X., Bai, H. and Zhang, Z. (2019) 'Current status and future prospects of PARP inhibitor clinical trials in ovarian cancer', Cancer Manag Res, 11, pp. 4371-4390.

Jo, U., Senatorov, I.S., Zimmermann, A., Saha, L.K., Murai, Y., Kim, S.H., Rajapakse, V.N., Elloumi, F., Takahashi, N., Schultz, C.W., Thomas, A., Zenke, F.T. and Pommier, Y. (2021) 'Novel and Highly Potent ATR Inhibitor M4344 Kills Cancer Cells With Replication Stress, and Enhances the Chemotherapeutic Activity of Widely Used DNA Damaging Agents', Mol Cancer Ther, 20(8), pp. 1431-1441.

Jossé, R., Martin, S.E., Guha, R., Ormanoglu, P., Pfister, T.D., Reaper, P.M., Barnes, C.S., Jones, J., Charlton, P., Pollard, J.R., Morris, J., Doroshow, J.H. and Pommier, Y. (2014) 'ATR inhibitors VE-821 and VX-970 sensitize cancer cells to topoisomerase i inhibitors by

disabling DNA replication initiation and fork elongation responses', Cancer Res, 74(23), pp. 6968-79.

Karnak, D., Engelke, C.G., Parsels, L.A., Kausar, T., Wei, D., Robertson, J.R., Marsh, K.B., Davis, M.A., Zhao, L., Maybaum, J., Lawrence, T.S. and Morgan, M.A. (2014) 'Combined inhibition of Wee1 and PARP1/2 for radiosensitization in pancreatic cancer', Clin Cancer Res, 20(19), pp. 5085-96.

Kaufman, B., Shapira-Frommer, R., Schmutzler, R.K., Audeh, M.W., Friedlander, M., Balmaña, J., Mitchell, G., Fried, G., Stemmer, S.M., Hubert, A., Rosengarten, O., Steiner, M., Loman, N., Bowen, K., Fielding, A. and Domchek, S.M. (2015) 'Olaparib monotherapy in patients with advanced cancer and a germline BRCA1/2 mutation', J Clin Oncol, 33(3), pp. 244-50.

Kim, H., George, E., Ragland, R., Rafail, S., Zhang, R., Krepler, C., Morgan, M., Herlyn, M., Brown, E. and Simpkins, F. (2017) 'Targeting the ATR/CHK1 Axis with PARP Inhibition Results in Tumor Regression in', Clin Cancer Res, 23(12), pp. 3097-3108.

Kim, M.K., James, J. and Annunziata, C.M. (2015) 'Topotecan synergizes with CHEK1 (CHK1) inhibitor to induce apoptosis in ovarian cancer cells', BMC Cancer, 15, p. 196.
Kreahling, J.M., Gemmer, J.Y., Reed, D., Letson, D., Bui, M. and Altiok, S. (2012) 'MK1775, a selective Wee1 inhibitor, shows single-agent antitumor activity against sarcoma cells', Mol Cancer Ther, 11(1), pp. 174-82.

Kim, H., Xu, H., George, E., Hallberg, D., Kumar, S., Jagannathan, V., Medvedev, S., Kinose, Y., Devins, K., Verma, P., Ly, K., Wang, Y., Greenberg, R.A., Schwartz, L., Johnson, N., Scharpf, R.B., Mills, G.B., Zhang, R., Velculescu, V.E., Brown, E.J. and Simpkins, F. (2020) 'Combining PARP with ATR inhibition overcomes PARP inhibitor and platinum resistance in ovarian cancer models', Nat Commun, 11(1), p. 3726.

Kodack, D.P., Farago, A.F., Dastur, A., Held, M.A., Dardaei, L., Friboulet, L., von Flotow, F., Damon, L.J., Lee, D., Parks, M., Dicecca, R., Greenberg, M., Kattermann, K.E., Riley, A.K., Fintelmann, F.J., Rizzo, C., Piotrowska, Z., Shaw, A.T., Gainor, J.F., Sequist, L.V., Niederst, M.J., Engelman, J.A. and Benes, C.H. (2017) 'Primary Patient-Derived Cancer Cells and Their Potential for Personalized Cancer Patient Care', Cell Rep, 21(11), pp. 3298-3309.

Kok, Y.P., Guerrero Llobet, S., Schoonen, P.M., Everts, M., Bhattacharya, A., Fehrmann, R.S.N., van den Tempel, N. and van Vugt, M.A.T.M. (2020) 'Overexpression of Cyclin E1 or Cdc25A leads to replication stress, mitotic aberrancies, and increased sensitivity to replication checkpoint inhibitors', Oncogenesis, 9(10), p. 88.

Koussounadis, A., Langdon, S.P., Um, I.H., Harrison, D.J. and Smith, V.A. (2015) 'Relationship between differentially expressed mRNA and mRNA-protein correlations in a xenograft model system', Sci Rep, 5, p. 10775.

Kraakman-van der Zwet, M., Overkamp, W.J., van Lange, R.E., Essers, J., van Duijn-Goedhart, A., Wiggers, I., Swaminathan, S., van Buul, P.P., Errami, A., Tan, R.T., Jaspers,

N.G., Sharan, S.K., Kanaar, R. and Zdzienicka, M.Z. (2002) 'Brca2 (XRCC11) deficiency results in radioresistant DNA synthesis and a higher frequency of spontaneous deletions', Mol Cell Biol, 22(2), pp. 669-79.

Krajewska, M., Fehrmann, R.S., Schoonen, P.M., Labib, S., de Vries, E.G., Franke, L. and van Vugt, M.A. (2015) 'ATR inhibition preferentially targets homologous recombination-deficient tumor cells', Oncogene, 34(26), pp. 3474-81.

Krokan, H.E. and Bjørås, M. (2013) 'Base excision repair', Cold Spring Harb Perspect Biol, 5(4), p. a012583.

Kubo, A., Nakagawa, K., Varma, R.K., Conrad, N.K., Cheng, J.Q., Lee, W.C., Testa, J.R., Johnson, B.E., Kaye, F.J. and Kelley, M.J. (1999) 'The p16 status of tumor cell lines identifies small molecule inhibitors specific for cyclin-dependent kinase 4', Clin Cancer Res, 5(12), pp. 4279-86.

Kusakabe, M., Onishi, Y., Tada, H., Kurihara, F., Kusao, K., Furukawa, M., Iwai, S., Yokoi, M., Sakai, W. and Sugasawa, K. (2019) 'Mechanism and regulation of DNA damage recognition in nucleotide excision repair', Genes Environ, 41, p. 2.

Kwok, M., Davies, N., Agathanggelou, A., Smith, E., Oldreive, C., Petermann, E., Stewart, G., Brown, J., Lau, A., Pratt, G., Parry, H., Taylor, M., Moss, P., Hillmen, P. and Stankovic, T. (2016) 'ATR inhibition induces synthetic lethality and overcomes chemoresistance in TP53- or ATM-defective chronic lymphocytic leukemia cells', Blood, 127(5), pp. 582-95.

Labidi-Galy, S.I., Papp, E., Hallberg, D., Niknafs, N., Adleff, V., Noe, M., Bhattacharya, R., Novak, M., Jones, S., Phallen, J., Hruban, C.A., Hirsch, M.S., Lin, D.I., Schwartz, L., Maire, C.L., Tille, J.C., Bowden, M., Ayhan, A., Wood, L.D., Scharpf, R.B., Kurman, R., Wang, T.L., Shih, I.M., Karchin, R., Drapkin, R. and Velculescu, V.E. (2017) 'High grade serous ovarian carcinomas originate in the fallopian tube', Nat Commun, 8(1), p. 1093.

Lau, W.M., Ho, T.H. and Hui, K.M. (2007) 'p16INK4A-silencing augments DNA damage-induced apoptosis in cervical cancer cells', Oncogene, 26(41), pp. 6050-60.

Langsfeld, E.S., Bodily, J.M. and Laimins, L.A. (2015) 'The Deacetylase Sirtuin 1 Regulates Human Papillomavirus Replication by Modulating Histone Acetylation and Recruitment of DNA Damage Factors NBS1 and Rad51 to Viral Genomes', PLoS Pathog, 11(9), p. e1005181.

Lord, C.J., McDonald, S., Swift, S., Turner, N.C. and Ashworth, A. (2008) 'A high-throughput RNA interference screen for DNA repair determinants of PARP inhibitor sensitivity', DNA Repair (Amst), 7(12), pp. 2010-9.

Lee, J., Kumagai, A. and Dunphy, W.G. (2001) 'Positive regulation of Wee1 by Chk1 and 14-3-3 proteins', Mol Biol Cell, 12(3), pp. 551-63.

Lee, E.K. and Matulonis, U.A. (2020) 'PARP Inhibitor Resistance Mechanisms and Implications for Post-Progression Combination Therapies', Cancers (Basel), 12(8).

Lei, J., Ploner, A., Elfström, K.M., Wang, J., Roth, A., Fang, F., Sundström, K., Dillner, J. and Sparén, P. (2020) 'HPV Vaccination and the Risk of Invasive Cervical Cancer', N Engl J Med, 383(14), pp. 1340-1348.

Leijen, S., van Geel, R.M., Pavlick, A.C., Tibes, R., Rosen, L., Razak, A.R., Lam, R., Demuth, T., Rose, S., Lee, M.A., Freshwater, T., Shumway, S., Liang, L.W., Oza, A.M., Schellens, J.H. and Shapiro, G.I. (2016a) 'Phase I Study Evaluating WEE1 Inhibitor AZD1775 As Monotherapy and in Combination With Gemcitabine, Cisplatin, or Carboplatin in Patients With Advanced Solid Tumors', J Clin Oncol, 34(36), pp. 4371-4380.

Leijen, S., van Geel, R.M., Sonke, G.S., de Jong, D., Rosenberg, E.H., Marchetti, S., Pluim, D., van Werkhoven, E., Rose, S., Lee, M.A., Freshwater, T., Beijnen, J.H. and Schellens, J.H. (2016b) 'Phase II Study of WEE1 Inhibitor AZD1775 Plus Carboplatin in Patients With TP53-Mutated Ovarian Cancer Refractory or Resistant to First-Line Therapy Within 3 Months', J Clin Oncol, 34(36), pp. 4354-4361.

Lewis, C.W., Jin, Z., Macdonald, D., Wei, W., Qian, X.J., Choi, W.S., He, R., Sun, X. and Chan, G. (2017) 'Prolonged mitotic arrest induced by Wee1 inhibition sensitizes breast cancer cells to paclitaxel', Oncotarget, 8(43), pp. 73705-73722.

Li, H., Liu, Z.Y., Wu, N., Chen, Y.C., Cheng, Q. and Wang, J. (2020) 'PARP inhibitor resistance: the underlying mechanisms and clinical implications', Mol Cancer, 19(1), p. 107.

Liang, L., Deng, L., Nguyen, S.C., Zhao, X., Maulion, C.D., Shao, C. and Tischfield, J.A. (2008) 'Human DNA ligases I and III, but not ligase IV, are required for microhomology-mediated end joining of DNA double-strand breaks', Nucleic Acids Res, 36(10), pp. 3297-310.

Lieber, M.R. (2010) 'NHEJ and its backup pathways in chromosomal translocations', Nat Struct Mol Biol, 17(4), pp. 393-5.

Lisio, M.A., Fu, L., Goyeneche, A., Gao, Z.H. and Telleria, C. (2019) 'High-Grade Serous Ovarian Cancer: Basic Sciences, Clinical and Therapeutic Standpoints', Int J Mol Sci, 20(4).

Mang, C., Birkenmaier, A., Cathomas, G. and Humburg, J. (2017) 'Endometrioid endometrial adenocarcinoma: an increase of G3 cancers?', Arch Gynecol Obstet, 295(6), pp. 1435-1440.

Lin, A.B., McNeely, S.C. and Beckmann, R.P. (2017) 'Achieving Precision Death with Cell-Cycle Inhibitors that Target DNA Replication and Repair', Clin Cancer Res, 23(13), pp. 3232-3240.

Lindahl, T. and Nyberg, B. (1972) 'Rate of depurination of native deoxyribonucleic acid', Biochemistry, 11(19), pp. 3610-8.

Liu, Q., Guntuku, S., Cui, X.S., Matsuoka, S., Cortez, D., Tamai, K., Luo, G., Carattini-Rivera, S., DeMayo, F., Bradley, A., Donehower, L.A. and Elledge, S.J. (2000) 'Chk1 is an essential kinase that is regulated by Atr and required for the G(2)/M DNA damage checkpoint', Genes Dev, 14(12), pp. 1448-59.

Liu, Y., Beyer, A. and Aebersold, R. (2016) 'On the Dependency of Cellular Protein Levels on mRNA Abundance', Cell, 165(3), pp. 535-50.

Liu, X., Shao, Z., Jiang, W., Lee, B.J. and Zha, S. (2017) 'PAXX promotes KU accumulation at DNA breaks and is essential for end-joining in XLF-deficient mice', Nat Commun, 8, p. 13816.

Liu, D., Keijzers, G. and Rasmussen, L. J. (2017) 'DNA mismatch repair and its many roles in eukaryotic cells', Mutat Res Rev, 773, pp. 174-187.

Li, H., Liu, Z., Wu, N., Chen, Y., Cheng, Q. and Wang, J. (2020) 'PARP inhibitor resistance: the underlying mechanisms and clinical implications', Mol Cancer, 19 (1) pp. 107.

Lord, C.J. and Ashworth, A. (2017) 'PARP inhibitors: Synthetic lethality in the clinic', Science, 355(6330), pp. 1152-1158.

Lord, C.J., McDonald, S., Swift, S., Turner, N.C. and Ashworth, A. (2008) 'A high-throughput RNA interference screen for DNA repair determinants of PARP inhibitor sensitivity', DNA Repair (Amst), 7(12), pp. 2010-9.

McCabe, N., Turner, N.C., Lord, C.J., Kluzek, K., Bialkowska, A., Swift, S., Giavara, S., O'Connor, M.J., Tutt, A.N., Zdzienicka, M.Z., Smith, G.C. and Ashworth, A. (2006) 'Deficiency in the repair of DNA damage by homologous recombination and sensitivity to poly(ADP-ribose) polymerase inhibition', Cancer Res, 66(16), pp. 8109-15.

McMullen, M., Karakasis, K., Madariaga, A. and Oza, A.M. (2020) 'Overcoming Platinum and PARP-Inhibitor Resistance in Ovarian Cancer', Cancers (Basel), 12(6).

Maclaine, N.J. and Hupp, T.R. (2009) 'The regulation of p53 by phosphorylation: a model for how distinct signals integrate into the p53 pathway', Aging (Albany NY), 1(5), pp. 490-502.

Magdalou, I., Lopez, B.S., Pasero, P. and Lambert, S.A. (2014) 'The causes of replication stress and their consequences on genome stability and cell fate', Semin Cell Dev Biol, 30, pp. 154-64.

Malentacchi, F., Turrini, I., Sorbi, F., Projetto, E., Castiglione, F., Fambrini, M., Petraglia, F., Pillozzi, S. and Noci, I. (2019) 'Pilot investigation of the mutation profile of PIK3CA/PTEN genes (PI3K pathway) in grade 3 endometrial cancer', Oncol Rep, 41(3), pp. 1560-1574.

Markowski, M.C. and Antonarakis, E.S. (2020) 'PARP inhibitors in prostate cancer: time to narrow patient selection?', Expert Rev Anticancer Ther, 20(7), pp. 523-526.

Martins, F.C., Santiago, I., Trinh, A., Xian, J., Guo, A., Sayal, K., Jimenez-Linan, M., Deen, S., Driver, K., Mack, M., Aslop, J., Pharoah, P.D., Markowetz, F. and Brenton, J.D. (2014) 'Combined image and genomic analysis of high-grade serous ovarian cancer reveals PTEN loss as a common driver event and prognostic classifier', Genome Biol, 15(12), p. 526.

Matson, L. (2021) '"The power of science": HPV vaccine proven to dramatically reduce cervical cancer', Cancer Research UK.

Massagué, J. (2004) 'G1 cell-cycle control and cancer', Nature, 432(7015), pp. 298-306.

Massey, A.J. (2016) 'Inhibition of ATR-dependent feedback activation of Chk1 sensitises cancer cells to Chk1 inhibitor monotherapy', Cancer Lett, 383(1), pp. 41-52.

Massey, A.J., Stephens, P., Rawlinson, R., McGurk, L., Plummer, R. and Curtin, N.J. (2016) 'mTORC1 and DNA-PKcs as novel molecular determinants of sensitivity to Chk1 inhibition', Mol Oncol, 10(1), pp. 101-12.

Michelena, J., Lezaja, A., Teloni, F., Schmid, T., Imhof, R. and Altmeyer, M. (2018) 'Analysis of PARP inhibitor toxicity by multidimensional fluorescence microscopy reveals mechanisms of sensitivity and resistance', Nat Commun, 9(1), p. 2678.

Middleton, F.K., Patterson, M.J., Elstob, C.J., Fordham, S., Herriott, A., Wade, M.A., McCormick, A., Edmondson, R., May, F.E., Allan, J.M., Pollard, J.R. and Curtin, N.J. (2015) 'Common cancer-associated imbalances in the DNA damage response confer sensitivity to single agent ATR inhibition', Oncotarget, 6(32), pp. 32396-409.

Middleton, F.K., Pollard, J.R. and Curtin, N.J. (2018) 'The Impact of p53 Dysfunction in ATR Inhibitor Cytotoxicity and Chemo- and Radiosensitisation', Cancers (Basel), 10(8).
Min, A., Im, S.A., Jang, H., Kim, S., Lee, M., Kim, D.K., Yang, Y., Kim, H.J., Lee, K.H., Kim, J.W., Kim, T.Y., Oh, D.Y., Brown, J., Lau, A., O'Connor, M.J. and Bang, Y.J. (2017) 'AZD6738, A Novel Oral Inhibitor of ATR, Induces Synthetic Lethality with ATM Deficiency in Gastric Cancer Cells', Mol Cancer Ther, 16(4), pp. 566-577.

Min, A., Im, S.A., Jang, H., Kim, S., Lee, M., Kim, D.K., Yang, Y., Kim, H.J., Lee, K.H., Kim, J.W., Kim, T.Y., Oh, D.Y., Brown, J., Lau, A., O'Connor, M.J. and Bang, Y.J. (2017) 'AZD6738, A Novel Oral Inhibitor of ATR, Induces Synthetic Lethality with ATM Deficiency in Gastric Cancer Cells', Mol Cancer Ther, 16(4), pp. 566-577.

Miserocchi, G., Mercatali, L., Liverani, C., De Vita, A., Spadazzi, C., Pieri, F., Bongiovanni, A., Recine, F., Amadori, D. and Ibrahim, T. (2017) 'Management and potentialities of primary cancer cultures in preclinical and translational studies', J Transl Med, 15(1), p. 229.

Mirza, M.R., Coleman, R.L., González-Martín, A., Moore, K.N., Colombo, N., Ray-Coquard, I. and Pignata, S. (2020) 'The forefront of ovarian cancer therapy: update on PARP inhibitors', Ann Oncol, 31(9), pp. 1148-1159.

Mirza, M.R., Monk, B.J., Herrstedt, J., Oza, A.M., Mahner, S., Redondo, A., Fabbro, M., Ledermann, J.A., Lorusso, D., Vergote, I., Ben-Baruch, N.E., Marth, C., Mądry, R., Christensen, R.D., Berek, J.S., Dørum, A., Tinker, A.V., du Bois, A., González-Martín, A., Follana, P., Benigno, B., Rosenberg, P., Gilbert, L., Rimel, B.J., Buscema, J., Balser, J.P., Agarwal, S., Matulonis, U.A. and Investigators, E.-O.N. (2016) 'Niraparib Maintenance Therapy in Platinum-Sensitive, Recurrent Ovarian Cancer', N Engl J Med, 375(22), pp. 2154-2164.

Moeglin, E., Desplancq, D., Conic, S., Oulad-Abdelghani, M., Stoessel, A., Chiper, M., Vigneron, M., Didier, P., Tora, L. and Weiss, E. (2019) 'Uniform Widespread Nuclear Phosphorylation of Histone H2AX Is an Indicator of Lethal DNA Replication Stress', Cancers (Basel), 11(3).

Mohni, K.N., Kavanaugh, G.M. and Cortez, D. (2014) 'ATR pathway inhibition is synthetically lethal in cancer cells with ERCC1 deficiency', Cancer Res, 74(10), pp. 2835-45.

Mohni, K.N., Thompson, P.S., Luzwick, J.W., Glick, G.G., Pendleton, C.S., Lehmann, B.D., Pietenpol, J.A. and Cortez, D. (2015) 'A Synthetic Lethal Screen Identifies DNA Repair Pathways that Sensitize Cancer Cells to Combined ATR Inhibition and Cisplatin Treatments', PLoS One, 10(5), p. e0125482.

Moore, K., Colombo, N., Scambia, G., Kim, B.G., Oaknin, A., Friedlander, M., Lisyanskaya, A., Floquet, A., Leary, A., Sonke, G.S., Gourley, C., Banerjee, S., Oza, A., González-Martín, A., Aghajanian, C., Bradley, W., Mathews, C., Liu, J., Lowe, E.S., Bloomfield, R. and DiSilvestro, P. (2018) 'Maintenance Olaparib in Patients with Newly Diagnosed Advanced Ovarian Cancer', N Engl J Med, 379(26), pp. 2495-2505.

Morgan, R.D., Clamp, A.R., Evans, D.G.R., Edmondson, R.J. and Jayson, G.C. (2018) 'PARP inhibitors in platinum-sensitive high-grade serous ovarian cancer', Cancer Chemother Pharmacol, 81(4), pp. 647-658.

Morice, P., Leary, A., Creutzberg, C., Abu-Rustum, N. and Darai, E. (2016) 'Endometrial cancer', Lancet, 387(10023), pp. 1094-1108.

Mukhopadhyay, A., Elattar, A., Cerbinskaite, A., Wilkinson, S.J., Drew, Y., Kyle, S., Los, G., Hostomsky, Z., Edmondson, R.J. and Curtin, N.J. (2010) 'Development of a functional assay for homologous recombination status in primary cultures of epithelial ovarian tumor and correlation with sensitivity to poly(ADP-ribose) polymerase inhibitors', Clin Cancer Res, 16(8), pp. 2344-51.

Mukhopadhyay, A., Plummer, E.R., Elattar, A., Soohoo, S., Uzir, B., Quinn, J.E., McCluggage, W.G., Maxwell, P., Aneke, H., Curtin, N.J. and Edmondson, R.J. (2012)

'Clinicopathological features of homologous recombination-deficient epithelial ovarian cancers: sensitivity to PARP inhibitors, platinum, and survival', Cancer Res, 72(22), pp. 5675-82.

Murai, J. and Pommier, Y. (2019) 'PARP trapping beyond homologous recombination and platinum sensitivity in cancers', Annual review of Cancer Biology, 3, pp. 131-150.

Murai, J., Huang, S.Y., Das, B.B., Renaud, A., Zhang, Y., Doroshow, J.H., Ji, J., Takeda, S. and Pommier, Y. (2012) 'Trapping of PARP1 and PARP2 by Clinical PARP Inhibitors', Cancer Res, 72(21), pp. 5588-99.

Murga, M., Bunting, S., Montaña, M.F., Soria, R., Mulero, F., Cañamero, M., Lee, Y., McKinnon, P.J., Nussenzweig, A. and Fernandez-Capetillo, O. (2009) 'A mouse model of ATR-Seckel shows embryonic replicative stress and accelerated aging', Nat Genet, 41(8), pp. 891-8.

Murga, M., Campaner, S., Lopez-Contreras, A.J., Toledo, L.I., Soria, R., Montaña, M.F., Artista, L., Schleker, T., Guerra, C., Garcia, E., Barbacid, M., Hidalgo, M., Amati, B. and Fernandez-Capetillo, O. (2011) 'Exploiting oncogene-induced replicative stress for the selective killing of Myc-driven tumors', Nat Struct Mol Biol, 18(12), pp. 1331-1335.

Murray, J., Thomas, H., Berry, P., Kyle, S., Patterson, M., Jones, C., Los, G., Hostomsky, Z., Plummer, E.R., Boddy, A.V. and Curtin, N.J. (2014) 'Tumour cell retention of rucaparib, sustained PARP inhibition and efficacy of weekly as well as daily schedules', Br J Cancer, 110(8), pp. 1977-84.

Myshko, D. and Grisham, R. (2021) 'KRAS Pathway Opens Door for Patients With Difficult-to-Treat Ovarian Cancer.', OncologyLive, 22.

Negritto, C. (2010) 'Repairing Double-Strand DNA Breaks.', Nature Education, 3(9).
Nero, C., Vizzielli, G., Lorusso, D., Cesari, E., Daniele, G., Loverro, M., Scambia, G. and Sette, C. (2021) 'Patient-derived organoids and high grade serous ovarian cancer: from disease modeling to personalized medicine', J Exp Clin Cancer Res, 40(1), p. 116.

Nguewa, P.A., Fuertes, M.A., Cepeda, V., Alonso, C., Quevedo, C., Soto, M. and PÈrez, J.M. (2006) 'Poly(ADP-ribose) polymerase-1 inhibitor 3-aminobenzamide enhances apoptosis induction by platinum complexes in cisplatin-resistant tumor cells', Med Chem, 2(1), pp. 47-53.

Nghiem, P., Park, P.K., Kim Ys, Y.S., Desai, B.N. and Schreiber, S.L. (2002) 'ATR is not required for p53 activation but synergizes with p53 in the replication checkpoint', J Biol Chem, 277(6), pp. 4428-34.

Ngoi, N.Y.L., Pham, M.M., Tan, D.S.P. and Yap, T.A. (2021) 'Targeting the replication stress response through synthetic lethal strategies in cancer medicine', Trends Cancer, 7(10), pp. 930-957.

Nguyen, T., Hawkins, E., Kolluri, A., Kmieciak, M., Park, H., Lin, H. and Grant, S. (2015) 'Synergism between bosutinib (SKI-606) and the Chk1 inhibitor (PF-00477736) in highly imatinib-resistant BCR/ABL$^+$ leukemia cells', Leuk Res, 39(1), pp. 65-71.

Nowsheen, S., Bonner, J.A. and Yang, E.S. (2011) 'The poly(ADP-Ribose) polymerase inhibitor ABT-888 reduces radiation-induced nuclear EGFR and augments head and neck tumor response to radiotherapy', Radiother Oncol, 99(3), pp. 331-8.

Ochi, T., Blackford, A.N., Coates, J., Jhujh, S., Mehmood, S., Tamura, N., Travers, J., Wu, Q., Draviam, V.M., Robinson, C.V., Blundell, T.L. and Jackson, S.P. (2015) 'DNA repair. PAXX, a paralog of XRCC4 and XLF, interacts with Ku to promote DNA double-strand break repair', Science, 347(6218), pp. 185-188.

O Donnell, R.L., McCormick, A., Mukhopadhyay, A., Woodhouse, L.C., Moat, M., Grundy, A., Dixon, M., Kaufman, A., Soohoo, S., Elattar, A., Curtin, N.J. and Edmondson, R.J. (2014) 'The use of ovarian cancer cells from patients undergoing surgery to generate primary cultures capable of undergoing functional analysis', PLoS One, 9(6), p. e90604.

Olsen, A.K., Lindeman, B., Wiger, R., Duale, N. and Brunborg, G. (2005) 'How do male germ cells handle DNA damage?', Toxicol Appl Pharmacol, 207(2 Suppl), pp. 521-31.

Oo, Z.Y., Stevenson, A.J., Proctor, M., Daignault, S.M., Walpole, S., Lanagan, C., Chen, J., Škalamera, D., Spoerri, L., Ainger, S.A., Sturm, R.A., Haass, N.K. and Gabrielli, B. (2018) 'Endogenous Replication Stress Marks Melanomas Sensitive to CHEK1 Inhibitors', Clin Cancer Res, 24(12), pp. 2901-2912.

Oplustilova, L., Wolanin, K., Mistrik, M., Korinkova, G., Simkova, D., Bouchal, J., Lenobel, R., Bartkova, J., Lau, A., O'Connor, M.J., Lukas, J. and Bartek, J. (2012) 'Evaluation of candidate biomarkers to predict cancer cell sensitivity or resistance to PARP-1 inhibitor treatment', Cell Cycle, 11(20), pp. 3837-50.

Oza, A.M., Estevez-Diz, M., Grischke, E.M., Hall, M., Marmé, F., Provencher, D., Uyar, D., Weberpals, J.I., Wenham, R.M., Laing, N., Tracy, M., Freshwater, T., Lee, M.A., Liu, J., Qiu, J., Rose, S., Rubin, E.H. and Moore, K. (2020) 'A Biomarker-enriched, Randomized Phase II Trial of Adavosertib (AZD1775) Plus Paclitaxel and Carboplatin for Women with Platinum-sensitive', Clin Cancer Res, 26(18), pp. 4767-4776.

Oza, A.M., Tinker, A.V., Oaknin, A., Shapira-Frommer, R., McNeish, I.A., Swisher, E.M., Ray-Coquard, I., Bell-McGuinn, K., Coleman, R.L., O'Malley, D.M., Leary, A., Chen, L.M., Provencher, D., Ma, L., Brenton, J.D., Konecny, G.E., Castro, C.M., Giordano, H., Maloney, L., Goble, S., Lin, K.K., Sun, J., Raponi, M., Rolfe, L. and Kristeleit, R.S. (2017) 'Antitumor activity and safety of the PARP inhibitor rucaparib in patients with high-grade ovarian carcinoma and a germline or somatic BRCA1 or BRCA2 mutation: Integrated analysis of data from Study 10 and ARIEL2', Gynecol Oncol, 147(2), pp. 267-275.

Paculová, H., Kramara, J., Šimečková, Š., Fedr, R., Souček, K., Hylse, O., Paruch, K., Svoboda, M., Mistrík, M. and Kohoutek, J. (2017) 'BRCA1 or CDK12 loss sensitizes cells to CHK1 inhibitors', Tumour Biol, 39(10), p. 1010428317727479.

Parsels, L.A., Karnak, D., Parsels, J.D., Zhang, Q., Vélez-Padilla, J., Reichert, Z.R., Wahl, D.R., Maybaum, J., O'Connor, M.J., Lawrence, T.S. and Morgan, M.A. (2018) 'PARP1 Trapping and DNA Replication Stress Enhance Radiosensitization with Combined WEE1 and PARP Inhibitors', Mol Cancer Res, 16(2), pp. 222-232.

Patel, R., Barker, H.E., Kyula, J., McLaughlin, M., Dillon, M.T., Schick, U., Hafsi, H., Thompson, A., Khoo, V., Harrington, K. and Zaidi, S. (2017) 'An orally bioavailable Chk1 inhibitor, CCT244747, sensitizes bladder and head and neck cancer cell lines to radiation', Radiother Oncol, 122(3), pp. 470-475.

Patel, A.G., Flatten, K.S., Schneider, P.A., Dai, N.T., McDonald, J.S., Poirier, G.G. and Kaufmann, S.H. (2012) 'Enhanced killing of cancer cells by poly(ADP-ribose) polymerase inhibitors and topoisomerase I inhibitors reflects poisoning of both enzymes', J Biol Chem, 287(6), pp. 4198-210.

Peasland, A., Wang, L.Z., Rowling, E., Kyle, S., Chen, T., Hopkins, A., Cliby, W.A., Sarkaria, J., Beale, G., Edmondson, R.J. and Curtin, N.J. (2011) 'Identification and evaluation of a potent novel ATR inhibitor, NU6027, in breast and ovarian cancer cell lines', Br J Cancer, 105(3), pp. 372-81.

Pennington, K.P., Walsh, T., Harrell, M.I., Lee, M.K., Pennil, C.C., Rendi, M.H., Thornton, A., Norquist, B.M., Casadei, S., Nord, A.S., Agnew, K.J., Pritchard, C.C., Scroggins, S., Garcia, R.L., King, M.C. and Swisher, E.M. (2014) 'Germline and somatic mutations in homologous recombination genes predict platinum response and survival in ovarian, fallopian tube, and peritoneal carcinomas', Clin Cancer Res, 20(3), pp. 764-75.

Perkhofer, L., Schmitt, A., Romero Carrasco, M.C., Ihle, M., Hampp, S., Ruess, D.A., Hessmann, E., Russell, R., Lechel, A., Azoitei, N., Lin, Q., Liebau, S., Hohwieler, M., Bohnenberger, H., Lesina, M., Algül, H., Gieldon, L., Schröck, E., Gaedcke, J., Wagner, M., Wiesmüller, L., Sipos, B., Seufferlein, T., Reinhardt, H.C., Frappart, P.O. and Kleger, A. (2017) 'ATM Deficiency Generating Genomic Instability Sensitizes Pancreatic Ductal Adenocarcinoma Cells to Therapy-Induced DNA Damage', Cancer Res, 77(20), pp. 5576-5590.

Petersen, S., Wilson, A.J., Hirst, J., Roby, K.F., Fadare, O., Crispens, M.A., Beeghly-Fadiel, A. and Khabele, D. (2020) 'CCNE1 and BRD4 co-amplification in high-grade serous ovarian cancer is associated with poor clinical outcomes', Gynecol Oncol, 157(2), pp. 405-410.

Pires, I.M., Olcina, M.M., Anbalagan, S., Pollard, J.R., Reaper, P.M., Charlton, P.A., McKenna, W.G. and Hammond, E.M. (2012) 'Targeting radiation-resistant hypoxic tumour cells through ATR inhibition', Br J Cancer, 107(2), pp. 291-9.

Plotz, G., Zeuzem, S. and Raedle, J. (2006) 'DNA mismatch repair and Lynch syndrome', J Mol Histol, 37 (5-7), pp. 271-283.

Plummer, E.R., Middleton, M.R., Jones, C., Olsen, A., Hickson, I., McHugh, P., Margison, G.P., McGown, G., Thorncroft, M., Watson, A.J., Boddy, A.V., Calvert, A.H., Harris, A.L., Newell, D.R. and Curtin, N.J. (2005) 'Temozolomide pharmacodynamics in patients with metastatic melanoma: dna damage and activity of repair enzymes O6-alkylguanine alkyltransferase and poly(ADP-ribose) polymerase-1', Clin Cancer Res, 11(9), pp. 3402-9.

Plummer, R., Jones, C., Middleton, M., Wilson, R., Evans, J., Olsen, A., Curtin, N., Boddy, A., McHugh, P., Newell, D., Harris, A., Johnson, P., Steinfeldt, H., Dewji, R., Wang, D., Robson, L. and Calvert, H. (2008) 'Phase I study of the poly(ADP-ribose) polymerase inhibitor, AG014699, in combination with temozolomide in patients with advanced solid tumors', Clin Cancer Res, 14(23), pp. 7917-23.

Plummer, R., Lorigan, P., Steven, N., Scott, L., Middleton, M.R., Wilson, R.H., Mulligan, E., Curtin, N., Wang, D., Dewji, R., Abbattista, A., Gallo, J. and Calvert, H. (2013) 'A phase II study of the potent PARP inhibitor, Rucaparib (PF-01367338, AG014699), with temozolomide in patients with metastatic melanoma demonstrating evidence of chemopotentiation', Cancer Chemother Pharmacol, 71(5), pp. 1191-9.

Plummer, R., Verheul, H.M., De Vos, F.Y.F.L., Leunen, K., Molife, L.R., Rolfo, C., Grundtvig-Sørensen, P., De Grève, J., Rottey, S., Jerusalem, G., Italiano, A., Spicer, J., Dirix, L., Goessl, C., Birkett, J., Spencer, S., Learoyd, M., Bailey, C. and Dean, E. (2018) 'Pharmacokinetic Effects and Safety of Olaparib Administered with Endocrine Therapy: A Phase I Study in Patients with Advanced Solid Tumours', Adv Ther, 35(11), pp. 1945-1964.

Rafiei, S., Fitzpatrick, K., Liu, D., Cai, M.Y., Elmarakeby, H.A., Park, J., Ricker, C., Kochupurakkal, B.S., Choudhury, A.D., Hahn, W.C., Balk, S.P., Hwang, J.H., Van Allen, E.M. and Mouw, K.W. (2020) 'Loss Confers Greater Sensitivity to ATR Inhibition Than PARP Inhibition in Prostate Cancer', Cancer Res, 80(11), pp. 2094-2100.

Rajeshkumar, N.V., De Oliveira, E., Ottenhof, N., Watters, J., Brooks, D., Demuth, T., Shumway, S.D., Mizuarai, S., Hirai, H., Maitra, A. and Hidalgo, M. (2011) 'MK-1775, a potent Wee1 inhibitor, synergizes with gemcitabine to achieve tumor regressions, selectively in p53-deficient pancreatic cancer xenografts', Clin Cancer Res, 17(9), pp. 2799-806.

Ray-Coquard, I., Vanacker, H., Le Saux, O. and Tredan, O. (2020) 'Overcoming resistance to PARP inhibitor in epithelial ovarian cancer, are we ready?', EBioMedicine, 61, p. 103046.

Reaper, P.M., Griffiths, M.R., Long, J.M., Charrier, J.D., Maccormick, S., Charlton, P.A., Golec, J.M. and Pollard, J.R. (2011) 'Selective killing of ATM- or p53-deficient cancer cells through inhibition of ATR', Nat Chem Biol, 7(7), pp. 428-30.

Restelli, V., Chilà, R., Lupi, M., Rinaldi, A., Kwee, I., Bertoni, F., Damia, G. and Carrassa, L. (2015) 'Characterization of a mantle cell lymphoma cell line resistant to the Chk1 inhibitor PF-00477736', Oncotarget, 6(35), pp. 37229-40.

Ricciardi, E., Baert, T., Ataseven, B., Heitz, F., Prader, S., Bommert, M., Schneider, S., du Bois, A. and Harter, P. (2018) 'Low-grade Serous Ovarian Carcinoma', Geburtshilfe Frauenheilkd, 78(10), pp. 972-976.

Rogakou, E.P., Pilch, D.R., Orr, A.H., Ivanova, V.S. and Bonner, W.M. (1998) 'DNA double-stranded breaks induce histone H2AX phosphorylation on serine 139', J Biol Chem, 273(10), pp. 5858-68.

Roy, R., Chun, J. and Powell, S.N. (2011) 'BRCA1 and BRCA2: different roles in a common pathway of genome protection', Nat Rev Cancer, 12(1), pp. 68-78.

Rundle, S., Bradbury, A., Drew, Y. and Curtin, N.J. (2017) 'Targeting the ATR-CHK1 Axis in Cancer Therapy', Cancers (Basel), 9(5).

Saldivar, J.C., Cortez, D. and Cimprich, K.A. (2017) 'The essential kinase ATR: ensuring faithful duplication of a challenging genome', Nat Rev Mol Cell Biol, 18(10), pp. 622-636.

Šalovská, B., Janečková, H., Fabrik, I., Karlíková, R., Čecháková, L., Ondrej, M., Link, M., Friedecký, D. and Tichý, A. (2018) 'Radio-sensitizing effects of VE-821 and beyond: Distinct phosphoproteomic and metabolomic changes after ATR inhibition in irradiated MOLT-4 cells', PLoS One, 13(7), p. e0199349

Sakai, W., Swisher, E. M., Karlan, B. Y., Agarwal, M. K., Higgins, J., Friedman, C., Villegas, E., Jacquemont, C., Farrugia, D. J., Couch, F. J., Urban, N. and Taniguchi, T. (2008) 'Secondary mutations as a mechanism of cisplatin resistance', Nature, 451 (7182), pp. 1116- 1120.

Sarkaria, J.N., Busby, E.C., Tibbetts, R.S., Roos, P., Taya, Y., Karnitz, L.M. and Abraham, R.T. (1999) 'Inhibition of ATM and ATR kinase activities by the radiosensitizing agent, caffeine', Cancer Res, 59(17), pp. 4375-82.

Sarni, D. and Kerem, B. (2017) 'Oncogene-Induced Replication Stress Drives Genome Instability and Tumorigenesis.', Int J Mol Sci., 18(7), p. 1339.

Schmitt, A., Knittel, G., Welcker, D., Yang, T.P., George, J., Nowak, M., Leeser, U., Büttner, R., Perner, S., Peifer, M. and Reinhardt, H.C. (2017) 'Deficiency Is Associated with Sensitivity to PARP1- and ATR Inhibitors in Lung Adenocarcinoma', Cancer Res, 77(11), pp. 3040-3056.

Schwanhäusser, B., Busse, D., Li, N., Dittmar, G., Schuchhardt, J., Wolf, J., Chen, W. and Selbach, M. (2011) 'Global quantification of mammalian gene expression control', Nature, 473(7347), pp. 337-42.

Schrempf, A., Slyskova, J. and Loizou, J.I. (2021) 'Targeting the DNA Repair Enzyme Polymerase θ in Cancer Therapy', Trends Cancer, 7(2), pp. 98-111.

Sears, C.R. and Turchi, J.J. (2012) 'Complex cisplatin-double strand break (DSB) lesions directly impair cellular non-homologous end-joining (NHEJ) independent of downstream damage response (DDR) pathways', J Biol Chem, 287(29), pp. 24263-72.

Seidman, J.D., Horkayne-Szakaly, I., Haiba, M., Boice, C.R., Kurman, R.J. and Ronnett, B.M. (2004) 'The histologic type and stage distribution of ovarian carcinomas of surface epithelial origin', Int J Gynecol Pathol, 23(1), pp. 41-4.

Serpico, A. F., D'Alterio, G., Vetrei, C., Monica, R. D., Nardella, L., Visconti, R. and Grieco, D. (2019) 'Wee1 Rather Than Plk1 Is Inhibited by AZD1775 at Therapeutically Relevant Concentrations', Cancers, 11 (6), pp. 819.

Setton, J., Zinda, M., Riaz, N., Durocher, D., Zimmermann, M., Koehler, M., Reis-Filho, J.S. and Powell, S.N. (2021) 'Synthetic Lethality in Cancer Therapeutics: The Next Generation', Cancer Discov, 11(7), pp. 1626-1635.

Shaheen, M., Allen, C., Nickoloff, J.A. and Hromas, R. (2011) 'Synthetic lethality: exploiting the addiction of cancer to DNA repair', Blood, 117(23), pp. 6074-82.

Shi, Q., Shen, L.Y., Dong, B., Fu, H., Kang, X.Z., Yang, Y.B., Dai, L., Yan, W.P., Xiong, H.C., Liang, Z. and Chen, K.N. (2018) 'The identification of the ATR inhibitor VE-822 as a therapeutic strategy for enhancing cisplatin chemosensitivity in esophageal squamous cell carcinoma', Cancer Lett, 432, pp. 56-68.

Shimada, M., Kigawa, J., Ohishi, Y., Yasuda, M., Suzuki, M., Hiura, M., Nishimura, R., Tabata, T., Sugiyama, T. and Kaku, T. (2009) 'Clinicopathological characteristics of mucinous adenocarcinoma of the ovary', Gynecol Oncol, 113(3), pp. 331-4.

Smith, H.L., Southgate, H., Tweddle, D.A. and Curtin, N.J. (2020) 'DNA damage checkpoint kinases in cancer', Expert Rev Mol Med, 22, p. e2.

Smith, H.L., Prendergast, L. and Curtin, N.J. (2020) 'Exploring the Synergy between PARP and CHK1 Inhibition in Matched', Cancers (Basel), 12(4).

Sørensen, C.S., Hansen, L.T., Dziegielewski, J., Syljuåsen, R.G., Lundin, C., Bartek, J. and Helleday, T. (2005) 'The cell-cycle checkpoint kinase Chk1 is required for mammalian homologous recombination repair', Nat Cell Biol, 7(2), pp. 195-201.

Sorensen, C.S. and SyljuÂsen, R.G. (2012) 'Safeguarding genome integrity: the checkpoint kinases ATR, CHK1 and WEE1 restrain CDK activity during normal DNA replication', Nucleic Acids Res, 40(2), pp. 477-86.

Southgate, H.E.D., Chen, L., Tweddle, D.A. and Curtin, N.J. (2020) 'ATR Inhibition Potentiates PARP Inhibitor Cytotoxicity in High Risk Neuroblastoma Cell Lines by Multiple Mechanisms', Cancers (Basel), 12(5).

Spagnolo, L., Rivera-Calzada, A., Pearl, L.H. and Llorca, O. (2006) 'Three-dimensional structure of the human DNA-PKcs/Ku70/Ku80 complex assembled on DNA and its implications for DNA DSB repair', Mol Cell, 22(4), pp. 511-9.

Srivastava, S., Tong, Y.A., Devadas, K., Zou, Z.Q., Chen, Y., Pirollo, K.F. and Chang, E.H. (1992) 'The status of the p53 gene in human papilloma virus positive or negative cervical carcinoma cell lines', Carcinogenesis, 13(7), pp. 1273-5.

Stodtmann, S., Nuthalapati, S., Eckert, D., Kasichayanula, S., Joshi, R., Bach, B.A., Mensing, S., Menon, R. and Xiong, H. (2021) 'A Population Pharmacokinetic Meta-Analysis of Veliparib, a PARP Inhibitor, Across Phase 1/2/3 Trials in Cancer Patients', J Clin Pharmacol, 61(9), pp. 1195-1205.

Stover, E.H., Konstantinopoulos, P.A., Matulonis, U.A. and Swisher, E.M. (2016) 'Biomarkers of Response and Resistance to DNA Repair Targeted Therapies', Clin Cancer Res, 22(23), pp. 5651-5660.

Stoepker, C., Faramarz, A., Rooimans, M.A., van Mil, S.E., Balk, J.A., Velleuer, E., Ameziane, N., Te Riele, H. and de Winter, J.P. (2015) 'DNA helicases FANCM and DDX11 are determinants of PARP inhibitor sensitivity', DNA Repair (Amst), 26, pp. 54-64.

Sultana, R., Abdel-Fatah, T., Perry, C., Moseley, P., Albarakti, N., Mohan, V., Seedhouse, C., Chan, S. and Madhusudan, S. (2013) 'Ataxia telangiectasia mutated and Rad3 related (ATR) protein kinase inhibition is synthetically lethal in XRCC1 deficient ovarian cancer cells', PLoS One, 8(2), p. e57098.

Sung, H., Ferlay, J., Siegel, R.L., Laversanne, M., Soerjomataram, I., Jemal, A. and Bray, F. (2021) 'Global Cancer Statistics 2020: GLOBOCAN Estimates of Incidence and Mortality Worldwide for 36 Cancers in 185 Countries', CA Cancer J Clin, 71(3), pp. 209-249.

Syljuåsen, R.G., Sørensen, C.S., Hansen, L.T., Fugger, K., Lundin, C., Johansson, F., Helleday, T., Sehested, M., Lukas, J. and Bartek, J. (2005) 'Inhibition of human Chk1 causes increased initiation of DNA replication, phosphorylation of ATR targets, and DNA breakage', Mol Cell Biol, 25(9), pp. 3553-62.

Swisher, E.M., Lin, K.K., Oza, A.M., Scott, C.L., Giordano, H., Sun, J., Konecny, G.E., Coleman, R.L., Tinker, A.V., O'Malley, D.M., Kristeleit, R.S., Ma, L., Bell-McGuinn, K.M., Brenton, J.D., Cragun, J.M., Oaknin, A., Ray-Coquard, I., Harrell, M.I., Mann, E., Kaufmann, S.H., Floquet, A., Leary, A., Harding, T.C., Goble, S., Maloney, L., Isaacson, J., Allen, A.R., Rolfe, L., Yelensky, R., Raponi, M. and McNeish, I.A. (2017) 'Rucaparib in relapsed, platinum-sensitive high-grade ovarian carcinoma (ARIEL2 Part 1): an international, multicentre, open-label, phase 2 trial', Lancet Oncol, 18(1), pp. 75-87.

Tang, H., Liu, Y., Wang, X., Guan, L., Chen, W., Jiang, H. and Lu, Y. (2018) 'Clear cell carcinoma of the ovary: Clinicopathologic features and outcomes in a Chinese cohort', Medicine (Baltimore), 97(21), p. e10881.

Thada, V. and Cortez, D. (2019) 'Common motifs in ETAA1 and TOPBP1 required for ATR kinase activation', J Biol Chem, 294(21), pp. 8395-8402.

Theriault, B.L., Portelance, L., Mes-Masson, A.M. and Nachtigal, M.W. (2013) 'Establishment of primary cultures from ovarian tumor tissue and ascites fluid', Methods Mol Biol, 1049, pp. 323-36.

Thomas, A., Redon, C.E., Sciuto, L., Padiernos, E., Ji, J., Lee, M.J., Yuno, A., Lee, S., Zhang, Y., Tran, L., Yutzy, W., Rajan, A., Guha, U., Chen, H., Hassan, R., Alewine, C.C., Szabo, E., Bates, S.E., Kinders, R.J., Steinberg, S.M., Doroshow, J.H., Aladjem, M.I., Trepel, J.B. and Pommier, Y. (2018) 'Phase I Study of ATR Inhibitor M6620 in Combination With Topotecan in Patients With Advanced Solid Tumors', J Clin Oncol, 36(16), pp. 1594-1602.

Thompson, L.H., Fong, S. and Brookman, K. (1980) 'Validation of conditions for efficient detection of HPRT and APRT mutations in suspension-cultured Chinese hamster ovary cells', Mutat Res, 74(1), pp. 21-36.

Toledo, L.I., Murga, M., Zur, R., Soria, R., Rodriguez, A., Martinez, S., Oyarzabal, J., Pastor, J., Bischoff, J.R. and Fernandez-Capetillo, O. (2011) 'A cell-based screen identifies ATR inhibitors with synthetic lethal properties for cancer-associated mutations', Nat Struct Mol Biol, 18(6), pp. 721-7.

Tominaga, Y., Li, C., Wang, R.H. and Deng, C.X. (2006) 'Murine Wee1 plays a critical role in cell cycle regulation and pre-implantation stages of embryonic development', Int J Biol Sci, 2(4), pp. 161-70.

Vítor, A.C., Huertas, P., Legube, G. and de Almeida, S.F. (2020) 'Studying DNA Double-Strand Break Repair: An Ever-Growing Toolbox', Front Mol Biosci, 7, p. 24.
Weber, A.M. and Ryan, A.J. (2015) 'ATM and ATR as therapeutic targets in cancer', Pharmacol Ther, 149, pp. 124-38.

Wang, Y., Li, J., Booher, R.N., Kraker, A., Lawrence, T., Leopold, W.R. and Sun, Y. (2001) 'Radiosensitization of p53 mutant cells by PD0166285, a novel G(2) checkpoint abrogator', Cancer Res, 61(22), pp. 8211-7.

Weaver, A.N., Cooper, T.S., Rodriguez, M., Trummell, H.Q., Bonner, J.A., Rosenthal, E.L. and Yang, E.S. (2015) 'DNA double strand break repair defect and sensitivity to poly ADP-ribose polymerase (PARP) inhibition in human papillomavirus 16-positive head and neck squamous cell carcinoma', Oncotarget, 6(29), pp. 26995-7007.

Wei, H. and Yu, X. (2016) 'Functions of PARylation in DNA Damage Repair Pathways', Genomics Proteomics Bioinformatics, 14(3), pp. 131-139.

Williamson, C.T., Miller, R., Pemberton, H.N., Jones, S.E., Campbell, J., Konde, A., Badham, N., Rafiq, R., Brough, R., Gulati, A., Ryan, C.J., Francis, J., Vermulen, P.B., Reynolds, A.R., Reaper, P.M., Pollard, J.R., Ashworth, A. and Lord, C.J. (2016) 'ATR inhibitors as a synthetic lethal therapy for tumours deficient in ARID1A', Nat Commun, 7, p. 13837.

Wilson, A.J., Sarfo-Kantanka, K., Barrack, T., Steck, A., Saskowski, J., Crispens, M.A. and Khabele, D. (2016) 'Panobinostat sensitizes cyclin E high, homologous recombination-proficient ovarian cancer to olaparib', Gynecol Oncol, 143(1), pp. 143-151

Wyatt, D.W., Feng, W., Conlin, M.P., Yousefzadeh, M.J., Roberts, S.A., Mieczkowski, P., Wood, R.D., Gupta, G.P. and Ramsden, D.A. (2016) 'Essential Roles for Polymerase θ-Mediated End Joining in the Repair of Chromosome Breaks', Mol Cell, 63(4), pp. 662-673.

Xiong, Y., Li, T., Assani, G., Ling, H., Zhou, Q., Zeng, Y., Zhou, F. and Zhou, Y. (2019) 'Ribociclib, a selective cyclin D kinase 4/6 inhibitor, inhibits proliferation and induces apoptosis of human cervical cancer in vitro and in vivo', Biomed Pharmacother, 112, p. 108602.

Xu, H., George, E., Kinose, Y., Kim, H., Shah, J.B., Peake, J.D., Ferman, B., Medvedev, S., Murtha, T., Barger, C.J., Devins, K.M., D'Andrea, K., Wubbenhorst, B., Schwartz, L.E., Hwang, W.T., Mills, G.B., Nathanson, K.L., Karpf, A.R., Drapkin, R., Brown, E.J. and Simpkins, F. (2021) 'copy number is a biomarker for response to combination WEE1-ATR inhibition in ovarian and endometrial cancer models', Cell Rep Med, 2(9), p. 100394.

Yamulla, R.J., Nalubola, S., Flesken-Nikitin, A., Nikitin, A.Y. and Schimenti, J.C. (2020) 'Most Commonly Mutated Genes in High-Grade Serous Ovarian Carcinoma Are Nonessential for Ovarian Surface Epithelial Stem Cell Transformation', Cell Rep, 32(9), p. 108086.

Yao, Y. and Dai, W. (2014) 'Genomic Instability and Cancer', J Carcinog Mutagen, 5.
Yeo, C.Q.X., Alexander, I., Lin, Z., Lim, S., Aning, O.A., Kumar, R., Sangthongpitag, K., Pendharkar, V., Ho, V.H.B. and Cheok, C.F. (2016) 'p53 Maintains Genomic Stability by Preventing Interference between Transcription and Replication', Cell Rep, 15(1), pp. 132-146.

Yazinski, S.A., Comaills, V., Buisson, R., Genois, M.M., Nguyen, H.D., Ho, C.K., Todorova Kwan, T., Morris, R., Lauffer, S., Nussenzweig, A., Ramaswamy, S., Benes, C.H., Haber, D.A., Maheswaran, S., Birrer, M.J. and Zou, L. (2017) 'ATR inhibition disrupts rewired homologous recombination and fork protection pathways in PARP inhibitor-resistant BRCA-deficient cancer cells', Genes Dev, 31(3), pp. 318-332.

Yin, Y., Shen, Q., Zhang, P., Tao, R., Chang, W., Li, R., Xie, G., Liu, W., Zhang, L., Kapoor, P., Song, S., Ajani, J., Mills, G.B., Chen, J., Tao, K. and Peng, G. (2017) 'Chk1 inhibition potentiates the therapeutic efficacy of PARP inhibitor BMN673 in gastric cancer', Am J Cancer Res, 7(3), pp. 473-483.

Appendix A

Expert Reviews in Molecular Medicine

cambridge.org/erm

Review

Cite this article: Smith HL, Southgate H, Tweddle DA, Curtin NJ (2020). DNA damage checkpoint kinases in cancer. *Expert Reviews in Molecular Medicine* **22**, e2, 1–15. https://doi.org/10.1017/erm.2020.3

Received: 21 August 2019
Revised: 25 February 2020
Accepted: 23 March 2020

Key words:
ATM; ATR; CDK1; CDK2; cell cycle; CHK1; CHK2; DNA damage response; p53; WEE1

Author for correspondence:
Nicola J. Curtin,
E-mail: nicola.curtin@ncl.ac.uk

© The Author(s), 2020. Published by Cambridge University Press

CAMBRIDGE UNIVERSITY PRESS

DNA damage checkpoint kinases in cancer

Hannah L. Smith[1], Harriet Southgate[2], Deborah A. Tweddle[2] and Nicola J. Curtin[1]

[1]Newcastle Centre for Cancer Faculty of Medical Sciences, Newcastle University, Newcastle upon Tyne, NE2 4HH, UK and [2]Wolfson Childhood Cancer Research Centre, Newcastle Centre for Cancer, Faculty of Medical Sciences, Newcastle University, Newcastle upon Tyne, NE1 7RU, UK

Abstract

DNA damage response (DDR) pathway prevents high level endogenous and environmental DNA damage being replicated and passed on to the next generation of cells via an orchestrated and integrated network of cell cycle checkpoint signalling and DNA repair pathways. Depending on the type of damage, and where in the cell cycle it occurs different pathways are involved, with the ATM-CHK2-p53 pathway controlling the G1 checkpoint or ATR-CHK1-Wee1 pathway controlling the S and G2/M checkpoints. Loss of G1 checkpoint control is common in cancer through *TP53*, *ATM* mutations, Rb loss or cyclin E overexpression, providing a stronger rationale for targeting the S/G2 checkpoints. This review will focus on the ATM-CHK2-p53-p21 pathway and the ATR-CHK1-WEE1 pathway and ongoing efforts to target these pathways for patient benefit.

Introduction

The DNA damage response (DDR) is essential to maintain genomic integrity in the face of a continuous onslaught of DNA damage from endogenous and environmental sources. Activation of this response involves the close coordination of DNA repair pathways and signalling to cell cycle arrest to allow repair and prevent DNA damage being copied (G1 and S-phase checkpoint) or transmitted to the next generation (G2/M checkpoint). The kinases ataxia-telangiectasia mutated (ATM) and ataxia-telangiectasia mutated and rad3 related (ATR) are DNA damage sensors that are at the apex of a phosphorylation and dephosphorylation cascade signalling to both cell cycle arrest via inactivation of cyclin-dependent kinases (CDKs) (Fig. 1), and DNA repair. ATM and ATR have overlapping but non-redundant activities with substantial cross-talk between the two pathways (Ref. 1). This review will describe the role of these signalling cascades and the development of drugs targeting them for anti-cancer therapy.

The role of ATM/CHK2 pathway in cell cycle checkpoints

ATM is activated in response to DNA double-strand breaks (DSBs) (Ref. 2). In undamaged cells, ATM exists as a dimer. Upon recruitment by the MRE11/RAD50/NBS1 (MRN) complex to DSBs, ATM autophosphorylates at serine 367 (ser367), serine 1893 (ser1893), serine 1981 (ser1981) and serine 2996 (ser2996) resulting in monomerisation and activation (Refs 3, 4). Active ATM phosphorylates many target proteins regulating DNA repair, cell cycle arrest and apoptosis including CHK2, p53 and H2AX (Ref. 5). ATM plays a crucial role in the activation of the G1/S cell cycle checkpoint, primarily mediated through p53 activity. The most important transducer of ATM signalling is CHK2, a kinase that signals to DNA repair, cell cycle arrest and apoptosis. ATM phosphorylates CHK2 on threonine 68 (thr68) causing CHK2 dimerisation and autophosphorylation of the kinase domain, required for full activation (Ref. 6).

Active CHK2 phosphorylates the Cdc25A and Cdc25C phosphatases, which results in their inactivation/degradation. This promotes cell cycle arrest as active cdc25A/C remove inhibitory phosphorylation on CDKs that drive cell cycle progression. Cdc25A dephosphorylates CDK2, promoting progression into S phase. Cdc25C also dephosphorylates CDK1, which is usually held in the inactive state via phosphorylation by WEE1 and Myt1, promoting the transition into M phase (Refs 1, 7, 8). Although ATM can signal to G2 arrest via CHK2, the cell cycle defects observed in ATM-deficient cells are primarily G1/S checkpoint deficiency (Refs 9–11).

CHK2 also causes cell cycle arrest by phosphorylating the tumour suppressor p53 on ser15 and ser20 resulting in p53 stabilisation and activation (Ref. 12). p53 is a transcription factor which, when active, initiates the transcription of genes involved in DNA repair, cell cycle arrest, apoptosis and metabolism as well as its own negative regulators (Ref. 13) for example, mouse double minute 2 (MDM2), a ubiquitin ligase that targets p53 for degradation (Ref. 14). In response to DNA damage, p53 is phosphorylated by many kinases including ATR and CHK1 as well as ATM and CHK2, contributing to cross-talk between the two pathways. This phosphorylation blocks the interaction between p53 and MDM2 leading to p53 protein accumulation (Ref. 15). Active p53 promotes the transcription of *CDKN1A*, which encodes the cyclin-dependent kinase inhibitor $p21^{CIP1/WAF1}$ (Ref. 16). p21 mediates p53-dependent G1 cell cycle arrest (Refs 17, 18). p53 activation also leads to the transcription of pro-apoptotic genes including *Puma*, *Noxa*, *BAX* and *Apaf1*, resulting in apoptotic cell death if the damage is sustained (Ref. 19). The regulation of p53-mediated G1 checkpoint arrest and/or apoptosis by the

Downloaded from https://www.cambridge.org/core. Newcastle University, on 15 Feb 2022 at 13:26:48, subject to the Cambridge Core terms of use, available at https://www.cambridge.org/core/terms. https://doi.org/10.1017/erm.2020.3

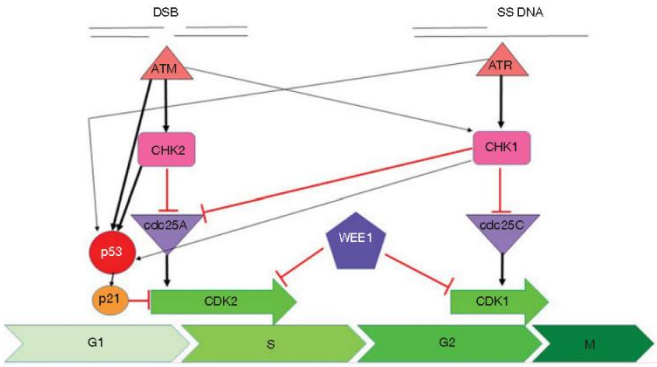


Fig. 1. Cell cycle checkpoint signalling. DNA double-strand breaks activate ATM, which phosphorylates and activates CHK2, which phosphorylates and inactivates cdc25A, preventing it from removing the inactivating phosphate on CDK2 thereby inhibiting S-phase entry and progression. Both ATM and CHK2 phosphorylate p53 resulting in transactivation of p21 to inhibit CDK2. SS-DNA (e.g. at stalled replication forks) activates ATR, which phosphorylates and activates CHK1, which phosphorylates and inactivates cdc25c, preventing it from removing the inactivating phosphate on CDK1 thereby inhibiting G2/M progression. There is substantial cross-talk between the two pathways with CHK1 also being a target of ATM and cdc25A a target of CHK1 and both ATR and CHK1 targeting p53. In addition, DNA damage activates WEE1 which phosphorylates and inactivates both CDK1 and CDK2. Black arrows indicate main activation pathways, grey ones are secondary pathways and red lines indicate inhibition.

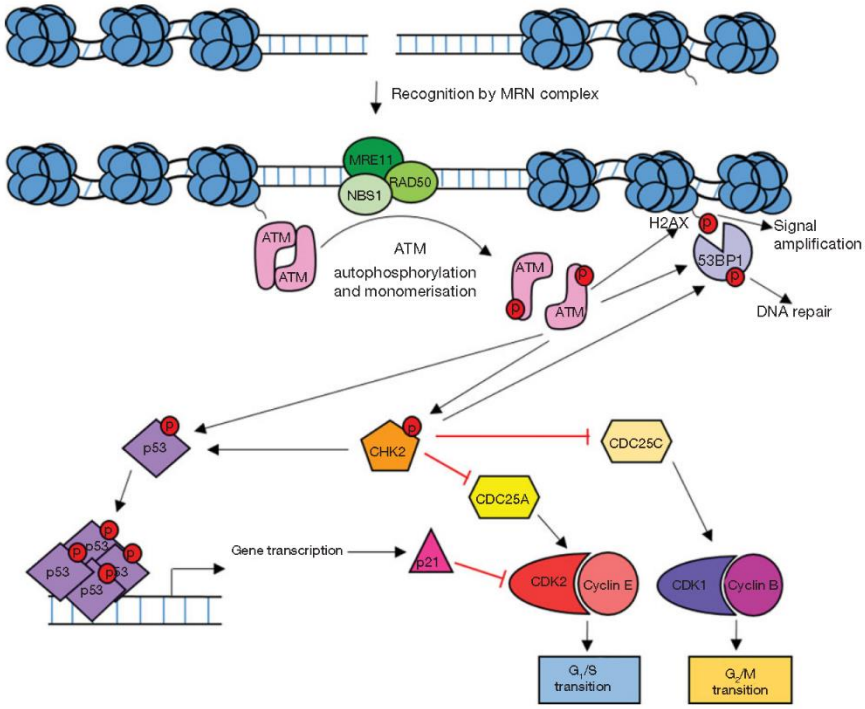


Fig. 2. Overview of ATM signalling in response to DNA damage. DNA double-strand breaks are recognised by the MRE11/RAD50/NBS1 (MRN) complex which recruits ATM leading to ATM activation. Active ATM phosphorylates the histone variant H2AX (γH2AX) leading to amplification and spreading of the damage signal. ATM-dependent phosphorylation of p53 and CHK2 leads to the activation of DNA repair processes and cell cycle arrest. Active p53 induces G_1 arrest through transcriptional activation of the CDKN1A gene which codes for the cyclin-dependent kinase (CDK) inhibitor p21. Active CHK2 also phosphorylates p53 as well as CDC25 phosphatases resulting in S and G_2 arrest. 53BP1 is recruited to γH2AX and phosphorylated by ATM and CHK2 leading to DNA repair.

DDR kinases is likely dependent on the context of the DNA damage, such as the type of DNA damage, cell cycle phase and molecular pathology of the cell type in question.

Figure 2 illustrates how the ATM/CHK2/p53 signalling pathway leads to cell cycle arrest and the maintenance of genome integrity. This pathway suppresses tumorigenesis and as a consequence, defects are often observed in cancer.

Role of ATM/CHK2 in DNA repair

Although not essential for the repair of the majority of DSBs, ATM activity is required for the repair of a subset of DSBs generally associated with heterochromatin (Ref. 20). In response to DNA DSBs and stalled replication forks the variant histone H2AX is phosphorylated at ser139 by DNA-PK, ATM and ATR resulting in the accumulation of γH2AX in the vicinity of the

Downloaded from https://www.cambridge.org/core. Newcastle University, on 15 Feb 2022 at 13:26:48, subject to the Cambridge Core terms of use, available at https://www.cambridge.org/core/terms. https://doi.org/10.1017/erm.2020.3

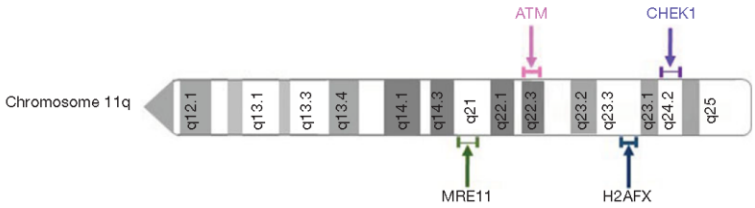


Fig. 3. Location of frequently deleted DNA damage response genes on chromosome 11q.

DNA lesion. In *ATM*-deficient cells, around 10–15% of DNA damage foci, identified by antibodies against γH2AX, are retained 72 hours after ionising radiation (IR) (Ref. 21). γH2AX recruits mediator of DNA damage checkpoint 1 (MDC1) (Ref. 22). Phosphorylation by ATM stabilises MDC1 on chromatin where it acts as a molecular scaffold recruiting chromatin modifiers to relax heterochromatin in the vicinity of the DSB (Ref. 23). More MRN complexes are recruited to the site of the DSB by the interaction between MDC1 and NBS1, which in turn recruits and activates further ATM kinases, resulting in amplification of the signal along chromatin (Refs 24, 25). ATM activation promotes DNA repair indirectly via both non-homologous end joining (NHEJ) and homologous recombination DNA repair (HRR), two prominent DSB repair pathways. ATM-dependent phosphorylation of 53BP1 recruited to damage markers on chromatin prevents DSB end resection, promoting NHEJ (Ref. 26). Conversely, ATM and CHK2 phosphorylate BRCA1 at the site of DNA damage (Ref. 27). BRCA1 plays a critical role in the initiation of HRR (described in the section 'Role in DNA repair') (Ref. 28). 53BP1 and BRCA1 show mutual antagonism and, although both proteins are present throughout the cell cycle, pathway dominance is largely governed by the cell cycle stage and cyclin-CDK activity (Refs 29, 30).

In addition to BRCA1, ATM-mediated regulation of nucleases is required for efficient DNA end resection and activation of ATR at DSBs (Refs 31, 32). ATR signalling is discussed in the section 'Role of ATR-CHK1-WEE1 in cell cycle checkpoints'. However, a direct role of ATM in DNA repair is unclear as ATM is dispensable for the repair of the majority of DNA DSBs, although it has an important role in initiating the chromatin remodelling cascade induced by phosphorylation of histone H2AX, and signalling to cell cycle checkpoint arrest (Ref. 22).

Pathway dysfunction in cancer

Aberrations in the *ATM* gene are commonly seen in cancer. Homozygous germline mutations in *ATM* result in ataxia telangiectasia (A-T), a well characterised recessive genetic disease which predisposes to the development of cancer (Ref. 33). Somatic mutations of *ATM* have been identified in many cancer types, most commonly lymphoid malignancies, suggesting that ATM loss contributes to tumorigenesis (Ref. 34). Loss of ATM expression has also been observed in many cancer types including colorectal cancer, breast cancer, non-small cell lung cancer, lung adenocarcinoma and pancreatic cancer (Refs 35–39). In addition to *ATM* mutation, *ATM* loss of heterozygosity (LOH) may arise through deletion of the long arm of chromosome 11 (11q). Interestingly, other DDR components are often co-deleted with *ATM*. Genes encoding MRE11, CHK1 and the histone variant H2AX are also located on chromosome 11q (Fig. 3), and are frequently deleted with ATM (Refs 40, 41). Allelic deletion of these genes may contribute to DNA damage repair deficiencies which could be targeted therapeutically. 11q deletion is commonly observed in breast cancer, chronic lymphocytic leukaemia (CLL), other lymphoid malignancies, and childhood neuroblastoma and is associated with poor survival (Refs 41–43).

CHK2 mutations, although less common than mutations in ATM, are also observed across cancer types including colon, kidney, breast and prostate cancer (Ref. 44). Homozygous germline *CHK2* mutation is rare and manifests in Li-Fraumeni syndrome, a cancer predisposition syndrome usually associated with mutations in the gene encoding p53, *TP53* (Ref. 45). Somatic mutations in *CHK2* have been observed across the entire amino acid sequence and lead to functionally null or unstable CHK2 protein.

The most commonly mutated gene across cancer types is *TP53*, which codes for the p53 protein. Around 80% of patients with Li-Fraumeni patients have germline mutations of *TP53* (Ref. 46). Somatic *TP53* mutations are observed in around 40% of all tumours (Refs 47, 48), the mutation rate varying between cancer types from nearly 100% in ovarian cancer to <10% for haematological malignancies (Ref. 47). Mutations in *TP53* result in a spectrum of p53 mutant proteins, from classical loss of transcriptional function to gain of function mutants which alter transcriptional networks and promote an oncogenic phenotype (Ref. 49).

As with *ATM*, *TP53* loss of heterozygosity through allelic deletion of chromosome 17p is frequently observed in cancer (Ref. 50). Loss of 17p is often accompanied by mutation of the other *TP53* allele, although 17p deletion alone has been shown to predict poor prognosis in some myeloid malignancies (Refs 51, 52).

Overall aberration in the ATM/CHK2/p53 axis frequently occurs in cancer. Targeting cancer-specific defects in this pathway could contribute to effective cancer treatments with reduced side effects.

Rationale for the development of inhibitors

Neither ATM nor CHK2 kinases are essential for life, indicating some redundancy with other DNA damage signalling and repair pathways.

In humans, *ATM* mutations lead to the autosomal recessive disease A-T. A-T patients are very radiosensitive and display increased adverse and sometimes fatal reactions to both radiotherapy and radio-mimetic chemotherapy (Ref. 33). In addition to the identification of *ATM* mutations in cancer (discussed in the section 'Pathway dysfunction in cancer'), heterozygous carriers also have an increased risk of developing cancer, particularly breast and lymphoid (Refs 34, 53). $ATM^{-/-}$ mice are viable and display many features of A-T including cerebellar dysfunction, infertility, radio-sensitivity and cancer predisposition (Refs 54, 55). Targeting ATM with small molecule inhibitors should sensitise cells to radio- and chemotherapy thus reducing the dose required and reducing off-target toxicities of these treatments. However,

Downloaded from https://www.cambridge.org/core. Newcastle University, on 15 Feb 2022 at 13:26:48, subject to the Cambridge Core terms of use, available at https://www.cambridge.org/core/terms.
https://doi.org/10.1017/erm.2020.3

systemic ATM inhibition could also lead to increased toxicity from chemotherapy agents. For example, combining chemotherapy with other DDR inhibitors, such as MGMT and PARP inhibitors, led to dose reductions of both the chemotherapy and DDR inhibitors owing to increased toxicity (Refs 56, 57). Radiotherapy is more targeted towards the tumour and as techniques become more precise with improving technology. ATM inhibitors may be particularly useful in this context.

CHK2 kinase is also not essential. *CHK2* knockout (KO) mice show little to no phenotype but, in contrast to ATM KO, are resistant to ionising radiation (IR) and have defects in p53-mediated apoptosis pathways (Ref. 58). However, cancer-prone phenotypes associated with the absence of CHK2 become apparent when other DDR genes, such as *CHK1*, *MRE11* and *NBS1*, are impaired (Ref. 59). $CHK1^{+/-}$ $CHK2^{-/-}$ mice show high levels of spontaneous damage and decreased apoptotic responses, increasing cancer susceptibility showing some degree of co-operation and redundancy. Overall, the context in which CHK2 inhibitors will have therapeutic benefit remains unclear.

Preclinical development of ATM inhibitors

Many small-molecule ATP-competitive inhibitors of ATM have been developed and generally act as radiosensitisers *in vitro* (Ref. 60). The first described potent and specific ATM inhibitor, KU55933, was developed by KuDos pharmaceuticals (now part of AstraZeneca) (Ref. 61). It enhanced the cytotoxicity of IR and topoisomerase I and II poisons, but its poor aqueous solubility and *in vivo* bio-availability precluded advanced preclinical testing. KU60019, a structural derivative of KU55933 with improved potency and aqueous solubility, effectively radiosensitised glioblastoma *in vivo* when directly injected into the tumour (Ref. 62), but still had poor *in vivo* bioavailability (Ref. 1). KU60019 caused greater radiosensitisation in p53 deficient tumours. However, using KU59403, another derivative of KU55933, in matched p53 functional and dysfunctional cell lines showed that the radio- and chemosensitising effects of ATM inhibition was not p53 dependent (Ref. 63). While the pharmacodynamic properties of KU59403 were still not suitable for oral administration, systemic *in vivo* studies in mice were carried out by intraperitoneal injection. As well as sensitizing to IR, KU59403 also sensitised tumours to topoisomerase I and II inhibitors, irinotecan and etoposide respectively, *in vivo*.

AZ32 is a moderately potent ATM inhibitor discovered by chemical library screening at AstraZenena. The chemistry is different from that of the KuDos compounds and has been shown to be orally bioavailable as well as capable of crossing the blood-brain barrier in mice (Ref. 64). *In vivo* optimisation of AZ32 led to the development of AZD1390 sensitised brain tumours to radiotherapy in preclinical models justifying translation into a clinical trial (section 'Clinical trials with ATM and CHK2 inhibitors') (Ref. 65).

In addition to AZD1390, the compound AZD0156 was developed by AstraZeneca following optimisation of a different lead scaffold (Ref. 66). AZD0156 shows good pharmacodynamic properties and is synergistic with the topoisomerase I inhibitor irinotecan and the PARP inhibitor olaparib in tumour xenograft models. AZD0156 has also entered a phase 1 clinical trial.

CP-466722, another selective ATM inhibitor, was identified by Pfizer and showed similar radio-sensitising properties to KU55933 (Ref. 67). *In vivo* studies were not possible because of the compound having a short half-life in mice ($t_{1/2} < 1$ hour).

In 2017, Dohmen *et al.* identified GSK635416A as a novel radio-sensitiser in non-small cell lung cancer (NSCLC) cell lines from a screen of published GlaxoSmithKline protein kinase inhibitors, which was shown to act through inhibition of ATM (Ref. 68). When combined with the PARP inhibitor olaparib, GSK635416A showed an additive radio-sensitizing effect. No *in vivo* studies have been published for this compound to date.

Preclinical development of CHK2 inhibitors

In contrast to CHK1 inhibitors, few CHK2-specific inhibitors have been developed. In general, they show modest anti-proliferative effects when compared with ATM, ATR and CHK1 kinase inhibitors (Ref. 69).

A screen of the AstraZeneca compound library yielded AZD7762 as a potent CHK1 inhibitor with equal potency against CHK2 (Ref. 70). This dual inhibitor will be discussed with other CHK1 inhibitors in the section 'Preclinical development of CHK1 inhibitors'.

A 2-arylbenzamidazole compound (ABI) was the first CHK2-specific inhibitor to be proposed, showing high selectivity (IC50 = 15 nM) over CHK1 (IC50 > 10 μM) (Ref. 71). However, CHK2 inhibition in cells by ABI was greatly reduced compared with cell-free assays achieving 42% inhibition of CHK2 at 5 μM. When used as a tool, the compound showed dose-dependent *radioprotection* in human CD4+ and CD8+ T-cells, similar to the radioresistance of CHK2 null mice.

Attenuation of IR-induced apoptosis was seen in mouse thymocytes after treatment with three other structurally distinct CHK2 inhibitors, VRX0466617 (Ref. 72), PV1019 (Ref. 73) and CCT241533 (Ref. 74). Another CHK2 inhibitor, BML-277 (CHK2 inhibitor II), first disclosed by Arienti *et al.* (Ref. 71), was shown to be radioprotective in human glioma cell lines (Ref. 75). These data are consistent with the observation that CHK2 KO mice are radioresistant (section 'Rationale for the development of inhibitors' (Ref. 58)). Studies in HT-29 (human colon cancer) cells and HeLa (human cervical cancer) cells treated with CCT241533 failed to show any impact on the radiomimetic bleomycin cytotoxicity (Ref. 76). Interestingly, BML-277 antagonised oxaloplatin cytoxicity in colorectal cancer cell lines (Ref. 77). In contrast, survival analysis by colony formation assay in U251 human glioblastoma cell line showed potentiation of IR by PV1019. Whether these contrasting observations reflect the differing molecular pathology of the cell lines remains to be determined.

Although the role of CHK2 inhibition in response to IR is unclear, there is some evidence that the combination of CHK2i with topoisomerase I poisons and poly (ADP)-ribose polymerase (PARP) inhibitors might be effective. PV1019 was shown to potentiate the cytotoxic effects of topotecan and camptothecin in ovarian cancer cell lines (Ref. 73). Potentiation of the effects of the PARP inhibitors rucaparib and olaparib was seen with the addition of CCT241533 (Ref. 76).

Clinical trials with ATM and CHK2 inhibitors

Three ATM inhibitors are currently being investigated in phase 1 clinical trials (Table 1). To date, no specific CHK2 inhibitor has progressed to clinical trials but phase 1 studies of AZD7762, the dual CHK1/CHK2 inhibitor have been undertaken in combination with gemcitabine. The results published from the completed trial showed that AZD7762 leads to cardiac toxicity leading to 2 further trials being terminated and the clinical progression of the inhibitor being discontinued (Ref. 78).

Role of ATR-CHK1-WEE1 in cell cycle checkpoints

The ATR-CHK1-WEE1 pathway activates both intra-S and G2/M checkpoint control in response to replication stress (RS) and DNA damage. RS is the momentary slowing or stalling of replication fork progression that can be caused by replication outstripping the rate of dNTP production or lesions in the DNA. ATR is

Downloaded from https://www.cambridge.org/core. Newcastle University, on 15 Feb 2022 at 13:26:48, subject to the Cambridge Core terms of use, available at https://www.cambridge.org/core/terms.
https://doi.org/10.1017/erm.2020.3

Table 1. ATM inhibitors currently in clinical trials

Drug name	Phase	Monotherapy/combination	Tumour type	NCT
M3541	I	In combination with palliative radiotherapy	Solid tumour	NCT03225105
AZD0156	I	In combination with olaparib, irinotecan, fluorouracil, folinic acid	Advanced solid tumours	NCT02588105
AZD1390	I	In combination with radiotherapy	Brain cancer	NCT03423628

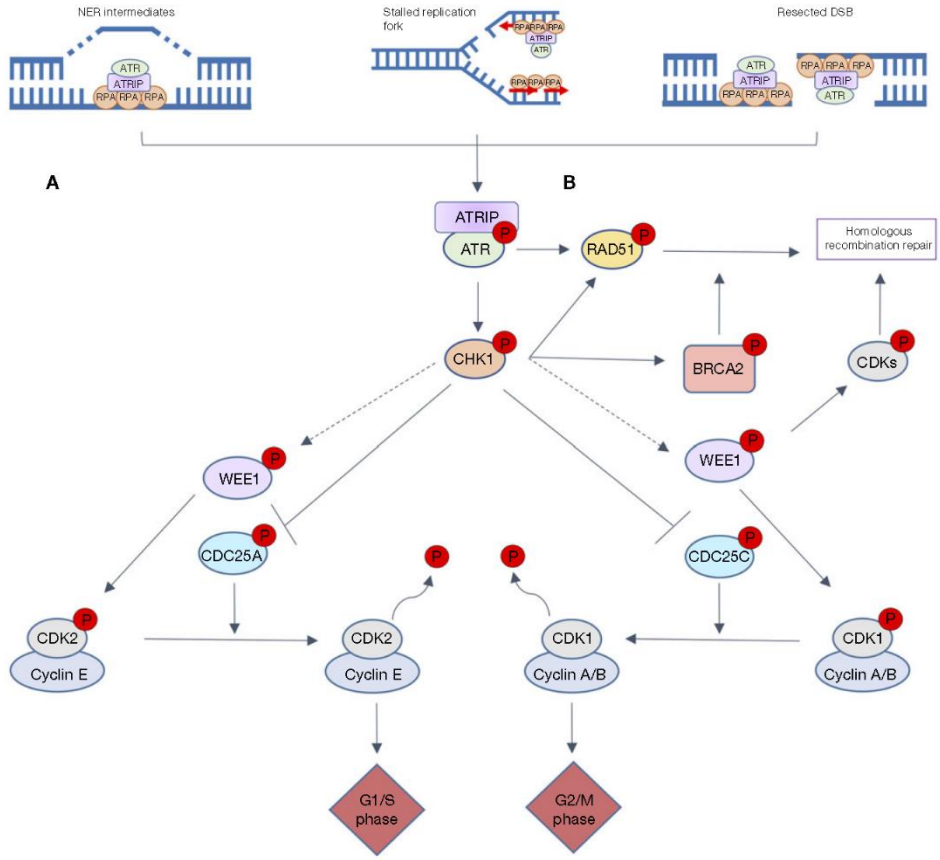


Fig. 4. Overview of ATR signalling in response to DNA damage. Resected double-strand breaks (DSBs), stalled replication forks and NER intermediates all lead to replication protein A (RPA) recruiting ATR via ATR-interacting protein (ATRIP). **A.** The ATR-CHK1 cascade is heavily involved in cell cycle checkpoint control. ATR activates CHK1 which causes the inactivating phosphorylation of both CDC25C and CDC25A, hence preventing the removal of inhibitory phosphorylation on CDK1 and 2, respectively. These lesions also activate WEE1, directly or via CHK1 (dashed grey arrows) to phosphorylate and inactivate CDK1 and 2. Progression through cell cycle G1/s and G2/M phases is reliant upon activation of CDK2/cyclin E and CDK1/cyclin A/B complexes, respectively. When WEE1 CHK1 or ATR are inhibited, CDK1 and CDK2 are activated so S-phase progression and mitotic entry occur with no delay to allow DNA repair. **B.** ATR, CHK1 and WEE1 also signal to key proteins involved in homologous recombination repair (HRR). ATR promotes repair protein RAD51 recruitment to DSBs and stalled replication forks, independent of BRCA. CHK1 phosphorylates key HRR proteins BRCA2 and RAD51. When activated WEE1 inhibitory phosphorylates CDKs, which play a key role in HRR end resection.

activated by a number of DNA damaging factors, including ultraviolet radiation, antimetabolite-induced dNTP depletion, topoisomerase poisons, alkylating agents or DNA crosslinking agents (Ref. 79). Many of these factors result in single-strand DNA (ss-DNA), which allows for the recruitment of ATR activating proteins TOPBP1 or ETAA1. Although ss-DNA arises primarily from RS it is also a result of resected DSBs and nucleotide excision repair (NER) intermediates. Replication protein A (RPA) coats the ss-DNA, protecting it from degradation and enabling recruitment of ATR via ATR-interacting protein (ATRIP). ATR is activated by either TOPBP1, which is recruited by interaction with MRN complex that resects DSB to give long ss-DNA overhangs and the 9-1-1 complex (a proliferating cell nuclear antigen (PCNA)-like clamp that binds SS-DS DNA

Downloaded from https://www.cambridge.org/core. Newcastle University, on 15 Feb 2022 at 13:26:48, subject to the Cambridge Core terms of use, available at https://www.cambridge.org/core/terms. https://doi.org/10.1017/erm.2020.3

junctions) or by ETAA1, which is recruited to ss-DNA by interaction with RPA (Ref. 80). Upon activation, ATR activates CHK1 by phosphorylation at serine 345 causing CHK1 to autophosphorylate at serine 296, to achieve full activation. Like CHK2, CHK1 causes the inactivating phosphorylation of CDC25A/C (Refs 81, 82), thereby preventing them from removing the inhibitory phosphorylation on CDK2 and 1, respectively (as described in Fig. 4). In yeast and xenopus, CHK1 phosphorylates and activates Wee1 kinase activity to phosphorylate, and hence inactivate, CDK 1 and 2 (Refs 83, 84). This is yet to be shown in mammalian cells. The net result of this kinase activation and phosphatase inhibition is inhibition of CDK2, and thus S-phase entry and progression, and inhibition of CDK1 preventing entry into mitosis.

Role in DNA repair

The ATR-CHK1-WEE1 cascade also plays a role in HRR, a high fidelity DSB repair pathway, restricted to late S and G2 phase as it uses the sister chromatid as a DNA template (Ref. 85). During HRR extensive DNA end-resection occurs, resulting in the ss-DNA overhang that leads to ATR activation. HRR is also responsible for the resolution of collapsed replication forks caused by RS – the prime activator of the ATR-CHK1-WEE1 pathway. It is therefore not surprising that these kinases are also associated with DNA repair by HRR (Ref. 86).

All three kinases in the cascade have demonstrated involvement in HRR. In *BRCA* defective cells, ATR can act independently of BRCA1 to recruit RAD51 to DSBs and stalled replication forks, inhibition of ATR disrupted RAD51 loading suggesting key involvement in HRR (Ref. 87). Similarly, CHK1 may promote HRR by phosphorylating key HRR components BRCA2 and RAD51 (Refs 81, 88). WEE1 is also involved in HRR owing to its inhibitory phosphorylation of CDKs upon activation. The resection of DNA ends, a necessary step in HRR is antagonised by CDK activity (Ref. 89), inhibition of CDK activity by WEE1 (or cdc25 inactivation downstream of CHK1) promotes HRR, therefore inhibition of either CHK1 or WEE1 will result in higher CDK activity and compromise HRR (Ref. 90).

Pathway dysfunction in cancer

The importance of the ATR-CHK1-WEE1 cascade is highlighted by the embryonic lethality of all three components (Refs 91–93). No humans are recorded as being born without these essential kinases but Seckel syndrome (SS) is a rare, autosomal recessive disorder owing to a hypomorphic mutation in *ATR*, resulting in delayed development but not cancer predisposition. SS mice are not cancer-prone, even when crossed with p53 defective mice (Ref. 94). There are contrasting data regarding the tumour predisposition of $ATR^{+/-}$ mice with one study reporting increased tumour incidence and others reporting no increase in tumour incidence (Refs 91, 95). $CHK1^{+/-}$ mice are not predisposed to tumourigenesis (Ref. 92), and no abnormalities are reported in adult $WEE1^{+/-}$ mice (Ref. 93).

The general consensus seems to be that complete loss of ATR, CHK1 or WEE1 signalling is incompatible with normal development but that compromising the pathway by hypomorphic mutation or heterozygous deletion does not predispose to tumour development. However, upregulation of the pathway in tumours may be indicators of poor prognosis. Two studies in breast cancer indicate that high pCHK1 levels correlated with local recurrence and worse cancer-specific survival (Refs 96, 97) and WEE1 overexpression have been observed in several tumour types: hepatocellular carcinoma (HCC), breast, glioblastoma, lung and colon (Ref. 98).

Rationale for targeting ATR-CHK1-WEE1

Cancer cells are considered to have higher levels of RS than normal cells. There are several causes for this: (i) increased expression of oncogenes or growth factor receptors that drive cells into S-phase, (ii) accelerated cell cycle progression owing to increased expression of CDKs or their cyclin partners or loss of their protein inhibitors, and (iii) loss of G1 checkpoint control (Refs 96–99). Additionally, RS results in genomic instability that is an enabling characteristic of cancer (Refs 100, 101), thereby creating a vicious circle. RS is the prime trigger for ATR-CHK1-WEE1 signalling and cancer cells are therefore highly dependent on this pathway (Refs 100, 102, 103). Thus, there is a potential to exploit the increased RS, coupled with the loss of G1 control, in cancer cells by targeting the ATR-CHK1-WEE1 pathway, without compromising normal cells with proficient G1 checkpoint control (Ref. 104).

In addition to their pivotal role in the S and G2/M cell cycle checkpoints, ATR-CHK1-WEE1 also promote HRR, as described above. Therefore, inhibiting these kinases has the potential to compromise HRR, thereby sensitising cells to DNA damaging anticancer agents.

Preclinical development of ATR inhibitors

An early study in 1998 found that overexpression of kinase-inactive ATR caused sensitivity to IR, cisplatin and methyl methanesulfonate (MMS) (Ref. 105). Caffeine was found to be a weak ATR inhibitor (1999) and, although it lacked specificity, it was still good enough to test the potential of ATR inhibition (Ref. 106). It was shown to inhibit ATR activity at a radio sensitising concentration (Ref. 107). Subsequently in 2002, Nghiem *et al.*, showed that expression of the kinase-dead ATR conferred sensitivity to multiple anti-cancer/DNA damaging agents (UV, hydroxyurea (HU), IR, cisplatin and aphidicolin). In terms of the potential of single-agent ATR inhibitors this study also showed that endogenous causes of replication stress (cyclin D, E, CDK2 overexpression or p53 inactivation by MDM2 or human papillomavirus (HPV) E6 expression) conferred sensitivity to kinase-dead ATR overexpression and/or caffeine (Ref. 108).

ATR inhibitor development was slow to take off from these early studies, possibly because of the difficulty in developing a cell-free assay. Nevertheless, in 2011, NU6027, originally developed as a CDK2 inhibitor, was found to be a more potent inhibitor of ATR that CDK2 in intact cells. NU6027 enhanced cisplatin and HU cytotoxicity in an ATR-dependent manner, and the major classes of DNA damaging anticancer drugs in MCF7 breast cancer cells, and attenuated G2 cell cycle arrest. Cells defective in HRR are exquisitely sensitive to PARP inhibitors and, in the first investigation of its kind, NU6027 inhibited HRR and increased PARP inhibitor cytotoxicity (Ref. 109).

In 2011 a novel ATRi screen identified ETP-46464 as an ATRi that had increased cytotoxicity in cells overexpressing cyclin E. It significantly sensitised cells to IR, abolishing the G2/M checkpoint in these cells, independent of p53 status (Ref. 110). In 2015, Teng *et al.*, went on to show that it also sensitised cells to cisplatin treatment (Ref. 111). However, ETP-46464 lacked specificity as it also inhibited mTOR, DNA-PKcs and P13Kα, and had poor *in vivo* pharmacological properties (Ref. 110).

AZ20 is an ATRi developed in 2013 from the P13K inhibitor, LY294002, with good potency and selectivity (Ref. 112). In acute myeloid leukaemia (AML) cell lines and patient samples, AZ20 acted synergistically with cytarabine, resulting in enhanced apoptosis and induced replication stress (Ref. 113). This drug also synergistically inhibited cell growth in combination with gemcitabine in pancreatic cancer cell lines (Ref. 114).

Downloaded from https://www.cambridge.org/core. Newcastle University, on 15 Feb 2022 at 13:26:48, subject to the Cambridge Core terms of use, available at https://www.cambridge.org/core/terms.
https://doi.org/10.1017/erm.2020.3

AZD6738 was developed from AZ20 in 2018, with improved aqueous solubility and excellent pharmacokinetic qualities (Ref. 115). It sensitised non-small cell lung cancer (NSCLC) cells and xenografts to cisplatin and gemcitabine (Ref. 116), and a panel of human cancer cells to radiation (Ref. 117). AZD6738 suppressed tumour growth and increased apoptosis in ATM defective cells (Ref. 118).

VE-821 was one of the first potent ATRi with greatly improved selectivity for ATR over other PI3K-like kinases discovered in 2011 (ATM, DNAPKcs, mTOR). VE-821, as a single agent, increased apoptosis in cancer cells versus non-cancerous cells (Ref. 119). VE-821 can sensitise cells to IR (Refs 120–122), gemcitabine and camptothecin (Refs 119, 123). However, the strongest synergy observed thus far is with platinum-based therapies cisplatin and carboplatin (Refs 119, 124). Interestingly, when used in combination with the PARPi veliparib, VE-821 further sensitised *BRCA* defective cells beyond the sensitivity already observed owing to HRR status (Ref. 124). In 2015 Middleton *et al.*, showed that defects in ATM, HRR (BRCA2, XRCC3) and BER (XRCC1) resulted in increased sensitivity to VE-821. Interestingly, defective Ku80 (involved in NHEJ) caused hypersensitivity to VE-821, but the loss of its binding subunit, DNA-PKcs, did not (Ref. 125).

M6620 (also known as VE-822/VX-970 developed in 2012 and, from the same chemical series as VE-821) was the first highly selective, potent ATR inhibitor to go into clinical trials and is currently in phase 2 trials. It potentiates a number of DNA damaging agents including carboplatin, cisplatin, gemcitabine, irinotecan and IR in a wide array of cancers (Refs 126–132). Nagel *et al.*, found that M6620 combined with cisplatin showed a better response *in vivo* than cisplatin combined with etoposide, another chemotherapeutic, providing a solid rationale for combining cisplatin and M6620 in the clinic and limiting inevitable side effects with combining two chemotherapeutic agents (Ref. 132). As with other ATR inhibitors, it was found that ATM conferred sensitivity to ATR, both *in vitro* and *in vivo* (Refs 128, 133).

In 2017 Wengner *et al.*, characterised a novel ATRi, BAY1895344, which inhibited cell proliferation in an array of human cancer cell lines as well as having a strong anti-tumour effect as monotherapy in xenograft models. Synergistic anticancer activity was reported when used in combination with Radium-223 in xenograft models (Ref. 134).

Preclinical development of CHK1 inhibitors

UCN-01 was a first-generation, potent CHK1 inhibitor originally developed in 1999 as a protein kinase C inhibitor (Ref. 135). *In vitro,* it abrogated G2 checkpoint control and sensitised p53 defective cancer cells to DNA damaging agents (cisplatin, camptothecin and IR). However, it has poor potency and specificity and struggled to bypass a radiation-induced G2/M checkpoint (Ref. 136).

In 2008 the biological effects of AZD7762, a potent dual CHK1 CHK2 inhibitor with equal potency against both kinases, was shown to result primarily from inhibition of CHK1 (Ref. 70). *In vitro* studies have demonstrated that AZD7762 potentiated the cytotoxic effects of the nucleoside analogue gemcitabine, topoisomerase inhibitors and cisplatin (Refs 137–141). These findings were reflected *in vivo* and AZD7762 showed good pharmacokinetics and tolerability in mice. However, the effect of dual CHK1/CHK2 inhibition showed no increased benefit compared with CHK1-specific targeting agents suggesting that most of the anti-tumour effects are through inhibition of CHK1.

PF-477736 is a potent ATP-competitive CHK1 inhibitor with >100-fold selectivity over CHK2 developed in 2008 (Ref. 142). It has potent single-agent activity in triple-negative breast and ovarian cancer cell lines (Ref. 143), as well as sensitising cells to chemotherapeutic drugs gemcitabine, carboplatin, doxorubicin, mitomycin C and toptotecan (Refs 142, 144–146). PF-477736 also sensitises HPV positive head and neck cancer cells to radiation (Ref. 147). PF-477736 caused synergistic cytotoxicity in combination with targeted therapies irutinib and bosutinib in mantle cell lymphoma (MCL) and chronic myeloid leukaemia (CML), respectively (Refs 148, 149). PF-477736 was more cytotoxic in p53 mutant and Myc-driven cancers (Refs 142, 150).

In 2017, a novel CHK1 inhibitor, MK-8776 (also known as SCH900776 and identified in 2011), abrogated IR-induced G2/M checkpoint activation, resulting in aberrant mitosis, and was a potent radiosensitiser in breast and cervical cell lines (Refs 151, 152). MK-8776 also radiosensitised non-small cell lung cancer and head and neck cancer cell lines, in p53 non-functional cells (Ref. 153). Montano *et al.*, reported that MK-8776 sensitised cells to an array of DNA damaging agents: HU (20–70 fold), cytarabine (15–35 fold) and gemcitabine (5–10 fold), with no sensitisation reported with cisplatin or 5-fluorouracil (5-FU) (Ref. 154). However, a later study by Herudkova *et al.* found that MK-8776 significantly sensitised cells to cisplatin and another platinum-based therapy, LA-12 (Ref. 155).

SRA737 (previously CCT244747, which was discovered in 2012) is a novel, potent, orally active CHK1 inhibitor, with good selectivity (Refs 156, 157). It was developed at the ICR and is active as a single agent in *MYCN*-driven neuroblastoma and in combination with IR, gemcitabine and irinotecan (Refs 156, 157). SRA737 has synergistic antitumour activity with the PARP inhibitors niraparib and olaparib in mammary and ovarian cancer cells *in vitro* and *in vivo* (Ref. 158).

In 2015 LY2606368, a specific CHK1 inhibitor with strong single-agent activity *in vitro* and *in vivo* was discovered (Refs 159–162). It demonstrated synergy with PARP inhibitors olaparib and BMN673 in ovarian and gastric cancer, respectively (Refs 163, 164) and potentiated cisplatin even in a panel of platinum-resistant human cancers cell lines (Refs 161, 165).

Pre-clinical development of WEE1i

Despite the key role for WEE1 in S and G2 arrest, very few small-molecule inhibitors have been developed. In 2001, PD0166285 was the first potent WEE1 inhibitor. It radiosensitised ovarian, colon, lung and ovarian tumour cells in a p53-dependent manner (Ref. 166). It was a potent radiosensitiser in glioblastoma, but a major limitation to its development is its inability to penetrate the blood-brain-barrier (Refs 167–169). Furthermore, PD0166285 was non-selective, it also inhibited CHK1, Src non-receptor tyrosine kinase, epidermal growth factor receptor (EGFR), platelet-derived growth factor β (PDGF-β) and fibroblast growth factor receptor-1 (FGFR-1) (Ref. 170).

In 2009 AZD1775/MK-1775 was discovered as a specific, potent WEE1 inhibitor that showed excellent selectivity (Ref. 171). It was effective as a single agent (Ref. 172), as well as in synergistically increasing the cytotoxicity of various DNA damaging agents (IR, gemcitabine, carboplatin, cisplatin, 5-FU, pemetrexed, doxorubicin and camptothecin), *in vitro* and *in vivo* (Refs 171, 173–176). Earlier studies reported p53 status as a determinant for sensitivity to AZD1775 (Refs 171, 174). However, more recent studies have shown MK-1775 cytotoxicity to be independent of p53 (Refs 172, 177). Heijink *et al.* carried out a genome-wide unbiased screen and concluded that the activity of DNA replication proteins, beyond p53, is a key determinant of WEE1 inhibitor sensitivity (Ref. 177).

Synergy between inhibitors of ATR-CHK1-WEE1

Studies of the combination of inhibitors of the pathway with one another have thus far shown potential. ATR inhibition by VE-821 and CHK1 inhibition by AZD7762 caused synergistic cell death *in*

Downloaded from https://www.cambridge.org/core. Newcastle University, on 15 Feb 2022 at 13:26:48, subject to the Cambridge Core terms of use, available at https://www.cambridge.org/core/terms.
https://doi.org/10.1017/erm.2020.3

vitro and *in vivo* (Ref. 178). VX-970 (VE-822) was well tolerated in combination with AZD7762 in mice and resulted in increased survival of tumour-bearing mice (Ref. 178). ATR inhibition by AZD6738 was also synergistic with WEE1 inhibition by AZD1775 in causing the accumulation of DNA damage, via forced mitotic entry, and growth inhibition. This combination also inactivated HRR- sensitising cells to cisplatin and PARP inhibition (Ref. 179). An anti-metastatic effect was observed *in vitro* when ATR inhibitors AZ06738 and ETP-46464 were combined with WEE1 inhibitor AZD1775 (Ref. 180).

CHK1 and WEE1 inhibitors are another well-tolerated, synergistic combination as demonstrated in several studies in a variety of different cancer models, a few examples are given here. CHK1 inhibitor MK-8776 sensitised AML cells to AZD1775 *ex-vivo* and the combination was effective against neuroblastoma xenografts (Refs 181, 182). A study by Hauge *et al.*, showed synergistic anti-tumour effects between the WEE1 inhibitor AZD1775 and CHK1 inhibitors AZD7762 and LY2603618. A combination of these inhibitors resulted in mitotic catastrophe and reduced cell survival because of the combined effects on S phase and DNA damage associated with unscheduled replication initiation (Ref. 183). Similarly, the combination of CHK1 inhibitor AZD7762 and WEE1 inhibitor AZD1775 caused increased cytotoxicity and apoptosis in metastatic melanoma cell lines (Ref. 184). Synergy was also reported with CHK1 inhibitor PF-477736 and WEE1 inhibitor AZD1775 in MCL cells (Ref. 185).

Pre-clinical synergy of ATR-CHK1-WEE1 inhibitors and PARP inhibitors

Inhibitors of the ATR-CHK1-WEE1 cascade have shown synergy with PARP inhibitors. Peasland *et al.*, were the first to show that the ATR inhibitor, NU6027, was synthetically lethal in combination with the PARP inhibitor, rucaparib in breast and ovarian cancer cells (Ref. 109). Subsequently, the ATR inhibitor VE-821 was found to sensitise *BRCA* mutant cells to veliparib (Ref. 125) and a synthetically lethal screen found VE-821 had profound synergy with PARP inhibition in both HRR competent and defective cells (Ref. 186). Kim *et al.*, showed that inhibiting PARP resulted in increased reliance on the ATR-CHK1 pathway for genomic stability and that the combination of olaparib with ATRi AZD6738 effectively reduced tumour burden in patient-derived xenografts of serous ovarian cancer (Ref. 187).

A series of PARP inhibitors (rucaparib, olaparib, veliparib and NU1025) synergised with various CHK1 inhibitors (UCN-01, AZD7762 and LY2603618) to increase DNA damage and apoptosis *in vitro* in breast cancer cells (Ref. 188). The PARPi olaparib in combination with CHK1 inhibitor MK-8776, supressed colony formation in *BRCA* mutant models to a greater degree than either inhibitor as a single agent (Ref. 187). The PARP inhibitor Talazoparib was also synergistic with LY2606368, both *in vitro* and *in vivo* in gastric cancer (Ref. 164). Similarly, LY2606368 also showed inhibited HRR function and synergised with olaparib to decrease cell survival in *BRCA* wild-type cells (Ref. 163).

Fewer studies have looked at PARP and WEE1 inhibition combined, perhaps owing to the availability of only one WEE1 inhibitor with the desired selectivity and specificity (AZD1775). AZD1775 has only been tested in combination with olaparib but these results have been promising and when used in combination, the inhibitors act synergistically to radiosensitise pancreatic, and *KRAS*-mutant NSCLC cells further than when either is used as a single agent (Refs 189, 190).

ATR inhibitors in clinical trials

M6620 (VE-822/VX-970) was the first ATR inhibitor to reach clinical trials. Thomas *et al.*, first reported ATR inhibition in combination with chemotherapy in patients, with the maximum dose of topotecan being well tolerated when used in combination with M6620 (Ref. 191). There are currently three active clinical trials using M6620, one of which is the first in a human study looking at the pharmacokinetics of M6620 in combination with gemcitabine, cisplatin, etoposide carboplatin and irinotecan (NCT02157792). A number of phase 1 and 2 studies are currently recruiting patients for the use of M6620 single agent and in combination with a number of DNA damaging agents including irradiation, cisplatin, carboplatin, gemcitabine, irinotecan and topotecan (see Table 2). Another selective, bioavailable ATR inhibitor currently in phase 1 and 2 trials is AZD6738. Of these trials, nine are investigating the use of AZD6738 with the PARP inhibitor olaparib, which has strong support from pre-clinical data (Ref. 187). The ATR inhibitor BAY1895344 is in a first in human phase I safety trial in patients with advanced solid tumours and lymphomas (NCT03188965). M4344/VX-803 is an orally bioavailable ATR inhibitor currently recruiting in phase 1 clinical trial where it will be used as a monotherapy and in combination with cisplatin, carboplatin or gemcitabine (NCT02278250). The ATR inhibitor BAY1895344 has recently shown to have anti-tumour activity and is well tolerated at active doses in cancers with defects in DDR, such as loss of ATM (Ref. 192) (NCT03188965).

CHK1 inhibitors in clinical trials

Although there is significant interest surrounding CHK1 inhibitors, clinical progression has often been hindered because of the lack of bio-availability and off-target effects (Ref. 157). UCN-01 was used in combination with carboplatin in a phase 1 study (NCT00036777) and progressed into phase 2 clinical trials in 2010 in patients with metastatic melanoma, but the trial was terminated prematurely because of discouraging results (NCT00072189). CHK1 inhibitors with greater specificity have now entered clinical evaluation. SRA737 is currently in phase 1/2 clinical trials, both as a monotherapy and in combination with gemcitabine +/− cisplatin (NCT02797964) (NCT02797977). MK-8776 is also in phase 1 and 2 trials as a monotherapy and in combination with gemcitabine, cytarabine and hydroxyurea (NCT00779584) (NCT01870596). Of the four clinical trials it is currently in, two have been completed, with one terminated and one withdrawn owing to a lack of patients (see Table 3). However, *in vitro* studies have shown MK-8776 to have a short half-life, as well as undergoing rapid demethylation *in vivo*, resulting in a less selective metabolite (MU379) (Ref. 193). Phase 1 clinical trials, in patients with advanced solid tumours, of PF-477736 in combination with gemcitabine were terminated early for business reasons, rather than safety concerns (NCT00437203). Prexasertib (LY2606368) is currently in phase 2 trials a monotherapy agent, specifically in patients with cancers that are p53 mutant, have DDR defects such as *BRCA* mutation, increased replication stress or CCNE1 amplification, as these are determinants of CHK1 inhibitor sensitivity (NCT02735980, NCT02203513, NCT03414047, NCT02873975). Prexasertib has also entered phase 1 and 2 clinical trials in combination with pemetrexed (NCT01296568, NCT00415636, NCT01139775, NCT00988858), gemcitabine (NCT01358968, NCT01341457, NCT01296568, NCT00839332) or cisplatin (NCT02555644, NCT01139775) but has currently only been in one clinical trial with a PARP inhibitor (NCT03057145), despite promising synergy being observed pre-clinically (Refs 163, 164).

WEE1 inhibitors in clinical trials

AZD17775 is the only WEE1 inhibitor to reach clinical development and is already in a number of phase 1 and 2 trials being used in combination with treatments such as carboplatin, gemcitabine, cisplatin, cytarabine and olaparib (Refs 194, 195, 196). Recently a dose-escalation trial of AZD1775 in

Downloaded from https://www.cambridge.org/core. Newcastle University, on 15 Feb 2022 at 13:26:48, subject to the Cambridge Core terms of use, available at https://www.cambridge.org/core/terms.
https://doi.org/10.1017/erm.2020.3

Table 2. ATR inhibitors currently in clinical trials

Drug name	Phase	Monotherapy/combination	Tumour type	NCT
M6620/ VX-970	I	In combination with whole brain radiotherapy	NSCLC, SCLC or neuroendocrine tumours that have metastasised to the brain	NCT02589522
		In combination with irinotecan hydrochloride	Solid metastatic tumours that are unable to be operated on	NCT02595931
		Assessing pharmacokinetics of M6620 in combination with gemcitabine, cisplatin, etoposide, carboplatin or irinotecan	First-in-human study, in patients with advanced solid tumours	NCT02157792
		As monotherapy or in combination with carboplatin and paclitaxel. A rollover study from VX13-970-002	Advanced solid tumours	NCT03309150
		In combination with chemoradiotherapy treatment (cisplatin and capecitabine)	Oesophageal cancer	NCT03641547
		In combination with cisplatin and radiotherapy	Locally advanced head and neck squamous cell carcinoma	NCT02567422
	II	In combination with avelumab and carboplatin	PARPi-resistant, recurrent, platinum-sensitive ovarian, primary peritoneal or fallopian tube	NCT03704467
		In combination with cisplatin or gemcitabine hydrochloride	Metastatic urothelial cancer	NCT02567409
		In combination with carboplatin +/− docetaxel	Metastatic castration-resistant prostate cancer	NCT03517969
		In combination with gemcitabine	Recurrent ovarian, primary peritoneal or fallopian tube	NCT02595892
		In combination with topotecan	Relapsed SCLC or extrapulmonary small cell cancer	NCT03896503
		Monotherapy	Advanced solid tumour	NCT03718091
		In combination with irinotecan	Metastatic or unresectable *TP53* mutant gastric or gastroesophageal junction cancer	NCT03641313
AZD6738	I	In combination with acalabrutinib	Relapsed/refractory aggressive Non-Hodgkins Lymphoma	NCT03527147
		Monotherapy	Head and neck squamous cell carcinoma	NCT03022409
		Monotherapy and in combination with palliative radiotherapy	Solid tumours	NCT02223923
		Monotherapy	Relapsed/refractory CLL, PLL or B cell lymphomas	NCT01955668
		In combination with gemcitabine	Advanced solid tumours	NCT03669601
		In combination with paclitaxel	Metastatic cancer failed standard chemotherapy	NCT02630199
		Monotherapy	Chronic myelomonocytic leukaemia or myelodysplastic syndrome	NCT03770429
	I/II	In combination with carboplatin, olaparib or durvalumab	Head and neck squamous cell carcinoma, advanced solid malignancy, NSCLC, gastric and breast cancer	NCT02264678
		Monotherapy and in combination with acalabrutinib	Relapsed or refractory high-risk CLL	NCT03328273
	II	Monotherapy	Neoadjuvant chemotherapy-resistant residual triple negative breast cancer	NCT03740893
		Monotherapy and in combination with PARPi olaparib	Renal cell carcinoma, urothelial carcinoma, pancreatic cancers and solid tumours that have spread to nearby tissue	NCT03682289
		In combination with PARPi olaparib	Recurrent ovarian cancer	NCT03462342
		In combination with PARPi olaparib	SCLC	NCT03428607
		In combination with PARPi olaparib	IDH1 and IDH2 mutant tumours	NCT03878095
		In combination with PARPi olaparib	Second- or third-line triple-negative breast cancer	NCT03330847
		In combination with PARPi olaparib	Resistant prostate cancer	NCT03787680
		In combination with PARPi olaparib	Advanced solid tumour	NCT02576444
		In combination with PARPi olaparib	Platinum refractory extensive-stage SCLC	NCT02937818
		In combination with immunotherapy durvalumab	Metastatic NSCLC which has progressed on an anti-PD-1 therapy	NCT03334617

(*Continued*)

Downloaded from https://www.cambridge.org/core. Newcastle University, on 15 Feb 2022 at 13:26:48, subject to the Cambridge Core terms of use, available at https://www.cambridge.org/core/terms. https://doi.org/10.1017/erm.2020.3

Table 2. (*Continued.*)

Drug name	Phase	Monotherapy/combination	Tumour type	NCT
		In combination with immunotherapy durvalumab	NSCLC with PD-1 immune checkpoint inhibitor resistance	NCT03833440
		In combination with immunotherapy durvalumab	Solid tumour, gastric cancer with failed secondary chemotherapy, melanoma patients	NCT03780608
BAY1895344	I	Monotherapy (first-in-human)	Advanced solid tumours and lymphomas	NCT03188965
M4344/ VX-803	I	Monotherapy and in combination with cisplatin, carboplatin and gemcitabine	Advanced solid tumours	NCT02278250

Table 3. CHK1 inhibitors currently in clinical trials

Drug name	Phase	Monotherapy/combination	Tumour type	NCT
MK-8776/ SCH900776	I	In combination with and without cytarabine	Acute leukaemia	NCT00907517
		In combination with hydroxyurea	Advanced solid tumours	NCT01521299
	II	In combination with and without cytarabine	Acute myeloid leukaemia	NCT01870596
LY2606368/ prexasertib	I	In combination with desipramine, pemetrexed or gemcitabine	Drug interaction study	NCT01358968
		In combination with gemcitabine	Solid tumours	NCT01341457
		In combination with pemetrexed or gemcitabine	Advanced/metastatic solid tumours	NCT01296568
		In combination with pemetrexed	Advanced/metastatic solid tumours	NCT00415636
		Monotherapy	Japanese patients with advanced solid tumour	NCT02514603
		Monotherapy	Paediatric solid tumours	NCT02808650
		In combination with ralimetanib	Advanced solid tumour	NCT02860780
		In combination with olaparib	Advanced solid tumour	NCT03057145
		In combination with cisplatin, cetuximab or radiotherapy	Head and neck cancer	NCT02555644
		In combination with PD-L1 inhibitor	Advanced solid tumours	NCT03495323
		In combination with cytarabine	Chronic/acute myeloid leukaemia	NCT02649764
	I/II	In combination with and without gemcitabine	Pancreatic cancer	NCT00839332
		In combination with cisplatin or pemetrexed	NSCLC	NCT01139775
	II	Monotherapy	Extensive stage SCLC	NCT02735980
		Monotherapy	Platinum resistant ovarian cancer	NCT03414047
		Monotherapy	Solid tumour with HRR defects or CCNE1 amplification	NCT02873975
		In combination with or without pemetrexed	Advanced or metastatic NSCLC	NCT00988858
		Monotherapy	*BRCA* mutant breast or ovarian cancer Triple-negative breast cancer HGSOC Castrate-resistant prostate cancer	NCT02203513

combination with gemcitabine and radiation showed promising results with good tolerability in patients with locally advanced pancreatic cancer (Ref. 197). The majority of clinical trials are still recruiting, suggesting this kinase inhibitor has exciting potential once trials have been completed and data is collected and analysed (Table 4).

DNA checkpoint kinase and immune checkpoint inhibitor combinations

Immune checkpoint inhibitors block the immunosuppressive mechanisms employed by cancers to prevent an effective anti-tumour immune response and have been found to be efficacious in many types of cancer. There is increasing evidence that tumour mutational burden increases the immunogenicity of cancers through the production of mutation-associated neoantigens, including those associated with microsatellite instability from defective DNA mismatch repair (Ref. 198). Damaged cytosolic DNA may also directly activate the immune system by stimulating interferon via the STING pathway (Stimulation of Interferon Genes) leading to enhanced immune checkpoint inhibitor responses in pre-clinical models. In ATM-deficient mice and patients with ataxia telangiectasia enhanced interferon production through the STING pathway has been observed (Ref. 198). ATM inhibition has recently been found to increase type 1 interferon signalling in a STING independent manner (Ref. 199). Clinical

Downloaded from https://www.cambridge.org/core. Newcastle University, on 15 Feb 2022 at 13:26:48, subject to the Cambridge Core terms of use, available at https://www.cambridge.org/core/terms. https://doi.org/10.1017/erm.2020.3

Table 4. WEE1 inhibitors currently in clinical trials

Drug name	Phase	Monotherapy/combination	Tumour type	NCT
AZD1775/ MK-1775	I	Monotherapy	Advanced/metastatic cancers	NCT02610075
		Monotherapy	Ovarian cancer, SCLC, other solid tumours	NCT02482311
		In combination with carboplatin and paclitaxel	Asian patients with advanced solid tumours	NCT02341456
		In combination with olaparib	Refractory solid tumours	NCT02511795
		In combination with irinotecan	RAS or BRAF mutated second-line metastatic colorectal cancer	NCT02906059
		In combination with either gemcitabine, cisplatin or carboplatin	Advanced solid tumours	NCT00648648
		In combination with either cisplatin and radiotherapy	Head and neck cancer	NCT03028766
	II	Monotherapy	Relapsed SCLC	NCT02593019
		In combination with docetaxel	NSCLC	NCT02087176
		In combination with carboplatin-paclitaxel	SCLC	NCT02513563
		In combination with cisplatin	Triple-negative metastatic breast cancer	NCT03012477
		In combination with cytarabine	Advanced acute myeloid leukaemia or myelodysplastic syndrome	NCT02666950

trials evaluating DNA damage repair inhibitors with immune checkpoint inhibitors are ongoing, including PARP, ATR and CHK1 inhibitors (Table 2).

Concluding remarks and future directions

Targeting DDR checkpoint signalling has evolved to the clinic based on sound scientific hypotheses and preclinical data. Early less specific inhibitors may have clouded the case for development but now more specific inhibitors are under investigation both as monotherapy and in combination with conventional cytotoxic chemotherapy or novel agents. The preclinical data suggest that targeting the ATR-CHK1-WEE1 pathway is likely to be more fruitful than targeting ATM and CHK2 signalling. To date, the most active combinations for each class of kinase inhibitor include ATR inhibitors with cis/carboplatin and CHK1 inhibitors with gemcitabine. A developing field is a potentiation with immune checkpoint inhibitors via several mechanisms of action. Identification of predictive biomarkers, particularly for monotherapy, however, has been challenging, for example, whether the presence of *TP53* mutations confers sensitivity.

The potential for some of these agents to be associated with second malignancy must not be forgotten, which is particularly a concern for young patients treated with these agents. Since defects in ATM and CHK2 are associated with tumours, but defects in ATR, CHK1 and WEE1 are not, one might predict that as single agents, inhibitors of the former might be associated with second malignancies but not the latter. However, in combination with cytotoxics already associated with second malignancies, the incidence is likely to be increased unless lower doses of the primary cytotoxic can be used in combination to achieve the same efficacy. Nevertheless, we must remember that the malignancies for which these agents are most likely to be used, especially in children, are the ones that are most difficult to cure with current strategies in which cure has yet to be achieved for the majority at any cost rather than at least cost.

Acknowledgements. This work was partly funded by the Children's Cancer & Leukaemia Group and Little Princess Trust and the JGWP foundation.

References

1. **Weber AM and Ryan AJ** (2015) ATM and ATR as therapeutic targets in cancer. *Pharmacology & Therapeutics* **149**(Suppl. C), 124–138.
2. **Maréchal A and Zou L** (2013) DNA damage sensing by the ATM and ATR kinases. *Cold Spring Harbor Perspectives in Biology* **5**, a012716.
3. **Kozlov SV *et al.*** (2011) Autophosphorylation and ATM activation: additional sites add to the complexity. *The Journal of biological chemistry* **286**, 9107–9119.
4. **Tanya TP** (2015) Mechanisms of ATM activation. *Annual Review of Biochemistry* **84**, 711–738.
5. **Shiloh Y and Ziv Y** (2013) The ATM protein kinase: regulating the cellular response to genotoxic stress, and more. *Nature Reviews Molecular Cell Biology* **14**, 197.
6. **Zannini L, Delia D and Buscemi G** (2014) CHK2 Kinase in the DNA damage response and beyond. *Journal of Molecular Cell Biology* **6**, 442–457.
7. **O'Connell MJ *et al.*** (1997) Chk1 is a wee1 kinase in the G2 DNA damage checkpoint inhibiting cdc2 by Y15 phosphorylation. *The EMBO Journal* **16**, 545–554.
8. **Chow JPH and Poon RYC** (2012) The CDK1 inhibitory kinase MYT1 in DNA damage checkpoint recovery. *Oncogene* **32**, 4778.
9. **Kastan MB *et al.*** (1992) A mammalian cell cycle checkpoint pathway utilizing p53 and GADD45 is defective in ataxia-telangiectasia. *Cell* **71**, 587–597.
10. **Beamish H *et al.*** (1996) Defect in multiple cell cycle checkpoints in ataxia-telangiectasia postirradiation. *Journal of Biological Chemistry* **271**, 20486–20493.
11. **Weber AM *et al.*** (2016) Phenotypic consequences of somatic mutations in the ataxia-telangiectasia mutated gene in non-small cell lung cancer. *Oncotarget* **7**, 60807–60822.
12. **Ou Y-H *et al.*** (2005) P53 C-terminal phosphorylation by CHK1 and CHK2 participates in the regulation of DNA-damage-induced C-terminal acetylation. *Molecular Biology of the Cell* **16**, 1684–1695.
13. **Fischer M** (2017) Census and evaluation of p53 target genes. *Oncogene* **36**, 3943.
14. **Wade M, Wang YV and Wahl GM** (2010) The p53 orchestra: Mdm2 and Mdmx set the tone. *Trends in cell Biology* **20**, 299–309.
15. **Roos WP and Kaina B** (2013) DNA damage-induced cell death: from specific DNA lesions to the DNA damage response and apoptosis. *Cancer Letters* **332**, 237–248.
16. **Abbas T and Dutta A** (2009) P21 in cancer: intricate networks and multiple activities. *Nature Reviews. Cancer* **9**, 400–414.
17. **Waldman T, Kinzler KW and Vogelstein B** (1995) P21 Is necessary for the p53-mediated G_1 arrest in human cancer cells. *Cancer Research* **55**, 5187–5190.

Downloaded from https://www.cambridge.org/core. Newcastle University, on 15 Feb 2022 at 13:26:48, subject to the Cambridge Core terms of use, available at https://www.cambridge.org/core/terms. https://doi.org/10.1017/erm.2020.3

18. **Deng C *et al.*** (1995) Mice lacking p21CIP1/WAF1 undergo normal development, but are defective in G1 checkpoint control. *Cell* **82**, 675–684.
19. **Bieging KT, Mello SS and Attardi LD** (2014) Unravelling mechanisms of p53-mediated tumour suppression. *Nature reviews. Cancer* **14**, 359–370.
20. **Goodarzi AA, Jeggo P and Lobrich M** (2010) The influence of heterochromatin on DNA double strand break repair: getting the strong, silent type to relax. *DNA Repair* **9**, 1273–1282.
21. **Goodarzi AA *et al.*** (2008) ATM signaling facilitates repair of DNA double-strand breaks associated with heterochromatin. *Molecular Cell* **31**, 167–177.
22. **Scully R and Xie A** (2013) Double strand break repair functions of histone H2AX. *Mutation Research/Fundamental and Molecular Mechanisms of Mutagenesis* **750**, 5–14.
23. **Blackford AN and Jackson SP** (2017) ATM, ATR, and DNA-PK: the trinity at the heart of the DNA damage response. *Molecular Cell* **66**, 801–817.
24. **Melander F *et al.*** (2008) Phosphorylation of SDT repeats in the MDC1 N terminus triggers retention of NBS1 at the DNA damage-modified chromatin. *The Journal of Cell Biology* **181**, 213–226.
25. **Spycher C *et al.*** (2008) Constitutive phosphorylation of MDC1 physically links the MRE11–RAD50–NBS1 complex to damaged chromatin. *The Journal of Cell Biology* **181**, 227–240.
26. **Panier S and Boulton SJ** (2013) Double-strand break repair: 53BP1 comes into focus. *Nature Reviews Molecular Cell Biology* **15**, 7.
27. **Greenberg RA** (2008) Recognition of DNA double strand breaks by the BRCA1 tumor suppressor network. *Chromosoma* **117**, 305–317.
28. **Prakash R *et al.*** (2015) Homologous recombination and human health: the roles of BRCA1, BRCA2, and associated proteins. *Cold Spring Harbor Perspectives in Biology* **7**, a016600–a00.
29. **Chen X *et al.*** (2011) Cell cycle regulation of DNA double-strand break end resection by Cdk1-dependent Dna2 phosphorylation. *Nature Structural & Molecular Biology* **18**, 1015–1019.
30. **Ceccaldi R, Rondinelli B and D'Andrea AD** (2016) Repair pathway choices and consequences at the double-strand break. *Trends in Cell Biology* **26**, 52–64.
31. **Jazayeri A *et al.*** (2006) ATM- and cell cycle-dependent regulation of ATR in response to DNA double-strand breaks. *Nature Cell Biology* **8**, 37–45.
32. **Myers JS and Cortez D** (2006) Rapid activation of ATR by ionizing radiation requires ATM and Mre11. *Journal of Biological Chemistry* **281**, 9346–9350.
33. **Rothblum-Oviatt C *et al.*** (2016) Ataxia telangiectasia: a review. *Orphanet Journal of Rare Diseases* **11**, 159–159.
34. **Choi M, Kipps T and Kurzrock R** (2016) ATM mutations in cancer: therapeutic implications. *Molecular Cancer Therapeutics* **15**, 1781–1791.
35. **Wang C *et al.*** (2017) ATM-deficient colorectal cancer cells are sensitive to the PARP inhibitor Olaparib(). *Translational Oncology* **10**, 190–196.
36. **Abdel-Fatah TMA *et al.*** (2014) Clinicopathological significance of ATM-Chk2 expression in sporadic breast cancers: a comprehensive analysis in large cohorts. *Neoplasia (New York, N.Y.)* **16**, 982–991.
37. **Petersen LF *et al.*** (2017) Loss of tumour-specific ATM protein expression is an independent prognostic factor in early resected NSCLC. *Oncotarget* **8**, 38326–38336.
38. **Villaruz LC *et al.*** (2016) ATM Protein is deficient in over 40% of lung adenocarcinomas. *Oncotarget* **7**, 57714–57725.
39. **Russell R *et al.*** (2015) Loss of ATM accelerates pancreatic cancer formation and epithelial-mesenchymal transition. *Nature Communications* **6**, 7677–7677.
40. **Ouillette P *et al.*** (2010) Aggressive chronic lymphocytic leukemia with elevated genomic complexity is associated with multiple gene defects in the response to DNA double-strand breaks. *Clinical Cancer Research* **16**, 835–847.
41. **Mlakar V *et al.*** (2017) 11q Deletion in neuroblastoma: a review of biological and clinical implications. *Molecular cancer* **16**, 114.
42. **Laake K *et al.*** (1999) Loss of heterozygosity at 11q23. 1 and survival in breast cancer: results of a large European study. *Genes, Chromosomes and Cancer* **25**, 212–221.
43. **Monni O and Knuutila S** (2001) 11q deletions in hematological malignancies. *Leukemia & Lymphoma* **40**, 259–266.
44. **Cybulski C *et al.*** (2004) CHEK2 Is a multiorgan cancer susceptibility gene. *American Journal of Human Genetics* **75**, 1131–1135.
45. **Lee SB *et al.*** (2001) Destabilization of CHK2 by a missense mutation associated with Li-Fraumeni syndrome. *Cancer Research* **61**, 8062–8067.
46. **Varley JM** (2003) Germline TP53 mutations and Li-Fraumeni syndrome. *Human Mutation* **21**, 313–320.
47. **Lawrence MS *et al.*** (2014) Discovery and saturation analysis of cancer genes across 21 tumour types. *Nature* **505**, 495.
48. **Bouaoun L *et al.*** (2016) TP53 Variations in human cancers: new lessons from the IARC TP53 database and genomics data. *Human Mutation* **37**, 865–876.
49. **Hainaut P and Pfeifer GP** (2016) Somatic TP53 mutations in the era of genome sequencing. *Cold Spring Harbor Perspectives in Medicine* **6**, a026179.
50. **Liu Y *et al.*** (2016) Deletions linked to TP53 loss drive cancer through p53-independent mechanisms. *Nature* **531**, 471–475.
51. **Fiskvik I *et al.*** (2013) Karyotyping of diffuse large B-cell lymphomas: loss of 17p is associated with poor patient outcome. *European Journal of Haematology* **91**, 332–338.
52. **Hallek M** (2017) Chronic lymphocytic leukemia: 2017 update on diagnosis, risk stratification, and treatment. *American Journal of Hematology* **92**, 946–965.
53. **Bartek J, Lukas J and Bartkova J** (2007) DNA Damage response as an anti-cancer barrier: damage threshold and the concept of 'conditional haploinsufficiency'. *Cell Cycle* **6**, 2344–2347.
54. **Barlow C *et al.*** (1996) Atm-deficient mice: a paradigm of ataxia telangiectasia. *Cell* **86**, 159–171.
55. **Xu Y and Baltimore D** (1996) Dual roles of ATM in the cellular response to radiation and in cell growth control. *Genes & Development* **10**, 2401–2410.
56. **Jiang X *et al.*** (2019) Current status and future prospects of PARP inhibitor clinical trials in ovarian cancer. *Cancer Management and Research* **11**, 4371.
57. **Rabik CA, Njoku MC and Dolan ME** (2006) Inactivation of O6-alkylguanine DNA alkyltransferase as a means to enhance chemotherapy. *Cancer Treatment Reviews* **32**, 261–276.
58. **Takai H *et al.*** (2002) Chk2-deficient mice exhibit radioresistance and defective p53-mediated transcription. *The EMBO Journal* **21**, 5195–5205.
59. **Niida H *et al.*** (2010) Cooperative functions of Chk1 and Chk2 reduce tumour susceptibility in vivo. *The EMBO Journal* **29**, 3558–3570.
60. **Brandsma I *et al.*** (2017) Directing the use of DDR kinase inhibitors in cancer treatment. *Expert Opinion on Investigational Drugs* **26**, 1341–1355.
61. **Hickson I *et al.*** (2004) Identification and characterization of a novel and specific inhibitor of the ataxia-telangiectasia mutated kinase ATM. *Cancer Research* **64**, 9152–9159.
62. **Biddlestone-Thorpe L *et al.*** (2013) ATM kinase inhibition preferentially sensitizes p53-mutant glioma to ionizing radiation. *Clinical Cancer Research* **19**, 3189–3200.
63. **Batey MA *et al.*** (2013) Preclinical evaluation of a novel ATM inhibitor, KU59403, in vitro and in vivo in p53 functional and dysfunctional models of human cancer. *Molecular Cancer Therapeutics* **12**, 959–967.
64. **Karlin J *et al.*** (2018) Orally bioavailable and blood–brain barrier-penetrating ATM inhibitor (AZ32) radiosensitizes intracranial gliomas in mice. *Molecular Cancer Therapeutics* **17**, 1637–1647.
65. **Durant ST *et al.*** (2018) The brain-penetrant clinical ATM inhibitor AZD1390 radiosensitizes and improves survival of preclinical brain tumor models. *Science Advances* **4**, eaat1719–eaeaat19.
66. **Pike KG *et al.*** (2018) The identification of potent, selective, and orally available inhibitors of ataxia telangiectasia mutated (ATM) kinase: the discovery of AZD0156 (8-{6-[3-(dimethylamino)propoxy]pyridin-3-yl}-3-methyl-1-(tetrahydro-2H-pyran-4-yl)-1,3-dihydro-2H-imidazo[4,5-c]quinolin-2-one). *Journal of Medicinal Chemistry* **61**, 3823–3841.
67. **Rainey MD *et al.*** (2008) Transient inhibition of ATM kinase is sufficient to enhance cellular sensitivity to ionizing radiation. *Cancer Research* **68**, 7466–7474.
68. **Dohmen AJC *et al.*** (2017) Identification of a novel ATM inhibitor with cancer cell specific radiosensitization activity. *Oncotarget* **8**, 73925–73937.
69. **Ronco C *et al.*** (2017) ATM, ATR, CHK1, CHK2 and WEE1 inhibitors in cancer and cancer stem cells. *Medicinal Chemistry Communications* **8**, 295–319.
70. **Zabludoff SD *et al.*** (2008) AZD7762, A novel checkpoint kinase inhibitor, drives checkpoint abrogation and potentiates DNA-targeted therapies. *Molecular Cancer Therapeutics* **7**, 2955–2966.

Downloaded from https://www.cambridge.org/core. Newcastle University, on 15 Feb 2022 at 13:26:48, subject to the Cambridge Core terms of use, available at https://www.cambridge.org/core/terms. https://doi.org/10.1017/erm.2020.3

71. **Arienti KL *et al.*** (2005) Checkpoint kinase inhibitors: SAR and radioprotective properties of a series of 2-arylbenzimidazoles. *Journal of Medicinal Chemistry* **48**, 1873–1885.
72. **Carlessi L *et al.*** (2007) Biochemical and cellular characterization of VRX0466617, a novel and selective inhibitor for the checkpoint kinase Chk2. *Molecular Cancer Therapeutics* **6**, 935–944.
73. **Jobson AG *et al.*** (2009) Cellular inhibition of checkpoint kinase 2 (Chk2) and potentiation of camptothecins and radiation by the novel Chk2 inhibitor PV1019 [7-nitro-1H-indole-2-carboxylic acid {4-[1-(guanidinohydrazone)-ethyl]-phenyl}-amide]. *Journal of Pharmacology and Experimental Therapeutics* **331**, 816–826.
74. **Caldwell JJ *et al.*** (2011) Structure-Based design of potent and selective 2-(quinazolin-2-yl)phenol inhibitors of checkpoint kinase 2. *Journal of Medicinal Chemistry* **54**, 580–590.
75. **Raso A *et al.*** (2012) Characterization of glioma stem cells through multiple stem cell markers and their specific sensitization to double-strand break-inducing agents by pharmacological inhibition of ataxia telangiectasia mutated protein. *Brain Pathology* **22**, 677–688.
76. **Anderson VE *et al.*** (2011) CCT241533 is a potent and selective inhibitor of CHK2 that potentiates the cytotoxicity of PARP inhibitors. *Cancer Research* **71**, 463–472.
77. **Pires IM, Ward TH and Dive C** (2010) Oxaliplatin responses in colorectal cancer cells are modulated by CHK2 kinase inhibitors. *British Journal of Pharmacology* **159**, 1326–1338.
78. **Sausville E *et al.*** (2014) Phase I dose-escalation study of AZD7762, a checkpoint kinase inhibitor, in combination with gemcitabine in US patients with advanced solid tumors. *Cancer Chemotherapy and Pharmacology* **73**, 539–549.
79. **Saldivar J, Cortez D and Cimprich K** (2017) The essential kinase ATR: ensuring faithful duplication of a challenging genome. *Nature Reviews Molecular Cell Biology* **18**, 622–636.
80. **Thada V and Cortez D** (2019) Common motifs in ETAA1 and TOPBP1 required for ATR kinase activation. *Journal of Biological Chemistry* **294**, 8395–8402.
81. **Rundle S *et al.*** (2017) Targeting the ATR-CHK1 axis in cancer therapy. *Cancers* **9**, 41.
82. **Lewis CW *et al.*** (2017) Prolonged mitotic arrest induced by Wee1 inhibition sensitizes breast cancer cells to paclitaxel. *Oncotarget* **8**, 73705–73722.
83. **Lin AB, McNeely SC and Beckmann RP** (2017) Achieving precision death with cell-cycle inhibitors that target DNA replication and repair. *Clinical Cancer Research* **23**, 3232–3240.
84. **Lee J, Kumagai A and Dunphy WG** (2001) Positive regulation of wee1 by Chk1 and 14-3-3 proteins. *Molecular Biology of the Cell* **12**, 551–563.
85. **Wyman C, Ristic D and Kanaar R** (2004) Homologous recombination-mediated double-strand break repair. *DNA Repair (Amst)* **3**, 827–833.
86. **Brown JS *et al.*** (2017) Targeting DNA repair in cancer: beyond PARP inhibitors. *Cancer Discovery* **7**, 20–37.
87. **Yazinski SA *et al.*** (2017) ATR Inhibition disrupts rewired homologous recombination and fork protection pathways in PARP inhibitor-resistant BRCA-deficient cancer cells. *Genes & Development* **31**, 318–332.
88. **Sørensen CS *et al.*** (2005) The cell-cycle checkpoint kinase Chk1 is required for mammalian homologous recombination repair. *Nature Cell Biology* **7**, 195–201.
89. **Buisson R *et al.*** (2017) Coupling of homologous recombination and the checkpoint by ATR. *Molecular Cell* **65**, 336–346.
90. **Krajewska M *et al.*** (2012) Forced activation of Cdk1 via wee1 inhibition impairs homologous recombination. *Oncogene* **32**, 3001.
91. **de Klein A *et al.*** (2000) Targeted disruption of the cell-cycle checkpoint gene ATR leads to early embryonic lethality in mice. *Current Biology* **10**, 479–482.
92. **Liu Q *et al.*** (2000) Chk1 is an essential kinase that is regulated by Atr and required for the G(2)/M DNA damage checkpoint. *Genes & Development* **14**, 1448–1459.
93. **Tominaga Y *et al.*** (2006) Murine Wee1 plays a critical role in cell cycle regulation and pre-implantation stages of embryonic development. *International Journal of Biological Sciences* **2**, 161–170.
94. **Murga M** (2009) A mouse model of ATR-Seckel shows embryonic replicative stress and accelerated aging. *Nature Genetics* **41**, 891–898.
95. **Brown EJ and Baltimore D** (2000) ATR Disruption leads to chromosomal fragmentation and early embryonic lethality. *Genes & Development* **14**, 397–402.
96. **Macheret M and Halazonetis TD** (2015) DNA replication stress as a Hallmark of cancer. *Annual Review of Pathology: Mechanisms of Disease* **10**, 425–448.
97. **Magdalou I *et al.*** (2014) The causes of replication stress and their consequences on genome stability and cell fate. *Seminars in Cell & Developmental Biology* **30**, 154–164.
98. **Berti M and Vindigni A** (2016) Replication stress: getting back on track. *Nature Structural & Molecular Biology* **23**, 103–109.
99. **Massague J** (2004) G1 cell-cycle control and cancer. *Nature* **432**, 298–306.
100. **Kotsantis P, Petermann E and Boulton SJ** (2018) Mechanisms of oncogene-induced replication stress: jigsaw falling into place. *Cancer Discovery* **8**, 537–555.
101. **Hanahan D and Weinberg RA** (2011) Hallmarks of cancer: the next generation. *Cell* **144**, 646–674.
102. **Syljuåsen RG *et al.*** (2005) Inhibition of human Chk1 causes increased initiation of DNA replication, phosphorylation of ATR targets, and DNA breakage. *Molecular and Cellular Biology* **25**, 3553–3562.
103. **Kitao H *et al.*** (2018) DNA Replication stress and cancer chemotherapy. *Cancer Science* **109**, 264–271.
104. **Kim J-Y *et al.*** (2015) Resveratrol analogue (E)-8-acetoxy-2-[2-(3, 4–diacetoxyphenyl) ethenyl]-quinazoline induces G2/M cell cycle arrest through the activation of ATM/ATR in human cervical carcinoma HeLa cells. *Oncology Reports* **33**, 2639–2647.
105. **Cliby WA *et al.*** (1998) Overexpression of a kinase-inactive ATR protein causes sensitivity to DNA-damaging agents and defects in cell cycle checkpoints. *The EMBO Journal* **17**, 159–169.
106. **Hall-Jackson CA *et al.*** (1999) ATR Is a caffeine-sensitive, DNA-activated protein kinase with a substrate specificity distinct from DNA-PK. *Oncogene* **18**, 6707–6713.
107. **Sarkaria JN *et al.*** (1999) Inhibition of ATM and ATR kinase activities by the radiosensitizing agent, Caffeine. *Cancer Research* **59**, 4375–4382.
108. **Nghiem P *et al.*** (2002) ATR Is not required for p53 activation but synergizes with p53 in the replication checkpoint. *Journal of Biological Chemistry* **277**, 4428–4434.
109. **Peasland A *et al.*** (2011) Identification and evaluation of a potent novel ATR inhibitor, NU6027, in breast and ovarian cancer cell lines. *British Journal of Cancer* **105**, 372–381.
110. **Toledo LI *et al.*** (2011) A cell-based screen identifies ATR inhibitors with synthetic lethal properties for cancer-associated mutations. *Nature Structural & Molecular Biology* **18**, 721–727.
111. **Teng P-n *et al.*** (2015) Pharmacologic inhibition of ATR and ATM offers clinically important distinctions to enhancing platinum or radiation response in ovarian, endometrial, and cervical cancer cells. *Gynecologic Oncology* **136**, 554–561.
112. **Foote KM *et al.*** (2013) Discovery of 4-{4-[(3R)-3-methylmorpholin-4-yl]-6-[1-(methylsulfonyl)cyclopropyl]pyrimidin-2-yl}-1H-indole (AZ20): a potent and selective inhibitor of ATR protein kinase with monotherapy in vivo antitumor activity. *Journal of Medicinal Chemistry* **56**, 2125–2138.
113. **Ma J *et al.*** (2017) Mechanisms responsible for the synergistic antileukemic interactions between ATR inhibition and cytarabine in acute myeloid leukemia cells. *Scientific Reports* **7**, 41950–41950.
114. **Liu S *et al.*** (2017) Inhibition of ATR potentiates the cytotoxic effect of gemcitabine on pancreatic cancer cells through enhancement of DNA damage and abrogation of ribonucleotide reductase induction by gemcitabine. *Oncology Reports* **37**, 3377–3386.
115. **Foote KM *et al.*** (2018) Discovery and characterization of AZD6738, a potent inhibitor of ataxia telangiectasia mutated and Rad3 related (ATR) kinase with application as an anticancer agent. *Journal of Medicinal Chemistry* **61**, 9889–9907.
116. **Vendetti FP *et al.*** (2015) The orally active and bioavailable ATR kinase inhibitor AZD6738 potentiates the anti-tumor effects of cisplatin to resolve ATM-deficient non-small cell lung cancer in vivo. *Oncotarget* **6**, 44289–44305.
117. **Dillon MT *et al.*** (2017) Radiosensitization by the ATR inhibitor AZD6738 through generation of acentric micronuclei. *Molecular Cancer Therapeutics* **16**, 25–34.
118. **Min A *et al.*** (2017) AZD6738, a novel oral inhibitor of ATR, induces synthetic lethality with ATM deficiency in gastric cancer cells. *Molecular Cancer Therapeutics* **16**, 566–577. research 78(13 Supplement), 838–38.
119. **Reaper PM *et al.*** (2011) Selective killing of ATM-or p53-deficient cancer cells through inhibition of ATR. *Nature Chemical Biology* **7**, 428–430.

Downloaded from https://www.cambridge.org/core. Newcastle University, on 15 Feb 2022 at 13:26:48, subject to the Cambridge Core terms of use, available at https://www.cambridge.org/core/terms. https://doi.org/10.1017/erm.2020.3

120. **Alsubhi N *et al.*** (2016) Chk1 phosphorylated at serine345 is a predictor of early local recurrence and radio-resistance in breast cancer. *Molecular Oncology* **10**, 213–223.
121. **Fujisawa H *et al.*** (2015) VE-821, an ATR inhibitor, causes radiosensitization in human tumor cells irradiated with high LET radiation. *Radiation Oncology (London, England)* **10**, 175–175.
122. **Šalovská B *et al.*** (2018) Radio-sensitizing effects of VE-821 and beyond: distinct phosphoproteomic and metabolomic changes after ATR inhibition in irradiated MOLT-4 cells. *PLoS One* **13**, e0199349–e49.
123. **Jossé R *et al.*** (2014) ATR Inhibitors VE-821 and VX-970 sensitize cancer cells to topoisomerase i inhibitors by disabling DNA replication initiation and fork elongation responses. *Cancer Research* **74**, 6968–6979.
124. **Huntoon CJ *et al.*** (2013) ATR inhibition broadly sensitizes ovarian cancer cells to chemotherapy independent of BRCA status. *Cancer Research* **73**, 3683–3691.
125. **Middleton FK *et al.*** (2015) Common cancer-associated imbalances in the DNA damage response confer sensitivity to single agent ATR inhibition. *Oncotarget* **6**, 32396–32409.
126. **Hall AB *et al.*** (2014) Potentiation of tumor responses to DNA damaging therapy by the selective ATR inhibitor VX-970. *Oncotarget* **5**, 5674–5685.
127. **Leszczynska KB *et al.*** (2016) Preclinical testing of an Atr inhibitor demonstrates improved response to standard therapies for esophageal cancer. *Radiotherapy and Oncology: Journal of the European Society for Therapeutic Radiology and Oncology* **121**, 232–238.
128. **Shi Q *et al.*** (2018) The identification of the ATR inhibitor VE-822 as a therapeutic strategy for enhancing cisplatin chemosensitivity in esophageal squamous cell carcinoma. *Cancer Letters* **432**, 56–68.
129. **Kurmasheva RT *et al.*** (2018) Initial testing (stage 1) of M6620 (formerly VX-970), a novel ATR inhibitor, alone and combined with cisplatin and melphalan, by the Pediatric Preclinical Testing Program. *Pediatric Blood & Cancer* **65**, e26825–n/a.
130. **Fordham SE *et al.*** (2018) Inhibition of ATR acutely sensitizes acute myeloid leukemia cells to nucleoside analogs that target ribonucleotide reductase. *Blood Advances* **2**, 1157–1169.
131. **Tu X *et al.*** (2018) ATR inhibition is a promising radiosensitizing strategy for triple-negative breast cancer. *Molecular Cancer Therapeutics* **17**, 2462–2472.
132. **Nagel R *et al.*** (2019) Inhibition of the replication stress response is a synthetic vulnerability in SCLC that acts synergistically in combination with cisplatin. *Molecular Cancer Therapeutics* **18**, 762–770.
133. **Schmitt A *et al.*** (2017) ATM deficiency Is associated with sensitivity to PARP1- and ATR inhibitors in lung adenocarcinoma. *Cancer Research* **77**, 3040–3056.
134. **Wengner AM *et al.*** (2018) Synergistic *in Vivo* activity of the ATR inhibitor BAY 1895344 in combination with the targeted alpha therapy radium-223 dichloride in a preclinical tumor model mimicking bone metastatic castration-resistant prostate cancer (mCRPC). *Cancer Research* **78**(13 Suppl), Abstract nr 838.
135. **Shapiro GI and Harper JW** (1999) Anticancer drug targets: cell cycle and checkpoint control. *The Journal of Clinical Investigation* **104**, 1645–1653.
136. **Graves PR *et al.*** (2000) The Chk1 protein kinase and the Cdc25C regulatory pathways are targets of the anticancer agent UCN-01. *Journal of Biological Chemistry* **275**, 5600–5605.
137. **Xiao Y *et al.*** (2013) Identification of preferred chemotherapeutics for combining with a CHK1 inhibitor. *Molecular Cancer Therapeutics* **12**, 2285–2295.
138. **Isono M *et al.*** (2017) Checkpoint kinase inhibitor AZD7762 strongly sensitises urothelial carcinoma cells to gemcitabine. *Journal of Experimental & Clinical Cancer Research: CR* **36**, 1–1.
139. **Xu H *et al.*** (2011) Checkpoint kinase inhibitor synergizes with DNA-damaging agents in G1 checkpoint-defective neuroblastoma. *International Journal of Cancer* **129**, 1953–1962.
140. **Gadhikar MA *et al.*** (2013) Chk1/2 inhibition overcomes the cisplatin resistance of head and neck cancer cells secondary to the loss of functional p53. *Molecular Cancer Therapeutics* **12**, 1860–1873.
141. **Bartucci M *et al.*** (2011) Therapeutic targeting of Chk1 in NSCLC stem cells during chemotherapy. *Cell Death and Differentiation* **19**, 768.
142. **Blasina A *et al.*** (2008) Breaching the DNA damage checkpoint via PF-00477736, a novel small-molecule inhibitor of checkpoint kinase 1. *Molecular Cancer Therapeutics* **7**, 2394–2404.
143. **Bryant C, Rawlinson R and Massey AJ** (2014) Chk1 inhibition as a novel therapeutic strategy for treating triple-negative breast and ovarian cancers. *BMC Cancer* **14**, 570–570.
144. **Kim MK, James J and Annunziata CM** (2015) Topotecan synergizes with CHEK1 (CHK1) inhibitor to induce apoptosis in ovarian cancer cells. *BMC Cancer* **15**, 196–196.
145. **Fang DD *et al.*** (2013) Combined gemcitabine and CHK1 inhibitor treatment induces apoptosis resistance in cancer stem cell-like cells enriched with tumor spheroids from a non-small cell lung cancer cell line. *Frontiers of Medicine* **7**, 462–476.
146. **Zhang C *et al.*** (2009) PF-00477736 mediates checkpoint kinase 1 signaling pathway and potentiates docetaxel-induced efficacy in Xenografts. *Clinical Cancer Research* **15**, 4630–4640.
147. **Busch C-J *et al.*** (2013) HPV-positive HNSCC cell lines but not primary human fibroblasts are radiosensitized by the inhibition of Chk1. *Radiotherapy and Oncology* **108**, 495–499.
148. **Restelli V *et al.*** (2015) Characterization of a mantle cell lymphoma cell line resistant to the Chk1 inhibitor PF-00477736. *Oncotarget* **6**, 37229–37240.
149. **Nguyen T *et al.*** (2015) Synergism between bosutinib (SKI-606) and the Chk1 inhibitor (PF-00477736) in highly imatinib-resistant BCR/ABL^{+} leukemia cells. *Leukemia Research* **39**, 65–71.
150. **Ferrao PT *et al.*** (2011) Efficacy of CHK inhibitors as single agents in MYC-driven lymphoma cells. *Oncogene* **31**, 1661.
151. **Suzuki M *et al.*** (2017) MK-8776, a novel Chk1 inhibitor, exhibits an improved radiosensitizing effect compared to UCN-01 by exacerbating radiation-induced aberrant mitosis. *Translational Oncology* **10**, 491–500.
152. **Zhou Z-R *et al.*** (2017) The Chk1 inhibitor MK-8776 increases the radiosensitivity of human triple-negative breast cancer by inhibiting autophagy. *Acta Pharmacologica Sinica* **38**, 513–523.
153. **Bridges KA *et al.*** (2016) MK-8776, a novel chk1 kinase inhibitor, radiosensitizes p53-defective human tumor cells. *Oncotarget* **7**, 71660–71672.
154. **Montano R *et al.*** (2013) Sensitization of human cancer cells to gemcitabine by the Chk1 inhibitor MK-8776: cell cycle perturbation and impact of administration schedule in vitro and in vivo. *BMC Cancer* **13**, 604.
155. **Herůdková J *et al.*** (2017) Chk1 inhibitor SCH900776 effectively potentiates the cytotoxic effects of platinum-based chemotherapeutic drugs in human colon cancer cells. *Neoplasia (New York, N.Y.)* **19**, 830–841.
156. **Walton MI *et al.*** (2012) CCT244747 Is a novel potent and selective CHK1 inhibitor with oral efficacy alone and in combination with genotoxic anticancer drugs. *Clinical Cancer Research: an Official Journal of the American Association for Cancer Research* **18**, 5650–5661.
157. **Patel R *et al.*** (2017) An orally bioavailable Chk1 inhibitor, CCT244747, sensitizes bladder and head and neck cancer cell lines to radiation. *Radiotherapy and Oncology: Journal of the European Society for Therapeutic Radiology and Oncology* **122**, 470–475.
158. **Booth L *et al.*** (2018) The CHK1 inhibitor SRA737 synergizes with PARP1 inhibitors to kill carcinoma cells. *Cancer Biology & Therapy* **19**, 786–796.
159. **King C *et al.*** (2015) LY2606368 causes replication catastrophe and antitumor effects through CHK1-dependent mechanisms. *Molecular Cancer Therapeutics* **14**, 2004–2013.
160. **Ghelli Luserna Di Rorà A *et al.*** (2016) Prexasertib, a Chk1/Chk2 inhibitor, increases the effectiveness of conventional therapy in B-/T- cell progenitor acute lymphoblastic leukemia. *Oncotarget* **7**, 53377–53391.
161. **Sen T *et al.*** (2017) CHK1 inhibition in small-cell lung cancer produces single-agent activity in biomarker-defined disease subsets and combination activity with Cisplatin or Olaparib. *Cancer research* **77**, 3870–3884.
162. **Lowery CD *et al.*** (2017) The checkpoint kinase 1 inhibitor prexasertib induces regression of preclinical models of human neuroblastoma. *Clinical Cancer Research* **23**, 4354–4363.
163. **Brill E *et al.*** (2017) Prexasertib, a cell cycle checkpoint kinases 1 and 2 inhibitor, increases in vitro toxicity of PARP inhibition by preventing Rad51 foci formation in BRCA wild type high-grade serous ovarian cancer. *Oncotarget* **8**, 111026–40.
164. **Yin Y *et al.*** (2017) Chk1 inhibition potentiates the therapeutic efficacy of PARP inhibitor BMN673 in gastric cancer. *American Journal of Cancer Research* **7**, 473–483.
165. **Hsu W-H *et al.*** (2019) Checkpoint kinase 1 inhibition enhances cisplatin cytotoxicity and overcomes cisplatin resistance in SCLC by promoting mitotic cell death. *Journal of Thoracic Oncology* **14**, 1032–1045.

Downloaded from https://www.cambridge.org/core. Newcastle University, on 15 Feb 2022 at 13:26:48, subject to the Cambridge Core terms of use, available at https://www.cambridge.org/core/terms. https://doi.org/10.1017/erm.2020.3

166. **Wang Y *et al.*** (2001) Radiosensitization of p53 mutant cells by PD0166285, a novel G_2 checkpoint Abrogator. *Cancer Research* **61**, 8211–8217.
167. **Mir SE *et al.*** (2010) In silico analysis of kinase expression identifies WEE1 as a gatekeeper against mitotic catastrophe in glioblastoma. *Cancer Cell* **18**, 244–257.
168. **PosthumaDeBoer J *et al.*** (2011) WEE1 Inhibition sensitizes osteosarcoma to radiotherapy. *BMC Cancer* **11**, 156–156.
169. **de Gooijer MC *et al.*** (2018) ATP-binding cassette transporters limit the brain penetration of Wee1 inhibitors. *Investigational New Drugs* **36**, 380–387.
170. **Panek RL *et al.*** (1997) In vitro pharmacological characterization of PD 166285, a new nanomolar potent and broadly active protein tyrosine kinase inhibitor. *Journal of Pharmacology and Experimental Therapeutics* **283**, 1433–1444.
171. **Hirai H *et al.*** (2009) Small-molecule inhibition of Wee1 kinase by MK-1775 selectively sensitizes p53-deficient tumor cells to DNA-damaging agents. *Molecular Cancer Therapeutics* **8**, 2992–3000.
172. **Kreahling JM *et al.*** (2012) MK1775, A selective Wee1 inhibitor, shows single-agent antitumor activity against sarcoma cells. *Molecular Cancer Therapeutics* **11**, 174–182.
173. **Hirai H *et al.*** (2010) MK-1775, a small molecule Wee1 inhibitor, enhances anti-tumor efficacy of various DNA-damaging agents, including 5-fluorouracil. *Cancer Biology & Therapy* **9**, 514–522.
174. **Rajeshkumar NV *et al.*** (2011) MK-1775, a potent Wee1 inhibitor, synergizes with gemcitabine to achieve tumor regressions, selectively in p53-deficient pancreatic cancer xenografts. *Clinical Cancer Research: an Official Journal of the American Association for Cancer Research* **17**, 2799–2806.
175. **Bridges KA *et al.*** (2011) MK-1775, a novel Wee1 kinase inhibitor, radiosensitizes p53-defective human tumor cells. *Clinical Cancer Research: an Official Journal of the American Association for Cancer Research* **17**, 5638–5648.
176. **Sarcar B *et al.*** (2011) Targeting radiation-induced G(2) checkpoint activation with the Wee-1 inhibitor MK-1775 in glioblastoma cell lines. *Molecular Cancer Therapeutics* **10**, 2405–2414.
177. **Heijink AM *et al.*** (2015) A haploid genetic screen identifies the G1/S regulatory machinery as a determinant of Wee1 inhibitor sensitivity. *Proceedings of the National Academy of Sciences of the United States of America* **112**, 15160–15165.
178. **Sanjiv K *et al.*** (2016) Cancer-specific synthetic lethality between ATR and CHK1 kinase activities. *Cell Reports* **14**, 298–309.
179. **Jin J *et al.*** (2018) Combined inhibition of ATR and WEE1 as a novel therapeutic strategy in triple-negative breast cancer. *Neoplasia (New York, N.Y.)* **20**, 478–488.
180. **Bukhari AB *et al.*** (2019) Inhibiting Wee1 and ATR kinases produces tumor-selective synthetic lethality and suppresses metastasis. *The Journal of Clinical Investigation* **129**, 1329–1344.
181. **Chaudhuri L *et al.*** (2014) CHK1 And WEE1 inhibition combine synergistically to enhance therapeutic efficacy in acute myeloid leukemia ex vivo. *Haematologica* **99**, 688–696.
182. **Russell MR *et al.*** (2013) Combination therapy targeting the Chk1 and Wee1 kinases shows therapeutic efficacy in neuroblastoma. *Cancer Research* **73**, 776–784.
183. **Hauge S *et al.*** (2017) Combined inhibition of Wee1 and Chk1 gives synergistic DNA damage in S-phase due to distinct regulation of CDK activity and CDC45 loading. *Oncotarget* **8**, 10966–10979.
184. **Magnussen GI *et al.*** (2015) Combined inhibition of the cell cycle related proteins Wee1 and Chk1/2 induces synergistic anti-cancer effect in melanoma. *BMC Cancer* **15**, 462–462.
185. **Chilà R *et al.*** (2015) Combined inhibition of Chk1 and Wee1 as a new therapeutic strategy for mantle cell lymphoma. *Oncotarget* **6**, 3394–3408.
186. **Mohni KN *et al.*** (2015) A synthetic lethal screen identifies DNA repair pathways that sensitize cancer cells to combined ATR inhibition and cisplatin treatments. *PLoS One* **10**, e0125482–e82.
187. **Kim H *et al.*** (2017) Targeting the ATR/CHK1 axis with PARP inhibition results in tumor regression in BRCA-mutant ovarian cancer models. *Clinical Cancer Research: an Official Journal of the American Association for Cancer Research* **23**, 3097–3108.
188. **Booth L *et al.*** (2013) PARP and CHK inhibitors interact to cause DNA damage and cell death in mammary carcinoma cells. *Cancer Biology & Therapy* **14**, 458–465.
189. **Karnak D *et al.*** (2014) Combined inhibition of Wee1 and PARP1/2 for radiosensitization in pancreatic cancer. *Clinical Cancer Research: an Official Journal of the American Association for Cancer Research* **20**, 5085–5096.
190. **Parsels LA *et al.*** (2018) PARP1 trapping and DNA replication stress enhance radiosensitization with combined WEE1 and PARP inhibitors. *Molecular Cancer Research: MCR* **16**, 222–232.
191. **Thomas A *et al.*** (2018) Phase I study of ATR inhibitor M6620 in combination with topotecan in patients with advanced solid tumors. *Journal of Clinical Oncology: Official Journal of the American Society of Clinical Oncology* **36**, 1594–1602.
192. **Bono JSD *et al.*** (2019) First-in-human trial of the oral ataxia telangiectasia and Rad3-related (ATR) inhibitor BAY 1895344 in patients (pts) with advanced solid tumors. *Journal of Clinical Oncology* **37**(15_suppl), 3007–3007.
193. **Samadder P *et al.*** (2017) Synthesis and profiling of a novel potent selective inhibitor of CHK1 kinase possessing unusual N-trifluoromethylpyrazole pharmacophore resistant to metabolic N-dealkylation. *Molecular Cancer Therapeutics* **16**, 1831–1842.
194. **Leijen S *et al.*** (2016) Phase II study of WEE1 inhibitor AZD1775 plus carboplatin in patients With TP53-mutated ovarian cancer refractory or resistant to first-line therapy within 3 months. *Journal of Clinical Oncology* **34**, 4354–4361.
195. **Oza AM *et al.*** (2015) An international, biomarker-directed, randomized, phase II trial of AZD1775 plus paclitaxel and carboplatin (P/C) for the treatment of women with platinum-sensitive, TP53–mutant ovarian cancer. *Journal of Clinical Oncology* **33**(15_suppl), 5506–5506.
196. **Lheureux S *et al.*** (2015) A randomized, placebo-controlled phase II trial comparing gemcitabine monotherapy to gemcitabine in combination with AZD 1775 (MK 1775) in women with recurrent, platinum-resistant epithelial ovarian, primary peritoneal, or Fallopian tube cancers: trial of princess Margaret, Mayo, Chicago, and California consortia. *Journal of Clinical Oncology* **33**(15_suppl), TPS5613–TPTPS13.
197. **Cuneo KC *et al.*** (2019) Dose escalation trial of the wee1 inhibitor Adavosertib (AZD1775) in combination with gemcitabine and radiation for patients with locally advanced pancreatic cancer. *Journal of Clinical Oncology* **37**, 2643–2650.
198. **Bever KM and Le DT** (2018) DNA repair defects and implications for immunotherapy. *The Journal of Clinical Investigation* **128**, 4236–4242.
199. **Zhang Q *et al.*** (2019) Inhibition of ATM increases interferon signaling and sensitizes pancreatic cancer to immune checkpoint blockade therapy. *Cancer research* **79**, 3940–3951.

Downloaded from https://www.cambridge.org/core. Newcastle University, on 15 Feb 2022 at 13:26:48, subject to the Cambridge Core terms of use, available at https://www.cambridge.org/core/terms. https://doi.org/10.1017/erm.2020.3

Appendix B

cancers

MDPI

Article

Exploring the Synergy between PARP and CHK1 Inhibition in Matched *BRCA2* Mutant and Corrected Cells

Hannah L Smith [1], Lisa Prendergast [2] and Nicola J Curtin [1,*]

[1] Newcastle Centre for Cancer, Translational and Clinical Research Institute, Faculty of Medical Sciences, Newcastle University, Newcastle upon Tyne NE2 4HH, UK; hannah.smith2@newcastle.ac.uk

[2] Cancer Research UK Drug Discovery Unit, Newcastle Centre for Cancer, Translational and Clinical Research Institute, Faculty of Medical Sciences, Newcastle University, Newcastle upon Tyne NE2 4HH, UK; Lisa.Prendergast@newcastle.ac.uk

* Correspondence: nicola.curtin@newcastle.ac.uk

Received: 31 January 2020; Accepted: 31 March 2020; Published: 4 April 2020

check for updates

Abstract: PARP inhibition results in the accumulation of DNA SSBs, causing replication stress (RS) and lesions that can only be resolved by homologous recombination repair (HRR). Defects in HRR, e.g., due to *BRCA2* mutation, confer profound sensitivity to PARP inhibitor (PARPi) cytotoxicity. In response to RS, CHK1 is activated to signal to S and G2/M cell cycle checkpoints and also to HRR. To determine the relative contribution of these two functions of CHK1 to survival following PARPi exposure, we investigated the effects of rucaparib (a PARPi) and PF-477736 (a CHK1 inhibitor) alone and in combination in cells with mutated and corrected *BRCA2*. The *BRCA2* mutated V-C8 cells were 1000× more sensitive to rucaparib cytotoxicity than their matched *BRCA2* corrected V-C8.B2 cells, but no more sensitive to PF-477736 despite having seven-fold higher levels of RS. PF-477736 caused a five-fold enhancement of rucaparib cytotoxicity in the V-C8.B2 cells, but no enhancement in the V-C8 cells. This differential sensitivity was not due to a difference in PARP1 or CHK1 expression or activity. PF-477736 increased rucaparib-induced RS (γH2AX foci) and completely inhibited RAD51 focus formation, indicating a profound suppression of HRR. Our data suggested that inhibition of HRR was the main mechanism of sensitisation to rucaparib, compounded with an inhibition of cell cycle checkpoints by PF-477736.

Keywords: PARP; ATR; CHK1; replication stress; homologous recombination DNA repair; cell cycle; cytotoxicity

1. Introduction

Replication stress (RS) is a key source of genomic instability, an enabling characteristic of cancer [1]. RS is increased in cancer due to an almost ubiquitous loss of G1 checkpoint control [2] and unrepaired DNA lesions encountering the replication fork. Poly(ADP-ribose) polymerase (PARP) is a key component of the DNA damage response by promoting DNA base excision repair/single-strand break repair (BER/SSBR) [3]. PARP is the first line of defence against the most common type of endogenous DNA damage, oxidative stress, a major contributor to RS. PARP inhibitors (PARPi) are a significant breakthrough in the treatment of cancer by exploiting cancer-specific defects in homologous recombination DNA repair (HRR), e.g., due to *BRCA* mutations. Toxicities associated with these drugs are generally mild [4]. Three PARPi are currently approved for the treatment of ovarian cancer, the success being largely due to the high frequency (>50%) of HRR defects in this cancer type [5–7].

The high levels of RS and loss of G1 control make cancer cells dependent on S and G2/M cell cycle checkpoint control [8]. Checkpoint kinase 1 (CHK1) is a pivotal checkpoint kinase signalling RS to cell cycle arrest through inactivation of cdc25A and cdc25C. Cdc25A and cdc25C are phosphatases that remove inactivating phosphates on CDK2 and CDK1, respectively. Since CDK2 is required for S-phase entry and progression and CDK1 is needed for mitosis, activation of CHK1 leads to S and G2/M arrest. CHK1 has also been shown to phosphorylate RAD51 and thus has key involvement in signalling to HRR, as well as halting the cell cycle to allow repair to occur [9,10].

CHK1 inhibitors have the potential to counteract HRR-mediated PARPi resistance [11]. Indeed, PARPi and CHK1 inhibitors have been shown to interact to cause increased cytotoxicity in breast and ovarian cancer cells, which was mediated by inhibition of HRR and increased DNA damage [12,13]. However, to date, no investigations have been carried out in paired HRR competent and HRR defective (HRD) cell lines to confirm this as the mechanism.

To better understand the mechanisms underlying the synergy between PARP and CHK1 inhibitors, we used paired *BRCA2* mutant (V-C8) and corrected (V-C8.B2) cells. We examined the effects of the clinically approved PARPi, rucaparib, and the CHK1 inhibitor, PF-477736, that has undergone clinical evaluation (NCT00437203) on target enzyme activity and inhibition, cell cycle control, DNA repair, and cytotoxicity. Our data suggest that CHK1 inhibition results primarily in an HRD phenotype, and this is synthetically lethal with PARP inhibition.

2. Results

2.1. V-C8 Cells Are More Sensitive to Rucaparib, but not PF-477736, and PF-477736 only Sensitised V-C8.B2 Cells to Rucaparib

Colony formation assays were used to determine the potency of rucaparib across V-C8 and V-C8.B2 cell lines. As expected, the HRD V-C8 cells were particularly sensitive to rucaparib (LC_{50} < 0.01 μM) and significantly more sensitive compared to matched HRR-competent V-C8.B2 cells (LC_{50} > 10 μM, $p < 0.001$) (Figure 1a). In contrast, no significant difference in cytotoxicity to PF-477736 (Figure 1b) was observed between the cell lines as both V-C8 and V-C8.B2 cells had similar LC_{50} (100.9 and 87.5 nM, respectively). This suggested that *BRCA2*/HRD status was not a determinant of sensitivity to CHK1 inhibitor PF-477736. Survival in V-C8 and V-C8.B2 cell was inhibited by less than 50% (44.0 ± 5.9 and 41.9 ± 3.5 %, respectively) at 50 nM PF-477736, so this concentration was used for further studies.

We next tested whether the CHK1 inhibitor could potentiate PARPi in HRR competent and defective cells. The survival of cells was evaluated when exposed to a range of rucaparib concentrations (V-C8, 0–0.3 μM, V-C8.B2, 0–30 μM, to account for increased sensitivity to rucaparib) with or without 50 nM PF-477736. In V-C8.B2 cells, co-incubation with PF-477736 decreased the LC_{50} of rucaparib 4.8-fold ± 2.7 (Figure 1c). PF-477736 did not sensitise HRD V-C8 cells to rucaparib (Figure 1d). This differential sensitisation of HRR functional and dysfunctional cells suggested PF-77736 was sensitising HRR competent cells by inhibiting HRR.

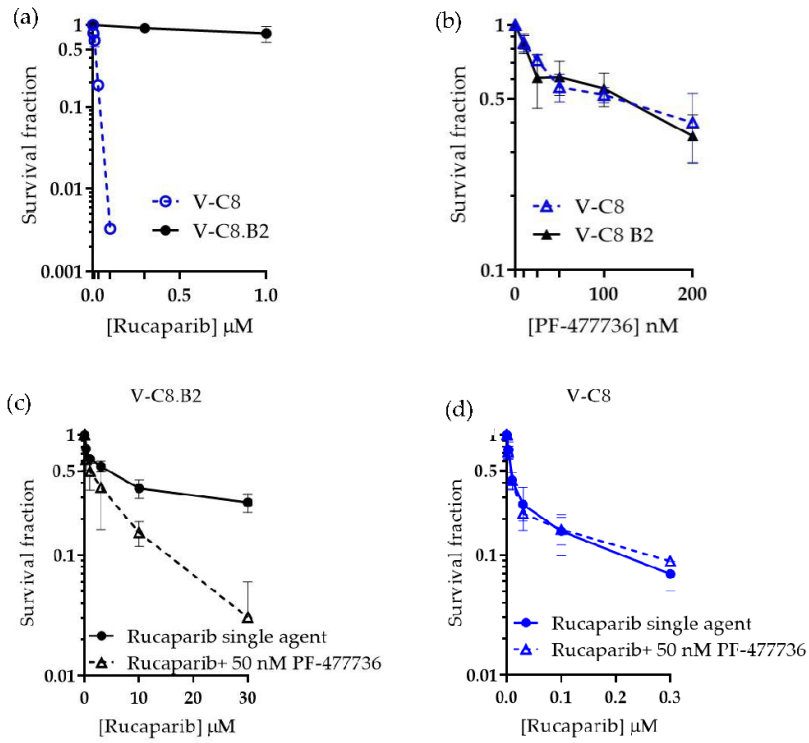


Figure 1. Differential cytotoxicity and synergy of rucaparib and PF-477736 in *BRCA2* mutant and corrected cells. V-C8 and V-C8.B2 cells were exposed to drugs at the indicated concentration for 24 h prior to replacement with drug-free medium for 7–10 days to allow colony formation. (**a**) Rucaparib, (**b**) PF-477736, (**c**) the combination of rucaparib with 50 nM PF-477736 in V-C8 B2 cells, and (**d**) the combination of rucaparib with 50 nM PF-477736 in V-C8 cells. Data are the mean and standard error of three independent experiments.

2.2. The Difference in Rucaparib Sensitivity Is not Due To Differential PARP-1 Expression between Cell Lines

To exclude differences in PARP1 expression, activity, or inhibition as factors contributing to the differential sensitisation to rucaparib by PF-477736, we measured PARP expression and activity in both cell lines. PARP1 levels were not substantially different between cell lines and were only modestly affected by rucaparib and PF-477736 (Figure 2a and Figure S1). Endogenous PAR levels were 2.3-fold higher in the HRD V-C8 cells compared to the V-C8.B2 cells (Figure 2b), possibly reflecting a higher level of endogenous DNA breakage activating PARP. There was no significant difference between the baseline PARP activity of both cell lines (Figure 2c). Rucaparib inhibited PARP activity to a similar extent in both V-C8 and V-C8.B2 cells with IC_{50} values of 59 and 53 nM, respectively (Figure 2d). In both cell lines, a concentration of 0.1 μM rucaparib inhibited PARP activity >95%. This concentration only killed 3% of V-C8.B2 cells compared with >99% of V-C8 cells, demonstrating that the differential cytotoxicity was determined by HRR status rather than the extent of PARP inhibition.

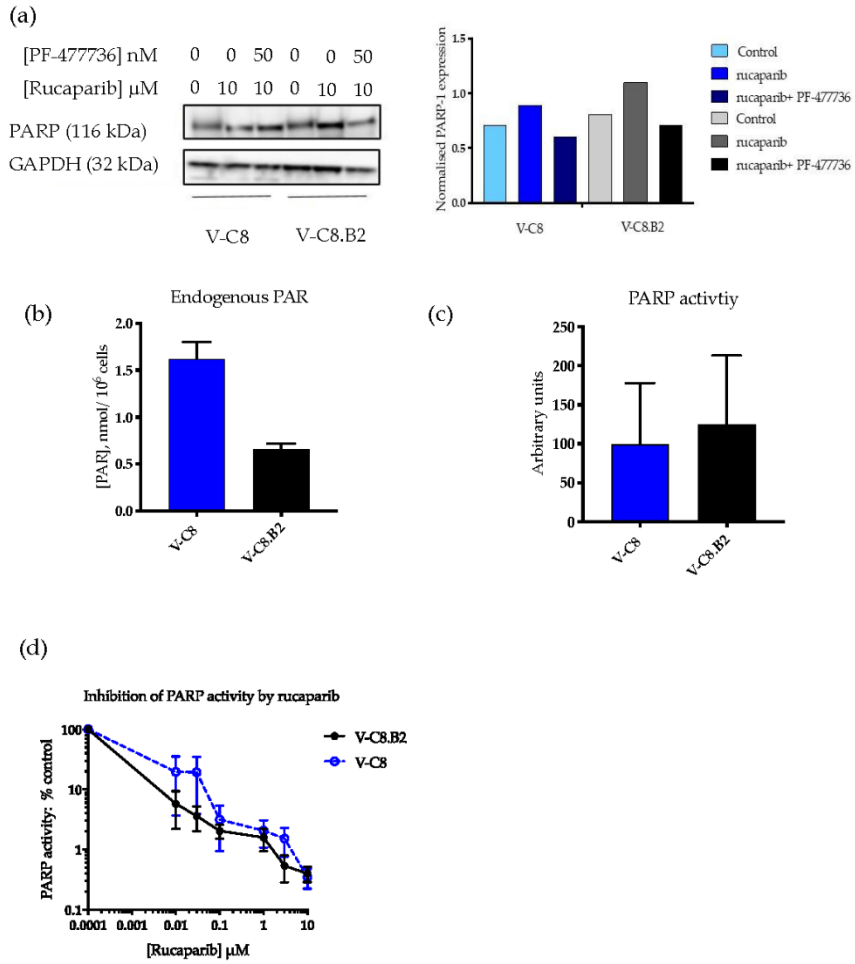


Figure 2. PARP-1 expression, activity, and inhibition by rucaparib in *BRCA2* mutant and corrected cells. (**a**) V-C8 and V-C8.B2 cells were exposed to drugs at the indicated concentration for 24 h prior to Western blot. Chemiluminescence was quantified using Syngene software. Bar charts are PARP-1 expression relative to the GAPDH loading control. Data are from a single representative experiment. (**b**) Endogenous PAR was measured in the absence of oligonucleotide and NAD+ by reference to a standard curve. Data are the mean and standard deviation of three independent experiments. (**c**) PARP activity (mean pixel values) was measured in the presence of oligonucleotide and NAD+. Data are the mean and standard deviation of three individual experiments. (**d**) PARP activity following exposure to increasing concentrations of rucaparib. Data are the mean and standard error of three individual experiments.

2.3. Rucaparib Activates CHK1 Similarly in Both Cell Lines, and This Activation Is Inhibited by PF-477736

Another possible explanation for the differential sensitisation by PF-477736 could have been a difference in the activation of CHK1 by rucaparib and a difference in the extent to which it was inhibited by PF-77736. The expression of CHK1 in the native and phosphorylated forms and downstream signalling to CDK1 were determined by Western blot (Figure 3a and Figure S2). CHK1 expression was slightly lower in V-C8 cells compared to V-C8.B2 cells, but this was not significant (Figure 3b). Rucaparib (10 μM) activated checkpoint signalling through ATR and CHK1 in both cell lines (Figure 3a). $CHK1^{S345}$ levels (indicating ATR activation) were increased 2.1-fold and 1.6-fold by rucaparib in V-C8 and V-C8.B2 cells, respectively. CHK1 activity ($CHK1^{S296}$) was increased by rucaparib to a similar extent in V-C8 and V-C8.B2 cells (1.5-fold and 1.6-fold, respectively) (Figure 3c). In both cell lines, PF-477736 (50 nM) inhibited this activation of CHK1, by 91.4% ± 12.2 in V-C8 cells and 75.6% ± 17.6 in V-C8.B2 cells. The difference in inhibition of $CHK1^{S296}$ by PF-477736 was not statistically significantly different between the two cell lines, suggesting this did not contribute towards the difference observed in sensitisation. Downstream of CHK1, PF-477736 similarly inhibited phosphorylation of CDK1 ($CDK1^{Y15}$) by 69.6% ± 24.8 in V-C8 cells and 56.88 % ± 26.1 in V-C8.B2 cells. Upstream of CHK1, PF-477736 activated ATR 2.1-fold ± 1.3 in V-C8 cells and 2.4-fold ± 1.2 in V-C8.B2 cells, suggesting an increased reliance on ATR when CHK1 was inhibited.

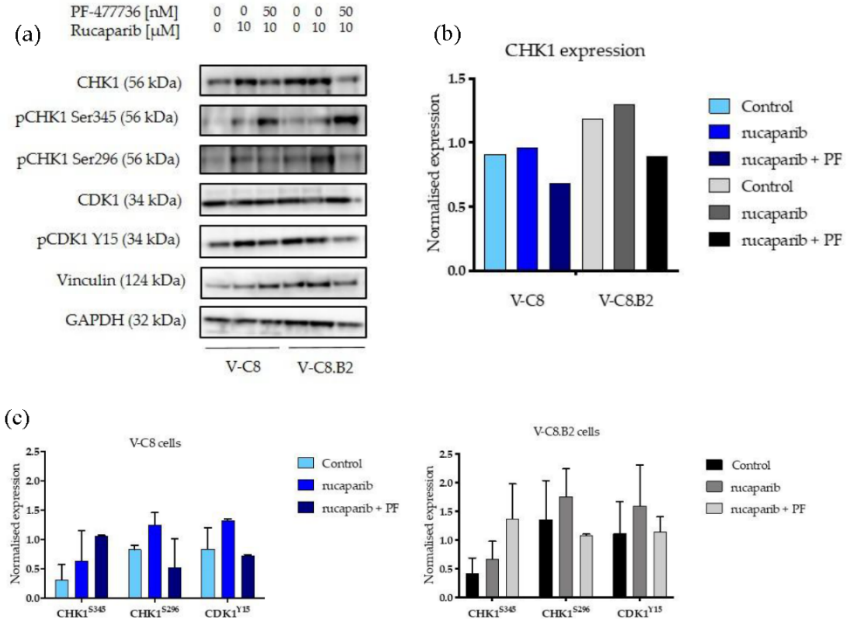


Figure 3. CHK1 expression, activation by rucaparib, and inhibition by PF-477736 in *BRCA2* mutant and corrected cells. Cells were exposed for 24 h to DMSO, rucaparib, or rucaparib and PF-477736 and analysed for $pCHK^{S345}$, CHK1, and $pCDK1^{Tyr15}$. Vinculin was used as a loading control for $pCHK^{S345}$, CHK1, $pCDK1^{Tyr15}$ and CDK1, and GAPDH was used as the loading control for $CHK1^{S296}$ (**a**) Western blot from a single representative experiment. (**b**) Densitometry was calculated using Syngene software of CHK1 expression normalised to Vinculin. (c) Normalised densitometry of phosphorylated CHK1 and CDK1. Data are the mean and standard deviation of three individual experiment.

2.4. Rucaparib Causes S-phase and G2 Accumulation, Which Is Attenuated by PF-477736

The effect of rucaparib and PF-477736 on the cell cycle was analysed to assess if the mechanism of sensitisation was by cell cycle checkpoint signalling. In V-C8.B2 cells, rucaparib caused a modest increase in S-phase (19.31%). Co-exposure to PF-477736 reduced the S-phase by 64.5% and G2/M by 33.6% compared to control cells, and this was accompanied by an increase in the sub-G1 fraction of 21.5%, suggesting that cells were progressing through S and G2/M with damaged DNA and dying, probably by mitotic catastrophe (Figure 4a).

2.5. Rucaparib Inhibition Leads to Increased DNA Damage and HRR, and PF-477736 Inhibits HRR

The induction of replication stress by rucaparib, resulting in collapsed replication forks following accumulation of endogenous DNA damage, is commonly measured by γH2AX phosphorylation. At baseline, untreated V-C8 cells had on average seven-fold more γH2AX foci/cell, compared to V-C8.B2 cells, reflecting their inability to resolve RS through HRR (Figure 4b). In V-C8.B2 cells, rucaparib increased γH2AX foci/cell 16-fold ($p < 0.0001$), PF-477736 caused a three-fold increase in γH2AX foci/cell ($p < 0.0001$), and the γH2AX foci/cell following the combination were higher still, but not significantly different from rucaparib alone.

In V-C8 cells, the already high levels of γH2AX foci were only increased by 20% by PF-477736 and 30% by rucaparib (Figure 4b, not significant). The combination increased the number of foci approximately three-fold ($p < 0.0001$). Due to the *BRCA2* mutation in these cells, they had very low levels of RAD51 foci, which were not increased by rucaparib or PF-477736 alone or in combination.

In marked contrast, in parallel with the induction of DNA breaks (γ-H2AX) in V-C8.B2 cells, rucaparib exposure caused an approximately 13-fold increase ($p < 0.0001$) in RAD51 foci in γ-H2AX-positive cells. Importantly, PF-477736 completely abrogated the rucaparib induction of RAD51 (significantly different from rucaparib alone, $p < 0.0001$), and the levels of foci were similar to control V-C8.B2 and the HRD V-C8 cells. These data indicated that the inhibition of CHK1 totally abolished HRR and led to a greater accumulation of collapsed replication forks.

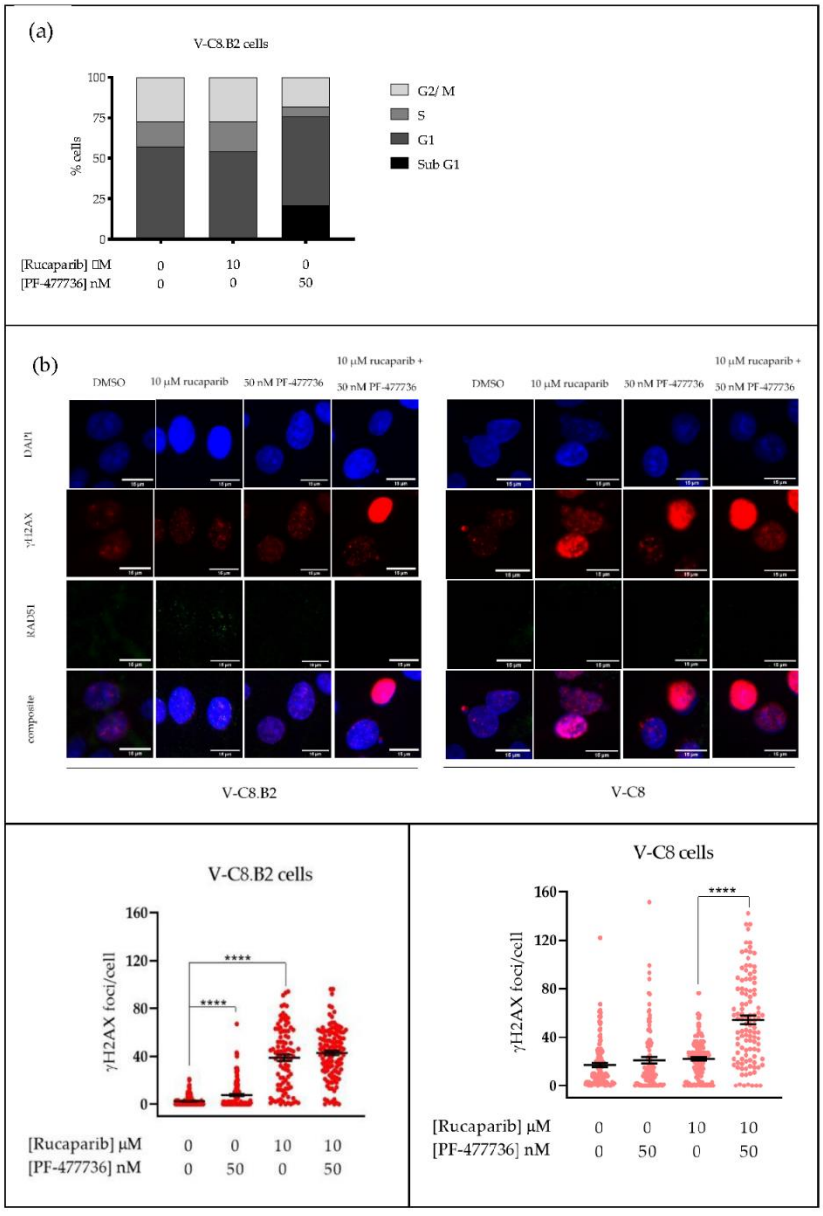


Figure 4. *Cont.*

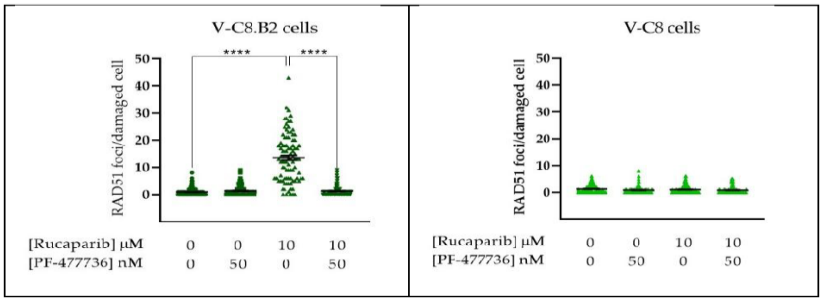


Figure 4. Impact of PF-477736 on cell cycle and homologous recombination repair (HRR) in rucaparib-treated cells. Cells were exposed for 24 h to DMSO, rucaparib, or rucaparib with PF-477736 at the indicated concentrations. (a) Cell cycle analysis of V-C8.B2 cells; data are from a single experiment. (b) Representative images are shown above quantified γH2AX and RAD51 foci, where each data point represents a single nucleus. RAD51 foci were only counted in cells with >mean γH2AX foci in untreated cells. Data are pooled from three independent experiments.

3. Discussion

Defects in either *BRCA1* or *BRCA2* have been known to result in a profound sensitivity to PARP inhibition since 2005 [14,15]. Rucaparib has previously been documented to be ≥1000× more cytotoxic to *BRCA2* mutant V-C8 cells compared to their matched *BRCA2* corrected V-C8.B2 cells (Patent WO/2005/012305), which we confirmed here. Interestingly, *BRCA2* was not a determinant of PF-477736 sensitivity. RS was thought to be a determinant of sensitivity to cell cycle checkpoint inhibitors, so this was somewhat surprising given that untreated V-C8 cell had seven-times more H2AX foci than V-C8.B2 cells. In previous studies, V-C8 cells were more sensitive to the ATR inhibitor VE-821 [16], possibly RS being a greater determinant of sensitivity to ATR than CHK1 inhibition.

Here, we confirmed that the observed difference in rucaparib sensitivity was not due to different PARP-1 expression levels or activity between the cell lines. This contrasts with previous reports of substantially higher levels of PARP activity in V-C8 compared to V-C8.B2 cells [17]. This may reflect differences in the method of detecting PARP activity. In our study, we used a GCLP-validated assay that has been used as a pharmacodynamic biomarker in PARPi clinical trials [18]. However, like this previous study, endogenous PAR levels were around two-fold higher in *BRCA2* mutant cells than wildtype, possibly indicating higher levels of endogenous DNA damage. In support of this hypothesis, there was approximately seven-times as much γH2AX foci formation in untreated *BRCA2* mutant V-C8 cells compared to *BRCA2* corrected V-C8.B2. The differential rucaparib sensitivity observed in cytotoxicity experiments was clearly due to *BRCA2* mutation and the synthetically lethal relationship between BER and HRR pathways. Therefore, it is interesting that PF-477736 only sensitised V-C8.B2 cells and not V-C8 cells to rucaparib, suggesting the CHK1 inhibitor was primarily acting on HRR.

We demonstrated that rucaparib induced RS to a higher extent in V-C8.B2 cells; however, this was most likely due to the high levels of RS in V-C8 control cells. CHK1 was activated to a similar extent by rucaparib in both V-C8 and V-C8.B2 cells, and PF-477736 caused a similar inhibition in both cell lines, so the differential sensitisation observed was not due to a greater activation or inhibition of the pathway. Rucaparib caused a similar increase in pCDK1^{Y15}, which was inhibited to a similar degree by PF-47736 in both cell lines, indicating that the downstream checkpoint signalling was intact and equally responsive to the two inhibitors in both cell lines. Therefore, this was not a factor in the differential sensitisation of VC8.B2 cells. Increased CHK^{S345} phosphorylation in both V-C8 and V-C8.B2 cells was also observed in response to CHK1 inhibition with PF-477736, suggesting upstream ATR activation as previously described [19,20].

Cell cycle analysis showed only a modest S-phase accumulation caused by rucaparib, probably associated with the increase in RS that was demonstrated by the increase in γH2AX (Figure 4). PF-477736 not only abolished this rucaparib-induced S-phase arrest, but also reduced both S- and G2-phases relative to untreated controls. This reduction in S and G2 was accompanied with a corresponding increase in the sub-G1 fraction, suggesting damaged cells were forced into mitosis before they could undertake repair, as has been reported for other PARP and CHK1 inhibitor combinations [21,22].

Although these data indicated that inhibition of cell cycle checkpoints by PF-477736 made a contribution to the cytotoxicity of rucaparib, this is unlikely to explain the differential sensitisation of the *BRCA2* corrected compared to the *BRCA2* mutant cells. We therefore tested the hypothesis that the primary mechanism of sensitisation was via PF-477736-mediated inhibition of HRR. As predicted, PF-477736 profoundly inhibited HRR, completely abolishing RAD51 foci formation. In a study of breast cancer cell lines, prexasertib synergised with the PARPi olaparib by causing S-phase arrest and inhibiting HRR/RAD51 foci [23]. In contrast, in high-grade serous *BRCA*-wildtype ovarian cancer cells, prexasertib synergised with olaparib by inhibiting G2/M arrest, as well as also inhibiting olaparib-induced RAD51 foci formation [13]. Clearly, the various molecular pathologies of these cells complicate the interpretation of the data.

4. Materials and Methods

4.1. Chemicals and Reagents

All chemicals and reagents used were obtained from Sigma-Aldrich, unless stated otherwise. Rucaparib was gifted from Pfizer Global R&D. Both rucaparib and PF-477736 (Selleckchem, Houston, TX, USA) were dissolved in dry DMSO at respective concentrations of 20 mM and 5 mM and stored at −80 °C before use.

4.2. Cell Culture

VC-8 and VC-8.B2 cells, a gift from Malgorzata Zdzienica, Leiden University [24], were maintained in exponential growth phase (<70–80% confluence) in DMEM with 10% foetal bovine serum (FBS; Thermo Fisher Scientific, Waltham, MA, USA) and incubated at 37 °C, 5% CO_2, and 95% humidity. VC8.B2 cells contained a BAC containing the *BRCA2* gene and maintained under selection with 200 µg/mL G-418 (Thermo Fisher Scientific, Waltham, MA, USA). Cells were mycoplasma free.

4.3. Cytotoxicity Assay

Exponentially growing cells were seeded at various densities in 6 well plates, allowing 3 different densities for each drug concentration estimated to give 20–200 colonies following drug treatment. After attachment, cells were exposed to various concentrations of rucaparib or PF-477736 alone or the combination of rucaparib ± 50 nM PF-477736 in DMSO or DMSO alone at a final concentration of 0.5% for 24 h. The medium was replaced with fresh medium and the cells left to incubate for 7–10 days to form colonies. The colonies were fixed in methanol:acetic acid (3:1) stained with 0.4% crystal violet, and colonies of >30 cells were counted by eye. Graphs were plotted using Graphpad Prism 6 software (San Diego, CA, USA).

4.4. Measurement of PARP Activity and Inhibition

Following incubation with rucaparib (0–10 µM) for 30 min, PARP activity was measured in permeabilised cells at 26 °C in the presence of 350 nM NAD+ and 10 mg/mL 12 mer palindromic oligonucleotide to activate the enzyme, as described previously [25,26]. Following transfer to a nitrocellulose membrane (GE Healthcare Life, Sciences, Amersham, Buckinghamshire, UK) the product, PAR, was measured with 10H anti-PAR monoclonal antibody (Enzo life sciences, Exeter, UK) overnight at 4 °C and HRP-conjugated goat anti-mouse secondary antibody (Dako, Santa Clara, CA, USA) diluted 1:1000 in PBS-Tween (PBS-T) 5%. Clarity Max ECL Western substrate (Bio-Rad, Hercules, CA,

USA) was added to the membrane, chemiluminescence imaged using the GBox and Genesys software (Syngene, Cambridge, UK), and quantified with reference to a standard curve of 0–25 pmol purified PAR (Enzo life sciences, Farmingdale, NY, USA) after subtraction of background reactions in the absence of NAD and oligonucleotide. Baseline PAR levels were measured using 50–100-times the cells used for inhibition experiments and with no oligonucleotide or NAD+ present. Purified PAR standard was diluted accordingly to a concentration of 0–25 pmol.

4.5. Measurement of CHK1 Activation and Inhibition by Western Blot

Exponentially growing cells in 100 mm dishes were exposed to media containing DMSO, 10 μM rucaparib, or 10 μM rucaparib and 50 nM PF-477736 for 24 h before extraction with 250 μL per dish of phosphosafe extraction reagent with protease cocktail inhibitor (Thermo Fisher Scientific, Waltham, MA, USA) at a 1:100 dilution per dish at 4 °C for 5–7 min, then scraped on ice into Eppendorf tubes. Following centrifugation at 8000× *g* for 10 min at 4 °C, the protein concentration of the supernatants was measured using a BCA protein assay kit (Thermo Fisher Scientific, Waltham, MA, USA) and diluted with deionised water to 0.5–1 mg/mL. XT sample buffer (Bio-Rad, Hercules, CA, USA) and XT reducing agent (Bio-Rad, Hercules, CA, USA) were added at constants of 25% and 0.5%, respectively. Samples were heated at 90 °C for 5 min, then 30 μg were loaded/well of 3–8% Criterion XT tris-acetate gels (Bio-Rad, Hercules, CA, USA), and the gel ran at 150V for approximately 1 h alongside HiMark pre-stained protein standard (Thermo Fisher Scientific, Waltham, MA, USA) in diluted 20× XT tricine with deionised water. The separated proteins were transferred onto a nitrocellulose membrane (Amersham, Buckinghamshire, United Kingdom) at 100 V for 1 h. The membrane was blocked for 1 h at room temperature in 5% milk in TBS-tween (TBST). Primary antibodies PARP-1 (#ab227244 Abcam, Cambridge, UK), vinculin (#4650), GAPDH (14C10 #2118), phospho-CHK1 (Ser296) (D3O9F #90178), phospho-Chk1 (Ser345) (#2341), and phospho-CDK1 (Tyr15) (10A11 #4539) were each diluted 1:1000 in TBS-Tween (TBS-T) and 5% bovine serum albumin (BSA) and left to incubate overnight at 4 °C (all obtained from Cell signalling, Massachusetts, United States except PARP-1). The membrane was cut into sections (approximately 30–45 kDa, 45–70 kDa, and 70–220 kDa), washed in TBS-T, before adding anti-rabbit goat polyclonal HRP secondary antibody (Cell Signaling Technology, Danvers, MA, USA) diluted 1:2000 in 5% skimmed milk in TBST at room temperature for 1 h. After washing with TBST, Clarity Max ECL Western substrate (Bio-Rad, Hercules, CA, USA) was applied to the membrane slices and chemiluminescence measured using Syngene software on the G-box.

4.6. Cell Cycle Analysis

Exponentially growing cells were exposed to DMSO, 10 μM rucaparib or 10 μM rucaparib with 50 nM PF-477736 for 24 h. Cells were washed twice with PBS, with each washing collected to ensure no loss of cells, before being trypsinised and harvested. Following centrifugation at 1500 rpm for 5 min, the supernatant was discarded, and the remaining cell pellet was resuspended in 1 mL ice cold PBS and centrifuged (3000 rpm, 5 min). The supernatant was removed, and 1 mL of 70% ethanol was added dropwise to the cell pellet. Samples remained at 4 °C for a minimum of 1 h. Prior to staining, cells were washed twice in PBS to remove ethanol before eventually being resuspended in 700 μL PBS. RNase was added to cells (12 μL of 1 mg/mL stock) alongside propidium iodide stain (20 μL of 1mg/mL stock). Cells were incubated in dark conditions at 37 °C for a minimum of 30 min. Analysis was carried out using Attune Nxt Cytometer. De Novo FCS Express 7 software was used to analyse the data.

4.7. Homologous Recombination Repair Assay

Cells were seeded at 0.5×10^5 cells/mL onto coverslips and incubated for 24 h before being exposed to either DMSO, 50 nM PF-477736, 10 μM rucaparib, or 10 μM rucaparib with 50 nM PF-477736 for 24 h. Cells were then washed with PBS and fixed with ice cold methanol for a minimum of 1 h at −20 °C. Coverslips were then washed with PBS 0.2% Triton-X-100 and blocked (2% BSA, 10% skimmed milk powder (Marvel, UK), 10% goat serum) for 1 h at room temperature before

being incubated with anti-RAD51 (Abcam, Cambridge, UK) diluted 1:500 in blocking buffer at 4 °C overnight. After washing in PBS, 0.2% Triton X-100 anti-phospho-histone H2AX (Merck, Branchburg, NJ, USA) was added to coverslips at 1:1000 and incubated for 1 h. After washing, secondary antibodies, Alexa Fluor 488 and Alexa Fluor 546 (ThermoFisher Scientific, Waltham, MA, USA), were added and incubated for 1 h, in dark conditions. Coverslips were washed then exposed to 0.5 µg/mL DAPI solution. Coverslips were mounted onto microscope slides using H-1400 hard set mounting media (Vector Laboratories, Burlingame, CA, USA). Slides were stored in dark conditions and left to dry prior to imaging. Cells were imaged using the Leica DM6 LED fluorescence microscope (Leica microsystems GmbH, Wetzlar, Germany). Images were analysed using Fiji ImageJ software [27]. In DMSO-treated cells, the mean γH2AX foci were calculated. Cells (control and treated) with more than the mean number of γH2AX foci in control cells were deemed γH2AX positive. RAD51 foci were only counted in γH2AX positive cells.

5. Conclusions

On the basis of our data in matched cell lines that differed only in their BRCA2 status, we proposed the model shown in Figure 5. That is, the RS caused by the accumulation of unrepaired SSB when PARP was inhibited led to collapse of replication forks. These lesions triggered activation of the ATR-CHK1 pathway that signals to cell cycle arrest, but the major contribution that CHK1 makes was to protect cells from PARPi cytotoxicity by promoting HRR. The use of a CHK1 inhibitor may therefore be useful not only for tumours that are intrinsically PARPi resistant due to functional HRR, but may also overcome acquired resistance to PARPi in BRCA mutant tumours that have restored HRR function. Recent studies with ovarian cancer PDX models demonstrated that the combination of the CHK1 inhibitor prexasertib with olaparib caused greater tumour growth delay and survival in both olaparib sensitive and resistant tumours [28]. Our data along with this PDX study may help in the interpretation of the results of clinical trials of PARPi-CHK1 inhibitor combinations, such as NCT03057145, in which olaparib is being investigated in combination with prexasertib.

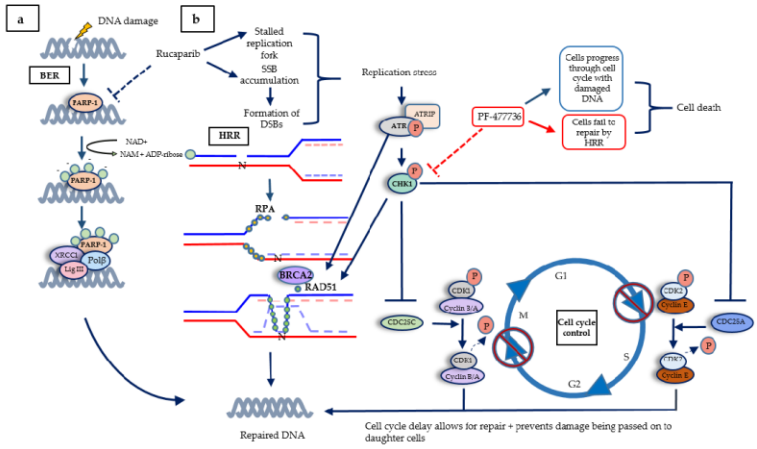


Figure 5. The DNA damage response, highlighting cross-talk between the cell cycle and DNA repair. (**a**) Base excision repair (BER) is the first line of defence when DNA damage occurs. PARP activation by SSB recruits XRCC1, Pol β, and Lig III to repair the DNA. (**b**) When PARP is inhibited, SSB accumulate, causing stalled replication forks, and single-ended DSBs, causing fork collapse. BRCA2 facilitates replacing RPA with repair protein RAD51, which subsequently forms a filament to search for the specific

homologous sequence on the sister chromatid as a template for repair and re-start. PARPi-induced replication stress activates ATR, which initiates a signalling cascade. ATR activates CHK1 by phosphorylation at serine 345, causing CHK1 to autophosphorylate at serine 296, to achieve full activation. CHK1 inactivates CDC25A/C, thereby preventing the removal of inhibitory phosphorylation on CDK2 and 1, respectively, thus preventing S-phase progression and mitosis. The pathway also promotes HRR as CHK1 activates BRCA2 and RAD51 by phosphorylation, and ATR also phosphorylates RAD51.

6. Patents

Helleday T and Curtin NJ. Therapeutic Compounds (PARP inhibitors in homologous repair/BRCA defective cancer) Patent Application Number PCT/GB2004/003183. Publication number WO 2005/012305 A2 Divisional application 16th April 2004 GB 0408524. WO2005012305A3.

Supplementary Materials: The following are available online at http://www.mdpi.com/2072-6694/12/4/878/s1: Figure S1: PARP1 expression in V-C8 and V-C8.B2 cells, Figure S2: CHK1 expression, activation by rucaaprib and inhibition by PF-477736 in V-C8 and V-C8.B2 cells.

Author Contributions: H.L.S. produced the data and wrote the manuscript; L.P. directed the research and edited the manuscript; N.J.C. conceived the project, directed the research and edited the manuscript. All authors have read and agreed to the published version of the manuscript.

Funding: This research was partly funded by the JGW Patterson foundation.

Conflicts of Interest: N.J.C. contributed to the development of rucaparib and obtained research funding from Agouron Pharmacurtical, Pfizer, and Clovis. By virtue of the two active patents and an original agreement between Cancer Research Technology, Newcastle University, and Agouron, she is in receipt of royalty payments, which she does not take personally; in the past, they have contributed to her research accounts, and a recent large sum has been used to set up a charitable fund within the local Community Foundation. https://www.communityfoundation.org.uk/group_grant/passionate-about-realising-your-potential/.

References

1. Hanahan, D.; Weinberg, R.A. Hallmarks of cancer: The next generation. *Cell* **2011**, *144*, 646–674. [CrossRef] [PubMed]
2. Massague, J. G1 cell cycle control and cancer. *Nature* **2004**, *432*, 298–306. [CrossRef] [PubMed]
3. Bai, P. Biology of Poly(ADP-Ribose) Polymerases: The Factotums of Cell Maintenance. *Mol. Cell* **2015**, *58*, 947–958. [CrossRef] [PubMed]
4. LaFargue, C.J.; Dal Molin, G.Z.; Sood, A.K.; Coleman, R.L. Exploring and comparing adverse events between PARP inhibitors. *Lancet Oncol.* **2019**, *20*, e15–e28. [CrossRef]
5. Mukhopadhyay, A.; Elattar, A.; Cerbinskaite, A.; Wilkinson, S.J.; Drew, Y.; Kyle, S.; Los, G.; Hostomsky, Z.; Edmondson, R.J.; Curtin, N.J. Development of a functional assay for homologous recombination status in primary cultures of epithelial ovarian tumor and correlation with sensitivity to poly(ADP-ribose) polymerase inhibitors. *Clin. Cancer Res.* **2010**, *16*, 2344–2351. [CrossRef]
6. Pepa, C.; Tonini, G.; Pisano, C.; Di Napoli, M.; Cecere, S.C.; Tambaro, R.; Facchini, G.; Pignata, S. Ovarian cancer standard of care: Are there real alternatives? *Chin. J. Cancer* **2015**, *34*, 17–27. [CrossRef]
7. Mirza, M.R.; Monk, B.J.; Herrstedt, J.; Oza, A.M.; Mahner, S.; Redondo, A.; Fabbro, M.; Ledermann, J.A.; Lorusso, D.; Vergote, I.; et al. Niraparib Maintenance Therapy in Platinum-Sensitive, Recurrent Ovarian Cancer. *N. Engl. J. Med.* **2016**, *375*, 2154–2164. [CrossRef]
8. Visconti, R.; Monica, R.D.; Grieco, D. Cell cycle checkpoint in cancer: A therapeutically targetable double-edged sword. *J. Exp. Clin. Cancer Res.* **2016**, *35*, 153. [CrossRef]
9. Sørensen, C.S.; Hansen, L.T.; Dziegielewski, J.; Syljuåsen, R.G.; Lundin, C.; Bartek, J.; Helleday, T. The cell-cycle checkpoint kinase Chk1 is required for mammalian homologous recombination repair. *Nat. Cell Biol.* **2005**, *7*, 195–201. [CrossRef]
10. Narayanaswamy, P.B.; Tkachuk, S.; Haller, H.; Dumler, I.; Kiyan, Y. CHK1 and RAD51 activation after DNA damage is regulated via urokinase receptor/TLR4 signaling. *Cell Death Dis.* **2016**, *7*, 2383. [CrossRef]
11. Haynes, B.; Murai, J.; Lee, J.M. Restored replication fork stabilization, a mechanism of PARP inhibitor resistance, can be overcome by cell cycle checkpoint inhibition. *Cancer Treat. Rev.* **2018**, *71*, 1–7. [CrossRef] [PubMed]

12. Booth, L.; Cruickshanks, N.; Ridder, T.; Dai, Y.; Grant, S.; Dent, P. PARP and CHK inhibitors interact to cause DNA damage and cell death in mammary carcinoma cells. *Cancer Biol. Ther.* **2013**, *14*, 458–465. [CrossRef] [PubMed]
13. Brill, E.; Yokoyama, T.; Nair, J.; Yu, M.; Ahn, Y.R.; Lee, J.M. Prexasertib, a cell cycle checkpoint kinases 1 and 2 inhibitor, increases in vitro toxicity of PARP inhibition by preventing Rad51 foci formation in BRCA wild type high-grade serous ovarian cancer. *Oncotarget* **2017**, *8*, 111026–111040. [CrossRef]
14. Bryant, H.E.; Schultz, N.; Thomas, H.D.; Parker, K.M.; Flower, D.; Lopez, E.; Kyle, S.; Meuth, M.; Curtin, N.J.; Helleday, T. Specific killing of BRCA2-deficient tumours with inhibitors of poly(ADP-ribose) polymerase. *Nature* **2005**, *434*, 913–917. [CrossRef] [PubMed]
15. Farmer, H.; McCabe, N.; Lord, C.J.; Tutt, A.N.; Johnson, D.A.; Richardson, T.B.; Santarosa, M.; Dillon, K.J.; Hickson, I.; Knights, C.; et al. Targeting the DNA repair defect in BRCA mutant cells as a therapeutic strategy. *Nature* **2005**, *434*, 917–921. [CrossRef]
16. Middleton, F.K.; Patterson, M.J.; Elstob, C.J.; Fordham, S.; Herriott, A.; Wade, M.A.; McCormick, A.; Edmondson, R.; May, F.E.; Allan, J.M.; et al. Common cancer-associated imbalances in the DNA damage response confer sensitivity to single agent ATR inhibition. *Oncotarget* **2015**, *6*, 32396–32409. [CrossRef] [PubMed]
17. Gottipati, P.; Vischioni, B.; Schultz, N.; Solomons, J.; Bryant, H.E.; Djureinovic, T.; Issaeva, N.; Sleeth, K.; Sharma, R.A.; Helleday, T. Poly(ADP-ribose) polymerase is hyperactivated in homologous recombinationdefective cells. *Cancer Res.* **2010**, *70*, 5389–5398. [CrossRef] [PubMed]
18. Plummer, R.; Jones, C.; Middleton, M.; Wilson, R.; Evans, J.; Olsen, A.; Curtin, N.; Boddy, A.; McHugh, P.; Newell, D.; et al. Phase I study of the poly(ADP-ribose) polymerase inhibitor, AG014699, in combination with temozolomide in patients with advanced solid tumors. *Clin. Cancer Res.* **2008**, *14*, 7917–7923. [CrossRef]
19. Massey, A.J. Inhibition of ATR-dependent feedback activation of Chk1 sensitises cancer cells to Chk1 inhibitor monotherapy. *Cancer Lett.* **2016**, *383*, 41–52. [CrossRef]
20. Syljuåsen, R.G.; Sørensen, C.S.; Hansen, L.T.; Fugger, K.; Lundin, C.; Johansson, F.; Helleday, T.; Sehested, M.; Lukas, J.; Bartek, J. Inhibition of human Chk1 causes increased initiation of DNA replication, phosphorylation of ATR targets, and DNA breakage. *Mol. Cell. Biol.* **2005**, *25*, 3553–3562. [CrossRef]
21. Yin, Y.; Shen, Q.; Zhang, P.; Tao, R.; Chang, W.; Li, R.; Xie, G.; Liu, W.; Zhang, L.; Kapoor, P.; et al. Chk1 inhibition potentiates the therapeutic efficacy of PARP inhibitor BMN673 in gastric cancer. *Am. J. Cancer Res.* **2017**, *7*, 473–483. [PubMed]
22. Kim, H.; George, E.; Ragland, R.; Rafail, S.; Zhang, R.; Krepler, C.; Morgan, M.; Herlyn, M.; Brown, E.; Simpkins, F. Targeting the ATR/CHK1 Axis with PARP Inhibition Results in Tumor Regression in BRCA-Mutant Ovarian Cancer Models. *Clin. Cancer Res.* **2017**, *23*, 3097–3108. [CrossRef] [PubMed]
23. Mani, C.; Jonnalagadda, S.; Lingareddy, J.; Awasthi, S.; Gmeiner, W.H.; Palle, K. Prexasertib treatment induces homologous recombination deficiency and synergizes with olaparib in triple-negative breast cancer cells. *Breast Cancer Res.* **2019**, *21*, 1–14. [CrossRef] [PubMed]
24. Kraakman-van der Zwet, M.; Overkamp, W.J.; van Lange, R.E.; Essers, J.; van Duijn-Goedhart, A.; Wiggers, I.; Swaminathan, S.; van Buul, P.P.; Errami, A.; Tan, R.T.; et al. Brca2 (XRCC11) deficiency results in radioresistant DNA synthesis and a higher frequency of spontaneous deletions. *Mol. Cell. Biol.* **2002**, *22*, 669–679. [CrossRef] [PubMed]
25. Plummer, E.R.; Middleton, M.R.; Jones, C.; Olsen, A.; Hickson, I.; McHugh, P.; Margison, G.P.; McGown, G.; Thorncroft, M.; Watson, A.J.; et al. Temozolomide pharmacodynamics in patients with metastatic melanoma: Dna damage and activity of repair enzymes O6alkylguanine alkyltransferase and poly(ADP-ribose) polymerase-1. *Clin. Cancer Res.* **2005**, *11*, 3402–3409. [CrossRef] [PubMed]
26. Canan, S.; Maegley, K.; Curtin, N.J. Strategies Employed for the Development of PARP Inhibitors. *Methods Mol. Biol.* **2017**, *1608*, 271–297.

27. Rueden, C.T.; Schindelin, J.; Hiner, M.C.; DeZonia, B.E.; Walter, A.E.; Arena, E.T.; Eliceiri, K.W. ImageJ2: ImageJ for the next generation of scientific image data. *BMC Bioinformatics* **2017**, *18*, 529. [CrossRef]
28. Parmar, K.; Kochupurakkal, B.S.; Lazaro, J.B.; Wang, Z.C.; Palakurthi, S.; Kirschmeier, P.T.; Yang, C.; Sambel, L.A.; Färkkilä, A.; Reznichenko, E.; et al. The CHK1 Inhibitor Prexasertib Exhibits Monotherapy Activity in High-Grade Serous Ovarian Cancer Models and Sensitizes to PARP Inhibition. *Clin. Cancer Res.* **2019**, *25*, 6127–6140. [CrossRef]



© 2020 by the authors. Licensee MDPI, Basel, Switzerland. This article is an open access article distributed under the terms and conditions of the Creative Commons Attribution (CC BY) license (http://creativecommons.org/licenses/by/4.0/).